Andrea Ciarmiello
Luigi Mansi
Editors

PET-CT and PET-MRI in Neurology

SWOT Analysis Applied to Hybrid Imaging

Springer

PET-CT and PET-MRI in Neurology

Andrea Ciarmiello • Luigi Mansi
Editors

PET-CT and PET-MRI in Neurology

SWOT Analysis Applied to Hybrid Imaging

Springer

Editors
Andrea Ciarmiello
Department of Nuclear Medicine
S. Andrea Hospital
La Spezia
Italy

Luigi Mansi
Department of Nuclear Medicine
Second University of Naples
Napoli
Italy

ISBN 978-3-319-31612-3 ISBN 978-3-319-31614-7 (eBook)
DOI 10.1007/978-3-319-31614-7

Library of Congress Control Number: 2016940200

Printed on acid-free paper

This Springer imprint is published by Springer Nature
The registered company is Springer International Publishing AG Switzerland

Foreword

Neuroimaging can be separated into two broad categories: (i) structural or anatomical imaging and (ii) functional or molecular imaging. Interestingly, one could claim that functional imaging preceded structural imaging by referring to the studies of the Italian neuroscientist Angelo Mosso, who invented the "human circulation balance" in Turin, during the late 1880s. This device could noninvasively measure the redistribution of blood during emotional and intellectual activity. Early in the twentieth century, Walter Dandy (while at Johns Hopkins in Baltimore) developed ventriculography and pneumoencephalography that allowed neurosurgeons for the first time to visualize structural changes in the ventricular system on x-rays that were caused by brain lesions. In the late 1920s, Egas Moniz, professor of neurology in Lisbon, introduced cerebral angiography, whereby both normal and abnormal blood vessels in and around the brain could be visualized with great accuracy (he received a Nobel Prize in 1949). More detailed anatomic images of the brain became available through computerized axial tomography (CAT or CT), which was introduced and refined in the 1960s and 1970s by Oldendorf, Hounfield, and Cormack. This effort translated a research instrument into a safer noninvasive clinical tomograph for imaging the skull and brain and other organs. CT is still extensively used today, which is reflected by the commonplace availability of CT scanners in most hospitals.

Imaging the brain with radiopharmaceuticals was developed in parallel to CT during the 1960s by Lassen, Ingvar, and Skinhoj in Scandinavia. Studies involving Xenon-133 inhalation to image cerebral blood flow used multiple external radiation detectors, plus mathematical algorithms to reconstruct two-dimensional radioactivity images (the forerunner of single-photon emission computed tomography (SPECT)). These blood flow images represented the first modern "functional neuroimaging," reflecting changes in cerebral blood flow from brain activation associated with speaking, reading, visual, or auditory perception and voluntary movement.

Positron emission tomography (PET) was initially developed by Gordon Brownell and William Sweet in the 1950s at the Massachusetts General Hospital, in Boston. A major expansion occurred in St. Louis, where the first positron imaging device was constructed by Ter-Pogossian, Hoffman, and Phleps. The first human PET scanner was developed in 1973 with a hexagonal array of detectors. The inclusion of short-lived oxygen-15-labeled water for PET imaging of cerebral blood flow (allowing multiple studies to be performed on the same subject), along with the ability to generate statistical

parametric maps (SPM) of cerebral activation, was an active area of research in the 1980s and 1990s. This was a major advance in neuroimaging and the assessment of cognitive function of the human brain, namely, the ability to image neural activity in specific brain structures while performing specific tasks, in both normal subjects and in individuals with specific neurological diseases. Currently, such studies are primarily performed using the MRI BOLD technique.

Concurrent with improvements in tomographic imaging technology, there was a parallel expansion in radiochemistry and radiopharmaceutical development for both SPECT and PET in the 1980s and 1990s, which continues to this day. Initially there was a focus on cerebral glucose utilization and neuroreceptor imaging (as PET imaging was limited by head-only tomographs at that time). With the advent of whole-body scanners, FDG PET imaging was rapidly adopted by oncologists to stage the extent and progression of disease and to monitor disease response to therapy. With the current focus on molecular-targeted medicine and individualized patient care, there is an expanding clinical demand to develop new target-specific radiopharmaceuticals for both diagnosis and therapy (theranostics), particularly in oncology where targeted radiopharmaceuticals are being used to assess the response to therapy.

Clinical magnetic resonance imaging (MRI)/magnetic resonance spectroscopy (MRS) was applied shortly after PET and provides both structural and functional images. The absence of radiation exposure and necessity of having a cyclotron and radiochemistry facility nearby, coupled with high-resolution images, were significant advantages and led to the rapid adoption of this imaging technology. Functional MRI/MRS (including BOLD, perfusion/diffusion, arterial spin labeling MRI, etc.) is increasingly being used and has led to MRI/MRS becoming the dominant neuroimaging modality over the past 15 years. This is reflected by the 25,000-plus clinical and research MRI scanners that exist worldwide.

Hyperpolarized MRI/MRS is a new imaging technology that provides a marked increase MRS signal from hyperpolarized molecules. It is currently a research tool that can be used to monitor metabolism, such as the conversion of pyruvate-to-lactate in tumors. This enhanced MRS molecular imaging strategy has evolved over the past decade, but remains technologically challenging. It requires the use of stable (nonradioactive) isotopes (e.g., 13C) for incorporation into specific molecules for hyperpolarization by a special hyperpolarization unit that has to be located close to the scanner, since hyperpolarized molecules decay rapidly (minutes).

In this prelude, I have briefly traced the rapidly evolving history of selected imaging modalities that have contributed to both structural and functional "neuroimaging." The benefits of the shift to hybrid PET/CT and PET/MR imaging are now widely recognized, and this shift is reflected in the title of this monograph and the individual contributions to this monograph.

New York, USA Ronald G. Blasberg, MD

Preface

The past decade has been characterized by fast technological growth. This led to the discovery of increasingly sophisticated diagnostic technologies in molecular imaging. Among these, positron emission tomography (PET) has been the imaging technique with the greatest clinical impact in oncology as well as in neurology and cardiology. Technological innovation has subsequently led to the introduction of hybrid modalities, such as PET/CT and more recently PET/MR.

New technologies are generally expensive, and some of the most frequently asked questions are relative to the cost effectiveness and the advantages of the new technology as compared to those previous. Generally, only several years after the introduction of a technology is there enough data to understand what the clinical impact and advantage of the new technology is.

Unfortunately, it is not always possible to wait too long before deciding whether to invest or not in a new technology. Therefore, a difficult problem to overcome is how to plan the acquisition of new technology in the presence of partial and little consolidated data. Without a planning strategy for healthcare development, there is the risk of acquiring potentially useless technology or by contrast wasting too much time before introducing a new useful technology in to clinical practice. In this book we have tried to apply the SWOT analysis to the evaluation of the strengths, weaknesses, opportunities, and threats of hybrid technologies.

SWOT analysis is a decision supporting tool designed for incorporating internal (strengths and weaknesses) and external (opportunities and threats) factors into organizational or technological change planning.

This analytical approach was previously used mainly in policy research to systematically analyze organizations' environments and only recently has been introduced in healthcare systems. When properly used, SWOT analysis may provide decision-makers a strong and structured basis for strategy development. SWOT analysis is performed through the collection of key informant perspectives, which are considered an essential part in achieving the identified objectives.

In this attempt, we have involved many researchers, clinicians, manufacturers, and decision-makers, a large group of experts, distributed around the world involved with different purposes in hybrid technologies. We are grateful to all of them for the essential contribution given to the achievement of this complex endeavor. We wish also to express our gratitude to the manufacturers who gave their contribution to the survey giving us the opportunity to

understand their point of view (Pier Paolo Buó, GE healthcare Srl; Sandro Paini, Philips Spa; Alessandra Tocchio, Siemens Healthcare Srl). Finally, we are grateful to decision-makers for time devoted to the survey, including their opinion of the analysis that gave us the opportunity to complete our data with the point of view of a relevant stakeholder. Finally, we wish to express our gratitude to Dr. Gianfranco Conzi for his significant contribution to the technological renovation project successfully carried out in our hospital.

La Spezia, Italy Andrea Ciarmiello

Contents

Part I

Basics

Physics of Hybrid Imaging

1

Girolamo Garreffa, Gisela Hagberg, and Luca Indovina

1.1 Introduction

The main purpose of multimodality imaging is to provide an advanced diagnostic tool by combining measurements of anatomy and physiology obtained with different techniques – in particular PET-TC and PET/MRI. Multimodality imaging can refer to two main fronts each characterized by the space-time context of data acquisition. Either such morphofunctional, multimodal images are generated by fusing images acquired with each technique separately and at different times or they may arise from truly contextual or simultaneous acquisitions. In this latter case, we are speaking of a hybrid system. There are many potential advantages of hybrid imaging, since ideally both anatomical and functional information can be obtained at the same time without any time delays between modalities and without any need for coregistration of the image information. Beyond this attractive prospect, there are some pivotal synergistic effects that come with the integration of multiple modalities, mainly relating to correcting PET data to yield truly quantitative information while maximizing the signal-to-noise ratio. In this chapter we shall briefly recall some basic physics concepts of each single and combined imaging technique: PET, CT, and MRI.

1.2 Position Emission Tomography (PET)

Positron emission tomography (PET) is an imaging modality, or radiotracer imaging technique, born in the early 1970s [1, 2] which has unique advantages as an investigative tool for studying biological functions at the molecular level. Tracer-molecules, labeled with radionuclide-emitting positrons (e^+), are injected into the subject under investigation with the aim to track biochemical and physiological processes in vivo. When a positron is emitted by a radionuclide, it will travel a few millimeters before interacting with an electron in the surrounding tissue causing the annihilation process: the two oppositely charged particles will be completely converted

G. Garreffa
Head of Applied Physics Section, Euro-Mediterranean Institute of Science and Technology I.E.ME.S.T., Palermo, Italy

G. Hagberg
Scheffler Group, MPI for Biological Cybernetics, University Hospital Tübingen, Tubingen, Germany

L. Indovina (✉)
Health Physics Unit, Fondazione Policlinico Universitario A. Gemelli, Rome, Italy
e-mail: luca.indovina@policlinicogemelli.it

A. Ciarmiello, L. Mansi (eds.), *PET-CT and PET-MRI in Neurology*,
DOI 10.1007/978-3-319-31614-7_1

into two photons emitted into opposite directions with a minimal energy of 511 keV (Fig. 1.1). The role of PET is to measure the exact position of the point of annihilation through detection of the two photons emitted during the annihilation process in coincidence and through detection of the exact time that the two photons travel before reaching a pair of detectors placed opposite to each other in a ring containing several such detector pairs in a PET device. Today, PET is able to detect the position of annihilation events (i.e., the position of radiolabeled molecules in the patient body) through the so-called time-of-flight (TOF) technology (Fig. 1.2). With time-of-flight PET imaging, the relative time difference (Δt) between the detection of the two annihilation photons is used to determine the most likely location (D) of the annihilation event along the line of annihilation or, using technical terminology, along the line of response (LOR) as follows:

$$D = c\Delta t / 2 \tag{1.1}$$

where c is the speed of light, i.e., the speed at which the annihilation photon travels toward the detector.

Radionuclides used in PET (most common are, e.g., ^{11}C, ^{18}F, ^{13}N, ^{15}O, ^{68}Ga) emit positrons because they are in a particular unstable nuclear composition. They emit a positron in order to decay to a stable nuclear state with a characteristic half-life, $T_{1/2}$ (h), which represents the time required to reduce the initial number of positron-emitting nuclei (i.e., the initial activity A_0) by one-half. The decay process is described by an exponential law arising from the circumstance that the number of events (decaying nuclei) per second is always proportional to the number of undecayed nuclei (i.e., $A(t)$) at a given time. Mathematically, this can be expressed as

$$A(t) = A_0 \exp\left(-\lambda t / T_{1/2}\right) \tag{1.2}$$

The half-life $T_{1/2}$ of different positron-emitting radionuclides ranges between 10^{-6}s and 10^{10} years. The activity, A, is measured in units of Becquerel (Bq) where 1 Bq = 1 decay event per s or also in Curie (Ci) where 1 Ci = $3.7 \cdot 10^{10}$ decay events per s, a common value in practice is 1 mCi = 37 MBq.

PET scanners consist of several rings of detector elements available to measure *coincidence events* from the annihilation process of positrons

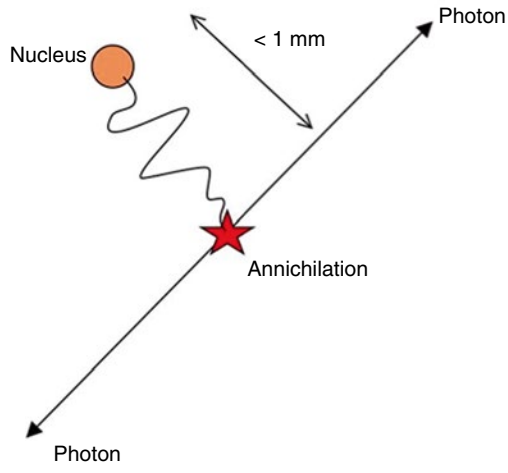

Fig. 1.1 Annihilation of positron and electron with production of two photons: generally after a submillimeter displacement from its origin

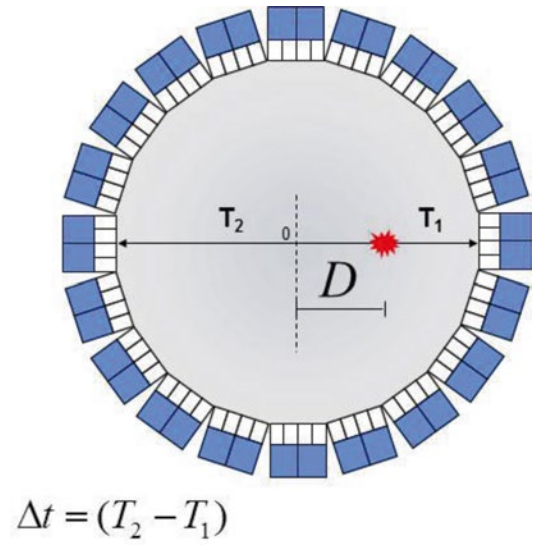

Fig. 1.2 Time-of-flight (*TOF*) technology: Δt is the time difference between the detection of the two annihilation photons used to determine the most likely location (D) of the annihilation event along the line of annihilation or, using technical terminology, along the line of response (*LOR*)

in the scanner. From the beginning of their clinical use, PET scanners were built with a number of detector rings that enabled an axial field of view ranging from 15 to 25 cm. PET images are generated from *true coincidences* measured in the detector elements and refer to a big number of photons. It means that PET images are performed avoiding *scattered and random coincidences*, which are discriminated and considered as background events (Fig. 1.3).

In the early years of PET systems, in an attempt to eliminate scatter and random coincidences, annular septa (~1 mm tick and radial width of 7–10 cm) made of tungsten or lead were inserted between rings. Only direct coincidence events between detector pairs placed in the same detector ring were recorded (2D data acquisition mode) reducing scatter coincidences to less than 10–15 %. In 2D mode (i.e., 2D PET), direct plane events or cross plane events are detected in order to maximize the number of events available to generate PET images. Considering the overall sensitivity, defined as the total true activity detected in the scanner in term of true coincidences with respect to the total activity present inside the scanner, the overall sensitivity in 2D mode is not bigger than 2 % or 3 % [3]. In more recent PET systems, to increase this value, septa are retractable or are not available at all (3D mode). All coincidence events from all possible combinations of detector pairs, regardless of position, are counted (Fig. 1.4). The 3D mode (i.e., 3D PET) increases the number of scattered coincidences to 30–40 % but also increases the overall sensitivity by a factor of almost 4–8.

Concluding this brief introduction to PET systems, it is important to highlight that PET imaging can be used for quantitative imaging. It means that physicians know that PET images are able to provide information regarding the specific activity (kBq/ml) contained in a specific volume of interest (VOI). To obtain quantitative data by PET, the number of true coincidence events has to be corrected for attenuation. Indeed, the 511 keV annihilation photons are attenuated, and this attenuation may differ between photons depending on the density and the composition of the tissue traversed before reaching the detector. In stand-alone PET imaging, a good scattering and attenuation correction can be achieved based on additional transmission scans, acquired by the use of rotating radiation rods as gamma ray sources (typically consisting of ^{68}Ga/^{68}Ge). The source is rotated around the scanner bore to uniformly expose all detector pairs to radiation, prior to image reconstruction and generation of correction maps [4]. However, for traditional transmission scans acquired by 3D PET, the increased amount of scattered radiation reduces the available signal-to-noise ratio to such a point that it is hardly possible to obtain an accurate attenuation correction using this approach.

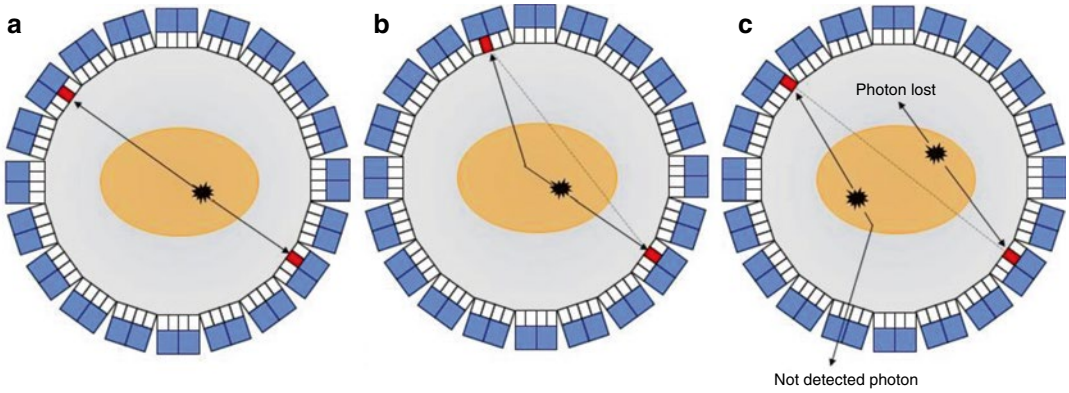

Fig. 1.3 Coincident events: true coincidence (**a**), scattered coincidence (**b**), and random coincidence (**c**) are plotted. Only true coincidences are able to give the exact annihilation position and they are used to generate PET images

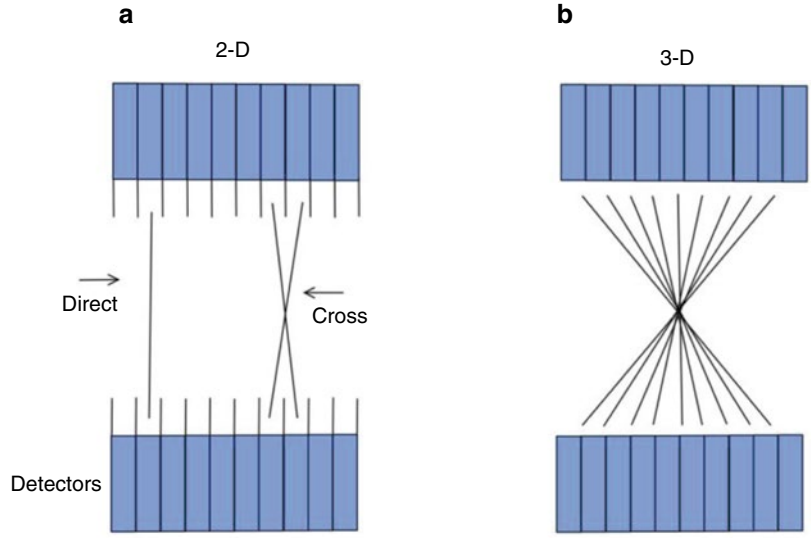

Fig. 1.4 (**a**) *2D* mode. True coincidence counts are obtained minimizing randoms and scatters. (**b**) *3D* mode. Coincidence events from all detector pairs are detected with much more random and scatter events

1.3 Computerized Tomography (CT)

CT is a diagnostic technique characterized by the possibility to acquire and reconstruct images of thin planar cross sections of the subject's body by means of appropriate measurements of X-ray attenuation through the section. These measurements are carried out by simultaneously rotating both the X-ray tube and the detector around the subject. The radiation attenuation is measured by taking into account that

$$I(d) = I_0 \exp(-\mu d) \tag{1.3}$$

where $I(d)$ is the radiation intensity after the X-ray beam has traversed a path of length d in a given material characterized by a *linear attenuation coefficient* μ and I_0 is the radiation intensity available before interacting with matter.

The CT image is generated after collecting a complete set of attenuation values (attenuation profile or projection values) at different rotational angles of the ray lines. Ideally the ray line consisting of the X-ray *tube detector*(*s*) pair(s) is perfectly parallel to each other and passes the tissue in transverse section planes with a defined thickness.

However, a body section is a not a homogeneous object due to the presence of different kinds of tissues. Along a single ray line, the measured attenuation is therefore the result of different contributions from all possible values of the attenuation coefficients μ_i and paths d_i for each tissue element i encountered. Then the resulting intensity I for a single line scan is

$$I = I_0 \exp(-\mu d) = I_0 \exp\left[-\left(\sum \mu_i d_i\right)\right] \tag{1.4}$$

It follows that the projection, P, can be obtained from

$$P = \ln(I / I_0) = \sum \mu_i d_i \tag{1.5}$$

The CT scanner uses these data to produce a digital image after the application of computational procedures to carry out the average μ for each voxel. This value is converted into a quantitative gray-level scale for each pixel, the Hounsfield units, and depends on density and atomic number of matter inside the corresponding elementary voxel.

1.4 PET/CT

The proposal to combine PET with CT was made in 1998 [5] with the idea to make use of CT images to derive accurate PET attenuation correction factors. The first prototype PET/CT

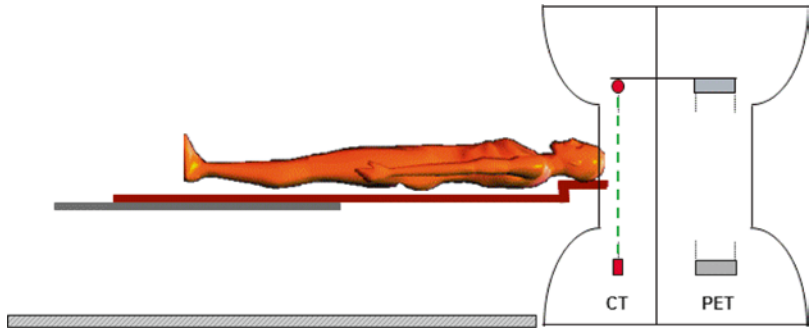

Fig. 1.5 PET/CT systems are combinations of stand-alone *CT* and *PET* scanners with a shared patient bed. They must be very accurately aligned

was indeed introduced in 2000 designed and built by CTI PET Systems in Knoxville, Tenn., USA (now Siemens Healthcare), and clinically evaluated at the University of Pittsburgh [6]. The PET/CT scanner combines two established modalities to build a new hybrid imaging technology. The two modalities CT and PET are complementary, with CT images useful to obtain anatomical information and PET to perform functional imaging. In practice, PET/CT systems are accurately aligned combinations of stand-alone CT and PET scanners with a shared patient bed (Fig. 1.5).

Owing to the link between the fate of radiation in matter at high and low energy, hybrid PET/CT imaging is highly advantageous for 3D PET techniques, since the complicated attenuation and scattering patterns of photons can be predicted from the CT scan. The reason behind this is the availability of a more sophisticated radiation source for the PET "transmission scans," namely, the rotating CT X-ray tube. By accurately correcting for the energy difference between the CT X-rays and the PET photon pair, the Hounsfield units of the CT scan can be (piecewise) linearly transformed into spatially fine-grained correction maps with minimal noise. To be used for attenuation correction, the CT data must thus be transformed to obtain an estimate of the attenuation coefficient at an energy of 511 keV. In practice, the attenuation map at 511 keV is estimated by linear scaling factors for bone and non-bone components based on the CT image values [7].

1.5 Magnetic Resonance (MR) Basic Physics

MR image contrast basically is the expression of a great number of tissue parameters, and the advantage of MRI, with respect to other imaging techniques, is based on the possibility to modify the weighting of these parameters according to clinical requirements. This, in terms of investigational tools, gives formidable opportunities ranging from morphological to functional methods. Tissue parameters that influence the MR signal are ρ, T_1 and T_2, diffusion, magnetic susceptibility, chemical shift difference between chemical compounds, the blood oxygen level-dependent effect, and perfusion, just to name a few. For the purpose of this section, we consider only the most significant parameters such as the *proton density* ρ, the *longitudinal* (*or spin lattice*) *relaxation time* T_1, and T_2 the *transversal* (*or spin-spin*) *relaxation time*.

The human body is primarily made of water and fat which have many hydrogen atoms, and the MR signal detected, in common MRI practice, is that produced by protons, the only particle in the nucleus of hydrogen atoms. The proton possesses a property called *spin I* which is associated with another property called *nuclear magnetic moment* μ defined as below:

$$\mu = \gamma \hbar \ I \tag{1.6}$$

where γ is the *gyromagnetic ratio* and its value for hydrogen is 26.7520 (10^7 rad/T s or 42.576 MHz/T), $\hbar = 1.054571800 \times 10^{-34}$ Js is the

reduced Planck constant, and $I=1/2$ is the (nuclear) spin quantum number.

In magnetic resonance imaging (MRI), the patient is placed in a strong uniform magnetic field, and the nuclear magnetic moments of hydrogen inside the patient body align with the direction of this field. According to the classical description, all magnetic moments (spins) of protons resemble a set of compass needles, and when a magnetic field is turned on, they align along the direction of the applied magnetic field from their initial random distribution, and if no further events occur, they will remain aligned with a constant precessional motion at angular frequency ω_0 (rad/s):

$$\omega_0 = \gamma B_0 \tag{1.7}$$

where B_0 is the applied uniform magnetic field. Dividing the right hand side of (Eq. 1.7) by 2π, we obtain the *resonance frequency* ν_0 or *Larmor frequency*. Due to some reasons that can be explained only by complicated statistical thermodynamics concepts, the total number of hydrogen nuclear spins is distributed on two categories: aligned (lower energy) and anti-aligned (higher energy) to magnetic field. At room temperature the number of spins at lower energy is slightly greater, and this difference produces the net macroscopic magnetization M_0 which is mainly responsible of the MR signal strength. For a magnetic field strength of 1.5 T, for example, the Larmor frequency of the hydrogen nuclear spin system is about 63 MHz and then in the radiofrequency (RF) range. Introducing a reference system (x, y, z), where B_0 is directed along z, at the equilibrium condition, the net macroscopic magnetization M_0 is aligned along z, where its component along z is the *longitudinal magnetization* M_z.

M_0 performs a precessional motion at frequency ν_0 and the component M_{xy}, called *transversal magnetization*, is zero. If an RF field (B_1) is applied at frequency ν_0, for a finite time t by using an antenna, or better, a coil with polarization along x, a rotation or flip of M_z is produced corresponding to

$$\theta = \gamma B_1 t \tag{1.8}$$

where θ is the flip angle from B_0 and t is the duration of RF pulse (Fig. 1.6).

The same coil used for excitation may be used also to detect MR signal since, according to the Faraday law, the transversal magnetization induces a magnetic flux variation and then a voltage in the coil. Immediately after the 90° pulse, M_z grows from zero toward its original equilibrium value according to the following equation:

$$M_z(t) = M_0\left[1-\exp(-t/T_1)\right] \tag{1.9}$$

where clearly results that M_z approaches M_0 after a given time determined by the time constant T_1, the *longitudinal relaxation time*, which is determined by interactions of the spin system with the tissue lattice.

The MR signal, corresponding to the voltage induced and detected in the coil, is proportional to the *amplitude of transverse magnetization* given by the following equation:

$$M_{xy}(t) = M_0 \exp(-t/T_2) \tag{1.10}$$

where T_2 represents the time constant that regulates the spin-spin relaxation process. After turning off the RF pulse, each spin interacts with its nearest neighbors, and this causes a spread of the effective magnetic field experienced by each spin and the global precession motion becomes incoherent. This process, in a time governed by T_2, gradually cancels the M_{xy} magnetization component produced by the RF pulse and is the main responsible of the MR signal as shown in Fig. 1.6.

To obtain an image, it is necessary to make the MR signal "spatially dependent" and then assigned the signal to a given position. For this purpose, three variable magnetic fields are introduced, called *magnetic field gradients s* or simply *gradients*. These variable fields are produced with separate coils built into the gantry, one for each canonical direction x, y, z. The gradients introduce a linear variation of the resonance frequency, or of the phase of the MR signal, in order to identify univocally the position where a specific MR signal is generated.

A series of RF and gradient pulses characterizes the *pulse sequence*, and through the selection

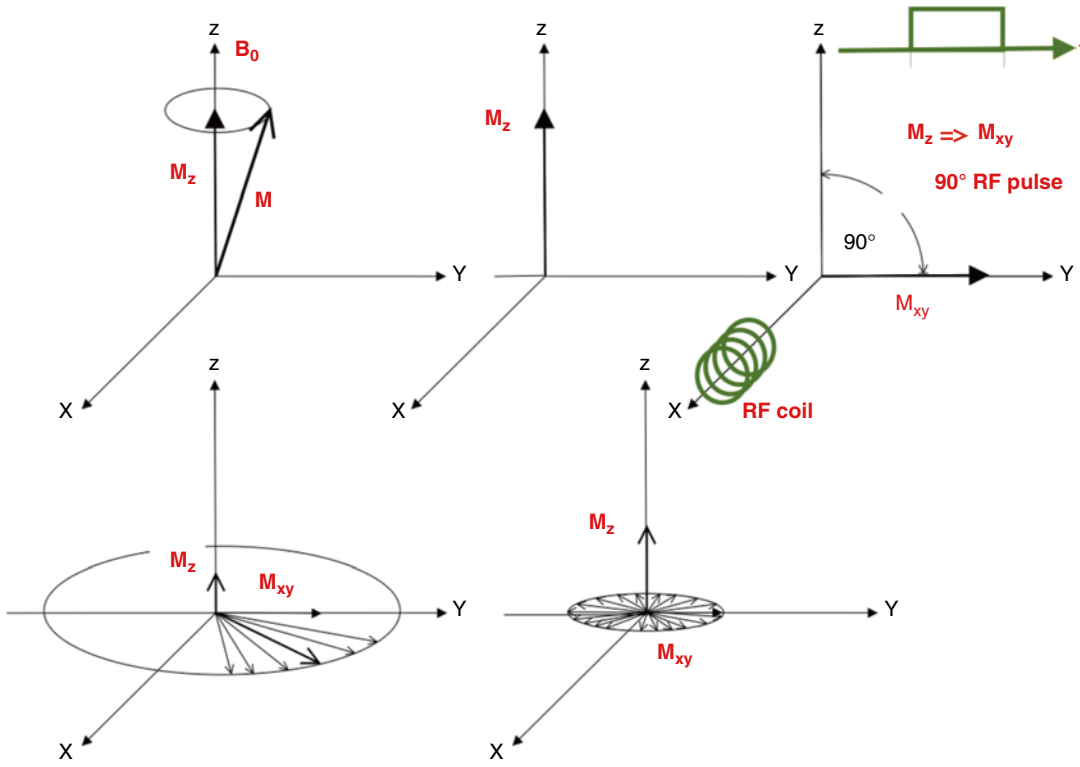

Fig. 1.6 From the *top left*: precession of macroscopic (net) magnetization M_0, which arises from all the individuals μ_i, under static uniform magnetic field applied along z; the resulting component M_z; flip of M_z immediately after application of 90° *RF* pulse with carrier at ν_0; evolution of M_z and M_{xy} after turning off RF pulse and loss of M_{xy} phase coherence characterized by T_2

of specific *scan parameters*, it is possible to compose the *scan protocol* and acquire the right MR signal suitable to form the right image for the specific diagnostic query.

Briefly and in conclusion, in magnetic resonance imaging (MRI), a radio frequency field is transmitted to the patient body part under investigation, and the consequent MR signal produced with a given scan protocol is then collected commonly by use of a district specific coil [8, 9].

1.6 PET/MRI

Historically, PET and MRI have been used as fused images [10] acquired on separate machines. Subsequently, the idea to integrate these techniques into a single machine was implemented [11–13]. The goal of this integration is that MR can provide anatomic information with high soft tissue contrast but without the additional radiation dose from CT. MR can also provide functional and anatomical information at the same time. The functional data obtained with both modalities can be complementary. The history of PET/MR brought us two possible solutions: systems that acquire images sequentially and those that can acquire images simultaneously (Fig. 1.7).

While PET and CT share a common ground in terms of radiation physics that leads to evident synergies, PET and MRI are rather complementary in their respective character. The effort to actually fuse these two techniques into a single one is propelled by the plethora of measurement parameters that can potentially be simultaneously gained but comes at the cost of tackling several, diverse challenges.

First of all, the main absorber of γ-photon energy, namely, bony structures, has poor visibility on conventional MR images. The water inside

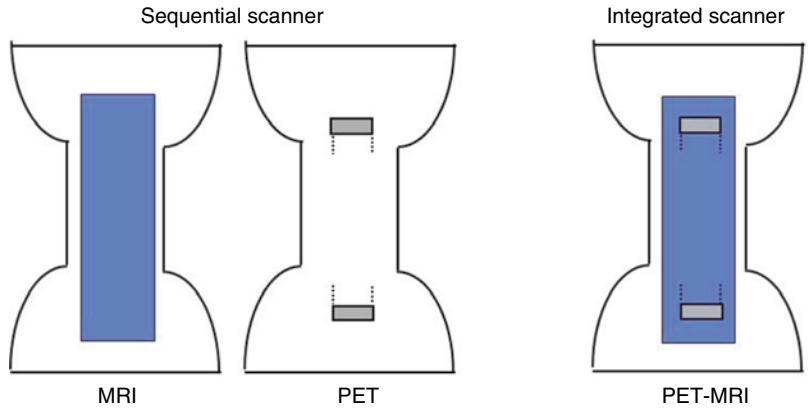

Fig. 1.7 Sequential or integrated PET/MR scanner

this tissue compartment has extremely short T_2 relaxation times – on the order of a few microseconds – compared to soft tissue structures, with T_2 times of several tenths of milliseconds. Therefore, conventional MRI techniques do not have the timing necessary to allow observation of the skeleton. However, emerging ultrashort (UTE) or even zero (ZTE) echo time techniques hold great promise to overcome this limitation and, provided a tight timing between NMR spin excitation and detection can be guaranteed in presence of PET-dedicated hardware, may positively impact hybrid MR/PET techniques in the near future.

An interesting interaction between the two modalities affects the range of the positron: the distance traveled prior to annihilation. The range is greater for high-energy positrons and ultimately determines the resolution available by PET, besides limitations set by detector design. Interestingly, it is influenced by the presence of an external magnetic field through a fundamental physical effect: the Lorentz force that acts upon the positively charged positron as it moves through the magnetic field. The magnetic force component of the Lorentz force, which does not take into account the influence of an electric field, is given by the cross product between the velocity vector, $\vec{v}$ of the particle with charge q, and the magnetic field vector according to

$$F = q\vec{\mathrm{v}} \times \vec{B} \tag{1.11}$$

The Lorentz force only acts perpendicular to the field, why a reduction of the positron range in this plane is expected and has been experimentally observed. On the contrary, a loss in PET resolution was reported in presence of an external magnetic field in planes oriented along the field lines, probably owing to partial deflection of positrons with skewed trajectories [14, 15]. The gain in actual resolution available in presence of fields up to 9.4 T was however modest, testifying that the LSO detector design currently used for MR/PET hybrid systems is the limiting factor for achieving the finest possible resolution, while very little the spatial uncertainty of the annihilation process has only a weak influence.

Last but not the least, an improvement of the PET quantification can be achieved by incorporating information regarding partial volume effects obtained from MRI in the image reconstruction. Generally, the goal of quantitative PET is to measure radiotracer concentration with uniform precision, but in case the structure is smaller than about twice the spatial resolution, the measured concentration will appear diluted. By incorporating the anatomical information from MRI, and the measured point spread function for each position within the field of view, the resolution loss occurring during reconstruction can be recovered, thus minimizing partial volume effects [16].

Taken together, even for PET/MRI systems several synergistic effects do exist despite their complementary character. Nevertheless, due to the mutual interference between hardware components in this kind of systems, continuous technological advances are necessary before these

can be fully exploited. Already when the very first hybrid scanners came up, different strategies that take into account the sensitivity of photomultiplier tubes (PMT) used in stand-alone PET scanners to the static magnetic field had to be developed. One option is to bring the information regarding scintillation events out of the magnet bore via optical fibers or via a split-magnet design [17, 18]. However, the field above which the PMT-based detection is no longer acceptable was found to be 10 mT and thus required optical fibers that were 3.5 m in length to get sufficiently away from a 1.5 T magnet. Generally, the energy resolution is worse the longer the wave guide. Under these circumstances, sensitivity is lost due to the decreased discriminatory power of the PET detection system. Another method, which eventually became the method of choice, was the use of solid state detectors, so-called avalanche photodiodes (APD). Although the amplification factor of APDs is only about 20 % of a PMT, the detection efficiency of the APD is still satisfactory, and the first generation detectors enabled the detection of 70 % of the events with an acceptable energy discrimination even when placed inside the field [19].

Contrary to the initial expectations, the PET electronics does not pose insurmountable problems for MRI. Magnetic field homogeneity can be maintained through standard second order shimming, and eddy currents induced by the presence of conductive material inside the bore can be compensated by the existing preemphasis hardware of the MR scanner. The loss in the signal-to-noise ratio of the MR signal during PET scanning was found to be minimal [20, 21]. Only during fMRI data acquisition, a greater MR signal drift was observed, since the presence of the PET hardware brought about a greater temperature increase.

The next generations of PET detectors are the silicon photomultipliers (SiPM) [22]. With respect to APD, they have a higher gain and lower temperature dependence, which improves PET signal-to-noise ratio on one hand, and are more robust against MRI-induced heating effects. What is even more interesting about these devices is that they are compatible with the PET time-of-flight technique, which potentially can bring about a huge improvement in localizing capability and hence an improved image resolution.

In the near future, the synergistic effects of hybrid PET/MRI scanners are expected to improve PET detection and quantification. On the one hand, advanced short echo time MRI techniques will improve attenuation and scatter correction, and on the other hand, emerging SiPM detection will enable the use of time-of-flight techniques and hereby further improve the precision and the sensitivity of PET detection. As known, the attenuation correction in PET/MRI is still currently being investigated [23, 24]: none of the integrated PET/MRI systems constructed to date incorporate a CT scanner or rotating transmission source, so this information must be somehow derived from the MRI image and/or any other available sources of information on attenuation like additional sources or PET emission data [25].

In conclusion, combined with parametric mapping of MRI-related parameter, future clinical practice in PET/MRI can thus expect to benefit from an improved truly multimodal tissue characterization.

References

1. U.S. Department of Energy TOoBaER (2010) A vital legacy biological and environmental research in the atomic age. Lawrence Berkeley National Laboratory, Berkeley
2. Cho ZH, Chan JK, Eriksson L (1976) Circular ring transverse axial positron camera for 3-dimensional reconstruction of radionuclides distribution. IEEE Trans Nucl Sci 23:613–622
3. Bergström M, Eriksson L, Bohm C, Blomqvist G, Litton J (1983) Correction for scattered radiation in a ring detector positron camera by integral transformation of the projections. J Comput Assist Tomogr 7(1):42–50
4. Cherry SR, Sorensen JA, Phelps ME (2003) Physics in nuclear medicine, 3rd edn. Saunders, Philadelphia
5. Kinahan PE et al (1998) Attenuation correction for a combined 3D PET/CT scanner. Med Phys 25(10):2046–2053
6. Beyer T, Townsend DW, Brun T et al (2000) A combined PET/CT scanner for clinical oncology. J Nucl Med 41:1369–1379
7. Carney JPJ, Townsend DW, Rappoport V, Bendriem B (2006) Method for transforming CT images for

attenuation correction in PET/CT imaging. Med Phys 33:976–983
8. Kuperman V (2000) Magnetic resonance imaging: physical principles and applications. Academic Press, New York, Chapters 1 & 4. ISBN 0124291503
9. Hashemi RH, Bradley Jr. WG, Lisanti CJ (2004) MRI the basics, 2nd edn. Lippincott Williams & Wilkins, Philadelphia. ISBN ISBN-13: 978-0-7817-4157-6, ISBN-10: 07817-4157-2
10. Hammer BE, Christensen NL, Heil BG (1994) Use of a magnetic field to increase the spatial resolution of positron emission tomography. Med Phys 21:1917–1920
11. Pelizzari CA, Chen GT, Spelbring DR, Weichselbaum RR, Chen CT (1989) Accurate three-dimensional registration of CT, PET, and/or MR images of the brain. J Comput Assist Tomogr 13:20–26
12. Shao Y, Cherry SR, Farahani K et al (1997) Simultaneous PET and MR imaging. Phys Med Biol 42:1965–1970
13. Shao Y, Cherry SR, Farahani K et al (1997) Development of a PET detector system compatible with MRI/NMR systems. IEEE Trans Nucl Sci 44:1167–1171
14. Shah NJ, Herzog H, Weirich C, Tellmann L, Kaffanke J, Caldeira L, Kops ER, Qaim SM, Coenen HH, Iida H (2014) Effects of magnetic fields of up to 9.4 T on resolution and contrast of PET images as measured with an MR-BrainPET. PLoS One 9(4):e95250. doi:10.1371/journal.pone.0095250, eCollection 2014
15. Kolb A, Sauter AW, Eriksson L, Vandenbrouke A, Liu CC, Levin C, Pichler BJ, Rafecas M (2015) Shine-through in PET/MR imaging: effects of the magnetic field on positron range and subsequent image artifacts. J Nucl Med 56(6):951–954. doi:10.2967/jnumed.114.147637
16. Baete K, Nuyts J, Van Laere K et al (2004) Evaluation of anatomy based reconstruction for partial volume correction in brain FDG-PET. Neuroimage 23(1):305–331
17. Lucas AJ, Hawkes RC, Ansorge RE et al (2006) Development of a combined micro PET-MR system. Technol Cancer Res Treat 5(4):337–341
18. Mackewn JE, Charles-Edwards G, Keevil S, Halsted P, Page R, Kelly M, Williams S, Hallett W, Marsden P (2007) Description and preliminary results of an MR-compatible PET system for molecular imaging studies. Proc Intl Soc Mag Reson Med 15:921
19. Pichler BJ, Swann BK, Rochelle J, Nutt RE, Cherry SR, Siegel SB (2004) Lutetium oxyorthosilicate block detector readout by avalanche photodiode arrays for high resolution animal PET. Phys Med Biol 49(18):4305–4319
20. Catana C, Procissi D, Wu Y, Judenhofer MS, Qi J, Pichler BJ, Jacobs RE, Cherry SR (2008) Simultaneous in vivo positron emission tomography and magnetic resonance imaging. Proc Natl Acad Sci U S A 105(10):3705–3710. doi:10.1073/pnas.0711622105
21. Judenhofer MS, Wehrl HF, Newport DF, Catana C, Siegel SB, Becker M, Thielscher A, Kneilling M, Lichy MP, Eichner M, Klingel K, Reischl G, Widmaier S, Röcken M, Nutt RE, Machulla HJ, Uludag K, Cherry SR, Claussen CD, Pichler BJ (2008) Simultaneous PET-MRI: a new approach for functional and morphological imaging. Nat Med 14(4):459–465. doi:10.1038/nm1700, Epub 2008 Mar 23
22. Weissler B, Gebhardt P, Lerche CW, Wehner J, Solf T, Goldschmidt B, Mackewn JE, Marsden PK, Kiessling F, Perkuhn M, Heberling D, Schulz V (2014) MR compatibility aspects of a silicon photomultiplier-based PET/RF insert with integrated digitization. Phys Med Biol 59(17):5119–5139
23. Bezrukov I, Mantlik F, Schmidt H, Schölkopf B, Pichler BJ (2013) MR-based PET attenuation correction for PET/MR imaging. Semin Nucl Med 43:45–59
24. Keereman V, Mollet P, Berker Y, Schulz V, Vandenberghe S (2013) Challenges and current methods for attenuation correction in PET/MR. MAGMA 26:81–98
25. Martinez-Möller A, Nekolla SG (2012) Attenuation correction for PET/MR: problems, novel approaches and practical solutions Z. Med Phys 22:299–310

Instrumentation

2

Michele Larobina, Carmela Nappi,
Valeria Gaudieri, and Alberto Cuocolo

2.1 Introduction

The remarkable innovation in molecular imaging and the introduction of advanced neurological diagnostic tools encouraged researchers and physicians in optimizing technological resources to approach brain diseases with increased accuracy of diagnosis. Computed tomography (CT), positron emission tomography (PET), and magnetic resonance (MR) imaging provide different and complementary information with both advantages and disadvantages. PET gives metabolic and molecular data, while CT offers high spatial resolution fiving detailed information at anatomical level, and MR enables investigation at morphological and functional levels also allowing diffusion imaging and spectroscopy [1]. In the attempt to overcome the limitations of standalone imaging methods, different modality combinations have been introduced.

In early 2000, PET/CT systems appeared in the diagnostic armamentarium and this tool is currently fully integrated in clinical routine. Several studies evaluating the diagnostic capability of PET/CT reported a higher accuracy of this hybrid imaging modality compared to PET and CT stand-alone modalities [2]. Although MR provides some advantages over CT such as superior soft tissue contrast, functional information and no ionizing radiation exposure, combining PET and MR has been extremely demanding due to the need to minimize any mutual interference between the two sophisticated systems. For this reason, a truly hybrid imaging tool, such as simultaneous PET/MR has been only recently introduced [3]. The PET/MR simultaneous approach enables to go beyond some limitations of current PET/CT scans, such as misregistration of attenuation (CT) and emission (PET) images due to spatial and temporal mismatch between CT and PET acquisition reducing the percentage of artifactual false-positive results. For the evaluation of neurologic and psychiatric disorders, the appealing opportunity to combine MR and PET to investigate pathophysiological patterns at the same time aroused great interest in both researchers and clinicians.

This chapter will give an overview of technological aspects of currently available diagnostic tools also focusing on hybrid instrumentation such as PET/CT and PET/MR.

2.2 CT

In a CT system, the X-ray attenuation properties of an anatomical volume are measured at various angles. These views or projections are then

M. Larobina • C. Nappi • V. Gaudieri • A. Cuocolo (✉)
Department of Advanced Biomedical Sciences,
Institute of Biostructure and Bioimaging,
National Council of Research, University of
Naples Federico II, Naples, Italy
e-mail: cuocolo@unina.it

A. Ciarmiello, L. Mansi (eds.), *PET-CT and PET-MRI in Neurology*,
DOI 10.1007/978-3-319-31614-7_2

combined to reconstruct the tomographic images of the volume. CT joins the tomographic imaging formation theory to the principle that an X-ray beam, when passes through human tissues, is attenuated as function of the tissue composition [4].

CT is one of the most common imaging modalities and is an essential part of a radiology department. Since its development in the early 1970s, this modality has been significantly upgraded over time. The essential components of CT tomography are the X-ray source and the detection system, mounted on a gantry in a diametrically opposite position. The gantry is able to rotate continuously around the patient. The X-ray source is a vacuum tube in which electrons, due to thermionic effect, are emitted by a cathode and accelerated with an electrical potential difference in the range of 80–140 kV and then brusquely broken by colliding with an anode made of a highly absorbing material (typically tungsten). X-rays are emitted due to the bremsstrahlung effect of electrons on the anode [5]. Once X-rays are collimated and filtrated, they are targeted to the volume of interest. Ultrafast ceramic scintillators that convert X-ray energy into visible light detect the X-rays transmitted through the imaged volume. Finally, the light generated is transformed into an electrical signal using solid-state sensors.

All modern CT systems are *spiral* and *multi-slice*. Spiral CT (or helical CT), introduced in the 1989, implies that, during the acquisition, the bed motion is synchronized with the movement of the gantry so that the trajectory of the source respect to the patient is a "spiral." This technique allows the acquisition of a volume without the temporal and spatial discontinuities of single-slice scanners. On the other hand, multi-slice CT, introduced in 1998, allows the simultaneous acquisition of several layers and of an entire volume with a further reduction of the scan time [6]. Currently, CT systems offer 16–320 slices, with a minimum slice thickness of 0.5 mm and a scan time less than half a second per rotation. Faster acquisitions reduce motion artifacts and enable a better temporal resolution, which is particularly useful for some clinical applications such as perfusion and angiography studies. Multi-slice CT uses multi-row detectors. The number of rows gives the number of layers obtainable with a single gantry rotation or, in other words, the volume covered in one rotation.

The introduction of multi-slice systems and the volumetric acquisition with sub-second scanning time represent the two main key points of the instrumentation development of CT in the recent years. Also dual-source CT scan, making use of a dual X-ray source working at different voltages or of a single source acting as a double one with a rapid voltage switching, allows to exploit the energy dependence of the X-ray attenuation properties improving tissue differentiation [7].

Despite of the remarkable success of CT in diagnostic imaging, due to the great potential to provide detailed clinical information, radiation exposure is still an issue. Therefore, industry is currently mainly focused on radiation dose reduction. Systems for automatic X-ray tube current modulation in function of different body regions, patient size, and age have been implemented in the novel generation of CT scanners. Nevertheless, the development of new reconstruction algorithms to improve image quality with minimum radiation exposure is an active area of research [8].

2.3 PET

The use of positron-emitting radionuclides for imaging was introduced in the early 1950s [9]. PET imaging is based on detection of gamma ray pairs generated from annihilation of a positron released by a radioactive compound that is intravenously injected into the body with an electron of the tissue itself avid of the biologically radioactive compound. In this annihilation process, the mass of the electron and the positron is transformed in energy as two gamma rays of 511 keV that move away from the annihilation point in opposite directions. By simultaneously recording their arrival by means of a system of detectors that surround the district examined is possible to identify a line within the field of view (FOV) along which the annihilation took place (line of response). Only the pairs of photons recorded by

opposite detectors within a certain temporal window are considered to come from the same annihilation (*coincidence*) and considered valid for the purpose of image formation.

During a PET acquisition, a large number of coincidences are recorded. The corresponding lines of response recorded within the FOV are ordered as set of parallel projections in a matrix called *sinogram*. Starting from the sinograms, similarly to other tomographic imaging modalities, a computer reconstructs the distribution of the radionuclide in the acquired volume running a reconstruction algorithm. The detection of the two gamma photons originating from annihilation by opposite detectors is also known as "electronic collimation."

The detection system of a PET scanner consists of one or more stationary rings of detectors surrounding the FOV [10]. The axial FOV typically covers a length between 15 and 25 cm. Detectors are made of scintillator materials with characteristics such as stopping power, light yield, and response time optimized for the detection of the high-energy PET photons. Bismuth germanate (BGO), lutetium orthosilicate (LSO), and lutetium yttrium orthosilicate (LYSO) are currently the most employed scintillator materials. Scintillators are coupled to an electronic system for position-sensitive photodetection. The information provided by this system is the position of the detected gamma photons and their energy. In time-of-flight (TOF) systems the difference in the arrival time of the two annihilation gamma photons is added as recorded data and used in the reconstruction process. In a PET scanner design, the detection system gives the main contribution in defining the spatial resolution and the other characteristics as sensitivity and count rate capability [11]. This latter characteristic is expressed as noise equivalent count (NEC) curve and the related peak NEC value, a measure of the maximum useful activity concentration within the FOV before starting with saturation effects.

Commercially available PET systems have a spatial resolution between 4 and 6 mm; the acquisition time for a single bed position is of a few minutes. Performance of detectors and electronics affect system sensitivity, which is also proportional to the size of the axial FOV. Over the past 30 years, major advances in PET technology were achieved with adoption of faster scintillators and associated electronics and development of more efficient reconstruction algorithms to better account the corrections needed for quantitative studies. Moreover, industry built up septaless systems that have established the PET as an intrinsically 3D technique allowing a gain of sensitivity by a factor of five with respect to the 2D acquisition [12], which translates into a reduction of the dose and/or a reduction of the acquisition time. Finally, the integration of PET and CT scan in a single device opened up to multimodality imaging [13].

2.4 MR

Since its introduction in the early 1980s, MR has become a gold standard for several applications due to its capability to image soft tissues with very high resolution and excellent contrast. Advances in hardware, new MR imaging strategies, and novel approaches to image analyses have paved the way to new application in neurologic field [14]. Nuclear spin is the key concept in MR imaging. This is an intrinsic property of each atom and its value depends on the atomic composition. Thus, abstractly, every element can be evaluated through MR. However, in medical application, MR imaging is based mostly on hydrogen nuclei (protons) due to their abundance in biological tissues. The application of an appropriate radio-frequency (RF) energy to the studied system placed into a strong static magnetic field results in an excitation of the protons (resonance absorption). Once the RF transmitter is turned off, protons return to their original equilibrium state, in a process known as relaxation, by emitting energy, which is recorded by the system through the receiver coil. This is a time-dependent process and is characterized by rate constants known as relaxation times, responsible for primary image contrast mechanism. Three main relaxation times can be measured, T1, T2, and T2*, together with proton density (PD) of the tissues [15].

The typical configuration of an MR scanner consists of four essential components: the magnet, the gradient system, the RF transmitter/receiver system, and the electronic data processing unit. The magnet generates a uniform static magnetic field that produces the polarization of the nuclear spins, making possible the phenomenon of resonance. The magnetic field strength impact on the signal-to-noise ratio (SNR), and therefore higher field strength provides higher resolution images. In addition to the magnetic field strength, a crucial parameter to obtain good image quality is the spatial homogeneity of the main magnetic field, which is achieved by using specific coils known as shim coils. Despite the availability of systems operating at 7 and 9.4 T in research field, nowadays the most used devices in clinics are provided with 1.5 T or 3 T magnets.

The magnetic field gradient system is a set of orthogonal coils used to modulate the main magnetic field, generating shifts in the resonance frequency that allow to spatially localize tissue signals. The maximum gradient strengths (measured in milliTesla per meter) affect spatial resolution, while the gradients' slew rate (measured in Tesla per meter per second) influence the acquisition speed [16]. The RF system is responsible for the excitation of the spin and signal detection and consists mainly of a transmitter coil and a receiver coil. Once the signal is recorded, it is digitized, amplified, and processed to obtain the final MR image. During an MR imaging study, the RF and gradient systems act according to the specification of the data acquisition protocol (*sequence*) defining the contrast type of the reconstructed images [17]. With an appropriate choice of the acquisition sequence, it is possible to acquire images in which the contrast is an expression of a wide range of physical and biological phenomena, including proton density, differences in relaxation rates (e.g., T1 weighted, T2 weighted), molecular motions (diffusion and perfusion) [18], magnetic susceptibility (sensitive to iron accumulation in tissues) [19], differences in chemical shift [20], and hemoglobin oxygenation (used in functional studies to detect brain neuronal activation) [21]. Furthermore, the possibility to detect specific molecules on the basis of subtle differences in their resonance frequencies allows performing in vivo MR spectroscopic studies, providing information at cellular and metabolic level.

2.5 PET/CT Integration

The development of PET/CT integrated devices represents a successful hardware solution for PET and CT image fusion [22–26]. Introduced on the market in the 2001, a PET/CT scanner typically consists of a PET and a CT modality joined together. The two modalities are housed in a common gantry (with the exception of some models proposed by Philips), with separated detection systems. The two units share the patient bed so the tomographic axis of the two scanners coincides, and images are perfectly superimposed. A sequential acquisition approach is provided for PET/CT imaging. According to standard protocols, the CT scan is performed first and then the bed is moved into the PET FOV to start the PET acquisition. In contrast to PET/MR integration, CT does not interfere with PET and vice versa.

The characteristics of the PET and CT component of the hybrid device are not different from those of a PET and CT stand-alone modality. In particular, the latest commercial PET/CT scanners combine the state of the art technology for both modalities with high-resolution 3D PET systems and multi-slice CT up to 128 slices. The reconstructed PET and CT images generated during the single imaging session are naturally co-registered and can be displayed side by side on a slice by slice bases or fused together either as slices or as volume. In this kind of integrated system, CT provides data for attenuation correction for the PET, resulting in a considerable saving of time in place of the longest and noisy PET transmission scan. However, the attenuation coefficients measured with the CT need to be scaled to the PET photon energy because the energy of the X-ray is much lower than the PET photon energy of 511 KeV. This conversion, typically accomplished with a bilinear transformation, may fail in the presence of contrast media and/or metallic

artifacts. Thus, PET data not corrected for attenuation are also provided.

Performances of PET/CT machines also rely on reconstruction algorithms. The use of iterative reconstruction algorithms allows an improvement of image quality (noise and spatial resolution) in respect to analytical methods (i.e., filtered back projection). Nowadays, all the manufactures provide iterative reconstruction algorithms for both PET and CT. These algorithms have enormous potential and a wider use of such tools is expected in the future. Currently, at least four industries offer PET/CT scanners: General Electric (GE), Philips, Siemens, and Toshiba. All CT scanners are multi-slice with spiral acquisition mode and all PET/CT models on the market acquire PET in 3D mode. The characteristics of commercially available PET/CT scans are summarized in Table 2.1.

GE offers three PET/CT models: *Discovery iQ*, *Discovery 610*, and *Discovery 710*. The Discovery iQ and the 610 have a detection system based on BGO (for the iQ with an innovative dual channel detection technology called Lightburst). The axial FOV is 15.6 cm for the 610 and can vary from 15.6 to 26.0 cm for the iQ depending on the number of detector rings. The iQ is offered in combination with a 16-slice CT, while the 610 can be configured with a CT up to 64 slices. The Discovery 710 has a LYSO-based PET detection system, has an axial FOV of 15.6 cm, offers time-of-flight capability, and can be combined with a CT up to 64 slices.

Siemens Healthcare offers three PET/CT models: *Biograph mCT*, *Biograph mCT Flow*, and *Biograph mCT 20 Excel*. All these models have a PET based on LSO detectors and have time-of-flight capabilities. The axial FOV can

Table 2.1 Characteristics of PET/CT scanners commercially available

	PET				CT			
	Detector material	Axial FOV (cm)	TOF	Sensitivity (cps/kBq)	Peak NECR	Slices (*n*)	Min slice thickness (mm)	Min rotation time (sec)
GE								
Discovery iQ	BGO[a]	15.6–26	No	8–22	36–120 kcps @ 11 kBq/ml	16	0.625	0.5
Discovery 610	BGO	15.6	No	10	76 kcps @ 15 kBq/ml	64/128	0.625	0.35
Discovery 710	LYSO	15.6	Yes	7.5	130 kcps @ 29.5 kBq/ml	16/64/128	0.625	0.35
Philips								
Ingenuity TF	LYSO	18	Yes	7.4	120 kcps @ 19 kBq/ml	64/128	0.625	0.4
Vereos	LYSO[b]	16.4	Yes	5.7	171 kcps @ 50 kBq/ml	64/128	0.625	0.4
Siemens								
Biograph mCT20 Excel	LSO	15–21	Yes	5.8–10.2	107–180 kcps @ 28 kBq/ml	20	0.4	0.3
Biograph mCT	LSO	15–21	Yes	5.8–10.2	107–180 kcps @ 28 kBq/ml	20/40/64/128	0.4	0.3
Biograph mCT flow	LSO	15–21	Yes	5.8–10.2	107–180 kcps @ 28 kBq/ml	20/40/64/128	0.4	0.3
Toshiba								
Celestion	Lu based	19.6	Yes	10.8	NA	16	0.5	0.5

FOV field of view, *TOF* time of flight, *NECR* noise equivalent count rate
[a]With proprietary Lightburst™ detector technology
[b]With proprietary Digital Photon-Counting technology

span from 16 to 21 cm, depending on the number of detector rings. For the mCT and the mCT Flow models, the associated CT can be purchased with 20/40/64 or 128 slices. The mCT 20 is provided only with a 20-slice CT version. The mCT Flow model has the special feature to do the PET acquisition with a continuous bed motion.

Philips Healthcare offers two PET/CT systems: *Ingenuity TF* and *Vereos*. The Ingenuity has an "open" gantry design with the CT and the PET units that, sliding on a rail, can get closer up to 30 cm or moved away up to one meter. Both the PET and CT models proposed have a PET detector system based on LYSO and have time-of-flight capability, with the Vereos featuring a fully digital photon detection technology. The axial FOV of the Ingenuity is 18 cm, while it is 16.4 cm for the Vereos. The Ingenuity can be furnished with a CT of 64 or 128 slices; the Vereos comes with a 128-slices CT.

Toshiba Medical System recently proposes a unique PET/CT model named *Celesteion*. The PET detection system relies on a lutetium-based system with time-of-flight capability and an axial FOV of 19.6 cm. The associated CT is a 16-slice model.

Although CT provides images with high spatial resolution, a low soft tissue contrast is still an important limitation. Therefore, the possibility of having an anatomical reference with an excellent soft tissue contrast, such that provided by MR, remains of great interest and lead the development of PET/MR integrated systems.

2.6 PET/MR Integration

Hybrid PET/MR systems represent a recent breakthrough in medical imaging and are currently under investigation. Despite the great interest and significant effort started already in the early 1980s, the integration of these two sophisticated methods (PET and MR) proved to be highly demanding and only recently found satisfactory technological solutions. To set up a truly simultaneous device, some challenging redesign of both subsystems was necessary. In the first place, there is the need to settle a space for the PET detection system within the MR. In addition, the intense static magnetic field, the time-varying magnetic field gradients, and the radio-frequency pulses, all essential for MR imaging, jeopardize the performance of PET detectors based on photomultiplier tubes (PMT) technology [27, 28]. At the same time, the presence of the PET detectors compromise MR efficiency. To overcome this limitation, a sequential approach has been proposed in the last decades from industry. Philips proposed a turntable system between MR and PET devices while a trimodality similar solution, consisting in a PET/CT and an MR stand-alone equipment has been introduced by GE. However, the sequential approach does not allow simultaneous acquisition. The PET and MR devices are separated and the total acquisition time will be the sum of the PET and MR acquisition. Yet, extra space to locate two devices, instead of a single scanner, is needed. For these reasons, this method does not take on completely the challenge. To set up a fully integrated PET/MR system, researchers and industry have been focused on developing a compact, MR-compatible, PET detector technology without compromising the bore-size of the device. A real breakthrough in hybrid technology was achieved in 2008 [29] developing MR-compatible PMT known as avalanche photodiodes (APD). Conventional PMT are influenced by the effect of the magnetic field on the electrons traveling in the vacuum tubes. In addition, the gradient fields, used for spatial encoding, generate unsolicited currents in PET detector conductive circuitry. These local current loops, known as eddy currents, hamper the homogeneity of the static field, leading to signal loss and distortions in the reconstructed images. Furthermore, eddy currents determine heating, which hinders the sensitive calibration of the PET detectors. On the other hand, MR requires uniformity of static field, as inhomogeneities can lead to artifacts in the reconstructed images and PET detectors also release unwanted signals that, even if tenuous, can be registered by the delicate MR reception. A few years ago, a simultaneous PET/MR prototype with APD detectors has been developed and made commercially available from Siemens. However, the required unwieldy electromagnetic interference shielding limits the field of view of the MR scanner leading to truncation effects. The worse timing

Table 2.2 Characteristics of PET/MR scanners commercially available

	PET								MR		
	Scintillator	Axial FOV (cm)	TOF	Sensitivity (cps/kBq)	Peak NECR	Energy resolution (%)	PET/MR acquisition mode	PET/MR bore (cm)	AC	Gradient (mT/m)	Slew rate (T/m/s)
GE											
Discovery PET/CT-MR	LYSO	15.7	Yes	7.5	139.1 kcps @ 29.0 kBq/ml	12.4	*Sequential*	70/70	CT based	50	200
Signa PET/MR	LYSO (SiPM based)	25	Yes	21	218 kcps @ 17.7 kBq/ml	11.5	*Simultaneous*	60/60	MR-based	40	150
Philips											
Ingenuity TF	LYSO	18	Yes	7.1	88.5 kcps @ 13.7 kBq/ml	12	*Sequential*	70/60	MR-based	45	200
Siemens											
Biograph mMR	LSO (APD based)	25.8	No	14.4	184 kcps @ 23.1 kBq/ml	10.3	*Simultaneous*	60/60	MR-based	45	200

FOV field of view, *TOF* time of flight, *AC* attenuation correction, *NECR* noise equivalent count rate

Table 2.3 Relative advantages and disadvantages of PET/CT and PET/MR

	Advantages	Disadvantages
PET/CT	High-resolution anatomy Fast imaging Simple attenuation correction	Radiation dose from CT Sequential acquisition with possible motion induced misalignment
PET/MR	High soft tissue contrast Simultaneous acquisition with truly integrated information No radiation dose from MR MR sequences protocol flexibility	Cost MR-based attenuation correction Patient compliance Contraindication in patients with passive or active ferromagnetic devices

of the APD signals due to lower gain and higher noise compared to PMT signals also limits the overall time resolution of the imaging device, leading thus to a wider time coincidence window. Additionally, an increased number of detected accidental coincidences will degrade image quality. More recently, silicon photomultipliers (SiPM) have been proposed as scintillator readout in PET applications since they combine a number of advantageous properties compared to other photodetectors such as PMT or APD. The SiPM architecture is based on an array of single-channel APD. Quantitative information about the number of incident photons is given by the output signal of the SiPM array which is the sum of the signals of the individual APD connected to each other through a polysilicon resistor. SiPM exhibits a superior performance in terms of timing, allowing TOF acquisition, and a similar performance to proportional APD in terms of energy resolution [30–32]. Lately a novel PET detector concept has been proposed using arrays of SiPM as photodetectors. With regard to the post processing, it has become necessary to develop and optimize MR-based attenuation correction of the PET data, and different solutions such as template-based method [33], atlas-based approach, segmentation-based method [34], and sequence-based approach [35] have been proposed. Nevertheless, each method is still under validation. With regard to safety, patient exposure to ionizing radiations is significantly reduced compared to PET/CT, while on the other hand, passive or active implants, or other ferromagnetic objects, or objects of unknown material (pellets, bullets), are associated with a potential risk for the PET/MR examination.

Nowadays, two truly integrated hybrid PET/MR scanners are commercially available: Siemens *Biograph mMR* that utilize APD technology and GE *Signa PET/MR* that proposed SiPM-based method. The PET detector ring is allocated in a gap approximately 10 cm wide, obtained by replacing the innermost radiofrequency coil with a narrow-bore version and keeping the main coil and gradients of the wide-bore systems. Characteristics of commercially available PET/MR design, all working at 3 T, are summarized in Table 2.2.

The relative advantages and disadvantages of PET/CT and PET/MR are summarized in Table 2.3.

References

1. Margolis DJ, Hoffman JM, Gambhir SS et al (2007) Molecular imaging techniques in body imaging. Radiology 245:333–356
2. Bar-Shalom R, Yefremov N, Israel O et al (2003) Clinical performance of PET/CT in evaluation of cancer: additional value for diagnostic imaging and patient management. J Nucl Med 44:1200–1209
3. Pichler BJ, Judenhofer MS, Pfannenberg C (2008) Multimodal imaging approaches: PET/CT and PET/MRI. Handb Exp Pharmacol 185:109–132
4. Kak AC, Slaney M (1988) Principles of computerized tomographic imaging. IEEE Press, New York
5. Kalender WA (ed) (2011) Computed tomography: fundamentals, system technology, image quality, application, 3rd edn. Erlangen, Publicis Publishing
6. Ohnesorge B, Flohr T (eds) (2006) Multi-slice and dual-source CT in cardiac imaging: principles-protocols-indications-outlook, 2nd edn. Heidelberg, Springer
7. Johnson TR (2009) Dual-energy CT: technical background. In: Reiser MF, Becker CR (eds) Multislice CT, 3rd edn. Springer, Heidelberg, pp 65–73
8. Willemink MJ, de Jong PA, Schilham AM et al (2013) Iterative reconstruction techniques for computed tomography Part 1: technical principles. Eur Radiol 23:1623–1631
9. Nutt R (2002) 1999 ICP Distinguished Scientist Award. The history of positron emission tomography. Mol Imaging Biol 4:11–26

10. Muehllehner G, Karp JS (2006) Positron emission tomography. Phys Med Biol 51:R117–R137
11. Moses WW (2011) Fundamental limits of spatial resolution in PET. Nucl Instrum Methods Phys Res A 648(Supplement 1):S236–S240
12. Bendriem B, Townsend DW (eds) (2013) The theory and practice of 3D PET, vol 32. Springer Science & Business Media, Dordrecht
13. Bischof Delaloye A, Carrió I, Silberman B et al (2007) White paper of the European Association of Nuclear Medicine (EANM) and the European Society of Radiology (ESR) on multimodality imaging. Eur J Nucl Med Mol Imaging 34:1147–1151
14. Frayne R, Goodyear BG, Sevick RJ et al (2003) Magnetic resonance imaging at 3.0 Tesla: challenges and advantages in clinical neurological imaging. Invest Radiol 38(7):385–402
15. Dale BM, Brown MA, Semelka RC (eds) (2015) MRI: basic principles and applications, 5th edn. Wiley-Blackwell, Hoboken
16. Turner R (1993) Gradient coil design: a review of methods. Magn Reson Imaging 11:903–920
17. Liang ZP, Lauterbur PC (2000) Principles of magnetic resonance imaging: a signal processing perspective. Wiley-IEEE Press, New York
18. Le Bihan D, Breton E, Lallemand D et al (1988) Separation of diffusion and perfusion in intravoxel incoherent motion MR imaging. Radiology 68:497–505
19. Reichenbach JR, Schweser F, Serres B, Deistung A (2015) Quantitative susceptibility mapping: concepts and applications. Clin Neuroradiol 25(Suppl 2):225–230
20. Ciobanu L, Solomon E, Frydman L et al (2015) fMRI contrast at high and ultrahigh magnetic fields: insight from complementary methods. Neuroimage 113:37–43
21. Barker PB, Hearshen DO, Boska MD (2001) Single-voxel proton MRS of the human brain at 1.5T and 3.0T. Magn Reson Med 45:765–769
22. Townsend DW, Beyer T, Blodgett TM (2003) PET/CT scanners: a hardware approach to image fusion. Semin Nucl Med 33:193–204
23. Schöder H, Erdi YE, Yeung HW et al (2003) PET/CT: a new imaging technology in nuclear medicine. Eur J Nucl Med Mol Imaging 30:1419–1437
24. Seemann MD (2004) PET/CT: fundamental principles. Eur J Med Res 9:241–246
25. Alessio AM, Kinahan PE, Karp JS et al (2004) PET/CT scanner instrumentation, challenges, and solutions. Radiol Clin North Am 42:1017–1032
26. Farwell MD, Pryma DA, Mankoff DA (2014) PET/CT imaging in cancer: current applications and future directions. Cancer 120:3433–3445
27. Delso G, Ter Voert E, Veit-Haibach P (2015) How does PET/MR work? Basic physics for physicians. Abdom Imaging 40:1352–1357
28. Ziegler SI, Pichler BJ, Schwaiger M et al (2001) A prototype high-resolution animal positron tomograph with avalanche photodiode arrays and LSO crystals. Eur J Nucl Med 28:136–143
29. Judenhofer MS, Wehrl HF, Pichler BJ et al (2008) Simultaneous PET-MRI: a new approach for functional and morphological imaging. Nat Med 14:459–465
30. Wehrl HF, Sauter AW, Pichler BJ et al (2015) Combined PET/MR: a technology becomes mature. J Nucl Med 56:165–168
31. Shah SN, Huang SS (2015) Hybrid PET/MR imaging: physics and technical considerations. Abdom Imaging 40:1358–1365
32. Delso G, Ziegler S (2009) PET/MRI system design. Eur J Nucl Med Mol Imaging 36(Suppl 1):S86–S92
33. Wagenknecht G, Kaiser HJ, Herzog H et al (2013) MRI for attenuation correction in PET: methods and challenges. MAGMA 26:99–113
34. Hofmann M, Bezrukov I, Schölkopf B et al (2011) MRI-based attenuation correction for whole-body PET/MRI: quantitative evaluation of segmentation- and atlas-based methods. J Nucl Med 5:1392–1399
35. Berker Y, Franke J, Schulz V et al (2012) MRI-based attenuation correction for hybrid PET/MRI systems: a 4-class tissue segmentation technique using a combined ultrashort-echo-time/Dixon MRI sequence. J Nucl Med 53:796–804

Quantitation and Data Analysis in Hybrid PET/MRI Systems

3

Isabella Castiglioni, Francesca Gallivanone, and Maria Carla Gilardi

3.1 Introduction

Image processing methods are used in medical imaging with the purpose to improve image quality and quantitative accuracy, to allow feature extraction and quantitative assessment of structural, physiological and functional parameters, supporting physicians in the diagnostic process and scientists in understanding underlying physiopathological mechanisms. The information obtained can be qualitative, semi-quantitative and quantitative, depending on the type of information and the way this information is processed and represented. In hybrid imaging, combining complementary imaging modalities, as PET/CT or PET/MRI, quantitation and data analysis methods may allow enhancing the information derived from each modality individually but also those obtained by the multimodal integration process.

The aim of this chapter is to investigate quantitation and data analysis issues, in the context of a SWOT analysis applied to hybrid brain imaging [1]. In particular, the strengths (S), weaknesses (W), opportunities (O) and threats (T) of PET/MRI with respect to PET/CT are considered. The SWOT matrix is presented in Table 3.1. The contents for each cell (S, W, O, T) are discussed below.

I. Castiglioni (✉) • F. Gallivanone • M.C. Gilardi
Institute of Molecular Bioimaging and Physiology, National Research Council (IBFM-CNR), Segrate, MI, Italy
e-mail: isabella.castiglioni@ibfm.cnr.it

3.2 Strengths

Two main areas of strength of PET/MRI with respect to PET/CT can be recognized, with an impact onto quantitation and data analysis.

3.2.1 MRI High Soft Tissue Contrast

MRI is superior to CT in providing images with high soft tissue contrast and spatial resolution, allowing partitioning brain into main tissue components (typically grey matter, white matter and cerebrospinal fluid). This anatomical information can be incorporated into the functional PET brain images and used to improve PET reconstruction and quantitation.

3.2.1.1 MRI-Guided PET Image Reconstruction

PET/MRI can take advantage of the availability of high-resolution segmented MRI anatomical images to improve PET image reconstruction by accounting for a priori structural information [2]. MRI information can be incorporated either during the PET image reconstruction process or by the use of post-reconstruction filtering and post-reconstruction deconvolution of the PET

A. Ciarmiello, L. Mansi (eds.), *PET-CT and PET-MRI in Neurology*,
DOI 10.1007/978-3-319-31614-7_3

Table 3.1 Quantitation and data analysis: SWOT matrix of PET/MRI with respect to PET/CT

Strengths (*S*)	*Weaknesses* (*W*)
MRI high soft tissue contrast MRI-guided reconstruction MRI-guided PVE correction PET quantitation and MRI-derived input function PET/MRI in combination	Attenuation correction Workflow
Opportunities (*O*)	*Threats* (*T*)
Advanced image processing and data analysis methods combined with multi-parametric and multimodal imaging	Niche markets and slow translation from research to clinical application

reconstructed images. Most methods require segmentation of MRI images, and several MRI segmentation methods have been developed for a number of different clinical and research applications. In particular, for brain studies, applications range from brain volumetry, radiation therapy and surgical planning of brain oncological lesions and image-guided real-time intervention procedures in the brain [3]. However, even if extensively validated in brain MRI studies, MRI segmentation is still a difficult task, because MR images are affected by noise and image artefacts. Other approaches recently developed [4] adopt voxel-wise methodologies to directly filter noise in PET brain images, by utilizing the local linear model between structural MRI and functional PET brain images, thus avoiding the need of segmentation/parcellation of the MRI images.

As in PET/CT, most PET/MRI systems currently employ iterative reconstruction algorithms for the PET images. As a strategy to improve spatial resolution and contrast of PET images, the point spread function (PSF) is often incorporated into the reconstruction software. Unfortunately, a drawback of this improvement is the generation of image artefacts, similar to ringing artefacts (e.g. overshoot at the boundary of body regions), causing an overestimation in PET quantitation, in particular for small lesions. While this problem is not specific to hybrid PET/MRI systems, there has been a recent important effort towards the development of alternative reconstruction algorithms. For example, Lougovski et al. [5] proposed a new approach to reconstruction based on the volume of response between two coincidence detectors instead of standard lines of responses. Such algorithm was implemented on a commercial PET/MRI scanner, being able to suppress Gibbs artefacts while maintaining the same level of spatial resolution and contrast as for reconstruction methods with PSF based on line of responses.

3.2.1.2 MRI-Guided PVE Correction

MRI data can be useful to improve the quantification of PET radiotracer concentration by correcting PET data for partial volume effect (PVE) [6, 7].

Among the several PVE correction methods using MRI as prior information, the most popular is the geometric transfer matrix (GTM) method [6], where MR images can be segmented to different non-overlapping regions representing different tissue types, and these regions are then used to correct for both the tissue fraction effect and the point response effect in an analytical approach. To mitigate the challenge of segmenting the entire object, projection-based tissue activity estimation methods have been proposed to compensate for the PVE, which only required the segmentation of a small number of tissues within a small region around the lesion (e.g. tumour) [8, 9].

Recently Yan et al. [4] proposed a filtering method for PVE by introducing an MRI anatomical image as a prior term performed on the voxel level without the need to segment MR images. The performance of the proposed method was assessed on a simultaneous hybrid PET/MRI system. The authors simulated an (18)FDG PET dynamic study of a cervical cancer patient, showing that MRI-guided filters are more effective in reducing noise on PET images than filters not incorporating MRI anatomical information. Furthermore, MRI-guided PET PVC reduces bias and coefficient of variation of PET images. As clinical effects, small brain structures can be better defined and manually delineated.

3.2.1.3 PET Quantification and MRI-Derived Input Function

The absolute quantification of physiological or biochemical parameters in PET requires the application of mathematical models describing the kinetics of the radiotracer and measurement of the tracer time-activity curve in plasma, the arterial input function (AIF). This function can be measured by invasive procedures on blood samples or non-invasively by estimating the time-activity curve from arterial images on the dynamic PET scan. However, extracting AIFs from PET images is challenging due to large PVE.

Simultaneous PET/MR can assist in a non-invasive extraction of accurate AIF, taking advantage from the use of dynamic MRI with high temporal and spatial resolution. In a recent work, Evans et al. [10] demonstrated that in hybrid PET/MRI, a co-injected bolus of MRI contrast agent and PET ligands could be tracked using fast MRI acquisitions. This protocol allowed the measurement of AIF from the concentration time curves of the MRI contrast images with a better spatial and time resolution than those obtained by using AIF from the PET images. The authors found that MRI and PET AIFs displayed similar character and that MRI AIFs showed a reduced PVE with respect to PET AIFs, thus demonstrating the advantage of using MRI.

Recently, a pilot study on a piglet model investigated the potentials of the hybrid PET/MRI systems for brain imaging, assessing minimally invasive approaches to measure global cerebral blood flow (CBF), in a model of newborn piglets [11]. Using a simultaneous acquisition of (15)O-water PET and single TI pulsed arterial spin labelling (ASL) MR, the authors showed that quantification of CBF is possible with low injected activity of (15)O-water by non-invasive image-derived input function from MR. The CBF method is proposed for future studies of the pathophysiology of focal brain injury, such as stroke and periventricular leukomalacia.

3.2.2 PET/MRI in Combination

The main challenge in a PET/MRI scanner is to combine the two modalities leading to added value information, without compromising their image quality. To this purpose, two approaches have been proposed: sequential scanning and simultaneous scanning. In sequential scanning, PET and MRI studies are performed sequentially on two independent systems, thus limiting the interaction between PET and MRI. This is a straightforward solution, allowing multi-parametric information coming from the two modalities to be recorded in a single study session (although not simultaneously) [2]. Simultaneous scanning is technologically more challenging, as it requires full integration of the two systems, but it guarantees spatial and temporal PET-MRI data registration.

Both approaches have the potential to study, in the time of a single examination and without moving the patient, a variety of neurological functions dependent on the radiotracer used in PET (tracers of blood flow, metabolism and neurotransmission) and the acquisition sequences employed in MRI (e.g. DWI, fMRI, spectroscopy, etc.), with the specific advantage of simultaneous over sequential scanning of being able to assess fast changing processes by PET and MRI at the same time.

The potentials of PET/MRI multi-parametric scanning have been discussed in several papers (e.g. [12]) for the study of dementia and other neurodegenerative disorders, brain tumours, epilepsy and neuropsychiatric diseases. The opportunity derived by combining advanced image processing and data analysis methods for the quantification of functional parameters and the extraction of features and information from such a large amount of data will be discussed in the Opportunity section.

3.3 Weaknesses (W)

PET/MRI presents elements of complexity with respect to PET/CT, offering potentials on one side but, on the other, turning out in points of weakness. Contrary to CT, the complexity of MRI signal does not allow a direct association to density maps, to be applied straightforward for attenuation correction of PET data, making attenuation correction and quantitation more difficult

for hybrid PET/MRI than for PET/CT systems. Moreover, PET/MRI technology requires complex acquisition protocols and long scan duration, in particular when multi-parametric or whole body MRI studies are required.

3.3.1 Attenuation Correction

Despite the potential clinical advantages of PET/MRI, quantification of PET images obtained in PET/MRI acquisitions remains an open issue due to wide biases in the measurements of radioactivity concentration in reconstructed PET images, mainly due to the lack of accurate MR-based attenuation correction (AC) methods of PET images.

The problem of developing AC methods based on MR imaging is related to the MR signal itself. In fact, AC in PET/CT is performed on the basis of CT images, where signal intensity is directly related to electron density, thus enabling direct translation of CT images to maps of attenuation coefficients μ. On the contrary, MR signal is related to proton density and tissue relaxation properties, which are difficult to translate into electron density information. In order to obtain an MR-based AC map of μ attenuation coefficients, the method currently in use in commercial PET/MR system is based on segmentation of MR images in tissue classes and in the assignment of tissue-specific attenuation coefficients to different segmented classes [13]. This method is implemented in most of the commercial PET/MR systems, using a technique known as "three-dimensional volume-interpolated breath-hold examination (3D Dixon-VIBE)". By deriving information from these acquisitions, the signal is segmented in various tissue classes, such as the soft tissue, lungs and air, AC maps are generated assigning proper attenuation coefficients to each class and the obtained maps are used for AC during PET reconstruction.

Several limitations arise using this approach. Various components of PET/MR scanners, such as the patient table and the RF coils, are transparent in MR images, and attenuation information on these structures cannot be obtained by MR image segmentation. In order to account for this, the inclusion of predefined attenuation maps obtained from CT scans of the scanner components has been evaluated. This implementation may suffer from potential misalignments between CT and MR acquisitions, impacting on the accuracy of the obtained AC maps. Another drawback of the Dixon-based MR-AC approach is that some body compartments, such as cortical bone, do not appear at MR imaging, and bone attenuation is approximated to that in soft tissue or air. Ultrashort echo time (UTE) MRI sequences or combined UTE/Dixon MRI sequences have been considered to better distinguish cortical bone, air and soft tissue in segmentation-based techniques [14, 15]. With the purpose to obtain a more accurate AC in bone, atlas-based AC methods have been proposed. In these methods, patient MR images are co-registered to an MR atlas, which is in turn co-registered to a CT atlas, providing proper attenuation coefficients then applied to patient PET images [16]. This method is particularly suitable for brain studies, where co-registration errors are minimized with respect to other body districts. In whole body studies, physiological and non-physiological movements, the presence of implants, as well as distortions due to pathology impact on the accuracy of the method by causing atlas misregistration errors. Multi atlas-based methods were explored in order to avoid co-registration problems in particular in whole body imaging [17].

Navalpakkam et al. [18] have proposed an AC method, based on the generation of synthetic CT images and attenuation maps, obtained using an epsilon-insensitive support vector regression, to produce a continuous set of attenuation coefficients. Furthermore, the use of additional PET data from scattered coincidences has been recently proposed to improve the quality of AC maps reconstructed from PET emission data [19].

In summary, AC in PET/MRI is still an unsolved issue and a variety of solutions are being proposed, in general remaining at a prototype level. In neurological imaging, MR-based AC is more effective, reproducible and accurate within 20 %, with major errors in cerebellum and temporal lobes [20].

3.3.2 Workflow

PET/MRI workflow must be properly planned depending on the type of PET/MRI scanner, the anatomical district and the disease under examination. Workflow includes patient preparation, PET scanning, MRI scanning for PET AC and dedicated MRI scans for multi-parametric imaging (including anatomical imaging). PET/MRI workflow is thus more complex than in PET/CT and in general more time consuming.

While the experiences in the use of PET/MRI increase, translation from research to clinical applications remains a slow process, and clinical standardized protocols are hard to be set up, with the aim to optimize the balance among acquisition time, image quality and the amount of signal that can be further processed to obtain relevant clinical information.

Some papers dealing with PET/MRI workflow have been published [21–23], mainly focusing on whole body studies. In fact, neuroimaging is facilitated in that an axial field of view corresponding to a single bed position is sufficient to cover the whole brain, and simpler protocols could be adopted. However, it may be of interest in brain imaging to set up long acquisition protocols, comprehensive of dynamic PET scanning and multiple complex MRI sequences in addition to the conventional ones (e.g. to combine functional PET, morphological and functional MRI data). The point is then to optimize acquisition time and image reconstruction to achieve the best image quality.

Regarding PET reconstruction, the choice of the reconstruction method and of the reconstruction parameters plays a pivotal role, as optimized reconstruction improves image quality, thus allowing shortening the acquisition time. An evaluation of the impact of reconstruction parameters on image quality and quantitative accuracy of brain PET images acquired on a current generation PET/MRI system can be found in Leemans et al. [24]. Phantom studies simulating clinical conditions were performed to assess image quality and quantitative accuracy in terms of image contrast and noise characteristics.

In general, an efficient and systematic implementation of quantitation and data analysis procedures would require standardized and optimized acquisition protocols. Image processing methods for data analysis and quantitation are thus currently still dedicated to the individual modality (PET and MRI independently), more than to hybrid imaging with the aim to process PET and MRI in combination.

3.4 Opportunities (O)

PET/MRI technology is evolving rapidly, taking advantage of the fast advances in PET and MRI separately and of the efforts dedicated to efficiently combine the two scanners in one. The physics of hybrid imaging and the instrumentation challenge are beyond the purpose of this chapter and are topics of previous chapters of this book. However, it is worth noting how the technological advances are leading to an enormous amount of complementary multi-parametric quantitative data which can be generated by PET/MRI and analysed with advanced image processing and data analysis methods, thus offering unique insights into opportunities to optimize care for individual patients.

With this aim, advanced image processing algorithms, independently developed for each single modality, can be employed for the automatic or semi-automatic extraction and combination of multimodal and multi-parametric biomarkers.

Concerning PET brain imaging, biomarkers such as glucose hypometabolism or brain b-amyloid load have been considered for the diagnosis and/or differential diagnosis of dementia. Statistical approaches, such as voxels-based statistical analysis using statistical parametric mapping (SPM), proved an improvement in clinical diagnostic accuracy of AD and high predictive power for conversion to AD [25].

Supervised whole brain automatic classification computerized methods are used for the detection of image patterns typical of specific diseases (e.g. dementia, psychiatric disorders) corresponding to sensitive biomarkers or to a combination of them. Among these methods, support vector machine (SVM) algorithms [26, 27] have been successfully used and widely

adopted for the automatic classification of medical images (e.g. for the classification of non-pathological vs. pathological images or for the classification of disease subtypes [28]). Specifically, when applied to structural MRI images, SVM shows high potentials in the classification of dementia and of dementia subtypes (e.g. [29]).

Among automated image processing methods, texture analysis approaches have been explored in more recent years, particularly in oncology, with the aim to identify and characterize tumour heterogeneity towards a personalized therapy treatment. Three-dimensional texture analysis (3D TA) of structural MR images has been shown to improve the diagnostic classification of childhood brain tumours [30]. Textural [18F]-fluoroethyl-L-tyrosine (FET) PET features have been assessed as biomarkers enabling to predict grading as well as tumour progression and patient survival in high-grade gliomas [31].

Moreover, advanced data processing methods can be employed for the best combination of multimodal and multi-parametric biomarkers measured by hybrid PET/MRI, profiting from an accurate spatial and/or temporal correlation of data. Among these methods, multivariate data analysis such as SVM classification, multi-kernel learning and artificial neural network are able to combine two or more different biomarkers measured by PET or MRI within the same classification model. For example, it has been shown that combining information from (18)FDG PET and MRI substantially improves early diagnosis of AD [32, 33] and differential diagnosis of AD and frontotemporal lobar degeneration [34]. Starting from these results, it is clear that such advanced multivariate analysis is highly promising in providing, in one single examination session of hybrid PET/MRI, new "profiles of biomarkers" of diseases [35].

3.5 Threats (T)

Quantitation and data analysis in PET/MRI do not suffer specific threats but those associated to the technique itself and thus in particular high complexity, high costs and limited market with respect to PET/CT.

While the advantages of PET/CT with respect to PET standalone systems have made immediately evident, e.g. anatomical localization and improved quantification of PET images, integrated PET/MRI scanners are just opening a new scenario in hybrid imaging. A number of PET/MRI integrated scanners are currently available for research purposes worldwide, but major threats are speculated that could cause these systems not to grow rapidly in number, if clear clinical benefits do not continue to be demonstrated. Many results are indicating that combined PET/MRI used with conventional clinical acquisition protocols shows comparable performance in the detection, diagnosis and location of suspected diseases in patients as compared to conventional PET/CT. The next step for PET/MRI is crucial in studying the added clinical benefit of introducing sophisticated MRI sequences to the diagnostic imaging protocols. Also, the exact role and potential utility of simultaneous data acquisition in specific research and clinical settings need to be defined. It may be that simultaneous PET/MRI will be best suited for clinical situations that are disease specific and organ specific, related to diseases of the children or in those patients undergoing repeated imaging, for whom cumulative radiation dose must be kept as low as reasonably achievable. If so, the simultaneous acquisition could bring advantages only for niches of patients.

Regarding image analysis and quantitation, the added clinical value of sophisticated processing methods is promising, but remains to be proved. A major threat may be represented by the misalignment between the speed typical of computer technologies and that of medical devices: development of software tools is currently very fast and dynamic, whereas their clinical implementation and acceptance, passing through validation and incorporation into commercial medical systems (time to market), is much slower and spans over much longer periods of time. There is a high risk that the opportunities offered by the integration and correlation of multimodal and multi-parametric parameters

coming from the more advanced image processing methods available in each imaging modality cannot be taken by clinicians, but only within groups devoted to research and with skills and expertise in image processing, thus limiting their clinical utility.

Conclusions

This paper attempts to analyse benefits and limitations of brain PET/MRI vs PET/CT, focussing attention on quantitation and data analysis issues and according to a SWOT methodology. Strengths, weaknesses, opportunities and threats are considered referring to data, experiences and opinions reported in the literature. PET/MRI is an intriguing technology, offering the unique possibility to simultaneously investigate brain structure and functioning from different perspectives. Image processing and data quantification methods play a key role in order to take full advantage from the multiple information which can be collected in a single study session, to make them more accurately quantitative and move towards the very topical paradigm of precision medicine, e.g. by the identification of biomarkers to be measured at the individual level. PET/MRI is a very challenging technology, as the complexity of both instrumentation and procedures require the development of novel operational models to face management issues and high costs. Image processing and data quantification methods may enter in this scenario by supporting a simplification of the procedures (making them more automatic and less operator dependent) and their translation from research to clinical applications.

References

1. Hill T, Westbrook R (1997) SWOT analysis: It's time for a product recall. Long Range Plann 30(1):46–52
2. Zaidi H, Del Guerra A (2011) An outlook on future design of hybrid PET/MRI systems. Med Phys 38(10):5667–5689
3. Despotović I, Goossens B, Philips W (2015) MRI segmentation of the human brain: challenges, methods, and applications. Comput Math Methods Med 2015:450341
4. Yan J, Lim JC, Townsend DW (2015) MRI-guided brain PET image filtering and partial volume correction. Phys Med Biol 60:961–976
5. Lougovski A, Hofheinz F, Maus J, Schramm G, Will E, van den Hoff J (2014) A volume of intersection approach for on-the-fly system matrix calculation in 3D PET image reconstruction. Phys Med Biol 59(3):561–577
6. Rousset OG, Ma Y, Evans AC (1998) Correction for partial volume effects in PET: principle and validation. J Nucl Med 39:904–911
7. Zaidi H, Ruest T, Schoenahl F, Montandon ML (2006) Comparative assessment of statistical brain MR image segmentation algorithms and their impact on partial volume correction in PET. Neuroimage 32(4):1591–1607
8. Moore SC, Southekal S, Park MA, McQuaid SJ, Kijewski MF, Müller SP (2012) Improved regional activity quantitation in nuclear medicine using a new approach to correct for tissue partial volume and spillover effects. IEEE Trans Med Imaging 31(2):405–416
9. Southekal S, McQuaid SJ, Kijewski MF, Moore SC (2012) Evaluation of a method for projection-based tissue-activity estimation within small volumes of interest. Phys Med Biol 57(3):685–701
10. Evans E, Sawiak SJ, Ward AO, Buonincontri G, Hawkes RC, Carpentera TA (2014) Comparison of first pass bolus AIFs extracted from sequential 18F-FDG PET and DSC-MRI of mice. Nucl Instrum Methods Phys Res A 734(B):137–140
11. Andersen JB, Henning WS, Lindberg U, Ladefoged CN, Højgaard L, Greisen G, Law I (2015) Positron emission tomography/magnetic resonance hybrid scanner imaging of cerebral blood flow using 15O-water positron emission tomography and arterial spin labelling magnetic resonance imaging in newborn piglets. J Cereb Blood Flow Metab 35(11):1703–1710
12. Werner P, Barthel H, Drzezga A, Sabri O (2015) Current status and future role of brain PET/MRI in clinical and research settings. Eur J Nucl Med Mol Imaging 42(3):512–526
13. Boellaard R, Quick HH (2015) Current image acquisition options in PET/MR. Semin Nucl Med 45(3):192–200
14. Aitken AP et al (2014) Improved UTE-based attenuation correction for cranial PET-MR using dynamic magnetic field monitoring. Med Phys 41(1):012302
15. Burgos N et al (2014) Attenuation correction synthesis for hybrid PET-MR scanners: application to brain studies. IEEE Trans Med Imaging 33(12):2332–2341
16. Hofmann M, Pichler B, Scholkopf B, Beyer T (2009) Towards quantitative PET/MRI: a review of MR based attenuation correction techniques. Eur J Nucl Med Mol Imaging 36(Suppl 1):S93–S104
17. Marshall HR et al (2013) Description and assessment of a registration-based approach to include bones for attenuation correction of whole-body PET/MRI. Med Phys 40(8):082509
18. Navalpakkam BK, Braun H, Kuwert T, Quick HH (2013) Magnetic resonance-based attenuation correction for PET/MR hybrid imaging using continuous valued attenuation maps. Invest Radiol 48(5):323–332

19. Berker Y, Kiessling F, Schulz V (2014) Scattered PET data for attenuation-map reconstruction in PET/MRI. Med Phys 41(10):102502
20. Dickson JC, O'Meara C, Barnes A (2014) A comparison of CT- and MR-based attenuation correction in neurological PET. Eur J Nucl Med Mol Imaging 41(6):1176–1189
21. Barbosa FG, von Schulthess G, Veit-Haibach P (2015) Workflow in simultaneous PET/MRI. Semin Nucl Med 45(4):332–344
22. von Schulthess GK, Veit-Haibach P (2014) Workflow considerations in PET/MR imaging. J Nucl Med 55(Suppl 2):19S–24S
23. Martinez-Möller A et al (2012) Workflow and scan protocol considerations for integrated whole-body PET/MRI in oncology. J Nucl Med 53(9):1415–1426
24. Leemans EL, Kotasidis F, Wissmeyer M, Garibotto V, Zaidi H (2015) Qualitative and quantitative evaluation of blob-based time-of-flight PET image reconstruction in hybrid brain PET/MR imaging. Mol Imaging Biol 17(5):704–713
25. Perani D et al (2016) Cross-validation of biomarkers for the early differential diagnosis and prognosis of dementia in a clinical setting. Eur J Nucl Med Mol Imaging 43(3):499–508
26. Vapnik V (2000) The nature of statistical learning theory. Springer, New York
27. Shawe-Taylor J, Cristianini N (2004) Kernel methods for pattern analysis. Cambridge University Press, Cambridge, UK
28. Focke NK et al (2011) Individual voxel-based subtype prediction can differentiate progressive supranuclear palsy from idiopathic Parkinson syndrome and healthy controls. Hum Brain Mapp 32(11):1905–1915
29. Klöppel S et al (2008) Automatic classification of MR scans in Alzheimer's disease. Brain 131(3):681–689
30. Fetit AE, Novak J, Peet AC, Arvanitits TN (2015) Three-dimensional textural features of conventional MRI improve diagnostic classification of childhood brain tumours. NMR Biomed 28(9):1174–1184
31. Pyka T et al (2015) Textural analysis of pre-therapeutic [18F]-FET-PET and its correlation with tumor grade and patient survival in high-grade gliomas. Eur J Nucl Med Mol Imaging 43(1):133–141
32. Hinrichs C, Singh V, Xu G, Johnson S (2009) MKL for robust multi-modality AD classification. Med Image Comput Comput Assist Interv 12(Pt 2):786–794
33. Zhang D, Wang Y, Zhou L, Yuan H, Shen D, Alzheimer's Disease Neuroimaging Initiative (2011) Multimodal classification of Alzheimer's disease and mild cognitive impairment. Neuroimage 55(3):856–867
34. Dukart J et al (2011) Combined evaluation of FDG-PET and MRI improves detection and differentiation of dementia. PLoS One 6(3):e18111
35. Hinrichs C, Singh V, Xu G, Johnson SC, Alzheimers Disease Neuroimaging Initiative (2011) Predictive markers for AD in a multi-modality framework: an analysis of MCI progression in the ADNI population. Neuroimage 55(2):574–589

Radiopharmaceuticals

4

Mattia Riondato and William C. Eckelman

4.1 Introduction

Radiotracers and radiopharmaceuticals for Nuclear Medicine imaging with applications in neurology have been implemented for more than 50 years, based on the research efforts of scientists in the academic world, hospitals, and industry. The first described imaging applications in humans were pioneered in the early 1950s in the USA for the detection of intracranial lesions and for the assessment of regional cerebral blood flow. Images were obtained using conventional gamma cameras, after administering inert radioactive gases by inhalation or radioactive metal complexes by injection. These agents were not aimed to detect any specific mechanism or molecular target, but they were used in the research setting for describing pathophysiological processes.

The strong efforts in radiochemistry, in addition to the technological improvements of the tomographic detection systems, contributed to enforce the interest for this emerging technique, and the first studies in a clinical setting were reported during the 1960–1970s. The potential impact to patient care boosted the need of new and more specific radiotracers. Thus, the development of new tracers for neuroimaging applications turned from using radioactive salts and known chelating agents to the modern concept of molecular neuroimaging. This latter model is based on the specific interaction between the imaging agent and the molecular structure or cellular process of interest, such as receptors, enzymes, transporters, or metabolic pathways. The emitting radionuclides contained within the agent provide a signal that can create an image if associated with the proper imaging system. After four decades of hard work in radiochemistry, hundreds of radiotracers containing different single photon and positron emitter nuclides have been developed and applied to the most common imaging modalities for the evaluation of brain function, accomplishing clinical and investigational requirements (Table 4.1). A number of them have been approved by authorities and are currently used in Nuclear Medicine departments by physicians for specific applications, showing a potential impact for direct patient care. The major clinical areas of application include cerebrovascular diseases, movement disorders, dementia, epilepsy, and brain tumors. Neuroimaging radiotracers are also employed for the study of other mental disorders such as schizophrenia, addiction, depression, and anxiety.

M. Riondato, PhD (✉)
Nuclear Medicine Department, S. Andrea Hospital, La Spezia, Italy
e-mail: mattia.riondato@asl5.liguria.it

W.C. Eckelman
Molecular Tracer LLC, Bethesda, MD 20814, USA

A. Ciarmiello, L. Mansi (eds.), *PET-CT and PET-MRI in Neurology*,
DOI 10.1007/978-3-319-31614-7_4

Table 4.1 Early PET and SPECT human brain studies

Date	PET	SPECT
1955		[^{85}Kr]Gas
1963		[^{133}Xe]Gas
1964		[^{99m}]TcO_4^-
1965	[^{68}Ga]EDTA	
1967	[^{15}O]Oxygen	
1969	[^{15}O]Water	
1975		[^{123}I]Iodoantipyrine
1976	[^{11}C]Methionine	
1977	[^{18}F]FDG [^{11}C]Tryptophan [^{11}C]Valine	
1981		N-isopropyl-[^{123}I] Iodoamphetamine ([^{123}I]IMP)
1983	N-[^{11}C]Methylspiperone [^{18}F]FDOPA	[^{123}I]IQNB
1984	[^{18}F]Cyclofoxy	
1985	[^{11}C]Raclopride [^{11}C]Carfentanil [^{11}C]Flumazenil	[^{99m}Tc]HMPAO
>1985	Many	Many

Unexpectedly, the expanded range of radiotracers hasn't been followed by a parallel introduction of radiopharmaceuticals, as tools for answering clinical needs. During the last decade, radiotracers in order to get approval for clinical use or marketing authorization have been facing implemented radiopharmaceutical requirements, similar to those that are broadly applied to all drugs. In particular, the increased awareness for the quality and safety of radiopharmaceuticals and the need for confirmation that the diagnostic agent has to provide clinically useful information contributed to make a widespread use of new agents very challenging.

Last but not least, the use of SPECT and PET neuroimaging is not restricted to the clinical or investigational field in the hospital Nuclear Medicine departments. During the last decades, this imaging technique has gained attention in neuroscience for the excellent capability to gain insight into disease mechanisms, describing the kinetics of the radiotracers and measuring target reserves, such as enzymes or receptors. For this reason, the standard methodology developed to study normal and pathological processes has been extended to support drug discovery in the universities and in the pharmaceutical industry. Neuroimaging with carbon-11 and fluorine-18 PET radiotracers has become a routine procedure for the development of biomarkers for novel central nervous system therapeutics. Using a PET-specific radiotracer identical to a drug candidate, brain penetration and target occupancy measurements can be defined. The drug interaction with a specific brain target can also be studied by competition, if a suitable radiopharmaceutical for the same target is available. Such information may have a substantial impact in a go/no-go decision on a set of drug candidates before first-in human studies and furthermore may produce a significant effect on the overall pipeline cost for drug development.

4.2 Brain SPECT and PET Radiotracers: A Journey More than 50 Years Long

From a historical perspective, the use of radiotracers for brain scanning began in the early 1950s for the localization and identification of tumor damage by Sweet and Brownell [1–3].

Several compounds incorporating radionuclides were synthesized in order to obtain stable agents with a low toxicity profile. Among these, the most satisfactory have been the positron emitters arsenic-74 as arsenate, copper-64 as versenate, and mercury-203 as neohydrin [4, 5]. These scanning agents were not required to have any specific interaction; they were able to permeate across the disrupted blood–brain barrier (BBB), thus allowing a rudimental detection of the membrane integrity and the lesion extensions with camera-type systems. Despite the raising interest for the methodology, these long half-life radionuclides displayed suboptimal characteristics for a clinical use. A few years later, driven by favorable nuclear properties, a radionuclide generator, and known chemistry, the researcher's attention shifted to the development of a suitable agent containing gallium-68 [6]. As a consequence of the available "ready to use" ^{68}Ga-EDTA (ethylenediaminetetraacetic acid) milked from the generator, and the introduction of new positron scintillator cameras [7, 8], hundreds of patients were investigated during the 1960s [9, 10]. Unfortunately, the enthusiastic consensus for gallium-68 imaging faded away during the 1970s, mainly because of the restricted use of first-generation ^{68}Ge/^{68}Ga generators and the parallel development of new emerging radionuclide tracers, such us single-photon emitters technetium-99m/iodine-123 and the positron emitting carbon-11/fluorine-18.

Since the dramatic change that occurred at Brookhaven National Laboratory in the late 1950s for the availability of ^{99}Mo/^{99m} Tc generators, the radiometal technetium-99m opened a new era in Nuclear Medicine as well as in early neuroimaging [11]. The ideal nuclear properties, the easy availability from a generator, and the flexible chemistry facilitated the introduction of this emerging radionuclide that is, at present, the most employed for Nuclear Medicine procedures worldwide. The first agents ^{99m}Tc-pertechnetate and ^{99m}Tc-DTPA (diethylenetriaminopentaacetic acid), as well as other gamma emitters radiotracers thallium-201 and gallium-67 citrate, were evaluated for pathologies with altered BBB due to tumors or traumas [12–14]. However, all these radiotracers had the relevant constraint that they could be employed in neurological disease just for the evaluation of an altered BBB.

In the late 1950s, a few years later from the initial brain tumor scanning, Munck and Lassen pioneered the assessment of cerebral blood flow (CBF) by using inert radioactive gases, thus providing the basis for regional CBF functional imaging. Evaluation in human brains was performed by administrating trace amounts of krypton-85 by inhalation or intravenous injection in saline solution [15, 16]. In the original methodology, blood samples were collected from bilateral jugular veins and counted, reflecting the global blood flow and oxygen use. The further advance was the measurement of the regional cerebral perfusion achieved by placing detectors on the patient's scalp, to determine radiotracer accumulation and clearance on a regional basis, thus opening the way for a more modern concept of CBF scanning using a noninvasive approach [17, 18].

In the 1960s, major improvements occurred using molecular [^{15}O]oxygen for regional oxygen extraction and perfusion assessments, also taking advantage of the increased performances of imaging systems due to the introduction of first-generation Anger cameras [19]. Ter-Pogossian and Brownell evaluated the radiotracer kinetics after a single breath by means of a pair of detectors. However, the first results were not satisfactory because of the difficult interpretation of the collected data [20, 21]. Some years later, radioactivity administration was modified by using continuous [^{15}O]oxygen inhalation, producing a "steady-state" brain distribution dependent on perfusion and oxygen extraction, as well as the physical decay of the radioisotope [22]. Nevertheless, this technique suffered for some important disadvantages such as a constant delivery of the radioactive gas and a long-time scan during which, it is assumed, no change in physiological status occurs. A more practical and suitable method for imaging was then introduced using an intravenous injection of [^{15}O]oxygen water instead of a labeled gas [23], becoming a standard procedure for rCBF assessment with PET. These methods have been used in clinical

settings since the 1980s in several clinical conditions including strokes, brain tumors, and Parkinson's disease [24–26]. Despite the fact that the early evaluations were much more qualitative than quantitative, these methodologies represent a milestone for neuroimaging because of the direct impact on patient healthcare.

An alternative to PET radiopharmaceuticals for the rCBF measurement was developed during the 1980s by the parallel and successfully investigational studies with iodine-123 and technetium-99m. These efforts resulted in the development of perfusion agents able to overpass the normal BBB, such as [^{123}I]iodoantipyrine, [^{123}I]IMP (l-3-[^{123}I]-iodo-α-methyl-tyrosine), [^{99m}Tc]HMPAO ([^{99m}Tc]exametazime), and [^{99m}Tc]ECD ([^{99m}Tc]bicisate). Most of them have reached an established clinical use for the evaluation of various neurological diseases such as dementia, Alzheimer's disease, epilepsy, stroke, and Parkinson's disease [27–30].

A fundamental advance for Nuclear Medicine applications was the application of fluoro-18-deoxyglucose ([^{18}F]FDG) to image cerebral glucose metabolism in 1976, destined to become the most important PET tracer to this day with indications for tumors and for identification of foci of epileptic seizures [31, 32]. [^{18}F]FDG, a glucose analog, is able to delineate the glucose metabolism, which is very active in the normal brain and often hyperreactive in tumors.

The promising results using a radiotracer able to interact with substrates, in addition to the early quantitative imaging applications, confirmed the full potential of this emerging technique in describing molecular processes on human brain in health and disease. A general enthusiasm and great expectation for the future were soon satisfied by a rapid increase in the development of new radioactive molecules, typically including the positron emitters carbon-11 and fluorine-18 and single-photon emitters iodine-123 and technetium-99m. The new generation of radiotracers were designed for displaying affinity for receptors, enzymes, or other biological structures thus defined as radioligands, for interacting with specific metabolic pathways or for reproducing the chemical structures of drugs incorporating a radionuclide with identical characteristics or with minimal modifications or at least retaining the key biochemistry. Among the expanded range of imaging molecules, the first widespread applications included the regional amino acid metabolism using native amino acids or derivatives labeled with carbon-11, like [^{11}C]methionine, leucine, and unnatural amino acids [33–35]. A few years later, fluorine-18 dihydroxyphenylalanine ([^{18}F]FDOPA), a dopamine synthesis pathway analog, and N-[^{11}C]methylspiperone, a radioligand for dopamine/serotonin receptors, were used to assess for the first time the neurotransmission function in humans [36, 37]. The mid- to late 1980s were characterized by a continuous introduction of new radioligands with major advances for the quantification of dopamine receptor subtypes ([^{11}C]raclopride, [^{11}C] Schering-23390), dopamine transporters ([^{11}C] nomifensine), central benzodiazepine receptors ([^{11}C]flumazenil), peripheral benzodiazepine receptors ([^{11}C]PK11195), opioid receptor agonists and antagonists ([^{11}C]carfentanil and [^{11}C] diprenorphine) [38–44], as well as for the enzyme monoamine oxidase type B ([^{11}C]deprenyl) [45]. A new field of research appeared to be very auspicious for more specific and useful clinical applications with PET chemistry imposing a dominate role in neuroimaging.

Radiotracer expansion certainly benefitted from an increased understanding of both physiological and pathological molecular processes, but the great effort of chemists, pharmacists, biologists, physicists, and physicians was key to the progress. The influx of scientists from various fields allowed the discovery and validation of new radiopharmaceuticals to achieve a vast array of targeted radiotracers. This great evolution was also facilitated by the increased availability of supporting technologies and infrastructures such as generators, cyclotrons, SPECT and PET scanners, and chemistry laboratories. In addition, the notable improvements in radiochemistry, mainly in labeling strategies for rapidly labeling molecules with high specific activity starting from the most popular short-life PET radionuclides, have boosted the design of new radiotracers claiming the important role this discipline is playing in this field.

During the 1990s, a progressive investigation focused on the improvement of the existing imaging, as well as in modulating and delineating neurotransmission systems other than dopaminergic and serotoninergic. [^{11}C]WAY-100635, [^{11}C]MDL-100907, and [^{11}C]McNeil-5652 were introduced, respectively, for a more selective evaluation of serotonin receptor subtypes 1a/2a distribution and for the SERT/5-HTT transporters [46–48]. Novel [^{11}C]NNC112, [^{11}C]FBL457, and [^{11}C]-β-CIT displayed high affinities, respectively, for dopamine receptor subtypes 1 and 2/3 and for dopamine transporters [49–51]. Beyond the dopaminergic/serotoninergic systems, new imaging agents were aimed at exploring acetylcholinesterase enzyme ([^{11}C]MP4A and [^{11}C]PMP) and nicotinic receptor reserves (2-[^{18}F]F-A85380), as well as vesicular monoamine transporter type 2 ([^{11}C]DTBZ) and ATP-binding cassette (ABC) transporters like P-glycoprotein ([^{11}C]verapamil) [52–56].

For many years, the development of target-specific agents has been strongly dominated by PET chemistry, given the relatively easy replacement of a carbon, an oxygen or nitrogen with a radioisotope conserving the original chemical structures. However, the major worldwide diffusion of SPECT scanners promoted the investigation for the development of agents containing a suitable single-photon emitter radionuclide. A number of radioiodinated tracers which bind CNS receptors were synthesized and introduced successfully as alternatives to PET tracers in clinical settings. Iodinated derivatives displayed excellent properties for the quantitative evaluation of the muscarinic ([^{123}I]IQNB, [^{123}I]iododexetimide), dopamine ([^{123}I]IBZM and [^{123}I]epidepride), and benzodiazepine ([^{123}I]iomazenil and [^{123}I]NNC-13-8241) receptor reserves and for dopamine/serotonin transporter function ([^{123}I]-β-CIT) [57–63]. Because of the intrinsic difficulties to incorporate a radiometal such as technetium-99m into small molecules, able to pass the normal BBB and conserving the affinity for a specific target, investigational studies were not as consistent as for the main PET tracers in neurology. The synthesis and evaluation of the first [^{99m}Tc]-labeled tropane analogs that display selective dopamine transporter binding were reported in 1996 and 1997 (TRODAT-1 and technepine), and [^{99m}Tc]TRODAT-1 has succeeded in entering evaluation for clinical approval a few years later [64–66].

From 2000 to the present, the range of radiotracers for studying biochemical and pathophysiological molecular mechanisms has been expanding continuously. New targets of interest for neurological applications have been explored, among which are norepinephrine transporters ([^{11}C]methyl reboxetine), neurokinin-1 ([^{18}F]SPA-RQ) and cannabinoid-1 ([^{18}F]MK-9470) receptors and Alzheimer-related proteins (beta-amyloid with [^{11}C]PiB (Pittsburgh compound B) and related fluorine analogs, and more recently tau protein and alpha-synuclein with [^{18}F]THK5105) [67–71]. The concomitant advances in PET technology and the scanner proliferation in industrialized countries corroborated to establish the role of imaging in both research and clinical settings to improve our understanding in diagnoses, monitoring disease progression, and the response to treatment.

Unfortunately, relatively few radiotracers have been translated into the clinical setting, due to high requirements and complex procedures for getting the approval from authorities and, not least, because of the high costs of the required infrastructures. In addition, the utility of carbon-11, incorporated in most of the developed compounds, is limited by its short radioactive half-life, and for this reason, its on-site production and use are essential. On the contrary, fluorine-18 radiotracers may be produced and distributed to local hospitals, making use of this technology more widely accessible. A notable and successful example on the evolution for a specific clinical need, although uncommon, is represented by the radiopharmaceuticals employed in amyloid PET imaging. The first published experimental data using a carbon-11 compound ([^{11}C]PiB) with affinity for amyloid plaques has been followed by the development and commercialization of fluorine-18 analogs ([^{18}F]florbetapir, [^{18}F]florbetaben, and [^{18}F]flutemetamol) in less than 10 years [72].

It is expected that in the future, brain imaging will continue to benefit from new radiotracers and radiopharmaceuticals, although research activities appear to be less optimistic with respect to the initial enthusiastic consensus [73]. However, the lack of appropriate radiotracers for unknown molecular brain mechanisms represents one of the major challenges for radiochemists in supporting Nuclear Medicine imaging to understand physiological processes and diseases and for application to drug development.

4.3 Radiotracer and Radiopharmaceutical Design for the Development of Brain Imaging Agents

From the 1920s, when George Charles de Hevesy coined the term "radiotracer" paving the way for the application in biomedical sciences, many imaging agents have been developed and applied in Nuclear Medicine [74]. Over the years, brain imaging studies have evolved to include single-photon-emitting (SPECT) and positron-emitting (PET) radiopharmaceuticals particularly used in the evaluation of brain tumors, central motor disorders, and cognitive disorders.

Based on their mechanism of action, SPECT and PET brain radiotracers are generally classified in two groups according to their capability to perfuse cerebral tissues or to interact with specific substrates. The first group comprises the substrate nonspecific agents able to cross BBB and trace dynamic processes for high-capacity systems. They represent an important class of radiotracers, which biodistribution correlates with cerebral blood flow or brain tissue permeability; thus, they are also defined as perfusion agents (e.g., [^{99m}Tc]HMPAO and PET [^{15}O]water).

The second group is referred to those radiotracers with specificity for biochemical targets susceptible to changes as function of disease states. These agents are dependent on the densities of the interested molecular targets such as receptors, enzymes, and transporters. Since they are usually present at very low concentrations and are susceptible to saturation, these targets are defined as low-density-easily saturated sites. Lately, a major interest has been devoted to this class of radiotracers, due to their capability of detecting targets at the molecular level.

Despite the relevant results achieved in research during the last decades, the range of radiotracers and radiopharmaceuticals used for brain imaging in clinical settings worldwide appears limited (Table 4.2). In 2013, Molecular Imaging and Contrast Agent Database (MICAD) reported 11 SPECT and almost 100 PET tracers that have been tested at least once in humans, with potential as brain imaging agents [75]. However, a very few of them have reached the clinical state. This is consistent with the general reduced trend of approval of new pharmaceuticals (including radiopharmaceuticals) by the National Regulatory Authorities responsible for human medicines that shows a constant decline in approvals after 2000. Regulatory aspects and clinical development have to be considered the main reasons for such a few introductions, together with the economic aspects. An estimate of time and costs for the clinical development of diagnostic agents has been reported by Nunn and more recently by Zimmermann, who calculated that a radiopharmaceutical has a cost of €20–60 million from the time the lead molecule is identified and takes 7–9 years to develop (Fig. 4.1) [76, 77]. A conventional therapeutic drug has a higher cost, approximately €82–300 million to develop over 10–15 years, but the related market is by far larger than that of imaging agents, thus generating a much higher return on investment [78]. It is therefore evident that the commercialization of diagnostic imaging agents will not generate the same income in a comparable amount of time.

In this scenario, academic investigators play a major role in the design and synthesis of diagnostic imaging agents whose development has to be in line with the emerging needs of the public

Table 4.2 Radiopharmaceuticals approved or registered by federal authorities

Common name	Common names, acronyms, and nomenclature	Process/target
Flow and perfusion		
[^{99m}Tc]ECD	[^{99m}Tc]-Bicisate	Metabolic trapping
[^{99m}Tc]HMPAO	[^{99m}Tc]-Exametazime	Metabolic trapping
[^{15}O]O_2		Oxygen diffusion
[^{15}O]H_2O		Water diffusion
[^{15}O]CO		Red blood cell labeling
[^{81m}Kr]Krypton		Diffusion
[^{133}Xe]Xenon		Diffusion
Tumor metabolism		
[^{18}F]FDG	2-Deoxy-2-fluoro-D-glucose	Glucose metabolism
[^{123}I]IMT	3-Iodo-L-α-methyl tyrosine	Amino acid transport
[^{11}C]Methionine	(S)-2-Amino-4-(methylthio)butanoic acid	Amino acid transport
[^{18}F]FET	Fluoroethyltyrosine	Amino acid transport
[^{11}C]Choline	2-Hydroxy-N,N,N-trimethylethanamonium	Cell membrane metabolism
[^{18}F]Methylcholine	2-Fluorooxyethyl(trimethyl)azanium	Cell membrane metabolism
[^{11}C]Acetate	[1-^{11}C]Acetate	Lipid metabolism
[^{18}F]FLT	3′-Deoxy-3′-fluorothymidine	DNA synthesis
[^{18}F]FMISO	Fluoranyl-3-(2-nitroimidazol-1-yl)propan2-ol	Hypoxia
[^{99m}Tc]MIBI	[^{99m}Tc]-Sestamibi	P-glycoprotein
[^{201}Tl]Thallium chloride		Potassium analog
Dopamine system		
[^{18}F]FDOPA	(2S)-2-amino-3-(2-fluoranyl-4,5-dihydroxyphenyl) propanoic acid	Dopamine synthesis
[^{123}I]FP-CIT (DaTscan)	Ioflupane(123I) 2-Carbomethoxy-8-(3-fluoropropyl)-3-(4-iodophenyl)tropane	Dopamine transporter
[^{123}I]E-IA-F-CIT	Altropane(123I) N-Iodoallyl-2-carbomethoxy-3-(4-fluorophenyl) tropane	Dopamine transporter
[^{99m}Tc] TRODAT-1	2-[2-[[(3S,4R)-3-(4-chlorophenyl)-8-methyl-8-azabicyclo[3.2.1]octan-4-yl]methyl-(2-sulfidoethyl) amino] acetyl]azanidylethanethiolate;oxo- technetium-99	Dopamine transporter
[^{123}I]Beta-CIT(DOPAScan)	Iometopane(123I) 2Beta-carbomethoxy-3beta-(4-iodophenyl)tropane	Dopamine transporter
[^{123}I]Epidepride	N-[[(2S)-1-ethylpyrrolidin-2-yl] methyl]-5-iodo-2,3-dimethoxybenzamide	Dopamine D2/D3 receptor
[^{123}I]ADAM	2-[2-[(Dimethylamino)methyl]phenyl] sulfanyl-5-iodanylaniline	Serotonin transporter
[^{11}C]Raclopride	(S)-3,5-Dichloro-N-((1-ethylpyrrolidin-2-yl) methyl)-2-hydroxy-6-methoxy-(S)-3,5-dichloro-N-((1-ethylpyrrolidin-2-yl) methyl)-2-hydroxy-6-methoxybenzamide	Dopamine D2 receptor
[^{123}I]IBZM	Iolopride(123I) N-[[(2S)-1-Ethylpyrrolidin-2-yl] methyl]-2-hydroxy-3-iodanyl-6-methoxybenzamide	Dopamine D2 receptor

(continued)

Table 4.2 (continued)

Common name	Common names, acronyms, and nomenclature	Process/target
N-[^{11}C]Methylspiperone	8-[4-(4-Fluorophenyl)-4-oxobutyl]-3-methyl-1-phenyl-1,3,8-triazaspiro[4.5] decan-4-one	Dopamine D2/5-HT_2 receptor
Receptor- and enzyme-binding ligands (other than for Dopamine system)		
[^{11}C]PK11195	1-(2-Chlorophenyl)-N-methyl-N-(1-methylpropyl)-3-isoquinolinecarboxamide	Translocator protein (TSPO)
[^{11}C]Flumazenil	4H-Imidazo(1,5-a)(1,4)benzodiazepine-3-carboxylic acid, 8-fluoro-5,6-dihydro-5-methyl-6-oxo-, ethyl ester	GABA receptor
[^{123}I]Iomazenil	Ethyl 7-iodo-5-methyl-6-oxo-4H-imidazo[1,5-a][1,4]benzodiazepine-3-carboxylate	GABA receptor
2-[^{18}F]F-A85380	2-Fluoro-3-[2(S)-2-azetidinylmethoxy]pyridine	nACh receptor
[^{11}C]MP4A	N-[^{11}C]Methylpiperidin-4-yl acetate	AChE activity
Plaque-binding ligands		
[^{11}C]PiB	2-(4′-[^{11}C] Methylaminophenyl)-6-hydroxybenzothiazole	Plaque acceptor
[^{18}F]Florbetapir (Amyvid)	4-{(E)-2-[6-(2-{2-[2-(18F)Fluoroethoxy]ethoxy}ethoxy)-3-pyridinyl]vinyl}-N-methylaniline	Plaque acceptor
[^{18}F]Flutemetamol (Vizamyl)	2-[3-(18F)Fluoro-4-(methylamino)phenyl]-1,3-benzothiazol-6-ol	Plaque acceptor
[^{18}F]Florbetaben (Neuraceq)	4-{(E)-2-[4-(2-{2-[2-(18F)Fluoroethoxy]ethoxy}ethoxy)phenyl]vinyl}-N-methylaniline	Plaque acceptor
Cisternography		
[^{111}In]Indium diethylenetriamine pentaacetic acid injection	Sodium;2-[bis[2-[bis(carboxylatomethyl)amino]ethyl]amino]acetate;indium-111	CSF transport

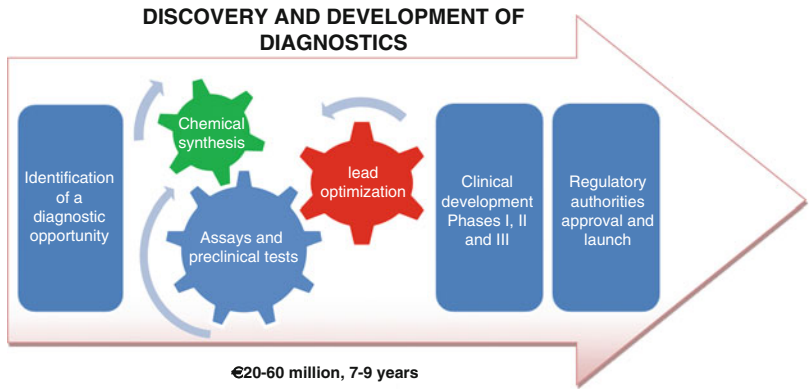

Fig. 4.1 Discovery and development process for a diagnostic (Adapted from FDA's Critical Path Initiative, cost and timeline numbers taken from Nunn and Zimmermann)

health system, but must be also economically sustainable for the diagnostic companies.

It is remarkable that within the few approved SPECT and PET agents in the last decade, most of them are brain imaging radiopharmaceuticals, with a tremendous increase of interest in the development of PET tracers for the diagnosis of neurodegenerative disorders. This shows that the current efforts, both from academia and industry, point toward a more accurate and early diagnoses of CNS pathologies in order to help clinical decisions that improve the effectiveness of medical care.

4.3.1 Radiopharmaceuticals for High-Capacity Systems or for Low-Density-Easily Saturated Sites

The design and the development of a radiopharmaceutical are strictly connected with its application: delineating a pathophysiological process or targeting a specific molecular structure.

The majority of the technetium-99m radiopharmaceuticals currently in use have been designed and developed for high-capacity systems. They are formulated from commercially available "instant kits" and pertechnetate-99m obtained from ^{99}Mo/^{99m}Tc generators. Each kit typically contains the ligand, the radionuclide has to be complexed, and an adequate quantity of reducing agent buffers to adjust the pH and to suit the labeling conditions, stabilizing agents and excipients. The radiotracer is thus obtained from the reaction between the ligands and the radionuclide in an appropriate oxidation state, resulting in a new stable coordinated system. The integral chemical structure for each complex, composed by the radionuclide core and ligands, is responsible for pharmacokinetic and pharmacodynamic properties. [^{99m}Tc]HMPAO and [^{99m}Tc]ECD are examples of kit-formulated radiopharmaceuticals for brain imaging routinely prepared in Nuclear Medicine worldwide [29, 30]. However, the amount of ligands contained in an "instant kit" is by far greater than that of technetium-99m, and it would saturate many low-capacity targets. This is the reason why these radiopharmaceuticals are primarily used for the imaging of high-capacity systems, such as regional cerebral blood flow, where saturation cannot be achieved. [^{99m}Tc]-kit-based radiopharmaceuticals are covering over 80 % of all Nuclear Medicine diagnostic procedures worldwide, with a noteworthy contribution to neuroimaging studies, although receptors and other molecular structures are subjects of major interest in brain imaging research at present.

Radiolabeled agents with high specificity for low-density-easily saturated sites are usually modeled on partial agonists and antagonists in the CNS therapeutic drug repertoire and lead compounds in the field of pharmaceutical research. Once the chemical structure of a potential new radiotracer has been identified for a specific biological target, the next step is to synthesize the desired compound by coupling an emitting nuclide suitable for imaging.

Many radiolabeled compounds with selectivity for receptors, enzymes, and transporters both for SPECT and PET brain imaging have been developed over more than 40 years of research. Among these, radiotracers based on positron emitters provide much useful information on neurophysiology and neuropharmacology of cholinergic, serotonergic, dopaminergic, GABA/benzodiazepine, opioid, and other neurotransmission systems [73]. Furthermore, PET methodology offers several advantages over SPECT, such as a higher sensitivity, better temporal and spatial resolution, shorter imaging protocols, and a lower patient dosimetry [79]. On the other hand, PET needs cyclotron and radiopharmacy facilities, which are expensive and require highly skilled personnel to operate.

SPECT radiotracers for low-density-easily saturated sites have a long history of radiochemistry research due to the relatively easy labeling with iodine-123 and the large availability of technetium-99m. A number of single-photon-emitting radiotracers for brain imaging have reached the clinical state and are commercially available in many countries. SPECT methodology is by far largely widespread compared with PET; therefore, it still plays a fundamental role allowing access to neuroimaging examinations in many conventional Nuclear Medicine centers worldwide. Recent technological improvements have reduced the gap between SPECT and PET [80], thus promoting the research and development of new single-photon-emitting radiotracers to satisfy the clinical need in Nuclear Medicine which are not supported by a PET cyclotron facility.

4.3.2 Challenges in Brain Imaging Radiotracer Development

The development of new diagnostic agents for brain imaging follows two main initial steps:

first the identification of the biological process indicative of the pathology to be investigated and second the identification of the molecular target best representing the process. This target will virtually represent the chemist's workbench for the design of the probe chemical structure.

During the pregenomic era, radiotracer design was based on in vitro assays, in vivo biodistribution studies, and autopsy data. This approach has been successful for a number of SPECT and PET agents with specificity for targets at molecular level, including most of the commonly applied radiopharmaceuticals (metabolic and receptor-binding tracers), but it does not represent the ideal approach for the design of early diagnostic agents [81].

However, considerable advances in molecular cell biology and the sequencing of the human genome opened the way for the postgenomic era with the advent of the new millennium. Ever since, new potential drug targets, as well as biomarkers, have become available from the genomics, proteomics, and single nucleotide polymorphisms (SNPs) findings [82]. Molecular imaging, as other fields in medicine, has gained benefit from the identification of new targets. This, together with the concomitant extended repertoire of tools and technologies, promoted the design of novel imaging probes for the application in Nuclear Medicine moving toward "precision medicine." In the future, the personalized imaging probes are expected to guide the treatment for patients (especially targeted treatments) and to significantly improve healthcare delivery and reduce its costs.

In this scenario, radiochemistry has maintained its crucial role, and the design and synthesis of novel radiotracers, which may become radiopharmaceuticals in clinical settings, are still considered one of the major challenges for radiopharmaceutical chemists.

The development of brain imaging radiotracers is not easy to carry out, especially if compared to other diagnostic agents, due to the extraordinary complexity of cerebral anatomy and biochemical functions [83, 84]. Radiotracer's pipeline has a typical bottleneck shape, where only a few of the numerous candidates synthesized will show suitable in vivo properties and eventually become radiotracers and then radiopharmaceuticals. When designing SPECT and PET radiotracers, the following key factors must be taken into account:

- Choice of the target indicative or representative of the pathology under investigation with consideration of an unmet need in the diagnosis of this pathology
- Identification of the lead compound/structure with specificity for the target
- Selection of the radionuclide
- Labeling strategy to synthesize the desired chemical structure

In addition, in order to allow the radioactivity to distribute within the brain and to quantify it with imaging techniques, radiotracers should ideally exhibit:

- Rapid and quantitative permeation through the blood–brain barrier (BBB)
- High affinity and selectivity for the target
- In vivo stability and absence of radioactive metabolites
- Favorable pharmacokinetic and pharmacodynamic properties in relation to radionuclide half-life

Other factors should also be considered in respect to the pharmaceutical requirements for human use, imposed by Drug Regulatory Authorities. Current radiopharmaceutical development shares much with standard drug discovery and development practices, and although diagnostic radiopharmaceuticals are generally administered only a few times in a patient's lifetime and the adverse reactions are extremely rare, the safety profile of a new radiotracer has to be demonstrated and validated. This assessment includes the evaluation of pharmacological and toxicological activity of the diagnostic preparation (including any component other than the labeled tracer) and the estimation of the absorbed radiation dose to prove a favorable risk-to-benefit ratio.

Last but not least, researchers should also keep in mind that, to be successful, radiopharmaceutical development should satisfy a specific clinical need with direct impact on patient disease treatment [85]. Although effectiveness of a radiotracer is required by regulatory authorities in order to get approval, a clear diagnosis of a pathologic status is most of the times difficult to achieve with brain imaging agents. An example is depicted by the recently introduced PET radiopharmaceuticals for quantitative imaging of beta-amyloid plaques [86]. Due to the occurrence of beta-amyloid deposition in normal elderly people and in clinical syndromes other than Alzheimer's disease (AD), amyloid quantification is an ambiguous indicator, even though plaques are one of the defining pathologic features of AD. Clinical trial studies have been designed to validate PET amyloid technology and to understand disease mechanisms, rather than to find new applications in clinical practice for an effective and early AD diagnoses. Therefore, the use of amyloid PET to clinically improve AD outcomes and to help medical decision-making has been long debated [87].

Recent efforts of researchers are aimed at identifying single targets that could be used for revealing and monitoring the progression of diseases. The discovery of new biomarkers for the accurate identification of a pathologic status will certainly assist radiochemists in their efforts to design and develop novel radiolabeled agents.

Since an ideal model of radiotracer development does not exist, we will now illustrate the main concepts for radiotracer design and development and their use for brain imaging, based on the research experience and some examples of successful applications in clinic settings.

4.3.3 True Radiotracers, Isotopic Radiotracers, and Analog Radiotracers

Labeling a desired biomolecule is not always an easy task. Since CNS molecules are always small in size (<500 Da) to cross the normal BBB, labeling may have a detrimental effect on the in vivo properties of the biomolecule and, eventually, on the final quality of the diagnostic image. Therefore, in the design of a new brain imaging radiotracer, particular attention has to be paid to the labeling strategy to obtain the desired molecular structure.

The process of coupling the radionuclide to the biomolecule can be achieved via the formation of covalent bonds for nonmetallic radioisotopes (such as carbon, nitrogen, oxygen, and the halogens) and dative bonds for metallic radionuclides (as technetium-99m or Indium-111).

The replacement of endogenous elements, such as carbon-12, oxygen-16, or nitrogen-15 with a radioisotope, is an appealing solution to avoid molecular perturbation due to the insertion of a radionuclide. Labeled compounds synthesized via isotopic substitution of organic molecules are defined as "true tracers," and their biochemical properties, including pharmacokinetics and pharmacodynamic properties, do not differ from those of the original biomolecule. [^{11}C]methionine, [^{11}C]acetate, and L-β-[^{11}C] DOPA are examples of true tracers (Fig. 4.2). The most important peculiarity of true radiotracers is their ability to study the components of a physiologic or pathologic process without disturbing the homeostatic system.

Isotopic substitution is also a convenient labeling approach for exogenous molecules with known pharmacologic activity, such as CNS drugs. In addition to the replacement of naturally occurring elements, other isotopes can be considered, for example, halogens. Fluorine-19 is not typically contained in endogenous molecules, but it is a common constituent of many pharmaceuticals, due to its contribution to improve drug bioavailability. Replacement with fluorine-18 can generate an "isotope tracer" identical to the chosen lead compound, which shares the same in vivo behavior without showing any pharmacological effect. The chemical structure of flumazenil, for example, allows the preparation of two isotope tracers: the carbon substituted [^{11}C]flumazenil ([^{11}C]FMZ) and the fluorine substituted [^{18}F]flumazenil ([^{18}F]FFMZ) (Fig. 4.2). They are both isotopic tracers of flumazenil with similar kinetic and binding behaviors, but with different

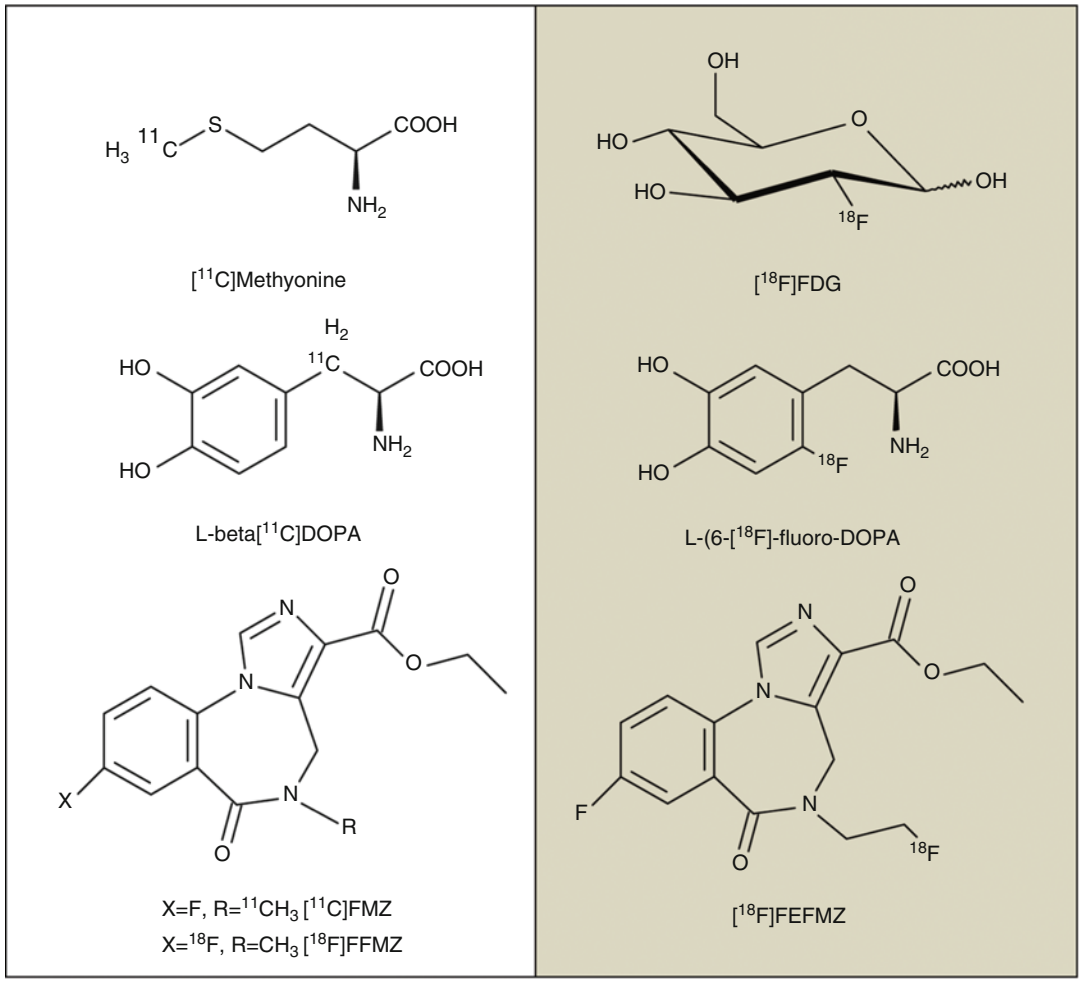

Fig. 4.2 Chemical structures for selected true tracers (and isotopic tracers) on the *left* and analog tracers on the *right*

radionuclide half-lives and perhaps different radioactive metabolites [88].

If the chosen radionuclide for radiolabeling does not have a stable isotope in its structure or it is not chemically convenient to replace, isotopic substitution is not an adequate strategy. This situation is extremely common, and to overcome this problem, labeling may be achieved by a chemical modification of the tracer structure, generating a derivative known as an "analog tracer." In order to assure a minimal molecular perturbation, substitution with a radiochemical scaffold of similar steric or electronic characteristics to the original molecule should be preferred. However, due to the labeling, the final radioactive molecule will be different from the native compound, and its binding affinity and selectivity for the target, as well as pharmacokinetic and pharmacodynamic properties, need to be tested for confirming its potential use as an imaging agent. For example, while L-β[^{11}C]DOPA is a true tracer for L-DOPA, [^{18}F]FDOPA L-(6-[^{18}F]-fluoro-DOPA) is an analog [^{18}F]-tracer, which differs for an additional fluorine in position 6 of the aromatic ring (Fig. 4.2). They are both used as biochemical probes to assess the rate of endogenous dopamine synthesis, although they have a different metabolism [89].

The biological behavior of an analog tracer is difficult to predict. However, considering the general small dimension of the interested

molecules, a modification in the chemical structure is often followed by an alteration of binding affinity and/or pharmacokinetic properties. A relevant number of studies demonstrating the variable influence of chemical modifications, due to labeling with different strategies, are reported in literature for many PET and SPECT radiotracers. Many analog tracers are produced by incorporating [^{18}F]alkyl scaffold of different lengths on N-, O-, or S-functions of the parent molecules. While N-[^{18}F]fluoroethyl flumazenil ([^{18}F]FEFMZ) maintained the specific binding to the benzodiazepine receptor, an N-[^{18}F]fluoropropyl derivative lost completely this affinity [90]. On the contrary, among the [^{18}F]-labeled spiperone analogs N-(2-[^{18}F]-fluoropropyl)-spiperone, the longer N-alkylated derivative showed improved binding and kinetic properties in comparison with N-(2-[^{18}F]-fluoroethyl)-spiperone [91].

In some special cases, analog tracers are desirable because they exhibit superior characteristics as imaging agents in comparison with true tracers, due to their in vivo behavior. A prominent example is depicted by [^{18}F]FDG, the most important analog tracer used for the assessment of glucose metabolism (Fig. 4.2). Once [^{18}F]FDG and glucose entered in the cell, they can either be transported back to the plasma or, as first metabolic step, they can equally be phosphorylated by hexokinase. In contrast, glucose continues along the glycolytic pathway for energy production while [^{18}F]FDG cannot enter glycolysis and becomes effectively trapped as FDG-6-phosphate, thus reaching a steady state. Therefore, [^{18}F]FDG is susceptible to metabolic trapping thus facilitating a PET study, while a glucose true tracer with carbon-11 or oxygen-15 produces many different radioactive metabolites, resulting in the need of image correction with mathematical models.

4.3.4 Common Radionuclides for Brain Imaging and Related Labeling Strategies

4.3.4.1 Carbon-11

Carbon-11, a positron emitter, is considered to be the preferable radionuclide for true tracer design, given the abundance of carbons in endogenous and exogenous molecules and the virtual versatility of organic chemistry labeling reactions. On the other hand, its fast decay (20.4 min) represents a major constraint in the clinical practice and imposes several requirements in the preparation and use of [^{11}C]-labeled compounds such as the presence of an in-house cyclotron and the development of a rapid procedure of radiolabeling, purification, and quality controls. As a rule of thumb, in order to be sustainable for clinical use, the production and release of [^{11}C]-radiotracers should be carried out within three half-lives of the radionuclide. This will afford manipulating enough radioactivity to allow the injection, distribution of the radionuclide, and the patient scanning according to the imaging protocol.

[^{11}C]-PET tracer production is currently based on the conversion of the irradiated in-target product [^{11}C]carbon dioxide or methane ([^{11}C]CO_2 or [^{11}C]CH_4) to a secondary reactive precursor (or synthon) that ensures labeling of suitable substrates in few minutes and with high yields. [^{11}C]methyl iodide and [^{11}C]methyl triflate are the most prominent examples of synthons for nucleophilic [^{11}C]methylation of primary and secondary alcohols, amines, and thiols, commonly applied for the production of many [^{11}C]radiotracers and radiopharmaceuticals, such as [^{11}C]methionine, [^{11}C]choline, [^{11}C]PIB, [^{11}C]raclopride, N-[^{11}C]methylspiperone, [^{11}C]carfentanil, and [^{11}C]McN-5652 [92]. When simple methylation is no longer a viable approach, the radionuclide has to be incorporated into the molecule with a different labeling strategy. [^{11}C]C-C bond formation is often required, especially for labeling molecules with functional groups such as carboxylic acids, ketones, amides, and imides. A common procedure is based on the direct reaction of target-prepared [^{11}C]CO_2 with a Grignard reagent to produce an intermediate, which can be hydrolyzed to give [carbonyl-^{11}C]carboxylic acids or converted to [carbonyl-^{11}C]amides [93]. In recent approaches, [^{11}C] carbonylation is also achieved through transition-metal-mediated reactions using [^{11}C]

methyl iodide, [^{11}C]cyanide, or [^{11}C]carbon monoxide, as secondary precursors. Several palladium-mediated cross-coupling reactions have been shown to be effective and very innovative approaches for preparing many [^{11}C] tracers. However, despite the availability of a large variety of synthetic strategies for [^{11}C]-radiotracers and radiopharmaceuticals, the majority of their production scale for clinical routine is limited to a few of the reactions described above [92, 93].

4.3.4.2 Fluorine-18

Another positron emitter widely used for the preparation of brain imaging agents is fluorine-18, the most important radionuclide for PET imaging. As mentioned above, fluorine is not typically present in endogenous molecules, in contrast to carbon and the most common heteroatoms. Its exceptional employment for in vivo imaging is primarily due to the minimal perturbation caused by its incorporation (similar to a hydroxyl substituent) into the final molecule, combined with advantageous physical half-life of 109.7 min, which permits multistep syntheses as well as a major flexibility in postproduction procedures. Furthermore, differently from carbon-11, it allows the distribution of [^{18}F]-labeled compounds within a few hours drive from the production site, thus attracting commercial interest.

[^{18}F]-fluorination strategies cover an important role in radiochemistry, and they are often used for the translation of [^{11}C]-radiotracers to [^{18}F]-analogs to overcome the main constraints in the manipulation of carbon-11 compounds. However, the approaches for incorporating a fluorine-18 in a molecule remain much more limited than those of carbon-11, due to the chemical nature of this element. The main synthetic strategies behind [^{18}F]-labeling can be classified into "direct fluorination," a one-step reaction, and "indirect fluorination," which requires a multistep synthetic procedure. The direct introduction of [^{18}F]fluorine into a molecule is often accomplished through a nucleophilic substitution reaction using no-carrier-added in-target-produced [^{18}F]fluoride, an enhancer for [^{18}F]nucleophilicity (Kryptofix-222) and a precursor with a good leaving group (triflate, mesylate, tosylate). After labeling, the crude reaction mixtures have to be purified by semipreparative HPLC or solid-phase extraction (SPE) techniques, to provide pure radiopharmaceuticals as sterile, pyrogen-free isotonic solutions suitable for intravenous injection. This simple method has the advantage to be easily adapted to many commercially available automated synthesizers, and due to the large availability of suitable precursors, it is routinely used to efficiently produce some of the most important [^{18}F]-radiotracers (some examples are [^{18}F]FDG, [^{18}F]FLT, [^{18}F]fallypride, and [^{18}F] FAZA). In addition, nucleophilic substitution may also be applied for the insertion of fluorine-18 into aromatic systems, such as for [^{18}F]flumazenil or [^{18}F]FDOPA, with high specific activity [94, 95].

Electrophilic fluorination using [^{18}F]F_2, produced by cyclotron irradiation, is an alternative direct strategy that was successfully developed in the early years of PET radiochemistry. Few clinical radiopharmaceuticals still rely on regioselective aromatic electrophilic [^{18}F]fluorination synthesis, for example [^{18}F]FDOPA [96]. Nevertheless, the general use of this labeling method is hampered by the low specific activity of the final [^{18}F]labeled compounds and a complicated high-pressure gas target, imposing a severe limitation for the development of targeted brain imaging agents.

When direct substitutions are not accessible, a common alternative is the "indirect [^{18}F]labeling via prosthetic groups." This process consists in the synthesis of a secondary small labeled precursor, typically a [^{18}F]fluoro-alkylating agent, which can be easily introduced into the molecule of interest. Prosthetic groups are versatile and they can react with the amine, amide, carboxylic, and phenolic groups of the "cold" precursors to obtain the [^{18}F]fluoro-alkylated radiotracers [97]. Among the most popular alkylating agents, [^{18}F]fluoro-methyl/ethyl/propyl bromine and tosylate have been used for the production of radiopharmaceuticals, such as [^{18}F]fluoromethyl and ethyl choline, [^{18}F]FET, and [^{18}F]FP-CIT [98, 99].

4.3.4.3 Iodine-123

Iodine-123 represents the main alternative to PET emitters for the design of target-specific radiotracers, thanks to its low energetic gamma emission and a half-life of 13.2 h suitable for SPECT imaging. Due to its easy and well-established chemistry, which allows its incorporation into a wide variety of molecules, iodine-123 holds a major interest in the development of radiotracers for nearly three decades. Furthermore, the advantageous half-life and the very high purity of iodine-123 starting radioactive material (which lead to high specific activity radiotracers) allow industrial production and delivery for hospital use over long distances although the highest radionuclidic purity I-123 requires a high-energy cyclotron.

Numerous small molecules have been studied as probes for brain receptors and enzymes, and iodine-123 has become the SPECT radionuclide of choice for development of conventional radiopharmaceuticals for brain imaging. However, iodine has a considerable dimension if compared with PET radionuclides (steric hindrance is similar to a methyl group), and therefore radiolabeling, depending on where iodine is incorporated, could deeply modify the kinetic and target affinity of the molecule. For instance, [^{123}I]-β-CIT, tropane-labeled derivative with relevant use in clinical setting, suffers serious drawbacks. It shows a low target selectivity, binding equally to both dopamine and serotonin transporters (DAT and SERT), and it has a slow kinetics which impose the operators to perform the imaging sessions within 24 h after bolus injection. [^{123}I]IPT and [^{123}I]PE2I have chemical structures similar to [^{123}I]-β-CIT, but they show much faster kinetics and improved selectivity for DAT versus SERT [100–102] (Fig. 4.3).

Radioiodination is the process that introduces a radioactive iodine into a chemical structure. Due to its relatively long half-life, the timing of the labeling reaction is only a minor limitation, and the production strategy focuses mainly on the one-step preparation and purification with high yield. Direct labeling is by far the most common method, based on the radionuclide insertion in an aromatic ring or vinylic groups using N-chloroamides. These reagents generate iodine cations from sodium iodide, which promptly react with activated groups through electrophilic substitution of good leaving groups. Radioiodination by demetallation, a commonly applied procedure, allows a regioselective labeling in almost a quantitative yield, preventing the formation of iodine side products that may be difficult to remove [103]. Some examples of the most important iodine-123 radiopharmaceutical for brain imaging are [^{123}I]-FP-CIT, [^{123}I]-β-CIT, [^{123}I]iomazenil, [^{123}I]IBZM, and [^{123}I]epidepride.

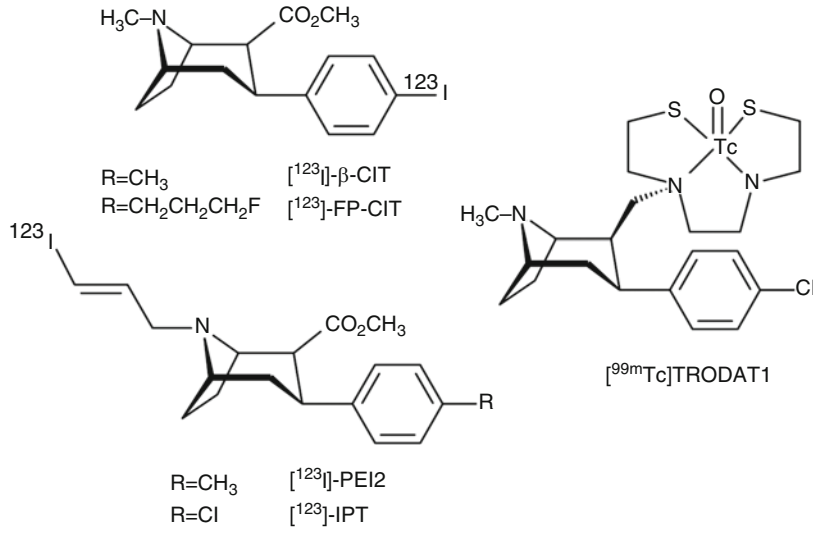

Fig. 4.3 Chemical structures for SPECT tropane derivatives [^{123}I]-β-CIT, [^{123}I]-FP-CIT, [^{123}I]-IPT, [^{123}I]-PE2I, and TRODAT1

Unfortunately, the production costs, especially those related to iodine-123 precursor, are still relatively high in comparison with other radionuclides, thus limiting the future interest for the development of new iodine-based radiotracer.

4.3.4.4 Technetium-99m

As an alternative to carbon-11, fluorine-18, and iodine-123, technetium-99m could be more widely used for the preparation of SPECT neuroimaging agents due to its relative low cost and easy availability. Different from the former radionuclides where a covalent attachment is required for radiolabeling, technetium-99m has to be incorporated through a chelation because of its metal nature. In the traditional labeling method, called the "pendant approach," the radiometal is stabilized through an external chelating system, covalently bonded to the bioactive molecule. Several CNS technetium imaging agents have been labeled using the pendant approach, which unfortunately often produces molecules suffering from metal core hindrance on receptor interaction and an overall excessive dimension which does not facilitate BBB crossing. This resulted in the development of very few technetium-99m radiotracers with suitable imaging properties and in only one agent, [^{99m}Tc]TRODAT-1, currently approved and used in clinical settings in Taiwan (Fig. 4.3) [64, 65, 104, 105].

To overcome constraints due to the presence of a voluminous external complex, technetium-99m "core" may be ideally incorporated within the chemical structure of the radiotracer. This strategy is defined as an "integrated approach," and the resulting molecule/chelated system has to both stabilize the radiometal and demonstrate affinity for the target. However, the insertion of such a foreign element causes dramatic modifications in the chemical properties of small molecules. This, together with the existent severe restrictions for the design of a brain imaging radiotracer, still represents an outstanding challenge for radiochemists and successful examples are rare. Researchers have been working for a long time on the development of new technetium-99m-based radiotracers, with major focus coordination chemistry (technetium can exist in different oxidation states) and labeling strategies, which play a major role for improving the critical issue of brain uptake. Many efforts have been made with the inert, compact, and versatile *fac*-[^{99m}Tc]tricarbonyl core after the year 2000 [106]. The interest for this new labeling approach was promoted by the development of a single vial freeze-dried kit for the preparation of [^{99m}Tc$(OH_2)_3(CO)_3]^+$, suitable for routine procedures in conventional Nuclear Medicine [107]. Despite the fact that penetration of the normal BBB remains a challenge for most of [^{99m}Tc]tricarbonyl radiotracers, not so much because of log P but due to molecular size, a few recent examples provided encouraging evidence that development of a promising brain imaging agent may be feasible [108, 109].

Certainly, to reduce the costs of brain receptor imaging, it would be desirable to have more technetium-based pharmaceuticals, rather than PET or iodine radiotracers. This, as mentioned above, would further allow a vast worldwide access to these brain diagnostic techniques, especially in developing countries where access to cyclotrons is still limited.

4.3.4.5 The Physical Half Life of a Radionuclide and the Biological Half Life of a Radiotracer

The half-life of the radionuclide in a radiotracer should correlate with the kinetic of the process to investigate. In other words, the radiotracer, after injection, should cross the BBB and interact quantitatively with the target, in a time frame that has to be consistent with the radionuclide half-life. Iodine-123 and technetium-99m allow extended imaging protocols due to their relatively long half-lives, and thus they may be employed to investigate slow kinetic processes. On the other hand, positron emitters with short half-lives, such as carbon-11 and fluorine-18, impose faster kinetics in order to gain maximum target uptake before a substantial radioactive decay occurs. Very short-lived nuclides, such as oxygen-15, are appropriate for preparing simple molecules with rapid kinetic to be used as perfusion agents as [^{15}O]water, [^{15}O]O_2, or [^{15}O]CO. An

optimized correlation between the half-life of a radionuclide and the process to investigate is also important in order to avoid unnecessary radiation burden to patients when long-lived radionuclide is used.

All these considerations are based on the assumption that a radiotracer is stable enough to reach the target intact. However, most radiotracers are significantly metabolized in vivo, and the assessment of the radiotracer metabolism, as well as the fate of its metabolites, is crucial for designing a successful application for diagnostic purposes.

Immediately after administration, radiotracers are susceptible to BBB selection and processing by an array of enzymes in the blood and other tissues. This may dramatically decrease the amount of labeled molecules and have a substantial impact on radiotracer distribution and target-to-nontarget ratio. The rate of metabolism determines the duration and efficacy of a radiotracer, also known as the biological half-life. It is key to note that external imaging detects the emitted photons, but contains no information on the chemical structure.

The ability of a molecule to cross the BBB depends on the balance between its passive transfer and its exit due to efflux pumps, such as P-glycoprotein (P-gp) and multidrug resistance-associated proteins [110, 111]. It is generally assumed that passive entry is facilitated for molecules with low weight (<500 Da) and moderate lipophilicity (typically measured octanol/water partition coefficient-logP) [112]. Hydrophilic or charged compounds are excluded by BBB, with some important exceptions for nutrients, such as choline or amino acids that can pass through active transporters. On the other hand, an excessive lipophilicity determines an increased binding to plasma proteins and nonspecific interaction with brain fats and proteins.

If an adequate brain entry is a key aspect for SPECT and PET radiotracers, in vivo stability is also crucial and it has to be also accurately evaluated. Drug metabolism, also known as xenobiotic metabolism, involves the biochemical modification of substances such as pharmaceuticals or radiotracers. Hydroxylation, N-demethylation, and oxidation are some of the most common enzyme-mediated reactions that may occur in vivo producing less lipophilic radioactive metabolites, which should then be excreted. The nature and degree for the metabolism of a radiolabeled compound are dependent upon its molecular structure, and especially for low-density-easily saturated sites, it can have a significant influence on the radioactive distribution and, eventually, on the reliability of the image scanning. In fact, tomographic systems detect the radionuclide signal regardless of its origin from the intact radiotracer, from a radiolabeled metabolic fragment or from the free radionuclide. This may result in a misleading acquired image due to the presence of several radioactive molecules. Since some of them are correlated to the parent chemical structure and compete for target occupancy, a biomathematical analysis is required for the quantization of regional brain radioactivity uptake [113].

Other common metabolic pathways for radiotracers involve the removal of [^{11}C]methyl or [^{18}F]fluoroethyl substituents from radiotracers or, in case of halogenated radiotracers, direct defluorination or deiodination [114]. Radiodefluorination is a relevant issue for [^{18}F]-radiotracers leading to the release of [^{18}F]fluoride in vivo, which is then accumulated in bone tissue. In particular for brain imaging, an undesired accumulation may produce PET images where tissue uptake near the skull is more difficult to interpret [115].

Radiotracer metabolism is not easy to predict, and although it remains an undesired effect, it does not always alter the final quality of the image. If radiotracer processing occurs outside of the CNS, all the resulting radioactive hydrophilic metabolites will be excluded by the BBB. [^{11}C] methyl-radiotracers, for example, are susceptible to demethylation leading to small polar radiometabolites (e.g., [^{11}C]formaldehyde) that don't interfere with brain uptake.

These considerations suggest that an effective molecular design has to take into account in order to prevent the formation of potential radioactive derivatives that may have negative consequences [114–116] for brain imaging. Several examples are reported in literature, where the chosen point of insertion of a radionuclide in the molecule

chemical structure will elicit radiotracer degradation to fragments that don't interact with the desired target or with lower permeability for BBB [117]. In the preparation of [^{11}C]volinanserin, a radiotracer with affinity for 5HT$_{2A}$ receptors, carbon-11 can be incorporated by methylation at the hydroxyl groups in positions 2 or 3 of the aromatic ring [118]. Both radiolabeled molecules are susceptible of enzymatic demethylation at position 3, but while the first results in the formation of lipophilic radioactive derivative that are able to cross the BBB and compete for target occupancy, the second is prone to produce a hydrophilic metabolite that is excluded from the brain (Fig. 4.4) [119, 120]. Labeling on position 3 is, in this case, the preferred choice.

The importance of inserting a radioisotope in different chemical groups and its influence on the radioactivity distribution in the brain have been also cleverly demonstrated with the 5-HT$_{1A}$ radioligand [^{11}C]WAY-100635 [121]. In this example, chemical structure enables carbon-11 insertion either in a methoxy group or in a carbonyl position (Fig. 4.4). Carbon-11 was first introduced through methylation, but since primary metabolic pathway in humans occurs through hydrolysis of the amide bond, [^{11}C]WAY-100635 metabolism resulted in the formation of an active metabolite with affinity for 5-HT$_{1A}$ binding and for α1-adrenergic receptors in the brain. In this case, metabolites were interfering with PET measurements. Only subsequently labeling position was modified into a carbonyl motif, thus avoiding [^{11}C]WAY-100635-labeled metabolites entering the brain and providing improved high PET signal and advantages in biomathematical modeling [122, 123].

A different approach for reducing the presence of radioactive metabolites is represented by the use of inhibitors for the enzyme responsible for the radiotracer major metabolic pathway. Carbidopa, for instance, a known inhibitor of aromatic amino acid decarboxylase, is clinically used for increasing total and specific brain tomographic activity per unit dose of [^{18}F]FDOPA [124]. Other inhibitors have been recently successfully tested although, due to the complexity of their metabolic pathways, the molecular design of a radiotracer remains the main measure for limiting the undesired metabolism [125, 126].

4.3.4.6 Specific Activity

Specific activity (SA) is one of the most important parameters (especially for radiotracers for low-density sites) to assess during radiotracer and radiopharmaceutical development, and it is

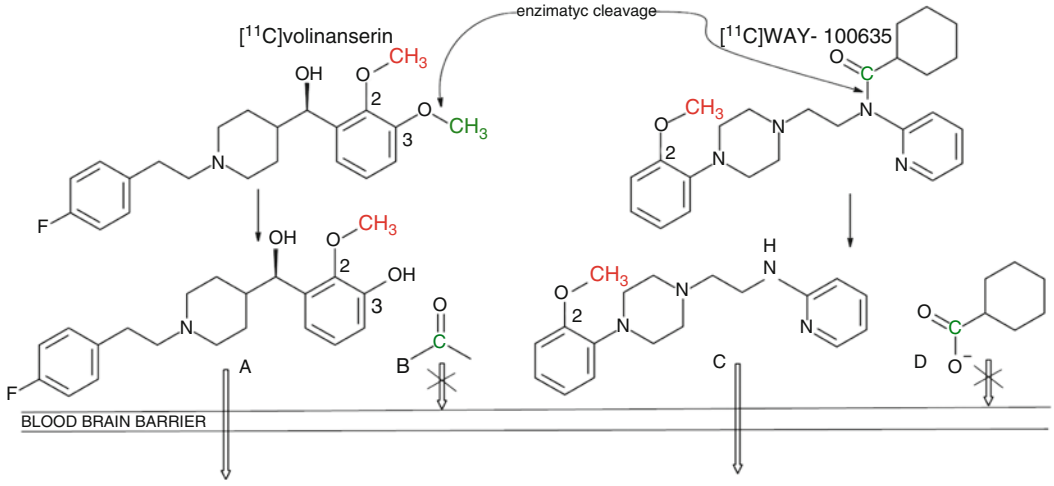

Fig. 4.4 [^{11}C]Volinanserin and [^{11}C]WAY-110635: choice of position of radiolabel as function of metabolism. Labeling with carbon-11 in red position produces for both tracers radiometabolites that interfere with the brain and specific receptor uptake (**a** and **c**). Labeling in green position produces "cold" metabolites that enter the brain, while radiometabolites are excluded by BBB (**b** and **d**)

defined as the amount of radioactivity per unit mass of a radiolabeled compound. This mass includes the mass of the radioactive product and the mass of its nonradioactive counterpart, determined typically by spectroscopic or electrochemical methods. SA is measured in Ci/μmol or GBq/μmol units, and for short-lived radionuclides, the time that the measurement of SA is key.

SA of a diagnostic agent must be congruent with the "radiotracer principle," where the overall mass of the administered tracer should be able to trace a process without inducing an unwanted biological response. This means that, for imaging studies, the amount of radioactivity to be administered has to be sufficiently high to allow the acquisition of good-quality images and low enough to prevent detector saturation and an excessive patient radiation exposure. At the same time, the radiopharmaceutical preparation, including all components, has to present a safe profile with low toxicity.

Every radioisotope or radioactive molecule is characterized by a specific SA; however, its evaluation may not be critical for all application with radiotracers. This is the case for true tracers (such as [^{11}C]acetate and [^{11}C]methionine) since the nonradioactive endogenous compounds are normally found in μM or higher concentrations in the organism and for high-capacity system radiotracers, such as agents for measuring regional cerebral blood flow, hypoxia, and glucose metabolism (e.g., [^{15}O]water or [^{18}F]FDG). In fact, due to the large capacity of these biological systems, radioactivity distribution is not significantly affected by the presence of relatively high concentration of "cold" molecules with identical or similar kinetic properties; thus, the acquired images may correctly represent organ functionalities or metabolic activities.

On the contrary, SA becomes crucial when the radioactive and nonradioactive molecules contained in the radiotracer batch may produce undesired pharmacodynamics–toxicological effects as well as target occupancy or saturation. Specific imaging applications, such as the study of toxic molecules behavior or the visualization of low-density receptors and enzymes in the brain, have to pay particular attention to SA. The required SA for a given radiotracer depends on the concentration of the interested low-capacity easily saturated sites, especially for receptors, which are typically in the range of 0.1–50 nM.

This has been recently demonstrated for [^{11}C] raclopride in an animal model study, where in case of a low specific activity radiotracer, significant receptor occupancy occurred by unlabeled dopamine, thus altering dramatically the target uptake [127].

Several factors may have a substantial impact on the final radiotracer SA. Ideally, the radionuclide employed for radiotracer development should be carrier-free, which means that it does not have to be contaminated by either stable radionuclides or other isotopes of the same element. Technetium-99m and iodine-123 closely match this property [128]. Furthermore, labeling should be carried out with a minimal amount of cold precursor, thus reducing the possibility of competition for target binding. Unfortunately, many fast reaction and high-labeling yields are achieved using a large excess of reagents; thus, the final preparation may contain biologically active impurities, such as residual precursor or side products from the labeling reaction, which were not removed by purification.

SA parameter is considered to be critical for many PET radiotracers. Although theoretical SA values for the most common used positron emitters are very high (340 TBq/μmol for carbon-11, 63 TBq/μmol for fluorine-18), these experimental values are usually very far from those obtained after radiotracer synthesis. The required SA for radiotracers that have to interact with receptors are generally in the range of 37–370 GBq/μmole, while lower SA may be adequate for enzyme-mediated molecular imaging studies. This decrease in SA is generally due to a dilution process with nonradioactive isotope, usually occurring in the radionuclide manipulation for the radiotracer preparation (from radionuclide production to labeling reaction). In fact, final specific activities of [^{18}F]- and [^{11}C]labeled radiotracers are extremely dependent on the production methods as well as the technologies, reagents, equipment, and procedures employed. Minimal alterations of experimental conditions can lead to

considerable effects on SA, especially when high values are required. For this reason, the same radiotracer may be produced with different values of SA depending on the production sites, and this produces the unpleasant consequence having different image quality from one PET center to another.

Therefore, considering the increasing expansion of PET radiopharmaceuticals and the influence of SA for neuroimaging studies, the establishment of harmonized protocols for each radiotracer production and use are certainly desirable. Furthermore, a definition of SA values for brain imaging radiotracers may also facilitate the approval of new radiopharmaceuticals for human use through regulatory authorities [129].

4.4 SPECT/PET Brain Imaging Radiopharmaceuticals

Radiopharmaceuticals and radiotracers for the investigation of neurological disorders with SPECT and PET have found many diagnostic applications. A large number of radiolabeled molecules have been developed, but only a few reached clinical state in Nuclear Medicine. After administration, typically by intravenous injection, the regional uptake and distribution of radioactivity are evaluated using tomographic systems. A selection of the most important radiopharmaceuticals routinely employed in clinical practice are reported in Table 4.2 and described as follows.

4.4.1 Flow and Perfusion

Radiopharmaceuticals applied in the evaluation of rCBF are transported by diffusion from the arterial vascular compartment into the normal brain tissue compartment. The distribution pattern depends on the interaction with brain tissue. Xenon-133 and krypton-81m for SPECT and [^{15}O]oxygen and [^{15}O]water for PET are freely diffusible and not trapped; thus, rCBF is evaluated by determination of the clearance rate of the tracer after a brief uptake period. [^{15}O]CO (carbon monoxide) is assumed to have a different mechanism, accumulating selectively in red blood cells when inhaled in tracer quantities. [^{15}O]CO labels hemoglobin in vivo forming carboxyhemoglobin, thus making possible the delineation of the cerebral vascular blood pool [130].

[^{99m}Tc]HMPAO and [^{99m}Tc]ECD are commonly used in clinical routine, and their use allows to monitor the changes of rCBF in various neurological diseases. Both complexes penetrate the intact BBB and their distribution correlates with rCBF. [^{99m}Tc]HMPAO retention is due to its chemical instability. After BBB penetration, technetium-99m dissociates forming complexes with intracellular proteins, rendering it unable to re-diffuse through the BBB and thus trapping radioactivity in the brain. The redox status of the tissue and the concentration of glutathione have been identified as critical parameters for this conversion [131]. [^{99m}Tc]ECD brain uptake is otherwise attributed to the enzymatic hydrolysis of an ester group and the formation of a hydrophilic metabolite, which cannot diffuse back out across the BBB, thus allowing SPECT imaging [132].

4.4.2 Tumor Metabolism

Despite the fact that [^{18}F]FDG is the "working horse" for diagnostic imaging studies in neuro-oncology (over 90 % are made with [^{18}F]FDG worldwide), other radiopharmaceuticals more tumor specific than [^{18}F]FDG are available. Among these, radiolabeled amino acid and choline derivatives (true tracers or analog tracers) are routinely employed for the diagnoses of primary and metastatic brain tumors. [^{11}C]methionine as well as other PET-labeled aromatic amino acid analogs, such as [^{18}F]FET and [^{18}F]FDOPA [133], are able to delineate the increased rates of amino acid transport by many tumor cells. [^{123}I]IMT, a gamma-emitting radiopharmaceutical, represents the SPECT clinical alternative due to similar in vivo behavior. Abnormal choline metabolism is another metabolic hallmark associated with oncogenesis and tumor progression. Choline is a cellular membrane phospholipid precursor that can be phosphorylated by the enzyme choline

kinase and further incorporated into phosphatidylcholine, a major phospholipid of all membranes. Radiolabeled choline derivatives are mainly used to diagnose prostate cancer; however, they have an established use for brain imaging [134].

[^{18}F]FLT, a nucleoside-labeled analog, is also employed as radiopharmaceutical in oncology and neuro-oncology. It is intracellularly phosphorylated by the thymidine kinase 1 (TK1), and the corresponding nucleoside monophosphate is not further metabolized. Since TK1 has a higher activity in proliferating tumor cells with respect to normal tissue, [^{18}F]FLT uptake represents an in vivo biomarker of proliferation activity [135].

^{201}Tl and [^{99m}Tc]MIBI are commonly used to image myocardial perfusion. Thallium-201 uptake in brain tumors is a result of a combination of factors, such as alterations in the BBB variability in the expression of the Na^+/K^+ pump and blood flow. [^{99m}Tc]MIBI accumulation depends on altered P-glycoprotein function on BBB and passive transport into tumor tissue mitochondria. Mainly in the past, cardiac radiopharmaceuticals have been widely used as neuro-oncological radiotracers, being able to be selectively incorporated by active proliferating cells comparing with normal brain tissue [133].

4.4.3 Dopaminergic System

Dopaminergic neurotransmission has a central role in many brain functions. The presynaptic nigrostriatal projection is the main location of the pathologic process in Parkinson's disease, and therefore, the assessment of disturbed dopamine synthesis is the main target for clinical studies. For measuring dopamine synthesis, the main radiopharmaceutical used is [^{18}F]FDOPA [89]. Postsynaptic receptors may also be involved in neurodegenerative disorders. The dopamine receptor family is composed by five subtypes, but the most studied is D2. N-[^{11}C]methylspiperone was one of the first radiotracer employed for the study of dopamine receptor reserve, but it also has affinity for 5-HT_2 receptors. The gold standard PET tracer for D2 receptors is [^{11}C]raclopride at present, which has allowed the analysis of central D2 receptors (although it also binds D3 receptors) [136]. For SPECT, [^{123}I]IBZN is the most widely used D2 receptor tracer, while for PET, [^{18}F]fallypride is especially suitable for investigation of extrastriatal D2 receptors.

The neural dopamine transporter (DAT) is a membrane-bound presynaptically located protein that regulates the concentration of dopamine in nerve terminals. The evaluation of the reuptake sites provides a measure of the density of dopaminergic nerve terminals. Several compounds have been shown to be antagonists of the monoamine reuptake system, and many tropane derivatives labeled with single-photon emitters are currently in use.

4.4.4 Other Neurotransmitting Systems

Acetylcholine is a neurotransmitter at cholinergic synapses that mediate functions on nicotinic and muscarinic receptors. Nicotinic receptors have been implied in many psychiatric and neurologic diseases, including depression and cognitive and memory disorders. 2-[^{18}F]F-A85380 is a potent and selective agonist suitable for imaging the nicotinic subtype $\alpha_4\beta_2$nACh receptors [54]. The muscarinic reserve, which is the dominant postsynaptic cholinergic receptor in the brain, has been targeted by many tracers for SPECT and PET. However, due to the lack of selectivity for the receptors subtypes, there are not radiopharmaceuticals in clinical state at present. On the contrary, the quantitative measurement of the acetylcholinesterase activity in the brain by radiolabeled acetylcholine analogs, such as [^{11}C]MP4A, has found broader application [52].

GABA is the most important inhibitory neurotransmitter which is altered in epilepsy, anxiety, and other psychiatric disorders. The radiopharmaceutical most widely used for central benzodiazepine-binding sites is the antagonist flumazenil labeled with carbon-11 or iodine-123 [43]. Another binding site for benzodiazepine in the brain is the peripheral benzodiazepine receptor (PBR), which is located in the mitochondrial

and nuclear subcellular fraction. The most frequently used radiopharmaceutical as the ligand for the PBRs is [^{11}C]PK11195, which is a valuable tool for imaging the activation of microglia in vivo [39].

4.4.5 Amyloid-Binding Ligands

The amyloid ligands in clinical use are the thioflavin T-derived [^{11}C]-Pittsburgh compound B (PIB) and [^{18}F]flutemetamol, [^{18}F]florbetaben, and [^{18}F]florbetapir [72]. [^{18}F]labeled analogs are approved by the Food and Drugs Administration (FDA) and European Medicines Agency (EMA) for the clinical evaluation of cognitive deficits in patients and available in the market.

4.4.6 Cisternography

Cisternography with [^{111}In]DTPA is indicated as an imaging agent to study the flow of cerebrospinal fluid (CSF) in the brain, to diagnose abnormalities in CSF circulation, to assess and help localize the site of CSF leakage, and to test the patency of or localize blocks in CSF shunts.

4.5 Future Brain Imaging Directions

An area of great excitement is the detection of neurotransmitter system fluctuations for the study of drug abuse or behavioral addictions. Addiction is the habitual compulsion to use a substance (i.e., alcohol, opiate, nicotine) or to engage in an activity without much regard for its detrimental effects on a person's physical, mental, financial, and social well-being (i.e., gambling, food, work, love). Brain imaging is a valuable tool that may help to establish addiction as a "disease," leading to the characterization of the involved neural circuitry in intoxication, withdrawal, and abstinence. Furthermore, the evidence of an altered neurotransmitter system may lead to the identification of a potential target for pharmacological treatments.

A key discovery has been the blunted striatal dopaminergic activity, at presynaptic and postsynaptic levels, in a variety of addictions [137]. Dopaminergic neurotransmission was found altered after repeated drug exposure, and the measurement of dopamine release has been described with SPECT and PET using the available radiopharmaceutical for dopamine receptors and DAT transporters.

While studies of addiction have been well established for the dopamine system, extension to other systems has been limited by the lack of suitable radiopharmaceuticals. However, within the past 10 years, and in particular in the last few years, promising tools have been made available for imaging fluctuations in 5-HT, endogenous opioids, GABA, and glutamate [73].

Conclusions

There are two main areas of research using PET-CT and PET-MRI imaging of neurological disease, namely, increasing the understanding of human biology and improving patient care through diagnostic imaging. Major advances have been made in understanding the complicated interactions in the brain. Although genetic and environmental factors are contributors to abnormalities, neurological and psychiatric diseases are not correlated with a single genetic abnormality. Ex vivo measurements using proteomic analysis of biopsy samples are most difficult in the brain giving external nuclear imaging an added value. As a result, measuring the changes in the biochemistry of the protein expression products and their neurotransmitters has become the province of nuclear imaging. The addition of anatomical instruments to PET and SPECT has made a tremendous difference in co-registering the small anatomical structures with the emitted radioactivity. SPECT/CT and SPECT/MRI have benefited more than PET/CT and PET/MRI given the lower resolution of SPECT [138].

The understanding of addiction, for example, has been enhanced by PET studies of receptor occupancy and synaptic neurotransmitter changes, especially for the dopamine system [139, 140].

Improving patient care through diagnostic imaging has been more difficult given the complexity of most diseases. The restrictions of patient tolerance and absorbed radiation dose have limited external imaging to one or two studies using probes for different biochemistry. The major achievements have been in monitoring general disease control points, mostly in tumors, or serving as a biomarker for potential drugs by measuring occupancy and changes in biochemistry as a function of disease progression or treatment. A case in point is the plaque imaging agents that are clearly biomarkers for the presence of plaque, but do not impact uniquely on diagnosing Alzheimer's disease. Overall, the combination imaging devices have increased the usefulness of radiopharmaceuticals by leading to more precise information for the location and the amount of radiopharmaceutical in specific areas of the brain.

Acknowledgments The authors thank Calogero D'Alessandria, Davide Camporese, and Benedetta Pagano for their collaboration on topics discussed in this chapter.

Glossary

Radionuclide A radioactive nuclide is an unstable form of a chemical element that decays by emitting particles, gamma radiation, or X-radiation.

Radioisotope An unstable isotope of an element that decays by emitting particles, gamma radiation, or X-radiation. The term, "radioisotopes," is limited to unstable atoms of the same element.

Radioindicator First used by Hevesy to describe the use of physiologic elements. It was used later to describe indicator dilution studies using radionuclides in cardiology.

Radiotracer This should be reserved for those radiolabeled compounds that contain a radioisotope of a stable element and not a radionuclide. The latter requires extensive validation to demonstrate that it is a radiotracer.

Radiopharmaceutical The term for a radiolabeled compound after approval or registration by a government agency. This nomenclature reflects the similar requirements for identity, purity, and safety that are required of pharmaceuticals.

References

1. Wrenn FR et al (1951) The use of positron emitting radioisotopes for the localization of brain tumors. Sciences 113:525
2. Brownell GL, Sweet WH (1953) Localization of brain tumors with positron emitters. Nucleonics 11:40
3. Seaman WB et al (1954) Localization of intracranial neoplasm with radioactive radioisotopes. Radiology 62:30
4. Sweet WH, Brownell GL (1955) Localization of intracranial lesions by scanning with positron-emitting arsenic. J Am Med Assoc 157(14):1183–1188
5. Brinkman CA et al (1962) Brain scanning with Mercury-203 labelled Neohydrin. J Neurosurg 19:644
6. Shealy CN et al (1964) Gallium-68 as a scanning agent for intracranial lesions. J Nucl Med 5:161–167
7. Gleason GI (1960) A positron cow. Int J Appl Radiat Isot 8:90–94
8. Greene MW, Tucker WD (1961) An improved gallium-68 cow. Int J Appl Radiat Isot 12:62
9. Anger HO, Gottschalk A (1963) Localization of brain tumors with the positron scintillation camera. J Nucl Med 4:326–330
10. Gottschalk A, Anger HO (1964) The sensitivity of the positron scintillation camera for detecting simulated brain tumors with gallium 68-EDTA. Am J Roentgenol Radium Ther Nucl Med 92:174–176
11. Richards P (1960) A survey of the production at Brookhaven National Laboratory of Radioisotopes for medical research. VII Rassegna Internazionale Elettronica e Nucleare, Rome, Italy. pp. 223–244.
12. Richards P (2002) Technetium-99m: the early days. In: Mazzi U (ed) Proceeding of the VIIth International Symposium on Technetium, Rhenium and other metals in Chemistry and Nuclear Medicine. servizi grafici editoriali snc, Padova, pp. 1–9
13. Ramsey RG, Quinn RG (1972) Comparison of accuracy between initial and delayed 99mTc-pertechnetate brain scans. J Nucl Med 13:131–134
14. Ryerson TW et al (1978) A quantitative clinical comparison of three 99mTechnetium labeled brain imaging radiopharmaceuticals. Radiology 127(2):429–432
15. Lassen NA, Munck O (1955) The cerebral blood flow in man determined by the use of radioactive krypton. Acta Physiol Scand 33(1):30–49
16. Munck O, Lassen NA (1957) Bilateral cerebral blood flow and oxygen consumption in man by use of krypton 85. Circ Res 5(2):163–168

17. Harper AM, Glass HI (1963) Measurement of cerebral blood-flow. Lancet 1(7293):1262–1263
18. Hoedt-Rasmussen K, Sveinsdottir E, Lassen NA (1966) Regional cerebral blood flow in man determined by intra-arterial injection of radioactive inert gas. Circ Res 18(3):237–247
19. Anger HO (1964) Scintillation camera with multichannel collimators. J Nucl Med 5:515–531
20. Ter-Pogossian MM et al (1969) The determination of regional cerebral blood flow by means of water labeled with radioactive oxygen 15. Radiology 93(1):31–40
21. Ter-Pogossian MM, Herscovitch P (1985) Radioactive oxygen-15 in the study of cerebral blood flow, blood volume, and oxygen metabolism. Semin Nucl Med 15(4):377–394
22. Jones T, Chesler DA, Ter-Pogossian MM (1976) The continuous inhalation of oxygen-15 for assessing regional oxygen extraction in the brain of man. Br J Radiol 49(580):339–343
23. Herscovitch P, Markham J, Raichle ME (1983) Brain blood flow measured with intravenous H2(15)O. I. Theory and error analysis. J Nucl Med 24(9):782–789
24. Lenzi GL, Frackowiak RS, Jones T (1982) Cerebral oxygen metabolism and blood flow in human cerebral ischemic infarction. J Cereb Blood Flow Metab 2(3):321–335
25. Lenzi GL et al (1978) Non-invasive regional study of chronic cerebrovascular disorders using the oxygen-15 inhalation technique. J Neurol Neurosurg Psychiatry 41(1):11–17
26. Lenzi GL et al (1978) Study of regional cerebral metabolism and blood flow relationships in man using the method of continuously inhaling oxygen-15 and oxygen-15 labelled carbon dioxide. J Neurol Neurosurg Psychiatry 41(1):1–10
27. Uszier JM et al (1975) Human CNS perfusion scanning with 123I-iodoantipyrine. Radiology 115(1):197–200
28. Kuhl DE et al (1982) Quantifying local cerebral blood flow by N-isopropyl-p-[123I]iodoamphetamine (IMP) tomography. J Nucl Med 23(3):196–203
29. Hammersley PA et al (1987) 99mTc-HMPAO as a tumour blood flow agent. Eur J Nucl Med 13(2):90–94
30. Leveille J et al (1989) Characterization of technetium-99m-L, L-ECD for brain perfusion imaging, Part 2: biodistribution and brain imaging in humans. J Nucl Med 30(11):1902–1910
31. Ido T et al (1978) Labeled 2-deoxy-D-glucose analogs. [18F]labeled 2-fluoro-2-deoxy-D-glucose, 2-fluoro-2-deoxy-D-mannose, 14C-2-deoxy-2-fluoro-D-glucose. J Label Comp Radio 14:175–183
32. Kuhl DE, Hoffman EJ, Phelphs ME, Ricci AR, Reivich M (1976) Design and application of the Mark IV scanning system for radionuclide computed tomography of the brain. IAEA Symp Med Radionuclide Imag 1:309–320
33. Comar D et al (1976) Labelling and metabolism of methionine-methyl-11 C. Eur J Nucl Med 1(1):11–14
34. Hubner KF et al (1981) Tumor detection with 1-aminocyclopentane and 1-aminocyclobutane C-11-carboxylic acid using positron emission computerized tomography. Clin Nucl Med 6(6):249–252
35. Barrio JR et al (1983) L-[1-11C]leucine: routine synthesis by enzymatic resolution. J Nucl Med 24(6):515–521
36. Garnett ES, Firnau G, Nahmias C (1983) Dopamine visualized in the basal ganglia of living man. Nature 305(5930):137–138
37. Wagner HN Jr et al (1983) Imaging dopamine receptors in the human brain by positron tomography. Science 221(4617):1264–1266
38. Jones AK et al (1988) Regional cerebral opioid receptor studies with [11C]diprenorphine in normal volunteers. J Neurosci Methods 23(2):121–129
39. Hashimoto K et al (1989) Synthesis and evaluation of 11C-PK 11195 for in vivo study of peripheral-type benzodiazepine receptors using positron emission tomography. Ann Nucl Med 3(2):63–71
40. Farde L et al (1986) Quantitative analysis of D2 dopamine receptor binding in the living human brain by PET. Science 231(4735):258–261
41. Halldin C et al (1986) Preparation of 11C-labelled SCH 23390 for the in vivo study of dopamine D-1 receptors using positron emission tomography. Int J Rad Appl Instrum A 37(10):1039–1043
42. Aquilonius SM et al (1987) In vivo evaluation of striatal dopamine reuptake sites using 11C-nomifensine and positron emission tomography. Acta Neurol Scand 76(4):283–287
43. Ehrin E et al (1984) Preparation and preliminary positron emission tomography studies of 11C-Ro 15–1788, a selective benzodiazepine receptor antagonist. Acta Pharm Suec 21(3):183–188
44. Frost JJ et al (1988) Mu-opiate receptors measured by positron emission tomography are increased in temporal lobe epilepsy. Ann Neurol 23(3):231–237
45. Fowler JS et al (1987) Mapping human brain monoamine oxidase A and B with 11C-labeled suicide inactivators and PET. Science 235(4787):481–485
46. Pike VW et al (1995) First delineation of 5-HT1A receptors in human brain with PET and [11C]WAY-100635. Eur J Pharmacol 283(1–3):R1–R3
47. Lundkvist C et al (1996) [11C]MDL 100907, a radioligand for selective imaging of 5-HT(2A) receptors with positron emission tomography. Life Sci 58(10):PL 187–PL 192
48. Suehiro M et al (1993) [11C](+)McN5652 as a radiotracer for imaging serotonin uptake sites with PET. Life Sci 53(11):883–892
49. Halldin C et al (1998) Carbon-11-NNC 112: a radioligand for PET examination of striatal and neocortical D1-dopamine receptors. J Nucl Med 39(12):2061–2068
50. Halldin C et al (1995) Carbon-11-FLB 457: a radioligand for extrastriatal D2 dopamine receptors. J Nucl Med 36(7):1275–1281
51. Halldin C et al (1996) [11C]beta-CIT-FE, a radioligand for quantitation of the dopamine transporter in

the living brain using positron emission tomography. Synapse 22(4):386–390
52. Iyo M et al (1997) Measurement of acetylcholinesterase by positron emission tomography in the brains of healthy controls and patients with Alzheimer's disease. Lancet 349(9068):1805–1809
53. Kilbourn MR et al (1996) In vivo studies of acetylcholinesterase activity using a labeled substrate, N-[11C]methylpiperdin-4-yl propionate ([11C] PMP). Synapse 22(2):123–131
54. Horti AG et al (1998) 2-[18F]Fluoro-A-85380, an in vivo tracer for the nicotinic acetylcholine receptors. Nucl Med Biol 25(7):599–603
55. Koeppe RA et al (1996) Kinetic evaluation of [11C] dihydrotetrabenazine by dynamic PET: measurement of vesicular monoamine transporter. J Cereb Blood Flow Metab 16(6):1288–1299
56. Elsinga PH et al (1996) Carbon-11-labeled daunorubicin and verapamil for probing P-glycoprotein in tumors with PET. J Nucl Med 37(9):1571–1575
57. Innis RB et al (1991) SPECT imaging of the benzodiazepine receptor: feasibility of in vivo potency measurements from stepwise displacement curves. J Nucl Med 32(9):1754–1761
58. Muller-Gartner HW et al (1992) Imaging muscarinic cholinergic receptors in human brain in vivo with Spect, [123I]4-iododexetimide, and [123I]4-iodolevetimide. J Cereb Blood Flow Metab 12(4):562–570
59. Holman BL et al (1985) Muscarinic acetylcholine receptors in Alzheimer's disease. In vivo imaging with iodine 123-labeled 3-quinuclidinyl-4-iodobenzilate and emission tomography. JAMA 254(21):3063–3066
60. Seibyl JP et al (1994) Whole-body biodistribution, radiation absorbed dose and brain SPECT imaging with iodine-123-beta-CIT in healthy human subjects. J Nucl Med 35(5):764–770
61. Kung HF et al (1990) In vivo SPECT imaging of CNS D-2 dopamine receptors: initial studies with iodine-123-IBZM in humans. J Nucl Med 31(5):573–579
62. Votaw JR et al (1995) Dosimetry of iodine-123-epidepride: a dopamine D2 receptor ligand. J Nucl Med 36(7):1316–1321
63. Foged C et al (1996) Development of 123I-labelled NNC 13–8241 as a radioligand for SPECT visualization of benzodiazepine receptor binding. Nucl Med Biol 23(3):201–209
64. Kung MP et al (1997) [99mTc]TRODAT-1: a novel technetium-99m complex as a dopamine transporter imaging agent. Eur J Nucl Med 24(4):372–380
65. Madras BK et al (1996) Technepine: a high-affinity 99m-technetium probe to label the dopamine transporter in brain by SPECT imaging. Synapse 22(3):239–246
66. Kung HF et al (2007) Clinical acceptance of a molecular imaging agent: a long march with [99mTc] TRODAT. Nucl Med Biol 34(7):787–789
67. Klunk WE et al (2004) Imaging brain amyloid in Alzheimer's disease with Pittsburgh Compound-B. Ann Neurol 55(3):306–319
68. Logan J et al (2007) Imaging the norepinephrine transporter in humans with (S, S)-[11C]O-methyl reboxetine and PET: problems and progress. Nucl Med Biol 34(6):667–679
69. Solin O et al (2004) Synthesis and characterization of a potent, selective, radiolabeled substance-P antagonist for NK1 receptor quantitation: ([18F] SPA-RQ). Mol Imaging Biol 6(6):373–384
70. Burns HD et al (2007) [18F]MK-9470, a positron emission tomography (PET) tracer for in vivo human PET brain imaging of the cannabinoid-1 receptor. Proc Natl Acad Sci U S A 104(23):9800–9805
71. Okamura N et al (2014) Non-invasive assessment of Alzheimer's disease neurofibrillary pathology using 18F-THK5105 PET. Brain 137(Pt 6):1762–1771
72. Mason NS, Mathis CA, Klunk WE (2013) Positron emission tomography radioligands for in vivo imaging of Abeta plaques. J Labelled Comp Radiopharm 56(3–4):89–95
73. Jones T, Rabiner EA (2012) The development, past achievements, and future directions of brain PET. J Cereb Blood Flow Metab 32(7):1426–1454
74. Myers WG (1979) Georg Charles de Hevesy: the father of nuclear medicine. J Nucl Med 20(6):590–594
75. Molecular Imaging and Contrast Agent Database (MICAD). Bethesda (MD): National Center for Biotechnology Information (US); 2004–2013. Available from: http://www.ncbi.nlm.nih.gov/books/NBK5330
76. Nunn AD (2006) The cost of developing imaging agents for routine clinical use. Invest Radiol 41(3):206–212
77. Zimmermann RG (2013) Why are investors not interested in my radiotracers. The industrial and regulatory constraints in the development of radiopharmaceuticals. Nucl Med Biol 40(2):155–166
78. Agdeppa ED, Spilker ME (2009) A review of imaging agent development. AAPS J 11(2):286–299
79. Rahmim A, Zaidi H (2008) PET versus SPECT: strengths, limitations and challenges. Nucl Med Commun 29(3):193–207
80. Ritt P, Kuwert T (2013) Quantitative SPECT/CT. Recent Results Cancer Res 187:313–330
81. Eckelman WC, Reba RC, Kelloff GJ (2008) Targeted imaging: an important biomarker for understanding disease progression in the era of personalized medicine. Drug Discov Today 13(17–18):748–759
82. Sharma V, Luker GD, Piwnica-Worms D (2002) Molecular imaging of gene expression and protein function in vivo with PET and SPECT. J Magn Reson Imaging 16(4):336–351
83. Laruelle M, Slifstein M, Huang Y (2003) Relationships between radiotracer properties and image quality in molecular imaging of the brain with positron emission tomography. Mol Imaging Biol 5(6):363–375
84. Van de Bittner GC, Ricq EL, Hooker JM (2014) A philosophy for CNS radiotracer design. Acc Chem Res 47(10):3127–3134

85. Gorovets A et al (2013) Efficacy considerations for U.S. Food and Drug Administration approval of diagnostic radiopharmaceuticals. J Nucl Med 54(8):1479–1484
86. Landau SM et al (2014) Amyloid PET imaging in Alzheimer's disease: a comparison of three radiotracers. Eur J Nucl Med Mol Imaging 41(7):1398–1407
87. Johnson KA et al (2013) Appropriate use criteria for amyloid PET: a report of the Amyloid Imaging Task Force, the Society of Nuclear Medicine and Molecular Imaging, and the Alzheimer's Association. J Nucl Med 54(3):476–490
88. Odano I et al (2009) [18F]flumazenil binding to central benzodiazepine receptor studies by PET–quantitative analysis and comparisons with [11C] flumazenil. Neuroimage 45(3):891–902
89. Torstenson R et al (1999) A comparison of 11C-labeled L-DOPA and L-fluorodopa as positron emission tomography tracers for the presynaptic dopaminergic system. J Cereb Blood Flow Metab 19(10):1142–1149
90. Shiue CY, Welch MJ (2004) Update on PET radiopharmaceuticals: life beyond fluorodeoxyglucose. Radiol Clin North Am 42(6):1033–1053, viii
91. Welch MJ et al (1988) N-(3-[18F]fluoropropyl)-spiperone: the preferred 18F labeled spiperone analog for positron emission tomographic studies of the dopamine receptor. Int J Rad Appl Instrum B 15(1):83–97
92. Miller PW et al (2008) Synthesis of 11C, 18F, 15O, and 13N radiolabels for positron emission tomography. Angew Chem Int Ed Engl 47(47):8998–9033
93. Scott PJ (2009) Methods for the incorporation of carbon-11 to generate radiopharmaceuticals for PET imaging. Angew Chem Int Ed Engl 48(33):6001–6004
94. Ryzhikov NN et al (2005) Preparation of highly specific radioactivity [18F]flumazenil and its evaluation in cynomolgus monkey by positron emission tomography. Nucl Med Biol 32(2):109–116
95. Shen B et al (2009) Automated synthesis of n.c.a. [18F]FDOPA via nucleophilic aromatic substitution with [18F]fluoride. Appl Radiat Isot 67(9):1650–1653
96. Fuchtner F, Steinbach J (2003) Efficient synthesis of the 18F-labelled 3-O-methyl-6-[18F]fluoro-L-DOPA. Appl Radiat Isot 58(5):575–578
97. Zhang MR, Suzuki K (2007) [18F]Fluoroalkyl agents: synthesis, reactivity and application for development of PET ligands in molecular imaging. Curr Top Med Chem 7(18):1817–1828
98. Wadsak W et al (2007) 18F fluoroethylations: different strategies for the rapid translation of 11C-methylated radiotracers. Nucl Med Biol 34(8):1019–1028
99. Lee SJ et al (2007) One-step high-radiochemical-yield synthesis of [18F]FP-CIT using a protic solvent system. Nucl Med Biol 34(4):345–351
100. Seibyl JP et al (1998) Iodine-123-beta-CIT and iodine-123-FPCIT SPECT measurement of dopamine transporters in healthy subjects and Parkinson's patients. J Nucl Med 39(9):1500–1508
101. Kim HJ et al (1997) Imaging and quantitation of dopamine transporters with iodine-123-IPT in normal and Parkinson's disease subjects. J Nucl Med 38(11):1703–1711
102. Emond P, Guilloteau D, Chalon S (2008) PE2I: a radiopharmaceutical for in vivo exploration of the dopamine transporter. CNS Neurosci Ther 14(1):47–64
103. Santos JS et al (2002) Radioiodination of proteins using prosthetic group: a convenient way to produce labelled proteins with in vivo stability. Cell Mol Biol (Noisy-le-Grand) 48(7):735–739
104. Heimbold I et al (2002) Synthesis, biological and autoradiographic evaluation of a novel Tc-99m radioligand derived from WAY 100635 with high affinity for the 5-HT(1A) receptor and the alpha1-adrenergic receptor. Nucl Med Biol 29(4):375–387
105. Hayne DJ et al (2015) Rhenium and technetium complexes that bind to amyloid-beta plaques. Dalton Trans 44(11):4933–4944
106. Schibli R, Schubiger PA (2002) Current use and future potential of organometallic radiopharmaceuticals. Eur J Nucl Med Mol Imaging 29(11):1529–1542
107. Alberto R et al (2001) Synthesis and properties of boranocarbonate: a convenient in situ CO source for the aqueous preparation of [(99m)Tc(OH(2))3(CO)3]+. J Am Chem Soc 123(13):3135–3136
108. Wang X et al (2014) Novel cyclopentadienyl tricarbonyl (99m)tc complexes containing 1-piperonylpiperazine moiety: potential imaging probes for sigma-1 receptors. J Med Chem 57(16):7113–7125
109. Saied NM et al (2015) Preparation and biodistribution of 1-((2-methoxyphenyl) piperazine)ferrocenecarboxamide labeled with technetium-99m as a potential brain receptor imaging agent. Eur J Med Chem 97:280–288
110. Lee G, Bendayan R (2004) Functional expression and localization of P-glycoprotein in the central nervous system: relevance to the pathogenesis and treatment of neurological disorders. Pharm Res 21(8):1313–1330
111. Dallas S, Miller DS, Bendayan R (2006) Multidrug resistance-associated proteins: expression and function in the central nervous system. Pharmacol Rev 58(2):140–161
112. Pike VW (2009) PET radiotracers: crossing the blood–brain barrier and surviving metabolism. Trends Pharmacol Sci 30(8):431–440
113. Zoghbi SS et al (2006) PET imaging of the dopamine transporter with 18F-FECNT: a polar radiometabolite confounds brain radioligand measurements. J Nucl Med 47(3):520–527
114. Kuchar M, Mamat C (2015) Methods to increase the metabolic stability of (18)F-radiotracers. Molecules 20(9):16186–16220

115. Giovacchini G et al (2005) 5-HT 1A receptors are reduced in temporal lobe epilepsy after partial-volume correction. J Nucl Med 46(7):1128–1135
116. Lundkvist C et al (1999) Different brain radioactivity curves in a PET study with [11C]beta-CIT labelled in two different positions. Nucl Med Biol 26(4):343–350
117. Carson RE et al (2003) Brain uptake of the acid metabolites of F-18-labeled WAY 100635 analogs. J Cereb Blood Flow Metab 23(2):249–260
118. Huang Y, Mahmood K, Mathis CA (1999) An efficient synthesis of the precursors of [11C]MDL 100907 labeled in two specific positions. J Labelled Comp Radiopharm 42:949–957
119. Scott DO, Heath TG (1998) Investigation of the CNS penetration of a potent 5-HT2a receptor antagonist (MDL 100,907) and an active metabolite (MDL 105,725) using in vivo microdialysis sampling in the rat. J Pharm Biomed Anal 17(1):17–25
120. Hinz R et al (2007) Validation of a tracer kinetic model for the quantification of 5-HT(2A) receptors in human brain with [(11)C]MDL 100,907. J Cereb Blood Flow Metab 27(1):161–172
121. Osman S et al (1996) Characterization of the radioactive metabolites of the 5-HT1A receptor radioligand, [O-methyl-11C]WAY-100635, in monkey and human plasma by HPLC: comparison of the behaviour of an identified radioactive metabolite with parent radioligand in monkey using PET. Nucl Med Biol 23(5):627–634
122. Pike VW et al (1996) Exquisite delineation of 5-HT1A receptors in human brain with PET and [carbonyl-11 C]WAY-100635. Eur J Pharmacol 301(1–3):R5–R7
123. Osman S et al (1998) Characterisation of the appearance of radioactive metabolites in monkey and human plasma from the 5-HT1A receptor radioligand, [carbonyl-11C]WAY-100635–explanation of high signal contrast in PET and an aid to biomathematical modelling. Nucl Med Biol 25(3):215–223
124. Timmers HJ et al (2007) The effects of carbidopa on uptake of 6-18F-Fluoro-L-DOPA in PET of pheochromocytoma and extraadrenal abdominal paraganglioma. J Nucl Med 48(10):1599–1606
125. Ryu YH et al (2007) Disulfiram inhibits defluorination of (18)F-FCWAY, reduces bone radioactivity, and enhances visualization of radioligand binding to serotonin 5-HT1A receptors in human brain. J Nucl Med 48(7):1154–1161
126. Tipre DN et al (2006) PET imaging of brain 5-HT1A receptors in rat in vivo with 18F-FCWAY and improvement by successful inhibition of radioligand defluorination with miconazole. J Nucl Med 47(2):345–353
127. Fischer K et al (2011) Noninvasive nuclear imaging enables the in vivo quantification of striatal dopamine receptor expression and raclopride affinity in mice. J Nucl Med 52(7):1133–1141
128. Eckelman WC, Bonardi M, Volkert WA (2008) True radiotracers: are we approaching theoretical specific activity with Tc-99m and I-123? Nucl Med Biol 35(5):523–527
129. Lapi SE, Welch MJ (2012) A historical perspective on the specific activity of radiopharmaceuticals: what have we learned in the 35 years of the ISRC? Nucl Med Biol 39(5):601–608
130. Martin WR, Powers WJ, Raichle ME (1987) Cerebral blood volume measured with inhaled C15O and positron emission tomography. J Cereb Blood Flow Metab 7(4):421–426
131. Jacquier-Sarlin MR, Polla BS, Slosman DO (1996) Oxido-reductive state: the major determinant for cellular retention of technetium-99m-HMPAO. J Nucl Med 37(8):1413–1416
132. Jacquier-Sarlin MR, Polla BS, Slosman DO (1996) Cellular basis of ECD brain retention. J Nucl Med 37(10):1694–1697
133. Palumbo B et al (2014) SPECT and PET serve as molecular imaging techniques and in vivo biomarkers for brain metastases. Int J Mol Sci 15(6):9878–9893
134. Giovannini E et al (2015) Clinical applications of choline PET/CT in brain tumors. Curr Pharm Des 21(1):121–127
135. Wardak M et al (2014) (1)(8)F-FLT and (1)(8) F-FDOPA PET kinetics in recurrent brain tumors. Eur J Nucl Med Mol Imaging 41(6):1199–1209
136. Elsinga PH, Hatano K, Ishiwata K (2006) PET tracers for imaging of the dopaminergic system. Curr Med Chem 13(18):2139–2153
137. Volkow ND et al (1997) Decreased striatal dopaminergic responsiveness in detoxified cocaine-dependent subjects. Nature 386(6627):830–833
138. Ritt P et al (2011) Absolute quantification in SPECT. Eur J Nucl Med Mol Imaging 38(Suppl 1):S69–S77
139. Volkow ND et al (2012) Addiction circuitry in the human brain. Annu Rev Pharmacol Toxicol 52:321–336
140. Bloomfield MA et al (2014) Dopamine function in cigarette smokers: an [(1)(8)F]-DOPA PET study. Neuropsychopharmacology 39(10):2397–2404

Contrast Media

5

Francesca Arena, Silvio Aime, and Francesco Blasi

Abbreviations

ASL	Arterial spin labeling
CEST	Chemical exchange
CNS	Central nervous system
CT	Computed tomography
DCE	Dynamic contrast enhancement
DOTATOC	1,4,7,10-tetraazacyclododecane-1,4,7,10-tetraacetic acid-tyrosine-3-octreotide
DTI	Diffusion tensor imaging
DTPA	Diethylene-triamine-pentacetate
DWI	Diffusion-weighted imaging
FDG	2-fluoro-2-deoxy-D-glucose
FET	Fluoroethyl-tyrosine
fMRI	Functional MRI
MRI	Magnetic resonance imaging
NMR	Nuclear magnetic resonance imaging
PET	Positron emission tomography
SPECT	Single-photon emission computed tomography
T1w	T1 weighted
T2*	T2 star
T2w	T2 weighted
FAZA	Fluoroazomycin-arabinoside

Diagnostic imaging has gained a pivotal role in medical science thanks to the development of noninvasive imaging strategies. Magnetic resonance, x-ray, and ultrasound have been used for decades in clinical practice to provide primarily anatomical information on both diseased and healthy tissues. Although traditional imaging is extremely useful to answer key questions about tissue alterations produced by a specific disease, it does not offer insight on the underlying mechanisms and molecular abnormalities that characterize the pathology. Differently, contrast-enhanced imaging takes advantage of the tissue contrast enhancement triggered by specific chemicals, namely, the contrast media, to obtain physiological and molecular information. Contrast media are indeed pharmaceuticals, with low or absent pharmacological activity, that enhance the visualization of radiological images by altering tissue contrast. After administration, contrast agents

F. Arena, PhD • F. Blasi, PhD
Department of Molecular Biotechnology and Health Sciences, University of Turin,
Via Nizza 52, Turin 10126, Italy

Center of Excellence for Preclinical Imaging,
BioIndustry Park "Silvano Furnero",
Via Ribes 5, Colleretto Giacosa 10010, Italy

S. Aime, PhD (✉)
Department of Molecular Biotechnology and Health Sciences, University of Turin,
Via Nizza 52, Turin 10126, Italy
e-mail: silvio.aime@unito.it

A. Ciarmiello, L. Mansi (eds.), *PET-CT and PET-MRI in Neurology*,
DOI 10.1007/978-3-319-31614-7_5

(CAs) may passively diffuse in the body (e.g., iodinated CAs for angiography), bind plasma proteins to enhance the vasculature (i.e., blood pool agents), distribute in the extravascular interstitial space (i.e., extracellular gadolinium-based CAs (GBCAs)), or target a biological substrate (i.e., molecular probes). Particularly, advances in the field of cell biology have boosted the discovery of new molecular targets that can be tracked noninvasively using molecular imaging, a novel diagnostic strategy that allows "in vivo characterization and measurement of the biological processes at the cellular and molecular level" [1]. Here, we will discuss the use of CAs in neurology with major focus on state-of-the-art diagnostic agents for magnetic resonance and nuclear imaging.

5.1 Contrast Agents for Magnetic Resonance Imaging

The contrast signal in magnetic resonance imaging (MRI) is the result of complex interplay between different chemical and physical factors, chiefly the longitudinal (T_1) and transversal (T_2) relaxation rate of water protons. MRI CAs can be classified in four groups of compounds based on their ability to prompt a tissue contrast enhancement. *Positive* CAs are based on paramagnetic metal ions (i.e., Gd^{3+}, Mn^{2+}) chelated to various nontoxic polyaminocarboxylic acids, either cyclic or linear. Paramagnetic complexes trigger a hyperintense (bright) signal in tissues where they accumulate. They are mainly used as extracellular agents that distribute in the blood and interstitial fluids, or as blood pool agents that bind natural macromolecules (e.g., serum albumin) to yield contrast enhancements especially for angiographic purposes. *Negative* CAs take advantage of superparamagnetic iron oxide particles (i.e., Fe_3O_4, γFe_2O_3) to generate a hypointense (dark) signal. These compounds are internalized by circulating macrophages thanks to their hydrophilic cover, allowing detection by MRI after passive diffusion to inflamed regions. Chemical exchange saturation transfer (CEST) molecules are a new class of MRI CAs that can provide physiological information about the tissue environment (e.g., metabolites concentration, pH, temperature). CEST CAs work by influencing the intensity of the bulk water signal through the transfer of saturated magnetization from an exchangeable pool of protons. Functional MRI CEST requires that protons are irradiated by a specific radiofrequency field centered at their absorption frequency, generating a frequency-encoded contrast able to detect more agents in the same image or responsive systems. Finally, endogenous molecules can be hyperpolarized (e.g., ^{13}C-pyruvate) to image their metabolic pathway and monitor cellular metabolism using fast MRI sequences.

GBCAs were the first class of NMR contrast media approved for clinical use in neurology [2]. Although sharing similar chemical features, they display different contrast enhancements, relaxivities, stabilities, and bindings to plasma proteins [3, 4] (Table 5.1). GBCAs are mainly used in neurology to highlight alterations in tissue perfusion, often as result of blood-brain barrier injury, particularly to enhance tumor contrast in patients with glioblastoma and to detect myelin injury in multiple sclerosis patients. Among new GBCAs currently tested, gadofluorine M accumulates in degenerating nerve fibers after experimental demyelination and multiple sclerosis in rodents, facilitating the visualization of CNS inflammatory events [7]. Activation-Guided Irradiation by X-rays (AGuIX) nanoparticles are new ultrasmall gadolinium-based systems that have been tested for MRI-guided radiotherapy for glioma treatment [8]. The nanoparticles accumulate at the tumor site, prompting greater contrast enhancement than the clinically approved gadoterate meglumine, as well as increased survival time after microbeam radiation therapy. Another important clinical application of GBCAs is vascular imaging. The new blood pool agent gadofosveset displays high relaxivity and long circulation time, improving blood vessel imaging and stenosis detection at the level of the head and neck with MR angiography [9]. Finally, gadolinium chelates linked to a targeting moiety can be used as molecular probes to visualize biochemical substrates using MRI. The myeloperoxidase (MPO)-sensitive molecular

Table 5.1 Gadolinium-based contrast agents commonly used for CNS imaging

Contrast agent	Commercial name (manufacturer)	Structure (charge)	Kinetic stability/Ktherm [5]	Relaxivity [6][a]
Gadopentate dimeglumine	Magnevist (Bayer Healthcare)	Linear (di-ionic)	<0.3/22.1	r_1 = 4.9–5.0 r_2 = 5.4–6.3
Gadoteridol	ProHance (Bracco)	Cyclic (nonionic)	>0.95/23.8	r_1 = 4.6 r_2 = 5.3
Gadodiamide	Omniscan (GE Healthcare)	Linear (nonionic)	<0.3/16.9	r_1 = 4.8 r_2 = 5.1
Gadobenate dimeglumine	MultiHance (Bracco)	Linear (di-ionic)	0.3–0.95/22.6	r_1 = 9.7–10.8 r_2 = 12.2–12.5
Gadoterate meglumine	Dotarem (Guerbet)	Cyclic (ionic)	>0.95/25.9	r_1 = 4.3 r_2 = 5.0
Gadobutrol	Gadovist (Bayer Healthcare)	Cyclic (nonionic)	>0.95/21.8	r_1 = 5.6 r_2 = NA

[a]Measured at 0.47 T in human serum or plasma (Gd^{3+} mM^{-1} s^{-1})

probe Gd-*bis*-5-hydroxytryptamide-DTPA (Gd-*bis*-5HT-DTPA) was used to target neuroinflammation after experimental autoimmune encephalomyelitis (EAE) and stroke in rodents [10, 11]. Importantly, compared to conventional GBCAs, Gd-*bis*-5HT-DTPA accumulation does not reflect passive CNS diffusion due to blood-brain barrier breakdown, but rather direct MPO-dependent MR enhancement, allowing in vivo imaging of neuroinflammation. Remarkably, Gd-*bis*-5HT-DTPA showed therapy monitoring capabilities in EAE mice treated with a specific MPO inhibitor [12].

Superparamagnetic iron oxide nanoparticles, either magnetite (Fe_3O_4) or maghemite (γ Fe_2 O_3) based, have been tested for more than two decades as MRI CAs. Although several compounds have been approved for clinical use, many have been discontinued or have limited global market (Table 5.2). According to their hydrodynamic diameter, the particles can be classified in standard (SPIO, 50–180 nm), ultrasmall (USPIO, 10–50 nm), and very small superparamagnetic iron oxide (VSPIO, <10 nm) particles. Thanks to their size and long circulation time, iron oxide particles are captured by circulating monocytes and then carried into the CNS where they accumulate at the inflammatory site. Although MR imaging cannot discriminate between endogenous (e.g., a hemorrhage after stroke or trauma) and exogenous (nanoparticles) iron signal, these agents have been used to detect several CNS lesions, including brain tumors, multiple sclerosis, and stroke [14, 15]. For example, ferumoxytol, initially approved for iron-replacement therapy in patients with chronic renal failure, has been used to detect various CNS pathologies by MRI, especially in patients with chronic kidney disease because of the lower toxicity compared to GBCAs [16]. Moreover, given the different mechanism of contrast enhancement (monocyte transport vs. passive diffusion), iron oxide nanoparticles have been used together with GBCAs to discriminate between multiple sclerosis lesions with different blood-brain barrier permeabilities [17]. Macrophage imaging with iron oxide nanoparticles is currently evaluated as a prognostic marker of disease progression in patients with early signs of multiple sclerosis (clinical trial code: NCT01567553). Iron oxide nanoparticles can also be conjugated to a targeting moiety to serve as MR molecular probes for endothelial vascular imaging. For example, USPIOs conjugated to vascular cell adhesion molecule-1 (VCAM-1)-binding peptides revealed vascular inflammation in animal models of arteriosclerosis and stroke [18, 19]. Recently, micro-sized particles of iron oxide (MPIOs) have been applied to endothelial molecular imaging because of their micron size range, the large payload of iron oxide (usually 0.1–1.6 pg/iron/MPIO particle), and the very short blood half-life (50–100 s) result in superior MR contrast compared to iron oxide nanoparticles. For example, MPIOs targeting VCAM-1 have been used to detect vascular

Table 5.2 Superparamagnetic iron oxide contrast agents

Contrast agent	Commercial name (manufacturer)	Coating agent	Size	Relaxivity [13][a]
Ferumoxides AMI-25	Feridex/Endorem (Guerbet)	Dextran T10	SPIO	$r_1 = 10.1$ $r_2 = 120$
Ferucarbotran SH U555A	Resovist (Bayer Healthcare)	Carboxydextran	SPIO	$r_1 = 9.7$ $r_2 = 189$
SH U 555C	Supravist (Bayer Healthcare)	Carboxydextran	USPIO	$r_1 = 10.7$ $r_2 = 38$
Feruglose NC-100150	Clariscan (GE Healthcare)	Pegylated starch	USPIO	NA
Ferumoxytol-10 AMI-227	Combidex/Sinerem (Guerbet)	Dextran T10, T1	USPIO	$r_1 = 9.9$ $r_2 = 65$
Ferumoxytol Code 7228	Feraheme (Guerbet)	Polyglucose sorbitol carboxymethyl ether	USPIO	$r_1 = 15$ $r_2 = 89$

[a]Measured at 1.5T in human serum or plasma ($Fe^{2+/3+}$ mM^{-1} s^{-1})

inflammation in mouse models of acute cerebral inflammation, chronic cerebral hypoperfusion, atherosclerosis, stroke, myocardial ischemia, Alzheimer's disease, and multiple sclerosis [20].

CEST imaging is a relatively new MRI contrast approach in which exogenous or endogenous compounds containing exchangeable protons are selectively saturated and, after transferring this saturation, indirectly detected through the water signal with enhanced sensitivity [21]. CEST MRI has been used to examine metabolites and tissue pH by endogenous contrast signal enhancement (e.g., amide proton transfer (APT)). pH-weighted MRI was performed after experimental stroke to assess tissue acidosis, showing feasibility to delineate ischemic penumbra [22, 23]. In patients with multiple sclerosis, APT-weighted CEST MRI revealed differences between healthy and degenerated white matter fibers, supporting the potential of this new technology for translation in CNS imaging [24].

Hyperpolarized MRI is a rapidly emerging and developing field of molecular imaging, and new hyperpolarized MRI CAs (e.g., ^{13}C-pyruvate, ^{13}C-lactate, ^{15}N-choline, ^{13}C-glutamine) have been used to monitor metabolic processes in healthy and pathologic CNS [25]. MR imaging following injection of hyperpolarized [1-^{13}C] pyruvate and [2-^{13}C] pyruvate was used to study brain metabolism in rats, by assessing the time courses of lactate and bicarbonate turnover and the transport of pyruvate through the BBB [26]. Quantitative assessment of ^{13}C-bicarbonate in tumor-bearing rat brain was recently performed by measuring the metabolism of pyruvate to acetyl coenzyme A mediated by pyruvate dehydrogenase [27]. The hyperpolarized compound 2-keto[1-^{13}C] isocaproate (KIC) was used to measure the branched-chain aminotransferase (BCAT) activity in the rat brain, a marker of metastatic cancer and a target of the proto-oncogene *c-myc* [28]. A recent clinical trial revealed a safe toxicological profile for [1-^{13}C] pyruvate, showing no dose-limiting toxicity even at the maximum dose of 0.43 mL/kg (230 mM [1-^{13}C] pyruvate) [29].

5.2 Contrast Agents for Nuclear Imaging

Nuclear imaging has gained a pivotal role in neurology since its clinical introduction due to the high sensitivity to detect brain pathologies and to investigate normal physiology and biochemical processes. Currently, the nuclear imaging techniques most often used in preclinical and clinical applications are positron emission tomography (PET) and single-photon emission computed tomography (SPECT), both based on the measurement of gamma-photons derived from the decay of a radioisotope. Therefore, PET or SPECT cameras detect the radioisotopes, which are usually incorporated into a molecule that is metabolically active (e.g., [^{18}F]-FDG for glucose metabolism imaging) or has targeting capabilities

(e.g., [^{68}Ga]-DOTATOC for neuroendocrine tumor imaging). The resulting drug, namely, the radiopharmaceutical, can be used as a contrast agent for nuclear imaging (radiotracer), targeted radiation therapy (radiotherapeutic), or combined diagnosis and treatment (radiotheranostic). Several new radiopharmaceuticals with translational potential have been proposed during the past few years, and some of them have already reached clinical adoption for imaging applications in neurology. For example, for Alzheimer's disease alone, three new PET radiotracers targeting beta-amyloid have been approved by the bureau of Food and Drug Administration (FDA) in the last 3 years (Amyvid, Eli Lilly, 2012; Vizamyl, GE Healthcare, 2013; Neuraceq, Piramal Imaging, 2014) [30]. A detailed review of radiotracers currently used in clinical practice has been reported in other chapters of this book and previously elsewhere [31]. Here, we will examine new radiotracers currently tested in preclinical settings, with particular emphasis on probes undergoing "first-in-human" exploratory trials.

Currently, many promising candidates are challenging the translational pipeline (Table 5.3). [^{18}F]-GE-180 (S-N,N-diethyl-9-(2-fluoroethyl)-5-methoxy 2,3,4,9-tetrahydro-1H-carbazole-4-carboxamide) is a tricyclic compound that binds with high-affinity to the activated glial cells marker translocator protein (TSPO 18 kDa), which dramatically increases after a neural injury [32]. Since neuroinflammation is involved in many neurodegenerative pathologies (e.g., multiple sclerosis, Parkinson's disease, stroke), molecular imaging of reactive glial cells is an important tool for both diagnosis and therapy monitoring with potential widespread diffusion in neurology and neuroscience [37]. [^{18}F]-GE-180 has some advantages compared to the standard TSPO marker [^{11}C]-(R)-PK11195, which has a low target-to-background contrast and low specificity and requires an on-site cyclotron for ^{11}C labeling [38]. In fact, [^{18}F]-GE-180 showed good metabolic stability and higher target uptake and specificity than [^{11}C]-(R)-PK11195 after administration in rats [32]. Moreover, [^{18}F]-GE-180 performed better in micro-PET imaging experiments than [^{11}C]-(R)-PK11195 in a model of LPS-induced neuroinflammation in rats [39] and showed higher ipsilateral TSPO uptake and lower contralateral background noise than [^{11}C]-(R)-PK11195 in a rat stroke model (middle cerebral artery occlusion) [40]. Specificity in vivo was confirmed by ex vivo autoradiography, binding experiments, and immunohistochemical stainings for activated microglia and astrocytes. Finally, a GMP-compliant, automated FASTlab synthesis and radiolabeling procedure has been already established (radiochemical yield 50 %, purity >95 %, specific activity 700–2000 GBq/μmol, high reproducibility across different radiopharmacies), in compliance with clinical human trial requirements [41]. [^{18}F]-GE-180 has already undergone a phase I trial in healthy volunteers and patients with multiple sclerosis (clinical trial code: NCT01738347), and a phase II trial in Alzheimer's disease patients is being planned. [^{124}I]-CLR1404 (18-(p-iodophenyl) octadecyl phosphocholine) is an alkylphosphocholine analog that accumulates in lipid rafts, highly abundant in cancer cells, allowing tumor imaging and therapy (in case of radioiodination with ^{131}I) [33]. Preclinical PET data showed high and selective uptake in a broad range of tumors, including glioblastoma and colon, breast, and pancreatic cancers. Particularly for glioma, [^{124}I]-CLR1404 was found to be more specific for detecting brain lesions than the gold standard [^{18}F]-FDG after administration in patients [33]. In fact, while FDG accumulates also in the normal brain and inflammatory cells, [^{124}I]-CLR1404 levels are high only in cancer cells, drastically increasing target-to-background contrast and therefore specificity of detection. Moreover, after radioiodination with ^{131}I, CLR1404 acts as a potent theranostic agent, showing radiation therapy efficacy in mouse xenograft tumor models [33]. In preclinical models of head and neck human cell-derived xenografts, [^{131}I]-CLR1404 in combination with external beam radiation therapy showed greater efficacy in reducing tumor growth than external radiation alone [42]. In a recent phase I human trial (clinical trial code: NCT00925275), [^{131}I]-CLR1404 administration in solid tumor patients didn't cause any severe

Table 5.3 New radiopharmaceuticals with clinical translation potential

Radiopharmaceutical	Biological target	Application in neurology
[^{18}F]-GE-180 [32]	Translocator protein 18 kDa (TSPO)	Microglia (neuroinflammation)
[^{124}I]-CLR1404 [33]	Cholesterol-rich lipid rafts	Cancer stem cells (glioblastoma)
[^{18}F]-MNI-659 [34]	Phosphodiesterase 10A	Early striatal degeneration (Huntington, Parkinson)
[^{64}Cu]-FBP8 [35]	Fibrin	Thrombosis, thromboembolism (stroke)
[^{11}C]-Martinostat [36]	HDACs 1–3, 6	Epigenetics (neural plasticity, memory, and aging)

adverse health effect and showed high stability of the radiopharmaceutical with no release of the isotope [43]. Dosimetry estimates obtained from SPECT images revealed that after administration of 740 MBq, the bone marrow is the dose-limiting organ (400 mSv). [^{18}F]-MNI-659 (2-(2-(3-(4-(2-fluoroethoxy)phenyl)-7-methyl-4-oxo-3,4-dihydroquinazolin-2-yl)ethyl)-4-isopropoxyisoindoline-1,3-dione) targets phosphodiesterase 10 A, an enzyme catalyzing the production of cyclic AMP, highly abundant in the medium spiny neurons of the corpus striatum [34]. Since medium spiny neuron degeneration is an early event in several human neurodegenerative diseases, including Parkinson and Huntington, [^{18}F]-MNI-659 may have broad applications in neurology [44]. After preclinical validation in nonhuman primates, [^{18}F]-MNI-659 was administered to healthy subjects showing high uptake in the striatum, fast clearance, and favorable dosimetry, with an effective dose of 0.024 mSv/MBq [34]. A subsequent trial in Huntington patients revealed that [^{18}F]-MNI-659 was capable of discriminating between different stages of the pathology, detecting also striatal degeneration in pre-Huntington patients [45]. PET imaging findings were confirmed by neurological assessments, with a strong inverse correlation between uptake and motor deficits. [^{64}Cu]-FBP8 is a short, cyclic peptide (FHC(*L*-4-hydroxyproline)(*L*-3-chlorotyrosine)DLCHIL-para-xylenediamine) conjugated with two NODAGA chelators (1,4,7-triazacyclononane,1-glutaric acid-4,7-acetic acid) that binds with high-affinity (400 nM) to fibrin, the main component of human thrombi [35]. [^{64}Cu]-FBP8 is produced in quantitative radiochemical yield (purity >99 %) with a specific activity of 6–12 GBq/μmol, has high metabolic stability (>90 % intact probe up to 4 h after intravenous administration in rats), has low affinity for fibrinogen and plasma proteins, and is cleared mostly by kidneys (plasma half-life: 14 min), features that make [^{64}Cu]-FBP8 a potential candidate for translation in clinical imaging of thrombosis. Thrombosis is the underlying cause of many cardiovascular diseases, including heart attack, stroke, deep vein thrombosis, and pulmonary embolism, which are leading causes of morbidity and mortality. Current diagnostic strategies rely on imaging modalities that are specific for distinct vascular territories, but a thrombus-specific whole-body imaging approach is still missing. Nonetheless, thromboembolic events such as stroke and pulmonary embolism would benefit from an imaging strategy capable of detecting the source thrombus and the culprit embolus with a single scan. When tested in a rat model of carotid artery thrombosis, [^{64}Cu]-FBP8 showed high target uptake and low off-target background, revealing thrombus location at both early and late time-points with high conspicuity. [^{64}Cu]-FBP7, a close analog of [^{64}Cu]-FBP8, detected extracranial and intracranial emboli in a model of embolic stroke in rats and allowed to visualize and quantify clot busting after administration of the thrombolytic drug recombinant tissue plasminogen activator (rtPA) [46]. A single whole-body PET/MRI scan was sufficient to pinpoint the location of multiple thrombi (carotid artery and femoral vein) after [^{64}Cu]-FBP8 administration in rats, confirming the potential of this new diagnostic strategy to

detect thrombosis in different body parts without the need of multiple examinations that can delay therapeutic interventions [47]. Moreover, probe uptake was greater in younger clots than in older ones and this was consistent with the amount of fibrin in these thrombi, showing that [^{64}Cu]-FBP8-PET may provide insight into clot composition and perhaps guide therapeutic strategies (i.e., thrombolysis vs. thrombectomy). Finally, human dosimetry estimates from rat biodistribution revealed an effective dose of 0.022 mSv/MBq for male and of 0.027 mSv/MBq for female, suggesting a low risk of radiogenic adverse health effects [48]. First-in-human clinical trials are scheduled for early 2016. [^{11}C]-Martinostat ((E)-3-(4-((((3r,5r,7r)-Adamantan-1-ylmethyl)(methyl)amino)methyl)-phenyl)-N-hydroxyacrylamide) is a hydroxamic acid with high brain penetration that targets the epigenetic key-modulator enzymes histone deacetylases (HDACs) [49]. HDACs are a family of enzymes involved in chromatin modification and epigenetic regulation of gene expression. Epigenetic dysregulation is implicated in several neurological and psychiatric conditions including neurodegenerative diseases, brain cancer, addiction, schizophrenia, and depression; therefore, HDAC imaging may be a valuable tool for both diagnosis and therapy monitoring [50]. [^{11}C]-Martinostat showed high target selectivity and nanomolar affinity for HDAC 1–3 and 6 in vitro (binding to recombinant enzyme) and ex vivo (blocking studies via autoradiography on rat brain sections) [49]. In vivo PET imaging conducted on rodents and nonhuman primates (baboons) revealed high brain penetration and target uptake, which was reverted by administration of the nonradioactive analog ^{12}C-Martinostat and the HDACs inhibitor CN54. Pharmacokinetic analyses showed that [^{11}C]-Martinostat has a fast arterial plasma clearance (peak 1 min after intravenous injection) and reaches maximum brain occupancy 20 min postinjection [36]. Volumes of distribution estimated from a two-compartmental model revealed values ranging from 30 to 55 mL/cc, with the highest radioactivity concentrations detected in the cortical regions, cerebellum, basal ganglia, and thalamus. Fast uptake of the probe from the bloodstream, high blood-brain barrier permeability, and slow washout kinetics further support clinical translation of [^{11}C]-Martinostat to quantify HDAC expression in the brain. [^{11}C]-Martinostat is currently being tested in healthy volunteers at Massachusetts General Hospital (Boston, USA).

5.3 Combined Use of MRI Contrast Agents and Radiopharmaceuticals for Hybrid Imaging

Hybrid PET/MR imaging is a tremendous tool for neurologists and neuroscientists to investigate normal physiology and pathologies of the brain. In fact, MRI is the top diagnostic imaging modality to assess brain morphology and FDG-PET represents the most common imaging strategy to evaluate brain metabolism. The clinical introduction of PET/MR integrated scanners has been a game changer in the field of medical imaging, particularly for neurologic applications. In fact, simultaneous MRI and PET acquisition offers several advantages compared to stand-alone modalities by providing complementary information about brain's anatomy, physiology, metabolism, and biochemisty [51, 52]. PET/MRI combines the exquisite anatomic details and high soft tissue contrast of MR with the high-sensitivity and absolute quantitative capabilities of PET, offering several advantages compared to the two modalities individually. Compared to PET/CT, the gold standard in clinical practice, PET/MRI exposes the patients to lower radiation risks (>50 % less ionizing radiation); has better tissue-to-noise contrast in the abdomen, pelvis, and brain; and can take advantage of several MR sequences and contrast media that may facilitate diagnosis and therapeutic choice [53]. Unlike hybrid PET/CT, PET/MRI can be performed simultaneously, offering spatial and temporal correlation of both signals and dynamic contrast enhancement. In clinical practice, PET/MR imaging using radiopharmaceuticals and MRI sequences without contrast media

enhancement has been gaining an important role for investigating and diagnosing brain pathologies [54]. For dementia imaging (e.g., Alzheimer's disease, mild cognitive impairments), PET may be used to assess hypometabolism (e.g., [^{18}F]-FDG) and amyloid deposition (e.g., [^{11}C]-Pittsburgh compound B, [^{18}F]-Florbetapir), while MR sequences can provide anatomical information on brain atrophy (T1/T2), white matter abnormalities (DTI), and cerebral perfusion and blood flow (ASL) [55]. For Parkinson's disease, dopaminergic system dysregulation can be imaged using [^{18}F]-DOPA or [^{11}C]-Raclopride (receptor agonist and antagonist, respectively), and [^{18}F]-FP/CIT (presynaptic dopamine transporter), while striatal increase of water diffusion (DWI) and iron accumulation (T2w, T2*) are MR markers of neuronal degeneration. Neuropathic pain can be evaluated by targeting the opioid system ([^{11}C]-Diprenorphine) and assessing functional hemodynamic response (fMRI) elicited by painful stimuli [56]. Thus, PET/MR imaging workup is now well consolidated and suited for longitudinal studies to examine the change of dynamic biomarkers and monitor disease progression. As an example, a recent 10-year long trial conducted on Alzheimer's disease patients showed that distinct phases of the pathology can be efficiently imaged using PET/MR biomarkers [57], providing information relevant not only to assess disease progression but also to monitor therapeutic efficacy. Differently, the combined use of PET radiopharmaceuticals and MR contrast agents is still limited, and just few examples can be found in recent clinical and basic science studies. Two recent clinical trials on glioma patients revealed good correlation between tumor metabolism ([^{18}F]-FET, amino acid metabolism) and blood volume (gadolinium-enhanced MRI) but poor colocalization between highly perfused and hypermetabolic areas [58, 59], providing complementary information about tumor heterogeneity. Another application of contrast-enhanced PET/MRI in neuro-oncology is the evaluation of blood-brain barrier disruption and metabolism. Larson and colleagues showed that multiparametric DCE-MRI and [^{18}F]-FDG-PET may help to discriminate tumor recurrences from radiation damage [60]. In fact, while recurrences are characterized by high [^{18}F]-FDG uptake and altered permeability due to blood-brain barrier disruption, areas with low metabolism but high permeability may be suggestive of lesions induced by radiation injury. In the preclinical field, molecular MRI using USPIO particles and [^{11}C]-PK11195 PET were used to image chronic neuroinflammation after experimental stroke in rats [61]. USPIO imaging shows areas with high phagocytic activity (i.e., macrophages), while [^{11}C]-PK11195 is a marker of activated glial cells (microglia and astrocytes). Multimodal analysis revealed that phagocytic activity (USPIO positive) was associated with tissue necrosis while tissue displaying only non-phagocytic inflammation ([^{11}C]-PK11195-positive) remained viable for several weeks after the onset, revealing diagnostic potential for this strategy to predict long-term tissue outcome after stroke. In a rat model of glioblastoma, sequential PET/MRI was used to visualize tumor metabolism ([^{18}F]-FDG), hypoxia ([^{18}F]-FAZA), and morphology (gadolinium-DTPA) [62]. Multiparametric imaging results were confirmed by ex vivo assessments, showing the feasibility of this multimodal approach to investigate non-invasively tumor biology. Another potential PET/MRI application involves the use of dual, bimodal probes targeting the same molecular moiety. Uppal and colleagues pioneered this methodology by labeling the MR fibrin-binding probe EP-2104R with ^{64}Cu [63]. The resulting dual fibrin-targeting probe showed good feasibility to detect arterial clots after experimental thromboembolism in rat, allowing simultaneous PET/MR molecular imaging of thrombosis. Lewis and collaborators developed a manganese-based dual-modality reporter gene to track stem cell trafficking in the brain [64]. Manganese-enhanced MRI successfully revealed the location of stem cells transplanted in the rat's brain, but authors found low PET [55] Mn uptake, detectable only by high-sensitivity ex vivo autoradiography. In summary, combined,

contrast-enhanced molecular PET/MRI is still a young technology that has been mainly used in neurology to assess tumor perfusion and metabolism. Targeted neuro PET/MR imaging is still mainly limited to PET tracers, while molecular MR imaging has not been implemented for patient imaging yet. Further studies are needed to fully exploit the diagnostic potential of combined molecular PET/MRI.

5.4 Final Remarks

Contrast media have gained a fundamental role in diagnostic imaging because of their ability to enhance radiological images and to provide multiparametric information about physiology, metabolism, and molecular targets. Contrast agents for magnetic resonance and nuclear imaging are indispensable tools for radiological assessments, and their use is increasing exponentially together with the diffusion of new diagnostic strategies and technologies. Although there have been terrific advancements in the field over the past 30 years, chemists and molecular imagers still have to face several challenges to improve the perks and to limit some of the pitfalls of contrast media [65]. Because of the inherent limited sensitivity of MR imaging, grams of contrast agents are usually administered to patients, raising potential toxicity risks. New gadolinium- and iron-loaded nanosystems, manganese-based agents, CEST and hyperpolarized probes, and new ^{19}F carriers may increase MR sensitivity and limit toxicity-related drawbacks. On the other side, potential radiogenic adverse effects always need to be taken into account for nuclear imaging probes, especially for those agents labeled with long-lived isotopes. The development of radiopharmaceuticals with improved pharmacokinetics and radiation dosimetry will be pivotal to support the diffusion of new nuclear imaging strategies. Finally, the design of specific combinations of magnetic resonance and nuclear imaging contrast agents for multimodal assessments (e.g., PET/MRI) may contribute to the diffusion in clinical practice of new diagnostic, molecular imaging approaches.

Acknowledgments Dr. Aime acknowledges MIUR (PRIN 2012SK7ASN) and AIRC (Investigator Grant IG 14565) for research support.

References

1. Weissleder R, Mahmood U (2001) Molecular imaging. Radiology 219:316–333
2. Bauer WM, Fenzl G, Vogl T, Fink U, Lissner J (1988) Indications for the use of Gd-Dtpa in Mri of the central nervous system – experiences in patients with cerebral and spinal-diseases. Invest Radiol 23:S286–S288
3. Aime S, Botta M, Fasano M, Terreno E (1998) Lanthanide(III) chelates for NMR biomedical applications. Chem Soc Rev 27:19–29
4. Caravan P, Ellison JJ, McMurry TJ, Lauffer RB (1999) Gadolinium(III) chelates as MRI contrast agents: structure, dynamics, and applications. Chem Rev 99:2293–2352
5. Idee JM, Port M, Robic C, Medina C, Sabatou M, Corot C (2009) Role of thermodynamic and kinetic parameters in gadolinium chelate stability. J Magn Reson Imaging 30:1249–1258
6. Giesel FL, Mehndiratta A, Essig M (2010) High-relaxivity contrast-enhanced magnetic resonance neuroimaging: a review. Eur Radiol 20:2461–2474
7. Bendszus M, Ladewig G, Jestaedt L, Misselwitz B, Solymosi L, Toyka K, Stoll G (2008) Gadofluorine M enhancement allows more sensitive detection of inflammatory CNS lesions than T2-w imaging: a quantitative MRI study. Brain 131:2341–2352
8. Le Duc G, Roux S, Paruta-Tuarez A, Dufort S, Brauer E, Marais A, Truillet C, Sancey L, Perriat P, Lux F, Tillement O (2014) Advantages of gadolinium based ultrasmall nanoparticles vs molecular gadolinium chelates for radiotherapy guided by MRI for glioma treatment. Cancer Nanotechnol 5:4
9. Essig M, Nikolaou K, Meaney JF (2007) Magnetic resonance angiography of the head and neck vessels. Eur Radiol 17(Suppl 2):B30–B37
10. Chen JW, Breckwoldt MO, Aikawa E, Chiang G, Weissleder R (2008) Myeloperoxidase-targeted imaging of active inflammatory lesions in murine experimental autoimmune encephalomyelitis. Brain 131:1123–1133
11. Breckwoldt MO, Chen JW, Stangenberg L, Aikawa E, Rodriguez E, Qiu S, Moskowitz MA, Weissleder R (2008) Tracking the inflammatory response in stroke in vivo by sensing the enzyme myeloperoxidase. Proc Natl Acad Sci U S A 105:18584–18589
12. Forghani R, Wojtkiewicz GR, Zhang YN et al (2012) Demyelinating diseases: myeloperoxidase as an imaging biomarker and therapeutic target. Radiology 263:451–460
13. Weinstein JS, Varallyay CG, Dosa E, Gahramanov S, Hamilton B, Rooney WD, Muldoon LL, Neuwelt EA (2010) Superparamagnetic iron oxide nanoparticles: diagnostic magnetic resonance imaging and potential

therapeutic applications in neurooncology and central nervous system inflammatory pathologies, a review. J Cereb Blood Flow Metab 30:15–35
14. Saleh A, Schroeter M, Ringelstein A, Hartung HP, Siebler M, Modder U, Jander S (2007) Iron oxide particle-enhanced MRI suggests variability of brain inflammation at early stages after ischemic stroke. Stroke 38:2733–2737
15. Vellinga MM, Engberink RDO, Seewann A, Pouwels PJW, Wattjes MP, van der Pol SMA, Pering C, Polman CH, de Vries HE, Geurts JJG, Barkhof F (2008) Pluriformity of inflammation in multiple sclerosis shown by ultra-small iron oxide particle enhancement. Brain 131:800–807
16. Farrell BT, Hamilton BE, Dosa E, Rimely E, Nasseri M, Gahramanov S, Lacy CA, Frenkel EP, Doolittle ND, Jacobs PM, Neuwelt EA (2013) Using iron oxide nanoparticles to diagnose CNS inflammatory diseases and PCNSL. Neurology 81:256–263
17. Dousset V, Brochet B, Deloire MSA, Lagoarde L, Barroso B, Caille JM, Petry KG (2006) MR imaging of relapsing multiple sclerosis patients using ultra-small-particle iron oxide and compared with gadolinium. Am J Neuroradiol 27:1000–1005
18. Michalska M, Machtoub L, Manthey HD, Bauer E, Herold V, Krohne G, Lykowsky G, Hildenbrand M, Kampf T, Jakob P, Zernecke A, Bauer WR (2012) Visualization of vascular inflammation in the atherosclerotic mouse by ultrasmall superparamagnetic iron oxide vascular cell adhesion molecule-1-specific nanoparticles. Arterioscler Thromb Vasc Biol 32:2350–2357
19. Frechou M, Beray-Berthat V, Raynaud JS, Meriaux S, Gombert F, Lancelot E, Plotkine M, Marchand-Leroux C, Ballet S, Robert P, Louin G, Margaill I (2013) Detection of vascular cell adhesion molecule-1 expression with USPIO-enhanced molecular MRI in a mouse model of cerebral ischemia. Contrast Media Mol Imaging 8:157–164
20. Montagne A, Gauberti M, Macrez R, Jullienne A, Briens A, Raynaud JS, Louin G, Buisson A, Haelewyn B, Docagne F, Defer G, Vivien D, Maubert E (2012) Ultra-sensitive molecular MRI of cerebrovascular cell activation enables early detection of chronic central nervous system disorders. Neuroimage 63:760–770
21. Guivel-Scharen V, Sinnwell T, Wolff SD, Balaban RS (1998) Detection of proton chemical exchange between metabolites and water in biological tissues. J Magn Reson 133:36–45
22. Sun PZ, Benner T, Copen WA, Sorensen AG (2010) Early experience of translating pH-weighted MRI to image human subjects at 3 Tesla. Stroke 41:S147–S151
23. McVicar N, Li AX, Goncalves DF, Bellyou M, Meakin SO, Prado MA, Bartha R (2014) Quantitative tissue pH measurement during cerebral ischemia using amine and amide concentration-independent detection (AACID) with MRI. J Cereb Blood Flow Metab 34:690–698
24. Dula AN, Asche EM, Landman BA, Welch EB, Pawate S, Sriram S, Gore JC, Smith SA (2011) Development of chemical exchange saturation transfer at 7 T. Magn Reson Med 66:831–838
25. Ross BD, Bhattacharya P, Wagner S, Tran T, Sailasuta N (2010) Hyperpolarized MR imaging: neurologic applications of hyperpolarized metabolism. Am J Neuroradiol 31:24–33
26. Marjanska M, Iltis I, Shestov AA, Deelchand DK, Nelson C, Ugurbil K, Henry PG (2010) In vivo 13C spectroscopy in the rat brain using hyperpolarized [1-(13)C]pyruvate and [2-(13)C]pyruvate. J Magn Reson 206:210–218
27. Park JM, Recht LD, Josan S, Merchant M, Jang T, Yen YF, Hurd RE, Spielman DM, Mayer D (2013) Metabolic response of glioma to dichloroacetate measured in vivo by hyperpolarized (13)C magnetic resonance spectroscopic imaging. Neuro Oncol 15:433–441
28. Karlsson M, Jensen PR, in 't Zandt R, Gisselsson A, Hansson G, Duus JO, Meier S, Lerche MH (2010) Imaging of branched chain amino acid metabolism in tumors with hyperpolarized 13C ketoisocaproate. Int J Cancer 127:729–736
29. Nelson SJ, Kurhanewicz J, Vigneron DB et al (2013) Metabolic imaging of patients with prostate cancer using hyperpolarized [1-(13)C]pyruvate. Sci Transl Med 5:198ra108
30. Sabri O, Seibyl J, Rowe C, Barthel H (2015) Beta-amyloid imaging with florbetaben. Clin Transl Imaging 3:13–26
31. Dierckx RA, Otte A, de Vries EFJ, van Waarde A, Leenders KL (2014) PET and SPECT in neurology. Springer, Berlin
32. Wadsworth H, Jones PA, Chau WF et al (2012) [18F]-GE-180: a novel fluorine-18 labelled PET tracer for imaging translocator protein 18 kDa (TSPO). Bioorg Med Chem Lett 22:1308–1313
33. Weichert JP, Clark PA, Kandela IK et al (2014) Alkylphosphocholine analogs for broad-spectrum cancer imaging and therapy. Sci Transl Med 6:240ra275
34. Barret O, Thomae D, Tavares A, Alagille D, Papin C, Waterhouse R, McCarthy T, Jennings D, Marek K, Russell D, Seibyl J, Tamagnan G (2014) In vivo assessment and dosimetry of 2 novel PDE10A PET radiotracers in humans: [18F]-MNI-659 and [18F]-MNI-654. J Nucl Med 55:1297–1304
35. Blasi F, Oliveira BL, Rietz TA, Rotile NJ, Day H, Looby RJ, Ay I, Caravan P (2014) Effect of chelate type and radioisotope on the imaging efficacy of 4 fibrin-specific PET probes. J Nucl Med 55:1157–1163
36. Wey HY, Wang C, Schroeder FA, Logan J, Price JC, Hooker JM (2015) Kinetic analysis and quantification of [11C]-Martinostat for in vivo HDAC imaging of the brain. ACS Chem Neurosci 6:708–715
37. Prinz M, Priller J (2014) Microglia and brain macrophages in the molecular age: from origin to neuropsychiatric disease. Nat Rev Neurosci 15:300–312
38. Chauveau F, Boutin H, Van Camp N, Dolle F, Tavitian B (2008) Nuclear imaging of neuroinflammation: a comprehensive review of [11C]-PK11195 challengers. Eur J Nucl Med Mol Imaging 35:2304–2319
39. Dickens AM, Vainio S, Marjamaki P, Johansson J, Lehtiniemi P, Rokka J, Rinne J, Solin O, Haaparanta-Solin M, Jones PA, Trigg W, Anthony DC, Airas L

(2014) Detection of microglial activation in an acute model of neuroinflammation using PET and radiotracers [11C]-(R)-PK11195 and [18F]-GE-180. J Nucl Med 55:466–472
40. Boutin H, Murray K, Pradillo J, Maroy R, Smigova A, Gerhard A, Jones PA, Trigg W (2015) [18F]-GE-180: a novel TSPO radiotracer compared to [11C]-R-PK11195 in a preclinical model of stroke. Eur J Nucl Med Mol Imaging 42:503–511
41. Wickstrom T, Clarke A, Gausemel I, Horn E, Jorgensen K, Khan I, Mantzilas D, Rajanayagam T, in 't Veld DJ, Trigg W (2014) The development of an automated and GMP compliant FASTlab Synthesis of [18F]GE-180; a radiotracer for imaging translocator protein (TSPO). J Labelled Comp Radiopharm 57:42–48
42. Morris ZS, Weichert JP, Saker J, Armstrong EA, Besemer A, Bednarz B, Kimple RJ, Harari PM (2015) Therapeutic combination of radiolabeled CLR1404 with external beam radiation in head and neck cancer model systems. Radiother Oncol 116:504–509
43. Grudzinski JJ, Titz B, Kozak K, Clarke W, Allen E, Trembath L, Stabin M, Marshall J, Cho SY, Wong TZ, Mortimer J, Weichert JP (2014) A phase 1 study of [131I]-CLR1404 in patients with relapsed or refractory advanced solid tumors: dosimetry, biodistribution, pharmacokinetics, and safety. PLoS One 9:e111652
44. Reiner A, Albin RL, Anderson KD, D'Amato CJ, Penney JB, Young AB (1988) Differential loss of striatal projection neurons in Huntington disease. Proc Natl Acad Sci U S A 85:5733–5737
45. Russell DS, Barret O, Jennings DL, Friedman JH, Tamagnan GD, Thomae D, Alagille D, Morley TJ, Papin C, Papapetropoulos S, Waterhouse RN, Seibyl JP, Marek KL (2014) The phosphodiesterase 10 positron emission tomography tracer, [18F]-MNI-659, as a novel biomarker for early Huntington disease. JAMA Neurol 71:1520–1528
46. Ay I, Blasi F, Rietz TA, Rotile NJ, Kura S, Brownell AL, Day H, Oliveira BL, Looby RJ, Caravan P (2014) In vivo molecular imaging of thrombosis and thrombolysis using a fibrin-binding positron emission tomographic probe. Circ Cardiovasc Imaging 7:697–705
47. Blasi F, Oliveira BL, Rietz TA, Rotile NJ, Naha PC, Cormode DP, Izquierdo-Garcia D, Catana C, Caravan P (2015) Multisite thrombus imaging and fibrin content estimation with a single whole-body PET scan in rats. Arterioscler Thromb Vasc Biol 35:2114–2121
48. Blasi F, Oliveira BL, Rietz TA, Rotile NJ, Day H, Naha PC, Cormode DP, Izquierdo-Garcia D, Catana C, Caravan P (2015) Radiation dosimetry of the fibrin-binding probe 64Cu-FBP8 and its feasibility for PET imaging of deep vein thrombosis and pulmonary embolism in rats. J Nucl Med 56:1088–1093
49. Wang C, Schroeder FA, Wey HY, Borra R, Wagner FF, Reis S, Kim SW, Holson EB, Haggarty SJ, Hooker JM (2014) In vivo imaging of histone deacetylases (HDACs) in the central nervous system and major peripheral organs. J Med Chem 57:7999–8009
50. Wang C, Schroeder FA, Hooker JM (2014) Visualizing epigenetics: current advances and advantages in HDAC PET imaging techniques. Neuroscience 264:186–197
51. Catana C, Drzezga A, Heiss WD, Rosen BR (2012) PET/MRI for neurologic applications. J Nucl Med 53:1916–1925
52. Drzezga A, Barthel H, Minoshima S, Sabri O (2014) Potential clinical applications of PET/MR imaging in neurodegenerative diseases. J Nucl Med 55:47S–55S
53. Catana C, Guimaraes AR, Rosen BR (2013) PET and MR imaging: the odd couple or a match made in heaven? J Nucl Med 54:815–824
54. Werner P, Barthel H, Drzezga A, Sabri O (2015) Current status and future role of brain PET/MRI in clinical and research settings. Eur J Nucl Med Mol Imaging 42:512–526
55. Besson FL, La Joie R, Doeuvre L, Gaubert M, Mezenge F, Egret S, Landeau B, Barre L, Abbas A, Ibazizene M, de La Sayette V, Desgranges B, Eustache F, Chetelat G (2015) Cognitive and brain profiles associated with current neuroimaging biomarkers of preclinical Alzheimer's disease. J Neurosci 35:10402–10411
56. Wey HY, Catana C, Hooker JM, Dougherty DD, Knudsen GM, Wang DJ, Chonde DB, Rosen BR, Gollub RL, Kong J (2014) Simultaneous fMRI-PET of the opioidergic pain system in human brain. Neuroimage 102(Pt 2):275–282
57. Yau WY, Tudorascu DL, McDade EM et al (2015) Longitudinal assessment of neuroimaging and clinical markers in autosomal dominant Alzheimer's disease: a prospective cohort study. Lancet Neurol 14:804–813
58. Filss CP, Galldiks N, Stoffels G, Sabel M, Wittsack HJ, Turowski B, Antoch G, Zhang K, Fink GR, Coenen HH, Shah NJ, Herzog H, Langen KJ (2014) Comparison of [18F]-FET PET and perfusion-weighted MR imaging: a PET/MR imaging hybrid study in patients with brain tumors. J Nucl Med 55:540–545
59. Henriksen OM, Larsen VA, Muhic A, Hansen AE, Larsson HB, Poulsen HS, Law I (2015) Simultaneous evaluation of brain tumour metabolism, structure and blood volume using [18F]-fluoroethyltyrosine (FET) PET/MRI: feasibility, agreement and initial experience. Eur J Nucl Med Mol Imaging 43(1): 103–112
60. Larsen VA, Simonsen HJ, Law I, Larsson HB, Hansen AE (2013) Evaluation of dynamic contrast-enhanced T1-weighted perfusion MRI in the differentiation of tumor recurrence from radiation necrosis. Neuroradiology 55:361–369
61. Walter HL, Walberer M, Rueger MA, Backes H, Wiedermann D, Hoehn M, Neumaier B, Graf R, Fink GR, Schroeter M (2015) In vivo analysis of neuroinflammation in the late chronic phase after experimental stroke. Neuroscience 292:71–80
62. Belloli S, Brioschi A, Politi LS, Ronchetti F, Calderoni S, Raccagni I, Pagani A, Monterisi C, Zenga F, Zara G,

Fazio F, Mauro A, Moresco RM (2013) Characterization of biological features of a rat F98 GBM model: a PET-MRI study with [18F]-FAZA and [18F]-FDG. Nucl Med Biol 40:831–840

63. Uppal R, Catana C, Ay I, Benner T, Sorensen AG, Caravan P (2011) Bimodal thrombus imaging: simultaneous PET/MR imaging with a fibrin-targeted dual PET/MR probe–feasibility study in rat model. Radiology 258:812–820
64. Lewis CM, Graves SA, Hernandez R, Valdovinos HF, Barnhart TE, Cai W, Meyerand ME, Nickles RJ, Suzuki M (2015) 52Mn production for PET/MRI tracking of human stem cells expressing divalent metal transporter 1 (DMT1). Theranostics 5:227–239
65. Terreno E, Castelli DD, Viale A, Aime S (2010) Challenges for molecular magnetic resonance imaging. Chem Rev 110:3019–3042

Part II

Most Frequent Clinical Applications

FDG-PET in Dementia

6

Marco Aiello, Carlo Cavaliere, M. Inglese, S. Monti, and Marco Salvatore

6.1 Neuropathology of Dementia

The word "dementia" derives from the Latin "de mens," meaning "without mind." This condition is referred to a wide spectrum of symptoms encompassing for memory impairment, personality changes, and emotive dysregulation [1]. For the majority of these cases (about 6–7 % in people aged 65 years and older) [2], the etiology and pathogenesis are not fully recognized.

Although clinical cognitive assessment represents the first and crucial step in the diagnostic patient's workflow, neuropathological examination is needed to characterize dementia subtypes, representing the "gold standard" in dementia diagnostics. This approach consists in a macro- and microscopic investigation of the brain post-mortem, although brain biopsy from a living patient can be considered a possible alternative, even if not justified in terms of risk/effectiveness [3].

Brain tissues can be stained with conventional (such as hematoxylin-eosin, Congo red, or different silver stains) and immunohistochemical (IHC) procedures. By IHC, specific abnormally configured proteins (e.g., tau, β-amyloid, α-synuclein, ubiquitin, transactivation-responsive DNA-binding protein 43 (TDP-43), or fused in sarcoma (FUS)) can be easily visualized and used as marker of dementia subtypes, grouped according to it, in "tauopathies," "synucleinopathies," "TDP-43 proteinopathies," and "FUS proteinopathies" [4–6] (see Table 6.1 for further details).

6.2 The Neuropathology of Alzheimer Disease

Typical macroscopic findings are represented by symmetric and diffuse cortical atrophy with ventricle enlargement. Depigmentation of the noradrenaline-producing pontine nucleus locus coeruleus (LC) is also frequently observed. Neurodegeneration spreads from the medial temporal lobe, containing the hippocampus and entorhinal cortex, and early involved by Alzheimer disease (AD) progression, to the temporal, the parietal, and eventually the occipital and frontal lobes in cases with a more severe impairment [7].

Typical microscopic findings are represented by neurofibrillary tangle (NFT) and neuritic plaque (NP) and in more severe cases by cortical neuronal loss and gliosis. These histological alterations are generally stained by IHC for hyperphosphorylated tau and β-amyloid aggregations.

M. Aiello (✉) • C. Cavaliere • M. Inglese
S. Monti • M. Salvatore
IRCCS SDN, Istituto Ricerca Diagnostica Nucleare,
Via E. Gianturco 113, Naples, Italy
e-mail: maiello@sdn-napoli.it

A. Ciarmiello, L. Mansi (eds.), *PET-CT and PET-MRI in Neurology*,
DOI 10.1007/978-3-319-31614-7_6

Table 6.1 Molecular features of dementias

Marker	Histological alteration	Pathology
Tau	Neurofibrillary tangle (NFT) and neuritic plaques (NP)	Alzheimer disease (AD) Frontotemporal lobar degeneration (FTLD) variants, including Pick's disease (PiD), corticobasal degeneration (CBD), and progressive supranuclear palsy (PSP)
β-Amyloid	NP cores and in small-vessel walls	Alzheimer disease (AD) Cerebral amyloid angiopathy (CAA)
α-Synuclein	Lewy bodies (LB) and Lewy neurites	Parkinson's disease (PD) Lewy body disease (LBD) Multiple system atrophy (MSA)
Ubiquitin/p62	NFT, NP, LB	Tau-negative FTLD Amyotrophic lateral sclerosis (ALS)
TDP-43	Ubiquitin/p62-positive intracellular inclusions	Tau-negative FTLD Amyotrophic lateral sclerosis (ALS)
FUS	Intracellular inclusions	FTLD variants

Few neuropathological systems are commonly used for AD staging, based on the topographic distribution of the microscopic lesions [8, 9], the semiquantitative assessment of NP frequency [10], or a combination of Braak and Consortium to Establish a Registry for Alzheimer's Disease (CERAD) grading scores, resulting in a likelihood rating for AD [11].

6.3 The Neuropathology of Vascular Dementia

Vascular dementia (VaD) is a heterogeneous condition that includes different forms depending from the vessel diameter (large- or small-vessel variants) or the pathogenetic mechanism (e.g., hypoxic hypoperfusion) determining vascular injury. Strategically located infarcts, like in thalamus or hippocampus, can determine cognitive impairment, not strictly dependent by the lesion size.

Due to high heterogeneity of histological alterations, no consensus statements exist for neuropathological staging systems in VaD.

6.4 The Neuropathology of Lewy Body Disease

Two major forms of Lewy body disease (LBD) exist: "dementia with Lewy bodies" (DLB) and "Parkinson's disease with dementia" (PDD). These subtypes are both macroscopically characterized by mild cortical atrophy, mainly in the frontal lobes, and by depigmentation of the LC and the substantia nigra and differentiated by parkinsonism symptoms.

Microscopically, the peculiar lesion is represented by Lewy body (LB) inclusions, positive-stained with α-synuclein antibodies. LB alterations early involve brainstem to spread in more severe cases to limbic structures and the neocortex.

Two neuropathological staging systems are commonly used for LBD: CDLB05 [12] and Braak PD system [13]. The former, divided in four stages, is a semiquantitative assessment that takes into account spatial distribution of Lewy-related pathology (no LBD, brainstem-predominant, limbic/transitional, or diffuse neocortical LBD). The latter, based on the topographic distribution of Lewy-related pathology, stratifies LBD patients in seven stages, 0 to six.

6.5 The Neuropathology of Frontotemporal Lobar Degeneration

Frontotemporal lobar degeneration (FTLD) is a heterogeneous group of pathologies, communed by macroscopic frontal and/or temporal lobe atrophy and microscopic neuronal loss and

gliosis [7]. According to IHC staining, FTLD subtypes may be divided into "tauopathies," "TDP-43 proteinopathies," "FUS proteinopathies," and other minor forms. Also in this case, due to high heterogeneity of FTLD family, no consensus statements exist for neuropathological staging systems.

6.6 FDG-PET Applications and Findings in Dementia

Positron emission tomography (PET) with 2-[fluorine-18]fluoro-2-deoxy-d-glucose (FDG) is a highly useful imaging modality for the diagnosis of neurodegenerative disorders [14–19]. FDG is an analog of glucose, the main energy substrate of the brain. After uptake and phosphorylation by hexokinase, FDG becomes trapped in neurons, allowing imaging and measurement of the cerebral metabolic rate for glucose, which is closely related to neuronal and synaptic function [14–16]. Characteristic patterns of altered metabolism seen at fluorodeoxyglucose-PET (FDG-PET) can markedly improve the clinical diagnosis for specific types of dementia such as frontotemporal dementia (FTD), AD, and DLB, each of which has characteristic metabolic signatures, although there is some overlap. After performing anatomic imaging concurrently with biochemical and laboratory investigations to exclude secondary causes, FDG-PET is the most widely available and useful biomarker to detect early neurodegenerative dementia, differentiate neurodegenerative dementias [20], or suggest comorbidity of other neurodegenerative diseases identifying the cause of cognitive impairment.

In healthy subjects, the most intense FDG uptake occurs in the subcortical putamen, caudate nucleus, and thalamus, followed by high uptake in the cortical gray matter. The globus pallidus typically demonstrates mild uptake, and the white matter is relatively photopenic. In the workup of patient with dementia, two key structures should be actively sought and evaluated: the cingulate gyrus and the overlying precuneus cortex. However, it is important to review the anatomic images before interpreting the PET study. Structural lesions may confound the interpretation; hence, proper inspection of the anatomic images will prevent false-positive errors, while in the absence of anatomic structural changes, the risk of false-positive is low and FDG-PEt allows early and differential diagnosis among neurodegenerative dementia.

A small study in which 14 AD patients were compared with 16 mild cognitive impairment (MCI) patients found that the former group had reduced cerebral glucose metabolism in the posterior cingulate cortex, precuneus, and inferior parietal and middle temporal lobes, whereas in MCI patients, hypometabolism occurred only in the posterior cingulate gyrus [21].

In one multicenter study, 548 elderly subjects—including 110 healthy subjects—underwent FDG-PET. Disease-specific patterns allowed correct classification in 95 % of patients with AD, 92 % of patients with DLB, 94 % of patients with FTD, and 94 % of healthy subjects [22].

A meta-analysis of 24 studies involving 1112 patients confirmed the ability of FDG-PET to help predict the conversion of MCI to Alzheimer disease [23]. FDG-PET can depict glucose metabolic changes that not only precede but also exceed the degree of atrophy as determined with volumetric MR imaging, including voxel-based morphometry [24, 25].

In the following, the characteristic metabolic patterns observed in various cases of dementia will be reviewed.

6.7 Alzheimer Disease

AD is the most common cause of dementia and FDG-PET plays an important role as biomarker since it is described as a "neuronal injury" biomarker [26, 27]. The earliest changes of hypometabolism are often seen in the posterior cingulate gyrus [28]. The classic pattern of impaired metabolism consists of involvement of the posterior cingulate gyri, precuneus, and posterior temporal and parietal lobes [29–33]. With respect to the two hemispheres, involvement may be asymmetric or unilateral; when interhemispheric asymmetry is present, its direction

is consistent across all involved regions. In addition, in nearly all cases, the posterior cingulate gyrus is preferentially involved [34, 35]. In moderate-to-severe stages of AD, hypometabolism spreads to the prefrontal association cortices and there may be frontal lobe involvement, but the anterior cingulate gyrus is spared and the metabolism in the basal ganglia, thalamus, primary sensorimotor cortices, posterior fossa, and cerebellum is relatively preserved despite disease progression. Because the magnitude of glucose metabolic reduction in the medial temporal lobe, including the hippocampus, is not as large as that in the posterior temporal or posterior cingulate cortices, a decrease in hippocampal glucose metabolism with progression from mild-to-moderate-stage AD is not usually demonstrated [36] despite obvious hippocampal atrophy at the early stage.

FDG-PET studies of AD dementia can be aimed not only at improving diagnosis, prognostic assessment, and/or therapeutic management of the disease but also at elucidating neurological substrates, either of fundamental pathophysiology or of associations observed between disease and genetic or environmental factors [37]. Using PET to assess cerebral glucose metabolism, Alexander at al. [38] compared AD patients matched for demographic characteristics and dementia severity but differing in estimated pre-AD intellectual ability, as defined by demographic-based intelligent quotient (IQ) estimates, as well as by performance on a test of reading words: they found that estimated IQs were inversely correlated with cerebral metabolism in the prefrontal, premotor, and left superior parietal regions. Figure 6.1 shows PET/MR images depicting the progression of temporal atrophy and hypometabolism at different stages of cognitive impairment. Also, genetic risk factor has been identified: the apolipoprotein E gene (APOE) is a risk factor for late-onset AD, while the APOE ε4 allele [39] increases the risk and decreases the average age of dementia onset. Patients with early-onset AD who were APOE ε4-positive showed a significant decrease in glucose metabolism in the medial temporal lobe compared with patients with APOE ε4-negative AD [40]. By contrast, in the late-onset group, there were no differences in the glucose metabolic reduction patterns between patients with APOE ε4-positive and APOE ε4-negative AD. These findings suggest that the APOE genotype has a differential effect on the distribution of glucose metabolism.

6.8 Dementia with Lewy Bodies

DLB is the second most common neurodegenerative disorder in patients over 65 years of age and manifests with a pattern of bilateral parietal and posterior temporal hypometabolism and posterior cingulate gyral hypometabolism similar to that seen in Alzheimer disease [41–43]. However, there can also be associated involvement of the occipital lobes, which are spared in Alzheimer disease [44–46]. If the occipital cortex is not involved, AD and DLB cannot be distinguished on the basis of their FDG metabolic signatures. These findings are also seen in patients with Parkinson's disease (PD) and PD with dementia [47] because DLB and PD with dementia are in the same disease entity, involving spread of Lewy bodies in the cerebral cortices: in this case, the differential diagnosis can be made through clinical symptoms that are slightly different.

6.9 Frontotemporal Lobe Degeneration

Frontotemporal lobe degeneration is a heterogeneous group of diseases involving frontal and/or anterior temporal lobe degeneration and associated dementia. Frontotemporal lobe degeneration includes FTD, semantic dementia, and progressive nonfluent aphasia. In FTD, frontal and anterior temporal glucose metabolism is decreased, though the medial temporal region and the subcortical structures, including the striatum and thalamus, are also affected [48]. Metabolic and atrophic changes occur in the bilateral frontal and temporal lobes, whereas the affected regions of metabolism are larger and more severe than those of atrophy in the frontal lobe [49]. In patients with semantic dementia, asymmetrically severely decreased temporal metabolism can be demonstrated on FDG-PET images. These areas can

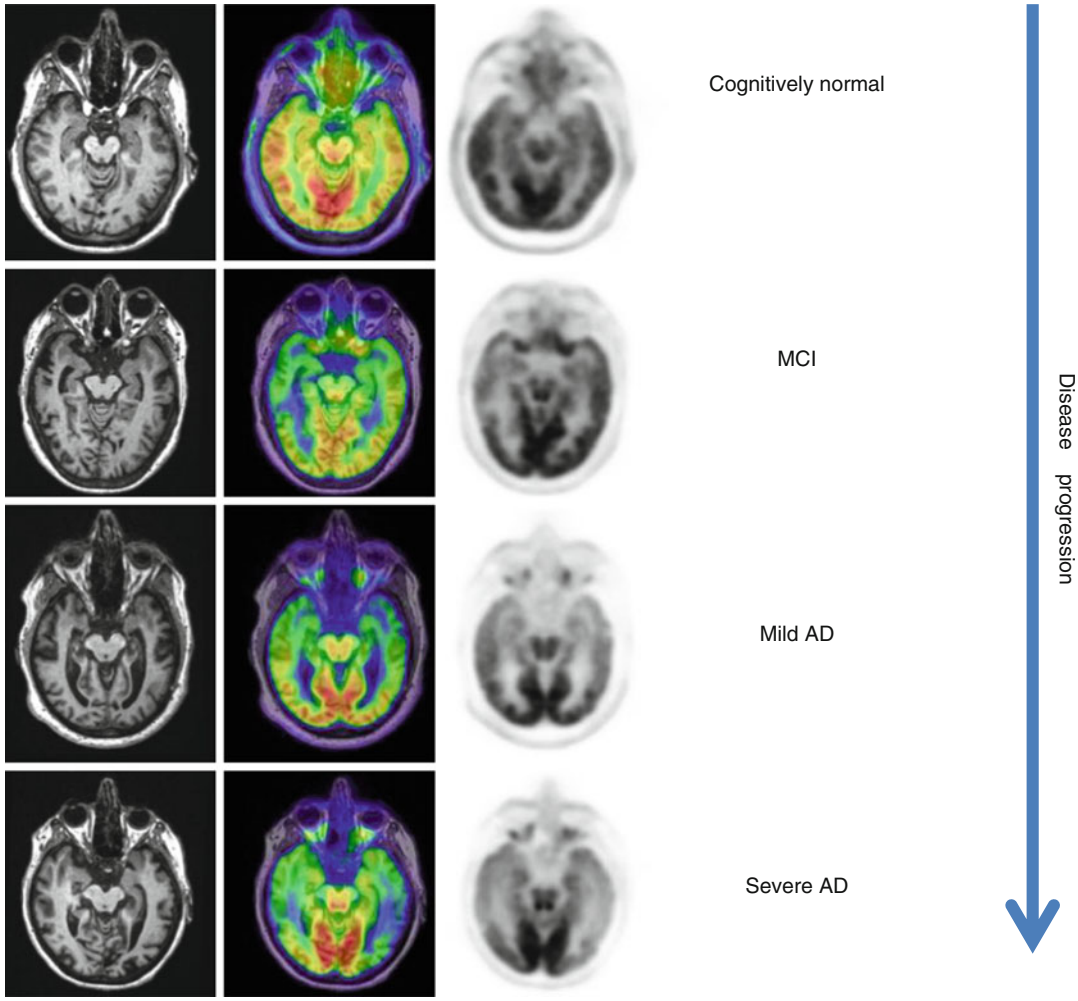

Fig. 6.1 PET/MR imaging showing the progression of temporal atrophy and hypometabolism at different stages of cognitive impairment (Images are courtesy of IRCCS SDN, Naples)

spread to the frontal and parietal cortices, though the degree of metabolism alteration is not as marked as in the anterior temporal cortices. Figure 6.2 shows PET/MR images of FT dementia.

6.10 Vascular Dementia

Vascular dementia is diagnosed with clinical symptoms and by detecting vascular lesions demonstrated by morphologic imaging, such as CT or MR [50–53]. As such, pure vascular dementia is not a PET-applicable dementia. However, vascular dementia is sometimes associated with AD or other neurodegenerative pathology, and these patients should be examined with FDG-PET to determine the comorbidity of AD or other neurodegenerative pathology. More likely, hypometabolism related to stroke is encountered incidentally in patients undergoing routine PET for oncologic indications when at least a portion of the involved area is within the field of view. The typical pattern consists of hypometabolism with abrupt margins in the territory of either the anterior, middle, or posterior cranial arteries, usually with evidence of encephalomalacia in the corresponding region on the

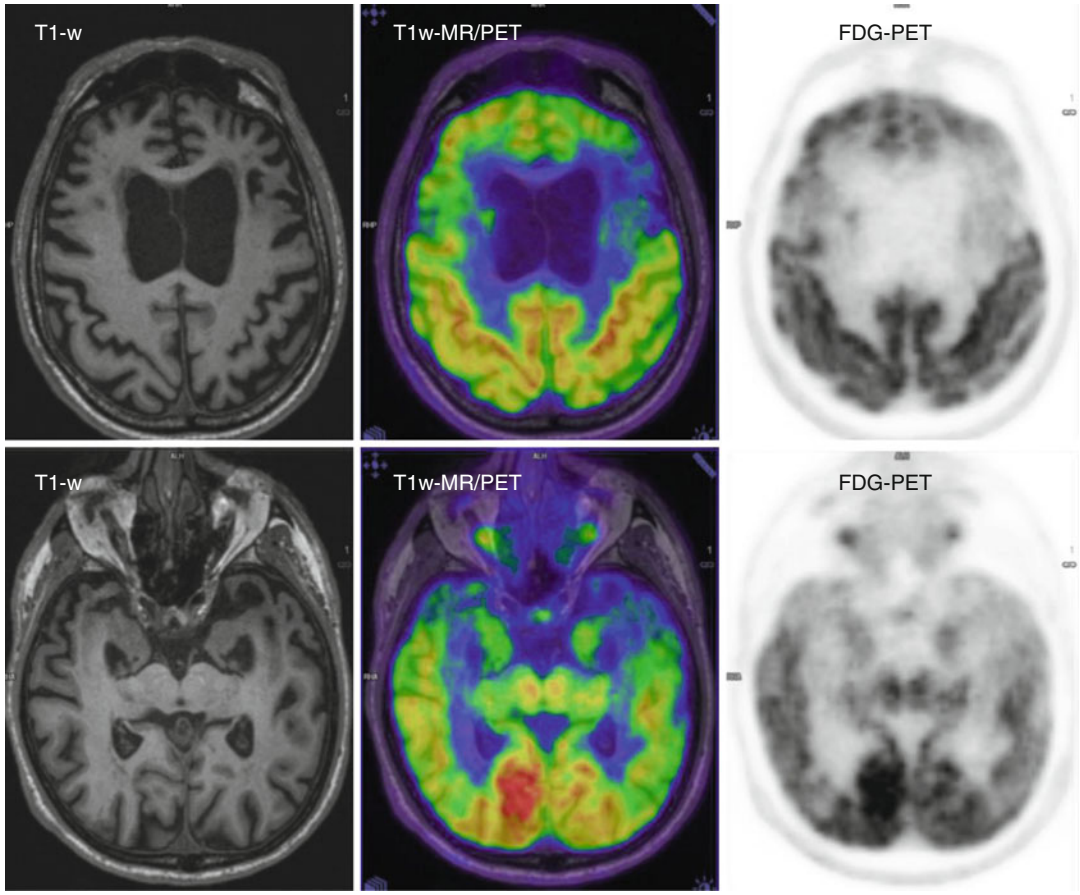

Fig. 6.2 PET/MR images of FT dementia. Male, 66 years old with diagnosis of frontotemporal dementia. Images show the typical FT dementia pattern: hypometabolism and atrophy of frontal (*top*) and temporal lobes (*bottom*); preserved metabolism of occipital and parietal cortices (Images are courtesy of IRCCS SDN, Naples)

CT images [52–54]. If the frontal lobe or internal capsule is involved, hypometabolism in the contralateral cerebellum may be seen due to crossed cerebrocerebellar diaschisis.

6.11 Structural Markers

Structural imaging has been receiving increasing interest as biomarker for cognitive impairment.

MRI is generally regarded as superior tool for brain imaging, as compared with CT; the main reason is the better soft tissue contrast of MR and, in addition, there are no ionizing radiations. Nevertheless, CT can be used for the evaluation of the brain atrophy in individuals who cannot receive MRI [58].

The clinical use of structural brain imaging confers substantial assistance in the early diagnosis of AD and is recommended for dementia diagnosis by major working groups involved in AD study [57, 58].

Hippocampal atrophy is a well-established early marker of AD [57] that correlates with impairments in memory function [56]. Furthermore, AD leads to progressive loss of brain volume throughout the cerebral cortex and other areas that is significantly greater in AD patients than age-matched controls and that correlates with the rate of cognitive deterioration [55].

Recent studies are focusing on a finer analysis where the hippocampus structure is characterized beyond its volume. In particular, hippocampal shape and subfield analysis are shown to be more sensitive in predicting pathological alterations [55].

Although the hippocampal and the whole brain atrophy rates are the most established structural markers for dementia progression, the estimation of the cortical thickness could represent a marker more specifically related to the evolution of AD and might be useful to evaluate the efficacy of new disease-modifying therapies [56].

On MR, white matter hyperintensities (WMH) and lacunas, frequently observed in the elderly (leukoaraiosis), are generally viewed as evidence of small-vessel disease. Fluid-attenuated inversion recovery (FLAIR) T2 weighted is considered the imaging gold standard for the classification and quantification of WMH load. Furthermore, diffusion-weighted imaging (DWI) can provide suitable information about the timing (acute or chronic) of WMH.

The Fazekas scale (FS) provides an overall impression of the presence of WMH in the entire brain. It is mainly scored on FLAIR or simply T2-weighted images dividing the white matter in periventricular and deep white matter, and each is given a grade depending on the size and confluence of lesions [57]. The Hachinski Ischemic Score (HIS) represents a brief clinical tool helpful in the differentiation of vascular dementia (HIS >7) [58]. Figure 6.3 shows a PET/MR study of VD with high WMH load, clearly visible in FLAIR, and HIS = 8.

6.12 Functional Markers

Dementia generally exhibits a specific regional pattern of altered brain perfusion.

In particular, perfusion estimated by arterial spin labeling (ASL) MR technique successfully revealed brain hypoperfusion in parietal areas and in the posterior cingulate cortex [59]. FTD shows frontal lobe hypoperfusion compared with AD [60].

ASL perfusion imaging has been shown to be suitable for early diagnosis of neurodegenerative diseases [59] in group comparisons, but it remains to determine its diagnostic confidence in individual patients. Moreover, it is interesting to exploit PET/MR hybrid imaging to understand the relationship between perfusion and glucose metabolism [61, 62].

Resting-state functional MRI (rs-fMRI) examination could provide further information about imaging alterations in dementia. New scenarios have been opened since Raichle introduced the term “default mode network” (DMN) to describe the brain function activity pattern during rest [63].

This DMN would include the relatively hypermetabolic brain areas of an individual that is not focused on any specific activity, entailing a relationship with the outside world, but is focused on task-independent introspection or self-referential thought. DMN is characterized by coherent neuronal slow (0.1 Hz) to very slow (0.01 Hz) oscillations of fMRI signal. DMN is deactivated during goal-oriented activity to leave space to other networks, specifically involved in a given task (so-called task-positive networks, or TPN). It is thought that during a specific task, the deactivated DMN and the TPN should be considered opposite elements of a single default network with anticorrelated components [64]. The DMN is not the only “low-frequency resting state.” The DMN is an interconnected and anatomically defined brain system showing a greater Blood Oxygenation Level Dependent (BOLD) fMRI activity during rest than during any attention-demanding task of a number of experimental paradigms [65, 66]. It has been shown that DMN changes during a visual-encoding task and is able during a nonspatial working memory task to distinguish between healthy aging, MCI, and mild AD. The degree of deactivation was lower in AD patients than in MCI patients and lower in MCI patients than in healthy controls [67]. By means of a simple sensorimotor processing task paradigm and fMRI, the decreased DMN activity in the posterior cingulate and hippocampus in healthy

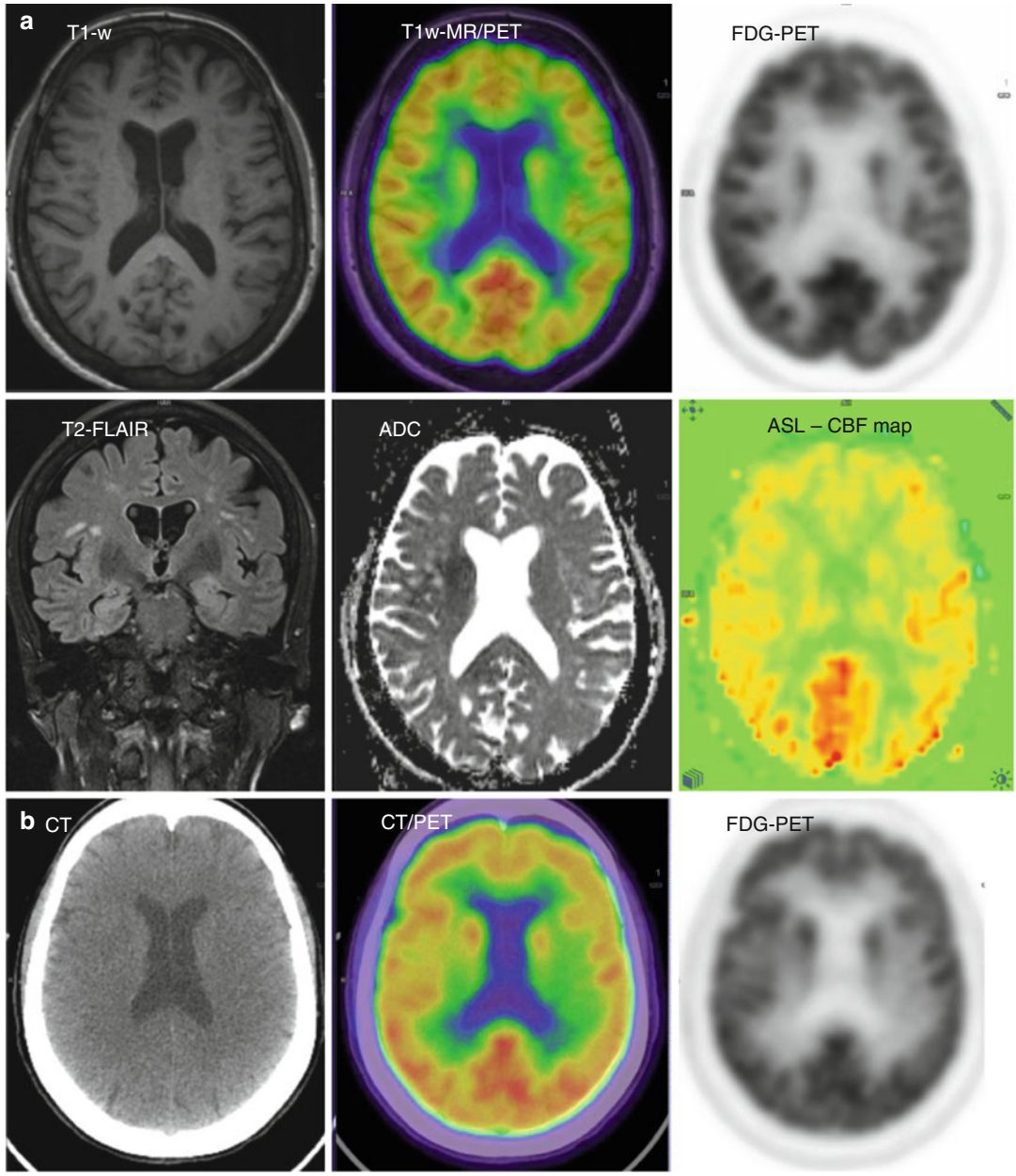

Fig. 6.3 Vascular dementia: PET/MR (**a**) vs. PET/CT (**b**), male patient, 67 years old, MMSE 17, CDR 2, Hachinski Score 8. The Hachinski Ischemic Scale is a tool widely used to identify a likely vascular component once a dementia diagnosis has been established. It is not itself a validated diagnostic tool. A score greater than 7 suggests vascular involvement. Main findings in MR/PET are mismatch between perfusion and metabolism in frontal area. Decreased frontal perfusion in absence of evident glucose metabolism in these areas. Images are courtesy of IRCCS SDN, Naples

aging subjects as compared to AD patients was sensitive and specific enough to differentiate between the two conditions and could therefore be a promising approach to identify AD [68].

Regional homogeneity (ReHo) is related to local functional connectivity and is another promising rs-fMRI metric sensible to alterations due to cognitive impairment [69, 70].

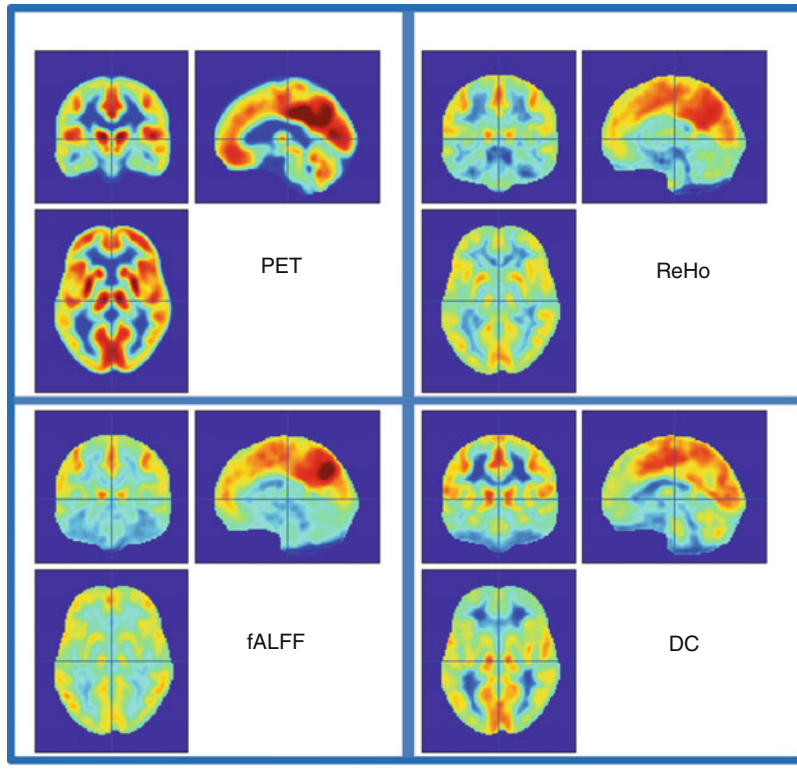

Fig. 6.4 Relationship between FDG-PET- and rs-fMRI-derived metrics. These pictures show the results of FDG-PET and different resting-state fMRI metrics (ReHO, Fractional Amplitude of Low Frequency Fluctuation (fALFF), and Degree Centrality (DC)) averaged over 23 neurologically health subjects simultaneously acquired on a PET/MR scanner. For further details and in-depth discussion, see [71]

Regarding simultaneous PET/MR imaging, it offers the unique opportunity to study and compare different imaging parameters at the same physiological conditions.

Aiello et al. [71] exploit PET/MR imaging to explore the relationship between the metabolic information provided by resting-state FDG-PET and resting-state BOLD fMRI (rs-fMRI) in neurologically healthy subjects. Their results show that the correlation between FDG-PET and rs-fMRI is significantly high, especially in DMN. Figure 6.4 depicts a visual comparison between rs-fMRI and FDG-PET voxel-wise maps carried out in this study.

6.13 Computer-Aided Diagnosis

The diagnostic performance of FDG-PET imaging could be improved exploiting well-established algorithms for the processing and analysis of PET images. To this aim, anatomic standardization of PET image sets is commonly performed by investigators to compare brain positron emission tomography images of different subjects voxel by voxel and for intersubject statistical analyses.

A key step for imaging software is registration algorithms. The registration of images aims to establish spatial correspondence between different modalities or different time points of each subjects' acquisition (co-registration) or between the image under examination and a spatial template (spatial normalization).

In the case of single modality, retrospective co-registration needs to be performed for visual comparison and voxel-wise analysis. In the case of hybrid acquisitions, different modalities (mainly PET/MR and PET/CT) could be considered intrinsically co-registered, but head displacements occurred during the

time-out between structural and functional acquisition could dramatically affect their spatial correspondence.

After image acquisition, following tomographic reconstruction with scatter correction and resolution recovery, attenuation correction is applied. Post-processing basically consists of image reorientation and normalization of uptake. Several Computer-Aided Diagnosis (CAD) software programs are available for brain image interpretation, all of which work on the same basic principle [72]. These programs are all designed to standardize brain images to account for individual variation in head size and shape and achieve correct alignment in the anterior commissure-posterior commissure plane. PET data are then normalized to a spatial template.

Spatial normalization of PET images could benefit from hybrid imaging; in fact, structural modalities such as CT and, mainly, MR provide more accurate normalization with respect to the PEt alone.

MRI-aided spatial normalization is more accurate than the one performed by using only PET images, given the better anatomical information and higher spatial resolution of MRI images [73]. Activity in each voxel is then normalized either globally or regionally [74]. Regional normalization is usually performed to a selected region (e.g., the cerebellum or pons) that is considered unlikely to be affected by the disease process [75].

The mapping of data to a brain FDG-PET template allows comparison of activity between individuals or groups of patients with use of statistical modeling, enabling the display of significant hypometabolic voxels on either two-dimensional cross-sectional images or 3D surface-rendered images and thereby facilitating pattern recognition, which is the key to the diagnosis. Use of automated voxel-based statistical mapping of the brain has been shown to increase diagnostic accuracy [76–78] first developed the 3D stereotactic surface projection system and used Z-score images to aid visual inspection of individual FDG images for diagnosing Alzheimer disease. The Z-score is the number of standard deviations from a database of age-matched control subjects ([normal mean - predicted value]/normal standard deviation). By using Z-score analysis, the magnitude of metabolic reduction across areas with different baseline (normal) metabolic activities can be compared and displayed with voxel-based color coding.

Statistical Parametric Mapping (SPM) is well documented, freely available and strongly supported by brain imaging community [79]. It offers quantitative voxel-by-voxel analysis in both functional [80, 81] and structural brain studies (voxel-based morphometry) [82]. SPM is the most popular method in voxel-based data analysis of functional brain data, for PET, SPECT, as well as fMRI. It is currently employed to reveal which parts of the brain are significantly activated by a task for a group of subjects or to find out which parts of the brain have a significant difference in cerebral blood flow or metabolism between healthy volunteers and patients [83]. First of all, spatial normalization, also known as anatomic standardization, was carried out in order to transform brain images of individual subjects into a standard brain [83]. Anatomic standardization analyzes subject groups, for which individual variations are treated statistically. The examination of a patient image in the standardized coordinate system to detect pixels above or below the normal range is a special case of a group analysis, because the patient is compared with a group of healthy volunteers and the result depends on the selection of the volunteers [83]. Spatial normalization uses a two-step approach: the affine transformation and the nonlinear warps. Firstly, the affine transformation that best maps the image to a template image in a standard space is calculated. The most employed templates are the stereotactic Talairach and Tournoux atlas (1988) and the Montreal Neurological Institute (MNI) template. The latter is based on averages of many MRI scans of healthy young adults and is used in SPM [84]. Figure 6.5 shows typical results of a normal database comparison of SPM analysis on FDG-PET images of AD subject.

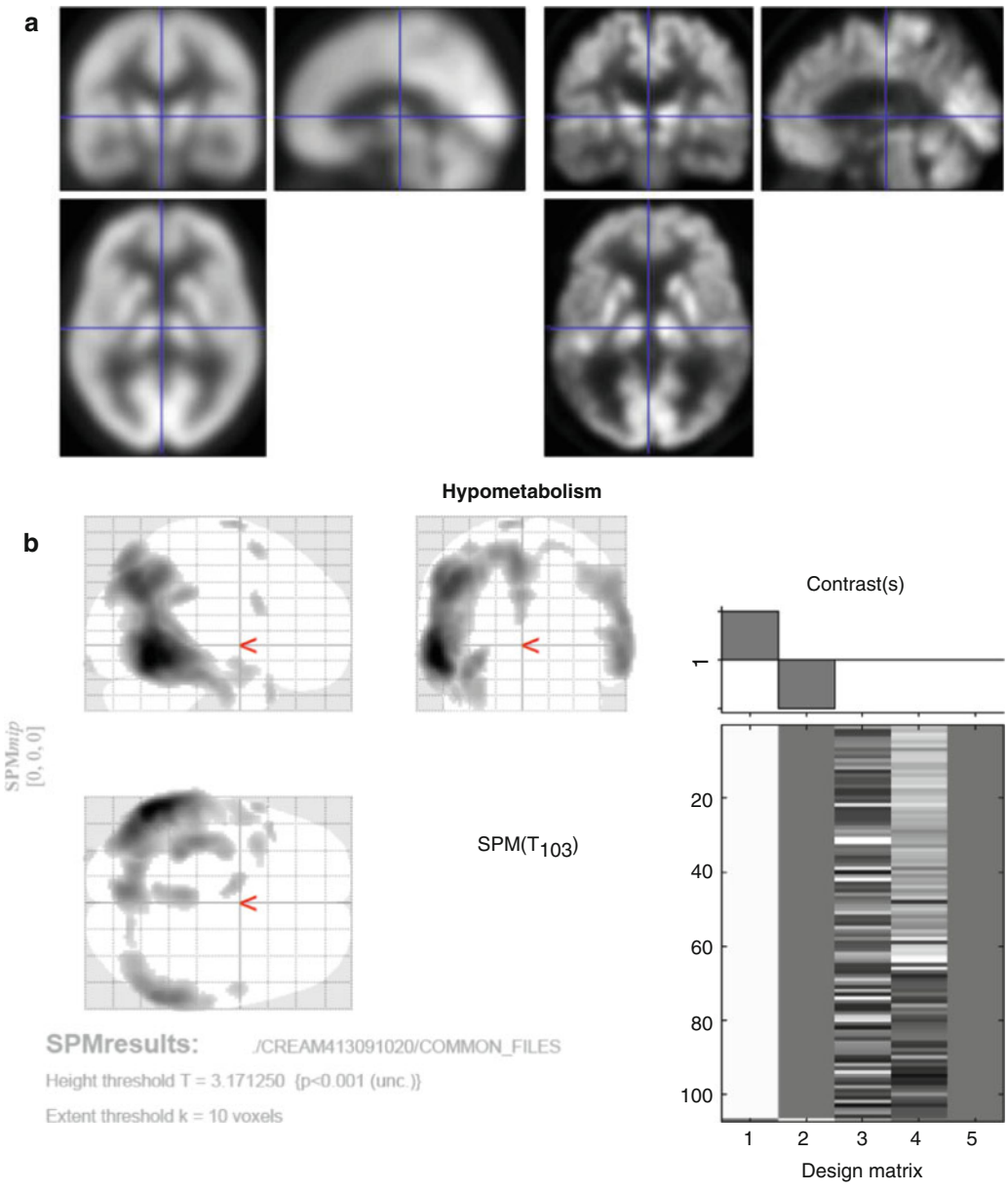

Fig. 6.5 Typical reporting of a SPM evaluation of FDG hypometabolism. (**a**) SPM's spatial normalization of a PET acquisition. PET image of single subject (*right*) normalized on SPM's PET template in MNI coordinates (*left*). (**b**–**c**) SPM results. Maximum intensity projections (**b**) and multi-slice overlay of SPM(t) map on MNI space. Voxels surviving statistical significance of $p<0.001$ are shown for the contrast patient < database of normality (hypometabolism). On the right of b, the design matrix of the two-sample *t*-test. Note the typical pattern of AD-related FDG hypometabolism. Pictures are rearranged from the report of SPM grid service of neu4grid platform (www.neu-grid4you.eu) funded by DG-CONNECT initiative

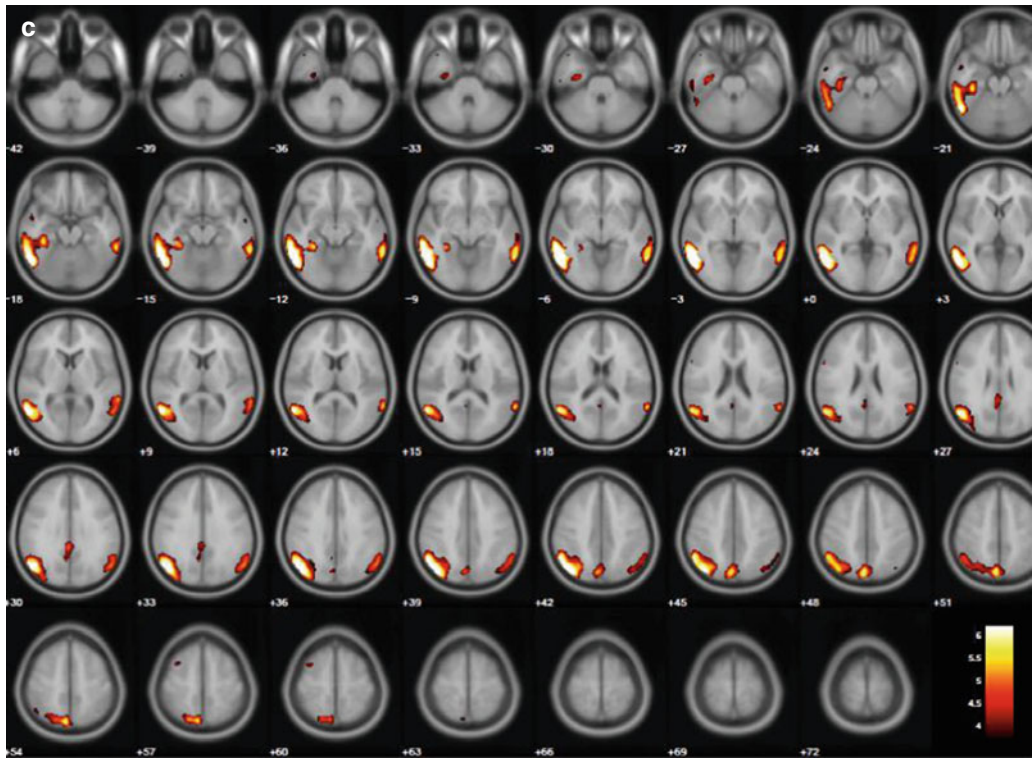

Fig. 6.5 (continued)

References

1. Alzheimer Europe (2010) Dementia: definition [Web site]. Available at: http://www.alzheimer-europe.org/EN/Glossary/dementia. Accessed 21 Jan 2011
2. Krishnan LL, Petersen NJ, Snow AL, Cully JA, Schulz PE, Graham DP et al (2005) Prevalence of dementia among Veterans Affairs medical care system users. Dement Geriatr Cogn Disord 20(4):245–253
3. Love S (2005) Neuropathological investigation of dementia: a guide for neurologists. J Neurol Neurosurg Psychiatry 76(Suppl V):v8–v14
4. Neumann M, Rademakers R, Roeber S, Baker M, Kretzschmar HA, Mackenzie IR (2009) A new subtype of frontotemporal lobar degeneration with FUS pathology. Brain 132(Pt 11):2922–2931
5. Dickson DW (2005) Required techniques and useful molecular markers in the neuropathologic diagnosis of neurodegenerative diseases. Acta Neuropathol 109(1):14–24
6. Kovacs GG, Budka H (2010) Current concepts of neuropathological diagnostics in practice: neurodegenerative diseases. Clin Neuropathol 29(5):271–288
7. Lowe J, Mirra SS, Hyman BT, Dickson DW (2008) Ageing and dementia. In: Love S, Louis DN, Ellison DW (eds) Greenfield's neuropathology, 8th edn. Hodder Arnold, London, pp 1031–1152
8. Braak H, Alafuzoff I, Arzberger T, Kretzschmar H, Del Tredici K (2006) Staging of Alzheimer disease-associated neurofibrillary pathology using paraffin sections and immunocytochemistry. Acta Neuropathol 112(4):389–404
9. Alafuzoff I, Arzberger T, Al-Sarraj S, Bodi I, Bogdanovic N, Braak H et al (2008) Staging of neurofibrillary pathology in Alzheimer's disease: a study of the BrainNet Europe Consortium. Brain Pathol 18(4):484–496
10. Mirra SS, Heyman A, McKeel D, Sumi SM, Crain BJ, Brownlee LM et al (1991) The Consortium to Establish a Registry for Alzheimer's Disease (CERAD). Part II. Standardization of the neuropathologic assessment of Alzheimer's disease. Neurology 41(4):479–486
11. National Institute on Aging, and Reagan Institute Working Group on Diagnostic Criteria for the Neuropathological Assessment of Alzheimer's Disease (1997) Consensus recommendations for the postmortem diagnosis of Alzheimer's disease. Neurobiol Aging (Suppl) 18(4):1–2
12. McKeith IG, Dickson DW, Lowe J, Emre M, O'Brien JT, Feldman H, for the Consortium on DLB (2005) Diagnosis and management of dementia with Lewy bodies: third report of the DLB consortium. Neurology 65(12):1863–1872
13. Braak H, Del Tredici K, Rüb U, de Vos RA, Jansen Steur EN, Braak E (2003) Staging of brain pathology

related to sporadic Parkinson's disease. Neurobiol Aging 24(2):197–211
14. Gallucci M et al (2008) Neurodegenerative diseases. Radiol Clin North Am 46(4):799–817
15. Coleman RE (2007) Positron emission tomography diagnosis of Alzheimer's disease. PET Clin 2(1):25–34
16. Silverman DHS, Alavi A (2005) PET imaging in the assessment of normal and impaired cognitive function. Radiol Clin North Am 43(1):67–77
17. Van Heertum RL, Tikofsky RS (2003) Positron emission tomography and single-photon emission computed tomography brain imaging in the evaluation of dementia. Semin Nucl Med 33(1):77–85, WB Saunders
18. Herholz K, Carter SF, Jones M (2014) Positron emission tomography imaging in dementia. Br J Radiol 80(2):S160–S167
19. Ishii K (2002) Clinical application of positron emission tomography for diagnosis of dementia. Ann Nucl Med 16(8):515–525
20. Ishii K (2014) PET approaches for diagnosis of dementia. AJNR Am J Neuroradiol 35(11): 2030–2038
21. Del Sole A et al (2008) Individual cerebral metabolic deficits in Alzheimer's disease and amnestic mild cognitive impairment: an FDG PET study. Eur J Nucl Med Mol Imaging 35(7):1357–1366
22. Mosconi L et al (2008) Multicenter standardized 18 F-FDG PET diagnosis of mild cognitive impairment, Alzheimer's disease, and other dementias. J Nucl Med 49(3):390–398
23. Yuan Y, Gu Z-X, Wei W-S (2009) Fluorodeoxyglucose–positron-emission tomography, single-photon emission tomography, and structural mr imaging for prediction of rapid conversion to Alzheimer disease in patients with mild cognitive impairment: a meta-analysis. AJNR Am J Neuroradiol 30(2):404–410
24. Chételat G et al (2008) Direct voxel-based comparison between grey matter hypometabolism and atrophy in Alzheimer's disease. Brain 131(1):60–71
25. Minoshima S et al (1999) Discordance between traditional pathologic and energy metabolic changes in very early Alzheimer's disease: pathophysiological implications. Ann N Y Acad Sci 893(1):350–352
26. McKhann GM et al (2011) The diagnosis of dementia due to Alzheimer's disease: recommendations from the National Institute on Aging-Alzheimer's Association workgroups on diagnostic guidelines for Alzheimer's disease. Alzheimers Dement 7(3):263–269
27. Albert MS et al (2011) The diagnosis of mild cognitive impairment due to Alzheimer's disease: recommendations from the National Institute on Aging-Alzheimer's Association workgroups on diagnostic guidelines for Alzheimer's disease. Alzheimers Dement 7(3):270–279
28. Minoshima S et al (1997) Metabolic reduction in the posterior cingulate cortex in very early Alzheimer's disease. Ann Neurol 42(1):85–94
29. Choo ILH et al (2007) Topographic patterns of brain functional impairment progression according to clinical severity staging in 116 Alzheimer disease patients: FDG-PET study. Alzheimer Dis Assoc Disord 21(2):77–84
30. Hirono N et al (2004) One-year change in cerebral glucose metabolism in patients with Alzheimer's disease. J Neuropsychiatry Clin Neurosci 16(4):488–492
31. Jagust WMRB et al (2007) What does fluorodeoxyglucose PET imaging add to a clinical diagnosis of dementia? Neurology 69(9):871–877
32. Langbaum JBS et al (2009) Categorical and correlational analyses of baseline fluorodeoxyglucose positron emission tomography images from the Alzheimer's Disease Neuroimaging Initiative (ADNI). Neuroimage 45(4):1107–1116
33. McMurtray AM et al (2008) Positron emission tomography facilitates diagnosis of early-onset alzheimer's disease. Eur Neurol 59(1–2):31–37
34. Ishii K et al (2006) Fully automatic diagnostic system for early-and late-onset mild Alzheimer's disease using FDG PET and 3D-SSP. Eur J Nucl Med Mol Imaging 33(5):575–583
35. Patterson JC et al (2009) Potential value of quantitative analysis of cerebral PET in early cognitive decline. Am J Alzheimers Dis Other Dement 23(6):586–592
36. Ishii K et al (1998) Relatively preserved hippocampal glucose metabolism in mild Alzheimer's disease. Dement Geriatr Cogn Disord 9(6):317–322
37. Phelps ME (2004) PET: molecular imaging and its biological applications. Springer Science & Business Media, New York
38. Alexander GE et al (1997) Association of premorbid intellectual function with cerebral metabolism in Alzheimer's disease: implications for the cognitive reserve hypothesis. Am J Psychiatry 154(2): 165–172
39. McKhann G et al (1984) Clinical diagnosis of Alzheimer's disease Report of the NINCDS-ADRDA Work Group* under the auspices of Department of Health and Human Services Task Force on Alzheimer's Disease. Neurology 34(7):939
40. Hirono N et al (2002) The effect of APOE ε4 allele on cerebral glucose metabolism in AD is a function of age at onset. Neurology 58(5):743–750
41. Colloby S, O'Brien J (2004) Functional imaging in Parkinson's disease and dementia with Lewy bodies. J Geriatr Psychiatry Neurol 17(3):158–163
42. Higuchi M et al (2000) Glucose hypometabolism and neuropathological correlates in brains of dementia with Lewy bodies. Exp Neurol 162(2):247–256
43. Ishii K et al (2004) Comparison of FDG-PET and IMP-SPECT in patients with dementia with Lewy bodies. Ann Nucl Med 18(5):447–451
44. Cordery RJ et al (2001) Dementia with Lewy bodies studied with positron emission tomography. Arch Neurol 58(3):505–508
45. Imamura T et al (2001) Occipital glucose metabolism in dementia with Lewy bodies with and without Parkinsonism: a study using positron emission tomography. Dement Geriatr Cogn Disord 12(3):194–197

46. Perneczky R et al (2008) Cerebral metabolic dysfunction in patients with dementia with Lewy bodies and visual hallucinations. Dement Geriatr Cogn Disord 25(6):531–538
47. Bohnen NI et al (2011) Cerebral glucose metabolic features of Parkinson disease and incident dementia: longitudinal study. J Nucl Med 52(6):848–855
48. Ishii K et al (1998) Cerebral glucose metabolism in patients with frontotemporal dementia. J Nucl Med 39(11):1875
49. Kanda T et al (2008) Comparison of grey matter and metabolic reductions in frontotemporal dementia using FDG-PET and voxel-based morphometric MR studies. Eur J Nucl Med Mol Imaging 35(12):2227–2234
50. Black S, Gao FQ, Bilbao J (2009) Understanding white matter disease imaging-pathological correlations in vascular cognitive impairment. Stroke 40(3 suppl 1):S48–S52
51. Doyle CA, Slater P (1995) Application of [3H] l-NG-nitro-arginine labelling to measure cerebellar nitric oxide synthase in patients with schizophrenia. Neurosci Lett 202(1):49–52
52. Kerrouche N et al (2006) 18FDG PET in vascular dementia: differentiation from Alzheimer's disease using voxel-based multivariate analysis. J Cereb Blood Flow Metab 26(9):1213–1221
53. Kuczynski B et al (2008) Cognitive and anatomic contributions of metabolic decline in Alzheimer disease and cerebrovascular disease. Arch Neurol 65(5):650–655
54. Mielke R, Heiss W-D (1998) Positron emission tomography for diagnosis of Alzheimer's disease and vascular dementia. Springer, Vienna
55. Marizzoni M et al (2015) Longitudinal reproducibility of automatically segmented hippocampal subfields: a multisite European 3 T study on healthy elderly. Hum Brain Mapp 36(9):3516–3527
56. Redolfi A et al (2015) Head-to-head comparison of two popular cortical thickness extraction algorithms: a cross-sectional and longitudinal study. PLoS One 10(3), e0117692
57. Fazekas F, Chawluk JB, Alavi A et al (1987) MR signal abnormalities at 1.5 T in Alzheimer's dementia and normal aging. AJR Am J Roentgenol 149(2):351–356
58. Moroney JT (1997) Meta-analysis of the Hachinski Ischaemic Score in pathologically verified dementias. Neurology 49:1096–1105
59. Xekardaki A et al (2014) Arterial spin labeling may contribute to the prediction of cognitive deterioration in healthy elderly individuals. Radiology 274(2):490–499
60. Du AT et al (2006) Hypoperfusion in frontotemporal dementia and Alzheimer disease by arterial spin labeling MRI. Neurology 67(7):1215–1220
61. Musiek ES et al (2012) Direct comparison of fluorodeoxyglucose positron emission tomography and arterial spin labeling magnetic resonance imaging in Alzheimer's disease. Alzheimers Dement 8(1):51–59
62. Aiello M et al (2014) Brain perfusion and glucose metabolism by simultaneous FDG-PET/MR-ASL in patients with cognitive disorders: initial experience. Proc Intl Soc Mag Reson Med
63. Raichle M et al (2001) A default mode of brain function. Proc Natl Acad Sci 98(2):676–682
64. Broyd SJ et al (2009) Default-mode network dysfunction in mental disorders: a systematic review. Neurosci Biobehav Rev 33:279–296
65. Buckner RL et al (2008) The brain's default network: anatomy, function and relevance to disease. Ann N Y Acad Sci 1124:1–38
66. Schulman GL et al (1997) Common blood flow changes across visual tasks: II Decreases in cerebral cortex. J Cogn Neurosci 9:648–663
67. Rombouts SA et al (2005) Altered resting state networks in mild cognitive impairment and mild Alzheimer's disease: an fMRI study. Hum Brain Mapp 26:231–239
68. Greicius MD et al (2004) Default-mode network activity distinguishes Alzheimer's disease from healthy aging: evidence from functional MRI. Proc Natl Acad Sci U S A 101:4637–4642
69. Zhang L et al (2012) Correlation of regional homogeneity and cognitive decline in Alzheimer's disease: a preliminary study. Proceedings of International Society of Magnetic Resonance in Medicine 20
70. Liu Y et al (2008) Regional homogeneity, functional connectivity and imaging markers of Alzheimer's disease: a review of resting-state fMRI studies. Neuropsychologia 46(6):1648–1656
71. Aiello M et al (2015) Relationship between simultaneously acquired resting-state regional cerebral glucose metabolism and functional MRI: A PET/MR hybrid scanner study. Neuroimage 113:111–121
72. Hosaka K et al (2005) Validation of anatomical standardization of FDG PET images of normal brain: comparison of SPM and NEUROSTAT. Eur J Nucl Med Mol Imaging 32(1):92–97
73. Gispert JD et al (2003) Influence of the normalization template on the outcome of statistical parametric mapping of PET scans. Neuroimage 19(3):601–612
74. Buchert R et al (2005) Adjusted scaling of FDG positron emission tomography images for statistical evaluation in patients with suspected Alzheimer's disease. J Neuroimaging 15(4):348–355
75. Yakushev I et al (2008) Choice of reference area in studies of Alzheimer's disease using positron emission tomography with fluorodeoxyglucose-F18. Psychiatry Res Neuroimaging 164(2):143–153
76. Minoshima S et al (1997) Metabolic reduction in the posterior cingulate cortex in very early Alzheimer's disease. Annals of neurology 42(1):85–94
77. Minoshima S et al (1994) Stereotactic PET atlas of the human brain: aid for visual interpretation of functional brain images. J Nucl Med 35(6):949–954
78. Minoshima S et al (1995) A diagnostic approach in Alzheimer's disease using three-dimensional stereotactic surface. J Nucl Med 36:1238–1248

79. Zaidi H et al (2006) Quantitative analysis in nuclear medicine imaging. Springer, New York
80. Friston KJ et al (1995) Statistical parametric maps in functional imaging: a general linear approach. Hum Brain Mapp 2:189–210
81. Friston KJ et al (1996) Detecting activations in PET and fMRI: levels of inference and power. Neuroimage 4:223–235
82. Ashburner J (2007) A fast diffeomorphic image registration algorithm. Neuroimage 38(1):95–113
83. Friston KJ et al (1995) Spatial registration and normalization of images. Hum Brain Mapp 3(3): 165–189
84. Brett M et al (2001) Using the Talairach atlas with the MNI template. Neuroimage 13:S85

Amyloid Imaging in Dementia and Related Disorders

7

V. Camacho and Ignasi Carrió

7.1 Introduction

Alzheimer's disease (AD) is the most common cause of cognitive impairment in the elderly that it accounts for about 70 % of cases of dementia. Less common causes include dementia with Lewy bodies (DLB) (about 15 %), frontotemporal lobar degeneration (FTLD) (more common in late middle age and the younger elderly), and vascular dementia [1]. AD may occur sporadically or as a result of rare genetic mutations that produce an autosomal dominant form of the disease. Initially, AD presents with amnesic memory impairment that progressively worsens with concomitant declines in other cognitive abilities and behaviors, which lead to the complete functional dependency that defines the dementia phase of the illness [2].

The pathological hallmarks of the disease are amyloid-β (Aβ) and tau aggregates, synaptic loss, and reactive gliosis [3]. Amyloid plaques are most abundant in the frontal cortex, cingulate gyrus, precuneus, and lateral parietal and temporal regions. There are relatively fewer plaques in the primary sensorimotor and occipital cortex and the mesial temporal areas, in contrast to neurofibrillary tangles, which are present in highest density in the mesial temporal areas, including the hippocampi [4].

AD dementia is now considered part of a continuum of clinical and biological phenomena, in which both AD pathological processes and clinical decline occur gradually over decades, with dementia representing the end stage. A model to explain the sequence of events has been proposed in which Aβ pathophysiological processes become abnormal first and downstream neuronal injury biomarkers become abnormal later [5]. The Aβ protein is produced from the cleavage of the amyloid precursor protein (APP) that occurs sequentially by the action of α-secretase or β-secretase (BACE-1) and γ-secretase. While the majority of APP is processed by α-secretase to result in non-amyloidogenic cleavage products, a proportion is cleaved by β-secretase and γ-secretase to result in the formation of Aβ peptides [6]. The predominant forms of Aβ peptides produced are Aβ40 and Aβ42, although Aβ aggregates have been shown to be directly toxic to neuronal cell cultures, the mechanism by which they exert their neurotoxic effects is still unclear [7]. In AD, these pathological processes have the early consequences of synaptic dysfunction and culminate later in neuronal loss. Amyloid burden correlates poorly with disease severity, suggesting a lesser role for insoluble Aβ fibrils, while soluble Aβ oligomers appear to play the major part in neurotoxicity [8].

V. Camacho (✉) • I. Carrió
Nuclear Medicine Department, Hospital de Sant Pau i la Santa Creu, Barcelona, Spain
e-mail: mcamachom@santpau.cat

A. Ciarmiello, L. Mansi (eds.), *PET-CT and PET-MRI in Neurology*,
DOI 10.1007/978-3-319-31614-7_7

In the last few decades, clinical diagnosis of AD has been made using the criteria defined by the Working Group of the National Institute of Neurological and Communicative Disorders and Stroke and the Alzheimer's Disease and Related Disorders Association [2]. In this criteria, the clinical diagnosis of AD could only be designated as "probable" while the patient was alive and could not be made definitively until Alzheimer's pathology had been confirmed postmortem; and the specificity of clinical criteria in differentiation of AD from other dementias was low [9]. In the *Revised Criteria for the Diagnosis of Alzheimer's Disease* [10] published in 2011, the core clinical criteria for AD continued to be essential in clinical practice but biomarkers were included to improve pathophysiological specificity in the diagnosis. Recently, the *International Working Group and the US National Institute on Aging-Alzheimer's Association* described criteria for diagnosis of AD, defining phenotypes and integrated biomarkers into the diagnostic process: pathological biomarkers (decreased $A\beta_{1-42}$ with increased T-tau or P-tau in CSF and increased retention on fibrillar amyloid PET) and topographical biomarkers (volumetric MRI and 18F-fluorodeoxyglucose-PET) [9].

Although the treatment of AD is symptomatic, with cholinesterase inhibitors (donepezil, galantamine, rivastigmine) or glutamate moderators (memantine), early diagnosis of AD is important to differentiate other causes of neurodegenerative diseases that cause dementia and to identify the patients that may benefit from treatment. Clinicians and patients and their families are increasingly seeking more accurate diagnostic and prognostic information. Clinical diagnosis alone has only moderate accuracy and requires the presence of dementia, but specific biomarkers, such as amyloid imaging, will allow more accurate diagnosis and earlier diagnosis when patients are only mildly symptomatic.

7.2 β-Amyloid Radiotracers

PET imaging with amyloid tracers provides important information about the extent of Aβ neuritic plaque burden in the brain; thus, amyloid PET is considered as a surrogate marker of brain fibrillar amyloid pathology in vivo [9]. The 11C-labeled Pittsburg compound B (11C-PIB), a thioflavin T derivated, was the first PET ligand to visualize selectively Aβ in living patients [11]. Histopathological studies demonstrated that 11C-PIB retention was correlated with postmortem findings [12]. However, the 20-min half-life of 11C limits its use to PET centers with a cyclotron despite its potential advantage for research. To overcome this limitation, several ligands labeled with 18Fluorine (18F), with a 110-min half-life, have been developed and replicating the results obtained with 11C-PIB.

Current amyloid 18F tracers belong to a variety of chemical classes such as thioflavin T (18F-flutemetamol), stilbenes (18F-florbetapir and 18F-florbetaben), and benzofuran derivates (18F-AZD4694) [13–16]. Although these tracers differ in how they bind to Aβ plaques, they exhibit high-affinity binding for fibrillar amyloid similar to that of 11C-PIB. Currently, three 18F-labeled amyloid tracers have been evaluated in clinical studies and approved for use by the Food and Drug Administration and the European Medicines Agency's Committee for Medicinal Products for Human Use: 18F-florbetapir (AMYViD TM®), 18F-flutemetamol (VizamylTM®), and 18F-florbetaben (NeuraCeqTM®). A negative brain amyloid scan shows a distinctive pattern of binding in white matter. In contrast, in a positive scan, uptake in cortical gray matter obscures the normal white matter pattern and shows binding extending to the outer edge of the brain (Fig. 7.1). White matter uptake is greater for 18F tracers than for 11C-PIB. In AD patients, the average cortical binding is similar to or less than the uptake in white matter, in contrast to 11C-PIB, which shows uptake about 30 % higher in cortex than in white matter [1].

7.3 Aβ Imaging in AD

In AD patients, the distribution of 11C-PIB uptake reflects the regional density of Aβ plaques [18]. Different studies have demonstrated, either by visual or by quantitative assessment, elevated

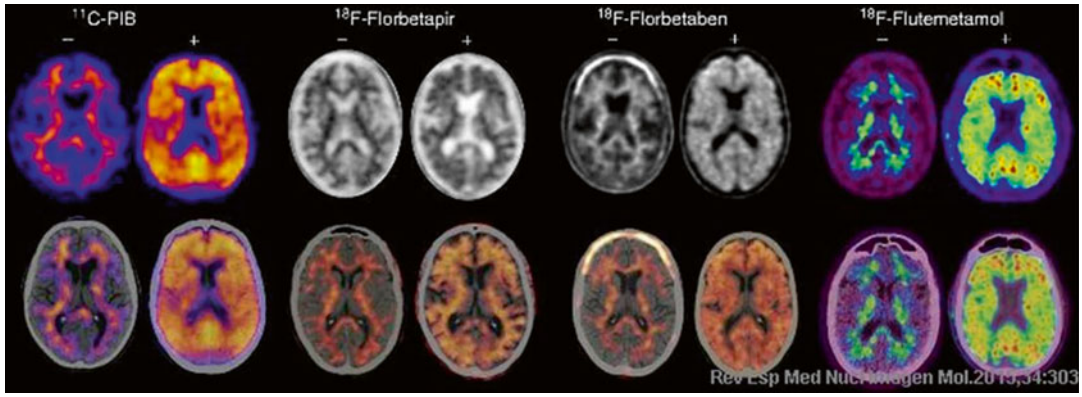

Fig. 7.1 Representative positive (+) and negative (−) PET (*top row*) and PET–CT (*down row*) images obtained with different Aβ radiotracers. From left to right: 11C-PIB, 18F-florbetapir, 18F-florbetaben, and 18F-flutemetamol (From Arbizu et al. [17], with permission from Elsevier)

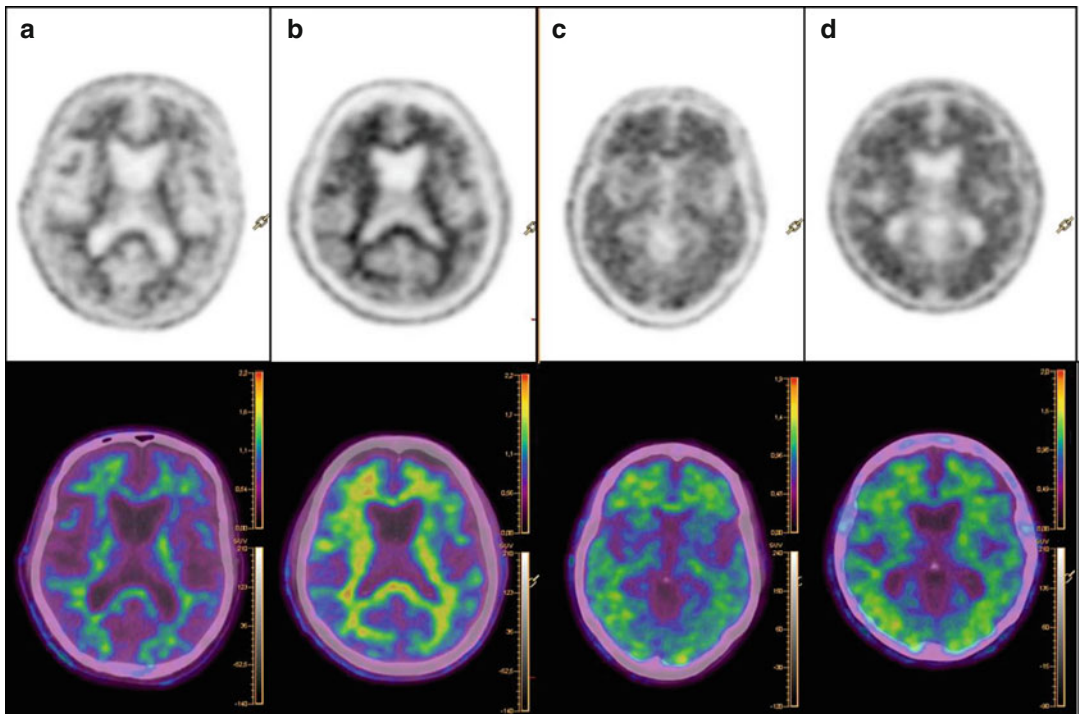

Fig. 7.2 Images of 18F-florbetapir PET (*top row*) and PET–CT (*down row*). Negative amyloid PET in healthy control (**a**) and in MCI patient (**b**) with a contrast between white and gray matter. Positive amyloid PET in MCI (**c**) and AD (**d**) patients with high cortical retention of tracer reflecting amyloid deposition

cortical retention of 11C-PIB in AD patients compared to healthy controls [11, 19] (Fig. 7.2). Similarly, other 18F-labeled tracers demonstrated a robust difference in cortical retention between AD and healthy controls [13, 20]. Recently, Chiotis et al. [21] investigated the role of age in the amyloid load of AD patients. In this study, age-related differences between groups were observed only in the putamen, where young AD patients showed significantly lower amyloid deposition in comparison to the older AD patients. This effect was observed in all diagnostic groups (healthy control (HC), MCI, AD), supporting an important role of the striatum in the age-related accumulation of Aβ.

Different studies indicate that Aβ imaging might allow accurate differential diagnosis of dementias [15, 22]. Villemagne et al. [15] demonstrated the utility of 18F-florbetaben to distinguish AD from other neurodegenerative disorders; specifically, 96 % of AD patients and 60 % of patients with MCI presented cortical retention of 18F-florbetaben; in contrast, only 9 % of patients with FTLD, 29 % of patients with DLB, 25 % of patients with vascular dementia, and 60 % of healthy controls presented cortical binding.

Interestingly, the regional distribution of 11C-PIB is not always the same. Patients with familial AD due to presenilin-1 mutations, familial AD, and cerebral amyloid angiopathy (CAA) due to reduplication of the APP present a very high 11C-PIB uptake in the striatum and relatively low cortical uptake [23]. This binding pattern is in contrast with the extensive cortical Aβ pathology found at autopsy in these patients, while the explanation for this atypical 11C-PIB pattern is not yet clear [24].

Most studies have found that Aβ binding is not associated with dementia severity and hypometabolism once the clinical diagnosis of AD has been reached, and there is no correlation between 11C-PIB binding and disease duration [25, 26]. These findings are consistent with the majority of clinicopathological studies that have not found a strong correlation between Aβ plaque burden and AD severity [27]. Jack et al. [28] reported that longitudinal clinical decline correlated strongly with brain atrophy rates but did not correlate with Aβ burden.

7.4 Aβ Imaging in Healthy Elderly

Neuropathological studies have reported a significant Aβ deposition in 25–45 % of the healthy elderly, and the extent and distribution of Aβ pathology may be indistinguishable from that found in AD. The prevalence of 11C-PIB positive in the healthy elderly increases each decade: at 60s, the prevalence of positive 11C-PIB is 12 % and at 80s increases at least to 50 % [1].

The ε4 allele of the apolipoprotein E (APOE-ε4) is associated with an increased risk of developing AD. Different studies demonstrated that the prevalence of 11C-PIB positive in the healthy elderly is strongly related to the presence of the APOE-ε4 allele, carried by 27 % of the general population [29]. In a recent meta-analysis, Jansen et al. [30] described that the age at onset of amyloid positivity was associated with cognitive status and the APOE genotype and at 90 years of age, about 40 % of the APOE-ε4 non-carriers and more than 80 % of APOE-ε4 carriers with normal cognition were amyloid positive. Elevated 11C-PIB binding in the healthy elderly is associated with a greater risk of cognitive decline and faster rate of brain atrophy, suggesting that Aβ imaging may be sensitive for detection of a preclinical AD state [31]. The rate of Aβ deposition increases slowly; in the healthy elderly with an 11C-PIB positive, the increase is on average 2–3 % per year and appears to be similar in MCI arriving at a plateau when AD is developed [32]. These results support that amyloid deposition starts 1 or 2 decades before onset of the clinical symptoms.

7.5 Amyloid PET in MCI

The term MCI due to AD is applied to a symptomatic predementia phase of AD. Thus, MCI due to AD is considered as a subset of the many causes of cognitive impairment that are not dementia, including impairments resulting from head trauma, substance abuse, or metabolic disturbance [33]. It is important to identify those symptomatic but nondemented individuals whose primary underlying pathophysiology is AD. Aβ imaging is useful in the early differential diagnosis of MCI. Different studies have shown a high amyloid deposition in 50–60 % individuals with MCI, who later progress to AD over 3–5 years of follow-up [34, 35]. Okello et al. [36] found that 11C-PIB-positive more rapid converters had a significantly increased Aβ burden in the anterior cingulate and frontal cortex compared to 11C-PIB-positive slower converters and nonconverters. On the other hand, patients with MCI

converting to AD during follow-up had greater 11C-PIB deposition in the posterior cingulate, lateral frontal cortex, temporal cortex, putamen, and caudate nucleus as compared to nonconverters. After a follow-up of 36 months, Doraiswamy et al. [37] described that subjects with 18F-florbetapir-positive scans presented with greater cognitive and global deterioration than 18F-florbetapir-negative subjects, regardless of diagnostic status. The higher amyloid deposition is correlated with the degree of memory impairment [38].

7.6 Aβ Related to Other Biomarkers

The *International Working Group and the US National Institute on Aging-Alzheimer's Association* report integrated biomarkers into the diagnostic process of AD [9]. The pathophysiological biomarkers are required for clinical diagnostic criteria and the topographical markers are recommended for the assessment of disease stage and progression. However, diagnostic and topographical biomarkers cannot be used as standalone test and should be interpreted in a larger clinical context that takes confounding factors into account.

7.6.1 CSF

The presence of low Aβ1–42 with increased T-tau or P-tau concentrations in CSF increases significantly the accuracy of AD diagnosis even at prodromal stage with a sensitivity of 90–95 % and a specificity of about 90 % [39]. An important concern is the large variability in CSF measures between laboratories, across techniques, and the lack of agreement on cutoff thresholds makes direct comparison of studies often difficult [40]. Although CSF biomarkers and Aβ imaging are pathophysiological biomarkers in the diagnosis of AD, they provide different information about AD pathophysiology. CSF Aβ1–42 measures soluble forms of Aβ and a low concentration suggests that significant parenchymal deposition has occurred, whereas Aβ imaging directly identifies fibrillar Aβ brain deposition. On the other hand, CSF T-tau and CSF P-tau reflect neuronal degeneration and hyperphosphorylation of tau in the brain, respectively.

Despite these discrepancies, a high degree of correlation exists between CSF markers of Aβ1–42 and tau and Aβ binding. Amyloid ligand retention on PET has consistently correlated inversely with CSF concentrations of Aβ1–42 [41] which supports the concept of a physiological link between CSF Aβ1–42 concentrations and brain amyloidosis, and it indicates that Aβ biomarkers are overall equally associated with clinical AD, both at the dementia stage and at the MCI stage. While this inverse relationship is consistent, there is not a perfect agreement between two markers, since some individuals have abnormal CSF Aβ1–42 concentrations with normal Aβ PET and vice versa [42]. Some studies have suggested that CSF Aβ abnormalities may precede fibrillar Aβ aggregation in the cortex especially in healthy elderly [41], and others suggest that Aβ imaging has greater specificity because CSF Aβ1–42 not always translates to cognitive decline or brain Aβ deposition [43]. Landau et al. [44] examined the agreement and disagreement between biomarkers of Aβ deposition in 374 individuals (AD, MCI, and healthy elderly) and observed a relatively small numbers of discordant subjects. Disagreement between CSF Aβ and 18F-florbetapir measurements may have been due to measurement problems such as errors introduced by PET image processing, the use of cutoffs with differing sensitivities and specificities, and standardization of CSF assays to the same set of cutoffs.

7.6.2 18F-FDG

18F-FDG PET has revealed glucose metabolic reductions in the parietotemporal, frontal, and posterior cingulate cortices to be the hallmark of AD and has a 90 % sensitivity in identifying AD [45]. 18F-FDG PET has been shown to have good sensitivity to follow disease evolution over time [46]. Hypometabolism in parietotemporal

and posterior cingulated cortex can be used to distinguish AD from other forms of dementia such as FTLD and DLB and from cerebrovascular disease [47]. Aβ PET and 18F-FDG PET presented similar accuracy to differentiate AD and FTLD [48].

Overall, the pattern of cortical metabolic changes has been useful to predict conversion from MCI to AD with a sensitivity of 95 % and a specificity of 79 % [49] and is related to cognitive impairment [50]. Although the accuracy of Aβ imaging and 18F-FDG in diagnosis of AD is similar, Li et al. reported a high accuracy of 18F-FDG than 11C-PIB in MCI patients [51]. In MCI patients, Aβ deposition was positively associated with hypometabolism in posterior brain regions, but not after conversion to AD, suggesting that there are interactions between Aβ deposition and metabolism during AD process and that a possible compensatory upregulation of posterior brain metabolism in the early phase may exist [52].

7.6.3 MRI

MRI, as well as 18F-FDG, is a biomarker of neurodegeneration that precedes and parallels cognitive decline. Medial temporal lobe atrophy is the best MRI marker at a prodromal stage of further progression to AD [53]; however, hippocampal volume is reduced in several conditions including old age and other neurodegenerative dementia [54]. The reliability of volumetric measures obtained from repeated MRI scans is high and allows the measurement of disease progression. Hippocampal loss occurs two or four times faster in patients with AD than in age-matched healthy controls [55]. The congruence between positive Aβ load and medial temporal atrophy is low, as these biomarkers play a different role in the physiopathology of AD [28]. This model of disease implies a complimentary role for MRI and amyloid clinical imaging, with each modality reflecting one of the major pathologies in Alzheimer's disease, amyloid dysmetabolism, and neurodegeneration. It also implies a complementary role in clinical trials: longitudinal measures with MRI might be preferred as an outcome measure to detect change in the underlying neurodegenerative pathology that tracks with clinical disease stage.

7.7 Amyloid PET in Other Conditions

7.7.1 Down's Syndrome

The typical neuropathological features of Alzheimer's disease, plaques and tangles, appear in virtually all patients with Down's syndrome (DS) over 40 years of age. Clinically, changes in cognitive performance and behavior appear to correlate with these neuropathological changes [56]. The prevalence of dementia in DS increased from 11 % between ages 40 and 49 to 77 % between 60 and 69 [57]. Aβ imaging has been used in DS as a model of the natural history of Aβ deposition in the brain (Fig. 7.3). In the literature, there are few studies using Aβ imaging in DS. These studies have reported widespread cortical binding in people with DS after over 40 years of age [58, 59]. Recently, Annuls et al. [60] reported that abnormal 11C-PIB load was strongly associated with clinical diagnosis of dementia without evidence of a substantial time window between abnormal 11C-PIB and cognitive decline. These results are in agreement with previous studies that reported absence of Aβ imaging in younger individuals although some single isolated cases presented with striatal binding [58]. Further studies are necessary to confirm these results because early detection of Aβ deposition prior to cognitive symptoms may modify therapies in these patients.

7.7.2 Cerebral Amyloid Angiopathy

CAA has been used as a general term to describe cerebrovascular amyloid deposition or cerebrovascular amyloidosis [61]. CAA is a common age-related cerebral small-vessel disease, characterized by progressive deposition of Aβ in the wall of small- to medium-sized arteries, arterioles, and

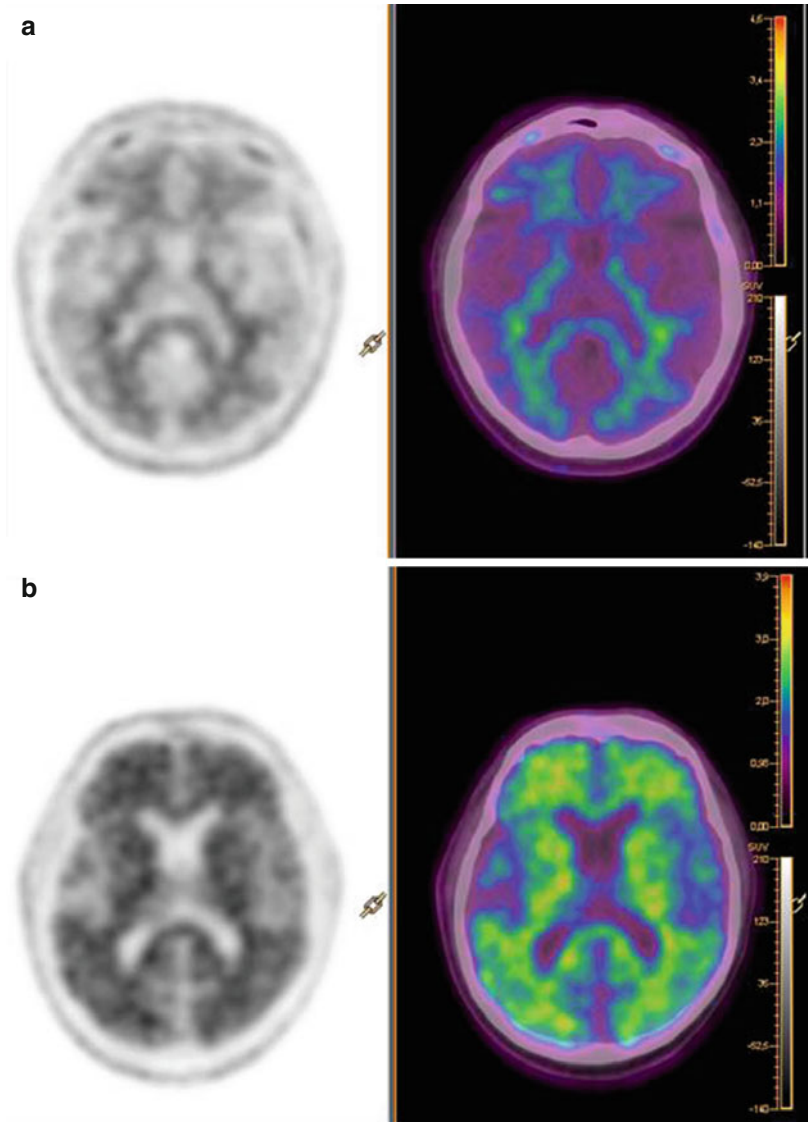

Fig 7.3 Images of 18F-florbetapir PET (*left*) and PET–CT (*right*) in DS patient without cortical amyloid burden (**a**) and in DS patient with high cortical amyloid burden. Amyloid PET in DS may help to identify patients with high amyloid deposition (**b**)

capillaries of the cerebral cortex and overlying leptomeninges. CAA is the major cause of spontaneous hemorrhagic stroke (intracerebral hemorrhage and microhemorrhages) and cognitive impairment in the elderly [62]. The prevalence of CAA increases with age and occurs in approximately half of elderly individuals [63]. The amyloid deposition pattern differs from AD in that the occipital cortex is more affected in CAA [64]. Although the Aβ PET has low specificity for CAA due to a higher 11C-PIB uptake in healthy elderly that may reflect incipient AD, a negative Aβ PET rules out CAA with a good sensitivity [65]. In addition, microhemorrhages may be associated with 11C-PIB retention. Gurol et al. [66] described in CAA patients with dementia that new related CAA hemorrhages preferentially occur at sites of increased 11C-PIB, suggesting that Aβ imaging may be useful in the prediction of incident hemorrhages in these patients.

7.7.3 Lewy Bodies Disease

DLB and Parkinson disease dementia (PDD) share pathologic findings that include cortical Lewy body accumulation, alpha-synuclein toxicity, and Aβ plaques and have similar clinical manifestations. DLB and PDD differ in the temporal sequence of symptoms and clinical features [67]. Different studies demonstrated Aβ deposition in Lewy body diseases (Villemagne 2014) (Fig. 7.4). In a recent meta-analysis, Ossenkoppele et al. [68] described that the prevalence of Aβ deposition in DLB is associated with APOE-ε4 and increased with age.

Several studies have found higher Aβ burden in DLB than in PDD [69, 70]; these results may suggest that amyloid burden contributes to cognitive impairment and it may relate to the relative timing of motor and cognitive findings. Foster et al. [70] reported high association between elevated 11C-PIB binding and worse global cognitive impairment in Lewy body disease, but there is no association with any other clinical or neuropsychological feature. They suggested that the presence of fibrillar amyloid-β does not distinguish between clinical subtypes of Lewy body-associated disorders, although larger numbers are needed to definitively rule out this association.

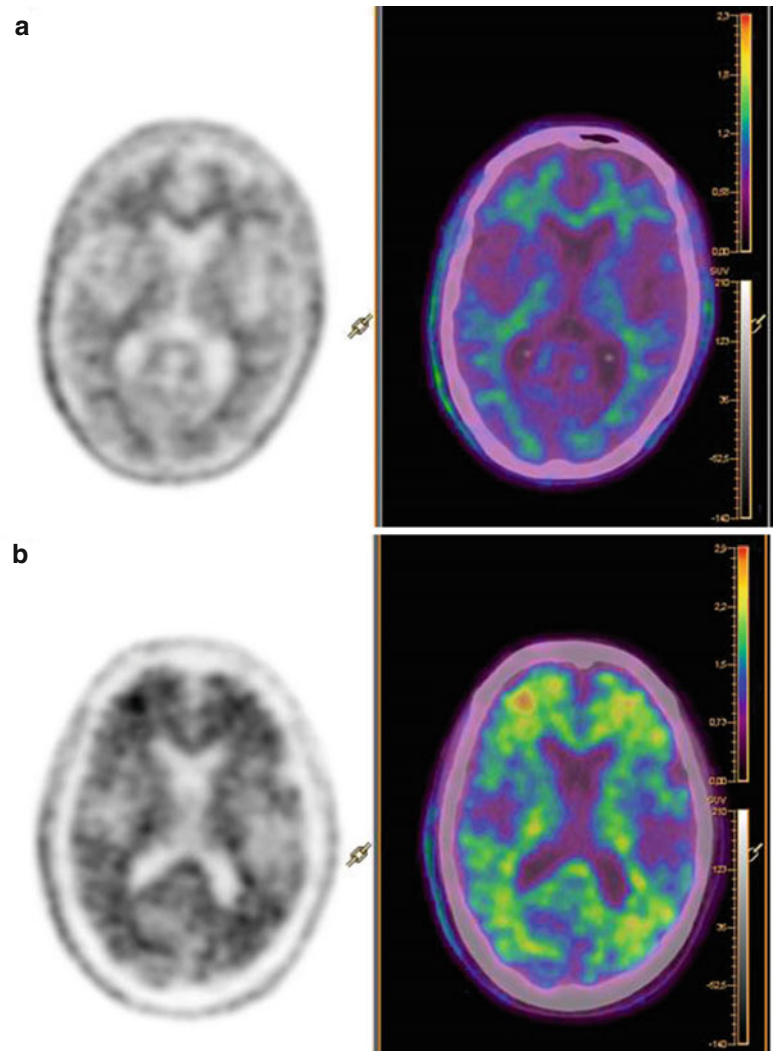

Fig. 7.4 Images of 18F-florbetapir PET (*left*) and PET–CT (*right*) in patient with DLB without cortical Aβ deposition (**a**) and in DLB patient with high cortical deposition (**b**)

7.7.4 Frontotemporal Lobar Degeneration

FTLD is the second most common cause of presenile dementia that typically presents with impairments in social, behavioral, and/or language function [71]. However, early diagnosis may be difficult due to the overlap between clinical features seen in FTLD and other neurodegenerative conditions such as AD. Many patients with pathologically confirmed FTLD are diagnosed with AD during life, and conversely, 10–40 % of patients clinically diagnosed with FTLD are found to have AD post-mortem [72].

In patients with FTLD, cortical Aβ load does not differ significantly from that of healthy controls; thus, Aβ imaging is a potential marker that can differentiate between FTLD and AD [15] (Fig. 7.5). Ravinovici et al. [48] observed that two tracers had similar accuracy in discriminating AD and FTLD, and 11C-PIB visual reads had a higher sensitivity for AD (89.5 %) than FDG visual reads (77.5 %) with similar specificity (11C-PIB 83 %, FDG 84 %). When scans were classified quantitatively, PIB had higher sensitivity (89 % vs. 73 %) while FDG had higher specificity (83 % vs. 98 %). A recent meta-analysis reported that the prevalence of Aβ positivity increased with age and APOE-ε4 in FTLD. An 18F-florbetapir study reported a patient with frequent cortical neuritic plaques and frontotemporal lobar degeneration with TDP4 inclusions. Probably the positive Aβ scans in patients diagnosed clinically of FTLD represent FTLD–AD comorbidity in the histopathology, with the FTLD component dominating the clinical presentation.

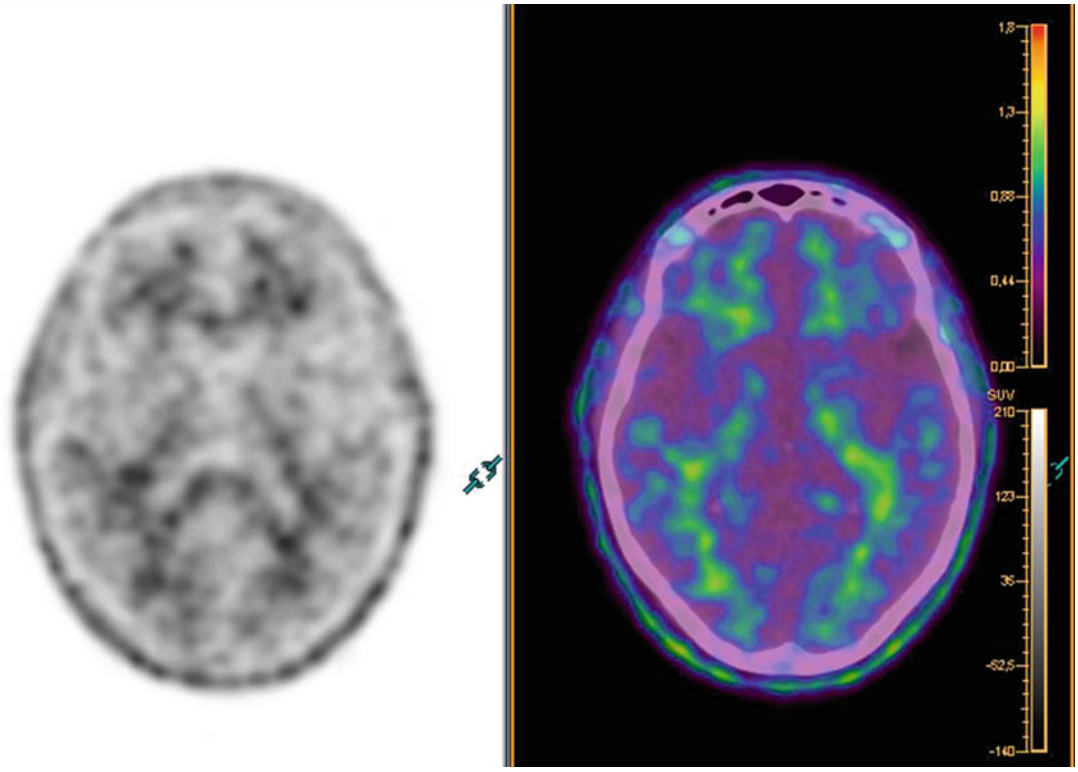

Fig 7.5 A representative negative18F-florbetapir PET (*left*) and PET–CT (*right*) in patient with frontotemporal lobar degeneration

7.7.5 Traumatic Brain Injury

There is increasing acceptance of epidemiological and pathophysiological links between traumatic brain injury (TBI) and the development of AD later in life and that Aβ plaques may be found in patients within hours following TBI [73]. It has also been suggested that a history of TBI accelerates the onset of AD [74]. Aβ plaques are found in up to 30% of patients who die in the acute phase following TBI. In contrast, in individuals dying of nonneurological causes, Aβ plaques tend to be confined to elderly individuals [75]. Different studies using Aβ imaging reported an increased Aβ deposition in gray matter in patients after TBI, at a range of times after TBI [76, 77]. The use of Aβ imaging following TBI provides us with the potential for understanding the pathophysiology of TBI, for characterizing the mechanistic drivers of disease progression of TBI, for identifying patients at high risk of accelerated AD, and for evaluating the potential of antiamyloid therapies.

7.8 Future Directions of Amyloid Imaging

There are pending issues in correlation between Aβ PET and the other biomarkers. Although the pathophysiological biomarkers have high correlation in the diagnosis of AD, there is not a perfect agreement with them. Some studies have suggested that CSF abnormalities may precede fibrillar brain Aβ deposition and others suggest that Aβ PET has greater specificity. These conflicting results indicate that further research is needed to discrepancies between in vivo Aβ measurements that it is important since the new criteria consider these markers as interchangeable in terms of diagnostic utility. On the other hand, while Aβ imaging measures molecular pathology, progression biomarkers (18F-FDG PET and MRI) measure the secondary effects of disease on brain structure and function. It also implies a complementary role in clinical diagnostic of AD, as well as in MCI patients.

Recently, several tau PET tracers have been developed [78, 79]. For use of tau PET as a biomarker of tau pathology in AD, PET tracers should have affinity PHF-tau and high selectivity for tau over amyloid-β and other protein deposits. PET tau imaging enables the longitudinal assessment of the spatial pattern of tau deposition and its relation to amyloid-β pathology and neurodegeneration. This technology could also be applied to the pharmacological assessment of anti-tau therapy, thereby allowing preventive interventions [80].

On the other hand, the application of Aβ imaging in pathologies of non-AD is subject of current active research, especially in non-AD diseases where Aβ deposition is present and may be involved in the disease pathogenesis (DLB, DS, CAA, TBI). Longitudinal studies are needed for early identification of non-AD diseases and for detection of Aβ deposition prior to cognitive symptoms that may modify therapies in these patients.

Actually, Aβ PET is contributing to the development of more effective therapies in clinical trials for AD. Several studies have incorporated amyloid PET as an outcome measure. In the phenserine trial [81] and in the solanezumab trials [82], no impact of therapy on Aβ deposition demonstrated by PET was observed. On the other way, in trials with other antiamyloid therapies, small to modest treatment reductions on brain amyloid by PET were shown [83–85]. Thus, the Aβ imaging has important implications for the future development and evaluation of disease-modifying therapies in clinical AD trials [86] and provides a potential prognostic time frames based on individual current Aβ burden. Furthermore, knowledge of the time frames associated with Aβ deposition is also relevant to design the therapeutic trials, allowing investigators to establish critical periods suitable for intervention along the disease pathway or estimate the duration of a specific trial.

References

1. Rowe CC, Villemagne VL (2013) Brain amyloid imaging. J Nucl Med Technol 41(1):11–18
2. McKhann G, Drachman D, Folstein M, Katzman R, Price D, Stadlan EM (1984) Clinical diagnosis of Alzheimer's disease: report of the NINCDS-ADRDA

Work Group under the auspices of Department of Health and Human Services Task Force on Alzheimer's Disease. Neurology 34(7):939–944
3. Villemagne VL, Ng S, Cappai R, Barnham KJ, Fodero-Tavoletti MT, Rowe CC et al (2006) La lunga attesa: towards a molecular approach to neuroimaging and therapeutics in Alzheimer's disease. Neuroradiol J 19(4):453–474
4. Braak H, Braak E (1997) Frequency of stages of Alzheimer-related lesions in different age categories. Neurobiol Aging 18(4):351–357
5. Jack CR, Knopman DS, Jagust WJ, Petersen RC, Weiner MW, Aisen PS et al (2013) Tracking pathophysiological processes in Alzheimer's disease: an updated hypothetical model of dynamic biomarkers. Lancet Neurol 12(2):207–216
6. Masters CL, Cappai R, Barnham KJ, Villemagne VL (2006) Molecular mechanisms for Alzheimer's disease: implications for neuroimaging and therapeutics. J Neurochem 97(6):1700–1725
7. Golde TE, Dickson D, Hutton M (2006) Filling the gaps in the abeta cascade hypothesis of Alzheimer's disease. Curr Alzheimer Res 3(5):421–430
8. Minati L, Edginton T, Bruzzone MG, Giaccone G (2009) Current concepts in Alzheimer's disease: a multidisciplinary review. Am J Alzheimers Dis Other Demen 24(2):95–121
9. Dubois B, Feldman HH, Jacova C, Hampel H, Molinuevo JL, Blennow K et al (2014) Advancing research diagnostic criteria for Alzheimer's disease: the IWG-2 criteria. Lancet Neurol 13(June): 614–629
10. McKhann GM, Knopman DS, Chertkow H, Hyman BT, Jack CR, Kawas CH et al (2011) The diagnosis of dementia due to Alzheimer's disease: recommendations from the National Institute on Aging-Alzheimer's Association workgroups on diagnostic guidelines for Alzheimer's disease. Alzheimers Dement 7(3):263–269
11. Klunk WE, Engler H, Nordberg A, Wang Y, Blomqvist G, Holt DP et al (2004) Imaging brain amyloid in Alzheimer's disease with Pittsburgh Compound-B. Ann Neurol 55(3):306–319
12. Ikonomovic MD, Klunk WE, Abrahamson EE, Mathis CA, Price JC, Tsopelas ND et al (2008) Post-mortem correlates of in vivo PiB-PET amyloid imaging in a typical case of Alzheimer's disease. Brain 131(Pt 6):1630–1645
13. Clark CM, Schneider JA, Bedell BJ, Beach TG, Bilker WB, Mintun MA et al (2011) Use of florbetapir-PET for imaging beta-amyloid pathology. JAMA 305(3):275–283
14. Koole M, Lewis DM, Buckley C, Nelissen N, Vandenbulcke M, Brooks DJ et al (2009) Whole-body biodistribution and radiation dosimetry of 18F-GE067: a radioligand for in vivo brain amyloid imaging. J Nucl Med 50(5):818–822
15. Villemagne VL, Ong K, Mulligan RS, Holl G, Pejoska S, Jones G et al (2011) Amyloid imaging with (18) F-florbetaben in Alzheimer disease and other dementias. J Nucl Med 52(8):1210–1217
16. Juréus A, Swahn B-M, Sandell J, Jeppsson F, Johnson AE, Johnström P et al (2010) Characterization of AZD4694, a novel fluorinated Abeta plaque neuroimaging PET radioligand. J Neurochem 114(3):784–794
17. Arbizu J, Garcia-Ribas G, Carrió I (2015) Recommendations for the use of PET imaging biomarkers in the diagnostic of neurodegenerative conditions associated with dementia: SEMNIM and SEN consensus. Rev Esp Med Nucl Imagen Mol 34(5):303–313
18. Braak H, Braak E (1991) Neuropathological stageing of Alzheimer-related changes. Acta Neuropathol 82(4):239–259
19. Ng S, Villemagne VL, Berlangieri S, Lee S-T, Cherk M, Gong SJ et al (2007) Visual assessment versus quantitative assessment of 11C-PIB PET and 18F-FDG PET for detection of Alzheimer's disease. J Nucl Med 48(4):547–552
20. Barthel H, Gertz H-J, Dresel S, Peters O, Bartenstein P, Buerger K et al (2011) Cerebral amyloid-β PET with florbetaben (18F) in patients with Alzheimer's disease and healthy controls: a multicentre phase 2 diagnostic study. Lancet Neurol 10(5):424–435
21. Chiotis K, Carter SF, Farid K, Savitcheva I, Nordberg A (2015) Amyloid PET in European and North American cohorts; and exploring age as a limit to clinical use of amyloid imaging. Eur J Nucl Med Mol Imaging 42(10):1492–1506
22. Fodero-Tavoletti MT, Cappai R, McLean CA, Pike KE, Adlard PA, Cowie T et al (2009) Amyloid imaging in Alzheimer's disease and other dementias. Brain Imaging Behav 3(3):246–261
23. Klunk WE, Price JC, Mathis CA, Tsopelas ND, Lopresti BJ, Ziolko SK et al (2007) Amyloid deposition begins in the striatum of presenilin-1 mutation carriers from two unrelated pedigrees. J Neurosci 27(23):6174–6184
24. Rabinovici G, Jagust W (2009) Amyloid imaging in aging and dementia: testing the amyloid hypothesis in vivo. Behav Neurol 21(1):117–128
25. Furst AJ, Rabinovici GD, Rostomian AH, Steed T, Alkalay A, Racine C et al (2012) Cognition, glucose metabolism and amyloid burden in Alzheimer's disease. Neurobiol Aging 33(2):215–225
26. Engler H, Forsberg A, Almkvist O, Blomquist G, Larsson E, Savitcheva I et al (2006) Two-year follow-up of amyloid deposition in patients with Alzheimer's disease. Brain 129(Pt 11):2856–2866
27. Guillozet al, Weintraub S, Mash DC, Mesulam MM (2003) Neurofibrillary tangles, amyloid, and memory in aging and mild cognitive impairment. Arch Neurol 60(5):729–736
28. Jack CR, Lowe VJ, Weigand SD, Wiste HJ, Senjem ML, Knopman DS et al (2009) Serial PIB and MRI in normal, mild cognitive impairment and Alzheimer's disease: implications for sequence of pathological events in Alzheimer's disease. Brain 132(Pt 5):1355–1365
29. Reiman EM, Chen K, Liu X, Bandy D, Yu M, Lee W et al (2009) Fibrillar amyloid-beta burden in cognitively normal people at 3 levels of genetic risk

for Alzheimer's disease. Proc Natl Acad Sci U S A 106(16):6820–6825
30. Jansen WJ, Ossenkoppele R, Knol DL, Tijms BM, Scheltens P, Verhey FRJ et al (2015) Prevalence of cerebral amyloid pathology in persons without dementia: a meta-analysis. JAMA 313(19):1924–1938
31. Mintun MA, Larossa GN, Sheline YI, Dence CS, Lee SY, Mach RH et al (2006) [11C]PIB in a nondemented population: potential antecedent marker of Alzheimer disease. Neurology 67(3):446–452
32. Villemagne VL, Burnham S, Bourgeat P, Brown B, Ellis KA, Salvado O et al (2013) Amyloid β deposition, neurodegeneration, and cognitive decline in sporadic Alzheimer's disease: a prospective cohort study. Lancet Neurol 12(4):357–367, Elsevier Ltd
33. Albert MS, DeKosky ST, Dickson D, Dubois B, Feldman HH, Fox NC et al (2011) The diagnosis of mild cognitive impairment due to Alzheimer's disease: recommendations from the National Institute on Aging-Alzheimer's Association workgroups on diagnostic guidelines for Alzheimer's disease. Alzheimers Dement 7(3):270–279
34. Kemppainen NM, Aalto S, Wilson IA, Någren K, Helin S, Brück A et al (2007) PET amyloid ligand [11C]PIB uptake is increased in mild cognitive impairment. Neurology 68(19):1603–1606
35. Forsberg A, Engler H, Almkvist O, Blomquist G, Hagman G, Wall A et al (2008) PET imaging of amyloid deposition in patients with mild cognitive impairment. Neurobiol Aging 29(10):1456–1465
36. Okello A, Koivunen J, Edison P, Archer HA, Turkheimer FE, Någren K et al (2009) Conversion of amyloid positive and negative MCI to AD over 3 years: an 11C-PIB PET study. Neurology 73(10):754–760
37. Doraiswamy PM, Sperling RA, Johnson K, Reiman EM, Wong TZ, Sabbagh MN et al (2014) Florbetapir F 18 amyloid PET and 36-month cognitive decline:a prospective multicenter study. Mol Psychiatry 19(9):1044–1051
38. Ong K, Villemagne VL, Bahar-Fuchs A, Lamb F, Chételat G, Raniga P et al (2013) (18)F-florbetaben Aβ imaging in mild cognitive impairment. Alzheimers Res Ther 5(1):4
39. Snider BJ, Fagan AM, Roe C, Shah AR, Grant EA, Xiong C et al (2009) Cerebrospinal fluid biomarkers and rate of cognitive decline in very mild dementia of the Alzheimer type. Arch Neurol 66(5):638–645
40. Fagan AM, Shaw LM, Xiong C, Vanderstichele H, Mintun MA, Trojanowski JQ et al (2011) Comparison of analytical platforms for cerebrospinal fluid measures of β-amyloid 1–42, total tau, and p-tau181 for identifying Alzheimer disease amyloid plaque pathology. Arch Neurol 68(9):1137–1144
41. Fagan AM, Mintun MA, Mach RH, Lee SY, Dence CS, Shah AR et al (2006) Inverse relation between in vivo amyloid imaging load and cerebrospinal fluid Abeta;42 in humans. Ann Neurol 59(3): 512–519
42. Jagust WJ, Landau SM, Shaw LM, Trojanowski JQ, Koeppe RA, Reiman EM et al (2009) Relationships between biomarkers in aging and dementia. Neurology 73(15):1193–1199
43. Mattsson N, Insel PS, Landau S, Jagust W, Donohue M, Shaw LM et al (2014) Diagnostic accuracy of CSF Ab42 and florbetapir PET for Alzheimer's disease. Ann Clin Transl Neurol 1(8):534–543
44. Landau SM, Lu M, Joshi AD, Pontecorvo M, Mintun MA, Trojanowski JQ et al (2013) Comparing positron emission tomography imaging and cerebrospinal fluid measurements of β-amyloid. Ann Neurol 74(6):826–836
45. Mosconi L (2005) Brain glucose metabolism in the early and specific diagnosis of Alzheimer's disease. Eur J Nucl Med Mol Imaging 32(4):486–510
46. Alexander GE, Chen K, Pietrini P, Rapoport SI, Reiman EM (2002) Longitudinal PET evaluation of cerebral metabolic decline in dementia: a potential outcome measure in Alzheimer's disease treatment studies. Am J Psychiatry 159(5):738–745
47. Mosconi L, Berti V, Glodzik L, Pupi A, De Santi S, de Leon MJ (2010) Pre-clinical detection of Alzheimer's disease using FDG-PET, with or without amyloid imaging. J Alzheimers Dis 20(3):843–854
48. Rabinovici GD, Rosen HJ, Alkalay A, Kornak J, Furst AJ, Agarwal N et al (2011) Amyloid vs FDG-PET in the differential diagnosis of AD and FTLD. Neurology 77(23):2034–2042
49. Silverman D (2003) Prognostic value of regional cerebral metabolism in patients undergoing dementia evaluation: comparison to a quantifying parameter of subsequent cognitive performance and to prognostic assessment without PET. Mol Genet Metab 80(3):350–355
50. Bohnen NI, Djang DSW, Herholz K, Anzai Y, Minoshima S (2012) Effectiveness and safety of 18F-FDG PET in the evaluation of dementia: a review of the recent literature. J Nucl Med 53(1):59–71
51. Li Y, Rinne JO, Mosconi L, Pirraglia E, Rusinek H, DeSanti S et al (2008) Regional analysis of FDG and PIB-PET images in normal aging, mild cognitive impairment, and Alzheimer's disease. Eur J Nucl Med Mol Imaging 35(12):2169–2181
52. Kemppainen N, Joutsa J, Johansson J, Scheinin NM, Någren K, Rokka J et al (2015) Long-term interrelationship between brain metabolism and amyloid deposition in mild cognitive impairment. Barthel H, editor. J Alzheimers Dis 48(1):123–133
53. Risacher SL, Saykin AJ, West JD, Shen L, Firpi HA, McDonald BC (2009) Baseline MRI predictors of conversion from MCI to probable AD in the ADNI cohort. Curr Alzheimer Res 6(4):347–361
54. Barkhof F, Polvikoski TM, van Straaten ECW, Kalaria RN, Sulkava R, Aronen HJ et al (2007) The significance of medial temporal lobe atrophy: a postmortem MRI study in the very old. Neurology 69(15):1521–1527

55. Lo RY, Hubbard AE, Shaw LM, Trojanowski JQ, Petersen RC, Aisen PS et al (2011) Longitudinal change of biomarkers in cognitive decline. Arch Neurol 68(10):1257–1266
56. Heston LL (1984) Down's syndrome and Alzheimer's dementia: defining an association. Psychiatr Dev 2(4):287–294
57. Visser FE, Aldenkamp AP, van Huffelen AC, Kuilman M, Overweg J, van Wijk J (1997) Prospective study of the prevalence of Alzheimer-type dementia in institutionalized individuals with Down syndrome. Am J Ment Retard 101(4):400–412
58. Handen BL, Cohen AD, Channamalappa U, Bulova P, Cannon SA, Cohen WI et al (2012) Imaging brain amyloid in nondemented young adults with Down syndrome using Pittsburgh compound B. Alzheimers Dement 8(6):496–501
59. Jennings D, Seibyl J, Sabbagh M, Lai F, Hopkins W, Bullich S et al (2015) Age dependence of brain β-amyloid deposition in Down syndrome: an [18F] florbetaben PET study. Neurology 84(5):500–507
60. Annus T, Wilson LR, Hong YT, Acosta-Cabronero J, Fryer TD, Cardenas-Blanco A et al (2015) The pattern of amyloid accumulation in the brains of adults with Down syndrome. Alzheimers Dement. Elsevier. In Press. doi: 10.1016/j.jalz.2015.07.490
61. Vinters HV (1987) Cerebral amyloid angiopathy. A critical review. Stroke 18(2):311–324
62. Charidimou A, Gang Q, Werring DJ (2012) Sporadic cerebral amyloid angiopathy revisited: recent insights into pathophysiology and clinical spectrum. J Neurol Neurosurg Psychiatry 83(2):124–137
63. Yamada M, Tsukagoshi H, Otomo E, Hayakawa M (1987) Cerebral amyloid angiopathy in the aged. J Neurol 234(6):371–376
64. Ly JV, Donnan GA, Villemagne VL, Zavala JA, Ma H, O'Keefe G et al (2010) 11C-PIB binding is increased in patients with cerebral amyloid angiopathy-related hemorrhage. Neurology 74(6):487–493
65. Baron J-C, Farid K, Dolan E, Turc G, Marrapu ST, O'Brien E et al (2014) Diagnostic utility of amyloid PET in cerebral amyloid angiopathy-related symptomatic intracerebral hemorrhage. J Cereb Blood Flow Metab 34(5):753–758
66. Gurol ME, Dierksen G, Betensky R, Gidicsin C, Halpin A, Becker A et al (2012) Predicting sites of new hemorrhage with amyloid imaging in cerebral amyloid angiopathy. Neurology 79(4):320–326
67. Lippa CF, Duda JE, Grossman M, Hurtig HI, Aarsland D, Boeve BF et al (2007) DLB and PDD boundary issues: diagnosis, treatment, molecular pathology, and biomarkers. Neurology 68(11):812–819
68. Ossenkoppele R, Jansen WJ, Rabinovici GD, Knol DL, van der Flier WM, van Berckel BNM et al (2015) Prevalence of amyloid PET positivity in dementia syndromes. JAMA 313(19):1939
69. Gomperts SN, Locascio JJ, Marquie M, Santarlasci AL, Rentz DM, Maye J et al (2012) Brain amyloid and cognition in Lewy body diseases. Mov Disord 27(8):965–973
70. Foster ER, Campbell MC, Burack MA, Hartlein J, Flores HP, Cairns NJ et al (2010) Amyloid imaging of Lewy body-associated disorders. Mov Disord 25(15):2516–2523
71. Ratnavalli E, Brayne C, Dawson K, Hodges JR (2002) The prevalence of frontotemporal dementia. Neurology 58(11):1615–1621
72. Varma AR, Snowden JS, Lloyd JJ, Talbot PR, Mann DM, Neary D (1999) Evaluation of the NINCDS-ADRDA criteria in the differentiation of Alzheimer's disease and frontotemporal dementia. J Neurol Neurosurg Psychiatry 66(2):184–188
73. Johnson VE, Stewart W, Smith DH (2010) Traumatic brain injury and amyloid-β pathology: a link to Alzheimer's disease? Nat Rev Neurosci 11(5):361–370
74. Plassman BL, Havlik RJ, Steffens DC, Helms MJ, Newman TN, Drosdick D et al (2000) Documented head injury in early adulthood and risk of Alzheimer's disease and other dementias. Neurology 55(8):1158–1166
75. Roberts GW, Gentleman SM, Lynch A, Murray L, Landon M, Graham DI (1994) Beta amyloid protein deposition in the brain after severe head injury: implications for the pathogenesis of Alzheimer's disease. J Neurol Neurosurg Psychiatry 57(4):419–425
76. Kawai N, Kawanishi M, Kudomi N, Maeda Y, Yamamoto Y, Nishiyama Y et al (2013) Detection of brain amyloid β deposition in patients with neuropsychological impairment after traumatic brain injury: PET evaluation using Pittsburgh Compound-B. Brain Inj 27(9):1026–1031
77. Hong YT, Veenith T, Dewar D, Outtrim JG, Mani V, Williams C et al (2014) Amyloid imaging with carbon 11-labeled Pittsburgh compound B for traumatic brain injury. JAMA Neurol 71(1):23–31
78. Fodero-Tavoletti MT, Furumoto S, Taylor L, McLean CA, Mulligan RS, Birchall I et al (2014) Assessing THK523 selectivity for tau deposits in Alzheimer's disease and non-Alzheimer's disease tauopathies. Alzheimers Res Ther 6(1):11
79. Villemagne VL, Fodero-Tavoletti MT, Masters CL, Rowe CC (2015) Tau imaging: early progress and future directions. Lancet Neurol 14(1):114–124
80. Okamura N, Harada R, Furumoto S, Arai H, Yanai K, Kudo Y (2014) Tau PET imaging in Alzheimer's disease. Curr Neurol Neurosci Rep 14(11):500
81. Kadir A, Andreasen N, Almkvist O, Wall A, Forsberg A, Engler H et al (2008) Effect of phenserine treatment on brain functional activity and amyloid in Alzheimer's disease. Ann Neurol 63(5):621–631
82. Doody RS, Thomas RG, Farlow M, Iwatsubo T, Vellas B, Joffe S et al (2014) Phase 3 trials of solanezumab for mild-to-moderate Alzheimer's disease. N Engl J Med 370(4):311–321
83. Ostrowitzki S, Deptula D, Thurfjell L, Barkhof F, Bohrmann B, Brooks DJ et al (2012) Mechanism

of amyloid removal in patients with Alzheimer disease treated with gantenerumab. Arch Neurol 69(2):198–207
84. Salloway S, Sperling R, Brashear HR (2014) Phase 3 trials of solanezumab and bapineuzumab for Alzheimer's disease. N Engl J Med 370(15):1460
85. Rinne JO, Brooks DJ, Rossor MN, Fox NC, Bullock R, Klunk WE et al (2010) 11C-PiB PET assessment of change in fibrillar amyloid-beta load in patients with Alzheimer's disease treated with bapineuzumab: a phase 2, double-blind, placebo-controlled, ascending-dose study. Lancet Neurol 9(4):363–372
86. Aisen PS (2009) Alzheimer's disease therapeutic research: the path forward. Alzheimers Res Ther 1(1):2

8 Movement Disorders: Focus on Parkinson's Disease and Related Disorders

Andrea Varrone, Sabina Pappatà, and Mario Quarantelli

8.1 Neuropathology and Pathophysiology of Movement Disorders and Relevance to Imaging

The pathological hallmark of PD is the presence of Lewy bodies in the cytoplasm of dopaminergic neurons and the loss of dopamine-containing cells in the substantia nigra. Lewy bodies are inclusions containing aggregates of alpha-synuclein, which is the misfolded protein characteristic of PD pathology. According to the Braak staging, the first pathological abnormalities are observed in the olfactory bulbs and the dorsal motor nucleus of the vagus nerve [1]. From those regions, alpha-synuclein pathology appears to spread in a caudal-to-rostral fashion, with subsequent involvement of other brainstem nuclei, such as the locus coeruleus, the raphe nuclei, and the substantia nigra, and finally of cortical regions, such as the anterior cingulate cortex, the insula, the amygdala, and the entorhinal cortex [1, 2]. At present, there is no available radioligand for imaging of alpha-synuclein deposition in vivo that has sufficient selectivity and affinity for alpha-synuclein aggregates [3]. Thus currently it is not possible to follow the development of alpha-synuclein pathology as it is the case for amyloid and tau imaging. However, the associated neuronal loss in the various brainstem nuclei and the loss of the axonal projections to the striatum and cortex can be examined in vivo with different radioligands targeting the monoaminergic systems. Alternatively, specific MR sequences can be used to examine the change of MR signal in the substantia nigra and locus coeruleus, and DTI tractography can be used to visualize nigrostriatal projections in vivo. The loss of nigrostriatal dopaminergic projections in PD is associated also with an imbalance between the direct and indirect pathway in the basal ganglia, which has been described in relation to the decreased thalamocortical input and might explain motor symptoms as rigidity and bradykinesia. The functional changes occurring in the basal ganglia circuit are associated with characteristic glucose metabolic abnormalities that result in the so-called PD covariance pattern. In addition to specific abnormalities of monoaminergic systems and of glucose metabolism, studies indicate also the presence of neuroinflammatory changes in the brain of PD patients, including microglia activation, which can be examined in vivo using PET imaging of the 18-kDa translocator protein (TSPO).

A. Varrone (✉)
Department of Clinical Neuroscience, Karolinska Institutet, Stockholm, Sweden
e-mail: andrea.varrone@ki.se

S. Pappatà • M. Quarantelli
Biostructure and Bioimaging Institute, National Research Council, Naples, Italy

A. Ciarmiello, L. Mansi (eds.), *PET-CT and PET-MRI in Neurology*,
DOI 10.1007/978-3-319-31614-7_8

MSA is another alpha-synucleinopathy characterized by the presence of glial cytoplasmic inclusions containing aggregates of alpha-synuclein accumulating in oligodendrocytes in the white matter of the striatum and the cerebellum, with associated involvement of the striatal and nigral neurons (striatonigral degeneration), the Purkinje cells of the cerebellum, the inferior olives, and the pontine nuclei (olivopontocerebellar atrophy). Jellinger et al. have provided a pathological classification of MSA [4], indicating the degree of severity of the aforementioned abnormalities and their clinical correlates that are conventionally referred to as MSA-P or MSA-C based on the prevalence of parkinsonian or cerebellar symptoms. Considering the involvement of the striatonigral pathway, the primary target of interest has been the dopaminergic system, both at the presynaptic (dopamine uptake or dopamine transporter) and postsynaptic site (D2 receptors). In addition, changes in glucose metabolism can be examined in the basal ganglia and cerebellum. Structural MRI permits to identify some specific signs of signal change both in the striatum and the pons. Diffusion-weighted imaging with MRI can sensitively detect changes in diffusion of the water molecules in the striatum and pontocerebellar region, associated to the degenerative process. Similarly as in PD, microglia activation can be examined with PET in the striatum of MSA patients.

The other two disorders that are of interest for this chapter are PSP and CBD. Both are conditions characterized by the presence of tau aggregates in the form of neurofibrillary tangles or other specific aggregates and are conventionally referred as tauopathies. There are different tau tandem repeats that can be found in different disorders. The three tandem repeats are typical of Pick disease, whereas the four tandem repeats are characteristic of CBD, PSP, and argyrophilic dementias. The tau aggregates found in Alzheimer's disease instead contain a mixture of three and four tandem repeats. PSP is typically characterized by three major clinical phenotypes: PSP-parkinsonism, Richardson's syndrome (RS), and pure akinesia with gate freezing (PAGF). In the case of PSP, a scoring of the tau pathology has been proposed by Williams et al., and it has been shown that the severity of tau abnormalities is greater in RS as compared with PSP-P and PAGF [5]. Besides neurofibrillary tangles, the other characteristic tau aggregates are the tufted astrocytes and the coiled bodies. The main brain regions where tau aggregates are typically found in PSP are the internal globus pallidus, the caudate nucleus, the substantia nigra, the subthalamic nucleus, the pons, the dentate nuclei of the cerebellum, the cerebellar white matter, and the frontal and parietal gray and white matter. The main pathological abnormalities that distinguish PSP from CBD are the presence of tufted astrocytes in PSP and the astrocytic plaques in CBD [6]. In addition, in PSP the pathology is more proximal and mainly localized in the basal ganglia, diencephalon, and brainstem, whereas in CBD pathological changes are more distal and tend to involve the cerebrum [7]. Imaging markers of interest for the assessment of PSP and CBD include dopamine uptake, dopamine transporter, and D2 receptors and in the case of PSP cholinesterase activity as marker of cholinergic projections from the brainstem to the thalamus, which are typically involved in PSP. FDG-PET shows characteristic patterns of hypometabolism in PSP and CBD. Neuroinflammatory changes have also been observed in the brain of PSP and CBD patients. New PET radioligands for tau imaging are under evaluation for their property to bind to four tandem repeats in PSP and CBD. Very preliminary results using PET and [^{11}C]PBB3, a new tau radiotracer with high selectivity and affinity for all the tau isoforms, showed increased binding in the basal ganglia, brainstem, thalamus, and cerebral cortex of a patient diagnosed as CBD, providing the first evidence of in vivo detection of tau aggregates in CBD [8]. Increased [^{18}F]FDDNP binding was also reported in subcortical and cortical regions of PSP patients, a pattern consistent with that of tau distribution in this disorder. [^{18}F]FDDNP however lacks sufficient specificity, selectivity, and affinity for tau as compared to Aβ aggregates [9]. Structural MRI can show characteristic findings of brainstem atrophy, and DWI has also been used to examine patterns of diffusion in the basal ganglia.

8.2 Main PET Applications and Findings in Parkinson's Disease and Related Disorders

The biochemical hallmark of PD is the loss of dopamine content in the striatal terminals due to the degeneration of dopaminergic nigrostriatal projections. Therefore, the dopaminergic system is the primary monoaminergic system affected in PD. However, considering the pathological staging reported by Braak et al., other nuclei of the brainstem seem to be affected early in the course of the disease. The raphe nuclei are highly enriched of serotonin-containing cells. Postmortem studies have reported a decrease of serotoninergic neurons in the medial raphe nuclei and a loss of serotonin markers (serotonin and serotonin transporter) in the striatum of PD patients. The degree of serotoninergic loss seems to be less severe than the loss of dopaminergic projections.

8.2.1 Monoaminergic Systems: Dopamine

In vivo PET studies have contributed to define the degree of dopaminergic and serotoninergic loss in relation to the disease onset and progression. Imaging markers for the presynaptic dopaminergic system include [^{18}F]fluorodopa and radioligands for the dopamine transporter (DAT) and for the vesicular monoamine transporter type 2 (VMAT2) (Fig. 8.1 and Table 8.1).

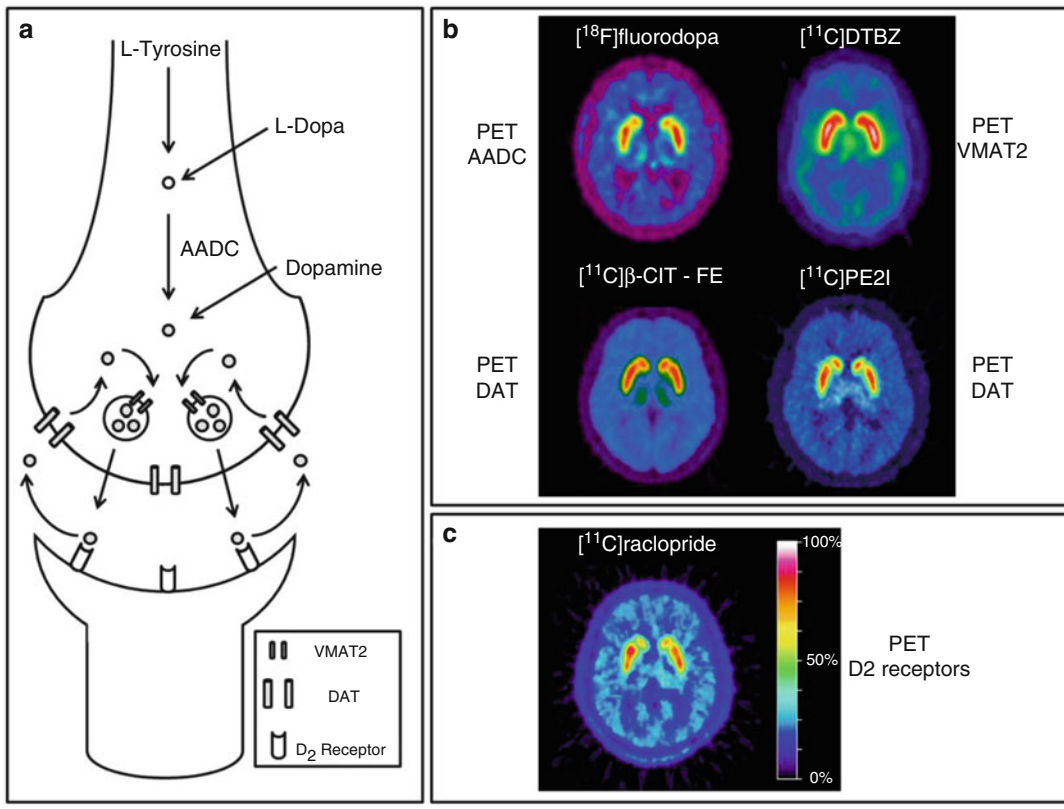

Fig. 8.1 Schematic representation of the dopamine synapse with (**a**) relevant presynaptic and postsynaptic targets for PET imaging. Representative images of different radioligands for imaging of the dopaminergic terminals. (**b**) [^{18}F]Fluorodopa (*AADC* aromatic amino acid decarboxylase), [^{11}C]DTBZ (VMAT2), and PET radioligands for the DAT. (**c**) [^{11}C]Raclopride (D2 receptor) (Reprinted with permission of Elsevier)

Table 8.1 PET radioligands for different dopaminergic targets of interest in movement disorders

Target	Radioligand	Synaptic location and parameter measured
AADC	[^{18}F]Fluorodopa	Presynaptic, dopamine uptake, and storage
DAT	[^{11}C]Methylphenidate	Presynaptic, dopamine reuptake from synaptic cleft
	[^{11}C]β-CFT	
	[^{11}C]PE2I	
	[^{18}F]β-CFT	
	[^{18}F]FP-CIT	
	[^{18}F]FECNT	
	[^{18}F]FE-PE2I	
VMAT2	[^{11}C]DTBZ	Presynaptic, dopamine reuptake in vesicles
	[^{18}F]DTBZ (AV-133)	
D2 receptor	[^{11}C]Raclopride	Postsynaptic on striatal neurons
	[^{18}F]Fallypride	
	[^{18}F]Desmethoxyfallypride	

PET studies with [^{18}F]fluorodopa and other presynaptic markers such as the DAT and the VMAT2 have shown that approximately 60–70 % of the dopaminergic terminals in the putamen are lost already at early stages of PD [10–22]. The caudate and the ventral striatum seem to be less affected as they receive the projections from the ventromedial part of the substantia nigra [23] and from the mesolimbic pathway that is less compromised in early stages of PD. The loss of dopaminergic projections is an exponential process occurring at a rate of approximately 6–10 % per year [21, 24–29]. The severity of the nigrostriatal dopaminergic deficit in the posterior putamen mostly correlates with some of the motor features of PD, such as bradykinesia and rigidity [16, 23], whereas the integrity of caudate projections correlates with working memory function [30] and with some personality traits such as novelty seeking [31] and harm avoidance [32]. Therefore, the dopaminergic dysfunction in PD seems to be not only associated with motor impairment but also with cognitive and behavioral aspects of the disease.

Newly developed ^{18}F-labeled tracers for the DAT and the VMAT2 such as [^{18}F]FE-PE2I and [^{18}F]FP-DTBZ are of potential interest as diagnostic markers in PD [20, 22]. The labeling with ^{18}F could allow for the distribution and use of the tracers in imaging centers having PET/CT systems, even without the cyclotron and radiochemistry units. The improved imaging characteristics of these new tracers combined with the improved resolution and sensitivity of the modern PET/CT and PET/MR systems would provide the possibility to examine the two targets, DAT and VMAT2, not only in the striatum but also in the substantia nigra (Fig. 8.2). Finally, the quantitative performance of PET might be of advantage in clinical trials aimed at using [^{18}F] fluorodopa, DAT, or VMAT2 imaging as biomarkers to assess imaging end points [33, 34].

The involvement of the dopaminergic system in PD is mainly confined to the presynaptic terminals, whereas the striatal neurons are only functionally affected by the loss of nigrostriatal input and decreased levels of striatal dopamine. In the very early stage of PD, there is indeed an increased availability of D2 receptors in the striatum measured with the radioligand [^{11}C]raclopride. This increased availability is most likely related to upregulation and/or reduced competition of the endogenous dopamine with the D2 receptor [35]. It has been shown that such increased availability tends to normalize with the L-dopa or dopaminergic treatment [36]. In PSP and MSA, there is involvement of striatal neurons depending upon the subtype or the stage of the disease. Therefore, D2 receptor imaging can demonstrate reduced postsynaptic D2 receptor

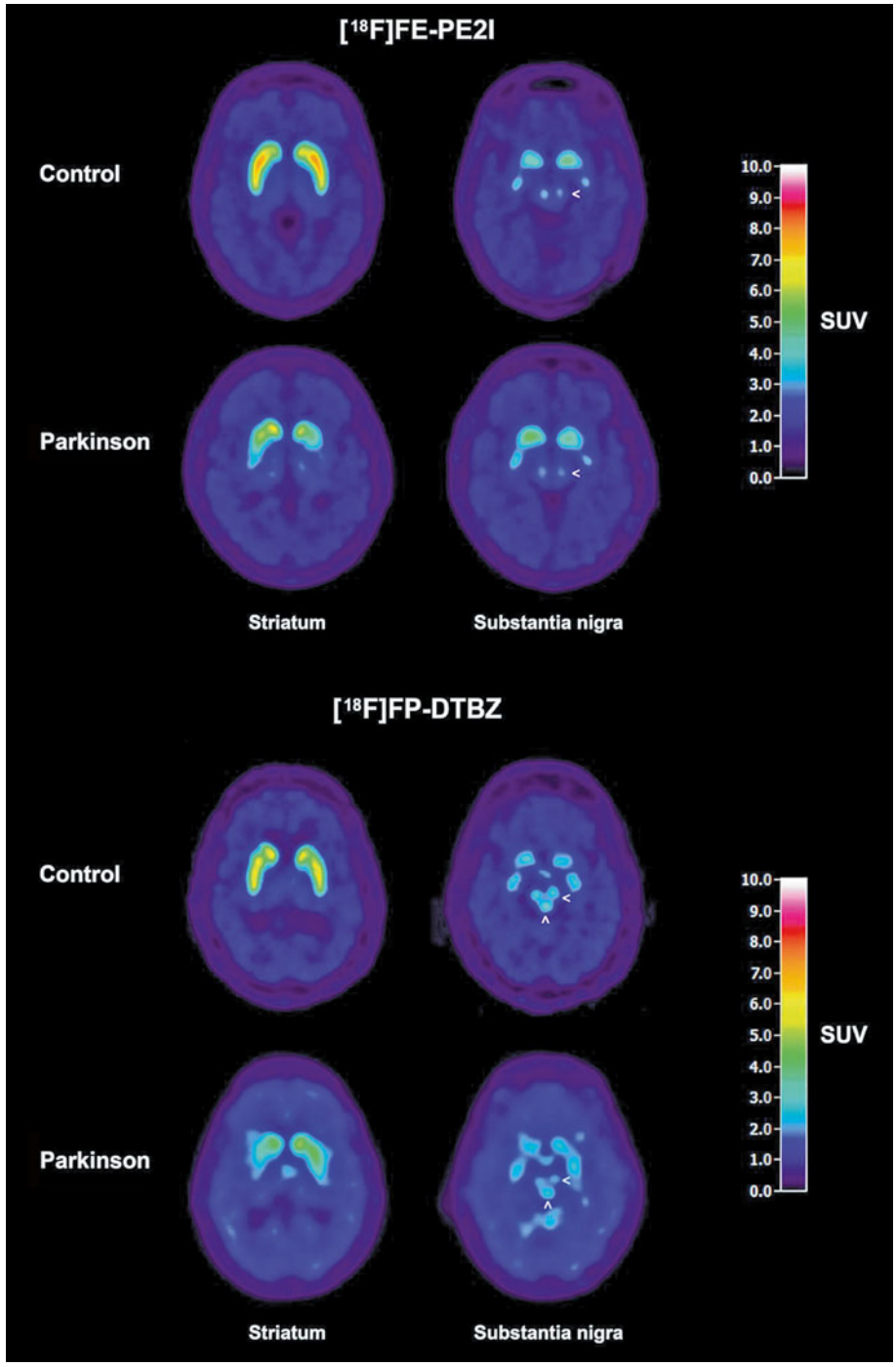

Fig. 8.2 Representative PET images of [^{18}F]FE-PE2I (*upper panel*) and [^{18}F]FP-DTBZ (*lower panel*) in control subjects and Parkinson's disease patients. The [^{18}F] FE-PE2I images were acquired using the high-resolution research tomograph (HRRT) at Karolinska Institutet and were smoothed with a Gaussian filter of 6 mm to reproduce the resolution of a clinical PET system (courtesy of Dr. Andrea Varrone). The [^{18}F]FP-DTBZ images were acquired at Molecular NeuroImaging (MNI), New Haven, CT, USA (courtesy of Dr. John Seibyl). The color scale corresponds to standard uptake value (SUV) units. The *arrow head* < indicates the binding to the DAT or VMAT2 in the dopaminergic cells of the substantia nigra; the *arrow head* ∧ indicates the binding to the VMAT2 in the serotoninergic cells in the raphe nuclei

availability in the striatum of MSA or PSP patients as compared with PD patients [37]. This difference can be also used as a diagnostic criterion to support the differential diagnosis between PD and MSA or PSP.

However, a certain overlap of dopamine D2 receptor availability might be present between PD patients and MSA or PSP patients. The accuracy of the differential diagnosis at individual level could be improved by using a multitracer approach (i.e., [^{11}C]raclopride + [^{18}F] FDG) [38, 39] or complementary information from a single-tracer study (i.e., blood flow + receptor binding for [^{11}C]raclopride) [40]. Besides the reference radioligand [^{11}C] raclopride, ^{18}F-labeled radioligands with higher affinity for the D2 receptor, [^{18}F]fallypride and [^{18}F]desmethoxyfallypride, have been developed [41]. A recent study in 37 patients with PD and 44 patients with atypical parkinsonian syndromes has shown that the measurement of [^{18}F]desmethoxyfallypride binding in the putamen had a sensitivity of 86.5 %, a specificity of 95.5 %, an accuracy of 91.4 %, and a positive predictive value of 94.1 % [42], similar to the values reported for FDG-PET [43].

8.2.2 Monoaminergic Systems: Serotonin

The involvement of the serotonin system in PD in vivo has been examined in several PET studies using different imaging markers of the serotonin systems. Most of the studies have been conducted with the serotonin transporter (5-HTT) radioligand [^{11}C]DASB [44–46], and additional few studies have been conducted with the 5-HT$_{1A}$ radioligands [^{11}C]WAY100635 or [^{18}F]MPFF [47, 48] or with the 5-HT$_{1B}$ radioligand [^{11}C]AZ10419369 [49]. PET studies with [^{11}C]DASB have shown that the 5-HTT availability is relatively more preserved than the dopaminergic function in early stages of the disease and that it decreases as the disease advances [46]. In early PD patients, there is approximately 30 % lower 5-HTT availability as compared with control subjects in the brainstem and basal forebrain, with the progressive involvement of the basal ganglia, amygdala, hippocampus, and anterior cingulate cortex in more advanced stages of the disease. The serotonin dysfunction globally seems not to be associated with the motor dysfunction [46]. However, PD patients with chronic fatigue have a marked reduction of 5-HTT availability in striatum and cortical areas compared with PD patients without fatigue symptoms [50], and the presence of depressive symptoms in PD patients seems to be positively associated with 5-HTT availability in the raphe nuclei and limbic regions [51, 52]. Therefore, some nonmotor symptoms such as chronic fatigue and depression seem to be associated with the serotonin function. PET studies with other markers of the serotonin system have contributed to support the involvement of the serotonin system in PD. Decreased 5-HT$_{1A}$ receptor availability in the raphe nuclei was found using [^{11}C] WAY100635 [47]. The 5-HT$_{1A}$ receptor availability in the raphe nuclei correlated with the severity of the tremor assessed with the Unified Parkinson´s Disease Rating Scale (UPDRS) [47]. Reduction of 5-HT$_{1A}$ receptor availability in several limbic brain regions in PD patients with depression was also reported using the radioligand [^{18}F]MPFF [48]. Finally, a recent study with the 5-HT$_{1B}$ receptor radioligand [^{11}C]AZ10419369 showed lower 5-HT$_{1B}$ receptor availability in the orbitofrontal cortex of PD patients without depression, suggesting an early involvement of serotonin function in PD not necessarily related with depressive symptoms [49]. Depression is a common nonmotor feature observed in PD patient, sometimes occurring also before the onset of the motor symptoms. Experience from clinical trials with serotonin reuptake inhibitors suggests that nonselective reuptake inhibitors can be also effective in the treatment of depression in PD. In agreement with this hypothesis are the results of the only one study with the nonselective monoaminergic transporter radioligand [^{11}C] RTI-32, demonstrating lower binding of [^{11}C]

RTI-32 in the locus coeruleus and limbic brain regions of depressed PD patients compared with nondepressed patients [53].

8.2.3 Enzymatic Activity in the Basal Ganglia

In parkinsonism there is alteration of the normal function of the basal ganglia-cortical circuit due to presynaptic denervation and loss of monoaminergic but also cholinergic terminals. In PD and PSP, the involvement of the nucleus basalis of Meynert determines a loss of cholinergic projections to the frontal cortex. Therefore, by measuring acetylcholinesterase activity with the PET radioligand [^{11}C] MP4A, it is possible to examine the loss of cholinergic projections to the frontal cortex in PD and PSP, compared with control subjects. In PSP, there is an additional involvement of the pedunculopontine nucleus (PPN) in the brainstem with consequent loss of thalamic cholinergic projections. According to this postmortem observation, in vivo PET studies revealed a decreased thalamic acetylcholinesterase activity in PSP patients as compared with controls and PD patients. This differential involvement of the thalamus and the cortex in PSP vs. PD has been suggested as potential marker to differentiate the two disorders [54].

Another important enzyme highly enriched in the striatal medium-sized spiny neurons (MSNs) is the phosphodiesterase 10A (PDE10A). PDE10A is the major regulator of cyclic AMP and cyclic GMP in the striatum both within the direct and indirect pathway. The PDE10A enzyme has been shown to be severely affected in Huntington's disease, due to the primary involvement of the MSNs. However, recently a decrease of PDE10A enzyme availability has been reported also in PD patients [55]. The decrease of PDE10A enzyme correlated with the duration of the disease and seemed to suggest an involvement of the cAMP/cGMP signaling pathway as the disease progresses. Additional studies are though needed to exclude a possible effect of antiparkinsonian pharmacological treatment on the PDE10A enzyme.

8.2.4 Neuronal Integrity and Glucose Metabolism

To our knowledge, there is only one study in PSP patients that has examined the integrity of cortical neurons using the radioligand [^{11}C]flumazenil. [^{11}C]Flumazenil is a marker of GABA-A receptors that are present on cortical GABAergic interneurons. The measurement of GABA-A receptor availability with [^{11}C]flumazenil is considered a marker of neuronal integrity. In PSP, decreased availability of GABA-A receptors has been found in the anterior cingulate cortex [56], a region in which glucose metabolism is also decreased. There seems not to be a loss of gray matter in the anterior cingulate [57], which might suggest that the loss of GABAergic signal and glucose metabolism in this region might be a result of subcortical deafferentation.

FDG-PET has been recently proposed also for the differential diagnosis of PD from atypical parkinsonian disorders. In PD patients a typical spatial covariance pattern of glucose metabolism has been described, with characteristic relative increase in glucose metabolism in the putamen and the cerebellum [58]. The expression of this pattern has been found also to correlate with dopaminergic dysfunction and with disease progression [59]. In atypical parkinsonian disorders, such as MSA, PSP, and CBD, there are characteristic and specific patterns of abnormalities in glucose metabolism. In MSA, there is a decrease in glucose metabolism in the putamen (in MSA-P variant) and in the cerebellar hemispheres (MSA-C variant) (Fig. 8.3). In PSP a decrease of glucose metabolism is found in the caudate nucleus, the brainstem, and the medial frontal cortex (Fig. 8.3). In CBD, an asymmetric decrease of glucose metabolism is found in the cortex (frontal and parietal including sensorimotor cortex) and in the striatum (Fig. 8.3). These patterns of abnormalities of glucose metabolism have been found to be specific for each disorder, with high sensitivity and specificity [43]. Therefore, FDG-PET can help support the differential diagnosis

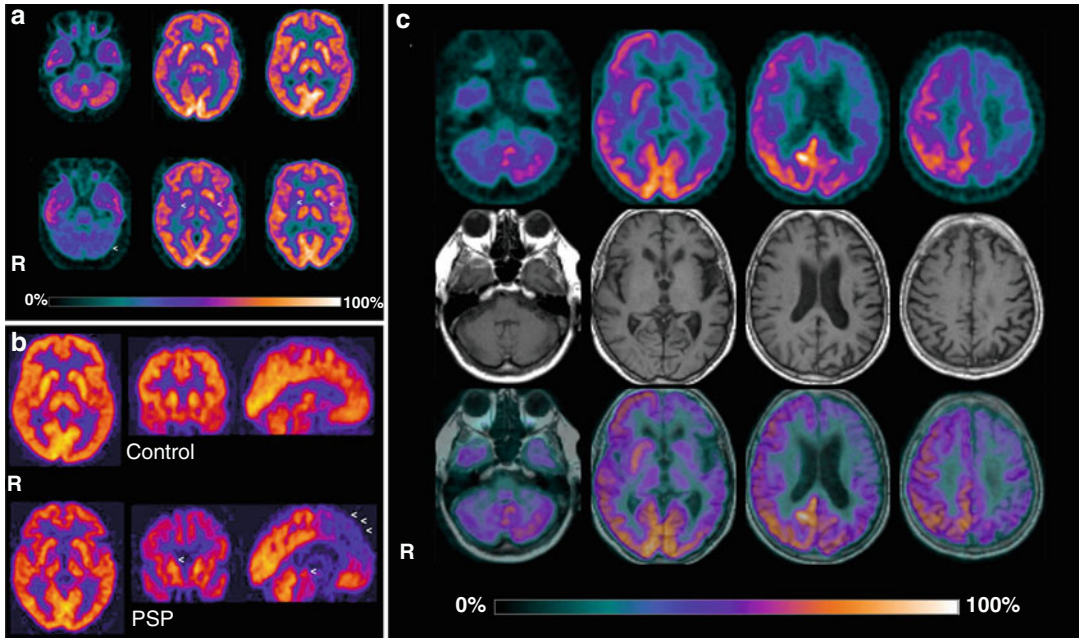

Fig. 8.3 *Left top panel* (**a**), FDG-PET images in a control subject (*Top row*) and a MSA patient (*Bottom row*), showing decreased glucose metabolism in the putamen and cerebellar hemispheres (*arrowheads*). *Left bottom panel* (**b**), FDG-PET images in a control subject and a PSP patient. The *arrowheads* indicate area of decreased glucose metabolism in the medial prefrontal cortex, striatum, and midbrain. *Right panel* (**c**), FDG-PET (*Top row*), MRI (*Middle row*), and fused PET-MRI images (*Bottom row*) in a patient with CBD

between PD and other parkinsonian disorders and could be considered an important diagnostic imaging tool for the neurologist and nuclear physicians [60].

8.2.5 Neuroinflammation: Imaging of the 18-kDa Translocator Protein (TSPO)

The 18-kDa translocator protein (TSPO) is a protein located on the inner mitochondrial membrane of different cells, such as microglia, monocytes, and astrocytes. The expression of TSPO is increased in case of microglia activation following acute or chronic pathological conditions, and TSPO PET imaging is considered a marker of microglia activation and neuroinflammation. In parkinsonian disorders, PET studies have been conducted with the TSPO radioligand [^{11}C]-*R*-PK11195 (Fig. 8.4). In PD patients, higher TSPO binding has been found in the following subcortical regions, striatum, thalamus, globus pallidus, and pons, and also in the frontal and cingulate cortex, compared with control subjects [61]. The [^{11}C]-*R*-PK11195 binding did not change significantly in those patients that underwent a follow-up PET measurement 18–24 months after the first examination, suggesting that the neuroinflammation in PD might be a stable process over time. Moreover, [^{11}C]-*R*-PK11195 binding in the midbrain has been found to correlate negatively with the DAT availability in the dorsal putamen and positively with the motor UPDRS, suggesting a link between neuroinflammation, dopaminergic deficit, and motor deficit [62]. Increased [^{11}C]-*R*-PK11195 binding was also reported in the striatum, globus pallidus, and thalamus of MSA patients, and in PSP patients increased binding was found in the same regions and also in the pons, midbrain, and frontal cortex [63, 64]. Interestingly, the striatal changes of water diffusivity measured with MRI in atypical parkinsonian patients and reflecting

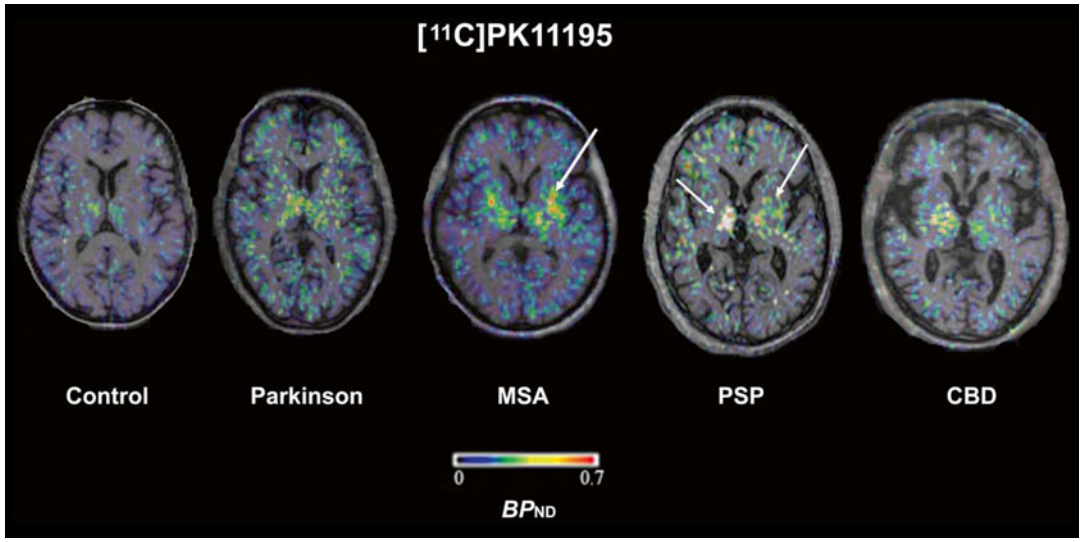

Fig. 8.4 Representative parametric images of binding potential of [11C]PK11195 in a control subject and in patients with different parkinsonian disorders. The *arrows* indicate areas of increased binding of [11C]PK11195 to TSPO (Courtesy of Dr. Alexander Gerhard, University of Manchester, UK. Reprinted with permission of Wolters Kluwer Health, Inc., John Wiley and Sons, and Elsevier)

microstructural damage correlate with microglial activation in the brainstem but not in the striatum, suggesting that microglial activation only in the brainstem regions contributes to tissue damage in these patients [65]. In addition, imaging of TSPO can be a suitable marker to examine treatment effects of anti-inflammatory drugs. In a clinical trial using minocycline in MSA patients, a small subgroup of patients were examined with [11C]-*R*-PK11195 PET before and after treatment. In those patients a decrease of [11C]-*R*-PK11195 binding was observed 6 months after treatment with minocycline [66]. Although minocycline did not show any clinical efficacy in MSA patients, the TSPO imaging sub-study suggested the possibility to monitor the anti-inflammatory effect on the microglia activation. This proof of mechanism was recently demonstrated in a study examining the effect of the myeloperoxidase (MPO) inhibitor AZD3241 on microglia activation in PD patients after 8 weeks of treatment and examined at baseline, 4 weeks, and 8 weeks of treatment with the TSPO radioligand [11C]PBR28 [67]. A statistically significant decrease of [11C]PBR28 binding by 15 % was observed in the active group, whereas no statistically significant changes were observed in the placebo group, suggesting that the inhibition of MPO leads to a decrease in microglia activation that can be detected in vivo with TSPO imaging [67].

8.3 Main MR Applications and Findings in Parkinson's Disease and Related Disorders

8.3.1 Conventional MRI

While conventional MRI has limited value in the diagnostic workup of typical PD [68], it can contribute to the exclusion of PD mimics, such as cerebrovascular disease, normal pressure hydrocephalus, or tumors [69], in patients with atypical parkinsonisms or in patients who fail to respond to therapeutic doses of L-dopa, conventional MRI.

In addition, specific signs may be present in atypical parkinsonian syndromes (APS) [70, 71] that can allow differential diagnosis.

In PSP, these signs include the "hummingbird" [72] and the "Mickey Mouse" [73, 74] or "morning glory flower" [75] signs (Fig. 8.5; both signs are expression of midbrain atrophy), while in MSA,

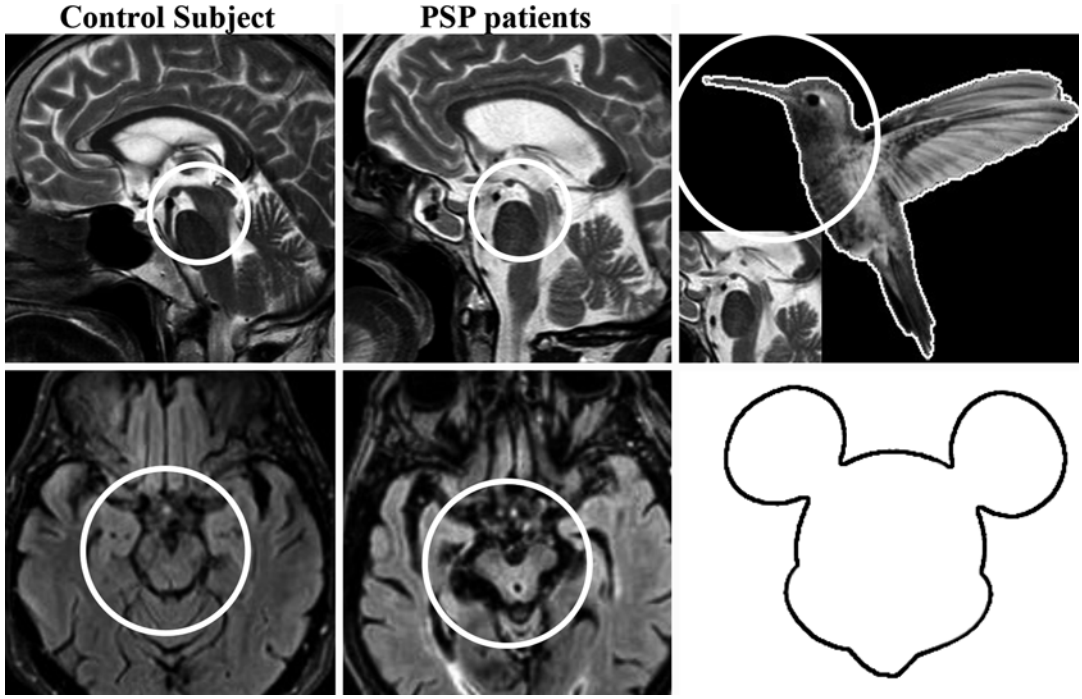

Fig. 8.5 Signs of midbrain atrophy in PSP at conventional MRI images. In sagittal images (*top row*), the hummingbird sign (also known as the penguin sign) refers to the characteristic shape that the atrophic midbrain assumes, resembling the head of a hummingbird (see circles on the *top row*). The Mickey Mouse sign refers to the shape of the midbrain in the axial plane (*bottom row*), where atrophy of the midbrain with relative sparing of tectum and cerebral peduncles results in this characteristic shape (see circle in the *bottom row*)

putaminal involvement can result in atrophy and hypointensity of the putamen on T2-weighted and T2*-weighted images [76], associated to a hyperintense rim on FLuid Attenuated Inversion-Recovery (FLAIR) sequences in the external capsule (Fig. 8.6a) [76, 77]. Of note, although the hyperintense rim sign is frequently seen also in normal controls at 3 tesla [78]; at 1.5 tesla it is highly specific for MSA-P, especially when it borders the posterior part of the putamen [79].

Conversely, the cerebellar involvement in MSA results in major vermian and cerebellar hemispheric atrophy [80], coupled to T2 hyperintensity of the middle cerebellar peduncles, the pontocerebellar, and pontine raphe fibers (Fig. 8.6b) [70, 80].

Of note, the hyperintensity of pontocerebellar and pontine raphe fibers, which results in the so-called "hot cross bun" sign, has been however reported also in vascular parkinsonism [81] and in variant Creutzfeldt-Jakob [82].

All these signs, however, although fairly specific, are usually more evident in the advanced phases of the disease, when the clinical picture is usually already sufficient to establish a diagnosis. Accordingly, advanced MR techniques are being explored to help differentiate APS from PD. These techniques include diffusion-weighted imaging (DWI), MR spectroscopy (MRS), and imaging of iron deposition by either R2* sequences or susceptibility-weighted imaging (SWI). In addition, volumetric techniques probing brain tissue changes by post-processing of 3-D-T1w volumes, which have allowed to highlight specific GM atrophy patterns in different parkinsonian syndromes, are also being explored to verify their diagnostic potential at single-subject level.

8.3.2 Diffusion-Weighted Imaging

In PD, diffusion alterations in SN consistent with neuronal loss have been detected in most studies [83], reaching a 100 % accuracy in separating PD

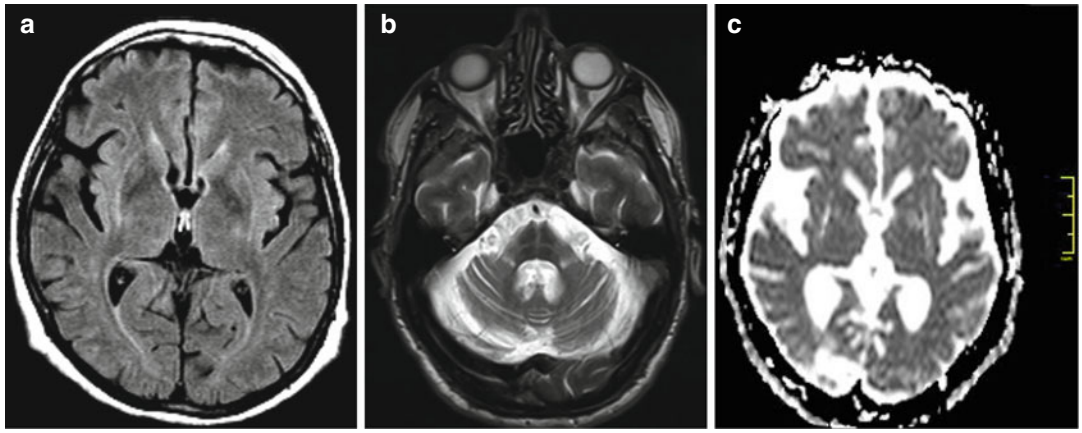

Fig. 8.6 (**a**) FLAIR image acquired at 1.5 tesla. Axial plane at the basal ganglia level in a MSA-P patient. A hyperintense rim surrounding the lateral margins of the putamen can be seen bilaterally, more prominent posteriorly on the right. (**b**) T2w axial plane at the MCP level in a MSA-C patient. Thinning and hyperintensity of both MCP, along with severe vermian and bilateral hemispheric cerebellar atrophy, can be seen. In addition, mild hyperintensity of the transverse pontocerebellar fibers and of the raphe results in the so-called "hot cross bun" sign. (**c**) ADM map. Axial plane at the basal ganglia level in a MSA-P patient. Increase diffusivity, consistent with neuronal loss and vacuolization, can be seen in the putamen bilaterally. Diffuse cortical and subcortical atrophy is also apparent

from healthy controls in early phases of the disease in one study [84], although these changes appear to be nonspecific as they do not allow to differentiate PD from APS [83].

In MSA, diffusion alterations have been quite consistently reported in the putamen [85–87] (Fig. 8.6c), pons, and cerebellum [87], compared to healthy controls. In addition, a significant progression of diffusion changes in the putamen has been shown in longitudinal studies [88, 89].

When considering also APS, increaseas of Apparent Diffusion Coefficient (ADC) in the Middle Cerebellar Peduncle (MCP) [90–92] and in the putamen [92, 93] and allows to differentiate the parkinsonian and cerebellar subtypes of MSA [94], and to separate MSA from both PSP and PD. On the other hand, increased ADC in midbrain and globus pallidus allowed to differentiate PSP from both PD and MSA [92].

Interestingly, the combination of morphometric and diffusion measures from a few critical structures (width and FA of the MCP and thickness of the pons) has been shown to provide added diagnostic value, allowing to differentiate MSA from PD with 92 % sensitivity and 96 % specificity [95], suggesting that these techniques provide complementary information to those conveyed by conventional MRI and volumetric analysis.

More heterogeneous patterns of diffusion alterations have been shown in CBD, where increased diffusivity has been however consistently reported in motor regions, SMA, cingulum, and thalamus [96, 97]. Although these regions were also affected in CBD, thus, it has been suggested that differences in the pattern of thalamic involvement (anteromedial nuclei in PSP, motor nuclei in CBD), greater involvement of SCP in PSP, and greater asymmetry of the supratentorial diffusion alterations may help to differentiate these two entities [97].

The acquisition of DWI weighted in diffusion along at least six noncollinear direction allows to calculate the diffusion tensor, defining in 3-D the major direction of diffusion for each voxel. From the tensor, streamlines of preferential diffusion can be reconstructed, which represent the direction of axons in each voxel, and specific WM bundles can be identified [98].

Tractographic analysis allows in principle to increase the specificity of the results by focusing on carefully chosen WM tracts, which are known to be selectively affected in the different diseases.

Accordingly, using a tractographic approach, reduced FA and increased ADC have been demonstrated in MCP and pontine crossing tracts in MSA, while PSP patients showed alterations in

the SCP and an extensive reduction of cortical projection fibers [99].

In addition, tractographic elaboration of high-resolution DTI more recently allowed to reliably isolate smaller WM bundles. Using this approach, increased diffusivity, coupled to reduced diffusion anisotropy, has been shown in the dentatorubrothalamic tracts of PSP patients [100] and in the nigrostriatal tracts of PD patients [99] (Fig. 8.7), in the latter being also highly asymmetric.

8.3.3 Imaging of Iron Deposition

Since early demonstrations of the possibility to measure signal changes due to abnormal iron distribution in MSA and PSP (increased in the putamen and less prominently in the caudate nucleus and lateral pars compacta of the substantia nigra) [101], several studies have focused on changes in either T2 or T2* in parkinsonian syndromes, with most studies showing increased R2* values in SNc of PD patients.

The recent introduction of SWI [102], with a significantly superior sensitivity to dephasing due to ferromagnetic substances, has further improved our capacity to detect iron accumulation in the SN [103–108], and following the same approach, increased iron content has been shown in putamen in MSA patients, as opposed to PD and PSP [107, 109, 110], while PSP patients show greater iron load in the globus pallidus and caudate nucleus, compared with PD, and in the thalamus, globus pallidus, red nucleus, and substantia nigra compared with MSA patients [109, 110].

However, overall accuracy at single-subject level in discriminating between PD, PSP, and MSA-P remained somewhat disappointing [111].

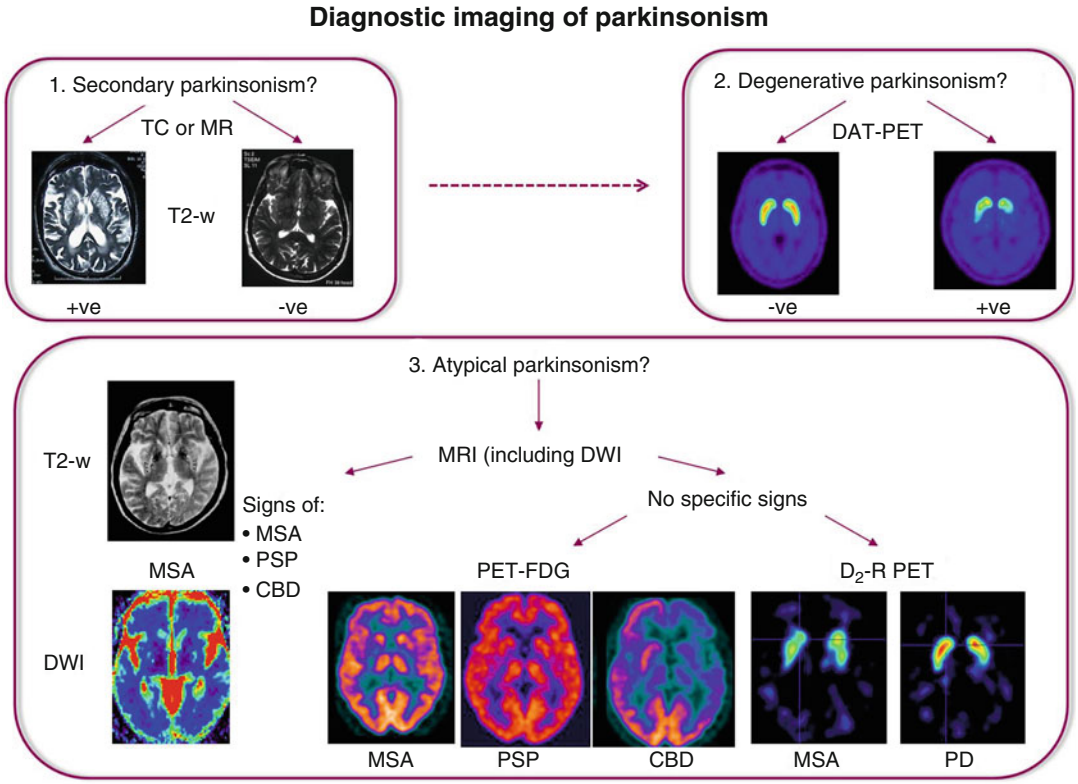

Fig. 8.7 Proposed diagnostic flowchart for the assessment of patients with clinical evidence of degenerative parkinsonism. MRI, FDG-PET, and DAT-PET images are provided by Dr. Andrea Varrone. DWI-MRI image is provided by Drs. Sabina Pappatà and Mario Quarantelli. Images of D2-PET are courtesy of Prof. Koen Van Laere

More recently, the introduction of ultrahigh fields has increased sensitivity to iron deposition in SN [112] and has allowed to study with greater sensitivity iron accumulation in SNpc nigrosome1 [113] (the largest nigrosome, where maximal cell loss occurs in PD). This approach has been then translated at 3 tesla, allowing a 94.6% accuracy in differentiating PD [114] or PD and APS [115] vs. Healthy Controls (HC).

Interestingly, selective loss of monoaminergic neurons has also been shown to be detectable at modified T1w images as a loss of the physiologic high signal of the SNpc and of the locus coeruleus, due to neuromelanin depletion, increased magnetization transfer effects, and iron load, with reported 82% sensitivity and 90% specificity in PD compared to HC [116].

When interpreting these results, it should be however considered that these techniques do not provide a quantitative measure of iron concentration, but are based on signal changes that are the net results of several phenomena, including among the others, besides the phase shifts introduced by the presence of ferromagnetic material, microstructural changes related to neuronal loss, vacuolization, and gliosis.

8.3.4 Magnetic Resonance Spectroscopy Imaging

MR spectroscopy has been used for neuronal loss and mitochondrial metabolic dysfunction, which are reflected by reductions in N-Acetyl-Aspartate (NAA) in cortical-basal ganglia networks. In addition, at higher field strengths, changes of Glu and GABA concentrations have been studied in the basal ganglia of PD patients, as putative markers of dysfunction of neuronal excitatory and inhibitory activities involved in the control of movements.

Conflicting results have been obtained in MRS studies carried out at 1.5 tesla, which have shown either no changes [117–120] or reduced NAA in basal ganglia [121, 122] and in several cortical regions [123–125] of PD patients.

Conversely, more consistent results have been obtained in APS, pointing at a potential role of MRS in the differential diagnosis of parkinsonisms. In particular, when comparing directly PD with different APS subtypes, reduced NAA [126] and NAA/Cho and NAA/Cr ratios [127, 128] have been found in the putamen and pallidum of MSA-P and PSP patients and in the pontine basis of MSA-C and MSA-P [128] patients, compared to PD.

Studies at higher fields have allowed to assess Glu/Gln and GABA in vivo, showing reduced Glu levels in the posterior cingulated gyrus [129], but not in the lentiform nucleus [130] of PD patients. In SN, reduced Glu levels have been shown in PD [131], with increases in GABA already in the mild stage of the disease [132] and a consequent strong increase of the GABA/Glu ratio [131].

Overall, despite the encouraging differences between groups highlighted, the diagnostic potential of MRS at the individual level remains to be proven.

8.3.5 Magnetization Transfer Imaging

Magnetization transfer imaging (MTI) probes tissue microstructure by exploiting the transfer between protons bound to large molecules, such as in myelin, and the mobile water protons.

Reduced MTR has been reported in the SN and putamen of PD patients already at the early stages of the disease, coupled to alterations in periventricular and parietal white matter [133, 134], and progression of the disease is associated to the involvement of caudate, pons, frontal white matter, and lateral thalamus [134].

When comparing PD and APS, differential patterns of MTR reduction have been shown [135]. In particular, an extensive involvement of globus pallidus and SN in PSP was found, which allowed to discriminate this groups from both MSA and PD patients, while MSA showed the lowest MTR in the putamen, allowing to discriminate between MSA and PD, although MSA and PSP groups somewhat overlapped.

8.3.6 Atrophy Studies

Several ROI-based analysis methods have been proposed to differentiate among PD and APS,

based on differential patterns of midbrain atrophy in PSP, asymmetric cortical atrophy in CBD, and putaminal/cerebellar atrophy in MSA-P/MSA-C.

In particular, the combined use of pons to midbrain and MCP/SCP ratios (MR parkinsonism index) has been proposed to distinguish PSP from other parkinsonian syndromes [136, 137].

On the other hand, reduced pontocerebellar volumes can be detected in MSA [138], while SN atrophy, although already present in early PD [139, 140], does not have sufficient sensitivity and specificity to discriminate between PD and APS, even when signal intensity differences are considered [141].

Finally, while atrophy of both parietal cortices and corpus callosum has been reported in CBD [142], these changes do not appear specific [143].

Compared to ROI-based analysis, voxel-based assessment of brain tissue loss has the advantages of not requiring a priori hypotheses and of being operator independent and has thus gained extensive use in the neuroimaging community. Its most diffuse implementation, voxel-based morphometry (VBM), has been shown to be suitable to detect cortical atrophy in temporal associative, limbic, paralimbic, frontal, and parietal regions in PD [144–147].

In PSP, GM loss is detected in the thalamus, midbrain, basal ganglia, and insular and frontal cortices [148], coupled to WM volume reductions in pons and midbrain and adjacent to the basal ganglia [149].

In MSA, significant reduction in the volume of the putamen is reported [150–152], along with frontal cortical involvement and cerebellar atrophy, the latter more prominent in the cerebellar variant of the disease [151, 153, 154].

Finally, asymmetric cortical atrophy remains the hallmark of CBD, with a less severe involvement of subcortical GM [155, 156].

In general, however, despite the clear differences in atrophy patterns across PD and APS subtypes, currently available studies do not support a sufficient sensitivity and specificity of VBM "as is" at single-subject level for a clinical use, apart from the differentiation of the PSP pattern from classic PD [157].

Furthermore, its performance in the early phases of these diseases, when differential diagnosis is an issue, remains to be proven.

Interestingly, however, recent studies based on large cohorts of PD patients suggest that support vector machines can be used to develop classification criteria for segmented MRI studies, reaching diagnostic accuracies above 90 % in differentiating PD from HC [158].

8.3.7 Future Trends

While conventional MRI has a reasonable specificity but lacks sufficient sensitivity in differentiating between parkinsonian syndromes, preliminary studies with advanced MRI techniques have shown a significant potential for differential diagnosis, especially when complementary techniques are applied. However, further data on the diagnostic accuracy of this approach in the earlier phases of the disease, as well as comparative studies (to disentangle the relative contributions of different techniques), are necessary to properly design integrated imaging protocols, to maximize differential diagnosis accuracy at single-subject level.

Furthermore, the impact of ultrahigh field MRI (providing superior sensitivity and resolution) and of hybrid PET/MRI scanners (allowing truly integrated structural and receptorial imaging) remains to be assessed.

8.4 Possibilities for Combined Applications

A proposed flowchart for diagnostic imaging of parkinsonism combining nuclear medicine and MRI is outlined in Fig. 8.7. A practical approach in case of suspected atypical parkinsonism would be to begin with MRI, including DWI to identify specific MRI findings suggestive of MSA, PSP, or CBD. In the absence of such findings, PET examination of glucose metabolism and/or D2 receptor imaging can help identify specific patterns of hypometabolism of D2 receptor loss suggestive of any of the above disorders. With the availability of hybrid PET/MR systems, the flowchart can be

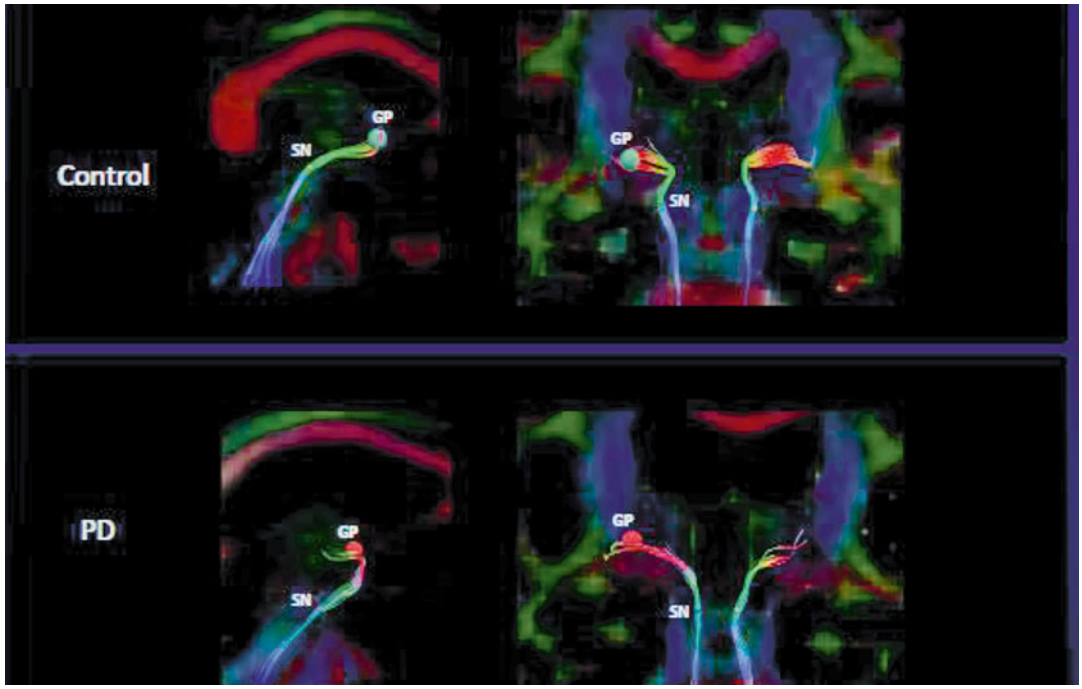

Fig. 8.8 Representative tract maps in a control subject and a PD patient (Courtesy of Drs. Yu Zhang and Norbert Shuff, University of California, San Francisco, USA)

simplified by considering only one imaging session in which structural MR, DWI, and PET can be done in a "one-stop shop" examination. Such approach would save time for scheduling the different examinations, sometimes performed in different departments, optimize patient compliance to the different procedures, and increase also the level of confidence in the diagnosis, giving the possibility to the radiologist and nuclear physician to review the images simultaneously and with high level of precision in the coregistration.

In patients in which the diagnosis of degenerative parkinsonism is in question, the present approach is to perform a structural brain scan (MRI as first choice) to rule out possible secondary causes of parkinsonism and DaTSCAN SPECT to examine DAT availability and confirm or exclude the presence of dopaminergic deficit. The availability of 18F-labeled radioligands for the DAT or VMAT2 in combination with the more wide access to PET or PET/CT systems might change the clinical scenario in the near future, giving the possibility to use PET instead of SPECT for examining the dopaminergic system in the clinical setting. The future availability of PET/MR systems will increase even more the possibility to use new DAT/VMAT2 radioligands for examining the dopaminergic system in suspected degenerative parkinsonism in combination with specific MR sequences to study the substantia nigra or DTI sequences to obtain tractography of the nigrostriatal tracts (Fig. 8.8). From a research perspective, the availability of specific radioligands for neuroinflammation combined with MR tractography could provide the possibility to examine in vivo the spread of neuroinflammatory changes along nigrostriatal or striatonigral pathways in PD and MSA.

8.5 Methodological Considerations and Future Directions

At present a major challenge is to develop specific radioligands for imaging alpha-synuclein deposition in vivo. If this challenge will be successful

and radioligands for visualizing alpha-synuclein deposits will be available, the combination of PET and MR will contribute to map precisely the distribution of alpha-synuclein in the brain of PD and MSA patients (in vivo staging) and also contribute to the understanding of the role of alpha-synuclein in the pathology of PD, considering the possibility to obtain functional, molecular, and metabolic information at the same time. To our knowledge there is only one study with the alpha-synuclein radioligand [^{11}C]BF-227 that has shown increased binding in several brain regions in MSA patients [159]. However, [^{11}C]BF-227 is not selective for alpha-synuclein as it binds also to amyloid-β and has also high-nonspecific binding, so it is not a suitable radioligand for imaging alpha-synuclein in vivo. Another aspect that is emerging more recently is the need to better characterize the binding of tau radioligands to four tandem repeats, characteristic of the tauopathies. At present, only [^{11}C]PBB3 has been shown to bind to tau aggregates present in CBD [8], but little information is available for other tau radioligands such as [^{18}F]807 or [^{18}F]THK5117 or [^{18}F]THK5351. The combination of PET and MRI can provide a detailed mapping of tau distribution in those tauopathies such as PSP and CBD that show inhomogeneous distribution of pathology. In addition, the intrinsic combination of PET and MRI could permit also PVE correction with improved accuracy of the quantification and mapping.

References

1. Braak H, Bohl JR, Muller CM, Rub U, de Vos RA, Del Tredici K (2006) Stanley Fahn Lecture 2005: the staging procedure for the inclusion body pathology associated with sporadic Parkinson's disease reconsidered. Mov Disord 21(12):2042–2051. doi:10.1002/mds.21065
2. Goedert M, Spillantini MG, Del Tredici K, Braak H (2013) 100 years of Lewy pathology. Nat Rev Neurol 9(1):13–24. doi:10.1038/nrneurol.2012.242, nrneurol.2012.242 [pii]
3. Shah M, Seibyl J, Cartier A, Bhatt R, Catafau AM (2014) Molecular imaging insights into neurodegeneration: focus on alpha-synuclein radiotracers. J Nucl Med 55(9):1397–1400. doi:10.2967/jnumed.113.136515
4. Jellinger KA, Seppi K, Wenning GK (2005) Grading of neuropathology in multiple system atrophy: proposal for a novel scale. Mov Disord 20(Suppl 12):S29–S36. doi:10.1002/mds.20537
5. Williams DR, Holton JL, Strand C, Pittman A, de Silva R, Lees AJ, Revesz T (2007) Pathological tau burden and distribution distinguishes progressive supranuclear palsy-parkinsonism from Richardson's syndrome. Brain 130(Pt 6):1566–1576. doi:10.1093/brain/awm104, 130/6/1566 [pii]
6. Yoshida M (2014) Astrocytic inclusions in progressive supranuclear palsy and corticobasal degeneration. Neuropathology 34(6):555–570. doi:10.1111/neup.12143
7. Dickson DW (1999) Neuropathologic differentiation of progressive supranuclear palsy and corticobasal degeneration. J Neurol 246(Suppl 2):II6–II15, doi:9246S006.415 [pii]
8. Maruyama M, Shimada H, Suhara T, Shinotoh H, Ji B, Maeda J, Zhang MR, Trojanowski JQ, Lee VM, Ono M, Masamoto K, Takano H, Sahara N, Iwata N, Okamura N, Furumoto S, Kudo Y, Chang Q, Saido TC, Takashima A, Lewis J, Jang MK, Aoki I, Ito H, Higuchi M (2013) Imaging of tau pathology in a tauopathy mouse model and in Alzheimer patients compared to normal controls. Neuron 79(6):1094–1108. doi:10.1016/j.neuron.2013.07.037
9. Kepe V, Bordelon Y, Boxer A, Huang SC, Liu J, Thiede FC, Mazziotta JC, Mendez MF, Donoghue N, Small GW, Barrio JR (2013) PET imaging of neuropathology in tauopathies: progressive supranuclear palsy. J Alzheimers Dis 36(1):145–153. doi:10.3233/JAD-130032
10. Snow BJ, Tooyama I, McGeer EG, Yamada T, Calne DB, Takahashi H, Kimura H (1993) Human positron emission tomographic [18F]fluorodopa studies correlate with dopamine cell counts and levels. Ann Neurol 34(3):324–330. doi:10.1002/ana.410340304
11. Burn DJ, Sawle GV, Brooks DJ (1994) Differential diagnosis of Parkinson's disease, multiple system atrophy, and Steele-Richardson-Olszewski syndrome: discriminant analysis of striatal 18F-dopa PET data. J Neurol Neurosurg Psychiatry 57(3):278–284
12. Sawle GV, Playford ED, Burn DJ, Cunningham VJ, Brooks DJ (1994) Separating Parkinson's disease from normality. Discriminant function analysis of fluorodopa F 18 positron emission tomography data. Arch Neurol 51(3):237–243
13. Rinne JO, Laihinen A, Nagren K, Ruottinen H, Ruotsalainen U, Rinne UK (1995) PET examination of the monoamine transporter with [11C]beta-CIT and [11C]beta-CFT in early Parkinson's disease. Synapse 21(2):97–103
14. Frey KA, Koeppe RA, Kilbourn MR, Vander Borght TM, Albin RL, Gilman S, Kuhl DE (1996) Presynaptic monoaminergic vesicles in Parkinson's disease and normal aging. Ann Neurol 40(6):873–884. doi:10.1002/ana.410400609

15. Kazumata K, Dhawan V, Chaly T, Antonini A, Margouleff C, Belakhlef A, Neumeyer J, Eidelberg D (1998) Dopamine transporter imaging with fluorine-18-FPCIT and PET. J Nucl Med 39(9):1521–1530
16. Rinne JO, Ruottinen H, Bergman J, Haaparanta M, Sonninen P, Solin O (1999) Usefulness of a dopamine transporter PET ligand [(18)F]beta-CFT in assessing disability in Parkinson's disease. J Neurol Neurosurg Psychiatry 67(6):737–741
17. Lee CS, Samii A, Sossi V, Ruth TJ, Schulzer M, Holden JE, Wudel J, Pal PK, de la Fuente-Fernandez R, Calne DB, Stoessl AJ (2000) In vivo positron emission tomographic evidence for compensatory changes in presynaptic dopaminergic nerve terminals in Parkinson's disease. Ann Neurol 47(4):493–503
18. Martin WR, Wieler M, Stoessl AJ, Schulzer M (2008) Dihydrotetrabenazine positron emission tomography imaging in early, untreated Parkinson's disease. Ann Neurol 63(3):388–394. doi:10.1002/ana.21320
19. Cumming P (2009) PET studies of DOPA utilization. In: Cumming P (ed) Imaging dopamine, 1st edn. Cambridge University Press, Cambridge, pp 54–79
20. Okamura N, Villemagne VL, Drago J, Pejoska S, Dhamija RK, Mulligan RS, Ellis JR, Ackermann U, O''Keefe G, Jones G, Kung HF, Pontecorvo MJ, Skovronsky D, Rowe CC (2010) In vivo measurement of vesicular monoamine transporter type 2 density in Parkinson disease with (18)F-AV-133. J Nucl Med 51(2):223–228. doi:10.2967/jnumed.109.070094, jnumed.109.070094 [pii]
21. Gallagher CL, Oakes TR, Johnson SC, Chung MK, Holden JE, Bendlin BB, McLaren DG, Xu G, Nickles RJ, Pyzalski R, DeJesus O, Brown WD (2011) Rate of 6-[18F]fluorodopa uptake decline in striatal subregions in Parkinson's disease. Mov Disord 26(4):614–620. doi:10.1002/mds.23503
22. Fazio P, Svenningsson P, Forsberg A, Jonsson EG, Amini N, Nakao R, Nag S, Halldin C, Farde L, Varrone A (2015) Quantitative analysis of (1)(8)F-(E)-N-(3-iodoprop-2-enyl)-2beta-carbofluoroethoxy-3beta-(4′-methyl-phenyl) nortropane binding to the dopamine transporter in Parkinson disease. J Nucl Med 56(5):714–720. doi:10.2967/jnumed.114.152421, jnumed.114.152421 [pii]
23. Jellinger KA (1999) Post mortem studies in Parkinson's disease – is it possible to detect brain areas for specific symptoms? J Neural Transm Suppl 56:1–29
24. Morrish PK, Sawle GV, Brooks DJ (1996) The rate of progression of Parkinson's disease. A longitudinal [18F]DOPA PET study. Adv Neurol 69:427–431
25. Morrish PK, Rakshi JS, Bailey DL, Sawle GV, Brooks DJ (1998) Measuring the rate of progression and estimating the preclinical period of Parkinson's disease with [18F]dopa PET. J Neurol Neurosurg Psychiatry 64(3):314–319
26. Nurmi E, Ruottinen HM, Kaasinen V, Bergman J, Haaparanta M, Solin O, Rinne JO (2000) Progression in Parkinson's disease: a positron emission tomography study with a dopamine transporter ligand [18F] CFT. Ann Neurol 47(6):804–808
27. Nurmi E, Ruottinen HM, Bergman J, Haaparanta M, Solin O, Sonninen P, Rinne JO (2001) Rate of progression in Parkinson's disease: a 6-[18F]fluoro-L-dopa PET study. Mov Disord 16(4):608–615
28. Brooks DJ, Frey KA, Marek KL, Oakes D, Paty D, Prentice R, Shults CW, Stoessl AJ (2003) Assessment of neuroimaging techniques as biomarkers of the progression of Parkinson's disease. Exp Neurol 184(Suppl 1):S68–S79
29. Nandhagopal R, Kuramoto L, Schulzer M, Mak E, Cragg J, Lee CS, McKenzie J, McCormick S, Samii A, Troiano A, Ruth TJ, Sossi V, de la Fuente-Fernandez R, Calne DB, Stoessl AJ (2009) Longitudinal progression of sporadic Parkinson's disease: a multi-tracer positron emission tomography study. Brain 132(Pt 11):2970–2979
30. Brooks DJ, Piccini P (2006) Imaging in Parkinson's disease: the role of monoamines in behavior. Biol Psychiatry 59(10):908–918. doi:10.1016/j.biopsych.2005.12.017, S0006-3223(06)00187-9 [pii]
31. Menza MA, Mark MH, Burn DJ, Brooks DJ (1995) Personality correlates of [18F]dopa striatal uptake: results of positron-emission tomography in Parkinson's disease. J Neuropsychiatry Clin Neurosci 7(2):176–179
32. Kaasinen V, Nurmi E, Bergman J, Eskola O, Solin O, Sonninen P, Rinne JO (2001) Personality traits and brain dopaminergic function in Parkinson's disease. Proc Natl Acad Sci U S A 98(23):13272–13277. doi:10.1073/pnas.231313198231313198 [pii]
33. Gill SS, Patel NK, Hotton GR, O'Sullivan K, McCarter R, Bunnage M, Brooks DJ, Svendsen CN, Heywood P (2003) Direct brain infusion of glial cell line-derived neurotrophic factor in Parkinson disease. Nat Med 9(5):589–595
34. Paul G, Zachrisson O, Varrone A, Almqvist P, Jerling M, Lind G, Rehncrona S, Linderoth B, Bjartmarz H, Shafer LL, Coffey R, Svensson M, Mercer KJ, Forsberg A, Halldin C, Svenningsson P, Widner H, Frisen J, Palhagen S, Haegerstrand A (2015) Safety and tolerability of intracerebroventricular PDGF-BB in Parkinson's disease patients. J Clin Invest 125(3):1339–1346. doi:10.1172/JCI79635, 79635 [pii]
35. Sawle GV, Playford ED, Brooks DJ, Quinn N, Frackowiak RS (1993) Asymmetrical pre-synaptic and post-synaptic changes in the striatal dopamine projection in dopa naive parkinsonism. Diagnostic implications of the D2 receptor status. Brain 116(Pt 4):853–867
36. Antonini A, Schwarz J, Oertel WH, Pogarell O, Leenders KL (1997) Long-term changes of striatal dopamine D2 receptors in patients with Parkinson's disease: a study with positron emission tomography and [11C]raclopride. Mov Disord 12(1):33–38. doi:10.1002/mds.870120107

37. Brooks DJ, Ibanez V, Sawle GV, Playford ED, Quinn N, Mathias CJ, Lees AJ, Marsden CD, Bannister R, Frackowiak RS (1992) Striatal D2 receptor status in patients with Parkinson's disease, striatonigral degeneration, and progressive supranuclear palsy, measured with 11C-raclopride and positron emission tomography. Ann Neurol 31(2):184–192. doi:10.1002/ana.410310209
38. Antonini A, Leenders KL, Vontobel P, Maguire RP, Missimer J, Psylla M, Gunther I (1997) Complementary PET studies of striatal neuronal function in the differential diagnosis between multiple system atrophy and Parkinson's disease. Brain 120(Pt 12):2187–2195
39. Ghaemi M, Hilker R, Rudolf J, Sobesky J, Heiss WD (2002) Differentiating multiple system atrophy from Parkinson's disease: contribution of striatal and midbrain MRI volumetry and multi-tracer PET imaging. J Neurol Neurosurg Psychiatry 73(5):517–523
40. Van Laere K, Clerinx K, D''Hondt E, de Groot T, Vandenberghe W (2010) Combined striatal binding and cerebral influx analysis of dynamic 11C-raclopride PET improves early differentiation between multiple-system atrophy and Parkinson disease. J Nucl Med 51(4):588–595. doi:10.2967/jnumed.109.070144, jnumed.109.070144 [pii]
41. Grunder G, Siessmeier T, Piel M, Vernaleken I, Buchholz HG, Zhou Y, Hiemke C, Wong DF, Rosch F, Bartenstein P (2003) Quantification of D2-like dopamine receptors in the human brain with 18F-desmethoxyfallypride. J Nucl Med 44(1):109–116
42. la Fougere C, Popperl G, Levin J, Wangler B, Boning G, Uebleis C, Cumming P, Bartenstein P, Botzel K, Tatsch K (2010) The value of the dopamine D2/3 receptor ligand 18F-desmethoxyfallypride for the differentiation of idiopathic and nonidiopathic parkinsonian syndromes. J Nucl Med 51(4):581–587. doi:10.2967/jnumed.109.071811, jnumed.109.071811 [pii]
43. Eckert T, Barnes A, Dhawan V, Frucht S, Gordon MF, Feigin AS, Eidelberg D (2005) FDG PET in the differential diagnosis of parkinsonian disorders. Neuroimage 26(3):912–921. doi:10.1016/j.neuroimage.2005.03.012, S1053-8119(05)00152-7 [pii]
44. Guttman M, Boileau I, Warsh J, Saint-Cyr JA, Ginovart N, McCluskey T, Houle S, Wilson A, Mundo E, Rusjan P, Meyer J, Kish SJ (2007) Brain serotonin transporter binding in nondepressed patients with Parkinson's disease. Eur J Neurol 14(5):523–528. doi:10.1111/j.1468-1331.2007.01727.x, ENE1727 [pii]
45. Albin RL, Koeppe RA, Bohnen NI, Wernette K, Kilbourn MA, Frey KA (2008) Spared caudal brainstem SERT binding in early Parkinson's disease. J Cereb Blood Flow Metab 28(3):441–444. doi:10.1038/sj.jcbfm.9600599, 9600599 [pii]
46. Politis M, Wu K, Loane C, Kiferle L, Molloy S, Brooks DJ, Piccini P (2010) Staging of serotonergic dysfunction in Parkinson's disease: an in vivo 11C-DASB PET study. Neurobiol Dis 40(1):216–221. doi:10.1016/j.nbd.2010.05.028, S0969-9961(10)00190-7 [pii]
47. Doder M, Rabiner EA, Turjanski N, Lees AJ, Brooks DJ (2003) Tremor in Parkinson's disease and serotonergic dysfunction: an 11C-WAY 100635 PET study. Neurology 60(4):601–605
48. Ballanger B, Klinger H, Eche J, Lerond J, Vallet AE, Le Bars D, Tremblay L, Sgambato-Faure V, Broussolle E, Thobois S (2012) Role of serotonergic 1A receptor dysfunction in depression associated with Parkinson's disease. Mov Disord 27(1):84–89. doi:10.1002/mds.23895
49. Varrone A, Svenningsson P, Forsberg A, Varnas K, Tiger M, Nakao R, Halldin C, Nilsson LG, Farde L (2014) Positron emission tomography imaging of 5-hydroxytryptamine1B receptors in Parkinson's disease. Neurobiol Aging 35(4):867–875. doi:10.1016/j.neurobiolaging.2013.08.025, S0197-4580(13)00370-9 [pii]
50. Pavese N, Metta V, Bose SK, Chaudhuri KR, Brooks DJ (2010) Fatigue in Parkinson's disease is linked to striatal and limbic serotonergic dysfunction. Brain 133(11):3434–3443. doi:10.1093/brain/awq268, awq268 [pii]
51. Boileau I, Warsh JJ, Guttman M, Saint-Cyr JA, McCluskey T, Rusjan P, Houle S, Wilson AA, Meyer JH, Kish SJ (2008) Elevated serotonin transporter binding in depressed patients with Parkinson's disease: a preliminary PET study with [11C]DASB. Mov Disord 23(12):1776–1780. doi:10.1002/mds.22212
52. Politis M, Wu K, Loane C, Turkheimer FE, Molloy S, Brooks DJ, Piccini P (2010) Depressive symptoms in PD correlate with higher 5-HTT binding in raphe and limbic structures. Neurology 75(21):1920–1927. doi:10.1212/WNL.0b013e3181feb2ab, 75/21/1920 [pii]
53. Remy P, Doder M, Lees A, Turjanski N, Brooks D (2005) Depression in Parkinson's disease: loss of dopamine and noradrenaline innervation in the limbic system. Brain 128(Pt 6):1314–1322. doi:10.1093/brain/awh445, awh445 [pii]
54. Shinotoh H, Namba H, Yamaguchi M, Fukushi K, Nagatsuka S, Iyo M, Asahina M, Hattori T, Tanada S, Irie T (1999) Positron emission tomographic measurement of acetylcholinesterase activity reveals differential loss of ascending cholinergic systems in Parkinson's disease and progressive supranuclear palsy. Ann Neurol 46(1):62–69
55. Niccolini F, Foltynie T, Reis Marques T, Muhlert N, Tziortzi AC, Searle GE, Natesan S, Kapur S, Rabiner EA, Gunn RN, Piccini P, Politis M (2015) Loss of phosphodiesterase 10A expression is associated with progression and severity in Parkinson's disease. Brain. doi:10.1093/brain/awv219, awv219 [pii]
56. Foster NL, Minoshima S, Johanns J, Little R, Heumann ML, Kuhl DE, Gilman S (2000) PET measures of benzodiazepine receptors in progressive supranuclear palsy. Neurology 54(9):1768–1773

57. Brenneis C, Seppi K, Schocke M, Benke T, Wenning GK, Poewe W (2004) Voxel based morphometry reveals a distinct pattern of frontal atrophy in progressive supranuclear palsy. J Neurol Neurosurg Psychiatry 75(2):246–249
58. Fukuda M, Edwards C, Eidelberg D (2001) Functional brain networks in Parkinson's disease. Parkinsonism Relat Disord 8(2):91–94, doi:S1353802001000220 [pii]
59. Huang C, Tang C, Feigin A, Lesser M, Ma Y, Pourfar M, Dhawan V, Eidelberg D (2007) Changes in network activity with the progression of Parkinson's disease. Brain 130(Pt 7):1834–1846. doi:10.1093/brain/awm086, awm086 [pii]
60. Varrone A, Asenbaum S, Vander Borght T, Booij J, Nobili F, Nagren K, Darcourt J, Kapucu OL, Tatsch K, Bartenstein P, Van Laere K (2009) EANM procedure guidelines for PET brain imaging using [18F]FDG, version 2. Eur J Nucl Med Mol Imaging 36(12):2103–2110. doi:10.1007/s00259-009-1264-0
61. Gerhard A, Pavese N, Hotton G, Turkheimer F, Es M, Hammers A, Eggert K, Oertel W, Banati RB, Brooks DJ (2006) In vivo imaging of microglial activation with [11C](R)-PK11195 PET in idiopathic Parkinson's disease. Neurobiol Dis 21(2):404–412. doi:10.1016/j.nbd.2005.08.002, S0969-9961(05)00226-3 [pii]
62. Ouchi Y, Yoshikawa E, Sekine Y, Futatsubashi M, Kanno T, Ogusu T, Torizuka T (2005) Microglial activation and dopamine terminal loss in early Parkinson's disease. Ann Neurol 57(2):168–175. doi:10.1002/ana.20338
63. Gerhard A, Banati RB, Goerres GB, Cagnin A, Myers R, Gunn RN, Turkheimer F, Good CD, Mathias CJ, Quinn N, Schwarz J, Brooks DJ (2003) [11C](R)-PK11195 PET imaging of microglial activation in multiple system atrophy. Neurology 61(5):686–689
64. Gerhard A, Trender-Gerhard I, Turkheimer F, Quinn NP, Bhatia KP, Brooks DJ (2006) In vivo imaging of microglial activation with [11C](R)-PK11195 PET in progressive supranuclear palsy. Mov Disord 21(1):89–93. doi:10.1002/mds.20668
65. Kobylecki C, Counsell SJ, Cabanel N, Wachter T, Turkheimer FE, Eggert K, Oertel W, Brooks DJ, Gerhard A (2013) Diffusion-weighted imaging and its relationship to microglial activation in parkinsonian syndromes. Parkinsonism Relat Disord 19(5):527–532. doi:10.1016/j.parkreldis.2013.01.017, S1353-8020(13)00052-7 [pii]
66. Dodel R, Spottke A, Gerhard A, Reuss A, Reinecker S, Schimke N, Trenkwalder C, Sixel-Doring F, Herting B, Kamm C, Gasser T, Sawires M, Geser F, Kollensperger M, Seppi K, Kloss M, Krause M, Daniels C, Deuschl G, Bottger S, Naumann M, Lipp A, Gruber D, Kupsch A, Du Y, Turkheimer F, Brooks DJ, Klockgether T, Poewe W, Wenning G, Schade-Brittinger C, Oertel WH, Eggert K (2010) Minocycline 1-year therapy in multiple-system-atrophy: effect on clinical symptoms and [(11)C] (R)-PK11195 PET (MEMSA-trial). Mov Disord 25(1):97–107. doi:10.1002/mds.22732
67. Jucaite A, Svenningsson P, Rinne JO, Cselenyi Z, Varnas K, Johnstrom P, Amini N, Kirjavainen A, Helin S, Minkwitz M, Kugler AR, Posener JA, Budd S, Halldin C, Varrone A, Farde L (2015) Effect of the myeloperoxidase inhibitor AZD3241 on microglia: a PET study in Parkinson's disease. Brain 138(Pt 9):2687–2700. doi:10.1093/brain/awv184, awv184 [pii]
68. NICE (2006) Parkinson's disease: diagnosis and management in primary and secondary care. http://www.nice.org.uk/guidance/cg35/resources/guidance-parkinsons-disease-pdf. Accessed 4 Apr 2015
69. Lees AJ, Hardy J, Revesz T (2009) Parkinson's disease. Lancet 373(9680):2055–2066. doi:10.1016/S0140-6736(09)60492-X
70. Massey LA, Micallef C, Paviour DC, O'Sullivan SS, Ling H, Williams DR, Kallis C, Holton JL, Revesz T, Burn DJ, Yousry T, Lees AJ, Fox NC, Jager HR (2012) Conventional magnetic resonance imaging in confirmed progressive supranuclear palsy and multiple system atrophy. Mov Disord 27(14):1754–1762. doi:10.1002/mds.24968
71. Tolosa E, Wenning G, Poewe W (2006) The diagnosis of Parkinson's disease. Lancet Neurol 5(1):75–86. doi:10.1016/S1474-4422(05)70285-4
72. Kato N, Arai K, Hattori T (2003) Study of the rostral midbrain atrophy in progressive supranuclear palsy. J Neurol Sci 210(1–2):57–60
73. Josephs KA (2007) Frontotemporal lobar degeneration. Neurol Clin 25(3):683–96, vi. doi:10.1016/j.ncl.2007.03.005
74. Righini A, Antonini A, De Notaris R, Bianchini E, Meucci N, Sacilotto G, Canesi M, De Gaspari D, Triulzi F, Pezzoli G (2004) MR imaging of the superior profile of the midbrain: differential diagnosis between progressive supranuclear palsy and Parkinson disease. AJNR Am J Neuroradiol 25(6):927–932
75. Adachi M, Kawanami T, Ohshima H, Sugai Y, Hosoya T (2004) Morning glory sign: a particular MR finding in progressive supranuclear palsy. Magn Reson Med Sci 3(3):125–132
76. Lee JY, Yun JY, Shin CW, Kim HJ, Jeon BS (2010) Putaminal abnormality on 3-T magnetic resonance imaging in early parkinsonism-predominant multiple system atrophy. J Neurol 257(12):2065–2070. doi:10.1007/s00415-010-5661-x
77. Schwarz J, Weis S, Kraft E, Tatsch K, Bandmann O, Mehraein P, Vogl T, Oertel WH (1996) Signal changes on MRI and increases in reactive microgliosis, astrogliosis, and iron in the putamen of two patients with multiple system atrophy. J Neurol Neurosurg Psychiatry 60(1):98–101
78. Lee WH, Lee CC, Shyu WC, Chong PN, Lin SZ (2005) Hyperintense putaminal rim sign is not a hallmark of multiple system atrophy at 3 T. AJNR Am J Neuroradiol 26(9):2238–2242
79. Tha KK, Terae S, Tsukahara A, Soma H, Morita R, Yabe I, Ito YM, Sasaki H, Shirato H (2012)

Hyperintense putaminal rim at 1.5 T: prevalence in normal subjects and distinguishing features from multiple system atrophy. BMC Neurol 12:39. doi:10.1186/1471-2377-12-39
80. Wenning GK, Colosimo C, Geser F, Poewe W (2004) Multiple system atrophy. Lancet Neurol 3(2):93–103
81. Muqit MM, Mort D, Miskiel KA, Shakir RA (2001) "Hot cross bun" sign in a patient with parkinsonism secondary to presumed vasculitis. J Neurol Neurosurg Psychiatry 71(4):565–566
82. Soares-Fernandes JP, Ribeiro M, Machado A (2009) "Hot cross bun" sign in variant Creutzfeldt-Jakob disease. AJNR Am J Neuroradiol 30(3), E37. doi:10.3174/ajnr.A1335
83. Cochrane CJ, Ebmeier KP (2013) Diffusion tensor imaging in parkinsonian syndromes: a systematic review and meta-analysis. Neurology 80(9):857–864. doi:10.1212/WNL.0b013e318284070c
84. Vaillancourt DE, Spraker MB, Prodoehl J, Abraham I, Corcos DM, Zhou XJ, Comella CL, Little DM (2009) High-resolution diffusion tensor imaging in the substantia nigra of de novo Parkinson disease. Neurology 72(16):1378–1384. doi:10.1212/01.wnl.0000340982.01727.6e
85. Schocke MF, Seppi K, Esterhammer R, Kremser C, Jaschke W, Poewe W, Wenning GK (2002) Diffusion-weighted MRI differentiates the Parkinson variant of multiple system atrophy from PD. Neurology 58(4):575–580
86. Schocke MF, Seppi K, Esterhammer R, Kremser C, Mair KJ, Czermak BV, Jaschke W, Poewe W, Wenning GK (2004) Trace of diffusion tensor differentiates the Parkinson variant of multiple system atrophy and Parkinson's disease. Neuroimage 21(4):1443–1451. doi:10.1016/j.neuroimage.2003.12.005
87. Ito M, Watanabe H, Kawai Y, Atsuta N, Tanaka F, Naganawa S, Fukatsu H, Sobue G (2007) Usefulness of combined fractional anisotropy and apparent diffusion coefficient values for detection of involvement in multiple system atrophy. J Neurol Neurosurg Psychiatry 78(7):722–728. doi:10.1136/jnnp.2006.104075
88. Seppi K, Schocke MF, Mair KJ, Esterhammer R, Scherfler C, Geser F, Kremser C, Boesch S, Jaschke W, Poewe W, Wenning GK (2006) Progression of putaminal degeneration in multiple system atrophy: a serial diffusion MR study. Neuroimage 31(1):240–245. doi:10.1016/j.neuroimage.2005.12.006
89. Pellecchia MT, Barone P, Vicidomini C, Mollica C, Salvatore E, Ianniciello M, Liuzzi R, Longo K, Picillo M, De Michele G, Filla A, Brunetti A, Salvatore M, Pappata S (2011) Progression of striatal and extrastriatal degeneration in multiple system atrophy: a longitudinal diffusion-weighted MR study. Mov Disord 26(7):1303–1309. doi:10.1002/mds.23601
90. Nicoletti G, Lodi R, Condino F, Tonon C, Fera F, Malucelli E, Manners D, Zappia M, Morgante L, Barone P, Barbiroli B, Quattrone A (2006) Apparent diffusion coefficient measurements of the middle cerebellar peduncle differentiate the Parkinson variant of MSA from Parkinson's disease and progressive supranuclear palsy. Brain 129(Pt 10):2679–2687. doi:10.1093/brain/awl166
91. Paviour DC, Thornton JS, Lees AJ, Jager HR (2007) Diffusion-weighted magnetic resonance imaging differentiates Parkinsonian variant of multiple-system atrophy from progressive supranuclear palsy. Mov Disord 22(1):68–74. doi:10.1002/mds.21204
92. Tsukamoto K, Matsusue E, Kanasaki Y, Kakite S, Fujii S, Kaminou T, Ogawa T (2012) Significance of apparent diffusion coefficient measurement for the differential diagnosis of multiple system atrophy, progressive supranuclear palsy, and Parkinson's disease: evaluation by 3.0-T MR imaging. Neuroradiology 54(9):947–955. doi:10.1007/s00234-012-1009-9
93. Baudrexel S, Seifried C, Penndorf B, Klein JC, Middendorp M, Steinmetz H, Grunwald F, Hilker R (2014) The value of putaminal diffusion imaging versus 18-fluorodeoxyglucose positron emission tomography for the differential diagnosis of the Parkinson variant of multiple system atrophy. Mov Disord 29(3):380–387. doi:10.1002/mds.25749
94. Pellecchia MT, Barone P, Mollica C, Salvatore E, Ianniciello M, Longo K, Varrone A, Vicidomini C, Picillo M, De Michele G, Filla A, Salvatore M, Pappata S (2009) Diffusion-weighted imaging in multiple system atrophy: a comparison between clinical subtypes. Mov Disord 24(5):689–696. doi:10.1002/mds.22440
95. Nair SR, Tan LK, Mohd Ramli N, Lim SY, Rahmat K, Mohd Nor H (2013) A decision tree for differentiating multiple system atrophy from Parkinson's disease using 3-T MR imaging. Eur Radiol 23(6):1459–1466. doi:10.1007/s00330-012-2759-9
96. Erbetta A, Mandelli ML, Savoiardo M, Grisoli M, Bizzi A, Soliveri P, Chiapparini L, Prioni S, Bruzzone MG, Girotti F (2009) Diffusion tensor imaging shows different topographic involvement of the thalamus in progressive supranuclear palsy and corticobasal degeneration. AJNR Am J Neuroradiol 30(8):1482–1487. doi:10.3174/ajnr.A1615
97. Whitwell JL, Schwarz CG, Reid RI, Kantarci K, Jack CR Jr, Josephs KA (2014) Diffusion tensor imaging comparison of progressive supranuclear palsy and corticobasal syndromes. Parkinsonism Relat Disord 20(5):493–498. doi:10.1016/j.parkreldis.2014.01.023
98. Catani M, Howard RJ, Pajevic S, Jones DK (2002) Virtual in vivo interactive dissection of white matter fasciculi in the human brain. Neuroimage 17(1):77–94
99. Nilsson C, Markenroth Bloch K, Brockstedt S, Latt J, Widner H, Larsson EM (2007) Tracking the neurodegeneration of parkinsonian disorders – a pilot study. Neuroradiology 49(2):111–119. doi:10.1007/s00234-006-0165-1
100. Surova Y, Nilsson M, Latt J, Lampinen B, Lindberg O, Hall S, Widner H, Nilsson C, van Westen D,

Hansson O (2015) Disease-specific structural changes in thalamus and dentatorubrothalamic tract in progressive supranuclear palsy. Neuroradiology. doi:10.1007/s00234-015-1563-z
101. Drayer BP, Olanow W, Burger P, Johnson GA, Herfkens R, Riederer S (1986) Parkinson plus syndrome: diagnosis using high field MR imaging of brain iron. Radiology 159(2):493–498. doi:10.1148/radiology.159.2.3961182
102. Haacke EM, Mittal S, Wu Z, Neelavalli J, Cheng YC (2009) Susceptibility-weighted imaging: technical aspects and clinical applications, part 1. AJNR Am J Neuroradiol 30(1):19–30. doi:10.3174/ajnr.A1400
103. Du G, Liu T, Lewis MM, Kong L, Wang Y, Connor J, Mailman RB, Huang X (2015) Quantitative susceptibility mapping of the midbrain in Parkinson's disease. Mov Disord. doi:10.1002/mds.26417
104. He N, Ling H, Ding B, Huang J, Zhang Y, Zhang Z, Liu C, Chen K, Yan F (2015) Region-specific disturbed iron distribution in early idiopathic Parkinson's disease measured by quantitative susceptibility mapping. Hum Brain Mapp. doi:10.1002/hbm.22928
105. Zhang W, Sun SG, Jiang YH, Qiao X, Sun X, Wu Y (2009) Determination of brain iron content in patients with Parkinson's disease using magnetic susceptibility imaging. Neurosci Bull 25(6):353–360. doi:10.1007/s12264-009-0225-8
106. Zhang J, Zhang Y, Wang J, Cai P, Luo C, Qian Z, Dai Y, Feng H (2010) Characterizing iron deposition in Parkinson's disease using susceptibility-weighted imaging: an in vivo MR study. Brain Res 1330:124–130. doi:10.1016/j.brainres.2010.03.036
107. Wang Y, Butros SR, Shuai X, Dai Y, Chen C, Liu M, Haacke EM, Hu J, Xu H (2012) Different iron-deposition patterns of multiple system atrophy with predominant parkinsonism and idiopathic Parkinson diseases demonstrated by phase-corrected susceptibility-weighted imaging. AJNR Am J Neuroradiol 33(2):266–273. doi:10.3174/ajnr.A2765
108. Lotfipour AK, Wharton S, Schwarz ST, Gontu V, Schafer A, Peters AM, Bowtell RW, Auer DP, Gowland PA, Bajaj NP (2012) High resolution magnetic susceptibility mapping of the substantia nigra in Parkinson's disease. J Magn Reson Imaging 35(1):48–55. doi:10.1002/jmri.22752
109. Han YH, Lee JH, Kang BM, Mun CW, Baik SK, Shin YI, Park KH (2013) Topographical differences of brain iron deposition between progressive supranuclear palsy and parkinsonian variant multiple system atrophy. J Neurol Sci 325(1–2):29–35. doi:10.1016/j.jns.2012.11.009
110. Lee JH, Han YH, Kang BM, Mun CW, Lee SJ, Baik SK (2013) Quantitative assessment of subcortical atrophy and iron content in progressive supranuclear palsy and parkinsonian variant of multiple system atrophy. J Neurol 260(8):2094–2101. doi:10.1007/s00415-013-6951-x
111. Gupta D, Saini J, Kesavadas C, Sarma PS, Kishore A (2010) Utility of susceptibility-weighted MRI in differentiating Parkinson's disease and atypical parkinsonism. Neuroradiology 52(12):1087–1094. doi:10.1007/s00234-010-0677-6
112. Cho ZH, Oh SH, Kim JM, Park SY, Kwon DH, Jeong HJ, Kim YB, Chi JG, Park CW, Huston J 3rd, Lee KH, Jeon BS (2011) Direct visualization of Parkinson's disease by in vivo human brain imaging using 7.0 T magnetic resonance imaging. Mov Disord 26(4):713–718. doi:10.1002/mds.23465
113. Lehericy S, Bardinet E, Poupon C, Vidailhet M, Francois C (2014) 7 Tesla magnetic resonance imaging: a closer look at substantia nigra anatomy in Parkinson's disease. Mov Disord 29(13):1574–1581. doi:10.1002/mds.26043
114. Noh Y, Sung YH, Lee J, Kim EY (2015) Nigrosome 1 detection at 3 T MRI for the diagnosis of early-stage idiopathic Parkinson disease: assessment of diagnostic accuracy and agreement on imaging asymmetry and clinical laterality. AJNR Am J Neuroradiol. doi:10.3174/ajnr.A4412
115. Reiter E, Mueller C, Pinter B, Krismer F, Scherfler C, Esterhammer R, Kremser C, Schocke M, Wenning GK, Poewe W, Seppi K (2015) Dorsolateral nigral hyperintensity on 3.0 T susceptibility-weighted imaging in neurodegenerative Parkinsonism. Mov Disord 30(8):1068–1076. doi:10.1002/mds.26171
116. Ohtsuka C, Sasaki M, Konno K, Koide M, Kato K, Takahashi J, Takahashi S, Kudo K, Yamashita F, Terayama Y (2013) Changes in substantia nigra and locus coeruleus in patients with early-stage Parkinson's disease using neuromelanin-sensitive MR imaging. Neurosci Lett 541:93–98. doi:10.1016/j.neulet.2013.02.012
117. Davie CA, Wenning GK, Barker GJ, Tofts PS, Kendall BE, Quinn N, McDonald WI, Marsden CD, Miller DH (1995) Differentiation of multiple system atrophy from idiopathic Parkinson's disease using proton magnetic resonance spectroscopy. Ann Neurol 37(2):204–210. doi:10.1002/ana.410370211
118. Cruz CJ, Aminoff MJ, Meyerhoff DJ, Graham SH, Weiner MW (1997) Proton MR spectroscopic imaging of the striatum in Parkinson's disease. Magn Reson Imaging 15(6):619–624
119. Tedeschi G, Litvan I, Bonavita S, Bertolino A, Lundbom N, Patronas NJ, Hallett M (1997) Proton magnetic resonance spectroscopic imaging in progressive supranuclear palsy, Parkinson's disease and corticobasal degeneration. Brain 120(Pt 9):1541–1552
120. Clarke CE, Lowry M, Horsman A (1997) Unchanged basal ganglia N-acetylaspartate and glutamate in idiopathic Parkinson's disease measured by proton magnetic resonance spectroscopy. Mov Disord 12(3):297–301. doi:10.1002/mds.870120306
121. Taylor-Robinson SD, Turjanski N, Bhattacharya S, Seery JP, Sargentoni J, Brooks DJ, Bryant DJ, Cox IJ (1999) A proton magnetic resonance spectroscopy study of the striatum and cerebral cortex in Parkinson's disease. Metab Brain Dis 14(1):45–55
122. Hu MT, Taylor-Robinson SD, Chaudhuri KR, Bell JD, Morris RG, Clough C, Brooks DJ, Turjanski N

(1999) Evidence for cortical dysfunction in clinically non-demented patients with Parkinson's disease: a proton MR spectroscopy study. J Neurol Neurosurg Psychiatry 67(1):20–26
123. Lucetti C, Del Dotto P, Gambaccini G, Bernardini S, Bianchi MC, Tosetti M, Bonuccelli U (2001) Proton magnetic resonance spectroscopy (1H-MRS) of motor cortex and basal ganglia in de novo Parkinson's disease patients. Neurol Sci 22(1):69–70
124. Camicioli RM, Korzan JR, Foster SL, Fisher NJ, Emery DJ, Bastos AC, Hanstock CC (2004) Posterior cingulate metabolic changes occur in Parkinson's disease patients without dementia. Neurosci Lett 354(3):177–180
125. Camicioli RM, Hanstock CC, Bouchard TP, Gee M, Fisher NJ, Martin WR (2007) Magnetic resonance spectroscopic evidence for presupplementary motor area neuronal dysfunction in Parkinson's disease. Mov Disord 22(3):382–386. doi:10.1002/mds.21288
126. Guevara CA, Blain CR, Stahl D, Lythgoe DJ, Leigh PN, Barker GJ (2010) Quantitative magnetic resonance spectroscopic imaging in Parkinson's disease, progressive supranuclear palsy and multiple system atrophy. Eur J Neurol 17(9):1193–1202. doi:10.1111/j.1468-1331.2010.03010.x
127. Federico F, Simone IL, Lucivero V, Mezzapesa DM, de Mari M, Lamberti P, Petruzzellis M, Ferrari E (1999) Usefulness of proton magnetic resonance spectroscopy in differentiating parkinsonian syndromes. Ital J Neurol Sci 20(4):223–229
128. Watanabe H, Fukatsu H, Katsuno M, Sugiura M, Hamada K, Okada Y, Hirayama M, Ishigaki T, Sobue G (2004) Multiple regional 1H-MR spectroscopy in multiple system atrophy: NAA/Cr reduction in pontine base as a valuable diagnostic marker. J Neurol Neurosurg Psychiatry 75(1):103–109
129. Griffith HR, Okonkwo OC, O'Brien T, Hollander JA (2008) Reduced brain glutamate in patients with Parkinson's disease. NMR Biomed 21(4):381–387. doi:10.1002/nbm.1203
130. Kickler N, Krack P, Fraix V, Lebas JF, Lamalle L, Durif F, Krainik A, Remy C, Segebarth C, Pollak P (2007) Glutamate measurement in Parkinson's disease using MRS at 3 T field strength. NMR Biomed 20(8):757–762. doi:10.1002/nbm.1141
131. Oz G, Terpstra M, Tkac I, Aia P, Lowary J, Tuite PJ, Gruetter R (2006) Proton MRS of the unilateral substantia nigra in the human brain at 4 tesla: detection of high GABA concentrations. Magn Reson Med 55(2):296–301. doi:10.1002/mrm.20761
132. Emir UE, Tuite PJ, Oz G (2012) Elevated pontine and putamenal GABA levels in mild-moderate Parkinson disease detected by 7 tesla proton MRS. PLoS One 7(1), e30918. doi:10.1371/journal.pone.0030918
133. Morgen K, Sammer G, Weber L, Aslan B, Muller C, Bachmann GF, Sandmann D, Oechsner M, Vaitl D, Kaps M, Reuter I (2011) Structural brain abnormalities in patients with Parkinson disease: a comparative voxel-based analysis using T1-weighted MR imaging and magnetization transfer imaging. AJNR Am J Neuroradiol 32(11):2080–2086. doi:10.3174/ajnr.A2837
134. Tambasco N, Belcastro V, Sarchielli P, Floridi P, Pierguidi L, Menichetti C, Castrioto A, Chiarini P, Parnetti L, Eusebi P, Calabresi P, Rossi A (2011) A magnetization transfer study of mild and advanced Parkinson's disease. Eur J Neurol 18(3):471–477. doi:10.1111/j.1468-1331.2010.03184.x
135. Eckert T, Sailer M, Kaufmann J, Schrader C, Peschel T, Bodammer N, Heinze HJ, Schoenfeld MA (2004) Differentiation of idiopathic Parkinson's disease, multiple system atrophy, progressive supranuclear palsy, and healthy controls using magnetization transfer imaging. Neuroimage 21(1):229–235
136. Quattrone A, Nicoletti G, Messina D, Fera F, Condino F, Pugliese P, Lanza P, Barone P, Morgante L, Zappia M, Aguglia U, Gallo O (2008) MR imaging index for differentiation of progressive supranuclear palsy from Parkinson disease and the Parkinson variant of multiple system atrophy. Radiology 246(1):214–221. doi:10.1148/radiol.2453061703
137. Morelli M, Arabia G, Messina D, Vescio B, Salsone M, Chiriaco C, Perrotta P, Rocca F, Cascini GL, Barbagallo G, Nigro S, Quattrone A (2014) Effect of aging on magnetic resonance measures differentiating progressive supranuclear palsy from Parkinson's disease. Mov Disord 29(4):488–495. doi:10.1002/mds.25821
138. Paviour DC, Price SL, Jahanshahi M, Lees AJ, Fox NC (2006) Regional brain volumes distinguish PSP, MSA-P, and PD: MRI-based clinico-radiological correlations. Mov Disord 21(7):989–996. doi:10.1002/mds.20877
139. Kashihara K, Shinya T, Higaki F (2011) Neuromelanin magnetic resonance imaging of nigral volume loss in patients with Parkinson's disease. J Clin Neurosci 18(8):1093–1096. doi:10.1016/j.jocn.2010.08.043
140. Ziegler DA, Wonderlick JS, Ashourian P, Hansen LA, Young JC, Murphy AJ, Koppuzha CK, Growdon JH, Corkin S (2013) Substantia nigra volume loss before basal forebrain degeneration in early Parkinson disease. JAMA Neurol 70(2):241–247. doi:10.1001/jamaneurol.2013.597
141. Jesse S, Kassubek J, Muller HP, Ludolph AC, Unrath A (2012) Signal alterations of the basal ganglia in the differential diagnosis of Parkinson's disease: a retrospective case-controlled MRI data bank analysis. BMC Neurol 12:163. doi:10.1186/1471-2377-12-163
142. Groschel K, Hauser TK, Luft A, Patronas N, Dichgans J, Litvan I, Schulz JB (2004) Magnetic resonance imaging-based volumetry differentiates progressive supranuclear palsy from corticobasal degeneration. Neuroimage 21(2):714–724. doi:10.1016/j.neuroimage.2003.09.070
143. Josephs KA, Tang-Wai DF, Edland SD, Knopman DS, Dickson DW, Parisi JE, Petersen RC, Jack

CR Jr, Boeve BF (2004) Correlation between antemortem magnetic resonance imaging findings and pathologically confirmed corticobasal degeneration. Arch Neurol 61(12):1881–1884. doi:10.1001/archneur.61.12.1881

144. Pereira JB, Ibarretxe-Bilbao N, Marti MJ, Compta Y, Junque C, Bargallo N, Tolosa E (2012) Assessment of cortical degeneration in patients with Parkinson's disease by voxel-based morphometry, cortical folding, and cortical thickness. Hum Brain Mapp 33(11):2521–2534. doi:10.1002/hbm.21378
145. Beyer MK, Janvin CC, Larsen JP, Aarsland D (2007) A magnetic resonance imaging study of patients with Parkinson's disease with mild cognitive impairment and dementia using voxel-based morphometry. J Neurol Neurosurg Psychiatry 78(3):254–259. doi:10.1136/jnnp.2006.093849
146. Biundo R, Formento-Dojot P, Facchini S, Vallelunga A, Ghezzo L, Foscolo L, Meneghello F, Antonini A (2011) Brain volume changes in Parkinson's disease and their relationship with cognitive and behavioural abnormalities. J Neurol Sci 310(1–2):64–69. doi:10.1016/j.jns.2011.08.001
147. Ramirez-Ruiz B, Marti MJ, Tolosa E, Bartres-Faz D, Summerfield C, Salgado-Pineda P, Gomez-Anson B, Junque C (2005) Longitudinal evaluation of cerebral morphological changes in Parkinson's disease with and without dementia. J Neurol 252(11):1345–1352. doi:10.1007/s00415-005-0864-2
148. Shi HC, Zhong JG, Pan PL, Xiao PR, Shen Y, Wu LJ, Li HL, Song YY, He GX, Li HY (2013) Gray matter atrophy in progressive supranuclear palsy: meta-analysis of voxel-based morphometry studies. Neurol Sci 34(7):1049–1055. doi:10.1007/s10072-013-1406-9
149. Yang J, Shao N, Li J, Shang H (2014) Voxelwise meta-analysis of white matter abnormalities in progressive supranuclear palsy. Neurol Sci 35(1):7–14. doi:10.1007/s10072-013-1512-8
150. Hauser TK, Luft A, Skalej M, Nagele T, Kircher TT, Leube DT, Schulz JB (2006) Visualization and quantification of disease progression in multiple system atrophy. Mov Disord 21(10):1674–1681. doi:10.1002/mds.21032
151. Minnerop M, Specht K, Ruhlmann J, Schimke N, Abele M, Weyer A, Wullner U, Klockgether T (2007) Voxel-based morphometry and voxel-based relaxometry in multiple system atrophy-a comparison between clinical subtypes and correlations with clinical parameters. Neuroimage 36(4):1086–1095. doi:10.1016/j.neuroimage.2007.04.028
152. Shigemoto Y, Matsuda H, Kamiya K, Maikusa N, Nakata Y, Ito K, Ota M, Matsunaga N, Sato N (2013) In vivo evaluation of gray and white matter volume loss in the parkinsonian variant of multiple system atrophy using SPM8 plus DARTEL for VBM. Neuroimage Clin 2:491–496. doi:10.1016/j.nicl.2013.03.017
153. Brenneis C, Seppi K, Schocke MF, Muller J, Luginger E, Bosch S, Loscher WN, Buchel C, Poewe W, Wenning GK (2003) Voxel-based morphometry detects cortical atrophy in the Parkinson variant of multiple system atrophy. Mov Disord 18(10):1132–1138. doi:10.1002/mds.10502
154. Brenneis C, Boesch SM, Egger KE, Seppi K, Scherfler C, Schocke M, Wenning GK, Poewe W (2006) Cortical atrophy in the cerebellar variant of multiple system atrophy: a voxel-based morphometry study. Mov Disord 21(2):159–165. doi:10.1002/mds.20656
155. Boxer AL, Geschwind MD, Belfor N, Gorno-Tempini ML, Schauer GF, Miller BL, Weiner MW, Rosen HJ (2006) Patterns of brain atrophy that differentiate corticobasal degeneration syndrome from progressive supranuclear palsy. Arch Neurol 63(1):81–86. doi:10.1001/archneur.63.1.81
156. Josephs KA, Whitwell JL, Dickson DW, Boeve BF, Knopman DS, Petersen RC, Parisi JE, Jack CR Jr (2008) Voxel-based morphometry in autopsy proven PSP and CBD. Neurobiol Aging 29(2):280–289. doi:10.1016/j.neurobiolaging.2006.09.019
157. Focke NK, Helms G, Scheewe S, Pantel PM, Bachmann CG, Dechent P, Ebentheuer J, Mohr A, Paulus W, Trenkwalder C (2011) Individual voxel-based subtype prediction can differentiate progressive supranuclear palsy from idiopathic Parkinson syndrome and healthy controls. Hum Brain Mapp 32(11):1905–1915. doi:10.1002/hbm.21161
158. Singh G, Samavedham L (2015) Unsupervised learning based feature extraction for differential diagnosis of neurodegenerative diseases: A case study on early-stage diagnosis of Parkinson disease. J Neurosci Methods 256:30–40. doi:10.1016/j.jneumeth.2015.08.011
159. Kikuchi A, Takeda A, Okamura N, Tashiro M, Hasegawa T, Furumoto S, Kobayashi M, Sugeno N, Baba T, Miki Y, Mori F, Wakabayashi K, Funaki Y, Iwata R, Takahashi S, Fukuda H, Arai H, Kudo Y, Yanai K, Itoyama Y (2010) In vivo visualization of alpha-synuclein deposition by carbon-11-labelled 2-[2-(2-dimethylaminothiazol-5-yl) ethenyl]-6-[2-(fluoro)ethoxy]benzoxazole positron emission tomography in multiple system atrophy. Brain 133(Pt 6):1772–1778. doi:10.1093/brain/awq091, awq091 [pii]

Psychiatric Disorders

9

Gilles N. Stormezand, Ronald J.H. Borra, Hans C. Klein, Peter Jan Van Laar, Ronald Boellaard, and Rudi A.J.O. Dierckx

9.1 Introduction

In the field of psychiatry, positron emission tomography (PET) imaging has attracted interest of researchers in a broad spectrum of diseases, such as depression, anxiety disorders, schizophrenia, and impulse control disorders. Being able to provide quantitative measurements of glucose metabolism, perfusion, and neurotransmitter functionality (e.g., neuroreceptors, transporters), PET provides useful information which adds to the differential diagnosis of diseases, as well as to understanding the neurobiological basis and determining neurotransmitter impairments. Functional imaging may further help to establish novel concepts and theoretic frameworks regarding diseases and to provide a rationale for specific pharmacological treatment. In psychiatric drug development, PET may play a role in the pharmacokinetic evaluation of a drug and in receptor occupancy studies, which helps to determine optimal dosing for further clinical trials. Finally, PET measurements may function as a biomarker, which could improve the selection of subjects entering clinical trials and provide an additional means of response evaluation. With the arrival of hybrid imaging, such as PET/CT and PET/MRI, simultaneous anatomical and functional biomarkers are obtained, which may be complementary in selected cases. Recent developments in functional MRI allow for different imaging combinations, such as the combined studies of cerebral perfusion and neurotransmitter systems. In this chapter, we will address the role of PET and anatomical imaging in various psychiatric disorders, with a particular focus on the separate PET and MRI findings and on potential applications of hybrid imaging.

G.N. Stormezand (✉) • R.J.H. Borra • R. Boellaard
Department of Nuclear Medicine & Molecular Imaging, Medical Imaging Center, University Medical Center, Groningen, The Netherlands
e-mail: g.n.stormezand01@umcg.nl

H.C. Klein
Program for Geriatric Psychiatry, University Center Psychiatry, Nuclear and Molecular Imaging, University Medical Center, Groningen, The Netherlands

P.J. Van Laar
Department of Radiology, University Medical Center, Groningen, University of Groningen, Groningen, The Netherlands

R.A.J.O. Dierckx
Department of Nuclear Medicine & Molecular Imaging, Medical Imaging Center, University Medical Center, Groningen, The Netherlands

Department of Radiology and Nuclear Medicine, Ghent University, Ghent, Belgium

9.2 Basics of PET-MRI

In many diseases of the brain in which functional or neurotransmission impairments predominate, macroscopic changes may not be apparent. In order to be sensitive to the cellular dysfunction

A. Ciarmiello, L. Mansi (eds.), *PET-CT and PET-MRI in Neurology*,
DOI 10.1007/978-3-319-31614-7_9

that is manifested by psychiatric disorders, it is necessary for imaging modalities to be able to visualize metabolic processes. PET tracers, usually labeled with short-lived isotopes [^{11}C] and [^{18}F], are particularly suited to this end. By selectively binding to different neuroreceptors in the brain, these tracers allow for in vivo assessment of receptor or transporter density or activity and of physiological activities in the brain. Alternatively, tracers are available which are able to target neuropathological processes, such as the activation of microglia (neuroinflammation), a feature which is commonly observed in neurodegenerative diseases, but may also be implicated in psychiatric disorders such as schizophrenia.

MRI on the other hand provides excellent soft tissue contrast, due to significant differences in the presence of free water molecules in the gray and white matter and the cerebrospinal fluid [1]. It offers the advantages that it is fully noninvasive (when performed without contrast agent) and that it does not expose subjects to ionizing radiation. Using MRI, micro- and macroscopical structural changes of the brain can be detected (sMRI), whereas functional MRI (fMRI) allows tracking of neural activity, not merely limited to activations of the brain but also to the connection of different parts of the brain. It is the combination of fMRI and PET imaging of neurotransmitter activity that has been highlighted in particular as a promising application of hybrid PET/MRI, helping to understand brain function in mental illnesses, and eventually guiding personalized therapies [2].

The simultaneous acquisition of both MRI and PET, i.e., the use of fully integrated PET/MRI systems, has come with several technical limitations and pitfalls, as described by Delso et al. [3]. The main challenge is that in order to provide quantitative PET measurements, PET/MRI has to rely on indirect MRI measurements to correct for attenuation in PET images. However, many technical solutions to address the abovementioned issue have been developed and will likely become available [4], which allows hybrid PET/MR to be used in the clinic as well as for scientific research. In the next section, we will describe PET and MRI findings in a selection of psychiatric disorders, attempting to identify potentially complementary applications.

9.3 Depression and Related Disorders

In depression, symptoms may consist of anhedonia, sleeping disorders, psychomotor agitation, fatigue, feelings of guilt, and cognitive disorders. A depressive episode may occur in major depressive disorder (MDD) and bipolar disorder (BD). One of the main challenges in the imaging of psychiatric disorders has been the highly heterogeneous nature of many psychiatric diseases, which potentially hampers the solid detection of brain regions involved in the process. This may particularly be the case in depressive disorders, in which a wide variety of clinical phenotypes may be present. Recently, most research focusing on functional imaging has been performed using (functional) MRI, whereas PET imaging has mostly been targeted at transporter and receptor imaging, providing a potentially complementary application for hybrid imaging, albeit still preserved for research purposes. We briefly discuss the main anatomical and functional imaging findings in depression using MRI and neurotransmitter findings using PET.

Several recent meta-analyses have appeared that have focused on MRI findings regarding anatomy [5–7], white matter integrity [8, 9], and fMRI [10] in MDD and are summarized in Table 9.1. All analyses suffered from the fact that both drug naive and medicated patients were included. Although studies initially employed a ROI-based analysis, more recently voxel-based morphometry techniques have been utilized which may reduce the bias of focusing on theoretically involved regions. Taken together, structural imaging findings point toward structural abnormalities in regions particularly involved in emotion control regulation such as the anterior cingulate and orbitofrontal and prefrontal cortex. Other regions showing significant reductions include the hippocampus and the striatum, although less consistently. The neurobiological basis of microstructural alterations in MDD has

Table 9.1 Summary of main findings of recent meta-analyses in MDD imaging using MRI

Series	No. of patients included	Modality	Main findings of patients with MDD vs. controls	Comments
Kempton (2011) [5]	9533 MDD, 8846 controls	sMRI	Lateral ventricle enlargement; larger cerebrospinal fluid volume; and smaller volumes of the basal ganglia, thalamus, hippocampus, frontal lobe, orbitofrontal cortex, and gyrus rectus	Both drug naive and medicated patients. Effect sizes were larger in patients experiencing a depressive episode than those in remission
Koolschijn (2009) [6]	2418 MDD, 1974 controls	sMRI	Large volume reductions in frontal regions, especially in the anterior cingulate and orbitofrontal cortex with smaller reductions in the prefrontal cortex. The hippocampus, the putamen, and caudate nucleus showed moderate volume reductions	Both drug naive and medicated patients. Significant study heterogeneity. ROI analysis
Iwabuchi (2015) [10]	455 MDD, 230 controls	fMRI	Increased regional homogeneity during paradigm-free resting state in the medial prefrontal cortex in depressed subjects	Both drug naive and medicated patients. Only studies conducted in China were included
Bora (2012) [7]	987 MDD, 937 HC.	sMRI	Significantly reduced gray matter in a cluster located in the rostral anterior cingulate cortex (ACC) was found. Gray matter reductions in the dorsolateral and dorsomedial prefrontal cortex	Both drug naive and medicated patients. Voxel-based morphometry
Murphy (2011) [9]	188 MDD, 221 HC	DTI	Increased WM FA values in the superior longitudinal fasciculus and increased FA values in the fronto-occipital fasciculus	Both drug naive and medicated patients. Increased FA value of the FOF was based on one study and was not consistently reported
Liao (2013) [8]	231 MDD, 261 controls	DTI	Decreased fractional anisotropy in the white matter in the right frontal lobe, right fusiform gyrus, left frontal lobe, and right occipital lobe. Fiber tracking showed that the main fascicles involved were the right inferior longitudinal fasciculus, right inferior fronto-occipital fasciculus, right posterior thalamic radiation, and interhemispheric fibers running through the genu and body of the corpus callosum	Both drug naive and medicated patients. Activation likelihood estimation (ALE). Relatively small group sizes

not been fully elucidated, yet there is evidence pointing toward a chronic elevation of cytokines [11]. DTI imaging has identified another putative mechanism; white matter changes in cortico-subcortical circuits, giving rise to disconnectivity. *Locally* reduced connectivity has further been implicated by the meta-analysis by Iwabuchi et al. [10], which according to the authors, is suggestive of increased participation of this region in default-mode-network-like functions.

Functional imaging using nuclear techniques (PET and SPECT) has usually been performed under resting conditions, yet MRI sequences are increasingly being evaluated in this setting. In this perspective, the use of arterial spin labeling sequences may especially be attractive, offering the advantage of using freely flowing water protons as an endogenous tracer. Using ASL, Duhameau and colleagues found hypoperfusion in the bilateral subgenual anterior cingulate cortex (sACC), left prefrontal dorsomedian cortex, left ACC, and left subcortical areas in depressed subjects [12]. The finding of reduced hypoperfusion of the sACC may be particularly relevant, since this region has not been consequently reported to be altered in anatomic imaging studies [5]. However, functional involvement of this region is supported by evidence in patients treated with deep brain stimulation in this region ($n=6$), in whom symptoms ameliorated over a sustained period in four out of six patients [13]. The observation of reduced activity of the sACC is also in line with the meta-analysis considering both fMRI, SPECT, and PET by Fitzgerald et al., who additionally reported hypoactivity in frontal gyri, the left superior temporal gyrus, insula, and the cerebellum, whereas hyperactivity was found in subcortical and limbic areas, as well as in medial and inferior frontal regions [14].

As mentioned previously, most PET studies in MDD have aimed to detect alterations in neurotransmitter systems, both in comparison to healthy controls and in response to pharmacological treatment. Impairments of the serotonergic system and dopaminergic system have often been implicated in the pathophysiology of depression, ever since the monoamine hypothesis was introduced. This hypothesis, which suggests that depression is caused by deficits in the serotonergic, dopaminergic, and noradrenergic neurotransmitter system, is nowadays regarded as an oversimplification [15]. Additional impairments such as relating to GABA – an inhibitory neurotransmitter – have been described. Klumpers et al. reported reduced binding of the $GABA_a$ benzodiazepine in the bilateral parahippocampal gyrus and the right temporal gyrus, using [^{11}C]-flumazenil [16]. The serotonergic system has been most widely studied in PET studies of MDD. Different radioligands are available to image the serotonin transporter (SERT), serotonin synthesis, and serotonin receptors.

Few studies have investigated serotonin synthesis in major depressive disorder using PET. In the largest study group (17 patients with MDD and 17 HC), reduced synthesis rates were observed in the bilateral cingulate and medial temporal lobe in females and the left cingulate lobe in males [17]. Concerning the SERT, studies have appeared usually comprising of small groups and have yielded inconsistent results, which were possibly due to confounding factors such as the heterogeneity of study groups (with many comorbidities), genetic polymorphisms, and seasonal changes. An interesting application of SERT imaging is targeted at measuring the SERT availability before and after treatment with serotonin reuptake inhibiting antidepressants, by means of which receptor occupancies can be determined at different doses. Ruhé et al., for example, performed a randomized, placebo-controlled dose-escalation study to show that the SERT occupancy remained relatively unchanged after true dose escalation relative to the placebo dose escalation, supporting a previously described flat dose response for SSRIs [18].

Results of dopamine synthesis studies are scarce, and reductions have not consistently been reported. For a detailed description of the results of studies on serotonergic and dopaminergic alterations between subjects with depressive disorders and healthy controls, the reader is referred to a recent review [15]. In general, the inconsistencies mentioned above seem to point

out that altered serotonergic and dopaminergic may be present in major depressive disorder but only in subsets. Therefore, more accurate phenotyping or genotyping of these subjects may eventually lead to more consistent results. In this light, hybrid PET/MRI imaging may play a role; impairments in neurotransmission may, for example, be more apparent in a subgroup who additionally show signs of reduced local connectivity of the dorsomedial prefrontal cortex (Table 9.1).

9.4 Anxiety Disorders

Anxiety disorders are characterized by developmentally inappropriate excessive fear and anxiety which lead to disturbances in several domains, such as in social, academic, or occupational environments. In DSM-V, anxiety disorders are a collection of disorders consisting of separation anxiety disorder, selective mutism, specific phobia, social anxiety disorder, panic disorder, panic disorder, agoraphobia, generalized anxiety disorder, substance-induced anxiety disorder, anxiety disorder due to another medical condition and other specified disorder, and unspecified anxiety disorder [19]. Anxiety disorders, regardless of the type, have an estimated lifetime prevalence of approximately 26 % [20]. Unlike in DSM-IV, obsessive-compulsive disorders (OCD) are no longer part of the list of anxiety disorders in DSM-V, but instead are mentioned separately under "obsessive-compulsive and related disorders." Indeed, a meta-analysis by Radua et al. gathering data on structural MRI has reported relatively increased bilateral gray matter volumes in the lenticular and caudate nuclei in subjects with OCD, whereas subjects with anxiety disorders tended more to show decreased gray matter volumes in the left lenticular nucleus [21]. The groups combined showed decreased bilateral gray matter volumes in the dorsomedial frontal/anterior cingulate gyri. The authors did note that some anxiety disorders, such as generalized anxiety disorder or specific phobias, were underrepresented in volumetric studies.

Specific phobias, however, have often been the subject of provocation studies using FDG PET or ^{15}O-H_2O. Specific phobias, as well as posttraumatic stress disorder, offer the "advantage" that anxiety responses can be induced by physiological means and thus measured at any given time. A meta-analysis by Fredrikson et al. has been performed in order to assess the within-group differences (at baseline and during fear induction) in subjects with specific and social phobias as well as posttraumatic stress disorder (PTSD) [22]. It was reported that specific regions, commonly attributed to the "fear network," such as the amygdala, midbrain, and insula, were consistently activated during fear provocation in both groups, whereas hypoactivation in the anterior cingulate cortex was observed in subjects with specific or social phobia and of the orbitofrontal cortex in subjects with PTSD. Another meta-analysis, which combined data derived from PET and SPECT studies with data from fMRI in the same categories of subjects (specific phobia, social anxiety phobia, and PTSD), showed consistent hyperactivation of only two regions – the amygdala and the insula. *Hypo*activation was only observed in specific regions in the PTSD group. Based on the results, the authors propose that hyperactivity in the amygdala and insula may be useful criteria for disorder categorization [23].

In the resting state, PET and SPECT studies have aimed to characterize alterations in neurotransmitter systems between patients and healthy controls, although relatively small in number and inconsistent results have been reported. These studies have focused on the postsynaptic D_2/D_3 dopamine receptor, $5HT1_a$ receptors, as well as the dopamine transporter (DAT), the serotonin transporter (SERT), and the benzodiazepine receptor (BZD). A recent comprehensive review reported that the most consistent findings include reduced benzodiazepine receptor activity in limbic and frontal regions and downregulation of 5HT1a receptors, mainly in limbic, striatal, and midbrain/thalamus regions [22]. A combination of fMRI and PET imaging of neurotransmitter systems may help to establish more consistent findings in this respect.

9.5 Schizophrenia Spectrum Disorders

In schizophrenia spectrum disorders, one or more of the following symptoms are present to variable degrees: delusions, hallucinations, disorganized thinking, grossly disorganized or abnormal motor behavior, and negative symptoms [19]. Psychosis is one of the hallmark features of schizophrenia spectrum disorders. Many years of structural brain research have led schizophrenia to well-established reductions in the brain volume. A meta-analysis by Haijma et al. including data of over 9000 patients with schizophrenia reported reduced intracranial, total brain and total gray matter volume, and total white matter volumes. Increased volume was only observed in the globus pallidus. Significant differences between medicated and antipsychotic naive patients were noted. Although unmedicated patients tended to show smaller gray matter volume reductions, volume reductions in the thalamus and caudate nucleus were more pronounced in treatment-naive patients. PET and SPECT studies of schizophrenia have mainly been driven by the putative involvement of the dopaminergic system, glutamate, and neuroinflammatory processes [24]. Regarding the dopaminergic system, investigations have targeted the postsynaptic D_2/D_3 receptor, presynaptic dopamine synthesis, and the dopamine transporter. An early meta-analysis by Laurelle et al. reported an increase of approximately 12% increase of D_2/D_3-receptor binding in medication-free patients with schizophrenia in comparison to healthy controls [25]. However, a more recent meta-analysis reported less consistent findings, with both increased, decreases, and no differences between subjects with schizophrenia and controls [26]. Possible explanations include competition at the receptor of the radiotracer with increased levels of endogenous dopamine resulting in lower D_2/D_3-receptor binding, or a medicated status, in which dopamine blockade might cause receptor regulation [24]. Increased dopamine synthesis capacity, assessed using [^{18}F]-DOPA, has been an often replicated finding and may also be correlated to disease severity. Amphetamine challenge studies, which measure differences between the pre- and postadmission of amphetamine, have indicated that medication-free subjects with schizophrenia show elevated striatal dopamine release. Finally, the dopamine transporter (DAT) does not seem to be implicated in schizophrenia [26].

Although PET tracers targeting glutamate release, such as [^{11}C]-APB688, are being developed and integrated into clinical research, most data converging on glutamate transmission has originated from MR spectroscopy. A recent meta-analysis has reported elevated GLX and glutamine levels in many regions of the brain, including the medial prefrontal cortex, the basal ganglia, and the anterior cingulate cortex. The authors conclude that disturbances in glutamate and glutamine neurotransmission are likely to be one of the factors underlying the pathophysiology of schizophrenia [26]. Another recent PET approach has aimed to quantify the activation of microglia (neuroinflammation) in schizophrenia, using the PET tracer [^{11}C]-(R)-PK11195. Indeed, increased specific binding was reported, particularly in the hippocampus [27]. Future studies using hybrid imaging may benefit from a strict patient selection, minimizing the mixture of medication naive and previously treated patients.

9.6 Substance-Related and Addictive Disorders

Addiction is a chronic relapsing disorder of the brain, characterized by a pattern of repetitive actions that are continued despite of adverse consequences, which may be linked to substances or behavior. Despite sharing potential clinical similarities to chemical addiction, difficulty presents when defining a pathologic addictive state of behavior, since eating, gaming, and sexual behavior may be considered normal behavior. In this respect, functional imaging modalities may help to establish neurobiological linkages between behavior addictions and substance use disorders. Currently, pathological gambling remains the only behavioral addiction included in DSM-V section "substance disorders and other addictive behaviors" [19], as it has been shown that there

are similarities between pathological gambling disorder and substance use disorder (SUD) [28, 29]. Although gaming addiction is increasingly prevalent, this condition is still under review for being considered as an entity in the DSM. Other potential addictions, such as sexual addiction or pornographic addiction, are not yet considered. A need for studies aiming to identify neurobiological correlates of hypersexuality disorders has been expressed in order to allow comparison to SUD [30]. Although a number of neuroimaging studies have focused on the direct effects on the brain of sexual arousal (e.g., visual stimuli, orgasms, sexual stimulation) [31–33], few have been conducted in the absence of sexual stimuli in potentially addicted subjects. Using diffusion tensor imaging (DTI), Miner and colleagues reported significantly higher superior frontal region mean diffusivity (MD) in subjects with compulsive sexual behavior ($n=16$) in comparison to controls ($n=8$). However, the DTI results were regarded inconsistent with impulse control disorders [34].

Altered dopamine transmission has been assumed to play a critical role in the pathogenesis of addiction [35]. Dopamine is a neurotransmitter that is present in a wide variety of animals, including both vertebrates and invertebrates. In the brain, this phenethylamine functions as a neurotransmitter, activating five receptor subtypes of dopamine receptors (D_1, D_2, D_3, D_4, and D_5), which are subdivided in two main classes of receptors, termed D_1-like (D_1, D_5) and D_2-like (D_2, D_3, D_4). In particular, D_2 receptors are associated with addiction-linked processes such as reward seeking, prediction, expectation, and motivation [36]. D_2-receptors are predominant in the striatum, in the core of the nucleus accumbens (NAc), and in the olfactory tubercle, but are also present in the prefrontal, cingulate, temporal, and entorhinal cortices, amygdala, hippocampus, hypothalamus, substantia nigra pars compacta, and ventral tegmental area (VTA) [37]. Functional imaging targeted at the mesolimbic dopaminergic system and its regulation by frontal regions has been applied in the field of pathological gambling and obesity [38–41], but has not been performed in sexual disorders such as pornography addiction.

Most drugs implicated in substance use disorder, e.g., chemical addiction, activate regions associated with the reward center, such as the mesolimbic and mesocortical dopamine systems, which consist of dopaminergic neurons in the ventral tegmental area and their projection regions, including the nucleus accumbens (ventral striatum) and medial prefrontal cortex [42]. Besides psychoactive drugs, several non-pharmacological rewards including gambling tasks [43], sex [44], playing video games [45], food [46], and even music [47] have been shown to generate significant dopamine release, which in turn might trigger addiction in vulnerable individuals. Involvement of the dopaminergic system in behavioral addictions has further been implicated by observations during agonistic dopaminergic treatment in patients with Parkinson's disease, which has been associated with hypersexuality disorder, and compulsive gambling and shopping [48, 49].

Positron emission tomography, using [^{11}C]-raclopride as a radioligand, enables functional assessment of D_2-receptor availability. Decreased [^{11}C]-raclopride binding has been a fairly consistent finding in studies assessing the D_2-receptor availability in the striatum in subjects addicted to different substances, including cocaine [50, 51], methamphetamine [52, 53], alcohol [54, 55], and heroin [56]. Few studies failed to report D_2-receptor-related differences in SUD compared to controls, particularly involving the direct effects alcohol and nicotine abuse [57–59]. Using dual tracer approaches, combining [^{18}F]-FDG (glucose analog, used to assess brain metabolism) and [^{11}C]-raclopride PET, decreased striatal binding availability in cocaine addicts has been linked with frontal hypometabolism, suggesting a deficit in prefrontal inhibitory signaling toward the striatum [60]. The opposite relationship, e.g., lower D_2-receptor availability correlating with higher prefrontal metabolism, has also been reported [61]. Stimulant administration in addicted individuals seems to increase metabolism in the orbital and medial prefrontal cortex to a larger extent than in controls, suggesting a normalization effect [62]. The prefrontal cortex has also been prone to gray matter volume

loss, as reported by a recent voxel-based morphometry meta-analysis [63].

Analogous to the above chemical addictions, several behavioral addictions, such as morbid obesity (food addiction) [41, 64] and pathological gambling [43], have been linked to decreased striatal D_2/D_3-receptor availability. In parallel to the previously described observations in cocaine addicts, decreased striatal D_2-receptor availability has been correlated with hypometabolism in prefrontal areas in subjects with morbid obesity [57]. In subjects with bulimia nervosa, striatal dopamine release after stimulant administration was associated with the frequency of binge eating, and there was a trend toward lower D_2-receptor availability [65]. Recently, reduced striatal D_2-receptor availability was shown in the dorsal striatum of subjects with compulsive Internet use [66]. From the latter study, it could however not be estimated which online activity is specifically related to the observed differences in D_2-receptor availability and is responsible for the reduced D_2-receptor availability.

There is evidence suggesting that repeated drug abuse over a prolonged period of time may result in maladaptive neural plasticity of the brain in vulnerable individuals, which might persist long time after withdrawal [67, 68]. Alternatively, there may be a primary deficit of the reward center, often referred to in the literature as the "reward deficiency syndrome," which might predispose an individual for developing future addictive behavior [69]. In this unifying concept, impulsive, addictive, and compulsive disorders, regardless of behavioral or chemical origin (e.g., alcoholism, cocaine dependency, food abuse, and sex addiction), are grouped based on shared neurochemical and genetic components. Polymorphisms at the D_2-receptor gene locus (DRD2), existing of the A1 and A2 allele, are held partly responsible for an individual vulnerability to develop substance abuse disorders [70] and have been linked to a deficiency to learn from errors [71]. It is suggested that a low number of D_2 receptors reflects a hypodopaminergic state, in which an individual seeks substances or behaviors that stimulate the dopaminergic system in order to achieve "normalization" [69]. Hybrid imaging approaches assessing the dynamics of reward processing in behavioral addictions may be able to shed more light on this issue.

9.7 Future Developments

As illustrated above, MRI and PET studies in the field of psychiatry have often yielded complementary results on different parameters such as brain volumetrics, neurochemistry, receptor density and/or occupancy, and glucose metabolism. The integration of simultaneous PET and MRI may offer several advantages, some of which related to image quality (e.g., using MRI to correct for partial volume effects or motion correction), yet the ability to achieve measurements of neuronal activity and neurotransmitter release at the same time in the setting of task processing or pharmacological interventions seems to add most value, even more so when temporal relationships are being investigated. Indeed, this advantage has already been captivated on by Mandeville et al., who performed simultaneous PET/fMRI experiments in rhesus monkeys to derive a receptor-based model for the analysis of dopamine-induced fMRI signals [72]. Temporal differences between both modalities were observed during a methamphetamine challenge, in which displacement of the PET ligand ($[^{11}C]$-raclopride) was slower than the evoked fMRI signal alterations, possibly due to receptor internalization. Another interesting study has correlated hemodynamic responses measured using the blood oxygenation-level-dependent (BOLD) signal with dynamic PET acquisitions of the opioid radioligand $[^{11}C]$-diprenorphine in eight healthy volunteers while applying pressure pain. The authors reported both modality-specific and overlapping networks (in the thalamus and striatum) involved in pain processing [73]. Complementary information from hybrid imaging has also been gathered by Wehrl et al. who found spatial and quantitative differences between activated regions as detected by fMRI and FDG PET during whisker pad stimulation in rats. These papers just illustrate the first applications of simultaneous

hybrid PET and MR imaging, providing for the first time a direct comparison of the temporal aspects of functional and molecular processes, which so far was not possible and was enabled by the development of hybrid PET/MR.

9.8 Summary and Conclusion

A large body of literature has covered the findings of anatomical and functional imaging with MRI, whereas PET studies have focused on functional imaging and alterations in neurotransmitter systems. Psychiatric conditions may present with considerable heterogeneity, both with respect to the clinical presentation and to neuroimaging findings, which has limited the consistency of these findings. Future studies may benefit from more accurate phenotyping and genotyping in order to be more sensitive to functional and neurotransmission impairments, e.g., by correlating a MRI-derived functional impairment to a specific neurotransmitter deficit measured with PET. PET and MRI, whether in combination or performed separately, may provide useful information in several domains. Neuroimaging may aid the selection of more homogeneous groups entering clinical trials, monitor pharmacological response, support new or existing concepts of diseases, and eventually guide pharmacological treatment by selecting patients that will most likely benefit. Recent developments in functional MRI allow for different imaging combinations, such as the combined studies of fMRI and neurotransmitter systems. Depending on the disorder and the goal of the examination, different combinations of imaging modalities can be selected which may be complementary. A PET/MRI hybrid imaging approach can be particularly valuable in the research field of psychiatry, as many single-modality studies have lacked (spatial and temporal) integration of different co-acting systems. Correlations between simultaneously acquired sets of MRI (e.g., volumetrics, fMRI, DTI, MRS) and PET (neurotransmission, neuronal activity) data may help to better understand the linkages between individual systems.

References

1. Neeb H, Zilles K, Shah NJ (2006) Fully-automated detection of cerebral water content changes: study of age- and gender-related H2O patterns with quantitative MRI. Neuroimage 29(3):910–922
2. Mier W, Mier D (2015) Advantages in functional imaging of the brain. Front Hum Neurosci 9:249
3. Delso G, Voert ET, Barbosa Fde G, Veit-Haibach P (2015) Pitfalls and limitations in simultaneous PET/MRI. Semin Nucl Med 45(6):552–559
4. Boellaard R, Quick HH (2015) Current image acquisition options in PET/MR. Semin Nucl Med 45(3):192–200
5. Kempton MJ, Salvador Z, Munafo MR, Geddes JR, Simmons A, Frangou S et al (2011) Structural neuroimaging studies in major depressive disorder. Meta-analysis and comparison with bipolar disorder. Arch Gen Psychiatry 68(7):675–690
6. Koolschijn PCMP, van Haren NEM, Lensvelt-Mulders GJLM, Hulshoff Pol HE, Kahn RS (2009) Brain volume abnormalities in major depressive disorder: a meta-analysis of magnetic resonance imaging studies. Hum Brain Mapp 30(11):3719–3735
7. Bora E, Fornito A, Pantelis C, Yücel M (2012) Gray matter abnormalities in major depressive disorder: a meta-analysis of voxel based morphometry studies. J Affect Disord 138(1–2):9–18
8. Liao Y, Huang X, Wu Q, Yang C, Kuang W, Du M et al (2013) Is depression a disconnection syndrome? Meta-analysis of diffusion tensor imaging studies in patients with MDD. J Psychiatry Neurosci 38(1):49–56
9. Murphy ML, Frodl T (2011) Meta-analysis of diffusion tensor imaging studies shows altered fractional anisotropy occurring in distinct brain areas in association with depression. Biol Mood Anxiety Disord 1(1):3-5380-1-3
10. Iwabuchi SJ, Krishnadas R, Li C, Auer DP, Radua J, Palaniyappan L (2015) Localized connectivity in depression: a meta-analysis of resting state functional imaging studies. Neurosci Biobehav Rev 51:77–86
11. Miller AH, Maletic V, Raison CL (2009) Inflammation and its discontents: the role of cytokines in the pathophysiology of major depression. Biol Psychiatry 65(9):732–741
12. Duhameau B, Ferré J, Jannin P, Gauvrit J, Vérin M, Millet B et al (2010) Chronic and treatment-resistant depression: a study using arterial spin labeling perfusion MRI at 3 Tesla. Psychiatry Res Neuroimaging 182(2):111–116
13. Mayberg HS, Lozano AM, Voon V, McNeely HE, Seminowicz D, Hamani C et al (2005) Deep brain stimulation for treatment-resistant depression. Neuron 45(5):651–660
14. Fitzgerald PB, Laird AR, Maller J, Daskalakis ZJ (2008) A meta-analytic study of changes in brain activation in depression. Hum Brain Mapp 29(6):683–695

15. Ruhé HG, Visser AKD, Frokjaer VG, Haarman BCM, Klein HC, Booij J (2014) PET and SPECT in psychiatry; Molecular imaging of depressive disorders. In: Dierckx RA, Otte A, De Vries EFJ, Van Waarde A, Den Boer JA (eds) PET and SPECT in psychiatry. Springer, Berlin Heidelberg, pp 93–172
16. Klumpers UM, Veltman DJ, Drent ML, Boellaard R, Comans EF, Meynen G et al (2010) Reduced parahippocampal and lateral temporal GABAA-[11C]flumazenil binding in major depression: preliminary results. Eur J Nucl Med Mol Imaging 37(3):565–574
17. Rosa-Neto P, Diksic M, Okazawa H, Leyton M, Ghadirian N, Mzengeza S et al (2004) Measurement of brain regional alpha-[11C]methyl-L-tryptophan trapping as a measure of serotonin synthesis in medication-free patients with major depression. Arch Gen Psychiatry 61(6):556–563
18. Ruhe HG, Booij J, v Weert HC, Reitsma JB, Franssen EJ, Michel MC et al (2009) Evidence why paroxetine dose escalation is not effective in major depressive disorder: a randomized controlled trial with assessment of serotonin transporter occupancy. Neuropsychopharmacology 34(4):999–1010
19. American Psychiatric Association (2013) Diagnostic and statistical manual of mental disorders, 5th edn. American Psychiatric Publishing, Arlington, VA
20. Kessler RC, Chiu WT, Demler O, Merikangas KR, Walters EE (2005) Prevalence, severity, and comorbidity of 12-month DSM-IV disorders in the National Comorbidity Survey Replication. Arch Gen Psychiatry 62(6):617–627
21. Radua J, van den Heuvel OA, Surguladze S, Mataix-Cols D (2010) Meta-analytical comparison of voxel-based morphometry studies in obsessive-compulsive disorder vs other anxiety disorders. Arch Gen Psychiatry 67(7):701–711
22. Fredrikson M, Faria V, Furmark T (2014) PET and SPECT in psychiatry; neurotransmission: a review of PET and SPECT studies in anxiety disorders. In: Dierckx RA, Otte A, De Vries EFJ, Van Waarde A, Den Boer JA (eds) PET and SPECT in psychiatry. Springer, Berlin Heidelberg, pp 349–370
23. Etkin A, Wager TD (2007) Functional neuroimaging of anxiety: a meta-analysis of emotional processing in PTSD, social anxiety disorder, and specific phobia. Am J Psychiatry 164(10):1476–1488
24. Klein HC, Doorduin J, van Berckel BN (2014) PET and SPECT in psychiatry; Molecular imaging in schizophrenia spectrum disorders. In: Dierckx RA, Otte A, De Vries EFJ, Van Waarde A, Den Boer JA (eds) PET and SPECT in psychiatry. Springer, Berlin Heidelberg, pp 453–462
25. Laruelle M (1998) Imaging dopamine transmission in schizophrenia. A review and meta-analysis. Q J Nucl Med 42(3):211–221
26. Salavati B, Rajji TK, Price R, Sun Y, Graff-Guerrero A, Daskalakis ZJ (2015) Imaging-based neurochemistry in schizophrenia: a systematic review and implications for dysfunctional long-term potentiation. Schizophr Bull 41(1):44–56
27. Doorduin J, de Vries EFJ, Willemsen ATM, de Groot JC, Dierckx RA, Klein HC (2009) Neuroinflammation in schizophrenia-related psychosis: a PET study. J Nucl Med 50(11):1801–1807
28. Petry NM (2006) Should the scope of addictive behaviors be broadened to include pathological gambling? Addiction 101(Suppl 1):152–160
29. Potenza MN (2006) Should addictive disorders include non-substance-related conditions? Addiction 101(Suppl 1):142–151
30. Kor A, Fogel Y, Reid RC, Potenza MN (2013) Should hypersexual disorder be classified as an addiction? Sex Addict Compulsivity 20(1–2):27–47. doi:10.1080/10720162.2013.768132
31. Huynh HK, Beers C, Willemsen A, Lont E, Laan E, Dierckx R et al (2012) High-intensity erotic visual stimuli de-activate the primary visual cortex in women. J Sex Med 9(6):1579–1587
32. Holstege G, Georgiadis JR, Paans AM, Meiners LC, van der Graaf FH, Reinders AA (2003) Brain activation during human male ejaculation. J Neurosci 23(27):9185–9193
33. Georgiadis JR, Kortekaas R, Kuipers R, Nieuwenburg A, Pruim J, Reinders AA et al (2006) Regional cerebral blood flow changes associated with clitorally induced orgasm in healthy women. Eur J Neurosci 24(11):3305–3316
34. Miner MH, Raymond N, Mueller BA, Lloyd M, Lim KO (2009) Preliminary investigation of the impulsive and neuroanatomical characteristics of compulsive sexual behavior. Psychiatry Res 174(2):146–151
35. Koob GF, Volkow ND (2010) Neurocircuitry of addiction. Neuropsychopharmacology 35(1):217–238
36. Wise RA (2006) Role of brain dopamine in food reward and reinforcement. Philos Trans R Soc Lond B Biol Sci 361(1471):1149–1158
37. Missale C, Nash SR, Robinson SW, Jaber M, Caron MG (1998) Dopamine receptors: from structure to function. Physiol Rev 78(1):189–225
38. Thanos PK, Michaelides M, Piyis YK, Wang GJ, Volkow ND (2008) Food restriction markedly increases dopamine D2 receptor (D2R) in a rat model of obesity as assessed with in-vivo muPET imaging ([11C] raclopride) and in-vitro ([3H] spiperone) autoradiography. Synapse 62(1):50–61
39. Linnet J, Peterson E, Doudet DJ, Gjedde A, Moller A (2010) Dopamine release in ventral striatum of pathological gamblers losing money. Acta Psychiatr Scand 122(4):326–333
40. Wang GJ, Geliebter A, Volkow ND, Telang FW, Logan J, Jayne MC et al (2011) Enhanced striatal dopamine release during food stimulation in binge eating disorder. Obesity (Silver Spring) 19(8):1601–1608
41. Wang GJ, Volkow ND, Logan J, Pappas NR, Wong CT, Zhu W et al (2001) Brain dopamine and obesity. Lancet 357(9253):354–357
42. Nestler EJ (1994) Hard target: understanding dopaminergic neurotransmission. Cell 79(6):923–926

43. Steeves TD, Miyasaki J, Zurowski M, Lang AE, Pellecchia G, Van Eimeren T et al (2009) Increased striatal dopamine release in Parkinsonian patients with pathological gambling: a [11C] raclopride PET study. Brain 132(Pt 5):1376–1385
44. Pfaus JG, Damsma G, Nomikos GG, Wenkstern DG, Blaha CD, Phillips AG et al (1990) Sexual behavior enhances central dopamine transmission in the male rat. Brain Res 530(2):345–348
45. Koepp MJ, Gunn RN, Lawrence AD, Cunningham VJ, Dagher A, Jones T et al (1998) Evidence for striatal dopamine release during a video game. Nature 393(6682):266–268
46. Small DM, Jones-Gotman M, Dagher A (2003) Feeding-induced dopamine release in dorsal striatum correlates with meal pleasantness ratings in healthy human volunteers. Neuroimage 19(4):1709–1715
47. Salimpoor VN, Benovoy M, Larcher K, Dagher A, Zatorre RJ (2011) Anatomically distinct dopamine release during anticipation and experience of peak emotion to music. Nat Neurosci 14(2):257–262
48. Weintraub D, Siderowf AD, Potenza MN, Goveas J, Morales KH, Duda JE et al (2006) Association of dopamine agonist use with impulse control disorders in Parkinson disease. Arch Neurol 63(7):969–973
49. Uitti RJ, Tanner CM, Rajput AH, Goetz CG, Klawans HL, Thiessen B (1989) Hypersexuality with antiparkinsonian therapy. Clin Neuropharmacol 12(5):375–383
50. Volkow ND, Wang GJ, Fowler JS, Logan J, Gatley SJ, Hitzemann R et al (1997) Decreased striatal dopaminergic responsiveness in detoxified cocaine-dependent subjects. Nature 386(6627):830–833
51. Martinez D, Broft A, Foltin RW, Slifstein M, Hwang DR, Huang Y et al (2004) Cocaine dependence and d2 receptor availability in the functional subdivisions of the striatum: relationship with cocaine-seeking behavior. Neuropsychopharmacology 29(6):1190–1202
52. Lee B, London ED, Poldrack RA, Farahi J, Nacca A, Monterosso JR et al (2009) Striatal dopamine d2/d3 receptor availability is reduced in methamphetamine dependence and is linked to impulsivity. J Neurosci 29(47):14734–14740
53. Volkow ND, Chang L, Wang GJ, Fowler JS, Ding YS, Sedler M et al (2001) Low level of brain dopamine D2 receptors in methamphetamine abusers: association with metabolism in the orbitofrontal cortex. Am J Psychiatry 158(12):2015–2021
54. Volkow ND, Wang GJ, Fowler JS, Logan J, Hitzemann R, Ding YS et al (1996) Decreases in dopamine receptors but not in dopamine transporters in alcoholics. Alcohol Clin Exp Res 20(9):1594–1598
55. Hietala J, West C, Syvalahti E, Nagren K, Lehikoinen P, Sonninen P et al (1994) Striatal D2 dopamine receptor binding characteristics in vivo in patients with alcohol dependence. Psychopharmacology (Berl) 116(3):285–290
56. Martinez D, Saccone PA, Liu F, Slifstein M, Orlowska D, Grassetti A et al (2012) Deficits in dopamine D(2) receptors and presynaptic dopamine in heroin dependence: commonalities and differences with other types of addiction. Biol Psychiatry 71(3):192–198
57. Spreckelmeyer KN, Paulzen M, Raptis M, Baltus T, Schaffrath S, Van Waesberghe J et al (2011) Opiate-induced dopamine release is modulated by severity of alcohol dependence: an [(18)F]fallypride positron emission tomography study. Biol Psychiatry 70(8):770–776
58. Montgomery AJ, Lingford-Hughes AR, Egerton A, Nutt DJ, Grasby PM (2007) The effect of nicotine on striatal dopamine release in man: A [11C]raclopride PET study. Synapse 61(8):637–645
59. Barrett SP, Boileau I, Okker J, Pihl RO, Dagher A (2004) The hedonic response to cigarette smoking is proportional to dopamine release in the human striatum as measured by positron emission tomography and [11C]raclopride. Synapse 54(2):65–71
60. Volkow ND, Fowler JS, Wang GJ, Hitzemann R, Logan J, Schlyer DJ et al (1993) Decreased dopamine D2 receptor availability is associated with reduced frontal metabolism in cocaine abusers. Synapse 14(2):169–177
61. Asensio S, Romero MJ, Romero FJ, Wong C, Alia-Klein N, Tomasi D et al (2010) Striatal dopamine D2 receptor availability predicts the thalamic and medial prefrontal responses to reward in cocaine abusers three years later. Synapse 64(5):397–402
62. Volkow ND, Wang GJ, Ma Y, Fowler JS, Wong C, Ding YS et al (2005) Activation of orbital and medial prefrontal cortex by methylphenidate in cocaine-addicted subjects but not in controls: relevance to addiction. J Neurosci 25(15):3932–3939
63. Ersche KD, Williams GB, Robbins TW, Bullmore ET (2013) Meta-analysis of structural brain abnormalities associated with stimulant drug dependence and neuroimaging of addiction vulnerability and resilience. Curr Opin Neurobiol 23(4):615–624
64. Volkow ND, Wang GJ, Telang F, Fowler JS, Thanos PK, Logan J et al (2008) Low dopamine striatal D2 receptors are associated with prefrontal metabolism in obese subjects: possible contributing factors. Neuroimage 42(4):1537–1543
65. Broft A, Shingleton R, Kaufman J, Liu F, Kumar D, Slifstein M et al (2012) Striatal dopamine in bulimia nervosa: a PET imaging study. Int J Eat Disord 45(5):648–656
66. Kim SH, Baik SH, Park CS, Kim SJ, Choi SW, Kim SE (2011) Reduced striatal dopamine D2 receptors in people with Internet addiction. Neuroreport 22(8):407–411
67. Nestler EJ (2014) Epigenetic mechanisms of drug addiction. Neuropharmacology 76 Pt B:259–268
68. Chen TJ, Blum K, Chen AL, Bowirrat A, Downs WB, Madigan MA et al (2011) Neurogenetics and clinical evidence for the putative activation of the brain reward circuitry by a neuroadaptagen: proposing an addiction candidate gene panel map. J Psychoactive Drugs 43(2):108–127

69. Blum K, Braverman ER, Holder JM, Lubar JF, Monastra VJ, Miller D et al (2000) Reward deficiency syndrome: a biogenetic model for the diagnosis and treatment of impulsive, addictive, and compulsive behaviors. J Psychoactive Drugs 32 Suppl:i–iv, 1–112
70. Noble EP (1994) Polymorphisms of the D2 dopamine receptor gene and alcoholism and other substance use disorders. Alcohol Alcohol Suppl 2:35–43
71. Klein TA, Neumann J, Reuter M, Hennig J, von Cramon DY, Ullsperger M (2007) Genetically determined differences in learning from errors. Science 318(5856):1642–1645
72. Mandeville JB, Sander CY, Jenkins BG, Hooker JM, Catana C, Vanduffel W et al (2013) A receptor-based model for dopamine-induced fMRI signal. Neuroimage 75:46–57
73. Wey HY, Catana C, Hooker JM, Dougherty DD, Knudsen GM, Wang DJ et al (2014) Simultaneous fMRI-PET of the opioidergic pain system in human brain. Neuroimage 102(Pt 2):275–282

PET/CT and PET/MRI in Neurology: Infection/Inflammation

10

Martina Sollini, Roberto Boni, Elena Lazzeri, and Paola Anna Erba

10.1 Introduction

For more than a century, X-ray was the only available modality allowing observation of inner workings of the human body. Today, a new generation of imaging devices is probing even deeper and transforming medicine in the process. Indeed, recent advances in imaging technology such as CT scans, MRIs, SPECT, and PET scans and other techniques have had a major impact on the diagnosis and treatment of disease. Nuclear medicine techniques for imaging inflammation and infection have enormously expanded gaining importance in the diagnostic setting as well as for prognostic implication and management of treatment. This important clinical role relies on the ability of functional imaging to pinpoint different components and phases of inflammatory and infectious diseases beside the pure morphological anomaly generally depicted by the majority of radiological imaging procedures. Indeed, the use of nuclear medicine techniques allows in vivo histological characterization of inflamed and infected tissues and highlights cells and phenomena principally involved, thus allowing definition of tailored personalized treatment.

Radiopharmaceuticals used in the field of inflammation and infection imaging have been developed to target specific phase of the pathophysiology of each process. Therefore, knowledge of the specific pathophysiology pathways will facilitate the understanding of their application as well as on their advantages and limitations.

A basic knowledge important to understand the complexity of inflammation and infection imaging is that, despite specific hallmarks, inflammation and infection are two distinct processes that often coexist. Inflammation is defined as a merely nonspecific immune response to a variety of stimuli such as trauma, ischemia, neoplasm, autoimmune disorders, as well as the invasion by microorganisms [1, 2]. Inflammation is part of the body's immune response that involves immune cells, blood vessels, and molecular mediators. The purpose of inflammation is to eliminate the initial cause of cell injury, clear out necrotic cells and tissues damaged from the original insult and the inflammatory process, and to initiate tissue repair. However, sometimes, inflammation can cause further inflammation; it can become self-perpetuating.

Neuroinflammation plays a central role in a variety of neurological diseases (i.e., cerebrovas-

M. Sollini, MD
Nuclear Medicine Unit, IRCCS MultiMedica, Sesto San Giovanni (Milan), Milan, Italy

R. Boni, MD • E. Lazzeri, MD, PhD
P.A. Erba, MD, PhD (✉)
Regional Center of Nuclear Medicine, University of Pisa, Via Savi, 56126 Pisa, Italy
e-mail: paola.erba@unipi.it

A. Ciarmiello, L. Mansi (eds.), *PET-CT and PET-MRI in Neurology*,
DOI 10.1007/978-3-319-31614-7_10

cular and demyelinating diseases), and it is a highly relevant diagnostic and therapeutic target, but several characteristics of the brain make both goals more difficult than at other sites. First, the BBB prevents most molecules from entering the brain. Thus, imaging probe and drug design need to bypass this challenge. Second, cranial bones complicate direct access to the brain for diagnostic (e.g., biopsy) or therapeutic (e.g., surgery) interventions and even distorts signal of certain (e.g., optical) imaging techniques. Lastly, the brain has very limited regeneration capacity, which makes secondary and tertiary prevention more difficult, so early diagnosis is of utmost importance. Molecular imaging techniques that noninvasively visualize specific targets of the inflammation cascade using specific and sensitive probes could be powerful tools to evaluate neuroinflammation in the preclinical and clinical settings. This could allow for more sensitive and earlier detection as well as for monitoring disease progression and response of patients to therapeutic interventions. Over the past decade, a plethora of molecular imaging agents have been developed and tested in animal models of neuroinflammation, and a few have been translated from bench to bedside. The most promising imaging techniques to visualize neuroinflammation include MRI, positron emission tomography (PET), single-photon emission computed tomography (SPECT), and optical imaging methods [3]. Figure 10.1a presents a schematic representation of possible targets in neuroinflammation.

On the other hand, infection is the process of invasion of an organism's body tissues by disease-causing agents, their multiplication, and the reaction of host tissues to these organisms and the toxins they produce. Infections are caused by different infectious agents including viruses, viroids, prions, bacteria, nematodes, arthropods, fungi, and other parasites. The host response to a microorganism usually begins with an inflammatory reaction and is followed by a humoral or cell-mediated immune response. Usually, the innate immune response which consists of blood vessel dilatation in the infected tissue increased circulation of immune cells, and their congregation allowed to keep the inflammatory reaction localized. When the innate immune response is amplified and dysregulated, the imbalance between pro-inflammatory and anti-inflammatory responses might result in sepsis. During sepsis, neuroinflammation and concomitant decrease of cerebral metabolism inducing early impairment of neuronal metabolism and activity have been described [4].

Radiopharmaceuticals localize into sites of infections by following one or more than one of the specific pathophysiological pathways. Since the advent of ^{67}Ga citrate for routine infection imaging in 1970s, a variety of agents have been developed and evaluated to detect areas of infection within the body. Two main groups of radiopharmaceuticals could be identified: agents for targeting microorganism (antimicrobial agents) and agents for targeting components of the immune response toward the infective agents. The theoretical advantage of using an antimicrobial agent is the selective targeting of the compound for microbial rather than human targets [5]. Therefore, such agents should be able to distinguish between inflammation due to infection with microbial pathogens and inflammation due to immune activity in circumstances where microbes are not involved. The prototype of this class of compounds is ^{99m}Tc-ciprofloxacin (^{99m}Tc-Infecton), an agent introduced in 1993 that has been extensively evaluated by many groups around the world in a wide range of scenarios. This radiopharmaceutical has been developed starting from ciprofloxacin hydrochloride, a synthetic broad-spectrum quinolone antibiotic which is taken up by Gram-positive and Gram-negative bacteria and inhibits DNA synthesis by binding to bacterial DNA gyrase. However, ciprofloxacin also binds reversibly to mammalian topoisomerase II but with 1000-fold lesser affinity [6]. Therefore, although the drug penetrates into white cells, it is not retained in the absence of bacterial infection. Following injection, only 20–30% of ciprofloxacin is bound to plasma proteins and the agent becomes widely distributed throughout the body. It is metabolized in the liver then eliminated by renal excretion during the first 24 h and via the bile over the next 5 days. More recently, several other antimicrobial agents have been radiolabeled and

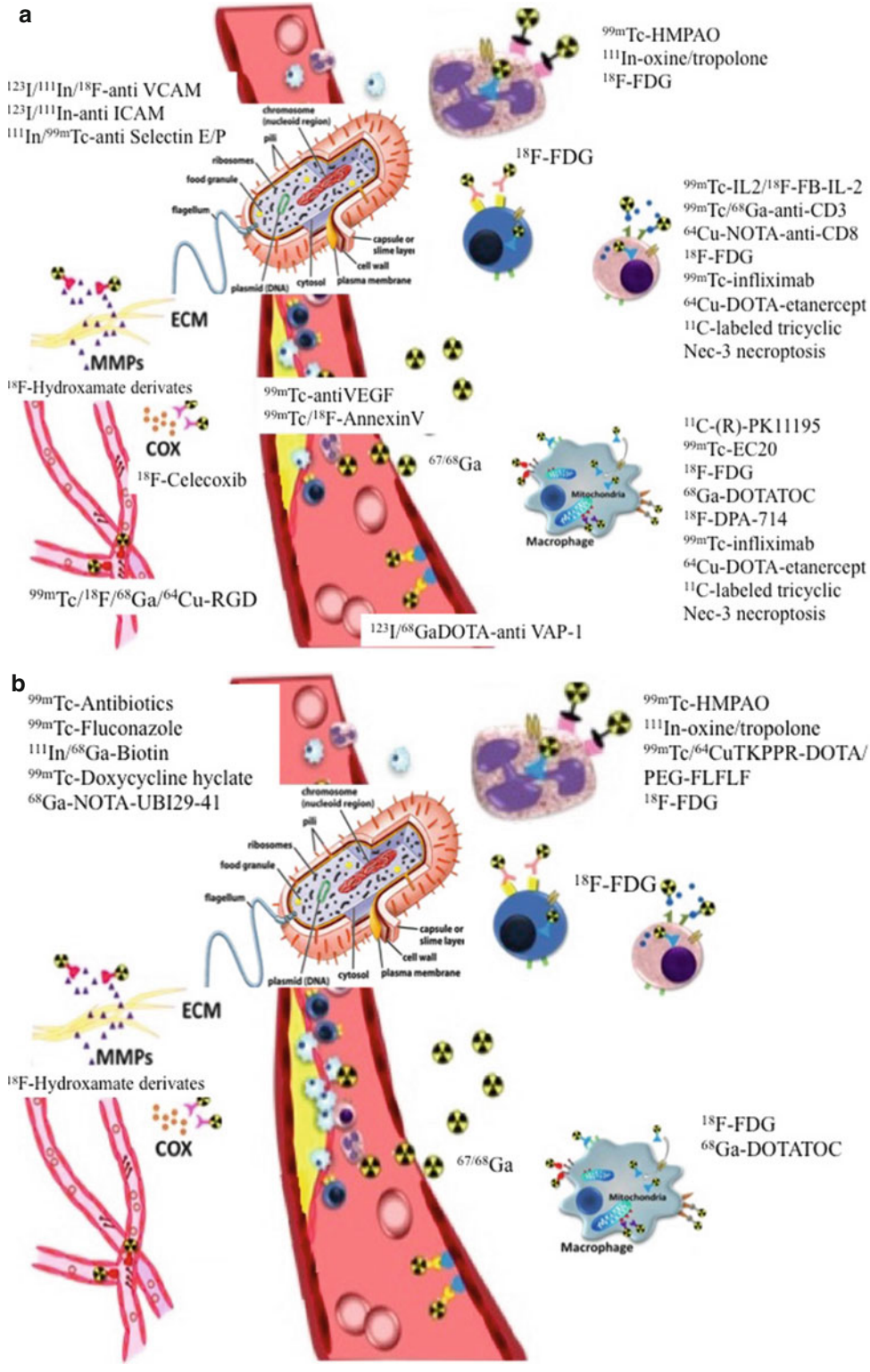

Fig. 10.1 (**a**) Schematic representation of possible target of inflammation. (**b**) Schematic representation of possible target of infection (Adapted from Wu et al. [286])

tested in animal models and patients with infections such as ^{99m}Tc-sparfloxacin and ^{99m}Tc-enrofloxacin, new-generation quinolones with enhanced activity against Gram-positive and mycobacteria; ^{99m}Tc-ceftizoxim, a third-generation cephalosporin antibiotic active against *S. aureus*, *Streptococci*, and Enterobacteriaceae; antituberculous agents (^{99m}Tc-isoniazid, ^{99m}Tc-ethambutol); or antifungal agents (^{99m}Tc-fluconazole, ^{99m}Tc-voriconazole, and ^{125}I-caspofungin) [5, 7, 8].

Another class of agents used to image infection after their radiolabeling are antimicrobial peptides. These molecules, produced by phagocytes, epithelial cells, endothelial cells, and many other cell types, are an important component of innate immunity against infection by a variety of pathogens [9]. These peptides show antibacterial, antiviral, and antifungal activities in vitro. Bacterial infections with *Staphylococcus aureus* and *Klebsiella pneumoniae* have been visualized in mice by ^{99m}Tc-labeled human neutrophil peptide-1 [10]. The basis of the antimicrobial activity of these peptides is the interaction of the cationic domains with the negatively charged surface of the microorganisms. The antimicrobial peptide ubiquicidin (TGRAKRRMQYNRR; 1693 Da) was originally isolated from mouse macrophage cells. This peptide is identical or highly homologous to S30, a protein that was purified from the small ribosomal subunit fraction of rat liver and shown to be present in various human and murine tissues [11]. Later, an identical UBI was isolated from human airway epithelial cells. This peptide was labeled with ^{99m}Tc, which targeted bacterial cells but not sterile inflammatory processes in experimental animals [12]. In later experiments, it also showed accumulation with high accuracy in fungal infections. More recently, UBI29-41 has been radiolabeled with ^{68}Ga-NOTA. In this study, ^{68}Ga-NOTA-UBI 29–41 exhibited significant uptake ratios between muscular infection and inflammation (Fig. 10.2), and further clinical evaluation of this novel metabolic tracer is proposed to investigate its potential use as a first-line PET/CT infection imaging agent [13].

A novel approach to bacterial-specific imaging targeting bacterial thymidine kinases is the use of a nucleoside analog 1-(2′-deoxy-2′-fluoro-b-D-arabinofuranosyl)-5-iodouracil (FIAU). FIAU was found to act as a substrate for *E. coli* thymidine kinase and after successful labeling with ^{125}I was able to image *E. coli* abscesses in mice and experimental infections with *E. faecalis*, *S. aureus*, *S. epidermidis*, and *S. pneumoniae* [14]. More recently, FIAU was radiolabeled with iodine-124 and used for PET/CT ([^{124}I]FIAU PET/CT) to test a small number of patients with suspected musculoskeletal infections (Fig. 10.3) [15].

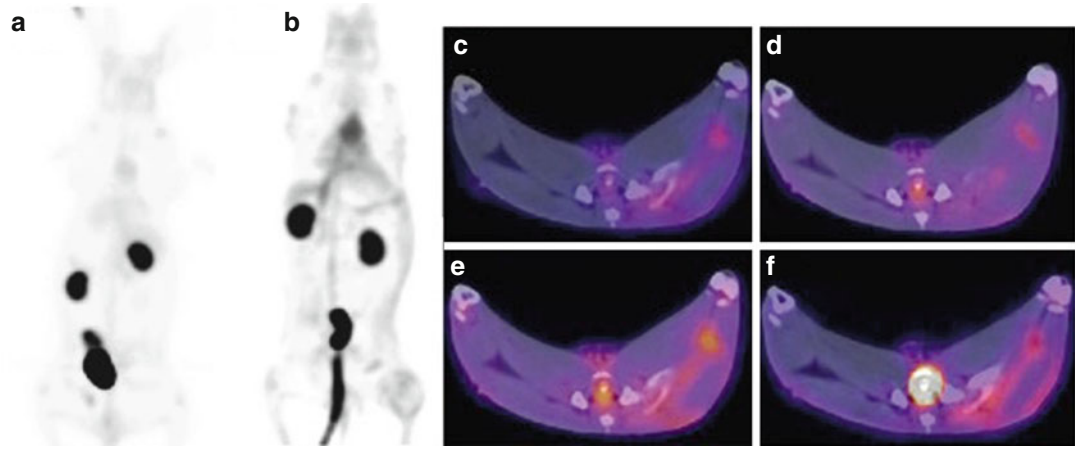

Fig. 10.2 Coronal PET images acquired at 60 min after intravenous injection of ^{68}Ga-NOTA-UBI29-41 into healthy rabbits (NZR-1) (**a**) and into rabbits with muscular infection (right thigh) and with sterile muscular inflammation muscle (left thigh) (NZR-2) (**b**). Axial PET/CT images displaying hind thighs 5 (**c**), 30 (**d**), 60 (**e**), and 90 (**f**) min after injection (Adapted from Ebenhan et al. [13])

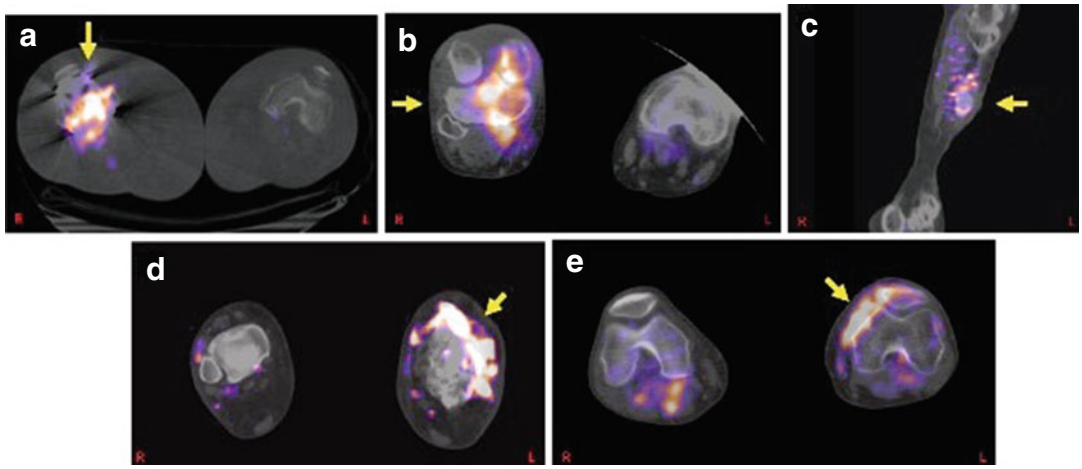

Fig. 10.3 [^{124}I]FIAU signal (*arrow*) in established infections as imaged by PET/CT obtained 2 h after radiotracer administration. In patients with (**a**) septic arthritis of the right knee, (**b**) septic arthritis of the right knee, (**c**) osteomyelitis of the left distal tibia, (**d**) cellulitis of the left lower extremity, (**e**) necrotizing septic arthritis of the left knee (Adapted from Diaz et al. [15])

Efforts to extend this technique to infections in other anatomical sites and other organisms that possess a suitable thymidine kinase are underway. Despite all the described, development of a true infection-specific imaging agent has yet to be identified and developed. Indeed, the majority of radiopharmaceuticals available for clinical use are targeting the immune response to the infective agents. Since granulocytes play an important role in the pathophysiology of infections, they represent one of the main targets for infection imaging. During infection, enhanced vascular permeability leads to the leakage of fluid and small molecules along with transudation or diapedesis of leukocytes. Therefore, such cells are the ones accumulating at the site of the infection [16]. The migration of granulocytes toward the sites of infection is a key process for infection imaging [17]. Such imaging agents localize both areas of inflammation as well as sites of infection, which makes the clinical interpretation somehow difficult [16]. Therefore, to achieve a differential diagnosis, accurate imaging acquisition protocols, sepcific interpretation and reading criteria are needed. For example, in the case of radiolabeled leukocyte imaging, time-dependent increase in radioactivity from early planar to delayed images is used for differentiation of physiologic accumulation of radiolabeled leukocytes in infectious sites as compared to the bone marrow and inflammatory sites which are characterized by a stable uptake of the radiolabeled cells over time. To this issue, acquisition of images in time mode, compensating for isotope decay at each time point and their analysis using the same scale frame to identify any focal area of activity that increases over time or shows a change in shape from early to late images, are recommended [18]. The advent of more sophisticate techniques such as PET/CT and PET/MRI scanners, presenting high spatial resolution and offering the potential advantage to combine functional data and morphological information, resulted crucial especially to image infection and inflammation of CNS. Nonetheless, literature on PET/CT and PET/MRI in CNS inflammation and infection is relatively scarce at this point in time, and it's essentially represented by case reports and small cohort of patients. Figure 10.4 represents an example of standard use of 99mTc-HMPAO-radiolabeled WBC with SPECT/CT acquisition in a patient with infection of the brain after surgery. Figure 10.1b presents a schematic representation of possible targets in neuroinfection.

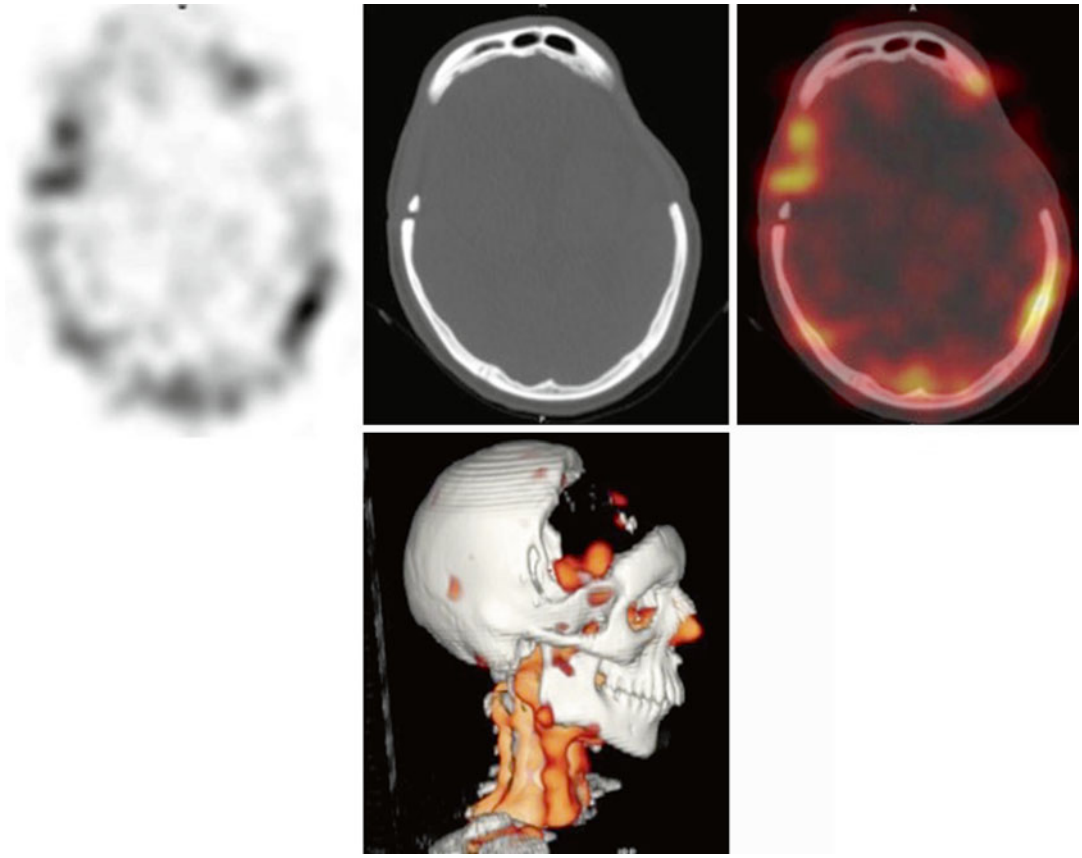

Fig. 10.4 ^{99m}Tc-HMPAO WBC SPECT/CT of a patient with brain infection after neurosurgery

The literature on CNS inflammation and infection imaging is relatively scarce at this point in time. There have been very few clinical studies performed, and most articles are case reports or involve only a small cohort of patients. The non-PET radiopharmaceuticals most used in CNS infection and inflammation are ^{99m}Tc-ethyl cysteinate dimer (^{99m}Tc-ECD) and radiolabeled leukocytes. The cerebral blood flow, assessed by ^{99m}Tc-ECD, is a surrogate marker of neuronal activity. ^{99m}Tc-ECD has shown useful results in CNS infection and inflammation (e.g., viral encephalitis) providing an accurate detection of subtle focal changes in uptake due to a superior contrast to background ratio of activity in white matter [16, 19]. Radiolabeled white blood cell (WBC) scan presents high specificity for infection [18, 20–23] and in CNS can be useful in solving diagnostic doubt between tumor and abscess [24–27]. An increasing amount of research has been performed on PET imaging in CNS infection and inflammation mainly using [^{18}F]FDG. Nonetheless, a major number of stand-alone PET papers have been published compared to hybrid PET/CT or PET/MRI in the evaluation of CNS.

10.2 Vasculitis

Cerebral vasculitis is inflammation of blood vessel walls that can occur with or without necrosis, leading to obstruction of the lumen, increased coagulation as consequence of the effects of proinflammatory cytokines, alteration of vascular tone, loss of neurologic function, and a wide variety of neurologic manifestations. CNS vasculitis occurs as part of a systemic vasculitis (inflammatory damage to the walls of large-,

medium-, small-, and variable-sized vessels). However, single-organ CNS vasculitis may also occur as an idiopathic disorder restricted to the CNS. In addition, vasculitis may be associated with systemic connective tissue disorders or may be secondary to infection, malignancy, drugs, or radiation therapy [28–30].

The pathophysiological hallmark of vasculitis is leukocyte infiltration of the vessel wall and reactive damage to mural structures and surrounding tissues, generally associated with ischemia. Arterial injuries at level of the smooth muscle cells located in the media with fragmentation of the internal elastic lamina, lymphocyte-macrophage transmural infiltration are the pathognomonic lesions [31].

Diagnosing vasculitis is challenging for physicians, especially in patients who present with nonspecific symptoms or signs of systemic inflammation. Symptoms of cerebral vasculitis may be neurologic, psychiatric, or both, and cognitive deterioration may be a leading feature. When the cerebral symptoms are part of a systemic disorder, the diagnosis may be easier, unless the cerebral symptoms are the first or only manifestation. Important clinical factors that merit consideration when suspected vasculitis as part of the differential diagnosis include patient age, gender, and ethnic origin. The presence of skin lesions, size of the involved vessel, involvement of other organs, use of medications, drug abuse, and the presence of neurologic signs (cognitive deterioration, focal deficits, transient ischemic attacks, stroke, and "thunderclap" headaches) should be also always considered. Imaging signs of cerebral vasculitis may be direct (e.g., vessel wall thickening and contrast material enhancement) or indirect (e.g., cerebral perfusion deficits, ischemic brain lesions, intracerebral or subarachnoid hemorrhage, and vascular stenosis) [32].

Doppler ultrasonography is highly sensitive in the detection of proximal arm and axillary vessels and carotid, finger, and temporal arteritis with sensitivity of about 85 % and specificity above 90 % when either edema, stenosis, or occlusion is present [33]. Whereas imaging methods restricted to luminal analysis like conventional angiography do not yield sufficient information about inflammatory vessel wall alterations [34], CT and MRI have been shown to detect vessel wall changes and luminal changes in LVV at the same time. CT is less sensitive than MRI in the assessment of cerebral vasculitis, with the exception of hemorrhage [35]. CT angiography can be used to evaluate both the vessel walls and the lumen and thus may show vessel wall alterations when the lumen is still unaffected at conventional catheter angiography. However, CT angiography cannot depict relatively small vessels. Arterial wall thickening and increased gadolinium contrast enhancement are the two typical MRI criteria for diagnosis of giant cell vasculitis (sensitivity and specificity of 81 % and 97 %). In case of cerebral vasculitis, MRI is the most commonly used imaging modality in the workup of patients. Standard MRI of the brain should include spin-echo T1- and T2-weighted imaging, fluid-attenuated inversion recovery (FLAIR) imaging, diffusion-weighted (DW) imaging, susceptibility-weighted (SW) imaging, routine time-of-flight MR angiography, and contrast-enhanced T1-weighted imaging. Contrast-enhanced high-resolution MR angiography and perfusion MR imaging may be applied in selected cases. T2-weighted images are used for the detection of ischemic or gliotic changes and frank infarction. FLAIR images improve the detection of lesions within the subarachnoid space and of ischemic white matter lesions, particularly lesions near the brain-CSF interface. Contrast-enhanced T1-weighted images may show leptomeningeal enhancement or associated intraparenchymal lesions. During the acute stage of infarction, DW MR imaging helps distinguish acute from chronic ischemic abnormalities. Within a few days, acute infarctions progress to a subacute stage with resultant angiogenesis and may enhance. In addition, wall thickening and intramural contrast material uptake are frequently seen in patients with active cerebral vasculitis affecting large brain arteries [35]. SW MR imaging aids in the detection of microhemorrhages associated with vasculitis [36].

[^{18}F]FDG-PET and PET/CT have emerged as a novel powerful imaging modality for the diagnosis and therapy monitoring of vasculitis [37]

with higher sensitivity in case of medium and large vessel vasculitis. Increased [^{18}F]FDG in the large cervical and thoracic vessels in giant cell arteritis (and Takayasu arteritis, TA) has been reported by many authors [38]. An overall sensitivity of 77–92 % and specificity of 89–100 % have been reported in several series of patients [39, 40]. [^{18}F]FDG uptake at the carotid artery has been reported in the presence of normal ^{67}Ga-citrate images [41] due to the better resolution of PET/CT systems. [^{18}F]FDG-PET and MRI perform similarly for the initial diagnosis, while for follow-up of immunosuppressive therapy, PET is preferable [42] demonstrating normalization of the site of [^{18}F]FDG uptake concordantly with the normalization of laboratory tests and symptoms [43, 44]. [^{18}F]FDG-PET/CT in TA is extremely useful for the definition of the extent of the disease (Fig. 10.5) since they may identify more vascular regions interested by active disease as compared to MRI, particularly in the early stage of the disease when the symptoms are nonspecific [45]. On the contrary, MR arteriography has the advantage of providing information about arterial stenosis and aneurysm formation. Subclinical involvement of large vessels in polymyalgia rheumatica has also been documented as increased uptake of [^{18}F]FDG in thoracic vessels and in the upper legs [46] and in the aorta and its major branches [47]. Different patterns of [^{18}F]FDG uptake may be evident: linear and continue in early disease, patchier in a linear fashion in later stage, typically in more sites as compared to clinical manifestation and also during immunosuppressive treatment and with negative CRP/ESR. Those patterns of uptake are associated with 92 % sensitivity, 100 % specificity, and 100 % positive predictive value, 85 % negative predictive value, and 94 % of accuracy for disease diagnosis [48]. Thus, [^{18}F]FDG-PET-CT could be invaluable to clinicians before treatment and in follow-up [49]. In conclusion, [^{18}F]FDG-PET is a sensitive and specific imaging modality for vasculitis diagnosis, particularly in early stages of the disease for the evaluation of disease extent and activity and for monitoring therapy efficacy. [^{18}F]FDG-PET performs excellently for large and medium vessel disease, while its performances may be decreased for small vessel disease where MR and MRI arteriography are preferred. The combination of [^{18}F]FDG-PET and MRI in terms of hybrid PET/MRI would offer not only sensitive evaluation of inflammatory processes in vessels as well as detailed morphological analysis in a single examination, but also reduce patient radiation dose in comparison to PET/CT, which might play an important role especially in young patients [50]. Up to now, few preliminary reports have dealt with the combined use of [^{18}F]FDG-PET and MRI in the evaluation of LVV as separate [42, 51] or "all-in-one" [50] procedures. Despite the very promising results reported in these publications, no many data are available about CNS vasculitis studied using

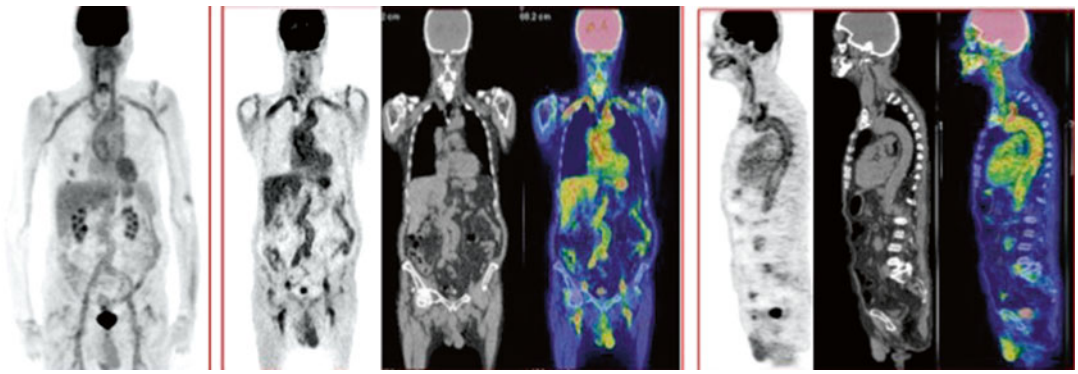

Fig. 10.5 Example of the pattern of [^{18}F]FDG uptake in a patient with large vessel vasculitis. Intense linear uptake along the wall of the aorta and epiaortic vessel is present and allowed to define the extent of the disease (Courtesy of Annibale Versari)

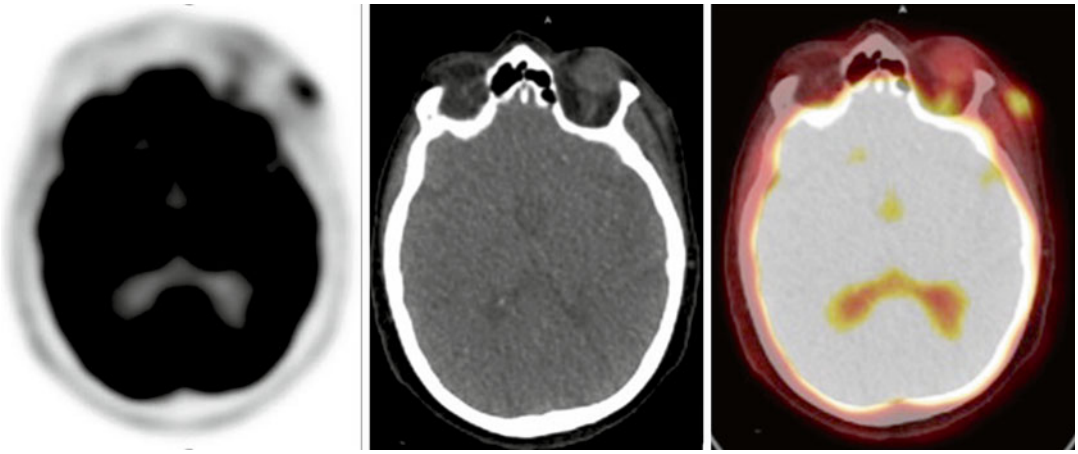

Fig. 10.6 Example of the pattern of [^{18}F]FDG uptake in a patient with vasculitis showing involvement of the left temporal artery

[^{18}F]FDG-PET/CT or PET/MRI. Rehak et al. [52] identified [^{18}F]FDG uptake directly in temporal and occipital arteries and even in smaller branches using a common hybrid PET/CT with a brain acquisition protocol. Figure 10.6 shows an example of [^{18}F]FDG-PET/CT in a patient with vasculitis with temporal artery involvement.

Activated macrophages and T lymphocytes are fundamental elements in the pathogenesis of GCA and TA [53]. Therefore, PK11195, a target agent that binds to the peripheral benzodiazepine receptor (PBR), a protein highly expressed in activated cells of the mononuclear phagocyte lineage, has been used for their clinical evaluation [54–59]. Indeed, since the early 1980s, [^{11}C]-PK11195 has been used for PET imaging of inflammatory diseases in the human brain on the basis of the low expression of PBRs in normal brain tissue and high expression in activated microglia, the resident phagocytes in brain tissue, during neuroinflammation [54, 57, 60–72].

10.3 Primary Angiitis of the CNS (PACNS)

PACNS is an idiopathic inflammatory disease of medium- to small-sized arteries affecting the CNS or peripheral nervous system, with no evidence of generalized inflammation [73]. It is most often observed in the fifth and sixth decades of life, and patients present with nonspecific symptoms such as acute or subacute confusion, headache, paresis, cranial neuropathy, hallucinations, or loss of consciousness [28, 74]. Imaging findings of PACNS are highly variable and nonspecific. CT may reveal areas of low attenuation suggestive of ischemic events. MRI is sensitive but not specific, showing discrete or diffuse supra- and infratentorial lesions involving the deep and superficial white matter. In addition, areas of infarct and hemorrhage may be seen. The lesions enhance in 90 % of cases [35, 73]. MR angiography is not informative, but occasionally may show vessel irregularities. DSA may show focal or multifocal segmental narrowing or occlusion or irregularities of both small- and medium-sized parenchymal and leptomeningeal blood vessels, collateral vessel formation, and prolonged circulation time. Case reports on the potential role of [^{18}F]MET PET coregistered with MRI have been reported (Fig. 10.7).

10.4 NeuroLES (NPSLE)

The most common neurological manifestation of lupus is headache, the cause of which can range from simple migraine to the so-called lupus-specific headache. Of much greater concern are grand mal seizures and psychosis however. Similarly, hemiplegia can be due to primary neu-

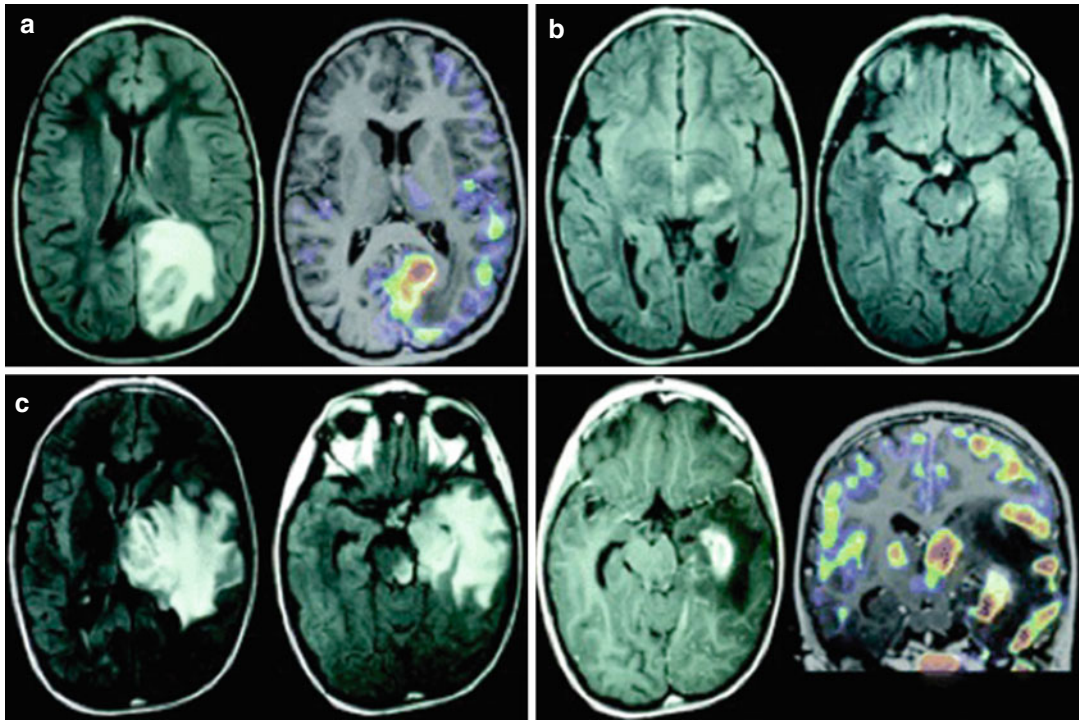

Fig. 10.7 Sequential brain [^{18}F]MET PET coregistered with MRI with fluid attenuation inversion recovery sequences and T1-weighted sequences coregistered. At presentation (**a**): increased uptake in left occipital pseudotumor that was reduced at 8 weeks (**b**) with the appearance of new left thalamic, mesiotemporal, and mesencephalic lesions. At 18 weeks, increase in size and MET uptake of the lesions (**c**). Stereotactic temporal brain biopsy under MRI and MET-PET guidance revealed SV granulomatous, nonnecrotic infiltration by T- and B-lymphocytes and multinucleated giant cells but no intranuclear viral inclusion or extravascular granulomas. Granulomatous SV PACNS was diagnosed (Adapted from Xavier De Tiège et al. [287])

rological involvement, secondary to hypertension or associated with the presence of antiphospholipid antibodies. Cerebellar disease and aseptic meningitis are much less common, but a variety of organic brain syndromes and impaired temporospatial orientation and pulmonary and intellectual deficit are well recognized and difficult to treat. The diagnosis of NPSLE is complex not only because of the variety of syndromes already mentioned but also because of the difficulty in differentiating active NPSLE from drug side effects and other unrelated pathology (e.g., cerebrovascular disease, depression, simple headache). Despite the countless attempts, no satisfactory diagnostic tool has yet been found. CT has largely been superseded by the more sensitive MRI, although CT is still in use for the emergency exclusion of cerebral hemorrhage. MRI is the current gold standard in the imaging assessment of NPSLE both for cerebrovascular and spinal pathologies [75]. T2-weighted images, in which edema is best visualized, show high-signal lesions that can be extensive or more focal, in keeping with the clinical pattern of disease. T1-weighted images are usually normal [75]. MRI is more likely to show abnormalities in focal neurological presentations than diffuse [75–78]. Periventricular lesions have been particularly associated with the antiphospholipid syndrome and can be impossible to differentiate on MRI from multiple sclerosis [79]. White matter hyperintensities increase with age in the general population and are also associated with hypertension; thus, it is not possible to differentiate NPSLE from other vasculopathies using conventional MRI [75]. The differentiation of acute active dis-

ease from old chronic lesions may be difficult [75]; however, the use of gadolinium may be helpful in delineating active inflammatory lesions [80]. Unfortunately, the finding of a normal MRI scan is common in NPSLE, and this has prompted the research of other MR-based techniques (e.g., spectroscopy) to increase sensitivity in the assessment of NPSLE; however, any of them are currently used in the clinical practice [75]. Positive results have been published about the metabolic characterization of NPSLE patients using PET/CT. The most prevalent and dramatic [^{18}F]FDG-PET/CT finding in NPSLE patients is parieto-occipital hypometabolism, probably due to the fact that this area represents a critical boundary among the three major intracerebral arteries [81]. Less frequently isolated parietal, cerebellar, or frontal hypometabolism could be visualized [81]. Other regions are rarely involved. In symptomatic patients, at least two brain regions show hypometabolism and cerebellar regions are usually affected [81]. Abnormalities in the parieto-occipital region are not pathognomonic for SLE with neuropsychiatric manifestation: they can also be found in the late whiplash syndrome or in dementia of the Alzheimer type [82]. The pathological mechanisms that underlie the findings in [^{18}F]FDG imaging may be heterogeneous. Depressed glucose use is currently thought to be the result of cerebral atrophy, infarctions, reduced density of cells, diaschisis (loss of function and electrical activity due to cerebral lesions in areas remote from the lesion but neuronally connected to it), or reduced [^{18}F]FDG uptake by cells. Metabolism and perfusion abnormalities uncovered by [^{18}F]FDG-PET and PET/CT imaging should therefore be interpreted with caution. Generalized neuronal loss, decreased neuronal density, and focal lesions due to chronic brain injury will result in hypometabolism and decreased perfusion [81]. Literature data suggested that the combination of PET and MRI can constitute a useful tool for assessing CNS involvement in SLE; in fact, while MRI scans are highly sensitive in detecting infarction (and especially white matter lesions), [^{18}F]FDG-PET is primarily indicated in patients with cerebral symptoms and insignificant MRI findings. Despite a lack of specificity, [^{18}F]FDG-PET proves to be even more sensitive than MRI in locating and diagnosing the extent of brain involvement in neuropsychiatric lupus, can identify fluctuations in regional cerebral metabolism even when no structural lesions are evident with MRI, and may also be helpful in the diagnosis of unclear cases (e.g., presence of only minor neuropsychiatric symptoms) [81]. Based on these premises, hybrid PET/MRI might offer a clear advantage to study NPSLE patients proving in a single examination all information necessary to assess CNS involvement.

10.5 Neurosarcoidosis

Sarcoidosis is a multisystem granulomatous disease of unknown etiology which may vary from acute forms to slow chronic and sometimes even asymptomatic illness. Clinical involvement of the CNS usually occurs early in the disease and is reported in approximately 5–15 % of cases [83]. As involvement of any part of the nervous system is possible, neurosarcoidosis may be difficult to diagnose due to its wide spectrum of clinical and radiological manifestations. Neurological features may be cranial neuropathy, papilledema, aseptic meningitis, hydrocephalus, seizures, psychiatric symptoms, cerebral and spinal sarcoid lesions, as well as peripheral neuropathy and skeletal muscle involvement [84]. MRI is sensitive for the detection of CNS lesions. Abnormalities usually found on MRI are multiple white matter lesions and meningeal enhancement [85]. Further proposed diagnostic criteria include laboratory support for CNS inflammation, ACE levels, and chest imaging, but definite diagnosis of sarcoidosis still has to be inferred from biopsy [86, 87]. Identifying a suitable site for biopsy can turn out to be difficult especially for patients with primary CNS involvement [88]. Therefore, diagnosis of neurosarcoidosis is often indirectly confirmed by other organ manifestations. Since systemic involvement is sometimes occult, [^{18}F]FDG-PET/CT may be useful to demonstrate systemic granuloma available for biopsy as well as to detect CNS involvement [88–90]. In fact, neurosarcoidosis modifies the stage of disease impacting in patient's

management, especially in cases of unknown and so far asymptomatic CNS manifestation, since a neurological involvement can result in a change of treatment. Additionally, [^{18}F]FDG-PET/CT can be used to monitor therapy responses since early metabolic changes in imaging uptake after initiation of corticosteroid therapy has been shown before than morphological changes on conventional imaging techniques [91].

10.6 Erdheim-Chester Disease

Erdheim-Chester disease (ECD) is a rare form of non-Langerhans' cell histiocytosis [92]. The clinical course of ECD is largely dependent on the extent and distribution of the disease. Some patients may be asymptomatic or have only mild and limited symptoms, while other patients may have a more aggressive form of the disease, with a poor prognosis, particularly when CNS and cardiovascular systems are involved [93, 94]. A reliable diagnosis of ECD can only be made if clinical, radiologic, and pathologic findings showing infiltration of involved tissues by CD68+ and CD1a− foamy histiocytes are considered together. None of the common investigations employed in ECD (e.g., CT, MRI, ^{99m}Tc bone scan) is able to provide a global assessment of the lesions during a single session. [^{18}F]FDG-PET/CT appears to be very advantageous in this regard [95].

[^{18}F]FDG-PET/CT scans presented good diagnostic performances both in the initial assessment of CNS ECD [95–97] and to evaluate treatment response (sensitivity = 66.7 % and 78.3 %; specificity = 92.3 % and 100 %) [95]. During the follow-up, [^{18}F]FDG-PET/CT can be used to monitor not only the number of lesions (Fig. 10.8) but also the SUV_{max} of the lesions, which reflects the underlying metabolic activity [95, 97]. Additionally, [^{18}F]FDG-PET/CT seems to be able to detect an early therapeutic response in CNS lesions compared to MRI [95].

10.7 Brain Abscess

Early diagnosis of brain abscess is important to choose the appropriate treatment approach. Differential diagnosis is complicated by both aspecific symptoms (intracranial pressure, focal neurological deficits, signs of infection) and CT/MRI lesion appearance of an intracerebral ring-enhancing lesion (common in infections and tumors). In particular, MRI has contributed greatly to the diagnosis of brain abscess. While brain

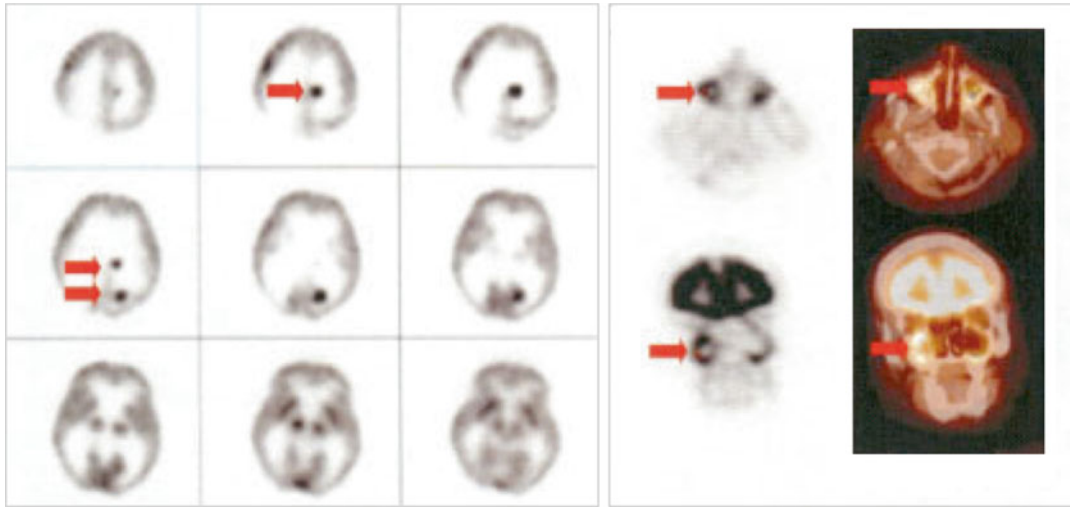

Fig. 10.8 Example of [^{18}F]FDG PET/CT images in a patient with Erdheim-Chester disease with neurologic involvement. Images show multiple cerebral uptake foci (*left panel*, *arrows*) as well as uptake in the right maxillary sinus (*right panel*, *arrows*) (Adapted from Arnaud et al. [95])

abscess displays a ring-enhancing lesion on contrast-enhanced T1-weighted images, it shows strong high signal on DWI. Treatment response in brain abscess has been monitored by showing the resolution of ring enhancement and the disappearance of the high signal on DWI. However, discordance between the signal intensity on the DWI and contrast enhancement is often found despite appropriate long-term intravenous antibiotics treatment. It has been reported that contrast enhancement did not disappear completely, although DWI demonstrated low signal on the follow-up examination [98]. A method that is capable of reliably evaluating treatment response would be of great benefit both for assessing the therapeutic outcome and for minimizing high-cost, long-term antibiotics with all of its known side effects. Technetium-99m HMPAO WBC has been demonstrated to be very useful for differentiating brain abscess from other types of intracerebral lesions, especially tumors, with high sensitivity, specificity, and accuracy for both ^{111}In-WBCs and ^{99m}Tc-HMPAO WBCs [24, 25, 27, 99]. Nevertheless, false-negative results have been reported in patients on high-dose steroid therapy [100] as well as weak or moderate activity in tumors (mostly at early images time) [100–102]. Literature data have demonstrated that PET/CT using different tracers, such as [^{18}F]FDG, ^{11}C-methionine or [^{18}F]fluoroethyl-L-tyrosine, [^{18}F]FET, and radiolabeled choline, can be used to image brain abscesses as well as device infections since they generally present high uptake [103–113] and suggested the use of [^{18}F]FDG to monitor treatment since it seems to directly reflect the degree of the inflammatory response [109, 114]. However, on record are individual patients showing [^{18}F]FDG and [^{18}F]FET uptake within a brain abscess and not in the contrast-enhancing walls [105] or around a brain abscess [106]. Nonetheless, high [^{18}F]FDG uptake may occur in cases of brain abscess, acute inflammatory demyelination, and neoplasm (Fig. 10.9) [115–117]. Nonetheless, since gray matter presents high [^{18}F]FDG uptake which increases over a 90-min time point after administration decreasing at later times [118], dual point images might be useful to evaluate the metabolic status and the extent of infectious disease [119].

10.8 Tuberculosis

Tuberculosis (TB) of the CNS is a highly devastating form of the disease which may involve parenchyma, meninges, skull, spinal, or any combination thereof [120]. MRI is generally considered superior to CT in detecting and assessing CNS TB [121]. Parenchymal involvement is most frequently seen in the form of a tuberculoma, which may be single or multiple. In the pediatric age group, it is seen more frequently in the cerebellum, whereas in adults, it has a predilection for the cerebral hemispheres and basal ganglion. The appearance of a tuberculoma varies on MRI depending on its stage of maturation [121]. A non-caseating granuloma is hyperintense on T2 and hypointense on T1 and shows solid enhancement, while a solid-caseating granuloma is usually hypointense on both T1 and T2 images. On CT, tuberculomas appear as round or lobulated soft tissue masses with varying attenuation and homogeneous or ring enhancement [122]. Miliary TB is often associated with TB meningitis and presents as small (<2 mm) foci of hyperintensity on T2 acquisitions, while after gadolinium administration, T1 images show numerous, round, small, homogeneous, enhancing lesions [121]. Contrast-enhanced MRI is also superior to CT for the evaluation of meningitis and its complications, including hydrocephalus [122]. Due to its high sensitivity to detect active lesions, [^{18}F]FDG-PET/CT plays an increasing role in TB populations. In fact, although in pulmonary TB differentiation between [^{18}F]FDG-avid malignancies and active TB lesions based on SUV_{max} is not possible (both demonstrate intense hypermetabolism with an overlap in SUV values when quantified) [123] not even dual-time-point imaging have been used [124], it may correct and evaluate extrapulmonary disease extent, impacting on the treatment plan, and it may be used to monitor treatment response [109, 125–128]. In CNS TB, dual point images might be useful to evaluate the extent of benign infectious disease [119]. [^{18}F]FDG-PET/CT has also been compared to ^{11}C-methionine PET/CT in the assessment of intracranial tuberculomas. Unexpectedly, despite the very different mechanism of uptake/action,

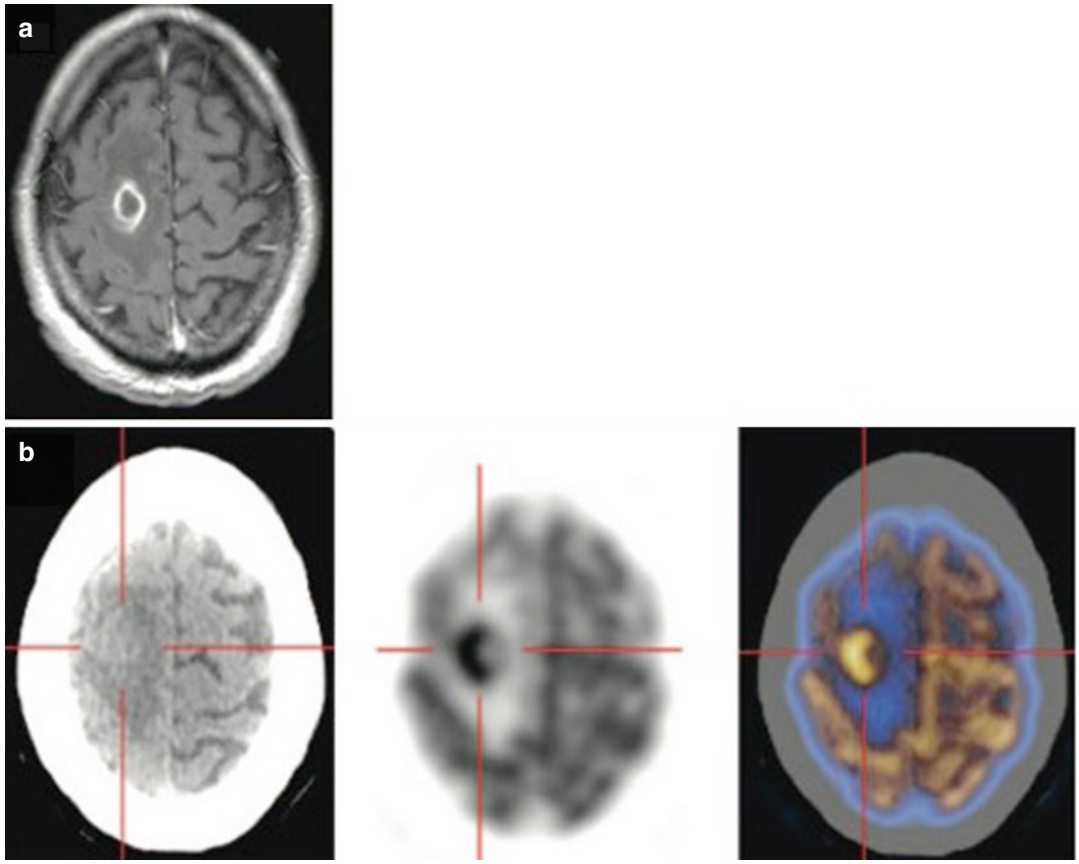

Fig. 10.9 Example of [^{18}F]FDG-PET CT scan in a patient with brain infection from *Nocardia*. [^{18}F]FDG-PET CT scan (**b**) of the brain shows increased uptake with a maximum SUV of the lesion of 11.0 (for comparison, maximum SUV of the contralateral normal gray matter was 9.5). Axial MRI, T1, postgadolinium (**a**) demonstrates a 2-cm ring-enhancing lesion in the right superior frontal lobe. CT (**b**, *left*) shows the frontal lobe lesion. The fused PET-CT image is shown at the *right* (Adapted from Mascarenhas et al. [112])

[^{18}F]FDG and ^{11}C-methionine PET/CT performed similar, although ^{11}C-methionine picked up much more lesions than [^{18}F]FDG. Moreover, as for malignant lesions, lesion delineation was superior on ^{11}C-methionine scans compared to [^{18}F]FDG ones [126]. Hence, in newly diagnosed, untreated patients, PET/CT specificity in distinguishing intracranial tuberculomas from neoplastic lesion seems to be limited using either ^{11}C-methionine or [^{18}F]FDG, but both these radiotracers can be used to assess the response to antitubercular treatment [126]. Despite those limitations, there are clinical situation where [^{18}F]FDG-PET may be very important for patient management. In cerebral disease resulting from *Mycobacterium tuberculosis* and appearing as a tuberculoma or tuberculous brain abscess (Fig. 10.10, the PET appearance is similar to bacterial brain abscess with hypometabolism or significant [^{18}F]FDG accumulation corresponding to the areas of enhanced at CT/MRI) [106, 109, 115, 129], whole-body images obtain at PET or PET/CT may be allowed to detect other tuberculous lesions and guided diagnosis.

10.9 HIV-Related Central Nervous System Disease

Despite the use of highly active antiretroviral therapy (HAART) that has led to reductions in the incidence of AIDS-related primary central

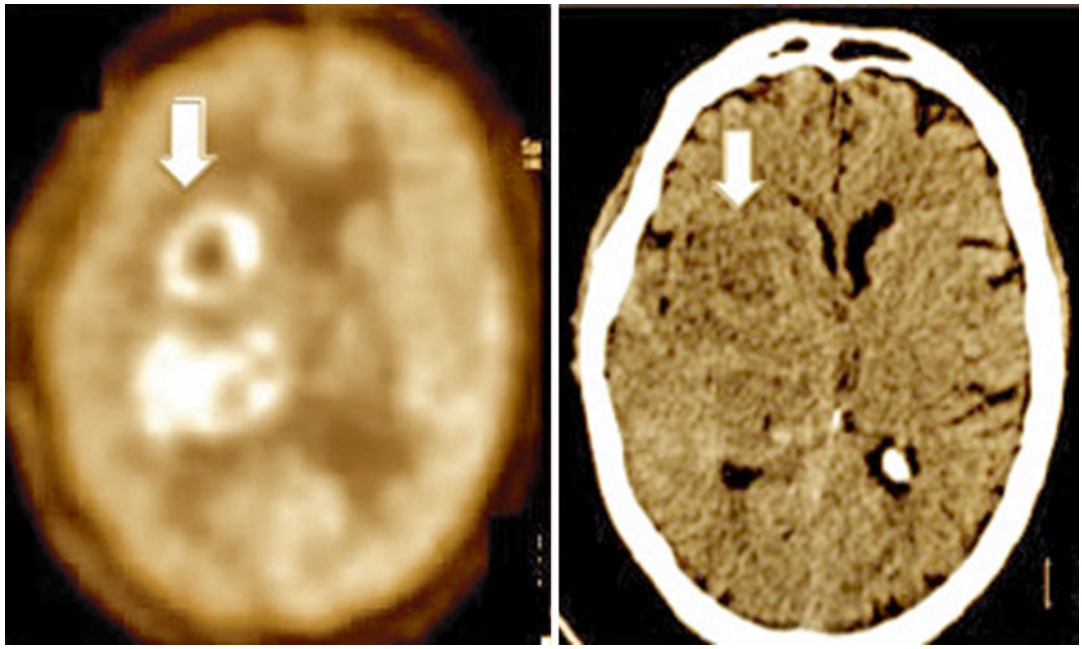

Fig. 10.10 [^{18}F]FDG PET/CT images of a patient with TBC presenting with right hemiparesis. PET images (*left panel*) show increased uptake within multiple doughnut lesions in the right basal ganglia and thalamus. CT images (*right panel*) show mass effect (Adapted from Harkirat et al. [288])

nervous system pathologies, the presence of neurological symptoms or signs in HIV-infected individual remains a diagnostic challenge if they do not have typical features on anatomical imaging or do not respond to subsequent empirical treatment. In this setting, a diagnostic test is needed, not only to establish the underlying diagnosis, but also to guide biopsy identifying the "optimal" site (i.e., the most easily accessible brain lesion) in order to increase accuracy and reduce the risk of complications [130]. Due to their immunosuppressed state, HIV-infected individual is prone to atypical infections and malignancies. The most common infections are toxoplasmosis [131], JC virus which can cause progressive multifocal leukoencephalopathy in the immunosuppressed, and mycobacterial infections [130]. HIV is also associated with a wide spectrum of vasculitides with various clinical presentations, including granulomatous angiitis, eosinophilic vasculitis, and nonspecific small-vessel vasculitis [132, 133]. Nonetheless, memory, behavioral problems, and all forms of dementia are a diagnostic challenge in this population since it is important to differentiate underlying dementia from potentially treatable causes such as infection, HIV encephalitis, and vasculitis [130].

Determining the nature of cerebral lesions is crucial for successful planning of further management and therapy. In evaluating the possible etiology of central neurological pathology, an important determining factor is the degree of immunosuppression [134]. First-line imaging includes CT and MRI with intravenous contrast agent. However, lesions are often indeterminate with regard to infection or malignancy, with no definite differentiating features [135, 136]. Advanced MRI techniques, including perfusion imaging, diffusion-weighted imaging, and MR spectroscopy, may be helpful in further differentiating the etiology of cerebral lesions, although toxoplasmosis demonstrates significant overlap with lymphoma such that apparent diffusion coefficient ratios cannot distinguish the two [137]. In addition, it is not uncommon for multiple pathologies to coexist [138, 139].

In patients with AIDS-related CNS complications (i.e., encephalopathy, encephalitis, PML, opportunistic infection, CNS lymphoma), sensitivity of leukocyte scintigraphy is reduced since opportunistic infections are characterized by low neutrophils recruitment. Thus, gallium-67 citrate and [^{18}F]FDG represent the most commonly used radiopharmaceuticals for HIV/AIDS population [140]. Also tallim-201 at brain SPECT has been initially used in case of brain abscess [141], but it has been demonstrated unreliable for the differential diagnosis of primary lymphoma from nonmalignant brain lesions in patients with AIDS [142]. Several studies indicated that [^{18}F]FDG can reliably distinguish CNS infections, such as toxoplasmosis, from lymphoma. In fact, both qualitative visual inspection and semiquantitative analysis (SUV within the lesion compared with SUV in a contralateral brain area) have demonstrated significant lower [^{18}F]FDG uptake in toxoplasmosis (Fig. 10.11) compared to lymphoma (no overlap of the uptake values) with value of sensitive and specific near 100 % when antitoxoplasmosis treatment is used [143–146]. The main clinical indication for nuclear medicine study in the presence of solitary brain mass is the differential diagnosis of the intracerebral cystic lesions appearing as hypodense ring enhancing at CT and MRI. High specific radiopharmaceutical as radiolabeled leukocyte is generally preferred for this purpose as well as for the evaluation of postoperative course of patients treated for brain abscesses. [^{18}F]FDG is the preferred radiopharmaceutical in case of HIV/AIDS patients with high risk of opportunistic infections. [^{18}F]FDG-PET/CT could be a helpful tool to differentiate between malignancy and infection as the metabolic activities of the pathologies can be different, potentially guiding patients' management [130, 143, 144, 146–148]. In vasculitis, the pattern of abnormal [^{18}F]FDG uptake has been considered more critical in differentiation than its level within lesions. Additionally, a whole-body scan may help in the interpretation of cerebral findings and may also demonstrate area(s) of increased glucose metabolism elsewhere in the body that are amenable to biopsy. This is particularly helpful in disseminated infection as demonstrated in patients with cavitating lung lesions and cerebral pathology, supporting the diagnosis of TB as an infectious cause for the brain lesions [130].

Lewitschnig et al. [130] evaluated 29 HIV-infected patients with brain [^{18}F]FDG-PET/CT. In the majority of cases (86 %), [^{18}F]FDG-PET/CT was required to differentiate infection from malignant causes of cerebral pathology. Cerebral toxoplasmosis was finally diagnosed in 11 patients. Ten of them presented focal or multifocal low-grade [^{18}F]FDG uptake (mean $SUV_{max} = 3.5$, range 1.9–5.8). Five patients with a final diagnosis of primary CNS lymphoma confirmed by biopsy showed focal lesions with high [^{18}F]FDG uptake (mean $SUV_{max} = 18.8$, range 12.4–29.9). There was no overlap in SUV_{max} measurements between patients with lymphoma and those with infective lesions. In five patients, [^{18}F]FDG-PET/CT findings were consistent with vasculitis which was confirmed in four cases (in the remaining case, final diagnosis concluded for degenerative corticobasal dementia), while in two cases, brain [^{18}F]FDG uptake was related to metastases from NSCLC and TB involvement. In 4/29 cases (toxoplasmosis, cerebrovascular accident, cerebral neuritis secondary to treponemal infection, and HIV encephalitis), PET/CT resulted false negative. Authors concluded remarking the usefulness of [^{18}F]FDG-PET/CT for differentiating between infection and primary CNS lymphoma and as helpful tool in the diagnostic work-up of patients with other HIV-related cerebral pathology. Additionally, PET/CT showing area(s) of increased glucose metabolism offered the advantage of identifying potential sites for biopsy.

Positive results using PET images to diagnose progressive multifocal leukoencephalopathy (PML) caused by JC virus have been reported by Shirai et al. [149] who suggested that the mismatch between [^{18}F]FDG and ^{11}C-methionine results may be useful for the early diagnosis and treatment of PML (Fig. 10.12). However, no data have been reported about the additional role of hybrid PET/CT or PET/MRI yet.

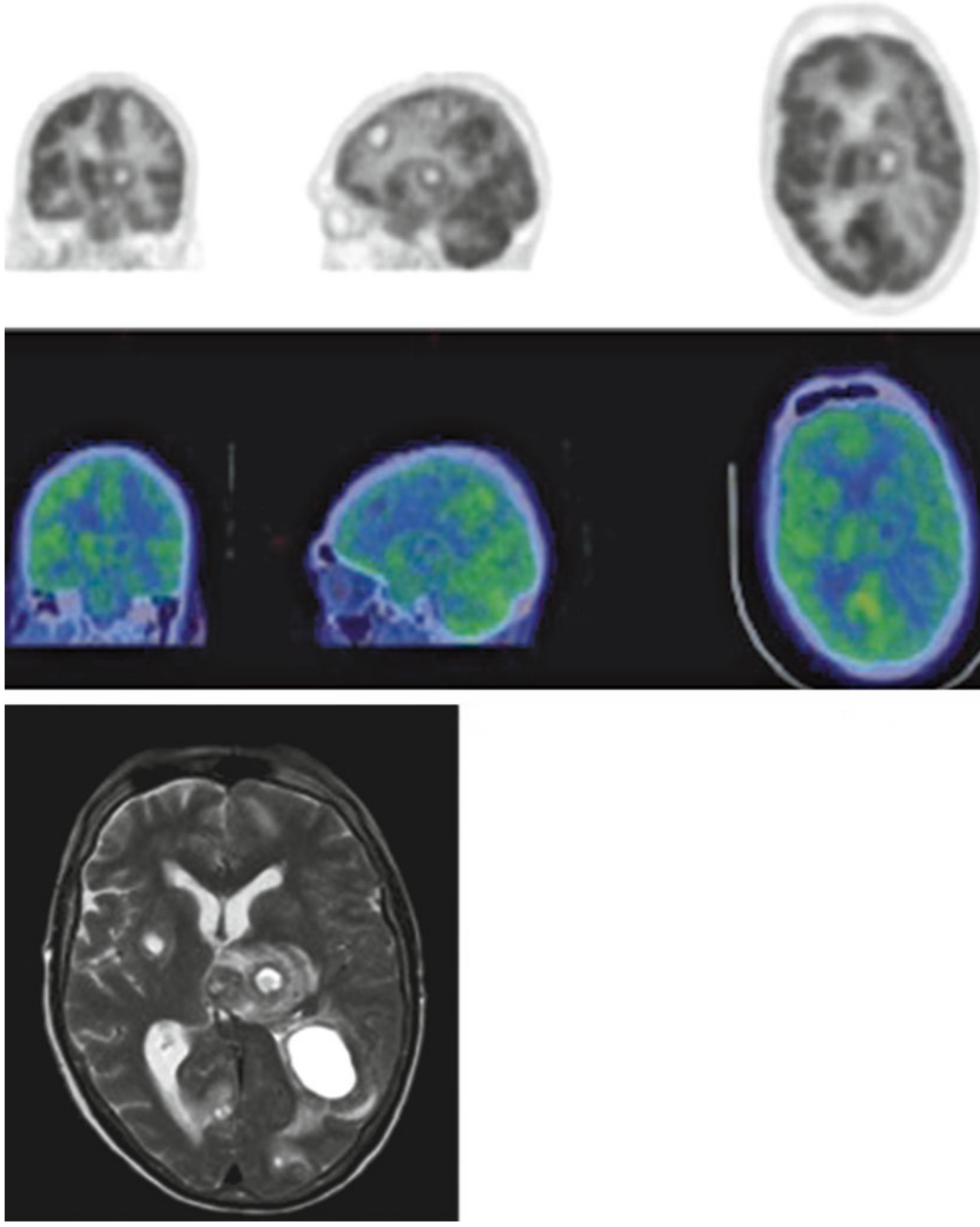

Fig. 10.11 A typical example of [^{18}F]FDG-PET/CT scan in a patient with toxoplasmosis. Multiple central photopenic lesions are shown at the emission images (*upper panel*). The corresponding T2-weighted MRI scan at the same level shows multifocal mass lesions (*lower panel*). *Middle panel* superimposed PET/CT images (Adapted from Lewitschnig et al. [130])

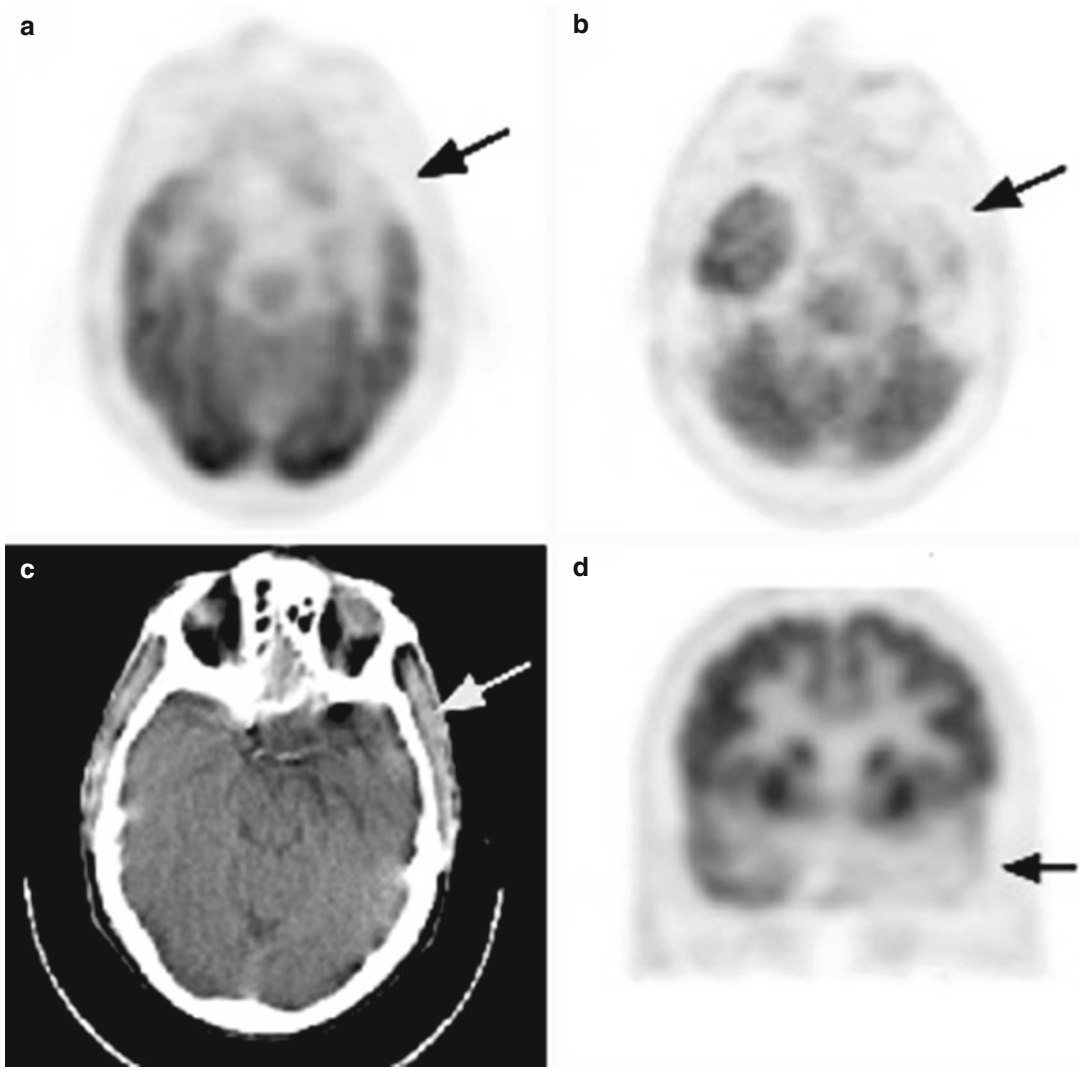

Fig. 10.12 Example of interictal cerebral [^{18}F]FDG PET/CT study in a patient with herpes simplex encephalitis causing acute viral leptomeningeal inflammation with a predilection for the temporal lobe. PET coronal slice at the level of the temporal lobes demonstrate extensive reduction in cerebral glucose metabolism (**a**, **b**, **d**), including the anterior hippocampus and amygdala. Associated hippocampal volume loss is present on the low-dose CT (**c**). As the metabolic sequelae of prior herpes simplex infection may become persistent despite antiviral therapy, with chronic cognitive, neuropsychiatric, and neurologic symptomatology, this diagnosis should be considered in cases with severe unilateral temporal lobe hypometabolism on FDG-PET imaging (Adapted from Wong et al. [235])

10.10 CNS Device Infection

Among the neurosurgical devices, the most used are ventricular shunts, Ommaya reservoirs, intracranial pressure devices, and implantable neurological stimulators. Ventriculostomy catheters or external ventricular drains (EVDs) are temporary devices, which permit therapeutic CSF drainage monitoring intracranial pressure, broadly used after closed head injuries, intracranial hemorrhage, or for hydrocephalus [150]. As for any other device, EVDs carry a risk of infection (0–27 %, dropped to 12 % adopting adequate protocol of EVD insertion/manipulation) [151–153]

represented in this case by ventriculomeningitis resulting from contamination of the drain during insertion, contamination of the drain system during routine care and manipulation, colonization of the drain at the insertion site by skin flora, or infection of the drain and CSF as a result of a surgical-site infection [150]. In the majority of cases, the diagnosis of ventriculomeningitis effectively is based on microbiologic results and be supported by CSF parameters, basic laboratory parameters, and clinical evaluation [150]. Radiological examinations, both CT and MRI, may have a role in EVD infection diagnosis only in selected cases [154]. In literature, there are not available data on the role of nuclear medicine techniques in this clinical setting.

Primary CSF shunts (shunt placement with no prior history of neurosurgical procedures) are most commonly placed in adults to treat idiopathic normal-pressure hydrocephalus; tumors, subarachnoid hemorrhage, head injury, and intraventricular hemorrhage are the most common causes requiring secondary shunt surgery. CSF shunt infection rate is similar to those of EVDs. The diagnostic principles of shunt infections are similar to those of ventriculomeningitis (CSF culture, Gram stain, chemistries, and cell count); blood cultures should always be performed [150]. Cerebral abscess and granuloma formation are very rare [155]. In case of distal catheter infection, CSF findings may be bland and abdominal echography or CT scan can be used to identify CSF-containing cysts suggestive for infection [150, 156, 157]. In case of shunt-related infection localized at CNS (i.e., abscess), CT scan and MRI may be helpful to identify abnormal findings suggestive for infection [158, 159]. The role of indium-111 leukocyte scan in primary, posttraumatic, and postsurgical infections (including patients with suspected ventriculoperitoneal shunt infections) has been evaluated resulting in high diagnostic accuracy [160]. Similar results have been published about the contribution of ^{99m}Tc-HMPAO leukocytes scintigraphy in the infections in skull neurosurgery including patients with intracerebral lesions, with suspected postsurgical infections, with suspected deep infection of the surgical wound, and with suspected ventriculoperitoneal shunt infections [22]. Particularly, in patients with suspected ventriculoperitoneal shunt infection, ^{99m}Tc-HMPAO leukocyte imaging correctly diagnosed infections without any false-positive findings [22]. In literature, only case reports reported the use of [^{18}F] FDG-PET/CT [161, 162] to detect ventriculoperitoneal shunt infection demonstrating valuable tool in case of high clinical suspicion when standard diagnostic modalities fail hardware infection diagnosis (Fig. 10.13).

Deep brain stimulators (DBS) are an effective option in the management of movement disorders and chronic pain. Incidence rate of DBS infection reported in literature ranges from 0.62 to 15 % reflecting the diversity of patient populations, the variety of surgical techniques adopted to implant DBS, varying use of antimicrobial prophylaxis treatment as well as the definition of infection used (involvement of the hardware and/or superficial skin infections at the incision sites) [150, 163]. Potential risk factors for developing DBS infection include age, scalp thickness, comorbidity, and surgical techniques. Battery exchanges can also lead to DBS infections. Infection can be localized at different part(s) of the DBS which are the internal pulse generator, the connector site, or the scalp where the lead exits the brain. Diagnosis of DBS infection is essentially based on clinical manifestations, but the identification of the microorganism responsible of infection is crucial to tailor treatments [150]. Favorable results were obtained by immunoscintigraphy using SPECT/CT acquisition (^{99m}Tc-sulesomab) [164], while no data on PET/CT or PET/MRI are available.

Ommaya reservoir is a closed system for continued access to the ventricular spaces indicated in case of tumor cysts or syrinx drainage, monitoring of CNS pressures and drug levels in CSF, direct instillation of agents into the CNS tumor bed, and treatment of leptomeningeal malignancies, cancer pain, and chronic/recurrent CNS infections [165]. The most common complication (2–23 %) of Ommaya reservoir is infection; nevertheless, late onset device infection has never been documented [166–168]. An Ommaya reservoir colonization can occur with any clinical signs of infection but a positive

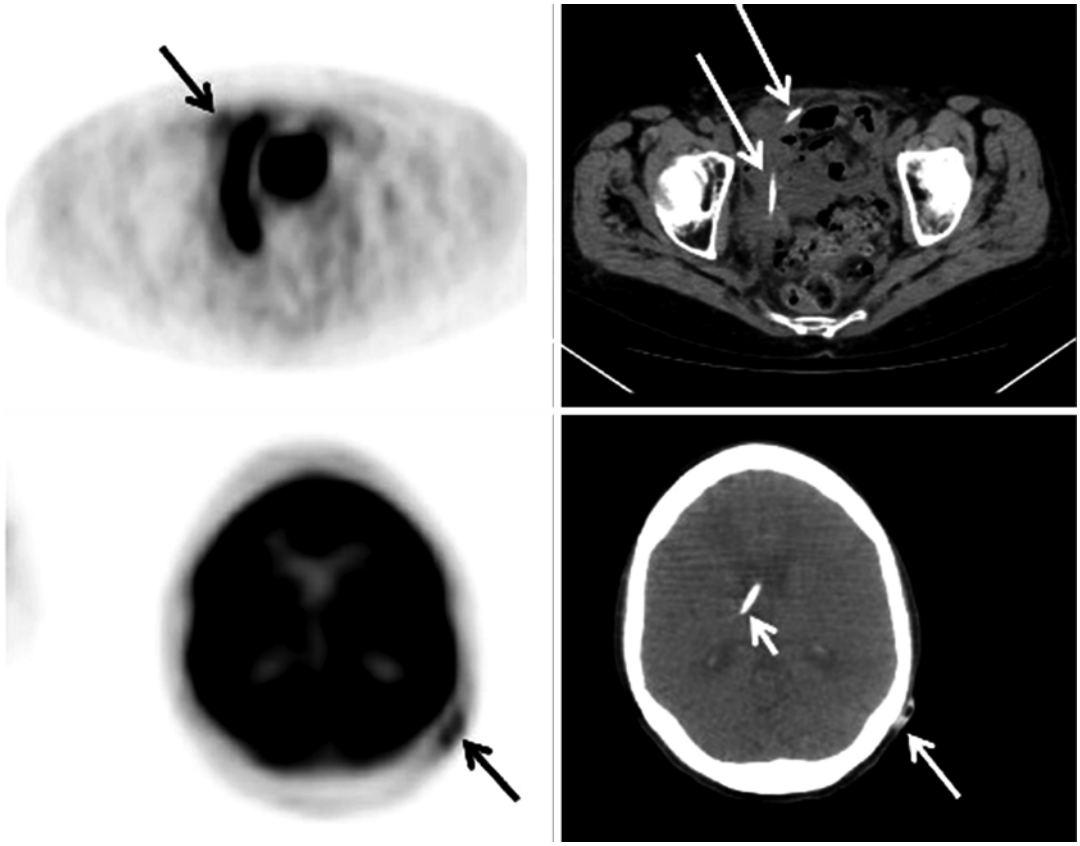

Fig. 10.13 Axial [^{18}F]FDG PET/CT images of the pelvis and head of a 75-year-old woman with lung cancer showing linear [^{18}F]FDG uptake along the pelvic end of the ventriculoperitoneal (VP)-shunt catheter and focal uptake in the VP-shunt reservoir in the scalp. The ventricular end of the VP-shunt catheter was seen in the right ventricle (*short white arrow*). No abnormal [18F]FDG uptake could be identified in the ventricular CSF, due to interruption from intense physiologic cerebral cortical [18F]FDG activity. Culture of the removed VP-shunt catheter demonstrated Gram-positive *Staphylococcus* (Adapted from Wan et al. [161])

ventricular culture. Blood cultures are generally negative in Ommaya reservoir infections [169]. In literature, there are not available data on the role of nuclear medicine techniques in this clinical setting.

10.11 Cochlear Implant Infections

Cochlear implantation (CI), nowadays, represents a treatment option in several condition including not only deafness but also patients with hearing still functioning in the low frequencies [170]. Due to the benefits of binaural hearing, bilateral CI has become the standard treatment over the last decade, and recently, it also demonstrated benefits in cases of unilateral deafness and severe tinnitus [170]. The most frequent CI complications are infections (1.7–16.6%) [171–173] related to the biofilm covering of the devices [174] (even though they are made from well-tolerated materials [175]), to the spread of microorganism into the inner ear during surgery, or to bacteremia [176]. CI infections include cutaneous necrosis and surgical wound dehiscence (immediately after or later surgery), otitis, cerebritis, and meningitis [172, 173]. Even it has been demonstrated that abnormal cochlear or auditory canal anatomy is a risk factor for meningitis in CI, the increased incidence of CI-related meningitis entails the drafting of some recommendations where the prophylactic vaccination against

Streptococcus pneumoniae has been scheduled before the implant [173, 177]. CI-related infection diagnosis is essentially clinical [176]. When an acute otitis media is suspected, the middle-ear fluid should be obtained for culture, and in case of clinical suspicion of meningitis, both middle-ear fluid and CFS cultures should be obtained [178]. Middle-ear mucosa biopsy specimens may also be obtained to diagnose biofilm-related otitis media [179]. Temporal bone radiographs are unsatisfactory in the detection of CI-related infection. In fact, although separation of the receiver/stimulator from the calvarium, a sign of the presence of underlying fluid, may be demonstrated on plain radiographs, this requires a tangential view necessitating careful patient positioning. In patients with suspected CI postoperative infection, CT is the technique of choice for detecting collections beneath the receiver/stimulator even though the images are masked by metallic artifacts [180]. Nuclear medicine imaging techniques have a limited role in CI infection diagnosis, especially in the acute forms. However, ^{99m}Tc-diphosphonate scintigraphy and [^{18}F]FDG-PET can be valuable tools in case of a late low-grade CI-related infection. In fact, in case of chronic osteomyelitis of the petrosal bone since the presence of minimal signs of infection is undetectable by radiology, nuclear medicine techniques may reveal the presence of radiopharmaceutical uptake [181].

10.12 Rhino-Orbital-Cerebral Mucormycosis

Mucormycosis is a life-threatening infection associated with severe morbidity and high mortality which may present clinically as rhino-orbital-cerebral mucormycosis (RCM), in a pulmonary, disseminated, gastrointestinal, and/or cutaneous form, with different patterns in pediatric and adults [182, 183]. The intracranial and orbital involvement could be associated with the onset of ophthalmoplegia, proptosis, orbital cellulitis, vision failures, and changes in mental behavior [184]. The initial radiologic diagnostic procedure in RCM should be MRI because of the low specificity and underestimation of the disease on the CT scan [185]. Early MRI findings of RCM included unilateral mucosal thickening and inflammatory soft tissue lesions in the sinonasal tract, while after disease progression, bone destruction and extra sinonasal extension can be seen in less than half cases. Absence of these findings may lead to a delay in diagnosis [186]. The helpful contribution of [^{18}F]FDG-PET/CT has been reported in the diagnostic workout of RCM [183, 187]. Particularly, the potential advantage of the use of [^{18}F]FDG-PET/CT seems to be its ability to detect active functional/metabolic changes reflecting inflammatory cell activity, before the onset of anatomical abnormalities assessed with the conventional radiological modalities, leading to an early diagnosis in the clinical suspicion of RCM [183]. However, the definite role of [^{18}F]FDG-PET/CT in this clinical setting remains to be determined, especially for discriminating inflammatory granulomatous disease from malignancy.

10.13 Malignant Otitis

Necrotizing external otitis (NEO) is a serious infection commonly found in diabetic and immunocompromised patients. It is not a neoplastic process and the term "malignant" is used in reference to the associated high mortality. Originating from the external auditory meatus (EAM), the infection may spread along the petrous bone and the skull base and become a skull base osteomyelitis (SBO) [176, 188, 189]. For some authors, the term NEO is equivalent to osteomyelitis of the skull base [190], whereas others consider NEO to be a generic term, including soft tissue and bone lesions [191, 192]. The role of imaging in NOE is to aid diagnosis, identify disease extent and any complications, as well as attempt to differentiate NOE from other conditions. CT evidence of osteolysis is a common finding, but it can be associated with various tumors and congenital lesions of the skull base hence CT cannot always provide a distinction between inflammatory and neoplastic processes. Bone sclerosis at the skull base can also be identified in NOE,

which may result from chronic osteomyelitis or following treatment initiation. Additionally, reports have suggested that follow-up CT examinations can evaluate treatment response; however, re-mineralization of the bone may not occur and, hence, CT is not always reliable for evaluating treatment response [193]. MRI can assess soft-tissue involvement in NOE and is the imaging technique of choice due to its superior contrast resolution [194]. On T1-weighted images, the EAM and soft tissues within the subtemporal region are thickened and demonstrate reduced T1 signal [194, 195]. The T2-weighted sequences return isointense or slightly hyperintense signal intensity. This is unlike the high signal that is noted in most inflammatory conditions with associated hyperemia and edema. The lower signal intensity on T2-weighted images is likely related to the nature of the underlying fibrotic and necrotizing pathological process [196, 197]. Following gadolinium contrast medium administration, there is typically diffuse enhancement, and focal areas of rim-enhancing inflammatory fluid collections may be identified. Middle ear, mastoid, and petrous apex involvement can be identified by changes in signal intensity on T2-weighted images [193]. Assessment of potential skull base and intracranial complications (meningitis, cerebritis, intracranial empyema, venous sinus thrombosis) is best served by MRI due to its ability to assess involvement of the medullary space of bone and identify subtle dural enhancement. Diffuse T1 hypointensity, T2 hyperintensity, and post-contrast enhancement within the central skull base relative to normal "fatty" bone marrow signal are indicative of central skull base osteomyelitis [198]. Identification of dural and leptomeningeal enhancement may signify spread to the meninges, and assessment of the dural venous sinuses (with CT or MR venography if necessary) should be undertaken to exclude venous thrombosis. Changes on MRI frequently lag behind clinical response, and similar to CT, MRI is not reliable for evaluating treatment response [193]. Scintigraphy may be used to localize the focus of NOE and osteomyelitis within the central skull base [193, 199–202]. No data are available on the use of PET/CT or PET/MRI in this specific field. However, promising results showed that [^{18}F]FDG positron emission tomography seems to be superior for detecting chronic osteomyelitis in the axial skeleton in comparison with immunoscintigraphy [203]. In particular, hybrid PET/MRI will provide relevant information on NEO in the future, guaranteeing better localization of the PET signal within soft tissues [204].

10.14 Bacteremia, Mycotic Aneurism, and Septic Emboli Foci

Patients with fever and/or elevated inflammatory parameters (e.g., ESR) pose a common diagnostic dilemma for many clinicians. Timely identification of metastatic complications of bloodstream infections due to spreading of the microorganisms to distant sites, although critical, is often difficult [41]. PET/CT may have diagnostic value in patients with nonspecific complaints and elevated inflammatory parameters by showing abnormal [^{18}F]FDG uptake suggestive of infection, malignancy, or auto-inflammatory disease. In FUO, PET/CT contributes to establishing a diagnosis in a high proportion of patients (36–69 % of cases) [205–207]. Causes of fever of unknown origin and elevated inflammatory parameters only partly overlap [208]. Besides physiologic uptake of brain [^{18}F]FDG severely hampers the delineation of disease in this organs, many authors suggest its usefulness in bloodstream infections also to assess the brain [41, 209–212].

A serious problem is the possibility of septic embolism in patients with cardiovascular infections, particularly in infectious endocarditis (IE). MSCT angiography is the first choice procedure in case of suspicions of cerebral septic embolism [213]. However, in case of subarachnoid and/or intraparenchymal hemorrhage, other vascular imaging, such as angiography, is required to diagnose/exclude a mycotic aneurysm if not detected on MSCT. MRI has a clear advantage in terms of sensitivity for the detection of cerebral lesions as compared to MSCT, also in

the setting of IE [214]. Cerebral MRI is in the majority of cases abnormal in IE patients with neurological symptoms [215]. It has higher sensitivity than MSCT in the diagnosis of the culprit lesion, in particular with regard to stroke, transient ischemic attack, and encephalopathy. MRI may also detect additional cerebral lesions that are not related to clinical symptoms [215]. Although detection of cerebral complications in IE may influence the clinical decisions, routine MRI screening is not recommended [216]. Nuclear medicine imaging has been reported very useful to detect septic embolism foci in patients with IE [18, 217, 218]. Growing interest has been reported in [^{18}F]FDG-PET/CT studies to rule out the extracardiac involvement in patients with IE. Interestingly, despite the limitations of this technique (e.g., relative low spatial resolution, gray matter uptake), it resulted useful and accurate also to diagnose septic embolism, including to the brain [217–221].

10.15 Creutzfeldt-Jakob Disease (CJD)

CJD is a rare and fatal prion disease of the CNS, caused by accumulation of the infectious prion PrPSc in the human brain, characterized by progressive rapid-onset dementia, myoclonus, and pyramidal and extrapyramidal tract motor signs [222]. Diagnosis of CJD can be challenging since the huge variability of the symptoms which can be observed, especially in its early stages, may simulate other common forms of dementia [223]. A noninvasive diagnostic test with high sensitivity and specificity could improve the accuracy in diagnosing prion diseases. In latest years, noninvasive techniques able to help clinicians to provide a definite diagnosis have been extensively evaluated [223]. According to international medical consensus, a definitive diagnosis is possible only through brain tissue pathological examination. The histological features include characteristic spongiform changes, neuronal cell loss, and gliosis in various regions of the brain. This neuronal damage is known to lead to glucose hypometabolism [222]. [^{18}F]FDG-PET/CT may be a useful tool for early diagnosis of CJD, as it may reveal a reduction in cellular glucose transport and metabolism in the cortex, cerebellum, and basal ganglia [224]. As one of the most sensitive modalities for investigating brain metabolism, [^{18}F]FDG-imaging has the potential to provide the earliest possible diagnosis of CJD; however, few data are available about the role of the hybrid [^{18}F]FDG-PET/CT in CJD [222, 223]. In the next future, we could predict even more advantages provided by PET imaging by creating an in vivo probe to label prion plaques, similar to that successfully developed for amyloid plaques in Alzheimer's disease [225] and eventually match information provided by PET imaging with MRI findings.

10.16 Encephalitis

In viral encephalitis and cerebellitis, the study of cerebral blood flow may have a prognostic significance. In fact, increased regional blood flow in various areas of the cerebral hemispheres, the typical finding of the acute phase generally returns to normal in the majority of the cases. A reduced regional blood flow at follow-up SPECT investigations is associated with poor clinical outcome probably as a consequence of neuronal death [226–231]. Some cases of encephalitis secondary to autoimmune or infectious disease imaged by PET/CT have been reported in literature. Autoimmune limbic encephalitis (ALE) is a rare disorder affecting the medial temporal lobe of the brain [232]. Voltage-gated potassium channel antibody-related limbic encephalitis (VGKC-LE) is a form of ALE manifesting as mood disorder (like depression) or bizzare thoughts and behaviors, frequently associated to seizures. Patients with VGKC-LE have been reported to have a normal brain MRI but bitemporal hypometabolism on brain [^{18}F]FDG-PET [233]; however, cases of correlations between [^{18}F]FDG-PET and MRI have also been described [234]. The only case of VGKC-LE imaged by hybrid [^{18}F]FDG-PET/MRI, confirming data previously reported [233], suggests the synergistic potential for identifying focal abnormalities that separately acquired single modality

testing might miss. Nonetheless, in literature different patterns of [^{18}F]FDG also in different forms of ALE as well as in Herpes simplex encephalitis (HSE) infection, varying from hyper- to hypometabolic to hypermetabolism, have been reported (Fig. 10.14) [235–237].

The mismatch between ^{11}C-acetate (no uptake) and [^{18}F]FDG (intense uptake) using PET/CT has been used to diagnose a case of encephalitis (Fig. 10.15) [238].

10.17 Atherosclerotic Plaque of Carotid

Atherosclerosis is a progressive disease. The origin of most acute vascular events is atherothrombosis, the formation of life-threatening clots, and it is currently accepted that plaque rupture and erosion are the major causes for atherothrombosis [239]. Atherosclerosis has been one of the most actively investigated fields in medical imaging. Atherosclerosis can be evaluated by using various imaging methods. Tissue perfusion, which can be evaluated on single-photon emission computed tomography (SPECT), computed tomography (CT), and magnetic resonance imaging (MRI), has been deemed as a functional imaging tool for atherosclerosis. More direct imaging of atherosclerosis is available by using angiography, CT, and MRI. Additionally, ultrasonography also may be used to evaluate atherosclerosis in some specific arteries, including the carotid artery. However, these imaging methods are based on the anatomical aspects of atherosclerosis and can hardly identify the activity and vulnerability of an atherosclerotic lesion, although information on plaque composition can be partially identified on CT or MRI.

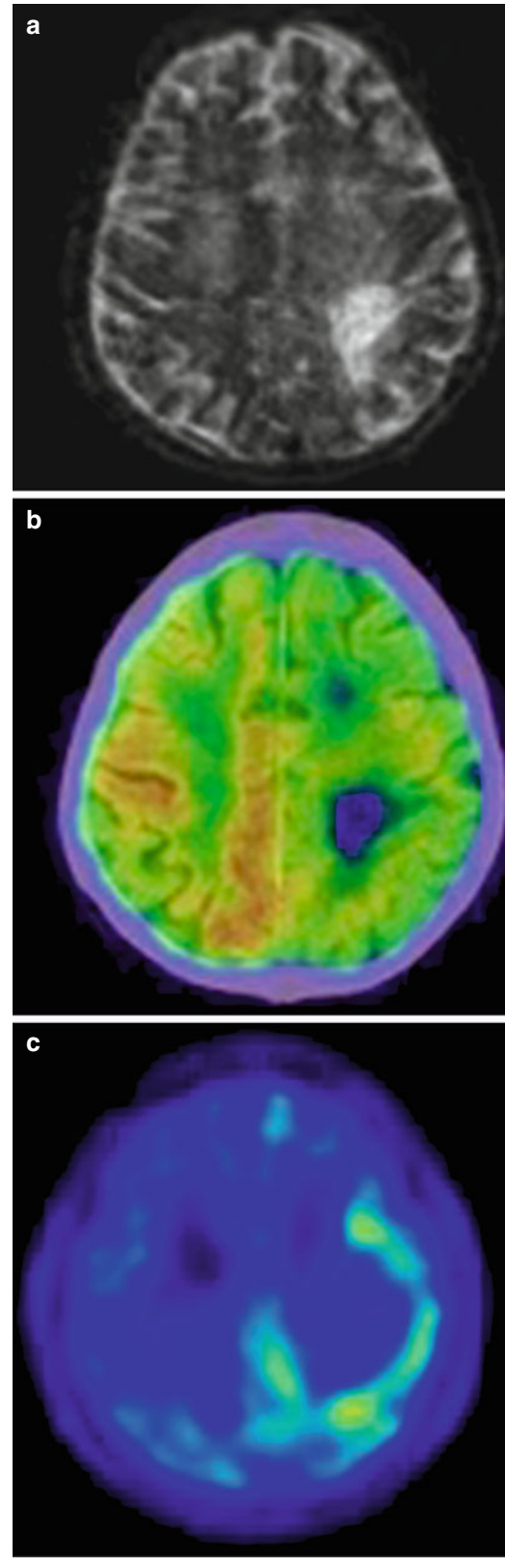

Fig. 10.14 Examples of ^{11}C-methionine (^{11}C-MET) and [^{18}F]FDG findings in the diagnosis of progressive multifocal leukoencephalopathy. Brain MRI image on admission (T2-weighted image) showing leukoencephalopathy of the left parietal lobe (**a**). [^{18}F]FDG uptake is decreased inside the lesion (**b**). ^{11}C-MET uptake is increased around the lesion (**c**) (Adapted from Shirai et al. [149])

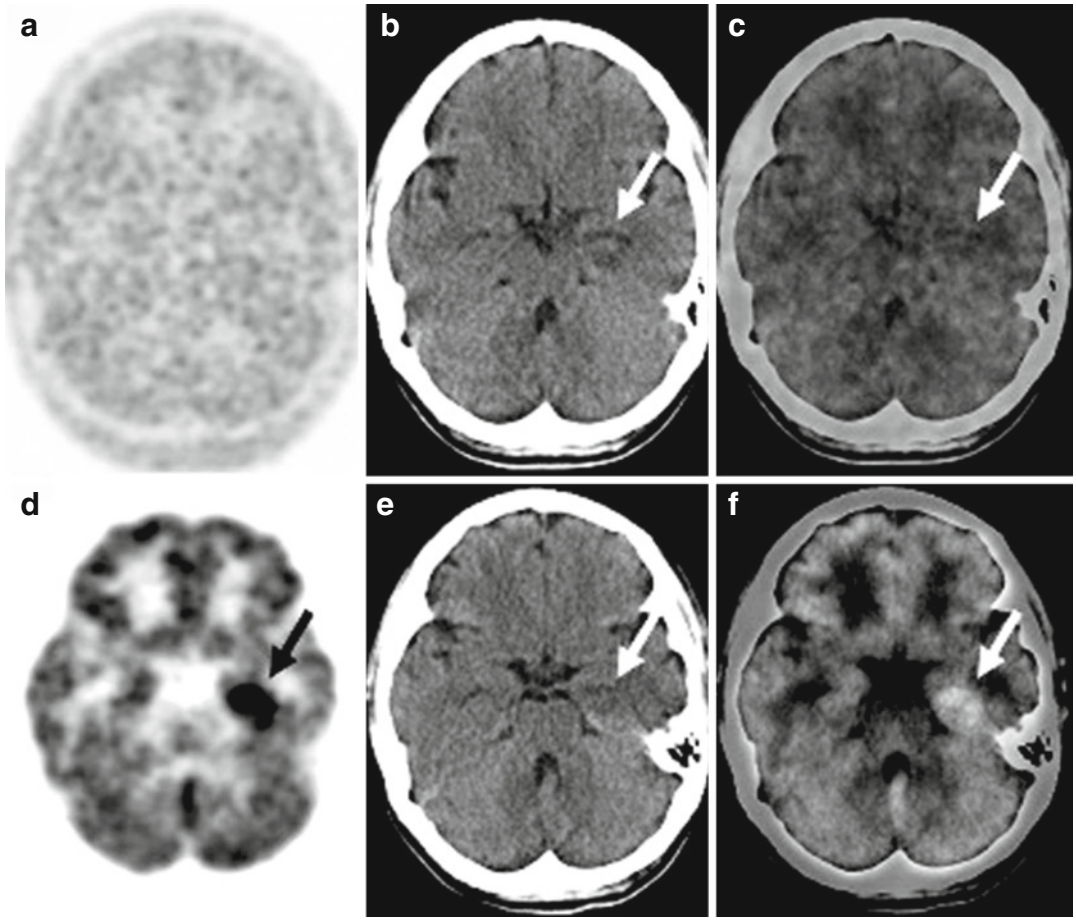

Fig. 10.15 Example of a patient with encephalitis diagnosed after dual tracer brain PET/CT study with [^{11}C]-acetate and [^{18}F]FDG. [^{11}C]-acetate images did not reveal any increased activity (**a**) in the hypodense lesion in the region of the left hippocampus revealed on the CT (**b**, *arrow*) and fused PET/CT (**c**, *arrow*) images. [^{18}F]FDG PET/CT scan of the brain was performed just after the completion of [^{11}C]-acetate imaging demonstrated intense activity (**d**), corresponding well to the hypodense lesion in the region of the left hippocampus both on the CT (**e**, *arrow*) and fused PET/CT (**f**, *arrow*) images (Adapted from Wang et al. [238])

Histological studies have demonstrated that vulnerable plaques have certain pathological characteristics that offer potential targets for identification. Structural features, such as positive remodeling, neovascularization, and intraplaque hemorrhage, can already be detected with noninvasive imaging [240]. Active, pathophysiological processes such as inflammation and microcalcification however represent additional drivers of vulnerability that have proven more challenging to identify noninvasively. Data from pathology of vulnerable plaques has lead to the recognition that plaque composition, more than degree of vessel occlusion, is the primary determinant of stability [241]. Therefore, the concept of the vulnerable plaque is a hallmark in atherosclerosis, and most of the pathogenesis mechanism and molecular targets in vulnerable plaque might be considered as targets for molecular imaging. The vulnerability of a plaque is characterized by a number of factors like a thin, collagen-poor fibrous cap, a large necrotic core, and abundant macrophages in the cap, whereas the luminal protrusion is not a marker of vulnerability [242]. Macrophages present in the developing plaque release cytokines and other factors that can weaken the fibrous cap, eventually leading to plaque instability and rupture [243, 244].

In fact, it has been observed that the pattern of distribution of macrophages correlates with degree of plaque instability [241]. Therefore, the ability to image plaques at high resolution to determine macrophage content and distribution could provide a means to noninvasively assess plaque vulnerability and degree of risk to rupture in inflamed arteries [241]. MRI shows the most promise for assessing both structure and lipid composition to evaluate plaque stability [245–247] offering the ability to perform both anatomical and functional examinations. The atherosclerotic plaque components can be differentiated using dedicated imaging sequences. T1-, T2-, and proton density-weighted imaging of carotid plaques allows for identification of the lipid-rich necrotic core, calcification, and intraplaque hemorrhage. The high spatial resolution of MRI even allows for identification and assessment of the fibrous cap. Additionally, adding specific contrast agents (e.g., paramagnetic gadolinium or iron oxide) which allow for visualization of processes in the atherosclerotic plaque at the molecular level, molecular imaging with MRI is also possible [248]. However, MRI lacks the sensitivity to screen large regions and atherosclerotic disease can occur anywhere in the vascular system. Multimodality imaging approach can be used to noninvasively map the distribution of macrophages in vivo allowing to combine the complementary strengths of each modality to better visualize features of interest [241].

PET imaging of atherosclerosis has so far focused primarily on [^{18}F]FDG. The first report on [^{18}F]FDG accumulation in the large arteries emerged in 2001 [249], and since then, a large body of evidence has materialized linking [^{18}F]FDG uptake to the macrophage contents of high-risk plaques (Fig. 10.16) [250–253]. A hunt for new and more specific tracers has started to target cell-mediated key molecular processes associated with the vulnerable atherosclerotic plaque. The most prominent of these targets include macrophage infiltration, apoptosis, hypoxia, and neoangiogenesis of the intima/media, but the clinical use of these tracers is very limited thus far [248]. Surface receptors expressed on macrophages were selected as imaging targets in early studies. Imaging probes for the IL-2 receptor [254] and scavenger receptors [255, 256] were labeled with ^{99m}Tc and tested in plaque imaging more than a decade ago. ^{99m}Tc-HYNIC-IL-2 is another IL-2 receptor targeting probe and recently has been utilized in a human study for carotid plaque imaging [257]. In more recent studies, chemokine receptors have been investigated. A peptide moiety of D-Ala1-peptide T-amide (DAPTA), which has an affinity for chemokine receptors, was also labeled with ^{64}Cu after conjugation with a comblike nanoparticle. ^{64}Cu-DAPTA-comb was reported to be an effective imaging probe for atherosclerosis [258]. Radiolabeled scavenger receptor (^{64}Cu-CD68-Fc) may help to target foam cell-rich plaques with high content of oxidized LDL, having the potential to identify unstable plaques and for risk stratification (Fig. 10.17) [259]. Small antibody fragment for vascular cell adhesion molecule (VCAM-1) [260] and peptide compounds for VCAM-1 [261] have relatively shorter half-lives in circulation and have been labeled with ^{99m}Tc and ^{18}F, respectively. There are other surface receptors of macrophages that have been utilized for plaque imaging. They also exhibited promising results in plaque imaging. The mannose receptor is also expressed on activated macrophages, particularly the M2 subtype, and its use has been attempted in plaque imaging with

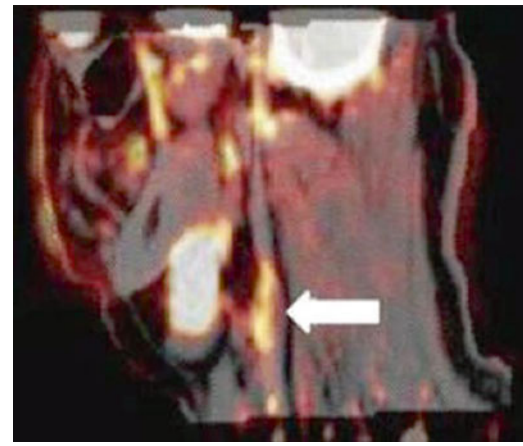

Fig. 10.16 Example of [^{18}F]FDG PET/CT scan in a patient with carotid atherosclerotic lesion in a male patient. *White arrow* show increased [^{18}F]FDG uptake at the level of the plaque in carotid artery (Adapted from Orbay et al. [289])

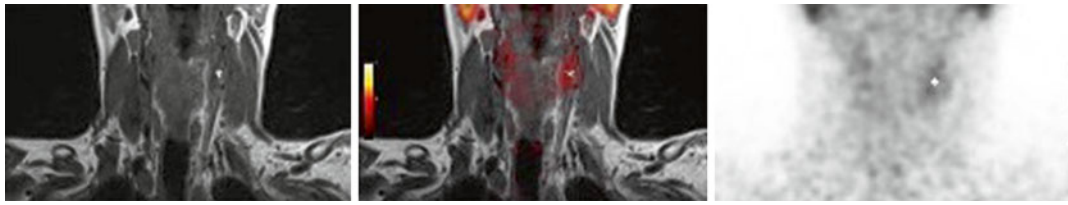

Fig. 10.17 Examples of [^{64}Cu]-DOTATATE PET/MRI of the neck region for visualization of the carotid arteries. T1-weighted MR image showing atherosclerotic plaque of the left internal carotid artery marked with *asterisk* (*left panel*). Combined PET/MRI of the same projection showing increased [^{64}Cu]-DOTATATE) uptake in the plaque (marked by *asterisk* in the *middle panel* images). Standalone PET image of the same projection showing [^{64}Cu]-DOTATATE biodistribution (*right panel*) (Adapted from Folke Pedersen et al. [285])

^{18}F-fluoro-D-mannose [262]. Fucoidan is a synthetic SLX-mimicking compound and increased ^{68}Ga-fucoidan uptake in atherosclerotic plaques in a proof-of-concept study [263]. Monocyte recruitment and migration in atherosclerotic plaques may be imaged by the direct radiolabeling of cells [264].

Apoptosis in the plaque occurs in macrophages or other cells as a result of active inflammation. Apoptosis can be visualized by radiolabeled annexin V, which binds to phosphatidylserine on the apoptotic cells' surfaces. In early studies, ^{99m}Tc-annexin V exhibited high uptake in atherosclerotic plaques [265–267].

Integrin αvβ3, a receptor for fibronectin and vitronectin, is expressed on activated endothelium and turn on angiogenic program by cross-talking with various growth factor receptors [268]. Intriguingly, a tri-peptide moiety of Arg-Gly-Asp (RGD) has a high affinity for integrin αvβ3 and has been utilized for angiogenesis imaging. ^{99m}Tc-NC100692, one of radiolabeled RGD compounds, exhibited high uptake in the atherosclerotic carotid artery in an animal model [269]. [^{18}F]Galacto-RGD PET/CT showed specific tracer accumulation in human atherosclerotic carotid plaques, which correlates with αvß3 expression. Integrin αvβ3 is expressed on macrophages as well as activated endothelium, and thus, this imaging visualizes both neoangiogenesis and macrophage accumulation in vulnerable plaques. VEGF receptor that is expressed on activated endothelium is another target for neoangiogenesis imaging. Recently, an antibody against VEGF receptor was labeled with ^{89}Zr and tested in carotid plaque PET imaging [270]. However, larger prospective studies are warranted to evaluate the potential of molecular imaging of αvß3 expression for clinical assessment of plaque inflammation [271].

In plaque, microcalcification represents additional drivers of vulnerability [272, 273]. Macroscopic deposits of calcium are associated with burnt-out and clinically stable disease. By contrast, the very early stages of microcalcification are associated with ruptured and high-risk lesions, in part because they identify inflamed plaques that have not yet healed and in part because microcalcification may directly weaken the cap surface [242, 274, 275]. ^{18}F-fluoride binds to regions of microcalcification prior to the presence of CT determined macrocalcification. ^{18}F-fluoride binds in relation to the exposed surface area of hydroxyapatite. This explains why uptake is proportionally greatest in the early, active stage of microcalcification while the plaque remains vulnerable to rupture. This stage precedes the potential development of stable, macroscopic calcification that is detected by traditional CT imaging. Studies have demonstrated a close association between ^{18}F-fluoride and both Framingham risk and CT calcium scores [276, 277]. Moreover in a recent work, ^{18}F-fluoride was used as marker of newly developing valvular calcium in aortic stenosis [277] with uptake predicting the progression of CT calcium scores at 1 year and once again correlating with histological markers of calcification activity [278]. The stage is now set for larger prospective trials to confirm whether ^{18}F-fluoride PET detects plaques with a propensity to rupture and in so doing identifies patients at risk of myocardial infarction. Additional studies will also help describe the natural history of this

marker of vulnerability and determine if this can be modified with targeted therapies. A recent study addressed the role of calcification by ^{18}F-NaF PET/CT and inflammation by [^{18}F]FDG PET/CT in the carotid plaques, symptomatic and asymptomatic, of patients with bilateral carotid atheromatosis and during the subacute phase of CVA. In this study, significant uptake of ^{18}F-NaF was found in carotid symptomatic plaques. From the association of ^{18}F-NaF uptake and symptomatology in the subacute phase of the CVA, it could be suggested that this tracer would identify the unstable plaques in risk of rupture. Of interest, lower ^{18}F-NaF uptake was found in plaques with larger calcium size, suggesting the calcium reached a "stable" stage after the mineralization process has ended in the atheroma plaque ("inactive" calcium) [277, 279]. Therefore, in these patients, the cause of the CVA could be hypothesized as being hemodynamic rather than thrombotic. Very different in plaques classified as grades II and III according to the calcification size, highest ^{18}F-NaF uptake was found as for the presence of more active calcification process at these stages (active calcification or "active" calcium). In grade I calcification, both processes, calcification and inflammation, show the same activity as expressed by ^{18}F-NaF TBR/^{18}F-FDG TBR indexes [280].

Hybrid [^{18}F]FDG-PET/MRI allows high sensitivity PET screening to identify putative lesions in a whole-body view and high resolution MRI for detailed mapping of biomarker expression in the lesions [241, 281, 282]. Integrated [^{18}F]FDG-PET/MR imaging has been compared to [^{18}F]FDG-PET/CT to evaluate carotid arteries in HIV patients with increased risk of atherosclerosis but without any symptoms of cardiovascular disease [283]. MR delineation of both the inner and outer walls of the carotid artery was superior to the CT however a high congruence between [^{18}F]FDG-uptake quantification using the two systems despite the inherent methodological differences between the two systems (e.g., method of attenuation correction) [283].

As for PET/CT imaging, other than [^{18}F]FDG tracers have been evaluated also in PET/MRI setting. In addition to PET-imaging tracers direct to target different molecular processes than glucose metabolism (e.g., somatostatin receptor), some molecules which combine functional data achievable using MRI to PET ones are under evaluation resulting in preclinical promising results, including probes designed to contain gadolinium or iron oxide and Cu-64 (PET) [241], as well as polymeric nanoparticle (e.g., ^{89}Zr-DNP) [284].

PET/MRI with ^{64}Cu-DOTATATE resulted promising in a small series of patients imaged before carotid endarterectomy. These results, although preliminary, suggested the potential role of ^{64}Cu-DOTATATE PET/MRI in the identification and characterization of vulnerable plaques accumulating in atherosclerotic plaques of the carotid artery (i.e., detecting alternatively activated macrophages) [285].

References

1. Boerman OC, Rennen H, Oyen WJ, Corstens FH (2001) Radiopharmaceuticals to image infection and inflammation. Semin Nucl Med 31:286–295
2. Rennen HJ, Boerman OC, Oyen WJ, Corstens FH (2001) Imaging infection/inflammation in the new millennium. Eur J Nucl Med 28:241–252
3. Pulli B, Chen J (2014) Imaging neuroinflammation – from bench to bedside. J Clin Cell Immunol 5:226
4. Semmler A, Hermann S, Mormann F, Weberpals M, Paxian SA, Okulla T et al (2008) Sepsis causes neuroinflammation and concomitant decrease of cerebral metabolism. J Neuroinflammation 5:38
5. Wareham D, Michael J, Das S (2005) Advances in bacterial specific imaging. Braz Arch Biol Technol 48:145–152
6. Das SS, Hall AV, Wareham DW, Britton KE (2002) Infection imaging with radiopharmaceuticals in the 21st century. Brazilian Arch Biol Technol 45:25–37
7. Siaens RH, Rennen HJ, Boerman OC, Dierckx R, Slegers G (2004) Synthesis and comparison of 99mTc-enrofloxacin and 99mTc-ciprofloxacin. J Nucl Med 45:2088–2094
8. Gomes Barreto V, Iglesias F, Roca M, Tubau F, Martín-Comín J (2000) Labelling of ceftizoxime with 99mTc. Rev Española Med Nucl 19:479–483
9. Zasloff M (2002) Antimicrobial peptides of multicellular organisms. Nature 415:389–395
10. Welling MM, Nibbering PH, Paulusma-Annema A, Hiemstra PS, Pauwels EK, Calame W (1999) Imaging of bacterial infections with 99mTc-labeled human neutrophil peptide-1. J Nucl Med 40: 2073–2080
11. Hiemstra PS, van den Barselaar MT, Roest M, Nibbering PH, van Furth R (1999) Ubiquicidin, a novel murine microbicidal protein present in the

cytosolic fraction of macrophages. J Leukoc Biol 66:423–428
12. Welling MM, Mongera S, Lupetti A, Balter HS, Bonetto V, Mazzi U et al (2002) Radiochemical and biological characteristics of 99mTc-UBI 29–41 for imaging of bacterial infections. Nucl Med Biol 29:413–422
13. Ebenhan T, Zeevaart JR, Venter JD, Govender T, Kruger GH, Jarvis NV et al (2014) Preclinical evaluation of 68Ga-labeled 1,4,7-triazacyclononane-1,4,7 -triacetic acid-ubiquicidin as a radioligand for PET infection imaging. J Nucl Med 55:308–314
14. Bettegowda C, Foss CA, Cheong I, Wang Y, Diaz L, Agrawal N et al (2005) Imaging bacterial infections with radiolabeled 1-(2′-deoxy-2′-fluoro-beta-D-arabinofuranosyl)-5-iodouracil. Proc Natl Acad Sci U S A 102:1145–1150
15. Diaz LA, Foss CA, Thornton K, Nimmagadda S, Endres CJ, Uzuner O et al (2007) Imaging of musculoskeletal bacterial infections by [124 I]FIAU-PET/CT. PLoS One 2:e1007
16. Petruzzi N, Shanthly N, Thakur M (2009) Recent trends in soft-tissue infection imaging. Semin Nucl Med 39:115–123
17. Tulchinsky M, Peters AM (2005) Leukocyte receptor-binding radiopharmaceuticals for infection and inflammation scintigraphy. J Nucl Med 46:718–721
18. Erba PA, Conti U, Lazzeri E, Sollini M, Doria R, De Tommasi SM et al (2012) Added value of 99mTc-HMPAO-labeled leukocyte SPECT/CT in the characterization and management of patients with infectious endocarditis. J Nucl Med 53:1235–1243
19. Kataoka H, Inoue M, Shinkai T, Ueno S (2007) Early dynamic SPECT imaging in acute viral encephalitis. J Neuroimaging 17:304–310
20. Prandini N, Lazzeri E, Rossi B, Erba P, Parisella MG, Signore A (2006) Nuclear medicine imaging of bone infections. Nucl Med Commun 27:633–644
21. Grippaudo FR, Pacilio M, Di Girolamo M, Dierckx RA, Signore A (2013) Radiolabelled white blood cell scintigraphy in the work-up of dermal filler complications. Eur J Nucl Med Mol Imaging 40:418–425
22. Liberatore M, Drudi FM, Tarantino R, Prosperi D, Fiore V, Missori P et al (2003) Tc-99m exametazime-labeled leukocyte scans in the study of infections in skull neurosurgery. Clin Nucl Med 28:971–974
23. Schillaci O (2009) Hybrid imaging systems in the diagnosis of osteomyelitis and prosthetic joint infection. Q J Nucl Med Mol Imaging 53:95–104
24. Rehncrona S, Brismar J, Holtås S (1985) Diagnosis of brain abscesses with indium-111-labeled leukocytes. Neurosurgery 16:23–26
25. Bellotti C, Medina M, Oliveri G, Ettorre F, Barrale S, Sturiale C et al (1988) Cerebral scintigraphy with 111indium oxine-labelled leukocytes in the differential diagnosis of intracerebral cystic lesions. Acta Neurochir Suppl 42:221–224
26. Palestro CJ, Swyer AJ, Kim CK, Muzinic M, Goldsmith SJ (1991) Role of in-111 labeled leukocyte scintigraphy in the diagnosis of intracerebral lesions. Clin Nucl Med 16:305–308
27. Grimstad IA, Hirschberg H, Rootwelt K (1992) 99mTc-hexamethylpropyleneamine oxime leukocyte scintigraphy and C-reactive protein levels in the differential diagnosis of brain abscesses. J Neurosurg 77:732–736
28. Garg A (2011) Vascular brain pathologies. Neuroimaging Clin N Am 21:897–926, ix
29. Néel A, Pagnoux C, Guillevin L, Hamidou M (2012) Central nervous system vasculitides: an update. Rev Med Interne 33:381–389
30. Alba MA, Espígol-Frigolé G, Prieto-González S, Tavera-Bahillo I, García-Martínez A, Butjosa M et al (2011) Central nervous system vasculitis: still more questions than answers. Curr Neuropharmacol 9:437–448
31. Gross WL, Trabandt A, Reinhold-Keller E (2000) Diagnosis and evaluation of vasculitis. Rheumatology (Oxford) 39:245–252
32. Küker W (2007) Cerebral vasculitis: imaging signs revisited. Neuroradiology 49:471–479
33. Blockmans D, De Ceuninck L, Vanderschueren S, Knockaert D, Mortelmans L, Bobbaers H (2007) Repetitive 18-fluorodeoxyglucose positron emission tomography in isolated polymyalgia rheumatica: a prospective study in 35 patients. Rheumatology 46:672–677
34. Andrews J, Al-Nahhas A, Pennell DJ, Hossain MS, Davies KA, Haskard DO et al (2004) Non-invasive imaging in the diagnosis and management of Takayasu's arteritis. Ann Rheum Dis 63:995–1000
35. Abdel Razek AAK, Alvarez H, Bagg S, Refaat S, Castillo M (2014) Imaging spectrum of CNS vasculitis. Radiographics 34:873–894
36. Poels MMF, Ikram MA, Vernooij MW (2012) Improved MR imaging detection of cerebral microbleeds more accurately identifies persons with vasculopathy. AJNR Am J Neuroradiol 33:1553–1556
37. Pipitone N, Versari A, Salvarani C (2008) Role of imaging studies in the diagnosis and follow-up of large-vessel vasculitis: an update. Rheumatology (Oxford) 47:403–408
38. Belhocine T, Blockmans D, Hustinx R, Vandevivere J, Mortelmans L (2003) Imaging of large vessel vasculitis with (18)FDG PET: illusion or reality? A critical review of the literature data. Eur J Nucl Med Mol Imaging 30:1305–1313
39. Bleeker-Rovers CP, Bredie SJH, van der Meer JWM, Corstens FHM, Oyen WJG (2003) F-18-fluorodeoxyglucose positron emission tomography in diagnosis and follow-up of patients with different types of vasculitis. Neth J Med 61:323–329
40. Meller J, Sahlmann C-O, Scheel AK (2007) 18F-FDG PET and PET/CT in fever of unknown origin. J Nucl Med 48:35–45
41. Bleeker-Rovers CP, Vos FJ, Wanten GJA, van der Meer JWM, Corstens FHM, Kullberg B-J et al (2005) 18F-FDG PET in detecting metastatic infectious disease. J Nucl Med 46:2014–2019

42. Meller J, Strutz F, Siefker U, Scheel A, Sahlmann CO, Lehmann K et al (2003) Early diagnosis and follow-up of aortitis with [(18)F]FDG PET and MRI. Eur J Nucl Med Mol Imaging 30:730–736
43. Tezuka D, Haraguchi G, Ishihara T, Ohigashi H, Inagaki H, Suzuki J et al (2012) Role of FDG PET-CT in Takayasu arteritis: sensitive detection of recurrences. JACC Cardiovasc Imaging 5:422–429
44. Otsuka H, Morita N, Yamashita K, Nishitani H (2007) FDG-PET/CT for diagnosis and follow-up of vasculitis. J Med Invest 54:345–349
45. Meller J, Grabbe E, Becker W, Vosshenrich R (2003) Value of F-18 FDG hybrid camera PET and MRI in early Takayasu aortitis. Eur Radiol 13:400–405
46. Blockmans D, Maes A, Stroobants S, Nuyts J, Bormans G, Knockaert D et al (1999) New arguments for a vasculitic nature of polymyalgia rheumatica using positron emission tomography. Rheumatology (Oxford) 38:444–447
47. Moosig F, Czech N, Mehl C, Henze E, Zeuner RA, Kneba M et al (2004) Correlation between 18-fluorodeoxyglucose accumulation in large vessels and serological markers of inflammation in polymyalgia rheumatica: a quantitative PET study. Ann Rheum Dis 63:870–873
48. Webb M, Chambers A, Al-Nahhas A, Mason JC, Maudlin L, Rahman L et al (2004) The role of 18F-FDG PET in characterising disease activity in Takayasu arteritis. Eur J Nucl Med Mol Imaging 31:627–634
49. Kobayashi Y, Ishii K, Oda K, Nariai T, Tanaka Y, Ishiwata K et al (2005) Aortic wall inflammation due to Takayasu arteritis imaged with 18F-FDG PET coregistered with enhanced CT. J Nucl Med 46:917–922
50. Einspieler I, Thürmel K, Pyka T, Eiber M, Wolfram S, Moog P et al (2015) Imaging large vessel vasculitis with fully integrated PET/MRI: a pilot study. Eur J Nucl Med Mol Imaging 42:1012–1024
51. Scheel AK, Meller J, Vosshenrich R, Kohlhoff E, Siefker U, Müller GA et al (2004) Diagnosis and follow up of aortitis in the elderly. Ann Rheum Dis 63:1507–1510
52. Rehák Z, Szturz P, Křen L, Fojtík Z, Staníček J (2014) Upsampling from aorta and aortic branches: PET/CT hybrid imaging identified 18F-FDG hypermetabolism in inflamed temporal and occipital arteries. Clin Nucl Med 39:e84–e86
53. Weyand CM, Goronzy JJ (2003) Medium- and large-vessel vasculitis. N Engl J Med 349:160–169
54. Venneti S, Lopresti B, Wiley C (2006) The peripheral benzodiazepine receptor in microglia: from pathology to imaging. Prog Neurobiol 80:308–322
55. Starosta-Rubinstein S, Ciliax BJ, Penney JB, McKeever P, Young AB (1987) Imaging of a glioma using peripheral benzodiazepine receptor ligands. Proc Natl Acad Sci U S A 84:891–895
56. Banati RB, Newcombe J, Gunn RN, Cagnin A, Turkheimer F, Heppner F et al (2000) The peripheral benzodiazepine binding site in the brain in multiple sclerosis: quantitative in vivo imaging of microglia as a measure of disease activity. Brain 123(Pt 1):2321–2337
57. Vowinckel E, Reutens D, Becher B, Verge G, Evans A, Owens T et al (1997) PK11195 binding to the peripheral benzodiazepine receptor as a marker of microglia activation in multiple sclerosis and experimental autoimmune encephalomyelitis. J Neurosci Res 50:345–353
58. Venneti S, Lopresti BJ, Wang G, Bissel SJ, Mathis CA, Meltzer CC et al (2004) PET imaging of brain macrophages using the peripheral benzodiazepine receptor in a macaque model of neuroAIDS. J Clin Invest 113:981–989
59. Raghavendra Rao VL, Dogan A, Bowen KK, Dempsey RJ (2000) Traumatic brain injury leads to increased expression of peripheral-type benzodiazepine receptors, neuronal death, and activation of astrocytes and microglia in rat thalamus. Exp Neurol 161:102–114
60. Charbonneau P, Syrota A, Crouzel C, Valois JM, Prenant C, Crouzel M (1986) Peripheral-type benzodiazepine receptors in the living heart characterized by positron emission tomography. Circulation 73: 476–483
61. Shah F, Hume SP, Pike VW, Ashworth S, McDermott J (1994) Synthesis of the enantiomers of [N-methyl-11C]PK 11195 and comparison of their behaviours as radioligands for PK binding sites in rats. Nucl Med Biol 21:573–581
62. Banati RB (2002) Visualising microglial activation in vivo. Glia 40:206–217
63. Pappata S, Cornu P, Samson Y, Prenant C, Benavides J, Scatton B et al (1991) PET study of carbon-11-PK 11195 binding to peripheral type benzodiazepine sites in glioblastoma: a case report. J Nucl Med 32: 1608–1610
64. Petit-Taboué MC, Baron JC, Barré L, Travère JM, Speckel D, Camsonne R et al (1991) Brain kinetics and specific binding of [11C]PK 11195 to omega 3 sites in baboons: positron emission tomography study. Eur J Pharmacol 200:347–351
65. Sette G, Baron JC, Young AR, Miyazawa H, Tillet I, Barré L et al (1993) In vivo mapping of brain benzodiazepine receptor changes by positron emission tomography after focal ischemia in the anesthetized baboon. Stroke 24:2046–2057; discussion 2057–8
66. Cagnin A, Myers R, Gunn RN, Lawrence AD, Stevens T, Kreutzberg GW et al (2001) In vivo visualization of activated glia by [11C] (R)-PK11195-PET following herpes encephalitis reveals projected neuronal damage beyond the primary focal lesion. Brain 124:2014–2027
67. Goerres GW, Revesz T, Duncan J, Banati RB (2001) Imaging cerebral vasculitis in refractory epilepsy using [(11)C](R)-PK11195 positron emission tomography. AJR Am J Roentgenol 176:1016–1018
68. Versijpt J, Debruyne JC, Van Laere KJ, De Vos F, Keppens J, Strijckmans K et al (2005) Microglial imaging with positron emission tomography and

atrophy measurements with magnetic resonance imaging in multiple sclerosis: a correlative study. Mult Scler 11:127–134
69. Hammoud DA, Endres CJ, Chander AR, Guilarte TR, Wong DF, Sacktor NC et al (2005) Imaging glial cell activation with [11C]-R-PK11195 in patients with AIDS. J Neurovirol 11:346–355
70. Gerhard A, Schwarz J, Myers R, Wise R, Banati RB (2005) Evolution of microglial activation in patients after ischemic stroke: a [11C](R)-PK11195 PET study. Neuroimage 24:591–595
71. Gerhard A, Pavese N, Hotton G, Turkheimer F, Es M, Hammers A et al (2006) In vivo imaging of microglial activation with [11C](R)-PK11195 PET in idiopathic Parkinson's disease. Neurobiol Dis 21: 404–412
72. Pavese N, Gerhard A, Tai YF, Ho AK, Turkheimer F, Barker RA et al (2006) Microglial activation correlates with severity in Huntington disease: a clinical and PET study. Neurology 66:1638–1643
73. Hajj-Ali RA, Calabrese LH (2013) Primary angiitis of the central nervous system. Autoimmun Rev 12: 463–466
74. Salvarani C, Brown RD, Hunder GG (2012) Adult primary central nervous system vasculitis: an update. Curr Opin Rheumatol 24:46–52
75. Peterson PL, Axford JS, Isenberg D (2005) Imaging in CNS lupus. Best Pract Res Clin Rheumatol 19:727–739
76. McCune WJ, MacGuire A, Aisen A, Gebarski S (1988) Identification of brain lesions in neuropsychiatric systemic lupus erythematosus by magnetic resonance scanning. Arthritis Rheum 31:159–166
77. Sibbitt WL, Sibbitt RR, Griffey RH, Eckel C, Bankhurst AD (1989) Magnetic resonance and computed tomographic imaging in the evaluation of acute neuropsychiatric disease in systemic lupus erythematosus. Ann Rheum Dis 48:1014–1022
78. Baum KA, Hopf U, Nehrig C, Stöver M, Schörner W (1993) Systemic lupus erythematosus: neuropsychiatric signs and symptoms related to cerebral MRI findings. Clin Neurol Neurosurg 95:29–34
79. Cuadrado MJ, Khamashta MA, Ballesteros A, Godfrey T, Simon MJ, Hughes GR (2000) Can neurologic manifestations of Hughes (antiphospholipid) syndrome be distinguished from multiple sclerosis? Analysis of 27 patients and review of the literature. Medicine (Baltimore) 79:57–68
80. Miller DH, Buchanan N, Barker G, Morrissey SP, Kendall BE, Rudge P et al (1992) Gadolinium-enhanced magnetic resonance imaging of the central nervous system in systemic lupus erythematosus. J Neurol 239:460–464
81. Curiel R, Akin EA, Beaulieu G, DePalma L, Hashefi M (2011) PET/CT imaging in systemic lupus erythematosus. Ann N Y Acad Sci 1228:71–80
82. Shapira Y, Weinberger A, Wysenbeek AJ (1996) Lymphadenopathy in systemic lupus erythematosus. Prevalence and relation to disease manifestations. Clin Rheumatol 15:335–338
83. Stern BJ, Krumholz A, Johns C, Scott P, Nissim J (1985) Sarcoidosis and its neurological manifestations. Arch Neurol 42:909–917
84. Hoitsma E, Faber CG, Drent M, Sharma OP (2004) Neurosarcoidosis: a clinical dilemma. Lancet Neurol 3:397–407
85. Smith JK, Matheus MG, Castillo M (2004) Imaging manifestations of neurosarcoidosis. AJR Am J Roentgenol 182:289–295
86. Zajicek JP, Scolding NJ, Foster O, Rovaris M, Evanson J, Moseley IF et al (1999) Central nervous system sarcoidosis – diagnosis and management. QJM 92:103–117
87. Joseph FG, Scolding NJ (2009) Neurosarcoidosis: a study of 30 new cases. J Neurol Neurosurg Psychiatry 80:297–304
88. Bolat S, Berding G, Dengler R, Stangel M, Trebst C (2009) Fluorodeoxyglucose positron emission tomography (FDG-PET) is useful in the diagnosis of neurosarcoidosis. J Neurol Sci 287:257–259, Elsevier B.V
89. Dubey N, Miletich RS, Wasay M, Mechtler LL, Bakshi R (2002) Role of fluorodeoxyglucose positron emission tomography in the diagnosis of neurosarcoidosis. J Neurol Sci 205:77–81
90. Kim HW, Won KS, Choi BW, Zeon SK (2010) Cerebral toxoplasmosis in a patient with AIDS on F-18 FDG PET/CT. Nucl Med Mol Imaging 44:75–77
91. Aide N, Benayoun M, Kerrou K, Khalil A, Cadranel J, Talbot JN (2007) Impact of [18F]-fluorodeoxyglucose ([18F]-FDG) imaging in sarcoidosis: unsuspected neurosarcoidosis discovered by [18F]-FDG PET and early metabolic response to corticosteroid therapy. Br J Radiol 80:e67–e71
92. Chester W (1930) Über Lipoidgranulomatose. Virchows Arch Pathol Anat Physiol Klin Med 279: 561–602
93. Haroche J, Amoura Z, Dion E, Wechsler B, Costedoat-Chalumeau N, Cacoub P et al (2004) Cardiovascular involvement, an overlooked feature of Erdheim-Chester disease: report of 6 new cases and a literature review. Medicine (Baltimore) 83: 371–392
94. Lachenal F, Cotton F, Desmurs-Clavel H, Haroche J, Taillia H, Magy N et al (2006) Neurological manifestations and neuroradiological presentation of Erdheim-Chester disease: report of 6 cases and systematic review of the literature. J Neurol 253: 1267–1277
95. Arnaud L, Malek Z, Archambaud F, Kas A, Toledano D, Drier A et al (2009) 18F-fluorodeoxyglucose-positron emission tomography scanning is more useful in follow-up than in the initial assessment of patients with Erdheim-Chester disease. Arthritis Rheum 60:3128–3138
96. Asabella AN, Cimmino A, Altini C, Notaristefano A, Rubini G (2011) (18)F-FDG positron emission tomography/computed tomography and (99m) Tc-MDP skeletal scintigraphy in a case of Erdheim-Chester disease. Hell J Nucl Med 14:311–312

97. Pereira Neto CC, Roman C, Johnson M, Jagasia M, Martin WH, Delbeke D (2004) Positron emission tomography/computed tomography of a rare xanthogranulomatous process: Erdheim-Chester disease. Mol Imaging Biol 6:63–67
98. Cartes-Zumelzu FW, Stavrou I, Castillo M, Eisenhuber E, Knosp E, Thurnher MM (2004) Diffusion-weighted imaging in the assessment of brain abscesses therapy. AJNR Am J Neuroradiol 25:1310–1317
99. Kim DG, Lee JI, Lee DS, Lee MC, Choi KS, Han DH (1995) 99mTc-HMPAO labeled leukocyte SPECT in intracranial lesions. Surg Neurol 44: 338–345
100. Schmidt KG, Rasmussen JW, Frederiksen PB, Kock-Jensen C, Pedersen NT (1990) Indium-111-granulocyte scintigraphy in brain abscess diagnosis: limitations and pitfalls. J Nucl Med 31:1121–1127
101. Balachandran S, Husain MM, Adametz JR, Pallin JS, Angtuaco TL, Boyd CM (1987) Uptake of indium-111-labeled leukocytes by brain metastasis. Neurosurgery 20:606–609
102. Spinelli F, Sara R, Milella M, Ruffini L, Sterzi R, Causarano IR et al (2000) Technetium-99m hexamethylpropylene amine oxime leucocyte scintigraphy in the differential diagnosis of cerebral abscesses. Eur J Nucl Med 27:46–49
103. Sasaki M, Ichiya Y, Kuwabara Y, Otsuka M, Tahara T, Fukumura T et al (1990) Ringlike uptake of [18F] FDG in brain abscess: a PET study. J Comput Assist Tomogr 14:486–487
104. Ishii K, Ogawa T, Hatazawa J, Kanno I, Inugami A, Fujita H et al (1993) High L-methyl-[11C]methionine uptake in brain abscess: a PET study. J Comput Assist Tomogr 17:660–661
105. Meyer MA, Frey KA, Schwaiger M (1993) Discordance between F-18 fluorodeoxyglucose uptake and contrast enhancement in a brain abscess. Clin Nucl Med 18:682–684
106. Dethy S, Manto M, Kentos A, Konopnicki D, Pirotte B, Goldman S et al (1995) PET findings in a brain abscess associated with a silent atrial septal defect. Clin Neurol Neurosurg 97:349–353
107. Mineura K, Sasajima T, Kowada M, Ogawa T, Hatazawa J, Uemura K (1997) Indications for differential diagnosis of nontumor central nervous system diseases from tumors. A positron emission tomography study. J Neuroimaging 7:8–15
108. Kang K, Lim I, Roh J-K (2007) Positron emission tomographic findings in a tuberculous brain abscess. Ann Nucl Med 21:303–306
109. Tsuyuguchi N, Sunada I, Ohata K, Takami T, Nishio A, Hara M et al (2003) Evaluation of treatment effects in brain abscess with positron emission tomography: comparison of fluorine-18-fluorodeoxyglucose and carbon-11-methionine. Ann Nucl Med 17:47–51
110. Huang Z, Zuo C, Guan Y, Zhang Z, Liu P, Xue F et al (2008) Misdiagnoses of (11)-choline combined with F-18-FDG PET imaging in brain tumours. Nucl Med Commun 29:354–358
111. Tan H, Chen L, Guan Y, Lin X (2011) Comparison of MRI, F-18 FDG, and 11C-choline PET/CT for their potentials in differentiating brain tumor recurrence from brain tumor necrosis following radiotherapy. Clin Nucl Med 36:978–981
112. Mascarenhas NB, Lam D, Lynch GR, Fisher RE (2006) PET imaging of cerebral and pulmonary Nocardia infection. Clin Nucl Med 31:131–133
113. Kracht LW, Friese M, Herholz K, Schroeder R, Bauer B, Jacobs A et al (2003) Methyl-[11C]-l-methionine uptake as measured by positron emission tomography correlates to microvessel density in patients with glioma. Eur J Nucl Med Mol Imaging 30:868–873
114. Park S-H, Lee S-W, Kang D-H, Hwang J-H, Sung J-K, Hwang S-K (2011) The role of f-fluorodeoxyglucose positron emission tomography in the treatment of brain abscess. J Korean Neurosurg Soc 49:278–283
115. Floeth FW, Pauleit D, Sabel M, Reifenberger G, Stoffels G, Stummer W et al (2006) 18F-FET PET differentiation of ring-enhancing brain lesions. J Nucl Med 47:776–782
116. McCarthy M, Yuan JB, Campbell A, Lenzo NP, Butler-Henderson K (2008) 18F-fluorodeoxyglucose positron emission tomography imaging in brain tumours: the Western Australia positron emission tomography/cyclotron service experience. J Med Imaging Radiat Oncol 52:564–569
117. Lau EWF, Drummond KJ, Ware RE, Drummond E, Hogg A, Ryan G et al (2010) Comparative PET study using F-18 FET and F-18 FDG for the evaluation of patients with suspected brain tumour. J Clin Neurosci 17:43–49
118. Spence AM, Muzi M, Mankoff DA, O'Sullivan SF, Link JM, Lewellen TK et al (2004) 18F-FDG PET of gliomas at delayed intervals: improved distinction between tumor and normal gray matter. J Nucl Med 45:1653–1659
119. Kim D, Kim CG, Park S (2010) Experience of dual time point brain F-18 FDG PET/CT imaging in patients with infectious disease. Nucl Med Mol Imaging 44:137–142
120. Rock RB, Olin M, Baker CA, Molitor TW, Peterson PK (2008) Central nervous system tuberculosis: pathogenesis and clinical aspects. Clin Microbiol Rev 21:243–261, table of contents
121. Trivedi R, Saksena S, Gupta RK (2009) Magnetic resonance imaging in central nervous system tuberculosis. Indian J Radiol Imaging 19:256–265
122. Skoura E, Zumla A, Bomanji J (2015) Imaging in tuberculosis. Int J Infect Dis 32:87–93, International Society for Infectious Diseases
123. Chang JM, Lee HJ, Goo JM, Lee H-Y, Lee JJ, Chung J-K et al (2006) False positive and false negative FDG-PET scans in various thoracic diseases. Korean J Radiol 7:57–69
124. Sathekge MM, Maes A, Pottel H, Stoltz A, van de Wiele C (2010) Dual time-point FDG PET-CT for differentiating benign from malignant solitary

pulmonary nodules in a TB endemic area. S Afr Med J 100:598–601
125. Harisankar C, Mittal BR, Bhattacharya A, Singh B (2010) FDG-PET/CT in diagnosis and early response evaluation of extra-pulmonary tuberculosis in a patient with aplastic anemia. J Postgrad Med 56:219–221
126. D'Souza MM, Sharma R, Jaimini A, Panwar P, Bansal A, Tripathi M et al (2012) Metabolic assessment of intracranial tuberculomas using 11C-methionine and 18F-FDG PET/CT. Nucl Med Commun 33:408–414
127. El Omri H, Hascsi Z, Taha R, Szabados L, El Sabah H, Gamiel A et al (2015) Tubercular meningitis and lymphadenitis mimicking a relapse of Burkitt's lymphoma on (18)F-FDG-PET/CT: a case report. Case Rep Oncol 8:226–232
128. Park I-N, Ryu J-S, Shim TS (2008) Evaluation of therapeutic response of tuberculoma using F-18 FDG positron emission tomography. Clin Nucl Med 33:1–3
129. Chung J-K, Kim YK, Kim S, Lee YJ, Paek S, Yeo JS et al (2002) Usefulness of 11C-methionine PET in the evaluation of brain lesions that are hypo- or isometabolic on 18F-FDG PET. Eur J Nucl Med Mol Imaging 29:176–182
130. Lewitschnig S, Gedela K, Toby M, Kulasegaram R, Nelson M, O'Doherty M et al (2013) 18F-FDG PET/CT in HIV-related central nervous system pathology. Eur J Nucl Med Mol Imaging 40:1420–1427
131. Wright D, Schneider A, Berger JR (1997) Central nervous system opportunistic infections. Neuroimaging Clin N Am 7:513–525
132. Velji AM (1986) Leukocytoclastic vasculitis associated with positive HTLV-III serological findings. JAMA 256:2196–2197
133. Saravanan M, Turnbull IW (2009) Brain: non-infective and non-neoplastic manifestations of HIV. Br J Radiol 82:956–965
134. Graham CB, Wippold FJ, Pilgram TK, Fisher EJ, Smoker WR (2000) Screening CT of the brain determined by CD4 count in HIV-positive patients presenting with headache. AJNR Am J Neuroradiol 21:451–454
135. Miller RF, Hall-Craggs MA, Costa DC, Brink NS, Scaravilli F, Lucas SB et al (1998) Magnetic resonance imaging, thallium-201 SPET scanning, and laboratory analyses for discrimination of cerebral lymphoma and toxoplasmosis in AIDS. Sex Transm Infect 74:258–264
136. Skiest DJ (2002) Focal neurological disease in patients with acquired immunodeficiency syndrome. Clin Infect Dis 34:103–115
137. Schroeder PC, Post MJD, Oschatz E, Stadler A, Bruce-Gregorios J, Thurnher MM (2006) Analysis of the utility of diffusion-weighted MRI and apparent diffusion coefficient values in distinguishing central nervous system toxoplasmosis from lymphoma. Neuroradiology 48:715–720
138. Gildenberg PL, Gathe JC, Kim JH (2000) Stereotactic biopsy of cerebral lesions in AIDS. Clin Infect Dis 30:491–499
139. Stenzel W, Pels H, Staib P, Impekoven P, Bektas N, Deckert M (2004) Concomitant manifestation of primary CNS lymphoma and toxoplasma encephalitis in a patient with AIDS. J Neurol 251: 764–766
140. Palestro CJ, Goldsmith SJ (1995) The role of gallium and labeled leukocyte scintigraphy in the AIDS patient. Q J Nucl Med 39:221–230
141. Kimizuka T, Ozaki Y, Sumi Y (2002) Thallium-201 accumulation in a patient with brain abscess. Ann Nucl Med 16:351–354
142. Licho R, Litofsky NS, Senitko M, George M (2002) Inaccuracy of Tl-201 brain SPECT in distinguishing cerebral infections from lymphoma in patients with AIDS. Clin Nucl Med 27:81–86
143. Hoffman JM, Waskin HA, Schifter T, Hanson MW, Gray L, Rosenfeld S et al (1993) FDG-PET in differentiating lymphoma from nonmalignant central nervous system lesions in patients with AIDS. J Nucl Med 34:567–575
144. Villringer K, Jäger H, Dichgans M, Ziegler S, Poppinger J, Herz M et al (1995) Differential diagnosis of CNS lesions in AIDS patients by FDG-PET. J Comput Assist Tomogr 19:532–536
145. Heald AE, Hoffman JM, Bartlett JA, Waskin HA (1996) Differentiation of central nervous system lesions in AIDS patients using positron emission tomography (PET). Int J STD AIDS 7:337–346
146. O'Doherty MJ, Barrington SF, Campbell M, Lowe J, Bradbeer CS (1997) PET scanning and the human immunodeficiency virus-positive patient. J Nucl Med 38:1575–1583
147. Liu Y (2011) Demonstrations of AIDS-associated malignancies and infections at FDG PET-CT. Ann Nucl Med 25:536–546
148. Sathekge M, Goethals I, Maes A, van de Wiele C (2009) Positron emission tomography in patients suffering from HIV-1 infection. Eur J Nucl Med Mol Imaging 36:1176–1184
149. Shirai S, Yabe I, Kano T, Shimizu Y, Sasamori T, Sato K et al (2014) Usefulness of (11)C-methionine-positron emission tomography for the diagnosis of progressive multifocal leukoencephalopathy. J Neurol 261:2314–2318
150. Stenehjem E, Armstrong WS (2012) Central nervous system device infections. Infect Dis Clin North Am 26:89–110
151. Friedman WA, Vries JK (1980) Percutaneous tunnel ventriculostomy. Summary of 100 procedures. J Neurosurg 53:662–665
152. Lozier AP, Sciacca RR, Romagnoli MF, Connolly ES (2002) Ventriculostomy-related infections: a critical review of the literature. Neurosurgery 51:170–181; discussion 181–2
153. Dasic D, Hanna SJ, Bojanic S, Kerr RSC (2006) External ventricular drain infection: the effect of a strict protocol on infection rates and a review of the literature. Br J Neurosurg 20:296–300
154. Takeuchi S, Takasato Y, Masaoka H, Hayakawa T, Otani N, Yoshino Y et al (2010) Hemorrhagic

encephalitis associated with Epstein-Barr virus infection. J Clin Neurosci 17:153–154
155. Arrese I, Nuñez AP, Rivas JJ, Lobato RD (2004) Delayed brain abscess as a complication of a CSF shunt. Neurocirugia (Astur) 15:472–475
156. Thet Y, Myint W, Myint W, Hughes D, Crowe AV, Banerjee A (2008) Ventriculo-peritoneal shunt infection in a patient on hemodialysis. Hemodial Int 12:319–321
157. Kolić Z, Kukuljan M, Bonifačić D, Vukas D (2010) CSF liver pseudocyst as a complication of a ventriculoperitoneal shunt. Wien Klin Wochenschr 122: 641–644
158. Khan SA, Gretchel A, Govender H, Hartzenberg B (2009) Brain abscess and granuloma formation as late complications of retained ventricular catheter. Neurol India 57:489–492
159. Stoodley P, Braxton EE, Nistico L, Hall-Stoodley L, Johnson S, Quigley M et al (2010) Direct demonstration of Staphylococcus biofilm in an external ventricular drain in a patient with a history of recurrent ventriculoperitoneal shunt failure. Pediatr Neurosurg 46:127–132
160. Medina M, Viglietti AL, Gozzoli L, Lucano A, Ravasi L, Lucignani G et al (2000) Indium-111 labelled white blood cell scintigraphy in cranial and spinal septic lesions. Eur J Nucl Med 27:1473–1480
161. Wan DQ, Joseph UA, Barron BJ, Caram P, Nguyen AP (2009) Ventriculoperitoneal shunt catheter and cerebral spinal fluid infection initially detected by FDG PET/CT scan. Clin Nucl Med 34:464–465
162. Rehman T, Chohan MO, Yonas H (2011) Diagnosis of ventriculoperitoneal shunt infection using [F-18]-FDG PET: a case report. J Neurosurg Sci 55:161–163
163. Hamani C, Lozano AM (2006) Hardware-related complications of deep brain stimulation: a review of the published literature. Stereotact Funct Neurosurg 84:248–251
164. Real R, Linhares P, Fernandes H, Rosas MJ, Gago MF, Pereira J et al (2011) Role of Tc-sulesomab immunoscintigraphy in the management of infection following deep brain stimulation surgery. Neurol Res Int 2011:817951
165. Sundaresan N, Suite ND (1989) Optimal use of the Ommaya reservoir in clinical oncology. Oncology (Williston Park) 3:15–22; discussion 23
166. Shapiro WR, Posner JB, Ushio Y, Chemik NL, Young DF (1977) Treatment of meningeal neoplasms. Cancer Treat Rep 61:733–743
167. Obbens EA, Leavens ME, Beal JW, Lee YY (1985) Ommaya reservoirs in 387 cancer patients: a 15-year experience. Neurology 35:1274–1278
168. Lishner M, Perrin RG, Feld R, Messner HA, Tuffnell PG, Elhakim T et al (1990) Complications associated with Ommaya reservoirs in patients with cancer. The Princess Margaret Hospital experience and a review of the literature. Arch Intern Med 150:173–176
169. Mechleb B, Khater F, Eid A, David G, Moorman JP (2003) Late onset Ommaya reservoir infection due to Staphylococcus aureus: case report and review of Ommaya Infections. J Infect 46:196–198
170. Sampaio ALL, Araújo MFS, Oliveira CACP (2011) New criteria of indication and selection of patients to cochlear implant. Int J Otolaryngol 2011:573968
171. Yu KC, Hegarty JL, Gantz BJ, Lalwani AK (2001) Conservative management of infections in cochlear implant recipients. Otolaryngol Head Neck Surg 125:66–70
172. Tambyraja RR, Gutman MA, Megerian CA (2005) Cochlear implant complications: utility of federal database in systematic analysis. Arch Otolaryngol Head Neck Surg 131:245–250
173. Achiques MT, Morant A, Muñoz N, Marco J, Llópez I, Latorre E et al (2010) Cochlear implant complications and failures. Acta Otorrinolaringol Esp 61: 412–417
174. Antonelli PJ, Lee JC, Burne RA (2004) Bacterial biofilms may contribute to persistent cochlear implant infection. Otol Neurotol 25:953–957
175. Hirsch BE, Blikas A, Whitaker M (2007) Antibiotic prophylaxis in cochlear implant surgery. Laryngoscope 117:864–867
176. Rubin Grandis J, Branstetter BF, Yu VL (2004) The changing face of malignant (necrotising) external otitis: clinical, radiological, and anatomic correlations. Lancet Infect Dis 4:34–39
177. de Miguel-Martínez I, Ramos-Macías A, Borkoski Barreiro S (2008) Efficacy of heptavalent pneumococcal conjugate vaccine in children with cochlear implant. Acta Otorrinolaringol Esp 59:2–5
178. Rubin LG, Papsin B (2010) Cochlear implants in children: surgical site infections and prevention and treatment of acute otitis media and meningitis. Pediatrics 126:381–391
179. Hall-Stoodley L, Hu FZ, Gieseke A, Nistico L, Nguyen D, Hayes J et al (2006) Direct detection of bacterial biofilms on the middle-ear mucosa of children with chronic otitis media. JAMA 296:202–211
180. Shpizner BA, Holliday RA, Roland JT, Cohen NL, Waltzman SB, Shapiro WH (1995) Postoperative imaging of the multichannel cochlear implant. AJNR Am J Neuroradiol 16:1517–1524
181. Hoep LS, Merkus P, van Schie A, Rinkel RNPM, Smit CF (2006) The value of nuclear scans in cochlear implant infections. Eur Arch Otorhinolaryngol 263:895–899
182. Gamaletsou MN, Sipsas NV, Roilides E, Walsh TJ (2012) Rhino-orbital-cerebral mucormycosis. Curr Infect Dis Rep 14:423–434
183. Altini C, Niccoli Asabella A, Ferrari C, Rubini D, Dicuonzo F, Rubini G (2015) (18)F-FDG PET/CT contribution to diagnosis and treatment response of rhino-orbital-cerebral mucormycosis. Hell J Nucl Med 18:68–70
184. Mohindra S, Mohindra S, Gupta R, Bakshi J, Gupta SK (2007) Rhinocerebral mucormycosis: the disease spectrum in 27 patients. Mycoses 50:290–296
185. Howells RC, Ramadan HH (2001) Usefulness of computed tomography and magnetic resonance in

fulminant invasive fungal rhinosinusitis. Am J Rhinol 15:255–261
186. Silverman CS, Mancuso AA (1998) Periantral soft-tissue infiltration and its relevance to the early detection of invasive fungal sinusitis: CT and MR findings. AJNR Am J Neuroradiol 19:321–325
187. Hot A, Maunoury C, Poiree S, Lanternier F, Viard JP, Loulergue P et al (2011) Diagnostic contribution of positron emission tomography with [18F]fluorodeoxyglucose for invasive fungal infections. Clin Microbiol Infect 17:409–417
188. Lucente FE, Parisier SC, Chandler JR (1996) Malignant external otitis (Laryngoscope. 1968; 78:1257–1294). Laryngoscope 106:805–807
189. Le Clerc N, Verillaud B, Duet M, Guichard J-P, Herman P, Kania R (2014) Skull base osteomyelitis: incidence of resistance, morbidity, and treatment strategy. Laryngoscope 124:2013–2016
190. Carfrae MJ, Kesser BW (2008) Malignant otitis externa. Otolaryngol Clin North Am 41:537–549, viii–ix
191. Tsikoudas A, Davis BC (2009) Benign necrotizing otitis externa. Ear Nose Throat J 88, E18
192. Patmore H, Jebreel A, Uppal S, Raine CH, McWhinney P (2010) Skull base infection presenting with multiple lower cranial nerve palsies. Am J Otolaryngol 31:376–380
193. Adams A, Offiah C (2012) Central skull base osteomyelitis as a complication of necrotizing otitis externa: imaging findings, complications, and challenges of diagnosis. Clin Radiol 67:e7–e16
194. Grandis JR, Curtin HD, Yu VL (1995) Necrotizing (malignant) external otitis: prospective comparison of CT and MR imaging in diagnosis and follow-up. Radiology 196:499–504
195. Sreepada GS, Kwartler JA (2003) Skull base osteomyelitis secondary to malignant otitis externa. Curr Opin Otolaryngol Head Neck Surg 11: 316–323
196. Kohut RI, Lindsay JR (1979) Necrotizing ("malignant") external otitis histopathologic processes. Ann Otol Rhinol Laryngol 88:714–720
197. Sando I, Harada T, Okano Y, Saito R, Caparosa RJ (1981) Temporal bone histopathology of necrotizing external otitis. A case report. Ann Otol Rhinol Laryngol 90:109–115
198. Chang PC, Fischbein NJ, Holliday RA (2003) Central skull base osteomyelitis in patients without otitis externa: imaging findings. AJNR Am J Neuroradiol 24:1310–1316
199. Strashun AM, Nejatheim M, Goldsmith SJ (1984) Malignant external otitis: early scintigraphic detection. Radiology 150:541–545
200. Stokkel MP, Takes RP, van Eck-Smit BL, Baatenburg de Jong RJ (1997) The value of quantitative gallium-67 single-photon emission tomography in the clinical management of malignant external otitis. Eur J Nucl Med 24:1429–1432
201. Redleaf MI, Angeli SI, McCabe BF (1994) Indium 111-labeled white blood cell scintigraphy as an unreliable indicator of malignant external otitis resolution. Ann Otol Rhinol Laryngol 103:444–448
202. Galletti F, Cammaroto G, Galletti B, Quartuccio N, Di Mauro F, Baldari S (2015) Technetium-99m ((99m)Tc)-labelled sulesomab in the management of malignant external otitis: is there any role? Eur Arch Otorhinolaryngol 272:1377–1382, Springer, Berlin Heidelberg
203. Termaat MF, Raijmakers PGHM, Scholten HJ, Bakker FC, Patka P, Haarman HJTM (2005) The accuracy of diagnostic imaging for the assessment of chronic osteomyelitis: a systematic review and meta-analysis. J Bone Joint Surg Am 87:2464–2471
204. Glaudemans AWJM, Quintero AM, Signore A (2012) PET/MRI in infectious and inflammatory diseases: will it be a useful improvement? Eur J Nucl Med Mol Imaging 39:745–749
205. Lorenzen J, Buchert R, Bohuslavizki KH (2001) Value of FDG PET in patients with fever of unknown origin. Nucl Med Commun 22:779–783
206. Bleeker-Rovers CP, Vos FJ, de Kleijn EMHA, Mudde AH, Dofferhoff TSM, Richter C et al (2007) A prospective multicenter study on fever of unknown origin: the yield of a structured diagnostic protocol. Medicine (Baltimore) 86:26–38
207. Balink H, Collins J, Bruyn GA, Bruyn G, Gemmel F (2009) F-18 FDG PET/CT in the diagnosis of fever of unknown origin. Clin Nucl Med 34:862–868
208. Vanderschueren S, Del Biondo E, Ruttens D, Van Boxelaer I, Wauters E, Knockaert DDC (2009) Inflammation of unknown origin versus fever of unknown origin: two of a kind. Eur J Intern Med 20:415–418
209. Vos FJ, Bleeker-Rovers CP, Sturm PD, Krabbe PFM, van Dijk APJ, Cuijpers MLH et al (2010) 18F-FDG PET/CT for detection of metastatic infection in gram-positive bacteremia. J Nucl Med 51:1234–1240
210. Tewari A, Padma S, Sundaram PS (2012) The diagnostic role of 18-fluorodeoxyglucocose-positron emission tomography/computed tomography in occult bacteremia searching underlying primary disease. Ann Indian Acad Neurol 15:336–338
211. Akiyama K, Karaki M, Samukawa Y, Mori N (2013) Blindness caused by septic superior ophthalmic vein thrombosis in a Lemierre Syndrome variant. Auris Nasus Larynx 40:493–496
212. Tseng J-R, Lin C-W, Chen S-H, Yen T-H, Lin P-Y, Lee M-H et al (2015) Clinical usefulness of ^{18}F-FDG PET/CT for the detection of infections of unknown origin in patients undergoing maintenance hemodialysis. J Nucl Med 56:681–687
213. Goddard AJP, Tan G, Becker J (2005) Computed tomography angiography for the detection and characterization of intra-cranial aneurysms: current status. Clin Radiol 60:1221–1236
214. Cruz-Flores S (2014) Neurologic complications of valvular heart disease. Handb Clin Neurol 119:61–73
215. Goulenok T, Klein I, Mazighi M, Messika-Zeitoun D, Alexandra JF, Mourvillier B et al (2013) Infective endocarditis with symptomatic cerebral complications:

contribution of cerebral magnetic resonance imaging. Cerebrovasc Dis 35:327–336
216. Bruun NE, Habib G, Thuny F, Sogaard P (2014) Cardiac imaging in infectious endocarditis. Eur Heart J 35:624–632
217. Van Riet J, Hill EE, Gheysens O, Dymarkowski S, Herregods M-C, Herijgers P et al (2010) (18)F-FDG PET/CT for early detection of embolism and metastatic infection in patients with infective endocarditis. Eur J Nucl Med Mol Imaging 37:1189–1197
218. Kestler M, Muñoz P, Rodríguez-Créixems M, Rotger A, Jimenez-Requena F, Mari A et al (2014) Role of 18F-FDG PET in patients with infectious endocarditis. J Nucl Med 55:1093–1098
219. Asmar A, Ozcan C, Diederichsen ACP, Thomassen A, Gill S (2014) Clinical impact of 18F-FDG-PET/CT in the extra cardiac work-up of patients with infective endocarditis. Eur Heart J Cardiovasc Imaging 15:1013–1019
220. Özcan C, Asmar A, Gill S, Thomassen A, Diederichsen ACP (2013) The value of FDG-PET/CT in the diagnostic work-up of extra cardiac infectious manifestations in infectious endocarditis. Int J Cardiovasc Imaging 29:1629–1637
221. Orvin K, Goldberg E, Bernstine H, Groshar D, Sagie A, Kornowski R et al (2015) The role of FDG-PET/CT imaging in early detection of extra-cardiac complications of infective endocarditis. Clin Microbiol Infect 21:69–76
222. Xing XW, Zhang JT, Zhu F, Ma L, Yin DY, Jia WQ et al (2012) Comparison of diffusion-weighted MRI with 18F-fluorodeoxyglucose-positron emission tomography/CT and electroencephalography in sporadic Creutzfeldt-Jakob disease. J Clin Neurosci 19:1354–1357, Elsevier Ltd
223. Caobelli F, Cobelli M, Pizzocaro C, Pavia M, Magnaldi S, Guerra UP (2014) The role of neuroimaging in evaluating patients affected by Creutzfeldt-Jakob disease: a systematic review of the literature. J Neuroimaging 6:1–12
224. Thomas A, Klein JC, Galldiks N, Hilker R, Grond M, Jacobs AH (2006) Multitracer PET imaging in Heidenhain variant of Creutzfeldt-Jakob disease. J Neurol 253:258–260
225. Macfarlane RG, Wroe SJ, Collinge J, Yousry TA, Jäger HR (2007) Neuroimaging findings in human prion disease. J Neurol Neurosurg Psychiatry 78:664–670
226. Kao CH, Wang SJ, Mak SC, Shian WJ, Chi CS (1994) Viral encephalitis in children: detection with technetium-99m HMPAO brain single-photon emission CT and its value in prediction of outcome. AJNR Am J Neuroradiol 15:1369–1373
227. San Pedro EC, Mountz JM, Liu HG, Deutsch G (1998) Postinfectious cerebellitis: clinical significance of Tc-99m HMPAO brain SPECT compared with MRI. Clin Nucl Med 23:212–216
228. Nara T, Nozaki H, Nishimoto H (1990) Brain perfusion in acute encephalitis: relationship to prognosis studied using SPECT. Pediatr Neurol 6:422–424
229. Daaboul Y, Vern BA, Blend MJ (1998) Brain SPECT imaging and treatment with IVIg in acute post-infectious cerebellar ataxia: case report. Neurol Res 20:85–88
230. Hirayama K, Sakazaki H, Murakami S, Yonezawa S, Fujimoto K, Seto T et al (1999) Sequential MRI, SPECT and PET in respiratory syncytial virus encephalitis. Pediatr Radiol 29:282–286
231. Park JW, Choi YB, Lee KS (2004) Detection of acute Epstein Barr virus cerebellitis using sequential brain HMPAO-SPECT imaging. Clin Neurol Neurosurg 106:118–121
232. Anderson NE, Barber PA (2008) Limbic encephalitis – a review. J Clin Neurosci 15:961–971
233. Gast H, Schindler K, Z'graggen WJ, Hess CW (2010) Improvement of non-paraneoplastic voltage-gated potassium channel antibody-associated limbic encephalitis without immunosuppressive therapy. Epilepsy Behav 17:555–557
234. Ances BM, Vitaliani R, Taylor RA, Liebeskind DS, Voloschin A, Houghton DJ et al (2005) Treatment-responsive limbic encephalitis identified by neuropil antibodies: MRI and PET correlates. Brain 128:1764–1777
235. Wong KK, Tolia B, Bohnen N (2008) Chronic sequelae of herpes simplex encephalitis demonstrated on interictal F-18 FDG PET/CT. Clin Nucl Med 33:443–444
236. Meyer MA, Hubner KF, Raja S, Hunter K, Paulsen WA (1994) Sequential positron emission tomographic evaluations of brain metabolism in acute herpes encephalitis. J Neuroimaging 4:104–105
237. Cistaro A, Caobelli F, Quartuccio N, Fania P, Pagani M (2014) Uncommon 18F-FDG-PET/CT findings in patients affected by limbic encephalitis: hyper-hypometabolic pattern with double antibody positivity and migrating foci of hypermetabolism. Clin Imaging 39:1–5, Elsevier Inc
238. Wang HC, Zhao J, Zuo CT, Zhang ZW, Xue FP, Liu P et al (2009) Encephalitis depicted by a combination of C-11 acetate and F-18 FDG PET/CT. Clin Nucl Med 34:952–954
239. Davies MJ, Richardson PD, Woolf N, Katz DR, Mann J (1993) Risk of thrombosis in human atherosclerotic plaques: role of extracellular lipid, macrophage, and smooth muscle cell content. Br Heart J 69:377–381
240. Noguchi T, Kawasaki T, Tanaka A, Yasuda S, Goto Y, Ishihara M et al (2014) High-intensity signals in coronary plaques on noncontrast T1-weighted magnetic resonance imaging as a novel determinant of coronary events. J Am Coll Cardiol 63:989–999
241. Jarrett BR, Correa C, Ma KL, Louie AY (2010) In vivo mapping of vascular inflammation using multimodal imaging. PLoS One 5:2–9
242. Bentzon JF, Otsuka F, Virmani R, Falk E (2014) Mechanisms of plaque formation and rupture. Circ Res 114:1852–1866
243. Tuzcu EM, Schoenhagen P (2003) Acute coronary syndromes, plaque vulnerability, and carotid artery

disease: the changing role of atherosclerosis imaging. J Am Coll Cardiol 42:1033–1036
244. Fuster V, Moreno PR, Fayad ZA, Corti R, Badimon JJ (2005) Atherothrombosis and high-risk plaque: part I: evolving concepts. J Am Coll Cardiol 46: 937–954
245. Fayad ZA (2001) The assessment of the vulnerable atherosclerotic plaque using MR imaging: a brief review. Int J Cardiovasc Imaging 17:165–177
246. Choudhury RP, Fuster V, Badimon JJ, Fisher EA, Fayad ZA (2002) MRI and characterization of atherosclerotic plaque: emerging applications and molecular imaging. Arterioscler Thromb Vasc Biol 22:1065–1074
247. Bhatia V, Bhatia R, Dhindsa S, Dhindsa M (2003) Imaging of the vulnerable plaque: new modalities. South Med J 96:1142–1147
248. Ripa RS, Kjær A (2015) Imaging atherosclerosis with hybrid positron emission tomography/magnetic resonance imaging. Biomed Res Int 2015:914516, Hindawi Publishing Corporation
249. Yun M, Yeh D, Araujo LI, Jang S, Newberg A, Alavi A (2001) F-18 FDG uptake in the large arteries: a new observation. Clin Nucl Med 26:314–319
250. Mizoguchi M, Tahara N, Tahara A, Nitta Y, Kodama N, Oba T et al (2011) Pioglitazone attenuates atherosclerotic plaque inflammation in patients with impaired glucose tolerance or diabetes a prospective, randomized, comparator-controlled study using serial FDG PET/CT imaging study of carotid artery and ascending aorta. JACC Cardiovasc Imaging 4:1110–1118
251. Rudd JHF, Warburton EA, Fryer TD, Jones HA, Clark JC, Antoun N et al (2002) Imaging atherosclerotic plaque inflammation with [18F]-fluorodeoxyglucose positron emission tomography. Circulation 105: 2708–2711
252. Graebe M, Pedersen SF, Borgwardt L, Højgaard L, Sillesen H, Kjaer A (2009) Molecular pathology in vulnerable carotid plaques: correlation with [18]-fluorodeoxyglucose positron emission tomography (FDG-PET). Eur J Vasc Endovasc Surg 37:714–721
253. Pedersen SF, Graebe M, Fisker Hag AM, Højgaard L, Sillesen H, Kjaer A (2010) Gene expression and 18FDG uptake in atherosclerotic carotid plaques. Nucl Med Commun 31:423–429
254. Annovazzi A, Bonanno E, Arca M, Alessandria CD, Marcoccia A, Spagnoli LG et al (2006) Original article. Eur J Nucl Med Mol Imaging 33:117–126
255. Elmaleh D, Narula J, Babich JW, Petrov A, Fischman AJ, Khaw B et al (1998) Rapid noninvasive detection of experimental atherosclerotic lesions with novel 99m Tc-labeled diadenosine tetraphosphates. Proc Natl Acad Sci U S A 95:691–695
256. Tepe G, Duda SH, Meding J, Brehme U, Ritter J, Hanke H et al (2001) Tc-99m-labeled endothelin derivative for imaging of experimentally induced atherosclerosis. Atherosclerosis 157:383–392
257. Glaudemans AWJM, Bonanno E, Galli F, Zeebregts CJ, De Vries EFJ, Koole M et al (2014) In vivo and in vitro evidence that 99m Tc-HYNIC-interleukin-2 is able to detect T lymphocytes in vulnerable atherosclerotic plaques of the carotid artery. Eur J Nucl Med Mol Imaging 41:1710–1719
258. Luehmann HP, Pressly ED, Detering L, Wang C, Pierce R, Woodard PK et al (2014) PET/CT imaging of chemokine receptor CCR5 in vascular injury model using targeted nanoparticle. J Nucl Med 55:629–634
259. Bigalke B, Phinikaridou A, Andia ME, Cooper MS, Schuster A, Wurster T et al (2014) PET/CT and MR imaging biomarker of lipid-rich plaques using [64Cu]-labeled scavenger receptor (CD68-Fc). Int J Cardiol 177:287–291, Elsevier Ireland Ltd
260. Broisat A, Toczek J, Dumas LS, Ahmadi M, Bacot S, Perret P et al (2014) Imaging is a sensitive and reproducible tool for the detection of inflamed atherosclerotic lesions in mice. J Nucl Med 55:1678–1685
261. Nahrendorf M, Keliher E, Panizzi P, Zhang H, Hembrador S, Figueiredo J et al (2009) 18F-4V for PET-CT imaging of VCAM-1 expression in inflammatory atherosclerosis. JACC Cardiovasc Imaging 2:1213–1222
262. Tahara N, Mukherjee J, De Haas HJ, Petrov AD, Tawakol A, Haider N et al (2014) 2-deoxy-2-[18F] fluoro-D-mannose positron emission tomography imaging in atherosclerosis. Nat Med 20:215–219
263. Li X, Bauer W, Israel I, Kreissl MC, Weirather J, Richter D et al (2014) Positron emission tomography for noninvasive characterization of vulnerable plaques. Arterioscler Thromb Vasc Biol 34:1661–1667
264. Kircher MF, Grimm J, Swirski FK, Libby P, Gerszten RE, Allport JR et al (2008) Noninvasive in vivo imaging of monocyte trafficking to atherosclerotic lesions. Circulation 117:388–395
265. Kolodgie FD, Petrov A, Virmani R, Narula N, Verjans JW, Weber DK et al (2003) Atheroma with radiolabeled annexin V: a technique with potential for noninvasive imaging of vulnerable plaque. Circulation 108:3134–3139
266. Johnson LL, Schofield L, Donahay T, Narula N, Narula J (2005) V imaging for in vivo detection of atherosclerotic lesions in porcine coronary arteries. J Nucl Med 46:1186–1194
267. Isobe S, Tsimikas S, Zhou J, Fujimoto S, Sarai M, Branks MJ et al (2006) Noninvasive imaging of atherosclerotic lesions in apolipoprotein E – deficient and low-density-lipoprotein receptor – deficient mice with annexin A5. J Nucl Med 47:1497–1506
268. Somanath PR, Malinin NL, Byzova TV (2009) Cooperation between integrin alphavbeta3 and VEGFR2 in angiogenesis. Angiogenesis 12:177–185
269. Razavian M, Marfatia R, Mongue-din H, Tavakoli S, Sinusas AJ (2011) Integrin targeted imaging of inflammation in vascular remodeling. Arterioscler Thromb Vasc Biol 31:2820–2826
270. Golestani R, Zeebregts CJ, Terwisscha van Scheltinga AGT, Lub-de Hooge MN, van Dam GM, Glaudemans AWJM et al (2013) Feasibility of

vascular endothelial growth factor imaging in human atherosclerotic plaque using (89)Zr-bevacizumab positron emission tomography. Mol Imaging 12: 235–243
271. Beer AJ, Pelisek J, Heider P, Saraste A, Reeps C, Metz S et al (2014) PET/CT imaging of integrin αvβ3 expression in human carotid atherosclerosis. JACC Cardiovasc Imaging 7:178–187
272. Virmani R, Burke AP, Farb A, Kolodgie FD (2006) Pathology of the vulnerable plaque. J Am Coll Cardiol 47
273. Narula J, Nakano M, Virmani R, Kolodgie F, Petersen R, Newcomb R et al (2013) Histopathologic characteristics of atherosclerotic coronary disease and implications of the findings for the invasive and noninvasive detection of vulnerable plaques. J Am Coll Cardiol 61:1041–1051
274. New SEP, Goettsch C, Aikawa M, Marchini JF, Shibasaki M, Yabusaki K et al (2013) Macrophage-derived matrix vesicles: an alternative novel mechanism for microcalcification in atherosclerotic plaques. Circ Res 113:72–77
275. Otsuka F, Sakakura K, Yahagi K, Joner M, Virmani R (2014) Has our understanding of calcification in human coronary atherosclerosis progressed? Arterioscler Thromb Vasc Biol 34:724–736
276. Derlin T, Wisotzki C, Richter U, Apostolova I, Bannas P, Weber C et al (2011) In vivo imaging of mineral deposition in carotid plaque using 18F-sodium fluoride PET/CT: correlation with atherogenic risk factors. J Nucl Med 52:362–368
277. Dweck MR, Chow MWL, Joshi NV, Williams MC, Jones C, Fletcher AM et al (2012) Coronary arterial 18F-sodium fluoride uptake: a novel marker of plaque biology. J Am Coll Cardiol 59:1539–1548
278. Dweck MR, Jenkins WSA, Vesey AT, Pringle MAH, Chin CWL, Malley TS et al (2014) 18F-sodium fluoride uptake is a marker of active calcification and disease progression in patients with aortic stenosis. Circ Cardiovasc Imaging 7:371–378
279. Cocker MS, Ardle M, Bch MB, Spence JD, Lum C, Hammond RR et al (2012) Imaging atherosclerosis with hybrid [18F] fluorodeoxyglucose positron emission tomography/computed tomography imaging: what Leonardo da Vinci could not see. J Nucl Cardiol 19:1211–1225
280. Quirce R, Martínez-Rodríguez I, Banzo I, Jiménez-Bonilla J, Martínez-Amador N, Ibáñez-Bravo S et al (2015) New insight of functional molecular imaging into the atheroma biology: 18F-NaF and 18F-FDG in symptomatic and asymptomatic carotid plaques after recent CVA. Preliminary results. Clin Physiol Funct Imaging 2015 Jul 3. doi: 10.1111/cpf.12254. [Epub ahead of print]
281. Fernández-Ortiz A, Jiménez-Borreguero LJ, Peñalvo JL, Ordovás JM, Mocoroa A, Fernández-Friera L et al (2013) The Progression and Early detection of Subclinical Atherosclerosis (PESA) study: rationale and design. Am Heart J 166:990–998
282. Rischpler C, Nekolla SG, Beer AJ (2013) PET/MR imaging of atherosclerosis: initial experience and outlook. Am J Nucl Med Mol Imaging 3:393–396
283. Pedersen SF, Ludvigsen TP, Johannesen HH, Löfgren J, Ripa RS, Hansen AE et al (2014) Feasibility of simultaneous PET/MR in diet-induced atherosclerotic minipig: a pilot study for translational imaging. Am J Nucl Med Mol Imaging 4:448–458
284. Majmudar MD, Yoo J, Keliher EJ, Truelove J, Iwamoto Y, Sena B et al (2013) Polymeric nanoparticle PET/MR imaging allows macrophage detection in atherosclerotic plaques. Circ Res 112:755–761
285. Folke Pedersen S, Vikjær Sandholt B, Høgild Keller S, Espe Hansen A, Ettrup Clemmensen A, Sillesen H et al (2015) 64Cu-DOTATATE PET/MRI for detection of activated macrophages in carotid atherosclerotic plaques: studies in patients undergoing endarterectomy. Arterioscler Thromb Vasc Biol 35:1696–1703
286. Wu C1, Li F, Niu G, Chen X (2013) PET imaging of inflammation biomarkers. Theranostics 3:448–466
287. De Tiège X, Van Bogaert P, Aeby A, Salmon I, Parpal H, Poppe AY, Maris C, Lanthier S (2011) Primary angiitis of the central nervous system: neurologic deterioration despite treatment. Pediatr 127
288. Harkirat S, Anana SS, Indrajit LK, Dash AK (2008) Pictorial essay: PET/CT in tuberculosis. Indian J Radiol Imaging 18:141–147
289. Orbay H, Hong H, Zhang Y, Cai W (2013) Positron emission tomography imaging of atherosclerosis. Theranostics 3:894–902

Brain Tumors

11

Giampiero Giovacchini, Victoria Salati, and Valentina Garibotto

11.1 Introduction

Primary brain tumors are a heterogeneous group of neoplasms, each with its own biology, prognosis, and treatment. Among primary brain tumors, gliomas constitute the most frequent pathologic finding. On the basis of histological features, gliomas are dived into low-grade (I and II) and high-grade (III and IV) tumors. Prognosis worsens as tumor grading increases. Brain tumors may remain asymptomatic for long periods. The most common symptom is headache. Focal symptoms or signs take place when the neoplasm compresses the nearby cerebral parenchyma.

In this chapter we will review the main features of neoplasms of the central nervous system (CNS), and we will focus on the use of positron emission tomography (PET) and single photon emission computed tomography (SPECT) and of hybrid techniques, particularly PET with computed tomography (PET/CT) and PET with magnetic resonance (PET/MR) in combination with various radiopharmaceuticals for the diagnosis, treatment, and follow-up of gliomas (Table 11.1).

G. Giovacchini (✉)
Institute of Radiology and Nuclear Medicine, Stadtspital Triemli, Zurich, Switzerland
e-mail: giovacchinig@yahoo.com

V. Salati • V. Garibotto
Department of Medical Imaging, Geneva University and Geneva University Hospitals, Geneva, Switzerland

11.2 Brain Tumor Imaging

11.2.1 Radiolabeled Amino Acids

The rate of protein synthesis is increased in proliferating brain tumors, which makes its measurement an important target for in vivo imaging. Uptake in the normal cortex of all labeled amino acids is very low and their role in mediating an inflammatory response is much less important than for glucose. Thus, high specificity could be predicted. Active transport through the natural amino acid carrier and, to some extent, blood–brain barrier (BBB) disruption represent the mechanisms of tracer uptake (Table 11.2).

^{11}C-Methionine Methionine, an essential sulfur amino acid, is necessary for growth and development. ^{11}C-Methionine (^{11}C-MET) is by far the amino acid most frequently used for brain tumor imaging.

Diagnostic Accuracy The overall sensitivity of ^{11}C-MET PET for distinguishing gliomas from nonmalignant lesions has been estimated to be around 75–95 %, with somewhat lower values reported in low-grade gliomas, where uptake

A. Ciarmiello, L. Mansi (eds.), *PET-CT and PET-MRI in Neurology*,
DOI 10.1007/978-3-319-31614-7_11

Table 11.1 Clinical indications to imaging gliomas

Pre-therapy
1. Diagnosis
2. Noninvasive tumor grading
3. Guidance for stereotactic biopsy
4. Surgical planning
5. Identification of metabolically active tumor (or biological target volume, BTV) for radiotherapy planning
Post-therapy
1. Identification of residual tumor
2. Differential diagnosis between tumor recurrence and radiation necrosis
3. Evaluation of response to chemotherapy
4. Prediction of survival

Table 11.2 Most common current radiotracers for brain tumor imaging

Biological process	Radiotracer
Glucose transport across BBB and metabolism	[^{18}F]-Fluodeoxyglucose ([^{18}F]-FDG)
Amino acid transport and protein synthesis	[^{11}C]-Leucine ^{11}C-Methionine (^{11}C-MET) [^{123}I]-Alpha-methyltyrosine ([^{123}I]-IMT) [^{18}F]-Fluoroethyltyrosine ([^{18}F]-FET) [^{11}C]-Alpha-methyltryptophan [^{18}F]-Proline
Amino acid transport and dopamine metabolism	[^{18}F]-Fluoro-L-3,4-dihydroxyphenylalanine ([^{18}F]-DOPA)
Cellular proliferation	3-Deoxy-3-[^{18}F]-fluorothymidine ([^{18}F]-FLT) [^{18}F]-2-Fluoro-5-methyl-1-beta-d-arabinofuranosyluracil ([^{18}F]-FMAU)
Lipid metabolism	^{11}C-Choline/ [^{18}F]-fluorocholine
Hypoxia	[^{18}F]-Fluoromisonidazole ([^{18}F]-FMISO) [^{123}I]-Iodoazomycin arabinoside ([^{123}I]-IAZA) [^{18}F]-Azomycin arabinoside ([^{18}F]-FAZA) [^{64}Cu]-Methylthiosemicarbazone ([^{64}Cu]-ATSM)
Somatostatin receptor type 2 expression in meningiomas	[^{68}Ga]-DOTATOC [^{68}Ga]-DOTATATE

may occasionally be negligible. More interestingly, specificity of ^{11}C-MET PET ranged between 87 and 100 % [35].

Grading On the other hand, the predictive value of ^{11}C-MET PET for grading is limited. Several studies showed that ^{11}C-MET is taken up by gliomas irrespective of grade and that there is sizeable overlap in uptake values between low-grade and high-grade gliomas. Semiquantitative analysis may help differentiating high-grade and low-grade gliomas in group analysis [35].

Prognosis In grades II and III gliomas, higher tumor to contralateral count ratios are associated with reduced survival. The prognostic power of ^{11}C-MET was stronger than that of [^{18}F]-fluorodeoxyglucose ([^{18}F]-FDG) [34, 58] (Fig. 11.1).

Tumor Extent Determination The critical factor in determining the edges of the tumors is the method used for distinguishing significant from negligible tracer uptake. There is currently no consensus on the best method. Visual qualitative and several semiquantitative methods have been adopted: fixed percent threshold value of tumor uptake, tumor/non-tumor ratios, standardized uptake values (SUV), and automatic software-based segmentation algorithms are some examples of such techniques. Integrating [^{11}C]-MET PET with MR images is useful for planning surgery, with ensuing clinical impact in about 80 % of the procedures. Integration of ^{11}C-MET PET with morphological imaging was also useful for defining the radiotherapy plan [45].

Tumor Biopsy Although the poor relation between ^{11}C-MET uptake and grading does not allow predicting the highest tumor grade, ^{11}C-MET PET may be used to reduce the number of required biopsy attempts and to reduce the risk of damaging functional areas in patients with brain tumors [45].

Tumor Recurrence Versus Radiation Injury Because of limitations of [^{18}F]-FDG for discriminating recurrent tumor from radiation injury,

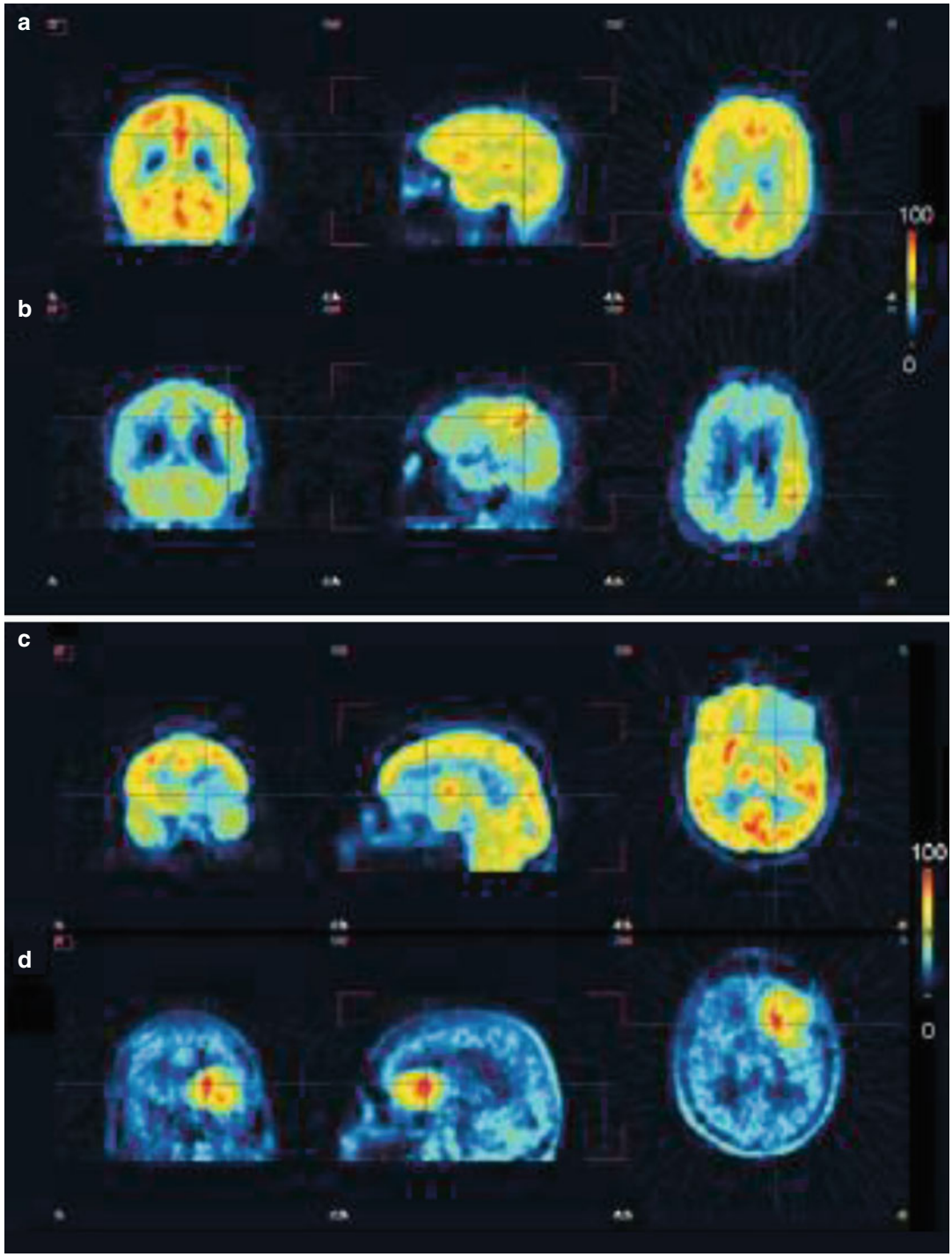

Fig. 11.1 Combined [^{18}F]-FDG (*upper row*) and ^{11}C-MET (*lower row*) PET studies. Patient #1 (**a**, **b**) displays tumor recurrence of the primary glioblastoma grade IV, which is easily detectable with ^{11}C-MET (**b**) but not on [^{18}F]-FDG (**a**). Patient #2 (**c**, **d**) is affected by a primary oligoastrocytoma grade II, which is hot on ^{11}C-MET PET (**d**) and cold on [^{18}F]-FDG PET (**c**) (Adapted from Van Laere et al. [58])

most authors prefer today using ^{11}C-MET PET. Comparative evaluations show a greater accuracy of ^{11}C-MET PET than [^{18}F]-FDG PET for the differential diagnosis [54].

11.2.2 O-(2-[^{18}F]-Fluoroethyl)-L-Tyrosine ([^{18}F]-FET) and 3-[^{123}I]-Alpha-Methyltyrosine ([^{123}I]-IMT)

[^{18}F]-FET is an artificial amino acid that is taken up into neoplastic cells, but it is not incorporated into proteins, in contrast to natural amino acids, such as ^{11}C-MET, which has a 15 % incorporation rate [26, 61].

[^{18}F]-FET PET was shown to be more accurate than [^{123}I]-alpha-methyltyrosine, [^{18}F]-FDG, [^{18}F]-fluorothymidine, and [^{18}F]-fluorocholine to detect brain tumors.

A recent meta-analysis of published data of 13 studies on the use of [^{18}F]-FET PET in primary brain tumor including 462 patients showed sensitivity and specificity of 82 % and 76 %, respectively. The mean and maximum tumor-to-background ratio (TBR_{mean} and TBR_{max}) were significantly lower in grade I–II gliomas as compared with III–IV gliomas [15].

The analysis of time–activity curves obtained through dynamic acquisition allows improving the differentiation between low- and high-grade gliomas. Early (<15 min) maximal uptake followed by a decreasing curve has been related to high-grade glioma, and late (>15 min) maximal uptake followed by a cumulative curve has been related to low-grade tumor [31].

[^{18}F]-FET imaging was also shown to have prognostic implications. In low-grade gliomas, baseline low [^{18}F]-FET uptake was predictive of longer time to progression and time to malignant transformation; on the contrary, high uptake predicted rapid conversion into a high-grade glioma [19]. [^{18}F]-FET can be used to quantify residual tumor volume after surgery, and postsurgical tumor volume determined by PET predicts progression-free and overall survival [44].

Table 11.3 Factors affecting uptake of radiopharmaceuticals in gliomas

1. Glucose metabolic rate
2. Protein synthesis rate
3. DNA proliferation rate
4. Membrane (lipid) proliferation rate
5. Blood–brain barrier integrity
6. Histological grade
7. Blood perfusion/blood volume
8. Expression of membrane transporters
9. Oxygen tissue concentration (hypoxia)
10. Dimension of the lesion (partial volume effect)
11. Radiotherapy treatment
12. Treatment with steroids or oncologic drugs
13. Necrotic areas
14. Expression of catecholamine binding sites

Some amino acid-derived radiopharmaceuticals (e.g., [^{123}I]-IMT) can also be labeled with single photon emitters for SPECT, allowing a less expensive, more widely accessible technique for imaging protein synthesis in brain tumors. As expected, worse tumor delineation was obtained in comparison to either ^{11}C-MET or [^{18}F]-FET. However, high [^{123}I]-IMT uptake post-tumor resection is associated with shorter survival [60] (Table 11.3).

Among other amino acid tracers, a growing important role is being played by [^{18}F]-fluorodopa ([^{18}F]-FDOPA), which is also sensitive to dopamine metabolism. Other than the high physiological uptake in the striatum, this tracer also displays low uptake in all the remaining brain areas. [^{18}F]-DOPA PET/CT is highly sensitive and specific for detection of glioma recurrence, it is superior to [^{18}F]-FDG, and it is especially advantageous in patients with low-grade gliomas [32, 53] (Figs. 11.2 and 11.3).

Tumor Proliferation Increased cell proliferation rate is a well-known hallmark of cancer. 3-Deoxy-3-[^{18}F]-fluorothymidine ([^{18}F]-FLT) offers the advantages of [^{18}F]-labeling and a favorable radiometabolite profile. Kinetic analysis showed that patients with brain tumors have increased tracer incorporation (K_i). In high-grade tumors where blood flow is also increased, the

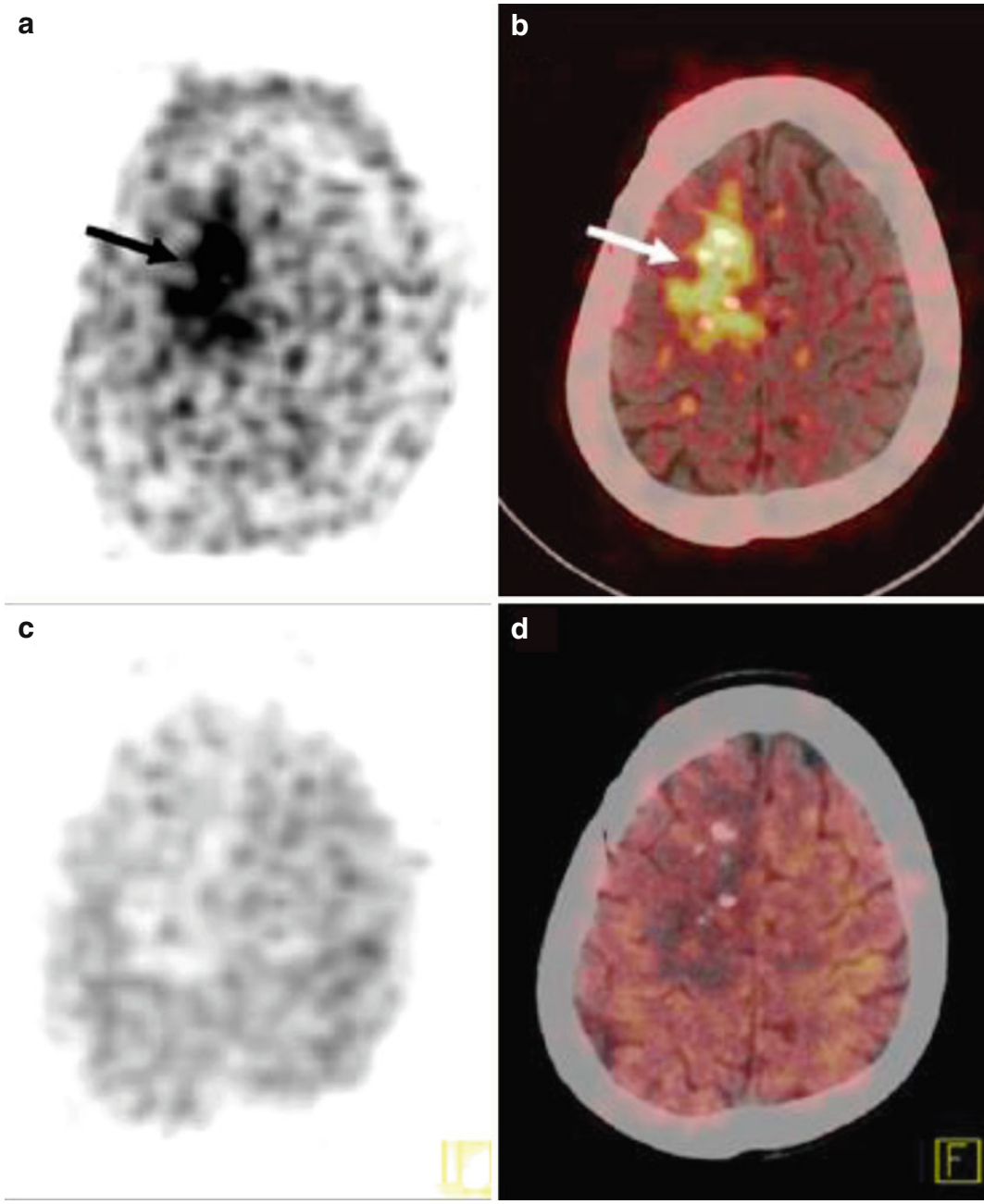

Fig. 11.2 Combined [^{18}F]-DOPA (*upper row*) and [^{18}F]-FDG (*lower row*) PET studies. A 27-year-old man with right frontal grade II oligoastrocytoma treated primarily with surgery and radiotherapy, presented with clinical suspicion of recurrence. Transaxial [^{18}F]-DOPA PET (**a**) and PET/CT (**b**) images show tracer accumulation in the right frontal lobe lesion (*arrows*) suggestive of recurrence. Transaxial [^{18}F]-FDG PET (**c**) and PET/CT (**d**) images show no abnormal focus of tracer uptake and are negative for recurrence. The patient underwent reoperation and was found to have recurrent grade III glioma (anaplastic astrocytoma) on histopathology (Adapted from Karunanithi et al. [32])

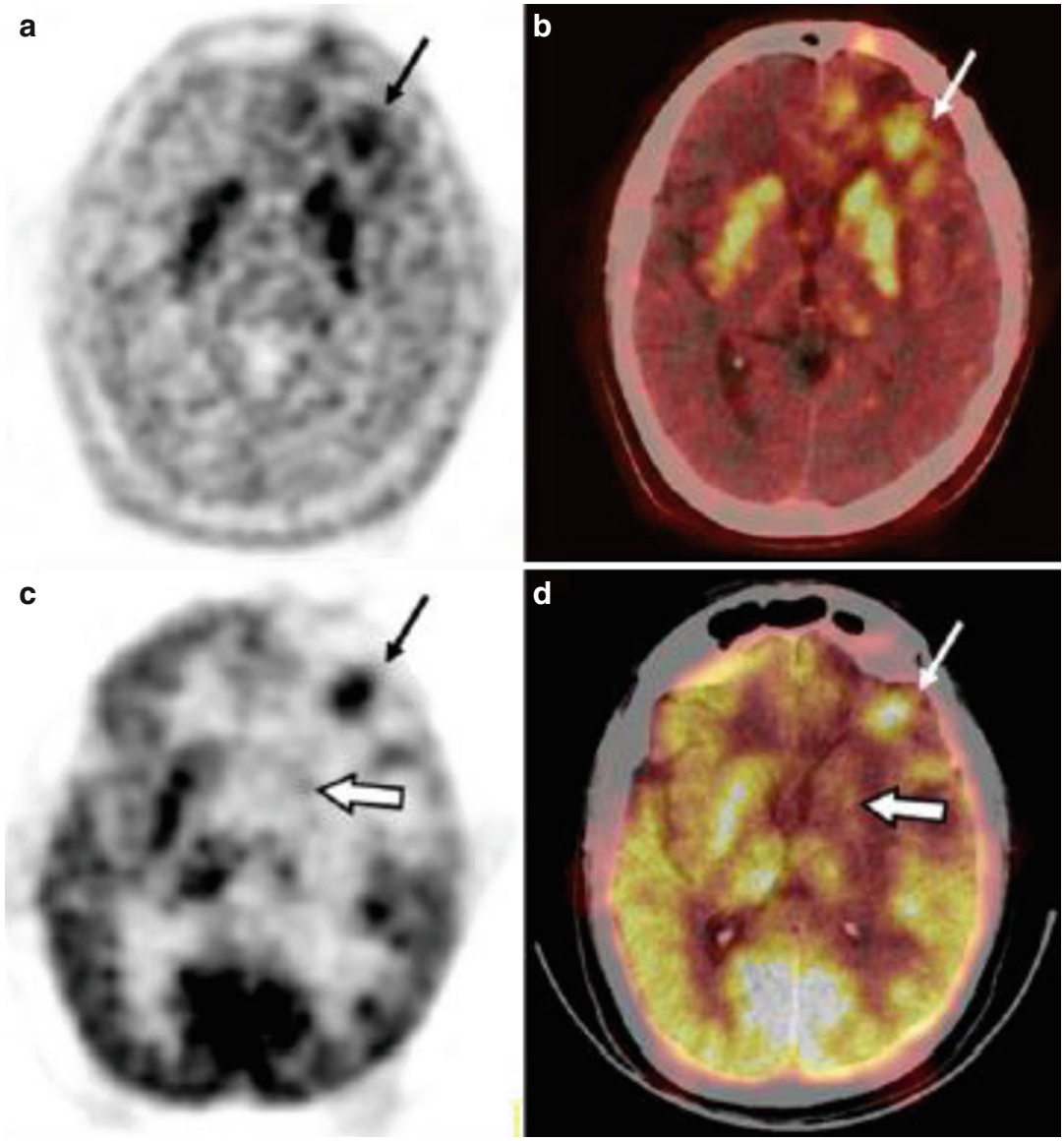

Fig. 11.3 Combined [^{18}F]-DOPA (*upper row*) and [^{18}F]-FDG (*lower row*) PET studies. A 44-year-old man with left frontal grade IV glioblastomas multiforme treated primarily with surgery, radiotherapy, and temozolomide. He presented 18 months later with progressive severe headache. Transaxial [^{18}F]-FDOPA PET (**a**) and PET/CT (**b**) images show tracer accumulation in the left frontal lesion (*arrow*), suggestive of recurrence. Transaxial [^{18}F]-FDG PET (**c**) and PET/CT (**d**) images also show tracer accumulation in a left frontal lesion (*small arrows*), suggestive of recurrence. The patient died within 5 months of PET/CT with progressive neurological weakness. Both [^{18}F]-FDOPA PET/CT and [^{18}F]-FDG PET/CT were true positive for recurrence in this patient. Note the decrease in [^{18}F]-FDG uptake in the ipsilateral striatum (*large arrows*) due to postradiotherapy changes (Adapted from Karunanithi et al. [32])

increased tracer incorporation may partially be related to blood flow rather than metabolism [38] (Table 11.4).

[^{18}F]-FLT had slightly lower (83 %) sensitivity than ^{11}C-MET (88 %) for detection of gliomas, and both tracers have a specificity of 100 %. SUV_{max} for ^{11}C-MET was significantly higher in high-grade gliomas than in low-grade gliomas, although there was a large overlap. For [^{18}F]-FLT, the group difference was larger. On the contrary, [^{18}F]-FLT was slightly superior to ^{11}C-MET for tumor grading [24].

Table 11.4 Most important favorable and unfavorable characteristics of common current radiopharmaceuticals for brain tumor imaging

	Advantages	Disadvantages
[^{18}F]-FDG	Easily available, overall good accuracy, good quality images Allows tumor grading Correlates with prognosis	High physiological uptake in the normal brain False positive by radiotherapy necrosis and infection Limited role for definition of radiotherapy plan
Amino acid tracers	Available for PET and some limited availability for SPECT Negligible uptake in the normal brain Optimal tumor delineation and contrast Uptake correlates with prognosis Very high negative predictive value for distinguishing recurrence from necrosis Useful for definition of radiotherapy plan	Tracer uptake is poorly affected by tumor grade Uptake may be similar in low-grade gliomas and nonmalignant tumors
[^{18}F]-FLT	Negligible uptake in the normal brain Optimal tumor delineation and contrast Superior to amino acid tracers for grading Allows differential diagnosis between tumor recurrence and necrosis	Uptake heavily affected by BBB integrity Kinetic analysis with metabolite correction may be required
Other tracers (radiolabeled choline, hypoxia tracers, serotonin receptor tracers)	Capability to investigate other metabolic pathways of brain tumor metabolism	Presently, still experimental in the clinical setting

11.2.3 [^{18}F]-Fluorodeoxyglucose ([^{18}F]-FDG)

PET with [^{18}F]-FDG allows measurement of the cerebral metabolic rate for glucose (CMRglc). [^{18}F]-FDG was the first PET tracer used for imaging brain tumors, and it is still widely used nowadays, after about 40 years. The 2-deoxyglucose model was defined by Sokoloff following autoradiographic experiments in rats [51]. Using arterial input function, dynamic scanning, and kinetic analysis, it is possible to obtain CMRglc (mg/100 g/min) [30, 51]. Using noninvasive approaches and a single static acquisition, SUV and the tumor/non-tumor ratio are the most commonly semiquantitative indices computed (Tables 11.5 and 11.6).

Diagnosis and Grading Early studies in brain tumor patients stressed the importance of the functional information provided by PET compared to morphologic neuroradiological techniques. Di Chiro et al. first used PET with [^{18}F]-FDG in 23 patients with cerebral gliomas. All ten high-grade gliomas demonstrated focal tracer uptake that was easily visible. The 13 low-grade gliomas had significantly lower CMRglc and no visible hot spot. In those early times, these results were considered as a major achievement because noninvasive grading of brain tumors was much less intuitive as nowadays. Sensitivity and specificity were 94 and 77 % [30] (Table 11.7).

Brain tumors may induce suppression of metabolic activity in the nearby normal and edematous tissue. Reduced glucose metabolism may occur also in the normal brain tissue remote, but functionally linked to the site of the tumor (crossed cerebellar diaschisis).

Tumor Recurrence Versus Radiation Necrosis Early studies showed that CMRglc was increased in patients with tumor recurrence and low in patients with necrosis [42]. Delayed imaging (90 min postinjection) increased the tumor-to-cortex contrast. Even though these results were confirmed in other studies, false positives were also reported because increased [^{18}F]-FDG accumulation may occur following radiotherapy.

The use of [^{18}F]-FDG for treatment planning remains controversial in light of the current

Table 11.5 Characteristics of quantitative and semiquantitative brain PET studies with [^{18}F]-FDG

	Quantitative studies	Qualitative studies
Arterial input function	Necessary	Not necessary
Acquisition	Dynamic (frames ranging from 30 s to 5 min for a total of 60 min)	Static (10–15 min acquisition 45-min postinjection)
Glycemia	Necessary	Not necessary
Parameters	CMRglc (mg/glc/100 g brain tissue)	Visual analysis SUV Tumor-to-non-tumor ratio
Data analysis	Time-consuming and technically challenging computer programming	None to simple (ROI analysis)
Diagnostic yield	Greater accuracy than semiquantitative analysis Greater clinical impact not proven	Sufficient for the vast majority of clinical cases
Metabolic specificity	Not specific for tumor	Not specific for tumor
Advantages/pitfalls	Potentially very accurate/logistically demanding	Simple derivation/sensitive to many parameters
Application	Preferred for research studies and group analysis	Preferred for clinical diagnostic routine and single-subject evaluation

Table 11.6 Sensitivity and specificity for diagnosis of brain gliomas/gliomas recurrence for most common PET tracers[a]

Tracer	Sensitivity (95 % CI)	Specificity (95 % CI)	Indication	Reference	Study
[^{18}F]-FDG	94 %	77 %	Diagnosis	[14]	Monocentric
[^{18}F]-FDG	75 %	81 %	Necrosis vs. recurrence	[11]	Monocentric
[^{18}F]-FDG	0.77 (0.66–0.85)	0.78 (0.54–0.91)	Necrosis vs. recurrence	[40]	Meta-analysis
[^{11}C]-MET	0.70 (0.50–0.84)	0.93 (0.44–1.0)	Necrosis vs. recurrence	[40]	Meta-analysis
[^{11}C]-MET	75–95 % (range)	87–100 % (range)	Diagnosis	[28]	Review
[^{18}F]-FET	0.82 (0.74–0.88)	0.76 (0.44–0.92)	Diagnosis	[15]	Meta-analysis
[^{18}F]-FLT	79 %	63 %	Diagnosis	[12]	Monocentric

[a]Note that these values should be taken cautiously because they depend from several variables, including gold standard, clinical indication, tumor grade and dimension, sample size, analysis method, and type of study (single center, multicenter, or meta-analysis). Multitracer single studies are generally more informative for the comparison between two tracers. For these reasons, only some explicative studies are cited

widespread use of amino acid tracers. [^{18}F]-FDG might be of special interest in high-grade gliomas exhibiting marked intratumoral heterogeneity where hot spots could be possible targets for dose escalation.

Prognostic Value and Response to Therapy

Several studies indicate that glucose metabolism, at initial presentation, at recurrence, or in response to therapy, is predictive of survival. The semiquantitative evaluation in pretreatment [^{18}F]-FDG PET provides significant additional prognostic information in newly diagnosed high-grade tumors, it is statistically more robust than the visual evaluation, and it is independent of traditional prognostic factors. The mean survival time of patients exhibiting high CMRglu was shorter than in patients with low CMRglu [43]. In the subgroup of high-grade gliomas, it was possible to divide patients into a group with low and another with high metabolic activity with 1-year survival rates of 78 % and 29 %, respectively [3].

PET was useful for monitoring the response to chemotherapy. A recent publication based on the National Oncologic PET Registry examined retrospectively data from 479 patients with primary brain tumors (72 %) or brain metastasis (28 %)

Table 11.7 Most common semiquantitative parameters, derivation, and main characteristics

Parameter	Derivation	Advantages	Disadvantages
Standardized uptake value (SUV)	ROI placed on any brain region. The uptake is normalized to the injected dose and body mass weight	Automatically computed	Sensitive to many parameters, primarily successful tracer injection, interval from injection time, and scan time, glycemia, and variation in the input function
Tumor-to-background ratio (TBR) or tumor-to-normal cortex ratio (T/N)	Ratio between the tumor ROI and the contralateral (or other reference) normal brain region	Many global biases that affect the SUV are canceled out as the ratio is computed	Influenced by perfusion/blood volume effects
Tumor-to-white matter ratio	Ratio between the tumor ROI and a reference white matter region	See above	See above Can only be applied to tumors that are strictly confined to gray matter
Parametric imaging	Kinetic analysis	Potentially very accurate	Very time consuming Sensitive to biases of the input function No clear advantage for the clinical routine. Used only in research protocols Examples: CMRglc for [^{18}F]-FDG or K_i for [^{18}F]-FLT

and found that overall, [^{18}F]-FDG PET imaging changed the intended management in 38 % of patients [29].

Radiolabeled Choline Choline is a phospholipid precursor and participates to membrane proliferation. The radiolabeled tracer (either ^{11}C-choline or [^{18}F]-fluorocholine) displayed an excellent capability to delineate the tumor contours due to the negligible uptake in the normal brain. However, increased tracer uptake may occur also in brain metastasis and meningiomas.

Presently there are discrepant findings on the issue whether increased lipid metabolism, as measured by PET/CT with radiolabeled, predicts [23, 41] or does not predict tumor grade [56]. Higher ^{11}C-choline uptake has been reported in high-grade gliomas compared to low-grade gliomas [23]. This result was confirmed in a multitracer study; tracer uptake was significantly higher in high-grade gliomas than in low-grade gliomas for ^{11}C-choline, but not for [^{18}F]-FDG [41]. However, ^{11}C-choline PET/CT could not reliably differentiate between low-grade gliomas and benign lesions because of the low uptake in low-grade tumors [41]. Another multitracer study compared ^{11}C-MET, ^{11}C-choline, and [^{18}F]-FDG. Whereas all three tracers showed a similar correlation between the tumor-to-normal cortex ratio and tumor grade in astrocytic and oligodendroglial tumors, ^{11}C-MET proved to best enable the straightforward visual localization of hot lesions [33].

Imaging Tumor Hypoxia Several bioreductive radiopharmaceuticals have been evaluated as hypoxia tracers. The common feature of these different tracers is that tissue binding increases as tissue oxygen decreases.

PET studies of brain tumor hypoxia are limited and focused mainly to the use of [^{18}F]-fluoromisonidazole ([^{18}F]-FMISO) [57]. Increased [^{18}F]-FMISO tumor uptake is generally found in the periphery but not in the necrotic center of glioblastomas multiforme. The latter finding is expected, because only peripheral viable cells are able to accumulate [^{18}F]-FMISO, and delivery to necrotic tissue is low [8].

Hypoxic volume measured with [^{18}F]-FMISO, that is, the voxels in the PET image with values higher than an arbitrary or predefined threshold, and the area of contrast enhancement in T1-weighted MR predict survival. [^{18}F]-FMISO uptake is greater in high-grade gliomas than in low-grade gliomas [52].

Imaging Somatostatin Receptors in Meningiomas Radiotracers able to visualize somatostatin receptors can be used for the delineation of meningiomas, based on the high expression of somatostatin receptor subtype 2 in these brain tumors [27]. The most commonly used tracer for this purpose is [^{68}Ga]-DOTATOC. PET imaging might detect lesions, with a higher sensitivity as compared with contrast-enhanced MRI, and help planning target volumes for radiation therapy, accurately distinguishing active meningioma tissue from surrounding postoperative tissue [1, 36]. The tracer has low intracranial background signal, given that somatostatin receptors are not expressed in the brain, except for the pituitary gland.

11.3 Additional Value of SPECT-CT and PET-CT Versus SPECT and PET Stand Alone

Radionuclide imaging has per se the capability of identifying disease in the early phase of disease, because biochemical dysfunctions typically occur before loss of structural function. Adding CT scan provides two major advantages: mainly it improved correction for attenuation of photons and secondarily it enables to locate on anatomical marks brain areas with abnormal functionality.

Low-dose CT is generally acquired with a tube current of 20–40 mA and tube voltage of about 120–140 kV; it is associated with low radiation doses of 1–4 mSv and is sufficient for anatomic referencing of SPECT lesions and attenuation correction [9]. The use of low-dose, nonenhanced spiral CT can be recommended in most SPECT/CT and PET/CT studies since virtually all patients referred to PET/CT or SPECT/CT will have already performed a diagnostic CT or MR. In the opposite case, diagnostic CT with contrast media should be performed [9].

So far, data on the added value of hybrid PET/CT and SPECT/CT over the stand-alone PET and SPECT remain rather limited. In general, individual CT scan-based attenuation correction may be particularly important for tracers with important regional variations in binding (such as [^{18}F]-FDOPA), but the same could apply to tracers that display more homogenous distribution, such as [^{18}F]-FDG or many amino acid tracers. It has been shown that attenuation correction based on individual CT scans produces more accurate results than attenuation correction based on ellipse-based Chang method [25].

One study showed that SPECT/CT could be useful to locate tumors in the presurgical setting and that this information could be transferred to the definition of the radiotherapy plan and for monitoring therapy. SPECT/CT technique allows to distinguish brain tumors and from other brain region with physiological uptake of the radiotracer, such as choroid plexus and venous sinuses, with a proven clinical impact on management in 43 % of patients [16].

11.4 PET/MRI: The New Modality of Choice for Brain Tumor Imaging?

PET/MRI tomographs represent the latest development in hybrid molecular imaging, opening new perspectives for clinical and research applications and attracting a large interest within the medical community [48, 59]. This new hybrid modality is expected to play a relevant role in a number of clinical applications in oncology, cardiology, and neuroimaging. Indeed, for brain imaging, MRI is the

"morphological" modality of choice for the investigation of brain lesions and clearly outperforms the non-contrast-enhanced CT which is usually coupled to PET studies in the current hybrid PET/CT examinations [18]. MRI provides not only an excellent soft tissue contrast, enhanced by the use of gadolinium-based contrast agents, but also visualizes white matter tracts, by diffusion tensor imaging (DTI), of utmost importance in surgical planning. In addition, a number of functional parameters can also be obtained by MRI, namely, perfusion, diffusion, and metabolic changes using MR spectroscopy.

11.4.1 PET/MRI Integrated Systems

Even if the idea of hybrid PET/MRI imaging is not new, and the first prototypes for small animal imaging date back to the early 1990s, the first hybrid acquisition in humans in a dedicated brain system has been realized in 2008 [49]. This is due to the major challenges arising when bringing these two technologies together, namely, the intrinsic incompatibility of photomultiplier technology with the magnetic field.

Different solutions have been adopted and can be grouped in two categories:

1. Simultaneous systems in which the PET is within the magnetic field and replacing the PET detection system, classically based on photomultipliers, by magnetic field-insensitive avalanche photodiodes or silicon-based elements [13, 47]
2. Sequential systems, in which each component (MRI and PET) is almost identical to standard standalone systems, provided proper electromagnetic shielding [62]

While the first solution has the clear advantage of simultaneous acquisition of both PET and MRI, with an overall reduction of total examination time, the second solution could be adopted without changes in the PET technology and allowed time-of-flight (TOF) imaging since the beginning. One of the two simultaneous tomographs currently available now also provides TOF technology [47].

11.4.2 PET/MRI Studies in Brain Oncology

Only a few studies have so far investigated the information provided by hybrid PET/MRI for brain tumor assessment and they are recapitulated in Table 11.8.

They overall show the feasibility of intracranial mass characterization by integrated PET/MRI also for presurgical and radiation therapy planning and also in pediatric patients (two studies targeted specifically this population). The majority of studies included patients with glioma and a subpopulation of patients with meningiomas, using a variety of PET tracers. The studies comparing PET/MRI output with PET/CT overall show that, despite systematic quantitative differences with PET/CT, mainly due to the attenuation correction strategy adopted, the image contrast and visual interpretation of the images obtained with PET/MRI are comparable to PET/CT.

The added value of integrated PET/MRI tomograph compared with the current standard (fused PET and MRI images acquired in separate sessions) has not been specifically investigated yet, and no cost-effectiveness studies are available yet.

Finally, most of these studies adopted fully diagnostic protocols of each modality, resulting in lengthy acquisitions. A key issue, to be addressed in future studies and with a wider practice with integrated tomographs, will be the identification of complementary/redundant information provided by PET and MRI, in order to develop truly integrated protocols that take advantage of the strongest assets of each modality, avoiding the duplication of data [4].

Hybrid PET/MRI systems are also the ideal setting for answering specific research questions,

Table 11.8 PET/MRI studies in brain tumors

Study	N of patients evaluated for intracranial lesions	Clinical indications	Type of PET-MR tomograph	Radiotracers	Results
Boss et al. [7]	4 adult patients	Staging	Simultaneous (whole-body 3 T MR with BrainPET insert, Siemens Healthcare)	[^{11}C]-MET	Comparison of DTI acquired simultaneously to PET or after the removal of the PET insert: the presence of the insert induces some artifacts but does not hinder diagnostic interpretation of DTI images
Boss et al. [6]	10 adult patients	Staging	Simultaneous (whole-body 3 T MR with BrainPET insert, Siemens Healthcare)	[^{11}C]-MET [^{68}Ga]-DOTATOC	Comparison with PET/CT data: PET/MRI data were strictly comparable, also for quantitative aspects and calculated tumor volumes
Schwenzer et al. [50]	28 adult patients	Staging and restaging	Simultaneous (whole-body 3 T MR with BrainPET insert, Siemens Healthcare)	[^{18}F]-FDG [^{11}C]-MET [^{68}Ga]-DOTATOC	Comparison of PET/MRI and PET/CT data: comparable tumor delineation with [^{11}C]-methionine; additional lesions were found in [^{68}Ga]-DOTATOC-PET images obtained with PET/MRI (presumably related to the higher resolution of the PET insert)
Neuner et al. [39]	4 adult patients	Staging and restaging of gliomas	Simultaneous (whole-body 3 T MR with BrainPET insert, Siemens Healthcare)	[^{18}F]-FET	Description of acquisition protocols, obtaining diagnostic quality and comprehensive evaluation of gliomas in one examination
Thorwarth et al. [55]	3 adult patients	Restaging and radiation therapy planning of atypical meningiomas	Simultaneous (whole-body 3 T MR with BrainPET insert, Siemens Healthcare)	[^{68}Ga]-DOTATOC	Description of adapted acquisition protocols and discussion of potential logistic and diagnostic benefits of integrated PET/MRI in radiation therapy planning of meningiomas
Garibotto et al. [22]	5 adult patients	Staging and radiotherapy planning	Sequential (Philips Ingenuity TF)	[^{18}F]-FET	Description of adapted acquisition protocols, obtaining diagnostic quality and comprehensive evaluation of gliomas in one examination

Table 11.8 (continued)

Study	N of patients evaluated for intracranial lesions	Clinical indications	Type of PET-MR tomograph	Radiotracers	Results
Bisdas et al. [5]	28 adult patients	Biopsy planning in gliomas	Simultaneous (Siemens mMR)	[^{11}C]-MET	Comparison of the areas of the metabolic imaging provided by [^{11}C]-MET PET and magnetic resonance spectroscopy: the maps overlap only partially with different results depending on tumor grade
Filss et al. [17]	36 adult patients	Staging and restaging	Simultaneous (whole-body 3 T MR with BrainPET insert, Siemens Healthcare)	[^{18}F]-FET	Comparison of [^{18}F]-FET uptake and perfusion-weighted MRI: significant differences in the spatial localization and size of metabolically active and hyperperfused tissue in gliomas
Preuss et al. [46]	4 pediatric patients	Biopsy planning	Simultaneous (Siemens mMR)	[^{11}C]-MET	Description of adapted acquisition protocols, obtaining all necessary data for surgical planning and neuronavigation in one single session
Fraioli et al. [20]	12 pediatric patients	Staging and restaging of astrocytic tumors	Simultaneous (whole-body 3 T MR with BrainPET insert, Siemens Healthcare)	[^{18}F]-Fluorocholine	Description of adapted acquisition protocols and discussion of potential logistic and diagnostic benefits of integrated PET/MRI in astrocytic brain tumors in children
Afshar-Oromieh et al. [2]	15 adult patients	Detection and radiation therapy volume definition of meningiomas	Simultaneous (Siemens mMR)	[^{68}Ga]-DOTATOC	Comparison of PET/CT and PET/MR: ideal diagnostic quality and lesion definition on PET/MRI images, despite systematic differences in quantitative parameters, possibly due to the later acquisition of PET/MRI images and to the different PET detectors

namely, about the similarity between functional measures obtained by PET and MRI. One study has specifically investigated areas of regional cerebral blood volume, estimated on perfusion-weighted MRI, and increased amino acidic uptake evaluated by [^{18}F]-FET PET, showing that the overlap between the two processes is limited in gliomas [17]. Another study evaluated the overlap between changes in MR spectroscopy and 11C-MET uptake, showing a partial overlap and different in low- and high-grade gliomas [5]. Overall, these preliminary studies underline the diversity of the information provided by the two modalities and the need for further cross-validation studies.

Advantages and challenges associated with this new hybrid modality, specifically concerning neuroimaging applications, have been previously addressed [10, 21].

We only briefly summarize here the main advantages of PET/MR hybrid imaging, as compared with standard PET/CT, which we could observe in our clinical practice:

- The availability of all relevant information in a single session, which reduces total examination time. The patient only has to be positioned once: this issue is particularly important for patients with limited compliance, such as children or patients with cognitive impairment due to neurodegenerative disorders or brain lesions. The single imaging session is also an advantage when additional procedures, such as anesthesia or sedation, are required. In general, patients and caregivers appreciate the opportunity of gathering all data in a single session.
  The acquisition at the same time of all image series also guarantees that all variables related to the disease evolution and to the treatment effects are strictly identical for all modalities, while PET and MRI acquired separately might easily have an interval of some days, with the possibility of relevant changes in some rapidly evolving biological phenomena
- A lower radiation exposure, by avoiding the CT acquisition currently used in PET/CT scans for attenuation measurement. This gain is of special interest in the pediatric population and in cases requiring repeated investigations.
- The systematic integration of PET and MRI for image interpretation. Fusion of images acquired on separate systems is standard practice and has already proven its importance and the diagnostic gain associated [37]. This can be ideally achieved by a combined hybrid acquisition, which minimizes fusion issues. In addition, the acquisition of all images in single session encourages truly multidisciplinary reading of the PET and MRI dataset, with an added value coming from the joined interpretation of the findings of the two modalities.

Conclusions

PET/CT can be used nowadays with several radiopharmaceuticals for imaging gliomas. At initial staging PEt allows identification of the metabolically active tumor volume, which is essential information to direct biopsy, for planning surgery and radiotherapy and can clarify an undetermined finding on MRI. PET can be used to assess noninvasively tumor grading: high metabolic activity is predictive of higher tumor grade and proliferative activity and it has negative prognostic value. Hardware-based coregistration of PET to CT is standard today, and it helps the differential diagnosis between tumor recurrence and radiation injury. When feasible, hardware- or software-based registration to MRI should also be performed. Increased PET activity combined with increased contrast enhancement or T1/T2 abnormalities is consistent with tumor recurrence; negligible PET activity is consistent with radiation necrosis.

[^{18}F]-FDG has high physiological brain uptake in gray matter und suffers from specificity, so that radiation necrosis can occasionally be indistinguishable from recurrent high-grade tumor. However, tumor [^{18}F]-FDG uptake has prognostic value.

Several radiopharmaceuticals were subsequently developed to explore biochemical processes other than glucose metabolism

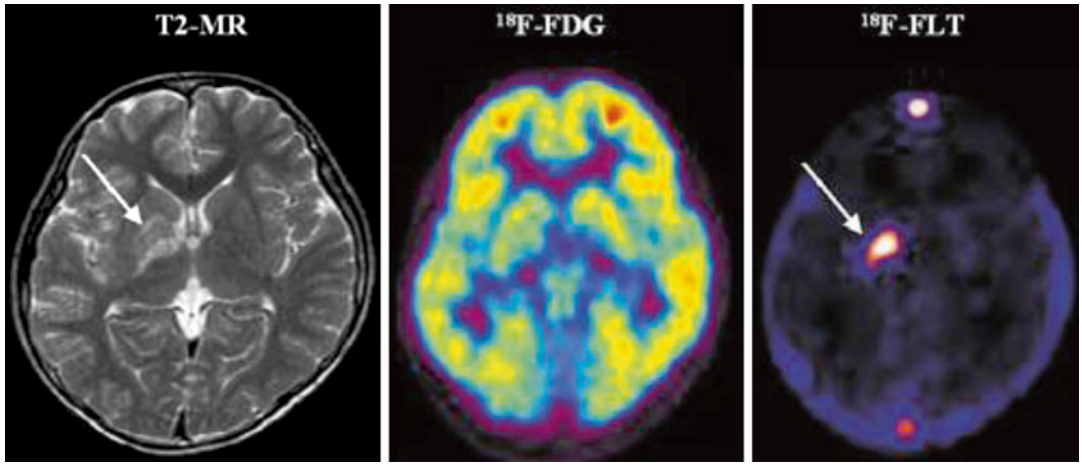

Fig. 11.4 An 11-year-old male with a germ cell tumor of the basal ganglia. MR shows subtle changes (*arrow*) in the right basal ganglia. On [^{18}F]-FDG PET, the right basal ganglia lesion shows slightly decreased uptake compared with the contralateral basal ganglia but increased uptake compared with normal *white matter*. [^{18}F]-FLT PET, however, reveals intensely increased uptake, suggesting the presence of a malignant tumor (*arrow*). Based on the [^{18}F]-FLT PET results, a stereotactic biopsy could be performed in the right basal ganglia (Adapted from Choi et al. [12])

that are associated to tumor growth. Amino acid tracers are sensitive to transport across the BBB and, to some extent, protein synthesis. Among these tracers, ^{11}C-MET is the one that is more widely used. Other promising tracers include [^{18}F]-FET and [^{18}F]-DOPA. For [^{18}F]-FET, a SPECT analog ([^{123}I]-IMT) exists that has lower diagnostic but similar prognostic values. Other than that, the role of SPECT/CT has today dramatically decreased. Physiological brain uptake of amino acids is low and they are less involved in inflammation in respect to [^{18}F]-FDG. Thus, their specificity for differentiating tumor recurrence vs. radiation necrosis is higher. However, amino acid tracers may be taken up similarly by low-grade tumors and high-grade tumors so that grading is not accurately predicted. They also have limited accuracy to distinguish low-grade gliomas from nonmalignant lesions. Virtually all amino acid tracers can be used for presurgical evaluation and to predict survival. For the clinical routine, the role of other tracers, such as hypoxia tracers and radiolabeled choline, is more uncertain (Fig. 11.4).

An ongoing technological development that may substantially increase the diagnostic accuracy of current PET tomographs and reduce logistical difficulties is the further development of PET/MRI tomographs. The studies performed so far have consistently shown that PET/MRI tomographs provide all relevant information for disease staging, biopsy, surgery, or radiation therapy planning in a single session, with adequate diagnostic quality despite the technical complexity of the hybrid design. As compared with PET/CT and MRI acquired separately, the hybrid design has mainly logistic and practical advantages: one single imaging session and identical conditions for both modalities. The diagnostic gain is still to be proven, even if the availability of high-resolution morphological imaging and functional/molecular imaging at the same time is expected to increase diagnostic confidence and possibly decrease false-positive and false-negative findings derived from each modality alone. Brain tumor imaging will clearly be one of the indications of choice for the new PET/MRI hybrid tomographs, where available (Fig. 11.5).

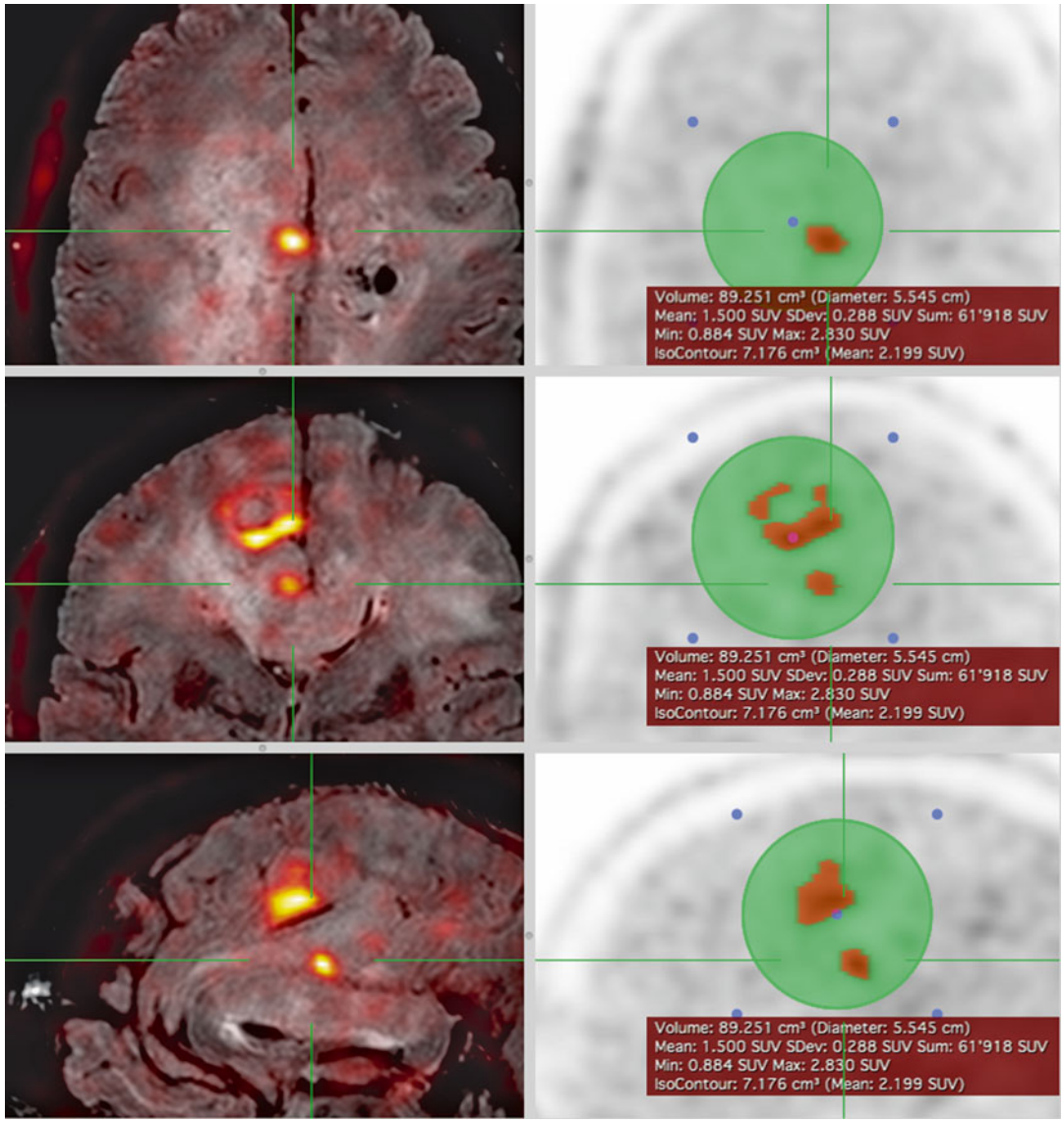

Fig. 11.5 PET/MRI images of [^{18}F]-FET in a 53-year-old glioblastoma patient, showing the fusion of FLAIR MRI and PET images (*left panel*) and the segmentation of the areas with the higher uptake (threshold set at 70% of the SUV_{max}) (*right panel*) (Geneva University Hospitals, Geneva, Switzerland)

References

1. Afshar-Oromieh A, Giesel FL et al (2012) Detection of cranial meningiomas: comparison of (6)(8) Ga-DOTATOC PET/CT and contrast-enhanced MRI. Eur J Nucl Med Mol Imaging 39(9):1409–1415
2. Afshar-Oromieh A, Wolf MB et al (2015) Comparison of (6)(8)Ga-DOTATOC-PET/CT and PET/MRI hybrid systems in patients with cranial meningioma: initial results. Neuro Oncol 17(2):312–319
3. Alavi JB, Alavi A et al (1988) Positron emission tomography in patients with glioma. A predictor of prognosis. Cancer 62(6):1074–1078
4. Barbosa Fde G, von Schulthess G et al (2015) Workflow in simultaneous PET/MRI. Semin Nucl Med 45(4):332–344
5. Bisdas S, Ritz R et al (2013) Metabolic mapping of gliomas using hybrid MR-PET imaging: feasibility of the method and spatial distribution of metabolic changes. Invest Radiol 48(5):295–301

6. Boss A, Bisdas S et al (2010) Hybrid PET/MRI of intracranial masses: initial experiences and comparison to PET/CT. J Nucl Med 51(8):1198–1205
7. Boss A, Kolb A et al (2010) Diffusion tensor imaging in a human PET/MR hybrid system. Invest Radiol 45(5):270–274
8. Bruehlmeier M, Roelcke U et al (2004) Assessment of hypoxia and perfusion in human brain tumors using PET with 18F-fluoromisonidazole and 15O-H2O. J Nucl Med 45(11):1851–1859
9. Buck AK, Nekolla S et al (2008) Spect/Ct. J Nucl Med 49(8):1305–1319
10. Catana C, Drzezga A et al (2012) PET/MRI for neurologic applications. J Nucl Med 53(12):1916–1925
11. Chao ST, Suh JH et al (2001) The sensitivity and specificity of FDG PET in distinguishing recurrent brain tumor from radionecrosis in patients treated with stereotactic radiosurgery. Int J Cancer 96(3):191–197
12. Choi SJ, Kim JS et al (2005) [18F]3'-deoxy-3'-fluorothymidine PET for the diagnosis and grading of brain tumors. Eur J Nucl Med Mol Imaging 32(6):653–659
13. Delso G, Furst S et al (2011) Performance measurements of the Siemens mMR integrated whole-body PET/MR scanner. J Nucl Med 52(12):1914–1922
14. Di Chiro G, DeLaPaz RL et al (1982) Glucose utilization of cerebral gliomas measured by [18F] fluorodeoxyglucose and positron emission tomography. Neurology 32(12):1323–1329
15. Dunet V, Rossier C et al (2012) Performance of 18F-fluoro-ethyl-tyrosine (18F-FET) PET for the differential diagnosis of primary brain tumor: a systematic review and Metaanalysis. J Nucl Med 53(2):207–214
16. Filippi L, Schillaci O et al (2006) Usefulness of SPECT/CT with a hybrid camera for the functional anatomical mapping of primary brain tumors by [Tc99m] tetrofosmin. Cancer Biother Radiopharm 21(1):41–48
17. Filss CP, Galldiks N et al (2014) Comparison of 18F-FET PET and perfusion-weighted MR imaging: a PET/MR imaging hybrid study in patients with brain tumors. J Nucl Med 55(4):540–545
18. Fink J, Muzi M et al (2015) Multi-modality brain tumor imaging – MRI, PET, and PET/MRI. J Nucl Med 56(10):1554–1561
19. Floeth FW, Pauleit D et al (2007) Prognostic value of O-(2-18F-fluoroethyl)-L-tyrosine PET and MRI in low-grade glioma. J Nucl Med 48(4):519–527
20. Fraioli F, Shankar A et al (2015) 18F-fluoroethylcholine (18F-Cho) PET/MRI functional parameters in pediatric astrocytic brain tumors. Clin Nucl Med 40(1):e40–e45
21. Garibotto V, Forster S et al (2013) Molecular neuroimaging with PET/MRI. Clin Transl Imaging 1(1):53–63
22. Garibotto V, Heinzer S et al (2013) Clinical applications of hybrid PET/MRI in neuroimaging. Clin Nucl Med 38(1):e13–e18
23. Hara T, Kondo T et al (2003) Use of 18F-choline and 11C-choline as contrast agents in positron emission tomography imaging-guided stereotactic biopsy sampling of gliomas. J Neurosurg 99(3):474–479
24. Hatakeyama T, Kawai N et al (2008) 11C-methionine (MET) and 18F-fluorothymidine (FLT) PET in patients with newly diagnosed glioma. Eur J Nucl Med Mol Imaging 35(11):2009–2017
25. Hayashi M, Deguchi J et al (2005) Comparison of methods of attenuation and scatter correction in brain perfusion SPECT. J Nucl Med Technol 33(4):224–229
26. Heiss P, Mayer S et al (1999) Investigation of transport mechanism and uptake kinetics of O-(2-[18F] fluoroethyl)-L-tyrosine in vitro and in vivo. J Nucl Med 40(8):1367–1373
27. Henze M, Schuhmacher J et al (2001) PET imaging of somatostatin receptors using [68GA]DOTA-D-Phe1-Tyr3-octreotide: first results in patients with meningiomas. J Nucl Med 42(7):1053–1056
28. Herholz K, Langen KJ et al (2012) Brain tumors. Semin Nucl Med 42(6):356–370
29. Hillner BE, Siegel BA et al (2011) Impact of dedicated brain PET on intended patient management in participants of the national oncologic PET Registry. Mol Imaging Biol 13(1):161–165
30. Huang SC, Phelps ME et al (1981) Error sensitivity of fluorodeoxyglucose method for measurement of cerebral metabolic rate of glucose. J Cereb Blood Flow Metab 1(4):391–401
31. Jansen NL, Graute V et al (2012) MRI-suspected low-grade glioma: is there a need to perform dynamic FET PET? Eur J Nucl Med Mol Imaging 39(6): 1021–1029
32. Karunanithi S, Sharma P et al (2013) 18F-FDOPA PET/CT for detection of recurrence in patients with glioma: prospective comparison with 18F-FDG PET/CT. Eur J Nucl Med Mol Imaging 40(7):1025–1035
33. Kato T, Shinoda J et al (2008) Metabolic assessment of gliomas using 11C-methionine, [18F] fluorodeoxyglucose, and 11C-choline positron-emission tomography. AJNR Am J Neuroradiol 29(6):1176–1182
34. Kim S, Chung JK et al (2005) 11C-methionine PET as a prognostic marker in patients with glioma: comparison with 18F-FDG PET. Eur J Nucl Med Mol Imaging 32(1):52–59
35. Kubota R, Kubota K et al (1995) Methionine uptake by tumor tissue: a microautoradiographic comparison with FDG. J Nucl Med 36(3):484–492
36. Milker-Zabel S, Zabel-du Bois A et al (2006) Improved target volume definition for fractionated stereotactic radiotherapy in patients with intracranial meningiomas by correlation of CT, MRI, and [68Ga]-DOTATOC-PET. Int J Radiat Oncol Biol Phys 65(1):222–227
37. Morana G, Piccardo A et al (2014) Value of 18F-3,4-dihydroxyphenylalanine PET/MR image fusion in pediatric supratentorial infiltrative astrocytomas: a prospective pilot study. J Nucl Med 55(5):718–723
38. Muzi M, Spence AM et al (2006) Kinetic analysis of 3'-deoxy-3'-18F-fluorothymidine in patients with gliomas. J Nucl Med 47(10):1612–1621
39. Neuner I, Kaffanke JB et al (2012) Multimodal imaging utilising integrated MR-PET for human brain tumour assessment. Eur Radiol 22(12):2568–2580

40. Nihashi T, Dahabreh IJ et al (2013) Diagnostic accuracy of PET for recurrent glioma diagnosis: a meta-analysis. AJNR Am J Neuroradiol 34(5):944–950, S941-911
41. Ohtani T, Kurihara H et al (2001) Brain tumour imaging with carbon-11 choline: comparison with FDG PET and gadolinium-enhanced MR imaging. Eur J Nucl Med 28(11):1664–1670
42. Patronas NJ, Di Chiro G et al (1982) Work in progress: [18F] fluorodeoxyglucose and positron emission tomography in the evaluation of radiation necrosis of the brain. Radiology 144(4):885–889
43. Patronas NJ, Di Chiro G et al (1985) Prediction of survival in glioma patients by means of positron emission tomography. J Neurosurg 62(6):816–822
44. Piroth MD, Holy R et al (2011) Prognostic impact of postoperative, pre-irradiation (18)F-fluoroethyl-l-tyrosine uptake in glioblastoma patients treated with radiochemotherapy. Radiother Oncol 99(2):218–224
45. Pirotte BJ, Levivier M et al (2009) Positron emission tomography-guided volumetric resection of supratentorial high-grade gliomas: a survival analysis in 66 consecutive patients. Neurosurgery 64(3):471–481
46. Preuss M, Werner P et al (2014) Integrated PET/MRI for planning navigated biopsies in pediatric brain tumors. Childs Nerv Syst 30(8):1399–1403
47. Queiroz MA, Delso G et al (2015) Dose optimization in TOF-PET/MR compared to TOF-PET/CT. PLoS One 10(7):e0128842
48. Ratib O, Beyer T (2011) Whole-body hybrid PET/MRI: ready for clinical use? Eur J Nucl Med Mol Imaging 38(6):992–995
49. Schlemmer HP, Pichler BJ et al (2008) Simultaneous MR/PET imaging of the human brain: feasibility study. Radiology 248(3):1028–1035
50. Schwenzer NF, Stegger L et al (2012) Simultaneous PET/MR imaging in a human brain PET/MR system in 50 patients-current state of image quality. Eur J Radiol 81(11):3472–3478
51. Sokoloff L, Reivich M et al (1977) The [14C]deoxyglucose method for the measurement of local cerebral glucose utilization: theory, procedure, and normal values in the conscious and anesthetized albino rat. J Neurochem 28(5):897–916
52. Swanson KR, Chakraborty G et al (2009) Complementary but distinct roles for MRI and 18F-fluoromisonidazole PET in the assessment of human glioblastomas. J Nucl Med 50(1):36–44
53. Talbot JN, Kerrou K et al (2007) FDOPA PET has clinical utility in brain tumour imaging: a proposal for a revision of the recent EANM guidelines. Eur J Nucl Med Mol Imaging 34(7):1131–1132, author reply 1133–1134
54. Terakawa Y, Tsuyuguchi N et al (2008) Diagnostic accuracy of 11C-methionine PET for differentiation of recurrent brain tumors from radiation necrosis after radiotherapy. J Nucl Med 49(5):694–699
55. Thorwarth D, Muller AC et al (2013) Combined PET/MR imaging using (68)Ga-DOTATOC for radiotherapy treatment planning in meningioma patients. Recent Results Cancer Res 194:425–439
56. Utriainen M, Komu M et al (2003) Evaluation of brain tumor metabolism with [11C]choline PET and 1H-MRS. J Neurooncol 62(3):329–338
57. Valk PE, Mathis CA et al (1992) Hypoxia in human gliomas: demonstration by PET with fluorine-18-fluoromisonidazole. J Nucl Med 33(12):2133–2137
58. Van Laere K, Ceyssens S et al (2005) Direct comparison of 18F-FDG and 11C-methionine PET in suspected recurrence of glioma: sensitivity, inter-observer variability and prognostic value. Eur J Nucl Med Mol Imaging 32(1):39–51
59. von Schulthess GK, Veit-Haibach P (2015) Guest editorial. Semin Nucl Med 45(3):189–191
60. Weber W, Bartenstein P et al (1997) Fluorine-18-FDG PET and iodine-123-IMT SPECT in the evaluation of brain tumors. J Nucl Med 38(5):802–808
61. Wester HJ, Herz M et al (1999) Synthesis and radiopharmacology of O-(2-[18F]fluoroethyl)-L-tyrosine for tumor imaging. J Nucl Med 40(1):205–212
62. Zaidi H, Ojha N et al (2011) Design and performance evaluation of a whole-body Ingenuity TF PET-MRI system. Phys Med Biol 56(10):3091–3106

Hybrid Imaging in Pediatric Central Nervous System Disorders

12

Giovanni Morana, Silvia Daniela Morbelli, Arnoldo Piccardo, Andrea Rossi, and Andrea Ciarmiello

12.1 Introduction

Modern neuroimaging techniques represent an essential tool in the evaluation of pediatric central nervous system disorders. The use of magnetic resonance imaging (MRI) has led to an enormous increase in our comprehensive knowledge of several pathological entities and currently represents the gold standard method because of its uniquely detailed tissue contrast differentiation and lack of invasiveness.

Positron emission tomography (PET) is emerging as a valuable imaging modality not competing with but rather complementing MRI. The simultaneous acquisition of morphologic and functional information with hybrid systems plays an increasingly important role to improve diagnostic accuracy, allowing to combine the advantages of different techniques in a single installation.

This chapter begins with some background information regarding imaging techniques and radiotracers. Then, the most relevant applications of hybrid imaging in pediatric central nervous system disorders are discussed, with emphasis on brain tumors and epilepsy, currently the main fields of applications. Finally, a brief discussion regarding other applications in pediatric neurology is provided.

12.2 Imaging Modalities

12.2.1 MRI

MRI scanners use magnetic fields and radio waves to form images of the body without exposure to ionizing radiation. MRI, unlike computed tomography (CT), is a collection of techniques that allow noninvasive evaluation of structural, biochemical, and functional aspects of the brain. The clinician can make many choices when an MRI examination is performed; when considering a specific pathological condition, it is important that the technique is "tailored" to identify the pathological substrate that is the subject of the investigation. There are many choices of imaging sequences, orientation, slice thickness, and imaging time, all of which can contribute to the optimization of the image. Magnetic resonance

G. Morana (✉) • A. Rossi
Neuroradiology Unit, Istituto Giannina Gaslini, Genoa, Italy
e-mail: giovannimorana@gaslini.org

S.D. Morbelli
Nuclear Medicine Unit, IRCCS AOU San Martino-IST, Genoa, Italy

A. Piccardo
Nuclear Medicine Unit, Ospedali Galliera, Genoa, Italy

A. Ciarmiello
Nuclear Medicine Department, Ospedale S. Andrea, La Spezia, Italy

A. Ciarmiello, L. Mansi (eds.), *PET-CT and PET-MRI in Neurology*,
DOI 10.1007/978-3-319-31614-7_12

techniques are traditionally classified as "conventional" or "advanced" depending of the morphological or functional attitude of the imaging study.

Conventional MRI with gadolinium-based contrast agents represents the current imaging modality of choice for evaluating pediatric brain disorders and provides excellent anatomic and morphologic imaging. Three-dimensional high-resolution data sets can be acquired, which allows reformatting of the two-dimensional image in any plane with any slice thickness, providing an optimal guide for neuronavigation systems. In addition to high-resolution structural imaging, advanced MRI techniques such as diffusion (including diffusion tensor imaging), perfusion, and spectroscopy allow to explore functional features including microstructure, hemodynamics, and metabolism [1].

Diffusion-weighted imaging (DWI) provides information regarding diffusion of water molecules in the section studied, from which quantitative values, the so-called apparent diffusion coefficient (ADC), can be calculated. DWI is quick and easy to obtain and, in less than 1-min scan time, provides noninvasive estimation of differences in cell density and tissue structure.

Diffusion-tensor imaging (DTI) provides information about both the rate and the direction of water motion through the measure of anisotropy, which is the tendency for water molecules to diffuse preferentially in some directions rather than equally in all directions. Water diffusion in white matter tends to be more facilitated in the direction of myelinated axons than in the orthogonal directions, and therefore, DTI is a sensitive method to normal white matter pathways (tractography) and their alterations in disease states that disrupt tract integrity [1, 2].

Perfusion-weighted imaging (PWI) measures hemodynamic properties of the brain at the microcirculation level. The two main methods of MR perfusion imaging in children include T2*-weighted dynamic susceptibility contrast-enhanced (DSC) perfusion and arterial spin labeling (ASL). DSC imaging requires the bolus intravenous administration of a paramagnetic contrast medium and the rapid acquisition of images over time during the first pass of contrast material through the capillary bed. Several parameters can be measured by DSC imaging, including cerebral blood volume (CBV), cerebral blood flow (CBF), and mean transit time (MTT). Of these, the relative cerebral blood volume (rCBV), which is the calculated CBV relative to the contralateral side, is the most widely used parameter derived from DSC and is considered a marker of angiogenesis [3]. Arterial spin labeling is a perfusion method for quantitatively measuring CBF by taking advantage of arterial water as a freely diffusible tracer. ASL is completely noninvasive and repeatable and is performed without gadolinium administration, thus bypassing concerns regarding gadolinium accumulation or nephrogenic systemic fibrosis. Despite its versatility, ASL suffers from certain limitations mainly related to the very low signal-to-noise ratio and post-processing issues, which have so far limited its routine clinical use [4].

MR spectroscopy (MRS) allows for noninvasive detection and estimation of normal and abnormal metabolites within brain tissue. Different patterns of metabolite concentrations are associated with increased cellular growth, neuronal loss, necrosis, or normal tissue. MRS is presently largely available on clinical MRI scanners and can be performed automatically in most situations [2].

Functional MRI (fMRI) is a functional neuroimaging procedure using MRI technology that allows for the noninvasive identification of sensory, motor, and cognitive functions by detecting changes associated with blood flow. This technique relies on the fact that cerebral blood flow and neuronal activation are coupled. When an area of the brain is in use, inflow of oxygenated blood to that region also increases. fMRI is increasingly employed to identify eloquent cortex to be spared during neurosurgery, principally the primary motor and sensory cortex and brain areas implicated in language and memory [5].

Of note, the abovementioned advanced MR techniques are not part of the standard examination of the brain and should be used as complementary tools to conventional MRI on a case-by-case basis.

12.2.2 PET/CT

PET/CT is an imaging modality combining in the same gantry a PET scanner and a CT scanner, allowing to acquire images derived from both modalities in a single session. This technology offers several advantages that may impact on the overall diagnostic performance.

The principal strength of PET/CT is the availability of CT images for attenuation correction, eliminating the need for time-consuming transmission scans. The use of the CT scanner to generate attenuation correction factors (ACFs) reduces the scan time by a significant amount and results in more accurate ACFs [6, 7]. Furthermore, multimodality imaging allows the two images to be acquired with the same geometry and body position with minimal delay between the two studies and without the need for external fiducial markers. After acquisition, images are reconstructed with the same slice thickness, realigned, and fused to generate a new image overlaying PET and CT data.

In children, preparation and acquisition procedures are very similar to those adopted for adult studies, but some considerations should be taken into account. Firstly, a full explanation of the scan should be given to the patient and parents. The need for sedation or anesthesia should be identified in advance, and an experienced anesthesiologist should be involved. The child should fast for at least 4–6 h before the study, especially in case of 18F-fluorodeoxyglucose (FDG) investigations, but should drink water to maintain good hydration. In case of FDG-PET/CT examinations, the blood glucose level should be assessed, and the preferred fasting blood glucose is below 120 mg/dl [8]. If a central line is used for tracer injection due to difficult peripheral access, it should be flushed with at least 20 ml of 0.9 % normal saline solution. The injected activity of FDG depends on the patient's weight and the type of acquisition. Acquisition in tridimensional (3D) mode is preferable due to its higher sensitivity. A minimum injected activity of 26 MBq has been introduced, and more in general the last version of EANM dosage card suggests injected activity according to body weight and mode scanning acquisition (2D or 3D) [9]. However, it is recognized that other ways of calculating the injected activity of FDG in children are possible (i.e., 6 MBq/kg body weight FDG in 2D mode scanning acquisition and 3 MBq/kg in 3D mode) [10]. Before the acquisition, the child should be encouraged to void.

Acquisition parameters depend largely on the detector and the type of scanner used; however, we suggest to acquire PET images in 3D mode, which has greater sensitivity and allows to achieve better image quality and higher signal-to-noise ratio. For FDG, a 15–20-min static acquisition should be performed about 45-min postinjection. The delay time between injection and scan is required to complete tracer redistribution between plasma and brain tissue compartment.

CT component of PET/CT should be used only for attenuation correction and anatomical localization of PET findings. To minimize dose exposure, we suggest to use the dose modulation method, enabling to adjust the mAs to the thickness of the body tissue while significantly reducing radiation exposure (about 25–35 %) without a corresponding reduction in image quality [11, 12].

12.2.3 PET/MR

PET/CT has been successfully established in clinical routine, but despite its diagnostic advantages, CT still provides limited soft-tissue contrast and exposes the patient to radiation doses. This is an important limitation in diagnostic pediatric studies. Indeed, the principal alternative source of anatomical information is MRI. The combined use of PET and MRI in children is therefore advisable and increasingly applied [13]. The first attempts to combine MRI and PET were performed with images acquired on separate scanners and subsequently co-registered by using proper softwares. This method works very well in pediatric neurological investigations, but it is of course time-consuming and may be, in some cases of "hostile anatomy" (e.g., after surgery and/or biopsy), error prone.

Integration of PET and MRI in one device maximizes patient comfort and minimizes examination time and sedation in very young patients and makes image registration more straightforward. However, combining MRI and PET in the same scanner has been very challenging due to known and potential crosstalk effects. On one hand, the static magnetic field prevents the normal operation of photomultiplier tubes and induces interference in the front-end electronics of PET detectors. On the other, the presence of the PET detector may induce inhomogeneities in the magnetic field, which can lead to artifacts on the MR images [14]. In addition, correct attenuation map for PET images is difficult to obtain by using MR [15].

At present, most of the abovementioned challenges have been solved with the introduction of the first integrated whole-body PET/MR scanner (Biograph mMR; Siemens Medical Solutions, Erlangen, Germany). This system is equipped with a 3-T magnet and high-resolution avalanche photodiode-lutetium oxyorthosilicate (LSO) PET detectors, which are integrated between the MR body coil and the gradient coils for simultaneous PET and MR acquisition, keeping mutual interference to a minimum [16]. For attenuation correction of the PET data, attenuation coefficient maps (air, lung, soft tissue, fat) are segmented from the fat and water images generated by a two-point Dixon MR sequence. Indeed, attenuation correction issue seems to be critical in brain imaging considering that cranial bone contributes to significantly attenuate the radioactivity. Thus, the introduction of this ultrashort echo time sequence is very important considering that this system permits to acquire signal from the bone to create attenuation maps [17, 18].

In addition to attenuation correction, this sequence can also be used for anatomical correlation of PET-positive lesions [19].

Following the Dixon sequence, a conventional and advanced diagnostic MRI data set can be acquired. The PET acquisition time is adapted to the measurement time of the MR examination. This does not lead to prolongation of data acquisition. Overall, a standard diagnostic PET/MR examination takes about 30–40 min depending on the applied MR sequences.

12.3 Radiotracers

The most widely used tracers in children with brain disorders are briefly reported here. A more detailed description of the clinical applications and results related to these or more specific tracers is discussed in the pathology-related sections.

12.3.1 Fluorodeoxyglucose

18F-FDG is a sensitive marker of brain metabolism mostly reflecting the metabolic demands of neuronal activity. Intravenously injected 18F-FDG is rapidly cleared from vascular to interstitial space and is then actively transported through cellular membranes into the cells by glucose transporter proteins (GLUTs). 18F-FDG is then phosphorylated by the enzyme hexokinase to 18F-FDG-phosphate but does not undergo significant further metabolism. This results in metabolic trapping in the cells [20, 21]. The physiological brain glucose metabolism and consequently the 18F-FDG brain uptake are very high, because glucose provides approximately 95 % of the required ATP and is also tightly connected to neuronal activity.

At present, 18F-FDG is the most commonly used (and widely available) PET tracer in pediatric epilepsy (see below). 18F-FDG was also the first PET tracer employed in children with brain tumors (see below). Glucose consumption is increased in brain tumors, especially in malignant gliomas; however, differentiating tumors from normal tissue or non-tumorous lesions is often difficult because of the high metabolism in normal cortex, resulting in low tumor-to-background contrast ratio. This is especially true for low-grade tumors in which the FDG uptake may be similar to that in normal white matter. On the other hand, hypermetabolic benign lesions such as pilocytic astrocytomas or choroid plexus papillomas can be characterized by high FDG uptake and are a potential pitfall when using FDG-PET for tumor grading. In addition, 18F-FDG is known to accumulate in macrophages and inflammatory tissue, often making

distinction between brain tumors and acute or chronic inflammatory processes difficult.

12.3.2 Amino-Acid Tracers

With the development of PET and PET/CT in clinical practice, alternative tracers to FDG have been introduced for pediatric brain tumor imaging. In this field, radiolabeled amino acids represent the first choice metabolic agents because of their low uptake in normal brain and relatively high uptake in brain tumors. Increased amino-acid uptake in brain tumors is not a direct measure of protein synthesis or dependent on blood-brain barrier breakdown but is rather related to increased transport mediated by type L amino-acid carriers [21]. Many natural amino acids and their synthetic analogs have been labeled and explored as tumor-imaging agents. 11C-methionine (MET) was the first probe employed in children with brain malignancies (see below), but its short half-life (20 min) limited its application to centers with an on-site cyclotron. More recently, 18F-labeled tracers have gained importance based on the possibility of their widespread application due to longer half-lives (110 min). Among them, 18F-dihydroxyphenylalanine (DOPA) and 18F-fluoroethyl-L-tyrosine (FET) are emerging as the two most promising tracers in pediatric brain tumor imaging (see below). Both probes show several similarities [22] with the exception of the specific 18F-DOPA uptake in the putamen and caudate nucleus. Unlike with 18F-FET, this latter aspect might potentially affect the ability to distinguish normal brain from adjacent tumor. On the other hand, 18F-DOPA uptake within the striatum gives the possibility to further stratify tumor uptake ratios through comparison with both the normal background levels and the striatum. No studies have so far compared 18F-DOPA and 18F-FET in children with brain tumors; however, this comparison has recently been performed in adults with brain gliomas at the time of diagnosis [23] and disease recurrence [24]. These studies confirmed that both tracers show comparable diagnostic results and can be successfully employed in low- and high-grade gliomas. Differently from DOPA, FET is a poor substrate to LAT1 and is more selectively transported through LAT2. Since it has been reported that LAT1 can be overexpressed in inflammation while LAT2 is more tumor selective, a higher risk for false-positive findings might be considered for DOPA than for FET [22].

In the field of epilepsy, 11C-methyl-L-tryptophan (AMT) has been employed in children with tuberous sclerosis. This tracer was developed to evaluate brain serotonin synthesis because in neurons that generate serotonin from tryptophan, AMT is converted to α-methyl-serotonin and is trapped in serotoninergic terminals [25]. Indeed it was found to be helpful in detecting epileptic foci because an increased uptake of AMT was discovered in epileptogenic tubers, which was attributed to an increased conversion and trapping of AMT via the inflammatory kynurenine pathway [26].

12.3.3 Choline

Choline is a precursor of phosphatidylcholine, which is the most important constituent of membrane lipids. When choline enters into tumor cells, it undergoes phosphorylation and after further biochemical processes, it is integrated into phospholipids. Due to the high metabolic rate of tumor tissue with consequent rapid biosynthesis of cell membranes, choline uptake in tumors is higher than in normal tissue [27]. Increased concentration of choline and its metabolites is also demonstrated by magnetic resonance spectroscopy studies in brain tumors. Very recently, 18F-choline has been employed in pediatric brain tumors (see below).

12.4 Pediatric Brain Tumors

12.4.1 Epidemiology and Clinical Findings

Pediatric brain tumors encompass a wide spectrum of heterogeneous neoplasms, each with its

own biology, prognosis, and treatment. Central nervous system tumors are the most common solid neoplasms in children and the second most common malignancy of childhood after leukemia. They represent the leading cause of death from cancer in pediatric oncology and comprise 20 to 25 % of all malignancies occurring among children under 15 years of age and 10 % of tumors occurring among 15–19-year-old children. In addition, survivors of childhood brain tumors often have severe neurological, neurocognitive, and psychosocial sequelae due to either the effects of the tumor or the treatment required to control it [28, 29].

The age-adjusted incidence rates of brain tumors tend to be highest in developed, industrial countries. However, the lower incidence of brain tumors in developing countries can be attributed to under-ascertainment [30].

Ionizing radiation is the only unequivocal risk factor that has been identified for glial and meningeal neoplasms. In particular, children treated with irradiation for acute lymphoblastic leukemia or patients treated with moderate doses of ionizing radiation for tinea capitis of the scalp have an elevated risk of developing gliomas. Although exposure to high-voltage power lines, the use of hair dyes, head trauma, and dietary exposure to nitrosourea compounds or other nutritional factors have all been described to increase the risk of brain tumors, these reports have not been confirmed by independent studies [30, 31].

There is a known relation between tumor location and age. Supratentorial tumors are more common in the first 2 years of life, whereas infratentorial neoplasms prevail between years 3 and 11. Supratentorial masses become again more common afterward. Another major difference from the adult population is the known prevalence of primitive intra-axial tumors, whereas extra-axial and secondary neoplasms are distinctly uncommon [32]. The clinical presentation depends heavily on the patient's age. Small infants present with macrocrania, difficult feeding, nausea, vomiting, and lethargy. Older children complain with signs of increased intracranial pressure, seizures, and focal neurological signs; generally, their clinical picture is not different from that of adults with central nervous system (CNS) tumors. Symptoms also are markedly dependent on tumor location. Patients with infratentorial tumors are likely to show marked nausea and vomiting due to involvement of the area postrema (emetic center), as well as cranial nerve palsies, truncal or cerebellar ataxia, and head tilt. Supratentorial tumors may generate seizures if the cortex is involved or may present with focal neurological signs due to specific regional involvement. Tumors located in specific areas, such as the sellar, suprasellar, and pineal regions, will present with specific signs, such as optic disturbances or endocrine dysfunction. High-grade, fast-growing tumors have early symptom onset, while slow-growing, small-sized tumors may remain asymptomatic for many years, especially if they are located in cerebral non-eloquent areas, such as the frontal lobe. In these cases, brain neoplasms can be an incidental finding at CT or MRI [32].

About 60–70 % of all pediatric brain tumors, including astrocytomas, medulloblastomas, and ependymomas, develop in the infratentorial compartment. The remaining 30–40 % of tumors are supratentorial and consist mainly of gliomas and craniopharyngiomas. The reason why pediatric brain tumors have a propensity to occur in the posterior fossa has not yet been elucidated.

When compared to their adult counterparts, pediatric low- and high-grade gliomas show significantly different frequencies of genomic alterations and divergent mechanisms of tumorigenesis [33, 34] and may be considered biologically distinct entities [35]. Concerning diffuse astrocytomas, mutations of IDH1/2 and TP53 are common in adults but rare in children. Adult diffuse astrocytomas show a higher degree of copy number change and carry a less favorable prognosis than their pediatric counterparts. Furthermore, hypermethylation of MGMT occurs only in adults. PTEN mutations and EGFR amplifications, which are frequent in adult primary glioblastoma, are less common in pediatric high-grade gliomas, which also arise de novo. The discovery of novel oncogenic driver mutations in histones H3.1 (position K27) and H3.3 (positions K27 and G34) as well as in the activin A receptor, type I

(ACVR1) is also a key finding in pediatric high-grade gliomas [33–36]. Finally, 5–10 % of brain tumors in childhood are thought to have a genetic predisposition, while such proportion is much lower in adults. Hereditary brain tumors occur in some familial cancer syndromes, such as the Li-Fraumeni syndrome, neurofibromatosis, tuberous sclerosis, rhabdoid tumor predisposition syndrome, nevoid basal cell carcinoma syndrome, von Hippel-Lindau disease, and Turcot's syndrome [37].

Treatment of children with CNS tumors is challenging and requires an integrated multidisciplinary approach that brings together different disciplines including neurosurgery, neuro-oncology, diagnostic imaging, neuropathology, and radiation medicine. Surgical resection represents the first-line treatment option and is a significant prognostic factor in the management of several pediatric CNS tumors. When complete surgical removal is not possible, biopsy or partial "debulking" may be performed, and adjuvant therapy with radiotherapy, chemotherapy, or a combination of both may be used. For malignant brain tumors (e.g., medulloblastoma, malignant glioma) and some lower-grade tumors, adjuvant therapy is performed even if a complete resection is achieved because of concerns about residual microscopic disease. Thus, surgery in combination with chemo- and/or radiotherapy is the mainstay of treatment for many pediatric brain tumors [38].

Advances in neurosurgical techniques, radiotherapy planning, and novel chemotherapeutics go hand in hand with an increasing demand for noninvasive diagnostic techniques. Conventional MRI can determine the location, presence of edema, mass effect, calcification, cyst formation, hemorrhage, vascularization, and contrast enhancement. Extra- and intra-axial brain tumors can also be discriminated quite accurately by anatomic imaging. However, conventional MRI suffers from certain limitations in distinguishing tumor from tumor mimics and in defining tumor type and grade and does not always allow precise delineation of tumor margins; differentiation between true tumor and treatment-induced changes, such as "pseudoprogression" or "pseudoresponse," is also extremely challenging, especially in the early phase of treatment monitoring. Furthermore, conventional MRI is unable to give information about the biological activity of the disease, thus limiting the clinical usefulness on therapeutic decision-making [39]. Advanced MRI techniques can partially overcome some of these limitations providing additional microstructural, hemodynamic, and metabolic information of brain tumors. However, several limitations regarding standardization, comparability, and reproducibility of data have limited their role so far, despite extensive application into various aspects of brain tumor imaging including tumor diagnosis, treatment planning, assessing response to treatment, and posttreatment surveillance. Additional imaging biomarkers capable of providing a more reliable, and possibly quantitative, evaluation of tumor biological activity are therefore needed in order to further improve the clinical management of affected patients.

12.4.2 Hybrid Imaging

12.4.2.1 PET/CT

The very first study in a relatively large sample of pediatric patients with brain tumors was performed by Hoffman et al. in 1992 [40]. They studied 17 pediatric patients with posterior fossa brain tumors with 18F-FDG PET. 18F-FDG uptake was visually ranked by two observers, and the results were correlated to tumor histology. Increased uptake was associated with more malignant and aggressive tumor types, while heterogeneous uptake was associated with previous therapy, including radiation therapy and chemotherapy. The authors concluded that 18F-FDG-PET would likely be an important adjunct in the management of pediatric posterior fossa tumors and predicted a rapid dissemination of PET technology for pediatric applications.

Nevertheless, PET has not become routinely used for the clinical management of pediatric brain tumors; the literature remains relatively scarce on this matter and the difference between adult and pediatric studies cannot be merely attributed to differences in prevalence of the disease [41].

Borgwardt et al. [42] studied 38 untreated pediatric patients with primary CNS tumors using PET with 18F-FDG and, when possible ($n=16$), with 15O-water at rest. Image processing included co-registration to MR in all patients. The 18F-FDG uptake in tumors was semiquantitatively calculated with a region-of-interest approach. They found a positive correlation between 18F-FDG uptake and malignancy grading. On the contrary, there was no correlation between 15O-water uptake and histological grade, a finding that was attributed to uncoupling between glucose metabolism and blood flow. Digital PET/MR co-registration combined to image fusion improved the information on the tumor location in 90 % of cases. PEt altered management in 77 % of patients with brain tumor.

Pirotte et al. reported their experience at the Erasme Hospital pediatric center where they examined about 400 pediatric patients with brain tumor with 18F-FDG and 11C-MET-PET between 1995 and 2005. In their retrospective analysis, they included 126 patients in whom pre- and postoperative MR imaging showed limitations for assessing the evolving nature of an incidental lesion, selecting targets for biopsy and delineating tumor tissue for surgical resection. In this group of patients (about one third of the whole case series), PET was expected to be most useful. They found that PET was helpful on several grounds, i.e., to (1) take a more appropriate decision in incidental lesions by detecting tumor/evolving tissue; (2) better differentiate indolent and active components of the lesion; (3) improve target selection and diagnostic yield of stereotactic biopsies, especially when performed in critical areas such as the brainstem or the pineal region; (4) provide prognostic information; (5) better delineate ill-defined tumor borders; (6) increase the number of tumor resections and the amount of tumor tissue surgically removed; (7) improve detection of tumor residues in the operative cavity at the early postoperative stage; (8) facilitate the decision of early second-look surgery for optimizing the radical resection; and (9) improve the accuracy of the radiosurgical dosimetry planning [41].

Utriainen et al. [43] used 18F-FDG and 11C-MET-PET to examine whether metabolic characteristics could be used as an index of clinical aggressiveness. SUV values for both tracers were compared with histopathology and selected histochemical features. The accumulation of both 18F-FDG and 11C-MET was significantly higher in high-grade than in low-grade tumors, but a considerable overlap was found. High-grade tumors showed higher proliferative activity and vascularity than low grades. In univariate analysis, 18F-FDG SUV, 11C-MET SUV, and apoptotic index were independent predictors of event-free survival.

Kruer et al. [44] examined with FDG-PET a cohort of 46 children/adolescents with low-grade astrocytomas (LGAs, WHO grade 1 or 2) in order to identify LGAs at risk for progressive disease (PD); they found that tumors with FDG hypermetabolism were significantly more likely to demonstrate aggressive behavior and PD.

A recent study evaluated the association of MRI and 18F-FDG-PET in pediatric diffuse intrinsic brain stem gliomas, demonstrating that if 18F-FDG uptake involves at least half the tumor, survival is poor [45]. More recently, a method of registering 18F-FDG-PET with MR permeability images was developed in children with brain tumors, mainly infiltrative gliomas [46].

Hipp et al. [47] compared the metabolic activity of pediatric brain tumors using FDG-PET and magnetic resonance spectroscopic imaging (MRSI) in 37 children diagnosed with a primary brain tumor using a voxel-wise comparison. Pediatric brain tumors were metabolically heterogeneous on FDG-PET and MRSI. Active tumor metabolism was observed more frequently using MRSI compared to FDG-PET, and agreement in tumor classification was weak ($\kappa=0.16$, $p=0.12$), with 42 % agreement (95 % CI = 25–61 %). Voxel-wise comparison for identifying the area of greatest metabolic activity showed overlap in the majority (62 %) of studies, though exact agreement between techniques was low (29.4 %, 95 % CI = 15.1–47.5 %). The authors concluded that FDG-PET and MRSI detect similar but not always identical regions of tumor activity, and there is little agreement in the degree of tumor metabolic activity between the two techniques.

Galldiks et al. [48] investigated the diagnostic accuracy of MET-PET for the differentiation between tumorous and non-tumorous lesions in 39 children and adolescents. MET-PET was able to distinguish brain tumors and non-tumorous brain lesions with a high sensitivity (83 %) and specificity (92 %). The authors suggested that MET-PET may be helpful when results of structural routine diagnostic procedures are not sufficient enough to obtain a treatment decision and planning.

In pediatric patients with central nervous system (CNS) germinomas, the diagnostic utility of 11C-MET was also recently demonstrated by Okochi et al. [49].

Despite these promising results, both 18F-FDG and MET-PET are still not routinely used for clinical evaluation of pediatric brain tumors. The physiologic high l8F-FDG uptake of the normal brain limits tumor detection, especially in low-grade gliomas [50], whereas short half-life (20 min) of 11C-MET limits its application to centers with an on-site cyclotron.

In the last few years, new fluorinated tracers have emerged as alternative radiolabeled compounds for characterizing pediatric brain tumors. Among them, 18F-DOPA was found to be a multi-targeted molecule in children, since it can be used for primary/recurrent brain tumors [51, 52]; for neuroblastoma diagnosis, prognosis, and surveillance [53, 54], including detection of CNS metastasis [55]; and in non-tumoral conditions such as congenital hyperinsulinism [56], with a potential impact on healthcare cost optimization.

Recent data suggest that multimodal 18F-DOPA PET/MR fusion imaging in children with infiltrative astrocytomas correlates reliably with WHO tumor grade and outcome, is useful for biopsy planning and posttreatment monitoring, and contributes to stratification of patients with diffuse astrocytomas and gliomatosis cerebri, thereby influencing their management [51].

Similar results have been reported for 18F-FET [57, 58]. In particular, ^{18}F-FET PET-guided surgical biopsy and resection [57], characterized undetermined brain lesions, detected tumor recurrence, and evaluated treatment response [58].

A very recent study compared metabolic information obtained by ^{18}F-DOPA PET/CT and ^{1}H-MRS in a population of children with supratentorial infiltrative gliomas or nonneoplastic brain lesions initially suspected to be gliomas on conventional MRI. Both MRS and 18F-DOPA PET provided useful complementary information for evaluating the metabolism of tumor and tumorlike brain lesions in children. In view of its better availability, lower costs, and lack of radiation exposure, MRS should be considered as the method of first choice in differentiating brain gliomas from nonneoplastic lesions. 18F-DOPA uptake better discriminated between low- and high-grade gliomas and was an independent predictor of progression-free survival and overall survival [59].

In the setting of posttreatment monitoring and particularly in patients treated with antiangiogenic agents, the significant contribution of multimodal co-registered MRI and 18F-DOPA PET/CT in early diagnosis of tumor "pseudoresponse" and nonenhancing tumor progression was demonstrated in a child with malignant transformation of ganglioglioma treated with bevacizumab [52].

Representative images of pediatric brain tumors studied with MRI and 18F-DOPA PET/CT are reported in Figs. 12.1, 12.2, 12.3, and 12.4.

12.4.2.2 PET/MR

Very few hybrid PET/MR imaging studies have been so far performed to evaluate pediatric brain tumors. Of note, one of the main advantages of the brain is that it is a static structure; thus, if brain MRI and PET/CT are performed within few days of each other, the chance that a brain tumor will change is extremely low. Therefore, PET/MR image fusion and co-registration allow optimal imaging of the brain when compared to body imaging. Nevertheless, total dose reduction and the possibility to perform both functional and morphological studies in the same clinical conditions while reducing total scan time represent the main advantage of hybrid PET/MR systems. In 2014, Preuss et al. [60] reported their experience in four patients aged 9–16 years who underwent hybrid PET/MRI scans employing 11C-MET and contrast-enhanced 3D-MR sequences for planning navigated biopsies. On the basis of their

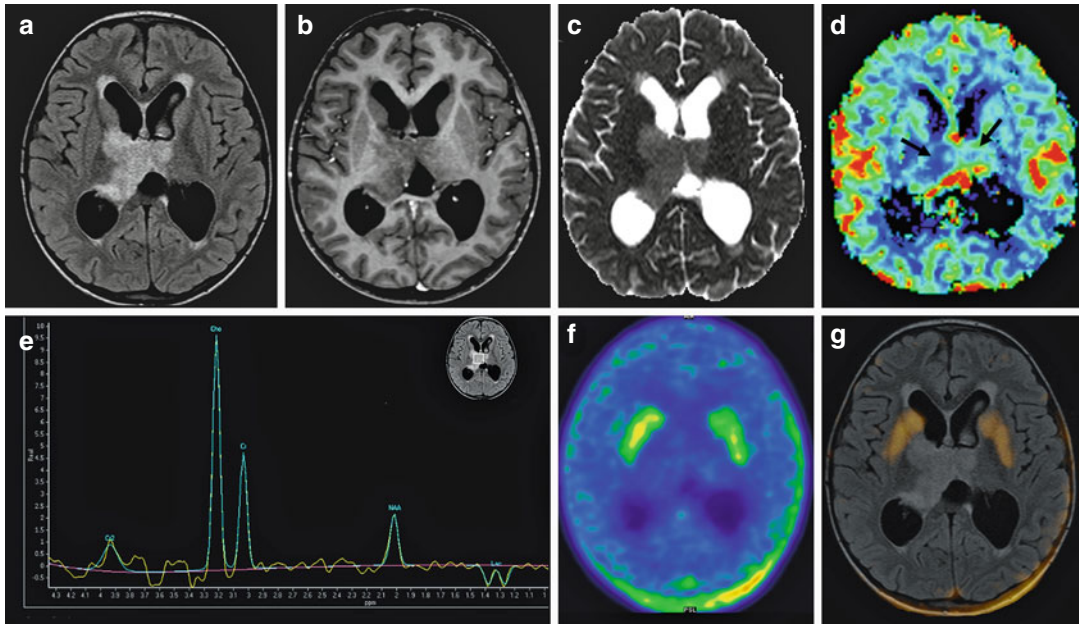

Fig. 12.1 Multimodal multiparametric diagnostic workup in a 6-year-old-boy with newly diagnosed diffusely infiltrating lesion. (**a**) Axial FLAIR image; (**b**) Gd-enhanced axial T1-weighted image; (**c**) Axial Apparent Diffusion Coefficient (ADC) map; (**d**) Axial relative cerebral blood volume (rCBV) map (dynamic susceptibility contrast-enhanced perfusion imaging); (**e**) single voxel MR spectroscopy (echo time 144 ms); (**f**) Axial 18F-DOPA PET/CT image; (**g**) fused PET/MRI image. Nonenhancing bithalamic diffusely infiltrating lesion, more prominent on the right (**a**, **b**). There is concomitant biventricular decompensated hydrocephalus due to bilateral stenosis of the foramina of Monro. The lesion shows increased diffusivity (**c**) and low perfusion (*arrows*, **d**). MR spectroscopy (**e**) demonstrates increased Cho/NAA and Cho/Cr ratios and a small lactate peak. No 18F-DOPA uptake is demonstrated (**f**, **g**). Biopsy revealed a grade II diffuse astrocytoma. In our experience, a great proportion of pediatric low-grade diffuse astrocytomas show absent or mild 18F-DOPA uptake in keeping with the indolent or slowly progressive behavior of these lesions

results, integrated PET/MRI scanner offered co-registered multimodal, high-resolution data for neuronavigation with reduced radiation exposure compared to PET/CT scans. One examination session provided all necessary data for neuronavigation and preoperative planning, avoiding additional anesthesia in the small patients.

Tsouana et al. [61] evaluated the efficacy of hybrid 18F-fluoroethyl-choline (FEC) PET/MRI as an imaging modality for diagnosis and assessment of treatment response and remission status in four patients with proven or suspected intracranial non-germinomatous germ cell tumors (NGGCT). In two patients, faint or absent choline avidity correlated with negative histology, whereas in other two patients, persistent choline avidity in the residual mass was suggestive of the presence of viable tumor, subsequently confirmed histologically. They concluded that 18F-FEC PET/MRI may be an effective imaging tool in detecting viable residual tumor in patients with intracranial NGGCT posttreatment.

Fraioli et al. [62] examined the feasibility of simultaneous acquisition of 18F-FEC PET and functional MRI (standardized uptake value [SUV]max/mean and apparent diffusion coefficient [ADC]mean), using a hybrid PET/MRI scanner, for diagnosis and response assessment in a cohort of 12 children with astrocytic brain tumors. They found complete concordance between standard cross-sectional MRI and functional 18F-FEC PET at diagnostic imaging. Choline (Cho) uptake was independently related to the histological grade of the tumor, and visual assessment based on Cho uptake and lesion enhancement pattern on MRI was similar. There was also a trend toward a negative correlation between SUV max/mean and ADC mean.

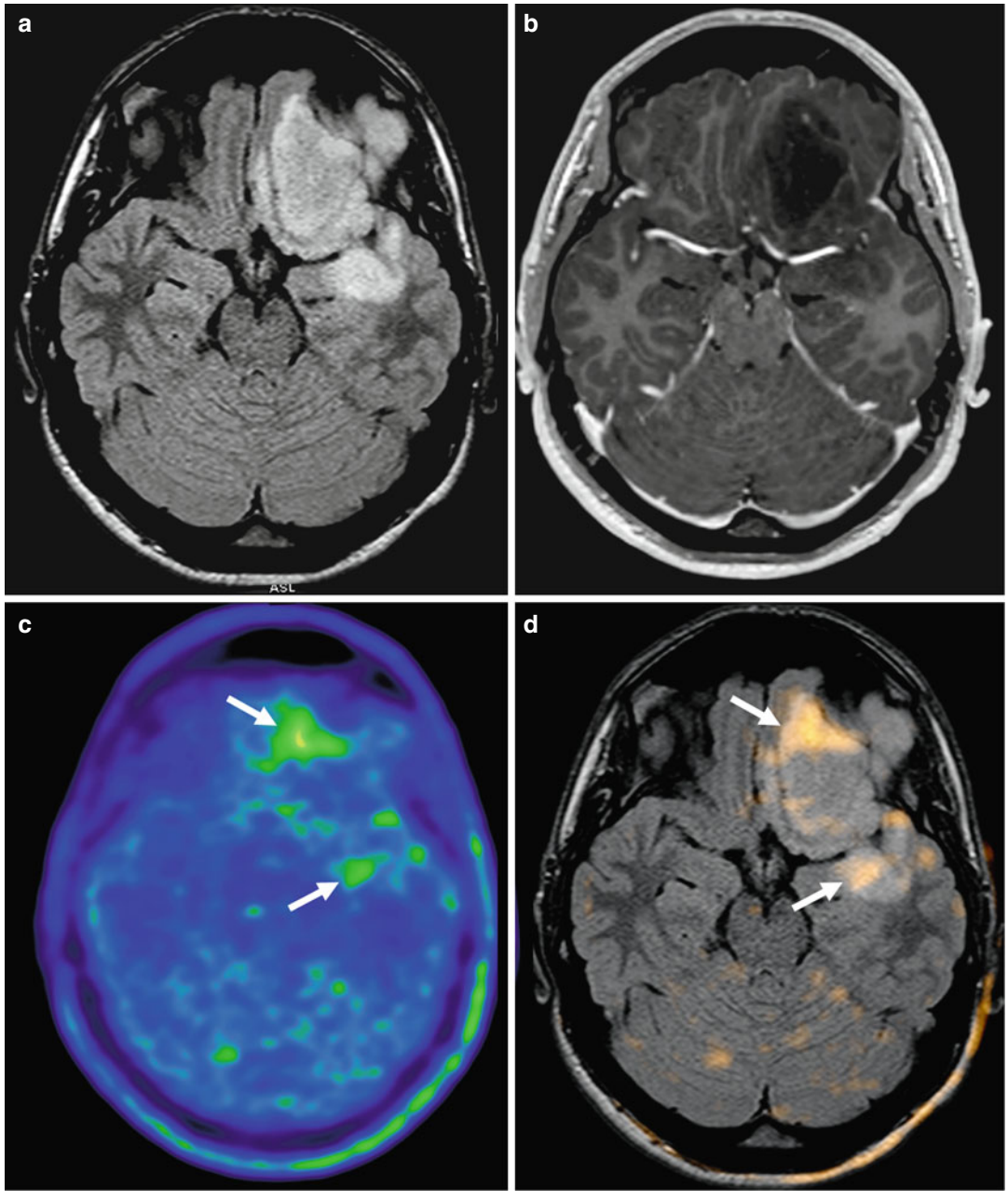

Fig. 12.2 Diffuse astrocytoma (WHO grade II) in a 17-year-old-boy. (**a**) Axial FLAIR image; (**b**) Gd-enhanced axial T1-weighted image; (**c**) axial 18 F-DOPA PET/CT image; (**d**) fused PET/MRI image. Left temporal-frontal nonenhancing diffusely infiltrating lesion (**a**, **b**) demonstrating focal areas of mildly increased 18F-DOPA uptake, in keeping with a low-grade diffuse astrocytoma

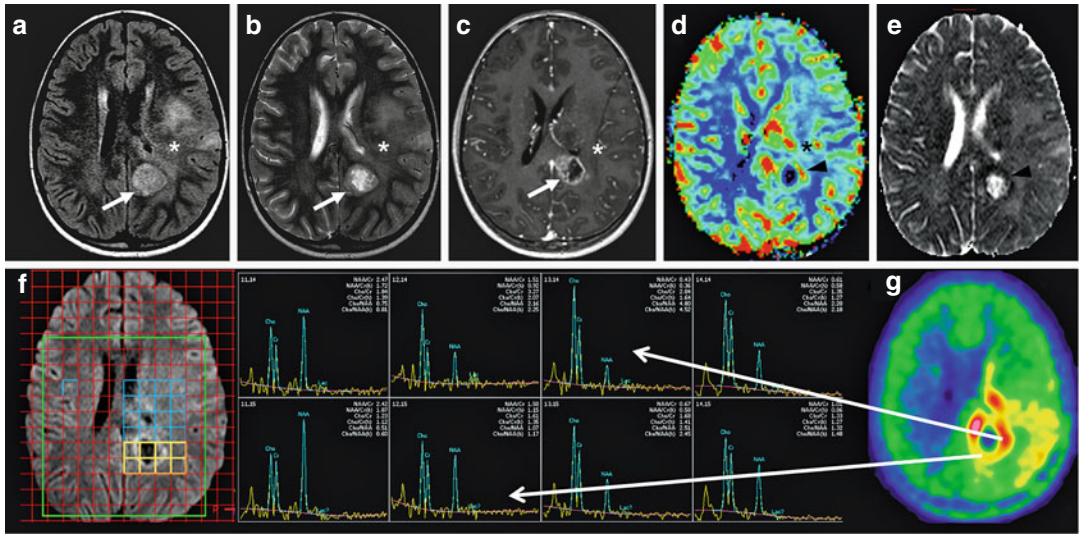

Fig. 12.3 Glioblastoma multiforme (WHO grade IV) in an 8-year-old boy. (**a**) Axial FLAIR image; (**b**) axial T2-weighted image; (**c**) Gd-enhanced axial T1-weighted image; (**d**) Axial relative cerebral blood volume (rCBV) map (dynamic susceptibility contrast-enhanced perfusion imaging); (**e**) Axial apparent diffusion coefficient (ADC) map; (**f**) Multi-voxel MR spectroscopy (echo time 144 ms); each of the eight spectra corresponds spatially to the *yellow boxes* on the anatomical image; (**g**) axial 18F-DOPA PET/CT image co-registered to MRI. Heterogeneous lesion located in the left frontal and parietal lobes characterized by a necrotic area (*arrow*, **a**–**c**) and a more prominent nonenhancing diffusely infiltrating component (*asterisk*, **a**–**c**). The lesion shows increased perfusion and restricted diffusion (*arrowhead*, **d**, **e**) along the margins of the necrotic component in keeping with increased vascularity and cellularity. Increased perfusion is also evident in the nonenhancing portion of the lesion (*asterisk*, **d**). Multivoxel MR spectroscopy (**f**) shows a more prominent increase of Cho/Cr and Cho/NAA ratios in the left lateral wall of the necrotic component. On 18F-DOPA PET (**g**) there is markedly increased uptake along the margins of the necrotic component as well as in the nonenhancing lesional component. Notice the spatial concordance of the metabolic information obtained by PET and MRS (*long white arrows*): increased DOPA uptake along the left lateral wall of the necrotic component corresponding to more prominent Cho/Cr and Cho/NAA ratios

12.5 Pediatric Epilepsy

12.5.1 Epidemiology and Clinical Findings

Epilepsy is one of the most frequent chronic neurological disorders, with an incidence of 50–100,000/year and a prevalence of 0.5–1 % [63].

Epileptic seizures result from abnormal patterns of excitability and synchrony among neurons in select brain areas, more often involving the cortex. There are many types of epileptic seizures [64]. Seizures with electrographic onset in a specific part of the brain and clinically limited to focal symptoms are named partial seizures. By contrast, generalized seizures and complex partial seizures are by definition associated with loss of consciousness and awareness, which is preserved in patients with simple partial seizures [64]. For a detailed description of epilepsy classification and syndromes, see Engel (2006) [64].

More than a half of epileptic patients respond to the first tried antiepileptic drug. However, around 20–25 % of patients do not respond to medications and are thus considered to have refractory epilepsy [65]. Refractory epilepsy can be treated with surgery in around 20 % of individuals [66]. Epilepsy surgery is thus performed in selected children with drug-resistant focal epilepsy. In this frame, multidisciplinary expertise is needed in evaluating the complex issues related to the wide range of epilepsy syndromes typical of pediatric patients. Presurgical evaluation aims to delineate the epileptogenic zone, which would correspond to the cortical area responsible for the generation of epileptic seizure [67]. Further aims

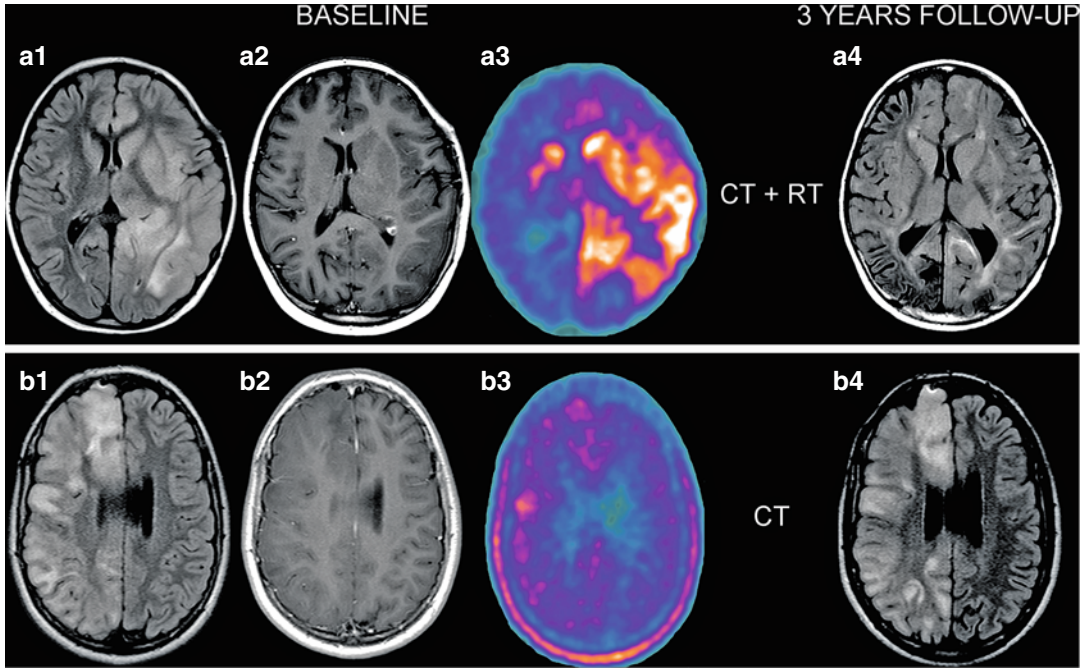

Fig. 12.4 Gliomatosis cerebri in two different adolescents. (**a**1, **b**1) axial FLAIR images; (**a**2, **b**2) Gd-enhanced axial T1-weighted images; (**a**3, **b**3) 18F-DOPA PET/CT images; (**a**4, **b**4) axial FLAIR images. *Left* (**a**1, **a**2) and *right* (**b**1, **b**2) hemispheric gliomatosis cerebri with similar extension and identical conventional MRI characteristics (diffuse hyperintensity on FLAIR and absence of contrast enhancement). The two lesions presented also identical histology (diffuse astrocytoma, WHO grade II). In both patients, biopsies had been performed before PET studies. Despite the identical histology and similar MRI findings, 18F-DOPA PET imaging revealed a different metabolic behavior of the two lesions, with heterogeneous and markedly increased uptake in one patient (**a**3) and absent to mild increased uptake in the other (**b**3). The first patient (*upper row*) was treated with a more aggressive treatment combining chemotherapy (CT) and radiotherapy (RT), whereas only CT was administered to the other patient (*lower row*). Despite the more aggressive treatment, on follow-up MRI studies, the first lesion progressed with the involvement of the contralateral hemisphere (**a**4) and after 3 years the patient died. The second lesion instead presented only minimal changes (**b**4) and the patient is still alive. In the first patient, biopsy underestimated the real nature of the lesion, probably due to sampling error. 18F-DOPA PET imaging, affording a more global view, was able to better stratify the biological nature of the two lesions, complementing MRI and histology

of the presurgical discussion are the identification of the risks of surgery and the estimate of the functional neurological outcome following surgery.

The comprehensive presurgical assessment of the patients includes clinical history and examination, MRI, electroencephalogram (EEG), and, in selected cases, functional imaging with SPECT and PET. In particular, brain MRI is the investigation of choice in children with epilepsy to screen for structural abnormalities, thus requiring a high-resolution MRI acquisition protocol [67]. In this framework, volumetry and relaxometry have shown greater accuracy for mesial temporal sclerosis [68]. This is particularly relevant for children as the majority of patients undergoing surgery have refractory partial seizures, mainly of temporal lobe origin (temporal lobe epilepsy (TLE)). Accordingly, the MRI protocol in pediatric patients is planned with a specific attention to the hippocampus. In addition to mesial temporal sclerosis detection, MRI is also useful to highlight tumors and malformations such as in tuberous sclerosis, a rare multisystem genetic disease that causes benign tumors to grow in the brain and in other organs.

Structural imaging remains negative or inconclusive in up to a quarter of patients studied for

presurgical evaluation [69]. More frequent reasons for an inconclusive MRI in the presurgical evaluation of children with epilepsy are (i) cortical malformations in children younger than 2 years (detection of the lesion hampered by immature myelination and poor white/gray matter differentiation); (ii) patients with multiple bilateral structural lesions, which are generally not all epileptogenic; and (iii) discordant results between MRI and EEG. These scenarios might be particularly relevant for extratemporal epilepsy and thus for pediatric patients, since extratemporal epilepsy is more frequent in children than in adults [70]. In these clinical settings, functional imaging with PET and SPECT can help in lateralizing or localizing the epileptogenic focus.

12.5.2 Hybrid Imaging

12.5.2.1 PET/CT

Historically, SPECT imaging using 99mTc-labeled compounds such as HMPAO and ECD that provide information about cerebral blood flow has been used to evaluate patients with epilepsy. In fact, it has been directly demonstrated that cortical blood flow significantly increases during a seizure [71]. These tracers distribute in few minutes to the brain, and then their distribution is stable for some hours. So, their kinetics is favorable for performing ictal imaging with the tracer injected immediately after seizure onset. Accordingly, ictal perfusion SPECT shows an area of hyperperfusion in the epileptogenic region, surrounded by an area of hypoperfusion that tends to enlarge at the end of the ictal phase. However, several different expertise and technical requirements are needed to perform and interpret an ictal SPECT. The procedure requires expert and vigilant video-EEG monitoring to immediately recognize the presence of a seizure, with the patients admitted in hospital for several days of continuous video. The staff needs to read the EEG and/or to identify the seizures with the habitual features of that patient; finally, the tracer needs to be injected within a few seconds, and the exact time of injection and the time of onset of the seizure need to be noted [72]. It is mandatory to perform interictal SPECT to compare baseline with ictal SPECT results by means of a dedicated software. SPECT ictal imaging of epilepsy requires a highly specialized setup with a multidisciplinary team, and thus it is not advisable to perform such type of studies at centers that do not have the necessary setup for proper acquisition and interpretation of the images [73].

For all these practical reasons, as well as for its better resolution, 18F-FDG-PET/CT has been increasingly used. 18F-FDG is indeed the most commonly used PET tracer in epilepsy as it allows to measure glucose metabolism, which is coupled with synaptic and neuronal activity [74]. However, the rapid changes occurring in neuronal activity and thus in glucose metabolism during the ictal state cannot be studied with the 18F-FDG-PET scan as it takes around 30 min for the tracer to be taken up by the brain and reach a steady state. Thus, 18F-FDG-PET is only performed as interictal examination. An interictal 18F-FDG-PET may be particularly useful and more practical when the aim is to define epileptogenic region lateralization (Fig. 12.5).

EEG monitoring at the time of the 18F-FDG-PET scan needs to be performed to exclude the presence of clinical or subclinical seizures that may occur during the 18F-FDG uptake time and that needs to be taken into account when interpreting the PET findings [73]. The epileptogenic region typically appears as an area of reduced tracer uptake in interictal 18F-FDG-PET/CT [75]. The area of interictal hypometabolism of FDG-PET is more often larger than the epileptogenic focus, probably expressing the abnormal function of closer areas involved by the first ictal spread. However, the mechanisms underlying the hypometabolism in epileptogenic cortex have not been clearly elucidated. Diaschisis, neuronal loss, and reduction in synaptic density have been alternatively advocated as possible underlying mechanisms [75]. In particular, it has been hypothesized that repeated seizures or dysfunctional epileptogenic cortex related to structural alterations such as dysplasia or tubers induce an inhibitory effect on the surrounding cortex [76]. In agreement with this hypothesis, it has been demonstrated that cortical hypometabolism

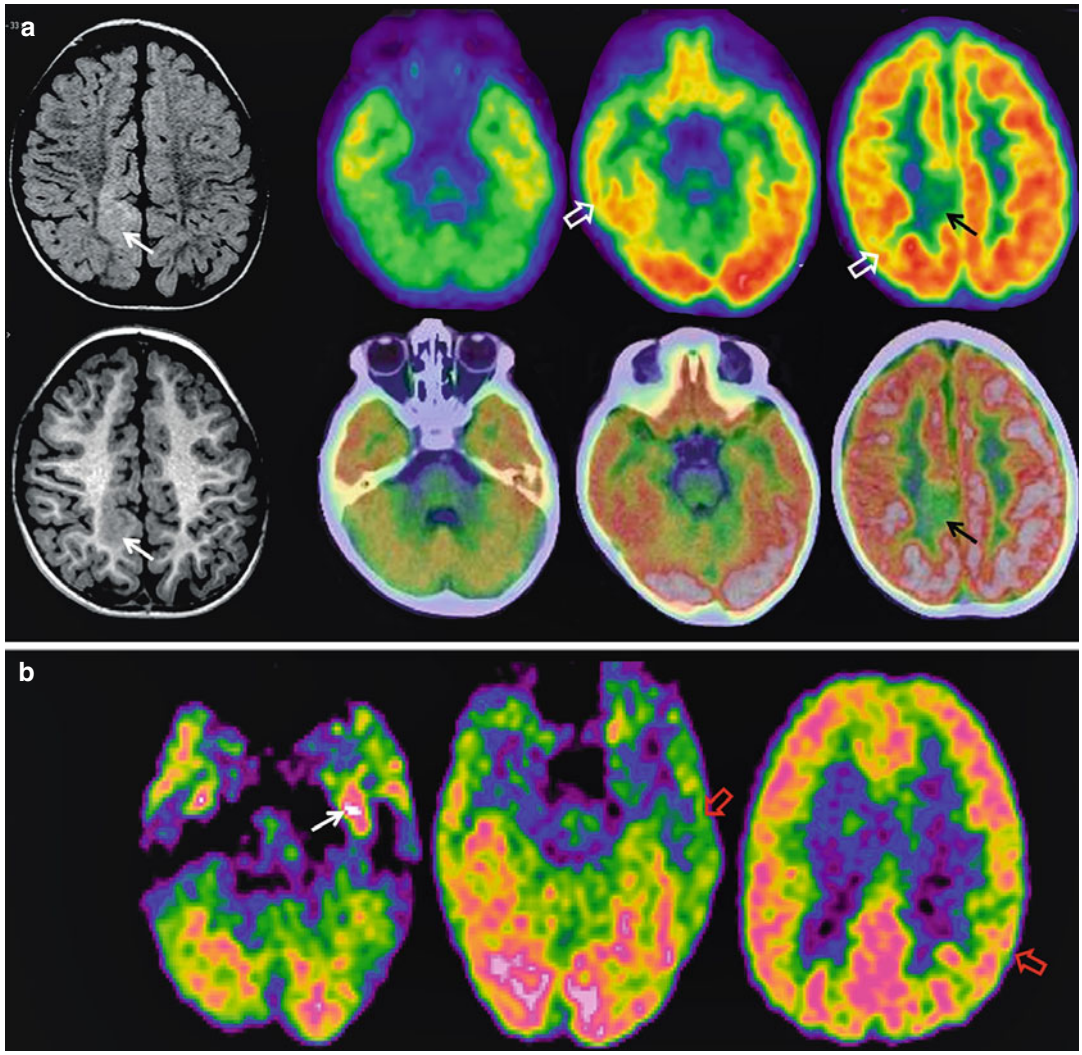

Fig. 12.5 (**a**) Interictal 18F-FDG PET in a 20-month-old patient with refractory epilepsy candidate to surgery. MRI shows a focal abnormality with blurring of the *gray-white* matter junction in the right medial frontal-parietal region in keeping with a focal cortical dysplasia (thin *white arrows*, *up and middle row*). PET scan shows an area of hypometabolism corresponding to the MRI lesion (*thin black arrows*, *upper and middle row*). Ipsilateral mild hypometabolism is also evident in both the right parietal and lateral temporal cortex (*open arrows*, *upper row*). No further areas of hypometabolism were detected, thus confirming side and localization of the focus epilepticus. (**b**) Ictal 18F-FDG PET in a 7-year-old patient with temporal lobe epilepsy. The scan was intended to be an interictal PET; however, the EEG monitoring showed repeated abnormalities soon after the injection of the tracer, thus revealing a subclinical seizure. In agreement with the occurrence of the seizure, an area of relative hypermetabolism (*thin white arrow*) was detected in the left medial temporal lobe, thus localizing the presence of the focus epilepticus (*open red arrows*)

correlates with the duration of the seizure. In fact, hypometabolism is usually present in 25 % of children with new-onset epilepsy and in up to 85 % of adults with intractable seizures [75, 77]. Furthermore, a relevant part of the more extended hypometabolism beyond the epileptogenic area certainly reflects the presence of diaschisis (i.e., ipsilateral thalamus and contralateral cerebellar cortex especially in case of frontal seizures). A further specific reason for hypometabolism in

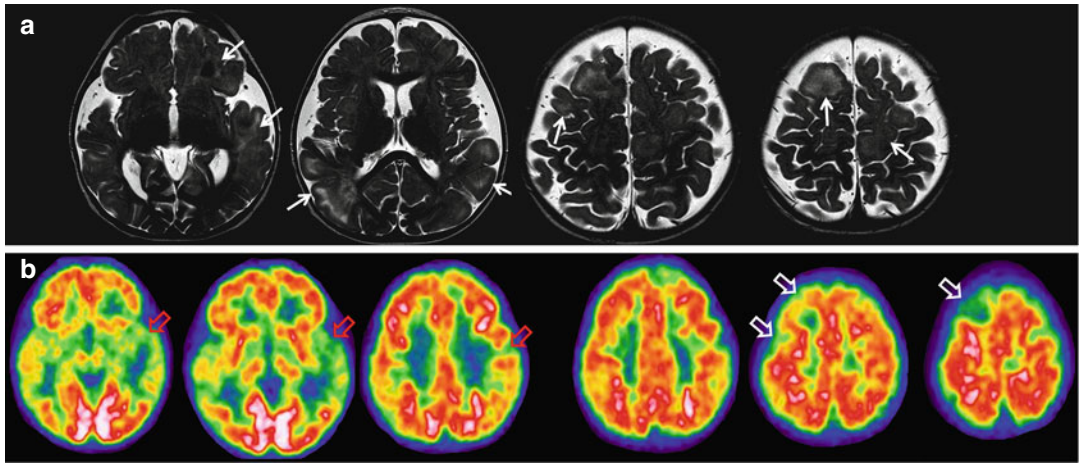

Fig. 12.6 A 2-year-old boy with refractory epilepsy due to tuberous sclerosis, candidate to surgical treatment. (**a**) MRI (T2-weighted images) shows several cortical tubers (*thin arrows*). (**b**) The child was submitted to an interictal 18 F-FDG PET to recognize the epileptogenic tuber. All the tubers correspond to sites of hypometabolism on PET (*red and white open arrows*); however, only the lesion located in the left temporal lateral cortex was surrounded by a significantly larger area of hypometabolism (diaschisis: *open red arrows*) and was thus suggested as the epileptogenic tuber

patients with tuberous sclerosis is related to the fact that cortical tubers comprise simplified dendritic arborizations [78], thus showing reduced metabolism. However, to recognize the epileptogenic tuber is important to evaluate the extension of the surrounding area of hypometabolism. In fact, in patients with more than one lesion, the tuber showing the higher ratio between the extension of hypometabolic area and its dimensions is more likely to be the epileptogenic tuber [78] (Fig. 12.6).

Finally, antiepileptic drugs may also decrease the absolute rates of glucose metabolism of the cerebral cortex [79].

Regardless of underlying cause of hypometabolism around the epileptogenic region, this evidence suggests that PET cannot be reliably used to precisely determine the surgical margin. Accordingly, especially in extratemporal lobe epilepsies, PET is more useful to guide the placement of intracranial electrodes (or in some cases to further guide the evaluation of MRI for the detection of subtle areas of cortical dysplasia). 18F-FDG-PET has a reported sensitivity of 85–90 % in the detection of the epileptic brain region in cases of TLE [80, 81]. In extratemporal lobe epilepsy, the role of 18-FDG-PET is less established. In fact, the percentage of inconclusive 18F-FDG-PET scans is higher than in patients with mesial or lateral temporal lobe involvement [82]. Finally, for both TLE and extratemporal epilepsy, visual inspection is the first step for the interpretation of the images with the aim to detect the presence of any hemispheric asymmetry of 18F-FDG distribution. Asymmetry index can also be calculated by means of regions of interest to identify the presence of homologue areas whose asymmetry index exceeds 10 % [83].

In recent years, it has been suggested that voxel-based whole-brain statistical analysis (i.e., with SPM) can improve the value of FDG-PET especially in patients with extratemporal lobe epilepsy, thus significantly increasing the sensitivity to the epileptogenic focus [84]. As a final remark, it should be underlined that, unlike with other clinical scenarios, hybrid PET/CT imaging has a less established added value over standalone PET in the presurgical management of children with epilepsy. In fact, the added value of CT in this context is lower, and PET images need to be viewed side-by-side with the subject's MRI and possibly co-registered with MRI.

Finally, new developments of PET technique in epilepsy are also related to the availability of other

PET tracers beyond 18F-FDG. 11C-Flumazenil (FMZ), an antagonist of the central benzodiazepine receptors/GABA, demonstrates the distribution of benzodiazepine receptors in the brain and might play a role in patients with TLE and normal MRI. In fact, a more accurate detection of asymmetrical uptake in the medial temporal lobe (compared with 18F-FDG-PET) has been demonstrated [81]. 11C-a-methyl-L-tryptophan, which measures tryptophan metabolism, is a promising tracer in patients with tuberous sclerosis [85]. In fact, it shows increased uptake in the epileptogenic cortex interictally, thus allowing a better detection of the epileptogenic lesion. Other tracers evaluated for PET imaging of epilepsy are able to bind the so-called translocator protein expressed on activated microglia, thus allowing the visualization of epilepsy related to neuroinflammation [73].

12.5.2.2 PET/MR

18F-FDG-PET/MRI off-line co-registration (Fig. 12.7) has demonstrated to provide more sensitivity than PEt alone in the detection of cortical epileptogenic lesions, thus improving the outcome of epilepsy surgery [86]. Chassoux and colleagues demonstrated that 87 % of patients with refractory epilepsy achieved seizure freedom after limited cortical resection guided by co-registered 18F-FDG-PET and MRI [87]. Salamon and colleagues demonstrated that including co-registered 18F-FDG-PET/MRI into the presurgical evaluation enhances the noninvasive identification and

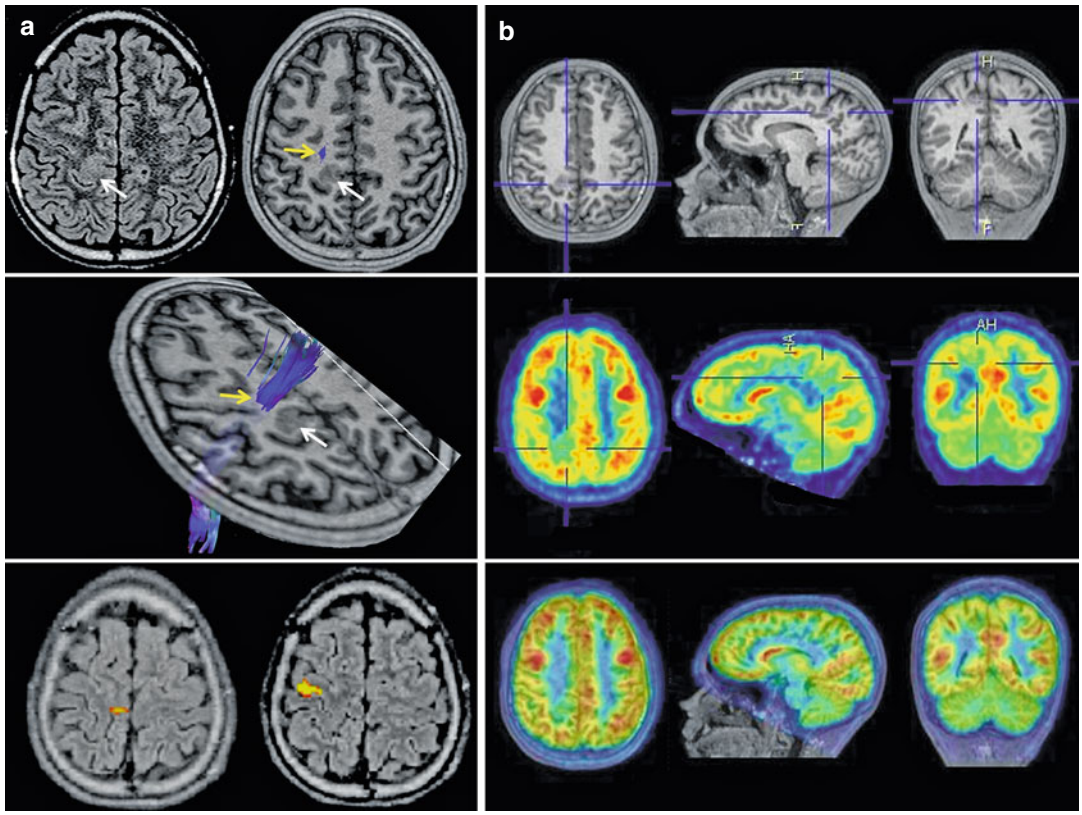

Fig. 12.7 Multimodal diagnostic workup in a 17-year-old boy with refractory epilepsy candidate to surgery. (**a**) Morphological FLAIR and T1-weighted MRI images show a focal cortical dysplasia in the right mesial perirolandic cortex (*white arrows, upper and middle rows*). Diffusion-tensor imaging (tractography) demonstrates the location of the motor component of the right corticospinal tract (*blue strip, yellow arrows, upper and middle rows*). Motor functional MRI study shows the cortical activation of the left foot and hand areas, which are located cranially to the lesion. (**b**) Off-line-fused interictal 18F-FDG PET/MRI performed with a dedicated software allows the detection of a small area of hypometabolism corresponding to the focal cortical dysplasia

successful surgical treatment of patients with cortical dysplasia, especially in case of discordant findings and/or in patients with normal MRI scans [86]. Similarly, Chandra and colleagues reported an added value of co-registered 18F-FDG-PET/MRI with diffusion imaging in patients with tuberous sclerosis [88]. In fact, they demonstrated that larger volumes of FDG-PET hypometabolism relative to MRI tuber size as well as higher ADC values identified epileptogenic tubers with improved accuracy compared with largest tuber by structural MRI.

In recent years, hybrid PET/MRI systems have become available offering a complementary combination of two modalities that have proven to be superior to the single modality approach in the diagnostic workup of several neurological disorders. However, there are no larger-scale studies to show the clinical role of PET/MRI in epilepsy surgery evaluation. To date, feasibility of hybrid PET/MRI for the detection of epileptogenic foci has been evaluated in small case series [89, 90]. Although the added value of hybrid PET/MRI still needs to be established in the clinical setting, some technical/practical improvement related to this method can be already defined for pediatric patients with epilepsy. In fact, lower radiation exposure and lower number of anesthesia are achieved with respect to a clinical workup including both MRI and PET/CT (in case of inconclusive MRI findings). Accordingly, the availability of PET/MRI may contribute to a more frequent use of 18F-FDG-PET in the presurgical workup of epilepsy [91].

12.6 Other Applications in Pediatric Neurology

Initial studies by Chugani et al. evaluated maturational changes in brain glucose metabolism in infants providing crucial information regarding the functional maturation of the human brain [92]. 18F-FDG-PET studies of infants with hypoxic-ischemic encephalopathy (HIE) were also performed, especially in the pre-DWI MRI era [93, 94]. A more recent study measuring cerebral glucose metabolism in 20 term infants with HIE after perinatal asphyxia demonstrated a high correlation between 18F-FDG hypometabolism and the severity of HIE and short-term outcome [95]. Very recently, the effects of mild hypothermia therapy for neonatal HIE on brain energy metabolism were evaluated with 18F-FDG-PET [96].

Sporadic PET studies, mainly in the form of case reports, have been performed in children with neurometabolic and degenerative disorders [97]. In Krabbe disease, marked 18F-FDG decrease in the left cerebral cortex and no uptake in the caudate heads were described in one child [98]. In X-linked adrenoleukodystrophy, 11C-[R]-PK11195 PET demonstrated increased tracer binding in the occipital, parietal, and posterior temporal white matter, in the genu of the corpus callosum, the bilateral posterior thalami, most of the posterior limb of the internal capsule, the bilateral cerebral peduncles, and the brainstem, indicating underlying neuroinflammation [99]. Serial 18F-FDG-PET studies have been performed in identical twins with Niemann-Pick disease type C, revealing a unique pattern consisting of severe hypometabolism of the frontal cortex bilaterally and in the bilateral parietal and temporal cortex [100]. In one child with type 1 glutaric aciduria, 18F-FDG-PET studies revealed a dramatic pattern of absent metabolic activity bilaterally in the striatum and diffuse cortical hypometabolism, most pronounced in the frontal-temporal region [101]. PET studies of glucose and oxygen utilization in children with mitochondrial diseases revealed that patients with cerebral and muscle disease had a lower ratio of oxygen-to-glucose consumption in the brain, suggesting the presence of aerobic glycolysis to lactate and other intermediate metabolites [102]. Marked bilateral 18F-FDG hypometabolism, particularly in calcarine, lateral, occipital, and temporal cortices and in the thalamus, has been reported in juvenile neuronal ceroid lipofuscinoses [103]. In type IV, 3-methylglutaconic aciduria progressive glucose hypometabolism from the basal ganglia and cerebellum to more diffuse hypometabolism with disease progression has been described [104]. In five patients with propionic academia, 18F-FDG-PET studies demonstrated increased

uptake in the basal ganglia and thalami, followed by decreased uptake in the basal ganglia at a later stage of the disease [105]. In infantile GM1 gangliosidosis, FDG-PET scan revealed a mild decrease in basal ganglia uptake and moderate to severe decrease in thalamic and visual cortex uptake [106]. In a child with 4-hydroxybutyric aciduria, FDG-PET scan showed a marked decrease in the cerebellar metabolism [107].

PET has also been used to evaluate neuropsychiatric disorders in childhood, such as attention deficit hyperactivity disorder, schizophrenia-related disorders, obsessive-compulsive disorder, autistic spectrum and related disorders, and anorexia nervosa [108, 109]. Villemagne et al. [110] studied glucose metabolism with PET in six girls with Rett syndrome aged 3–15 years of age. They found a consistent decrease in the occipital visual association areas and relative increase in tracer uptake in the frontal and temporal regions when related to the whole brain in the group of patients between 3 and 8 years of age. In addition, glucose metabolism was relatively increased in the cerebellum.

Inflammatory neurological diseases have also been investigated using FDG and 11C-[R]-PK11195 PET. In Rasmussen's encephalitis, FDG-PET imaging typically reveals marked hypometabolism restricted to the predominantly affected cerebral hemisphere associated with a hypometabolic contralateral cerebellar hemisphere [111]. However, unilateral marked hypermetabolism in the affected cerebral hemisphere and basal ganglia with subnormal contralateral cerebral activity and crossed cerebellar diaschisis have also been described [112].

Aron [113] evaluated two patients with Sydenham's chorea with PET scans in the active phase of the disease, showing hypermetabolic changes of the caudate nuclei and putamen. The scan reverted to normal in the recovery phase.

Very recently, 11C-[R]-PK11195 PET has been employed to evaluate neuroinflammatory changes in basal ganglia and thalamus in children with clinically diagnosed pediatric autoimmune neuropsychiatric disorders associated with streptococcal infection (PANDAS) and Tourette syndrome. Binding potential values, suggesting underlying activated microglia-mediated neuroinflammation, were found to be increased in bilateral caudate and lentiform nucleus in children with PANDAS and in bilateral caudate nuclei only in children with Tourette syndrome [114].

Conclusions

PET imaging combined with MRI, either by off-line co-registration or via hybrid PET/MR systems, plays an increasingly important role in the evaluation of pediatric patients with brain tumors and epilepsy.

In the field of brain tumor imaging, PET with amino-acid tracers can be helpful to overcome some limitations of conventional MRI, complementing advanced MRI techniques. This is especially true for selected pediatric brain tumors, such as diffusely infiltrating lesions where complete surgical removal may be impossible or ethically unacceptable and where tissue biopsy can lead to inaccurate results when biopsy samples are not taken from the most malignant region. In the field of epilepsy, 18F-FDG-PET has an established role in complementing MRI especially for those patients with inconclusive MRI studies. However, no convincing evidence of the role of PET imaging in other fields has emerged so far.

The integration of information obtained by MRI and PET should be performed by diagnostic imaging specialists (neuroradiologist and nuclear medicine physicians) working in close collaboration with each other, so as to properly appreciate and integrate the whole amount of diagnostic information, to extrapolate subtle diagnostic data, and to offer clinicians a more comprehensive and useful array of data. Since fully integrated PET/MRI hybrid systems are progressively becoming more available on the market, preliminary knowledge gathered through off-line co-registration of PET and MRI data will be important in order to optimize the yield of hybrid systems when they eventually become part of a standard clinical diagnostic pathway.

Simultaneous PET/MRI is expected to play an increasing role in pediatric diagnostic

imaging and to improve children's care by reducing radiation dose while also reducing the number of procedures performed under sedation and their duration. It also has the potential to provide new and more specific/sensitive metabolic and topographic disease assessment [115].

References

1. Vossough A, Nabavizadeh SA (2011) Functional imaging based diagnostic strategy: intra-axial brain masses. In: Scott HF, Feroze BM (eds) Functional neuroradiology, principles and clinical application. Springer, New York, pp 197–220
2. Rossi A, Gandolfo C, Morana G et al (2010) New MR sequences (diffusion, perfusion, spectroscopy) in brain tumours. Pediatr Radiol 40:999–1009
3. Mabray MC, Barajas RF Jr, Cha S (2015) Modern brain tumor imaging. Brain Tumor Res Treat 3:8–23
4. Deibler AR, Pollock JM, Kraft RA et al (2008) Arterial spin-labeling in routine clinical practice, part 1: technique and artifacts. AJNR Am J Neuroradiol 29:1228–1234
5. Gaillard WD (2004) Functional MR, imaging of language, memory, and sensorimotor cortex. Neuroimaging Clin N Am 14:471–485
6. Kinahan PE, Townsend DW, Beyer T, Sashin D (1998) Attenuation correction for a combined 3D PET/CT scanner. Med Phys 25:2046–2053
7. Kinahan PE, Hasegawa BH, Beyer T (2003) X-ray-based attenuation correction for positron emission tomography/computed tomography scanners. Semin Nucl Med 33:166–179
8. Stauss J, Franzius C, Pfluger T et al (2008) Guidelines for 18F-FDG PET and PET-CT imaging in paediatric oncology. Eur J Nucl Med Mol Imaging 35:1581–1588
9. Lassmann M, Biassoni L, Monsieurs M, EANM Dosimetry and Paediatrics Committees et al (2008) The new EANM paediatric dosage card: additional notes with respect to F-18. Eur J Nucl Med Mol Imaging 35:1666–1668
10. Holm S, Borgwardt L, Loft A et al (2007) Paediatric doses-a critical appraisal of the EANM paediatric dosage card. Eur J Nucl Med Mol Imaging 34:1713–1718
11. Paterson A, Frush DP, Donnelly LF (2001) Helical CT of the body: are settings adjusted for pediatric patients. Am J Roentgenol 176:297–301
12. Arch ME, Frush DP (2008) Pediatric body MDCT: a 5-year follow-up survey of scanning parameters used by pediatric radiologists. AJR Am J Roengenol 191:611–617
13. Kim S, Salamon N, Jackson HA et al (2010) PET imaging in pediatric neuroradiology: current and future applications. Pediatr Radiol 40:82–96
14. Delso G, Ziegler S (2009) PET/MRI system design. Eur J Nucl Med Mol Imaging 36(Suppl 1):S86–S92. doi:10.1007/s00259-008-1008-6
15. Disselhorst JA, Bezrukov I, Kolb A et al (2014) Principles of PET/MR imaging. J Nucl Med 55(Suppl 2):2S–10S [Epub ahead of print]
16. Hirsch FW, Sattler B, Sorge I et al (2013) PET/MR in children. Initial clinical experience in paediatric oncology using an integrated PET/MR scanner. Pediatr Radiol 43:860–875
17. Berker Y, Franke J, Salomon A et al (2012) MRI-based attenuation correction for hybrid PET/MRI systems: a 4-class tissue segmentation technique using a combined ultrashort-echo-time/Dixon MRI sequence. J Nucl Med 53:796–804
18. Keereman V, Fierens Y, Broux T et al (2010) MRI-based attenuation correction for PET/MRI using ultrashort echo time sequences. J Nucl Med 51:812–818
19. Eiber M, Martinez-Möller A, Souvatzoglou M et al (2011) Value of a Dixon-based MR/PET attenuation correction sequence for the localization and evaluation of PET-positive lesions. Eur J Nucl Med Mol Imaging 38:1691–1701
20. la Fougère C, Suchorska B, Bartenstein P et al (2011) Molecular imaging of gliomas with PET: opportunities and limitations. Neuro Oncol 13:806–819
21. Heiss WD, Raab P, Lanfermann H (2011) Multimodality assessment of brain tumors and tumor recurrence. J Nucl Med 52:1585–1600
22. Galldiks N, Langen KJ, Pope WB (2015) From the clinician's point of view – what is the status quo of positron emission tomography in patients with brain tumors? Neuro Oncol 17:1434–1444
23. Lapa C, Linsenmann T, Monoranu CM et al (2014) Comparison of the amino acid tracers 18F-FET and 18F-DOPA in high-grade glioma patients. J Nucl Med 55:1611–1616
24. Kratochwil C, Combs SE, Leotta K et al (2014) Intra-individual comparison of ^{18}F-FET and ^{18}F-DOPA in PET imaging of recurrent brain tumors. Neuro Oncol 16:434–440
25. Diksic M, Tohyama Y, Takada A (2000) Brain net unidirectional uptake of alpha-[14C]methyl-L-tryptophan (alpha-MTrp) and its correlation with regional serotonin synthesis, tryptophan incorporation into proteins, and permeability surface area products of tryptophan and alpha-MTrp. Neurochem Res 25:1537–1546
26. Chugani DC, Chugani HT, Muzik O et al (1998) Imaging epileptogenic tubers in children with tuberous sclerosis complex using alpha-[11C]methyl-L-tryptophan positron emission tomography. Ann Neurol 44:858–866
27. Gulyás B, Halldin C (2012) New PET radiopharmaceuticals beyond FDG for brain tumor imaging. Q J Nucl Med Mol Imaging 56:173–190
28. Muller S, Susan C (2009) Pediatric brain tumors: current treatment strategies and future therapeutics approaches. Neurotherapeutics 6:570–586

29. Heath JA, Zacharoulis S, Kieran MW (2012) Pediatric neuro-oncology: current status and future directions. Asia Pac J Clin Oncol 8:223–231
30. Ohgaki H, Kleihues P (2005) Population-based studies on incidence, survival rates, and genetic alterations in astrocytic and oligodendroglial gliomas. J Neuropathol Exp Neurol 64:479–489
31. DeAngelis LM (2001) Brain tumors. N Engl J Med 344:114–123
32. Tortori-Donati P, Rossi A, Biancheri R, Garrè ML, Cama A (2005) Brain tumors. In: Tortori-Donati P (ed) Pediatric neuroradiology. Springer, Berlin, pp 329–436
33. Jones DT, Mulholland SA, Pearson DM et al (2011) Adult grade II diffuse astrocytomas are genetically distinct from and more aggressive than their paediatric counterparts. Acta Neuropathol 121:753–761
34. Paugh BS, Qu C, Jones C et al (2010) Integrated molecular genetic profiling of pediatric high-grade gliomas reveals key differences with the adult disease. J Clin Oncol 28:3061–3068
35. Nishikawa R (2010) Pediatric and adult gliomas: how different are they? Neuro Oncol 12:1203–1204
36. Gajjar A, Bowers DC, Karajannis MA et al (2015) Pediatric brain tumors: innovative genomic information is transforming the diagnostic and clinical landscape. J Clin Oncol 33:2986–2998
37. Reilly KM (2009) Brain tumor susceptibility: the role of genetic factors and uses of mouse models to unravel risk. Brain Pathol 19:121–131
38. Pollack IF (2011) Multidisciplinary management of childhood brain tumors: a review of outcomes, recent advances, and challenges. J Neurosurg Pediatr 8:135–148
39. Piccardo A, Morana G (2014) Role of amino acid PET tracers in pediatric brain tumors. In: Cistaro A (ed) Atlas of PET/CT in pediatric patients. Springer, Milan, pp 157–163
40. Hoffman JM, Hanson MW, Friedman HS et al (1992) FDG-PET in pediatric posterior fossa brain tumors. J Comput Assist Tomogr 16:62–68
41. Pirotte B, Acerbi F, Lubansu A et al (2007) PET imaging in the surgical management of pediatric brain tumors. Childs Nerv Syst 23:739–751
42. Borgwardt L, Højgaard L, Carstensen H et al (2005) Increased fluorine-18 2-fluoro-2-deoxy-D-glucose (FDG) uptake in childhood CNS tumors is correlated with malignancy grade: a study with FDG positron emission tomography/magnetic resonance imaging coregistration and image fusion. J Clin Oncol 23:3030–3037
43. Utriainen M, Metsähonkala L, Salmi TT et al (2002) Metabolic characterization of childhood brain tumors: comparison of 18F-fluorodeoxyglucose and 11C-methionine positron emission tomography. Cancer 95:1376–1386
44. Kruer MC, Kaplan AM, Etzl MM Jr et al (2009) The value of positron emission tomography and proliferation index in predicting progression in low-grade astrocytomas of childhood. J Neurooncol 95:239–245
45. Zukotynski KA, Fahey FH, Kocak M et al (2011) Diffuse intrinsic brain stem glioma: a report from the pediatric brain tumor consortium. J Nucl Med 52:188–195
46. Zukotynski KA, Fahey FH, Vajapeyam S et al (2013) Exploratory evaluation of MR permeability with 18F-FDG PET mapping in pediatric brain tumors: a report from the pediatric brain tumor consortium. J Nucl Med 54:1237–1243
47. Hipp SJ, Steffen-Smith EA, Patronas N et al (2012) Molecular imaging of pediatric brain tumors: comparison of tumor metabolism using ^{18}F-FDG-PET and MRSI. J Neurooncol 109:521–527
48. Galldiks N, Kracht LW, Berthold F et al (2010) [11C]-L-methionine positron emission tomography in the management of children and young adults with brain tumors. J Neurooncol 96:231–239
49. Okochi Y, Nihashi T, Fujii M et al (2014) Clinical use of (11)C-methionine and (18)F-FDG-PET for germinoma in central nervous system. Ann Nucl Med 28:94–102
50. Uslu L, Donig J, Link M et al (2015) Value of 18F-FDG PET and PET/CT for evaluation of pediatric malignancies. J Nucl Med 56:274–286
51. Morana G, Piccardo A, Milanaccio C et al (2014) Value of 18F-3,4-dihydroxyphenylalanine PET/MR image fusion in pediatric supratentorial infiltrative astrocytomas: a prospective pilot study. J Nucl Med 55:718–723
52. Morana G, Piccardo A, Garrè ML et al (2013) Multimodal magnetic resonance imaging and 18F-L-dihydroxyphenylalanine positron emission tomography in early characterization of pseudoresponse and nonenhancing tumor progression in a pediatric patient with malignant transformation of ganglioglioma treated with bevacizumab. J Clin Oncol 31:e1–e5
53. Piccardo A, Lopci E, Conte M et al (2012) Comparison of 18F-DOPA PET/CT and 123IMIBG scintigraphy in stage 3 and 4 neuroblastoma: a pilot study. Eur J Nucl Med Mol Imaging 39:57–71
54. Piccardo A, Puntoni M, Lopci E et al (2014) Prognostic value of 18F-DOPA PET/CT at the time of recurrence in patients affected by neuroblastoma. Eur J Nucl Med Mol Imaging 41:1046–1056
55. Piccardo A, Morana G, Massollo M et al (2015) Brain metastasis from neuroblastoma depicted by 18F-DOPA PET/CT. Nucl Med Mol Imaging 49:241–242. doi:10.1007/s13139-015-0322-8
56. Ribeiro MJ, De Lonlay P, Delzescaux T et al (2005) Characterization of hyperinsulinism in infancy assessed with PET and 18F-fluoro-L-DOPA. J Nucl Med 46:560–566
57. Misch M, Guggemos A, Driever PH et al (2015) (18) F-FET-PET guided surgical biopsy and resection in children and adolescence with brain tumors. Childs Nerv Syst 31:261–267
58. Dunkl V, Cleff C, Stoffels G et al (2015) The usefulness of dynamic O-(2-18F-fluoroethyl)-L-tyrosine PET in the clinical evaluation of brain tumors in children and adolescents. J Nucl Med 56:88–92

59. Morana G, Piccardo A, Puntoni M et al (2015) Diagnostic and prognostic value of 18F-DOPA PET and 1H-MR spectroscopy in pediatric supratentorial infiltrative gliomas: a comparative study. Neuro Oncol. 17:1637–1647
60. Preuss M, Werner P, Barthel H et al (2014) Integrated PET/MRI for planning navigated biopsies in pediatric brain tumors. Childs Nerv Syst 30:1399–1403
61. Tsouana E, Stoneham S, Fersht N et al (2015) Evaluation of treatment response using integrated 18F-labeled choline positron emission tomography/magnetic resonance imaging in adolescents with intracranial non-germinomatous germ cell tumours. Pediatr Blood Cancer 62:1661–1663
62. Fraioli F, Shankar A, Hargrave D et al (2015) 18F-fluoroethylcholine (18F-Cho) PET/MRI functional parameters in pediatric astrocytic brain tumors. Clin Nucl Med 40:e40–e45
63. Sander JW (2003) The epidemiology of epilepsy revisited. Curr Opin Neurol 16:165–170
64. Engel J Jr (2006) Report of the ILAE classification core group. Epilepsia 47:1558–1568
65. Berg AT, Langfitt J, Shinnar S et al (2003) How long does it take for partial epilepsy to become intractable? Neurology 60:186–190
66. Meiners LC, Valk J, Jansen GH, van Veelen CW (1999) MR contribution in surgery of epilepsy. Eur Radiol 9:493–507
67. Stokes T, Shaw EJ, Juarez-Garcia A, Camosso-Stefinovic J, Baker R (2004) Clinical Guidelines and Evidence Review for the Epilepsies: diagnosis and management in adults and children in primary and secondary care. In The epilepsies: clinical practice guideline. Royal College of General Practitioners, London
68. Jackson GD, Connelly A, Duncan JS et al (1993) Detection of hippocampal pathology in intractable partial epilepsy: increased sensitivity with quantitative magnetic resonance T2 relaxometry. Neurology 43:1793–1799
69. Berg AT, Vickrey BG, Langfitt JT et al (2003) The multicenter study of epilepsy surgery: recruitment and selection for surgery. Epilepsia 44:1425–1433
70. Wyllie E, Comair YG, Kotagal P et al (1998) Seizure outcome after epilepsy surgery in children and adolescents. Ann Neurol 44:740–748
71. Horsley V (1892) An address on the origin and seat of epileptic disturbance: delivered before the Cardiff Medical Society. Br Med J 1:693–696
72. Pittau F, Grouiller F, Spinelli L et al (2014) The role of functional neuroimaging in pre-surgical epilepsy evaluation. Front Neurol 5:31
73. Patil S, Biassoni L, Borgwardt L (2007) Nuclear medicine in pediatric neurology and neurosurgery: epilepsy and brain tumors. Semin Nucl Med 37:357–381
74. Magistretti PJ, Pellerin L (1999) Astrocytes couple synaptic activity to glucose utilization in the Brain. News Physiol Sci 14:177–182
75. Kumar A, Chugani HT (2013) The role of radionuclide imaging in epilepsy, Part 1: sporadic temporal and extratemporal lobe epilepsy. J Nucl Med 54:1775–1781
76. Kumar A, Semah F, Chugani HT, Theodore WH (2012) Epilepsy diagnosis: positron emission tomography. Handb Clin Neurol 107:409–424
77. Gaillard WD, Kopylev L, Weinstein S et al (2002) Low incidence of abnormal 18FDGPET in children with new-onset partial epilepsy: a prospective study. Neurology 58:717–722
78. Szelies B, Herholz K, Heiss WD et al (1983) Hypometabolic cortical lesions in tuberous sclerosis with epilepsy: demonstration by positron emission tomography. J Comput Assist Tomogr 7:946–953
79. Theodore WH (1988) Antiepileptic drugs and cerebral glucose metabolism. Epilepsia 29(Suppl 2):S48–S55
80. Knowlton RC, Laxer KD, Ende G et al (1997) Presurgical multimodality neuroimaging in electroencephalographic lateralized temporal lobe epilepsy. Ann Neurol 42:829–837
81. Ryvlin P, Bouvard S, Le Bars D et al (1998) Clinical utility of flumazenil-PET versus [18F] fluorodeoxyglucose-PET and MRI in refractory partial epilepsy: a prospective study in 100 patients. Brain 121:2067–2081
82. Casse R, Rowe CC, Newton MD et al (2002) Positron emission tomography and epilepsy. Mol Imaging Biol 4:338–351
83. Muzik O, Chugani DC, Shen C et al (1998) Objective method for localization of cortical asymmetries using positron emission tomography to aid surgical resection of epileptic foci. Comput Aided Surg 3:74–82
84. Drzezga A, Arnold S, Minoshima S et al (1999) 18F-FDG PET studies in patients with extratemporal and temporal epilepsy: evaluation of an observer-independent analysis. J Nucl Med 40:737–746
85. Kumar A, Asano E, Chugani HT (2011) alpha-[11C]-methyl-L-tryptophan PET for tracer localization of epileptogenic brain regions: clinical studies. Biomark Med 5:577–584
86. Salamon N, Kung J, Shaw SJ et al (2008) FDG-PET/MRI coregistration improves detection of cortical dysplasia in patients with epilepsy. Neurology 71:1594–1601
87. Chassoux F, Rodrigo S, Semah F et al (2010) FDG-PET improves surgical outcome in negative MRI Taylor type focal cortical dysplasias. Neurology 75:2168–2175
88. Chandra PS, Salamon N, Huang J et al (2006) FDG-PET/MRI coregistration and diffusion-tensor imaging distinguish epileptogenic tubers and cortex in patients with tuberous sclerosis complex: a preliminary report. Epilepsia 47:1543–1549
89. Catana C, Drzezga A, Heiss W-D, Rosen BR (2012) PET/MRI for neurologic applications. J Nucl Med 53:1916–1925
90. Garibotto V, Heinzer S, Vulliemoz S et al (2013) Clinical applications of hybrid PET/MRI in neuroimaging. Clin Nucl Med 38:e13–e18

91. Werner P, Barthel H, Drzezga A, Sabri O (2015) Current status and future role of brain PET/MRI in clinical and research settings. Eur J Nucl Med Mol Imaging 42:512–526
92. Chugani HT, Phelps ME (1986) Maturational changes in cerebral function in infants determined by 18FDG positron emission tomography. Science 231:840–843
93. Suhonen-Polvi H, Ruotsalainen U, Ahonen A et al (1991) Positron emission tomography in asphyxiated infants. Preliminary studies of regional cerebral glucose metabolism using 18F-FDG. Acta Radiol Suppl 376:173
94. Lou HC (1988) Perinatal hypoxic–ischaemic brain damage and intraventricular haemorrhage. Baillieres Clin Obstet Gynaecol 2:213–220
95. Thorngren-Jerneck K, Ohlsson T, Sandell A et al (2001) Cerebral glucose metabolism measured by positron emission tomography in term newborn infants with hypoxic ischemic encephalopathy. Pediatr Res 49:495–501
96. Luo M, Li Q, Dong W et al (2014) Evaluation of mild hypothermia therapy for neonatal hypoxic-ischaemic encephalopathy on brain energy metabolism using 18F-fluorodeoxyglucose positron emission computed tomography. Exp Ther Med 8:1219–1224
97. Mohan KK, Chugani DC, Chugani HT (1999) Positron emission tomography in pediatric neurology. Semin Pediatr Neurol 6:111–119
98. Al-Essa MA, Bakheet SM, Patay ZJ et al (2000) Clinical and cerebral FDG PET scan in a patient with Krabbe's disease. Pediatr Neurol 22:44–47
99. Kumar A, Chugani HT, Chakraborty P, Huq AH (2011) Evaluation of neuroinflammation in X-linked adrenoleukodystrophy. Pediatr Neurol 44: 143–146
100. Kumar A, Chugani HT (2011) Niemann-Pick disease type C: unique 2-deoxy-2[^{18}F] fluoro-D-glucose PET abnormality. Pediatr Neurol 44:57–60
101. Awaad Y, Shamoto H, Chugani HT (1996) Hemidystonia improved by baclofen and PET scan findings in a patient with glutaric aciduria Type 1. J Child Neurol 11:167–169
102. Frackowiak RSJ, Herold S, Petty RK et al (1988) The cerebral metabolism of glucose and oxygen measured with positron emission tomography in patients with mitochondrial diseases. Brain 111:1009–1024
103. Iannetti P, Messa C, Spalice A et al (1994) Positron emission tomography in neuronal ceroid lipofuscinosis (Jansky-Bielschowsky disease): a case report. Brain Dev 16:459–462
104. Al-Essa M, Bakheet S, Al-Shamsan L et al (1999) 18Fluoro-2-deoxyglucose (18FDG) PET scan of the brain in type IV 3-methylglutaconic aciduria: clinical and MRI correlations. Brain Dev 21:24–29
105. Al-Essa M, Bakheet S, Patay ZJ et al (1999) 18Fluoro-2-deoxyglucose (18FDG) PET scan of the brain in propionic acidemia: clinical and MRI correlations. Brain Dev 21:312–317
106. Al-Essa MA, Bakheet SM, Patay ZJ et al (1999) Cerebral fluorine-18 labeled 2-fluoro-2-deoxyglucose positron emission tomography (FDG PET), MRI, and clinical observations in a patient with infantile G(M1) gangliosidosis. Brain Dev 21:559–562
107. Al-Essa MA, Bakheet SM, Patay ZJ et al (2000) Clinical, fluorine-18 labeled 2-fluoro-2-deoxyglucose positron emission tomography (FDG PET), MRI of the brain and biochemical observations in a patient with 4-hydroxybutyric aciduria; a progressive neurometabolic disease. Brain Dev 22:127–131
108. O'Tuama LA, Dickstein DP, Neeper R, Gascon GG (1999) Functional brain imaging in neuropsychiatric disorders of childhood. J Child Neurol 14:207–221
109. van Kuyck K, Gérard N, Van Laere K et al (2009) Towards a neurocircuitry in anorexia nervosa: evidence from functional neuroimaging studies. J Psychiatr Res 43:1133–1145
110. Villemagne PM, Naidu S, Villemagne VL et al (2002) Brain glucose metabolism in Rett Syndrome. Pediatr Neurol 27:117–122
111. Chipparini L, Granata T, Farina L et al (2003) Diagnostic imaging in 13 cases of Rasmussen's encephalitis: can early MRI suggest the diagnosis? Neuroradiology 45:171–183
112. Shetty-Alva N, Novotny EJ, Shetty T, Kuo PH (2007) Positron emission tomography in Rasmussen's encephalitis. Pediatr Neurol 36:112–114
113. Aron AM (2005) Sydenham's Chorea: Positron Emission Tomographic (PET) scan studies. J Child Neurol 20:832–833
114. Kumar A, Williams MT, Chugani HT (2015) Evaluation of basal ganglia and thalamic inflammation in children with pediatric autoimmune neuropsychiatric disorders associated with streptococcal infection and tourette syndrome: a positron emission tomographic (PET) study using 11C-[R]-PK11195. J Child Neurol 30:749–756
115. Purz S, Sabri O, Viehweger A et al (2014) Potential pediatric applications of PET/MR. J Nucl Med 55(Suppl 2):32S–39S

Part III

Less Frequent Clinical Applications

Multimodality Imaging of Huntington's Disease

13

Andrea Ciarmiello and Giampiero Giovacchini

13.1 Genetics of Huntington's Disease

13.1.1 Genetics

Huntington's disease (HD) is a hereditary autosomal dominant neurodegenerative disorder associated with progressive functional and brain structural changes, which inexorably lead to death. HD is caused by a mutation of the IT15 gene (HTT) on chromosome 4 that codes for a protein called the huntingtin protein [1]. HTT gene is composed by trinucleotide repeats (CAG). Normal subjects have a gene length that varies between 10 and 35 repeats [2], whereas HD individuals may show a CAG expansion ranging from 36- to over 120-folds.

Such degree of expansion determines the onset of Huntington's and other poly(CAG) diseases and the age at which these might occurs. It has been demonstrated that gene expansions ranging between 36 and 39 repeats do not necessarily predict the development of Huntington's disease, while development of the typical symptoms is always expected with extensions over 40 repeats [3] (Table 13.1). A higher expansion of the CAG tract is associated with earlier onset of disease; moreover, family-based studies have shown that the disease features the tendency to become progressively more aggressive and appear earlier as it passes down through successive generations [4]. The mutant form of the huntingtin protein is overexpressed by HTT gene-positive subjects. The progressive increase of intranuclear inclusions of huntingtin and ubiquitin fragments, which may precede by many years the clinical evidence of disease, determines HD phenotype [5].

13.2 Main Clinical Features of Huntington's Disease

Worldwide prevalence and mean incidence of Huntington's disease are, respectively, 2.7 per 100,000 and 0.38 per 100,000 per year [6].

Studies conducted in different countries show significant differences in prevalence between populations, with a lower prevalence in Asia compared to Europe, Canada, and North America and which are likely explained by the presence of huntingtin gene haplotypes [6].

HD is diagnosed on the basis of motor symptoms, psychiatric disorder, and dementia, yet

A. Ciarmiello (✉)
Department of Nuclear Medicine, S. Andrea Hospital, La Spezia, Italy
e-mail: andrea.ciarmiello@asl5.liguria.it

G. Giovacchini
Institute of Radiology and Nuclear Medicine, Stadtspital Triemli, Zurich, Switzerland

A. Ciarmiello, L. Mansi (eds.), *PET-CT and PET-MRI in Neurology*,
DOI 10.1007/978-3-319-31614-7_13

Table 13.1 CAG repeat expansion and probability to develop Huntington's disease. The table shows that a gene expansion ranging between 36 and 39 repeats is not necessarily associated to clinical onset, whereas development of the typical symptoms is always expected with extensions over 40 repeats

CAG repeats number	Classification	Disease status
<26	Normal	Unaffected
27–35	Intermediate	Unaffected
36–40	Reduced penetrance	+/– Affected
>40	Full penetrance	Affected

behavioral and neuropsychological changes may begin insidiously many years before the onset of the disease [7, 8].

The first motor manifestations of HD generally begin with chorea, a rapid and involuntary movement involving the face, trunk, and limbs. Initially movements are mild and not easily recognizable as the possible sign of a neurological disease. At this stage subjects are often unaware of the movements that seem to be part of purposeful actions. A recent study reported that almost 50 % of patients are unaware of motor symptoms despite the Unified Huntington's Disease Rating Scale (UHDRS) motor score being consistent with onset of motor HD [9]. Upon diagnosis, motor symptoms are generally associated with abnormal eye movements, especially in younger diseased subjects, while cognitive impairment is a characteristic component of the late stage of disease [10]. However, psychiatric disorders that commonly occur in Huntington's disease are often clinically evident even before the onset of motor signs [11].

13.3 PET Imaging in Huntington's Disease

13.3.1 Metabolic Imaging

PET metabolic imaging has greatly contributed to the understanding of biomolecular brain changes in HD, providing tools to improve the estimation of the age of disease onset and evaluate its progression over time. First HD molecular imaging studies date back to the early 1980s when using 18-fluorine labeled glucose radiotracer (18F-FDG) and PET (18F-FDG-PET) and demonstrated cell dysfunction mainly involving the caudate nucleus of gene-positive subjects [12]. Such pioneering studies showed the presence of a significant hypometabolism in the caudate nucleus of Huntington's gene mutation carriers, as compared to subjects unaffected by the mutation [12]. Further studies showed that the metabolic dysfunction of the caudate nucleus was present in asymptomatic subjects at risk for Huntington's disease [13]. Moreover dysfunction of the caudate nucleus was reported in a population of gene-positive subjects who showed no signs of cortical or caudate atrophy thus demonstrating that glucose hypometabolism preceded tissue loss [14]. Figure 13.1 shows the metabolic differences between 30 gene-negative subjects and a cohort of 71 gene mutation carriers at different stages of the disease. Analysis was performed under statistical parametric mapping (SPM). HD patients had lower 18F-FDG uptake in the striatum bilaterally as compared to healthy controls [15]. With the identification of the gene mutation responsible for HD, several studies were conducted on asymptomatic gene mutation carriers of different ages. These studies helped to understand that asymptomatic subjects far from disease onset feature a normal striatal metabolism which however begins to increase as the so-called zone of onset is approached [16]. Correlation of metabolic change occurring in the striatum with the expected time to onset is shown in Fig. 13.2. This figure illustrates the statistical map showing significantly hypometabolic brain regions obtained by introducing in the analysis the time to onset in years and rendered on SPM template normalized in a standard anatomical space.

Most affected regions were detected in caudate and putamen bilaterally. The linear correlation between glucose metabolism and time (Fig. 13.3) suggested the use of striatum metabolism in combination with CAG repeat number and subject age to improve accuracy of predicting model for age at onset [17].

Striatum metabolic impairment can be considered a strong indicator of disease at progression.

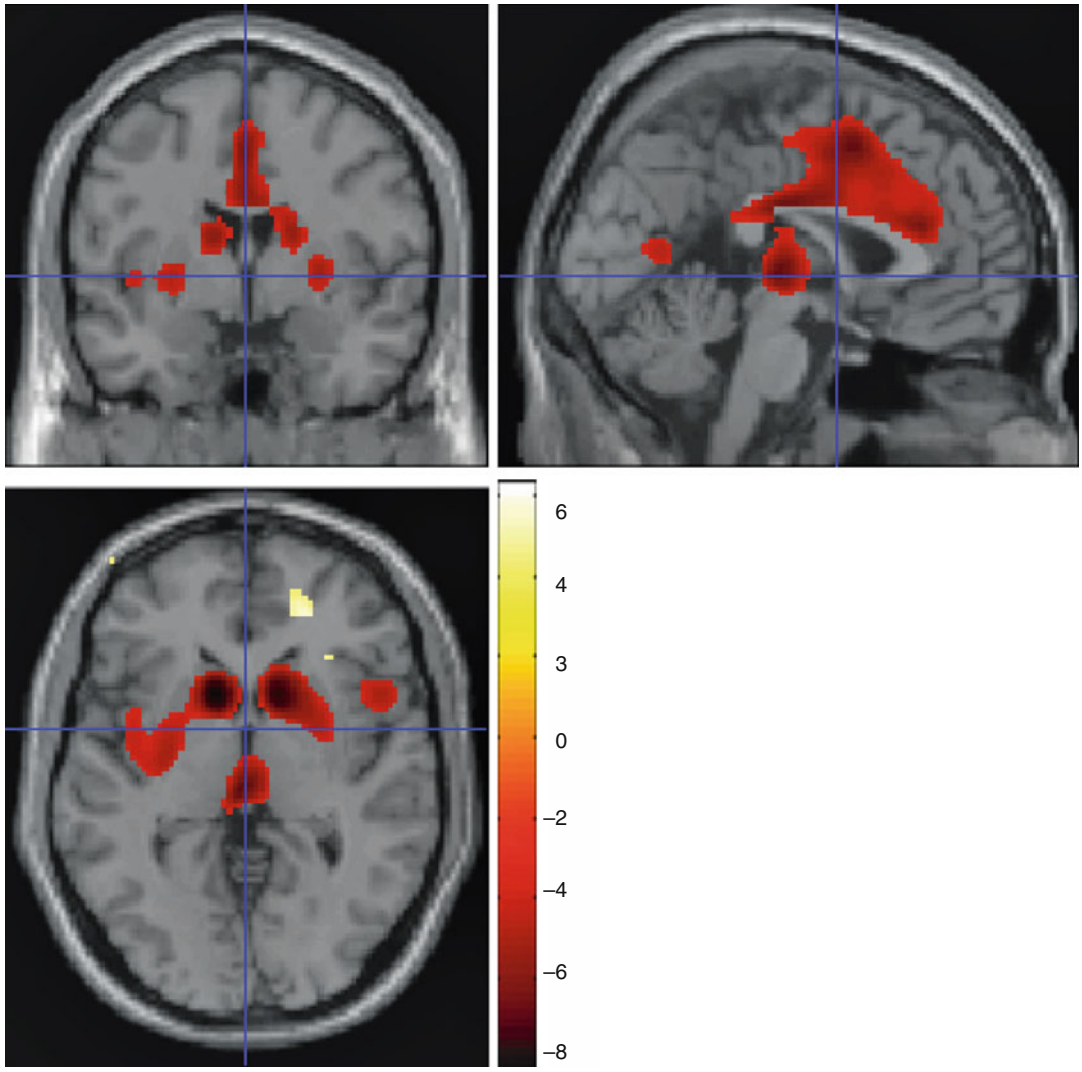

Fig. 13.1 18F-FDG-PET symptomatic gene-positive carriers vs. gene-negative subjects. Group comparisons were made using statistical parametric mapping. Brain areas showing significant reduced metabolism in symptomatic gene mutation carriers were rendered on single T1 SPM template. Statistical map was threshold at P corr = 0.05 with cluster extent >100

This finding was published by Young et al. in one of the first PET studies conducted in HD subjects. Authors found a positive correlation between caudate metabolism and subjects' overall functional capacity ($r = 0.906$; $p < 0.001$) in a group of fifteen symptomatic drug-free gene mutation carrier [18]. In Huntington's disease, cognitive impairment is almost always associated with motor disorders. Among the cognitive impairments, memory disorders are always clinically noticeable in HD. Berent et al. reported a significant correlation between neuropsychological memory score and caudate metabolism in HD population not evident in gene-negative subjects [19]. This evidence was also confirmed by more recent studies on animal model [20]. The striatum is undoubtedly the brain structure involved earliest and most heavily by the disease, but is certainly not the only one. Longitudinal studies have shown a progressive metabolic

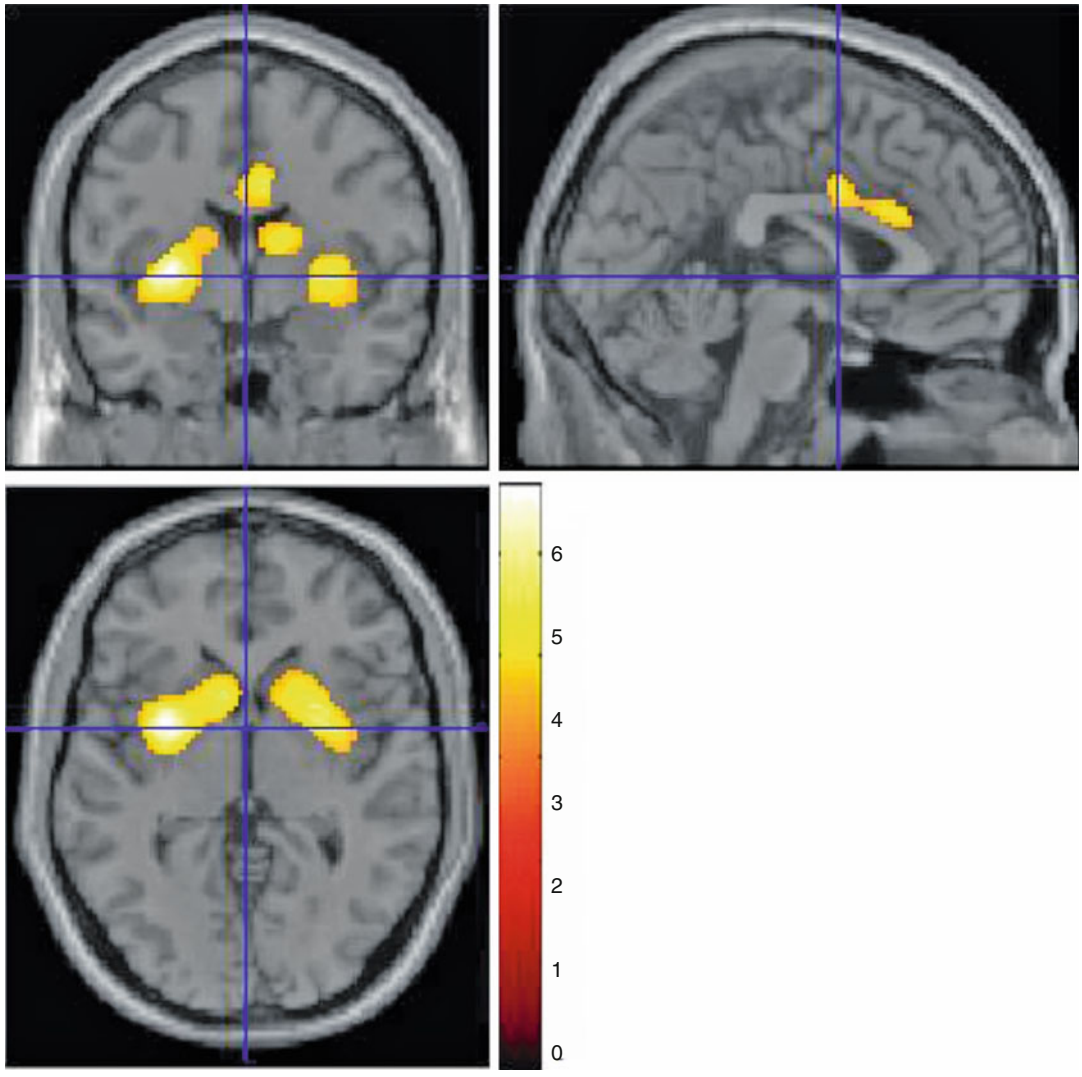

Fig. 13.2 Correlation of metabolic change with expected time to onset in preclinical gene mutation carrier. Analysis was made using statistical parametric mapping. Brain areas showing significant hypometabolism were rendered on single T1 SPM template. Statistical map was threshold at P corr = 0.05 with cluster extent >100

decline involving frontal, parietal, and temporal lobes in a cohort of 10 asymptomatic and 21 symptomatic gene mutation carriers [15]. The thalamus may be activated in presymptomatic gene carriers approaching the zone of onset as results of metabolic deactivation involving caudate nucleus or other cortical network nodes [21]. In accordance with the model of brain default mode (BDM) network [22], Feigin in 2007 described a relation between medial temporal and striatal hypometabolism and occipital metabolic activation [21]. Although striatal and cortical hypometabolism have been reported by many authors in Huntington's disease, it is not completely clear whether it is connected to the neuronal dysfunction or neuron loss. In the first hypothesis, the metabolic defect would lead to the death of neurons, whereas in the second cell loss and consequent atrophy would result in a false signal loss. Another point to consider is the relatively low spatial resolution of PET scanners. In fact even the most modern ones have a spatial

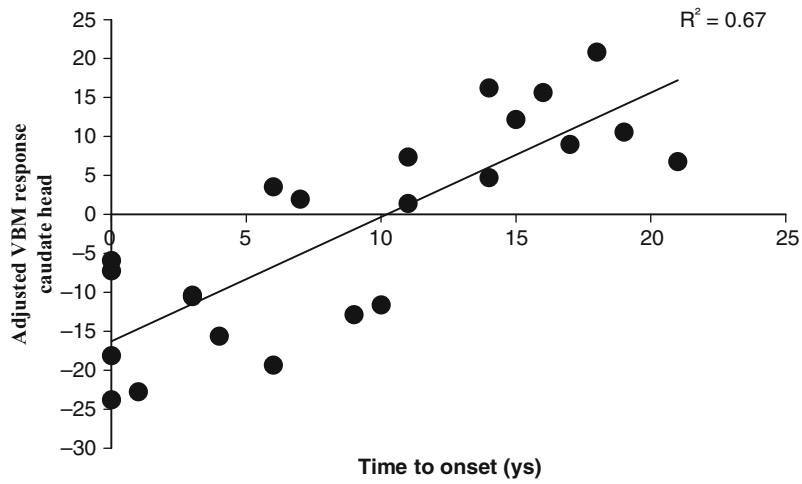

Fig. 13.3 Correlation of metabolic change with time in preclinical gene mutation carrier. Caudate head metabolism was found to correlate significantly with the expected time to disease onset

resolution that is unlikely less than 4–5 mm at full width at half maximum (FWHM). Therefore, for those brain structures the size of which approach that of the scanner's resolution, the tracer concentration is influenced by the radioactivity of the surrounding regions [23]. This effect, known as partial volume effect (PVE), is particularly critical when imaging subjects with structural abnormalities (e.g., atrophy). In these cases it would be necessary to separate the "true estimate" due to the metabolic defect by the "false estimate" given by atrophy [24]. To overcome these problems, the partial volume effects are generally corrected using an MR-based coregistration approach [25].

13.3.2 Receptorial Imaging

In addition to metabolism, HD studies have widely addressed the dopaminergic system as well. D1 and D2 dopamine receptors represent the major receptors subtypes expressed in the striatum of the adult brain. Dopamine receptors provide a pathway between the striatum and the output nuclei of the basal ganglia in a direct and indirect fashion [26]. Unbalanced activities of these pathways are reported to be associated to a heterogeneous group of movement abnormalities including Parkinson's disease and other forms of dystonias [27]. Raclopride has a high affinity for D2 receptor and has been therefore one of the most widely used tracers for receptor imaging. ^{11}C-Raclopride PET-based studies reported significant decrease of D2 receptor binding potential in symptomatic gene mutation carriers [28]. Interestingly, authors reported a significant correlation between D2 receptor density decrease and disease progression, thus pointing to the specific binding estimate as a possible biomarker of disease progression [28]. In asymptomatic gene-positive subjects, D2 receptor density decrease is significantly associated with CAG repeat number [16]. Moreover, serial ^{11}C-raclopride PET scan in asymptomatic HD showed an annual loss of receptor density of approximately 2% [29]. Andrews et al. reported that asymptomatic HD showing clinical evidence of disease progression had twice as higher receptor density decrease compared to non converted gene-positive subjects [29]. Similar studies confirmed the receptor density changes in asymptomatic HD but did not find any significant increased rate of receptor density around the zone of onset [30]. Striatal dopamine receptor decrease is also associated to cognitive performance in HD. Receptor binding as assessed by ^{11}C-raclopride PET significantly correlates with cognitive performance. Lawrence et al. reported a strong correlation between binding potential and memory performance (Spearman's rank correlation = 0.71; $P > 0.01$) [31]. Significant changes of dopamine receptor density have also been described in cortical areas as results of possible cortical neuronal damage.

Cortical dopaminergic dysfunction is a common finding in premanifest – as well as symptomatic – HD gene mutation carriers. Cortical areas most frequently involved in binding decreases were found in temporal and frontal lobes and have been associated with cognitive impairment [32]. A significant association was reported between D2 receptor cortical binding and scores on tests assessing attention and executive functions. Authors found that subjects with decreased binding had worse cognitive performance than subjects with normal dopamine receptor binding, independently from striatal D2 dysfunction [33].

In addition to changes in the postsynaptic, a decrease in presynaptic dopamine transporters was also reported. A ^{11}C-beta-CIT-PET-based study reported decreased striatal binding in gene-positive subject as compared with normal controls. Statistical comparison revealed a significant decrease in both caudate (53 %; $p = 0.02$) and putamen (55 %; $P < 0.02$) in gene positive as compared to gene-negative subjects [28]

13.3.3 Inflammation Imaging

Another feature associated with a variety of neurodegenerative disorders including Parkinson's disease (PD), Alzheimer's disease (AD), amyotrophic lateral sclerosis (ALS), almost all of the tauopathies [34], and Huntington's disease is neuroinflammation. Imaging of neuroinflammation is mainly based on the measure of activated microglia that may play a relevant role in neuronal damage and death.

The molecular target of neuroinflammation is an 18 kDa protein translocator protein (TSPO) located on the outer membrane of mitochondria. TSPO is overexpressed by activated microglia and is involved in many functions including apoptosis [35]. PK11195 has a high affinity for TSPO and has been used as tracer of inflammation imaging. Increased binding of ^{11}C-PK11195 has been reported in several neurodegenerative diseases such as dementia and multiple sclerosis [36]. Increased striatum binding of ^{11}C-PK11195 was reported in asymptomatic gene-positive subjects [37]. Authors also reported a strong correlation between ^{11}C-PK11195 striatal increase and the estimated age at onset in premanifest HD subjects [37]. Increased striatal binding of ^{11}C-PK11195 was reported also in HD patients which significantly correlated with disease severity as assessed by Unified Huntington's Disease Rating Scale score [38]. Besides striatum, increased binding of PK11195 in prefrontal cortex and anterior cingulate showed the presence of significant microglia activation in brain regions different from striatum [38].

13.4 MR Imaging in Huntington's Disease

13.4.1 Structural MR Imaging

The pathological hallmark of HD is the progressive atrophy of brain tissues which primarily involves the caudate nucleus and putamen [39, 40]. Several authors report a significant volume reduction of both the caudate nucleus and the putamen in manifest HD compared to normal subjects [41, 42]. In gene-positive subjects, striatal volume decrease is an early pathological event which begins many years before the disease onset. Aylward et al. reported a significant correlation between volumes of all basal ganglia structures as measured by MRI and estimated the years to onset showing that gene-positive subjects who were close to the onset had significantly lower caudate and putamen volume compared to controls [43]. Striatal volume loss also correlates with CAG repeat expansion and disease duration [44]. The clinical manifestations of the disease depend on the striatum structure most affected: motor disorders correlate with atrophy of the putamen, whereas caudate atrophy mainly correlates with cognitive impairment [41, 42].

Alongside the involvement of deep nuclei, there is also a progressive volume reduction of the cortical gray matter. Volume decrease of cortical gray matter has been reported in the premanifest, as well as in symptomatic, gene-positive subject [45]. Cortical thinning

increases progressively in the course of the disease and correlates with clinical measures of motor and cognitive impairment. Rosas et al. reported a significant relationship between TFC and cortical thinning in motor, supero-parietal cortex and the cuneus [46]. Investigating on the possible association between caudate volume and cognitive status, Rosas found a significant correlation between caudate volume and cognitive performance as measured by neuropsychological tests as verbal fluency, symbol digit, and Stroop color-word [46].

White matter (WM) atrophy has been described in gene-positive subjects. In a premanifest population, WM was reported to be significantly lower in subjects far from the estimated age at onset, compared to healthy controls [15]. Ciarmiello et al. also described a significant correlation between WM volume decrease and estimated years to onset [15]. WM volume reduction in symptomatic patients has been associated to decline in motor and cognitive performance [47].

As years pass HD subjects undergo the combined effect of GM and WM loss, which results in a significant relative increase of CSF volume. Indeed CSF volume, corrected for head size (fCSF), starts to increase in the presymptomatic stage progressing through the advanced stages of disease (Fig. 13.4). The yearly increase of fCSF is linearly correlated to CAG repeat number in gene-positive preclinical and affected subjects ($R2=0.24$, $P=0.0043$) [48]. fCSF also was found associated with a decreasing disability scale score and an increasing clinical severity of HD calculated as loss of TFC score unit/year [48]. Findings reported so far suggests that MR volumetric changes may be useful to improve the prediction of disease onset in preclinical gene-positive subjects and to assess treatment efficacy in experimental trials in manifest HD.

13.4.2 Functional MR Imaging

Studies on resting state networks have demonstrated structural and functional connectivity disruption in several dementia, motor disorders, and other major neurodegenerative diseases [49–52]. In fact, functional magnetic resonance imaging (fMRI) is capable of detecting the brain's response to stimuli, i.e., the blood oxygen level-dependent signal fluctuations of the brain's resting state activity and reactivation.

Studies on brain network under resting conditions have evidenced a widespread reduced connectivity in presymptomatic and symptomatic HD gene mutation carriers which can be found in premanifest and manifest gene mutation carriers [53]. By means of independent component analysis, Werner et al. reported a significant alteration of resting functional connectivity in HD and reported main changes to be found in the prefrontal cortex, thalamus, and caudate nucleus. Moreover, it was found that frontoparietal connectivity was reported to be inversely correlated

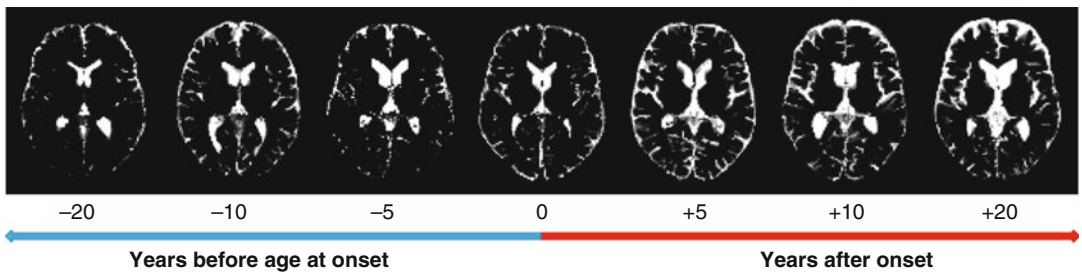

Fig. 13.4 Progressive stage-dependent cerebrospinal fluid compartment increase. Axial segmented map of cerebrospinal fluid obtained from magnetic resonance imaging scan in gene-positive Huntington's disease subjects at different stages of the disease. The volume of cerebrospinal fluid (*white color*) increases progressively from early premanifest to the advanced disease stages as a result of *gray* and *white* matter loss

with TFC score, which translates from a clinical point of view as a more severe disability [54].

Several fMRI studies reported altered functional brain connectivity in presymptomatic and manifest HD gene mutation carriers. Brain network changes are characterized by a progressive deactivation of the striatum and activation of different clusters widespread in the frontal and parietal cortex. Cortical activation is recognized as mechanism to offset neuronal loss in premanifest subjects in proximity of the onset area and in symptomatic HD. Premanifest subjects approaching the estimated age at onset showed a reduced striatal activation and a significantly increased frontal parietal activation than gene-positive individuals still far from onset and normal controls [55]. Dorsolateral prefrontal cortex (DLPFC) network is involved in executive functions and in working memory. Activation level of dorsolateral prefrontal cortex is positively correlated to UHDRS cognitive subscore [55]. As compared to control, premanifest gene mutation carriers showed longitudinal increased activation in the left DLPFC and medial frontal cortex which represent a compensatory response to early clinical changes occurring in proximity of disease onset [56]. In symptomatic HD brain network changes are dominated by cortical compensatory activation in response to the progressive deactivation affecting critical nodes of the network. DLPFC and anterior cingulate are the brain network regions most frequently involved and whose signal changes correlate with disease severity as measured by UHDRS [56–58].

Cognitive and mood disorders are associated with altered frontoparietal association. Reduced functional association between left premotor and medial prefrontal cortex in presymptomatic gene-positive subjects is associated to cognitive and mood impairment which increase significantly when first clinical signs of disease became noticeable [59]. Network connectivity begins to change very soon in the life of the of gene-positive carriers. Early changes start years before onset and continue through all the stages of disease thus suggesting a possible role as biomarker in experimental therapeutics.

13.5 Future Directions

In the last decades, PET and MRI have changed dramatically the paradigm of the functioning brain in many neurodegenerative diseases including HD. In the attempt to precisely map the brain regions related to each function, evidences led researchers to a new paradigm of the brain where functions are distributed in cortical nodes located in different lobes. Until few years ago, Huntington's disease was considered specifically related to caudate nucleus functional and structural changes but now the evidence obtained by new imaging technologies has allowed to understand that other brain structures are involved in the neurodegenerative process. New information on the molecular biology of neurodegeneration in patients with Huntington's could derive from the use of new hybrid imaging devices that allow the simultaneous scan of structural and functional images [60, 61]. The new challenge will be to visualize multiparametric functional images obtained by PET and fMRI or spectroscopy in the anatomical context derived by MR. The availability of MR images may used to limit some drawback of standalone PET imaging. As pointed out by several authors, there are some critical points related to the characteristics of PET modality to take into account. Among them, the low spatial resolution of the scanner and the partial volume effect may be sources of error thus limiting the accuracy of the PET estimates.

Such drawbacks may, however, be overcome by increasingly available hybrid technologies such as PET/CT and PET/MR. New studies focusing on HD performed on hybrid modality should incorporate into processing design and analysis information derived from both modalities. This approach would allow us to correct metabolic or receptorial measure taking into account the structural abnormalities of the brain (e.g., atrophy). Simultaneous acquisition of structural and functional images would also help to correct the effects of PET low spatial resolution.

References

1. (1993) A novel gene containing a trinucleotide repeat that is expanded and unstable on Huntington's disease chromosomes. The Huntington's Disease Collaborative Research Group. Cell 72(6):971–983
2. Kremer B et al (1994) A worldwide study of the Huntington's disease mutation. The sensitivity and specificity of measuring CAG repeats. N Engl J Med 330(20):1401–1406
3. Walker FO (2007) Huntington's disease. Lancet 369(9557):218–228
4. Norremolle A et al (1995) Correlation between magnitude of CAG repeat length alterations and length of the paternal repeat in paternally inherited Huntington's disease. Clin Genet 47(3):113–117
5. Davies SW et al (1997) Formation of neuronal intranuclear inclusions underlies the neurological dysfunction in mice transgenic for the HD mutation. Cell 90(3):537–548
6. Pringsheim T et al (2012) The incidence and prevalence of Huntington's disease: a systematic review and meta-analysis. Mov Disord 27(9):1083–1091
7. Paulsen JS et al (2001) Clinical markers of early disease in persons near onset of Huntington's disease. Neurology 57(4):658–662
8. Rosenblatt A et al (2003) Predictors of neuropathological severity in 100 patients with Huntington's disease. Ann Neurol 54(4):488–493
9. McCusker EA et al (2013) Unawareness of motor phenoconversion in Huntington disease. Neurology 81(13):1141–1147
10. Snowden J et al (2001) Longitudinal evaluation of cognitive disorder in Huntington's disease. J Int Neuropsychol Soc 7(1):33–44
11. van Duijn E et al (2008) Cross-sectional study on prevalences of psychiatric disorders in mutation carriers of Huntington's disease compared with mutation-negative first-degree relatives. J Clin Psychiatry 69(11):1804–1810
12. Kuhl DE (1984) Imaging local brain function with emission computed tomography. Radiology 150(3):625–631
13. Mazziotta JC et al (1987) Reduced cerebral glucose metabolism in asymptomatic subjects at risk for Huntington's disease. N Engl J Med 316(7):357–362
14. Hayden MR et al (1986) Positron emission tomography in the early diagnosis of Huntington's disease. Neurology 36(7):888–894
15. Ciarmiello A et al (2006) Brain white-matter volume loss and glucose hypometabolism precede the clinical symptoms of Huntington's disease. J Nucl Med 47(2):215–222
16. Antonini A et al (1996) Striatal glucose metabolism and dopamine D2 receptor binding in asymptomatic gene carriers and patients with Huntington's disease. Brain 119(Pt 6):2085–2095
17. Ciarmiello A et al (2012) 18F-FDG PET uptake in the pre-Huntington disease caudate affects the time-to-onset independently of CAG expansion size. Eur J Nucl Med Mol Imaging 39(6):1030–1036
18. Young AB et al (1986) PET scan investigations of Huntington's disease: cerebral metabolic correlates of neurological features and functional decline. Ann Neurol 20(3):296–303
19. Berent S et al (1988) Positron emission tomographic scan investigations of Huntington's disease: cerebral metabolic correlates of cognitive function. Ann Neurol 23(6):541–546
20. Kirch RD et al (2013) Early deficits in declarative and procedural memory dependent behavioral function in a transgenic rat model of Huntington's disease. Behav Brain Res 239:15–26
21. Feigin A et al (2007) Thalamic metabolism and symptom onset in preclinical Huntington's disease. Brain 130(Pt 11):2858–2867
22. Raichle ME, Snyder AZ (2007) A default mode of brain function: a brief history of an evolving idea. Neuroimage 37(4):1083–1090, discussion 1097–9
23. Hoffman EJ, Huang SC, Phelps ME (1979) Quantitation in positron emission computed tomography: 1. Effect of object size. J Comput Assist Tomogr 3(3):299–308
24. Fazio F, Perani D (2000) Importance of partial-volume correction in brain PET studies. J Nucl Med 41(11):1849–1850
25. Quarantelli M et al (2004) Integrated software for the analysis of brain PET/SPECT studies with partial-volume-effect correction. J Nucl Med 45(2):192–201
26. Levey AI et al (1993) Localization of D1 and D2 dopamine receptors in brain with subtype-specific antibodies. Proc Natl Acad Sci U S A 90(19):8861–8865
27. Karimi M, Perlmutter JS (2015) The role of dopamine and dopaminergic pathways in dystonia: insights from neuroimaging. Tremor Other Hyperkinet Mov (N Y) 5:280
28. Ginovart N et al (1997) PET study of the pre- and post-synaptic dopaminergic markers for the neurodegenerative process in Huntington's disease. Brain 120(Pt 3):503–514
29. Andrews TC et al (1999) Huntington's disease progression. PET and clinical observations. Brain 122(Pt 12):2353–2363
30. van Oostrom JC et al (2009) Changes in striatal dopamine D2 receptor binding in pre-clinical Huntington's disease. Eur J Neurol 16(2):226–231
31. Lawrence AD et al (1998) The relationship between striatal dopamine receptor binding and cognitive performance in Huntington's disease. Brain 121(Pt 7):1343–1355
32. Pavese N et al (2003) Progressive striatal and cortical dopamine receptor dysfunction in Huntington's disease: a PET study. Brain 126(Pt 5):1127–1135
33. Pavese N et al (2010) Cortical dopamine dysfunction in symptomatic and premanifest Huntington's disease gene carriers. Neurobiol Dis 37(2):356–361
34. Ciarmiello A (2011) Imaging of neuroinflammation. Eur J Nucl Med Mol Imaging 38(12):2198–2201

35. Sutter AP et al (2002) Specific ligands of the peripheral benzodiazepine receptor induce apoptosis and cell cycle arrest in human esophageal cancer cells. Int J Cancer 102(4):318–327
36. Cagnin A et al (2001) In-vivo measurement of activated microglia in dementia. Lancet 358(9280):461–467
37. Politis M et al (2011) Microglial activation in regions related to cognitive function predicts disease onset in Huntington's disease: a multimodal imaging study. Hum Brain Mapp 32(2):258–270
38. Pavese N et al (2006) Microglial activation correlates with severity in Huntington disease: a clinical and PET study. Neurology 66(11):1638–1643
39. Rosas HD et al (2001) Striatal volume loss in HD as measured by MRI and the influence of CAG repeat. Neurology 57(6):1025–1028
40. Paulsen JS et al (2008) Detection of Huntington's disease decades before diagnosis: the Predict-HD study. J Neurol Neurosurg Psychiatry 79(8):874–880
41. Harris GJ et al (1992) Putamen volume reduction on magnetic resonance imaging exceeds caudate changes in mild Huntington's disease. Ann Neurol 31(1):69–75
42. Harris GJ et al (1996) Single photon emission computed tomographic blood flow and magnetic resonance volume imaging of basal ganglia in Huntington's disease. Arch Neurol 53(4):316–324
43. Aylward EH et al (1996) Basal ganglia volume and proximity to onset in presymptomatic Huntington disease. Arch Neurol 53(12):1293–1296
44. Aylward EH et al (1997) Longitudinal change in basal ganglia volume in patients with Huntington's disease. Neurology 48(2):394–399
45. Tabrizi SJ et al (2011) Biological and clinical changes in premanifest and early stage Huntington's disease in the TRACK-HD study: the 12-month longitudinal analysis. Lancet Neurol 10(1):31–42
46. Rosas HD et al (2008) Cerebral cortex and the clinical expression of Huntington's disease: complexity and heterogeneity. Brain 131(Pt 4):1057–1068
47. Hobbs NZ et al (2010) The progression of regional atrophy in premanifest and early Huntington's disease: a longitudinal voxel-based morphometry study. J Neurol Neurosurg Psychiatry 81(7):756–763
48. Squitieri F et al (2009) Distinct brain volume changes correlating with clinical stage, disease progression rate, mutation size, and age at onset prediction as early biomarkers of brain atrophy in Huntington's disease. CNS Neurosci Ther 15(1):1–11
49. Wang K et al (2007) Altered functional connectivity in early Alzheimer's disease: a resting-state fMRI study. Hum Brain Mapp 28(10):967–978
50. Sheline YI, Raichle ME (2013) Resting state functional connectivity in preclinical Alzheimer's disease. Biol Psychiatry 74(5):340–347
51. Hacker CD et al (2012) Resting state functional connectivity of the striatum in Parkinson's disease. Brain 135(Pt 12):3699–3711
52. Baik K et al (2014) Dopaminergic modulation of resting-state functional connectivity in de novo patients with Parkinson's disease. Hum Brain Mapp 35(11):5431–5441
53. Dumas EM et al (2013) Reduced functional brain connectivity prior to and after disease onset in Huntington's disease. Neuroimage Clin 2:377–384
54. Werner CJ et al (2014) Altered resting-state connectivity in Huntington's disease. Hum Brain Mapp 35(6):2582–2593
55. Wolf RC et al (2007) Dorsolateral prefrontal cortex dysfunction in presymptomatic Huntington's disease: evidence from event-related fMRI. Brain 130(Pt 11):2845–2857
56. Poudel GR et al (2015) Functional changes during working memory in Huntington's disease: 30-month longitudinal data from the IMAGE-HD study. Brain Struct Funct 220(1):501–512
57. Thiruvady DR et al (2007) Functional connectivity of the prefrontal cortex in Huntington's disease. J Neurol Neurosurg Psychiatry 78(2):127–133
58. Georgiou-Karistianis N et al (2014) Functional magnetic resonance imaging of working memory in Huntington's disease: cross-sectional data from the IMAGE-HD study. Hum Brain Mapp 35(5):1847–1864
59. Unschuld PG et al (2012) Depressive symptoms in prodromal Huntington's disease correlate with Stroop-interference related functional connectivity in the ventromedial prefrontal cortex. Psychiatry Res 203(2-3):166–174
60. Ciarmiello A et al (2014) Hybrid SPECT/CT imaging in neurology. Curr Radiopharm 7(1):5–11
61. Mansi L, Ciarmiello A (2014) Perspectives on PET/MR imaging: are we ready for clinical use? J Nucl Med 55(4):529–530

Neuroimaging in Amyotrophic Lateral Sclerosis

14

Angelina Cistaro

14.1 Introduction

Amyotrophic lateral sclerosis (ALS) is a neurodegenerative process with a not yet fully understood etiology, resulting in progressive muscle paralysis [1]. It is the most frequent motor neuron disorder in adults characterized by a progressive alteration in the upper motor neurons located in the brain and lower motor neurons in the brainstem and spinal cord, with variable involvement of extramotor brain regions [2].

The cause of ALS is still unknown and no disease-modifying treatments are available, apart from the antiglutamatergic drug riluzole, which increases survival by about 2–3 months without affecting muscle strength [3]. Progression is always fatal, leading to death from respiratory failure after a median of evolution of 36 months from onset [4, 5].

The neuropathological hallmark of ALS is, along with corticospinal tract degeneration, a selective loss of anterior horn cells of the spinal cord and cells in lower motor cranial nerve nuclei [6].

The main clinical variants of ALS include primary muscular atrophy (PMA), primary lateral sclerosis (PLS), and progressive bulbar palsy (PBP) [1].

Each patient differs in their body region of onset, disease progression, and the combination of upper and lower motor neurons involved, meaning that onset and disease course in ALS are heterogeneous [7, 8]. In two-thirds of patients, the onset is at the spinal level, generally hypotrophy and weakness of limbs muscles; in one-third the onset is at bulbar level, dysphagia and dysarthria being the first symptoms [6]. Besides clinical heterogeneity, underlying pathophysiology in ALS seems to be similarly variable. Monogenetic traits have been identified in familial cases, as well as complex traits with contributions from multiple genetic and environmental factors [9]. Additionally, the same genetic error can result in different clinical phenotypes, while different genotypes can produce the same clinical phenotype.

Five to ten percent of cases are familial, with dominant inheritance of the pathological trait in almost all cases [5]. The list of genes linked to familial ALS is currently growing dramatically, from the description of the first mutations in the superoxide dismutase gene (SOD1) in 1993 to the last description of the C9orf72 gene that appears to be one of the most important genetic factors in frequency in Western Europe [5], followed by SOD1, TARDBP, and FUS mutations [10]. The relationship between ALS and genetic factors is continuously being strengthened by such findings [5, 11].

A. Cistaro
Positron Emission Tomography Centre,
IRMET, Affidea, Turin, Italy
e-mail: a.cistaro@irmet.com

A. Ciarmiello, L. Mansi (eds.), *PET-CT and PET-MRI in Neurology*,
DOI 10.1007/978-3-319-31614-7_14

In the remaining sporadic ALS cases, the pathophysiology remains unresolved. Several pathways have been proposed, with mitochondrial dysfunction, protein aggregate formation, excitotoxicity, axonal transport malfunction, mutant-derived oxidative damage, lack of growth factors, and inflammation all purported to play a role in the motor neuron death process [12].

There is a growing body of evidence demonstrating that ALS is a multisystem neurological disorder. Autopsy studies have shown that degeneration of central nervous system structures is not restricted to the primary motor cortex and the pyramidal tract [13–16]. In addition to motor signs, cognitive signs are detected by neuropsychological tests in about 50 % of patients with sporadic ALS, and typical frontotemporal dementia (FTD) occurs in approximately 10 % of the patients [17, 18]. Association of ALS and FTD occurs in the majority of *C9ORF72*-linked familial ALS (FALS) [19, 20].

Atypical clinical features can be associated, defining "ALS plus" [21] syndromes with signs and symptoms involving the sensory (particularly in *SOD1*-linked FALS) [22–31], extrapyramidal [23, 32–40], cerebellar [32, 41], ocular [42, 43], and autonomic [44] systems.

Due to its clinical heterogeneity and the lack of biological markers to diagnose ALS, the delay between the first symptoms and the diagnosis is evaluated at 9–13 months [21], justifying the interest for objective neuroimaging markers of upper motor neuron (UMN) involvement.

Diagnostic workup is complex. Currently, the diagnosis of ALS is based on clinical history and examination, electrodiagnostic tests [45], neuroimaging including computed tomography (CT) or magnetic resonance imaging (MRI) of the brain and spinal cord myelogram, clinical laboratory tests, muscle and/or nerve biopsy, and genetic testing [1].

The combination of upper motor neuron (UMN) and lower motor neuron (LMN) impairment that cannot be explained by any other disease process by means of the diagnostic workup, together with progression, is suggestive of ALS [46].

The diagnostic delay is increased in patients who present isolated lower motor neuron (LMN) signs [5]. In fact, the presence of central signs may allow confirming the diagnosis of ALS, but this is not the case in all patients, notably because the severity of peripheral signs can mask central signs, decreasing their detectability [47]. Furthermore, it has been estimated that clinical UMN signs are absent at first examination in 7–10 % of patients who further develop full-blown ALS [48, 49]. This is particularly true of patients diagnosed with progressive muscular atrophy (PMA), for whom upper motor neuron degeneration is evident only on postmortem examination [50].

Appropriate investigations are needed to rule out ALS-mimicking conditions, such as multifocal motor neuropathy and Kennedy's disease, which are unrelated disorders that may present similar clinical features to ALS or its variants [46, 51] and are considered to be responsible for diagnostic error in 5–10 % of cases [52, 53]. Also some cervical spondylotic myelopathies may be sometimes confused with ALS, in particular when the patients present spasticity and hyperreflexia in the lower limbs and concomitant muscle atrophy and fasciculations of the upper limbs. In this case MRI may help rule out spinal cord compression [54].

Diagnostic accuracy for ALS would improve if upper motor neuron deficits could be established objectively [8]. Current clinical practice uses neuroimaging to exclude conditions with similar clinical presentations to ALS, but not to either confirm or facilitate the diagnosis of ALS. An objective upper motor neuron imaging marker could shorten diagnostic delay and reduce the proportion of misdiagnosed cases [55]. Furthermore, there is an unmet need to find specific and early biomarkers to help to diagnose and characterize phenotype or progression [4].

Moreover, imaging in ALS could identify the involvement of extramotor brain regions, such as degenerative changes in frontotemporal brain region [56]. Such changes are associated with behavioral and cognitive deficits, which are mild in up to 32 % of cases and moderate to severe in up to 19 % of cases [57]. These cognitive and behavioral deficits are similar to those found in frontotemporal dementia (FTD), which forms a

clinicopathological spectrum with ALS as up to 15 % of patients with ALS meet the criteria for FTD [55].

In the last decades, neuroimaging by the positron emission tomography (PET) and magnetic resonance imaging has contributed to the knowledge of functional chances occurring in ALS in combination with both cognitive and motor impairments [58].

The purpose of ALS imaging is twofold. The first is to further progress our understanding of disease pathology and pathophysiology, in which group analysis is appropriate, and the second is to develop an imaging-based technology that enhances individualized diagnostic accuracy beyond the best clinical practice. Based on the critical appraisal of the shortcomings and achievements of recent ALS imaging studies, optimized study recommendations can be outlined.

14.2 Positron Emission Tomography and Magnetic Resonance Imaging in Amyotrophic Lateral Sclerosis

The combination of different MRI techniques and PET (Fig. 14.1) imaging might improve sensitivity and specificity for ALS. MRI also allows structure and function in ALS to be associated via the combination of resting-state functional MRI with diffusion tensor imaging and voxel-based morphometry.

Since early studies with nuclear imaging in ALS, patient demonstrated the reduction of glucose metabolism in the motor cortex [59].

In 1988 Di Chiro and coworkers [53], using PET with 18F-FDG, reported a generalized cerebral glucose hypometabolism in amyotrophic lateral sclerosis (ALS) patients with upper motor neuron signs. Furthermore, they showed that no significative cerebral hypometabolism was seen in the four ALS patients with only signs of lower motor neuron involvement. However in this last group although not significative, the hypometabolism suggests that there is cortex hypofunction due to the loss of signal from lower motor neuron throughout corticospinal trait. This is partially consistent with the status of spinal LMNs, which degenerate after their target tissue is lost by axotomy [53]. It has been shown that each degenerated dendritic branch represents a loss of contact with at least four or five other Betz cells via dendritic bundles. The authors concluded that the hypometabolism noted with FDG-PET in anatomically "healthy" cortex may reflect such a loss of synapses in the cortical network extending beyond the motor-sensory cortical regions. This hypometabolism could be functional inhibition or inactivation of relatively healthy neurons or functional disturbance due to focal lesion of the

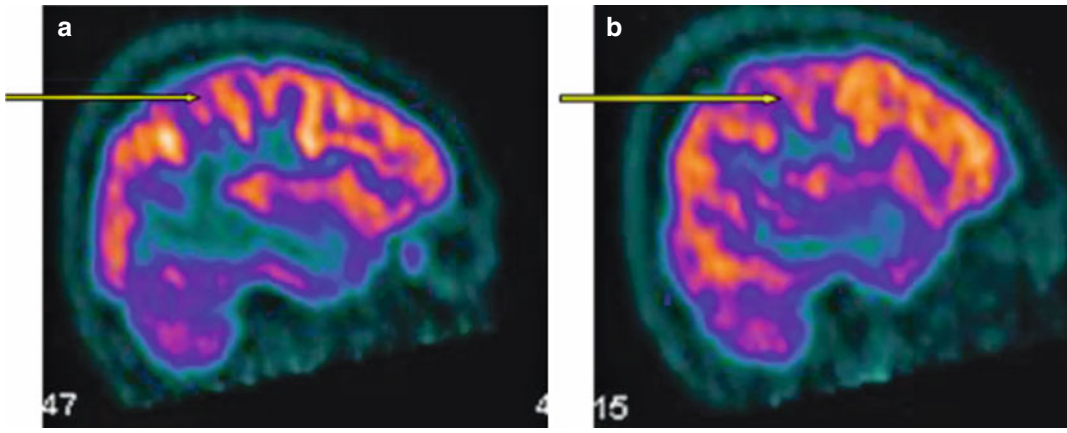

Fig. 14.1 Brain sagittal PET/CT images in ALS patient. (**a**) Sagittal normal metabolic representation of right motor cortex (*yellow raw*). (**b**) Hypometabolic left motor cortex (*yellow raw*)

motor cortex. These mechanisms could explain the decrease of regional glucose use in extramotor areas in ALS patients with upper motor neuron signs and the substantial normal distribution of glucose metabolism in ALS patients with only lower motor neuron signs, since in this last case the motor cortex is not primary affected.

Using the [11C]flumazenil, an antagonist at the benzodiazepine subunit of the $GABA_A$ receptor, expressed from pyramidal neurons and interneurons in all cerebral cortex, Lloyd and colleagues [60] reported in ALS patient a reduced binding in ALS involving motor/premotor areas but also extramotor areas, particularly the bilaterally prefrontal regions, bilaterally parietal cortex and visual association cortex, left motor/premotor cortex, Broca's area, and right temporal cortex. Reduced binding of [11C]flumazenil may reflect loss of cortical pyramidal and interneurons, which are thought to bear GABAA receptors, or it may reflect the downregulation of postsynaptic GABAA receptor expression in intact neurons. As the prefrontal cortex has few pyramidal cells, the loss of these in isolation is unlikely to explain our findings. Additionally, changes in flumazenil volumes of distribution in the primary motor cortex were less striking than those in the premotor and prefrontal areas, suggesting that the decreases are more likely to reflect loss of interneuronal function. The conclusion of the study supports the concept that ALS is a multisystemic degenerative disease.

Abrahams et al. [61] documented an altered metabolism in the frontal lobe even in non-demented ALS, assessing the cerebral blood flow (rCBF) by means of PET scan, performed during word generation and word repetition, in a group of patients with ALS and in a second non-ALS patient group with a cognitive impairment, both compared with healthy controls. The ALS patients showed an impaired activation in cortical and subcortical regions involving the dorsolateral prefrontal cortex; lateral premotor cortex; medial, prefrontal, and premotor cortices; and insular cortex bilaterally and the anterior thalamic nuclear complex. Similarly the non-ALS patient group demonstrated a relatively unimpaired pattern of activation. These data are expressions of an extramotor neuronal involvement in some non-demented ALS patients that develop probably along a thalamo-frontal association pathway.

In 2012 Cistaro et al. [62] reported a study of 32 ALS patients, 13 bulbar onsets and 19 spinal onsets, with probable laboratory-supported or definite ALS according to El Escorial ALS revised criteria consecutively matched with 22 healthy controls. Highly significant relative decreases in metabolism were found in large frontal and parietal regions in the bulbar-onset patients as compared with the spinal-onset patients and the controls, suggesting a differential metabolic and neuropsychological state between the two conditions. Reduced relative prefrontal and frontal metabolism is exclusive to patients with bulbar onset who were suffering from significantly reduced verbal fluency, confirming the higher rate of frontal impairment in this group. Relatively increased midbrain metabolism was found for the first time in both groups and appears to be the metabolic trait in ALS (Fig. 14.2). This ^{18}F-FDG-PET investigation provided unprecedented evidence of relatively increased metabolism in the amygdalae, midbrain, and pons in ALS patients as compared with control subjects, possibly due to local activation of astrocytes and microglia.

Meanwhile, Carrara and colleagues [63], the neuroradiological component of our group, described in T1 magnetization transfer contrast (MTC) an hyperintense signal intensity along the corticospinal tract and in posterior aspect of the body of the corpus callosum (CC) as a possible distinct phenotype of presentation of disease with prominent upper motor neuron involvement, such as PLS. In 37 % of patients studied, they found regional differences in white matter fractional anisotropy (FA) between patients with T1 MTC hyperintense signal intensity and patients without it. Patients with T1 MTC abnormal signal intensity showed lower FA strictly limited to the motor network and the posterior aspect of the body of the CC without extramotor FA reductions, whereas patients without this sign showed FA reductions in several confluent regions within and outside the CST and in the whole CC. The authors concluding suggest that the T1 MTC

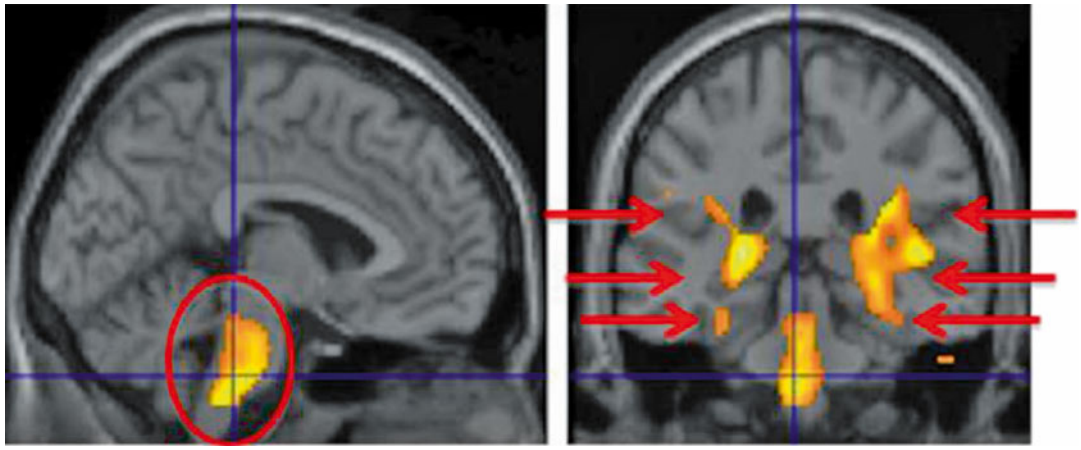

Fig. 14.2 Statistical parametric mapping (SPM) PET findings in sporadic ALS patients compared to controls. Statistically significant differences ($p<0.001$) are highlighted on a MRI T1 template: *left sagittal view and right coronal view*. Relative increase of 18F-FDG metabolism in the midbrain, pons, and corticospinal trait

sequence should be included in the diagnostic workup of patients with ALS.

The concept that the corpus callosum seems to be involved in the disease and that it can be used to support the diagnosis has been suggested from Filippini and coworkers [64]. They studied a group of 24 heterogeneous patients with ALS of variable UMN involvement clinically using DTI at 3 T MRI. This study demonstrated a consistent involvement of the CC and rostral corticospinal trait across the group of patients with ALS, including those with little clinical UMN involvement, supporting the concept of an independent cerebral pathogenic process in ALS. While CC involvement might relate to interhemispheric spread, it might equally reflect secondary damage due to independent bilateral cortical processes. Matched regional radial diffusivity increase supported the concept of anterograde degeneration of callosal fibers observed pathologically. A post hoc group comparison model incorporating significant values for fractional anisotropy, radial diffusivity, and gray matter was 92 % sensitive, 88 % specific, and 90 % accurate.

Agosta et al. [65] tested the diffusion tensor MRI diagnostic accuracy in distinguishing two motor neuron disease variants: primary lateral sclerosis (PLS), which has a slower rate of progression and a more benign prognosis, and ALS, the more common form of motor neuron disease. All patients showed a distributed pattern of abnormalities of the motor system, including the corticospinal tracts and corpus callosum. PLS patients showed a more severe damage to the rostral portions of the CST, motor callosal fibers, and subcortical white matter underlying the primary motor cortices. In PLS patients, damage to the CC midbody correlated with the severity of upper motor neuron clinical burden. The most predictive variable to distinguish motor neuron disease from controls was fractional anisotropy of the CC-primary motor cortex, which was able to classify correctly 79 % of MND patients versus controls, with the highest classification accuracy in PLS (90 %). This underscores that PLS, despite its distinct clinical phenotype and long survival, still lies within the wider MND spectrum. Whether the CC diffusivity may be a novel marker to increase confidence in an early diagnostic separation of PLS from ALS still needs to be investigated.

14.3 C9ORF72 Gene and Amyotrophic Lateral Sclerosis

While the majority of ALS cases appear sporadically in the population, 10 % of patients have a positive family history of ALS or frontotemporal

dementia (ALS-FTD), a related form of neurodegeneration. Recently, a GGGGCC hexanucleotide repeat expansion in the C9ORF72 gene, located on chromosome 9p21, has been demonstrated to be the commonest cause of familial amyotrophic lateral sclerosis (ALS) and to account for 5–10 % of apparently sporadic ALS [66].

In 2014 Cistaro and colleagues [67] evaluated the [18F]FDG PET pattern in a series of 15 ALS patients with the C9ORF72 hexanucleotide repeat expansion with sporadic ALS patients with (12 pts) or without (30 pts) comorbid frontotemporal dementia and 40 normal subjects. We found that ALS patients with the C9ORF72 mutation as compared to ALS patients with no genetic mutation show relative hypometabolism in the thalamus, basal ganglia, and limbic cortex and relative hypermetabolism in the occipital cortex, midbrain, and bilateral cerebellum. These alterations are consistent with the unique symptom constellation in patients carrying the C9ORF72 hexanucleotide repeat expansion and emphasize the "systemic" nature of lesions related to this mutation even in the early clinical phases of the disorder. ALS patients with the C9ORF72 hexanucleotide repeat expansion had a more widespread central nervous system involvement than ALS patients without genetic mutations, with or without comorbid FTD, consistent with their more severe clinical picture.

In the same year, Van Laere [68] evaluated the possible presence of specific metabolic signature at FDG PET imaging in a large group of patients (81 pts) with suspected diagnosis of ALS. After a complex diagnostic workup, including genetic screening, seven patients were diagnosed with primary lateral sclerosis and four patients received diagnosis of progressive muscular atrophy. In 70 subjects diagnosis of ALS was made, and patients were divided in two subgroups: the first one carrying C9orf72 mutations and second one without mutations. Hypometabolism was evidenced in the perirolandic region and with variable degree in the prefrontal cortex in the majority of patients. Noteworthy patients carrying C9orf72 mutation demonstrated discrete relative hypometabolism in the thalamus and posterior cingulate when compared with C9orf72-negative ALS patients.

Cistaro et al. [69] try to identify a 18F-FDG PET and MR profiles in 18 familial ALS patients: 1 FUS, 8 C9orf72, 4 SOD1, 4 TDP-43, 1 MATR3, and 1 ORF/TDP-43. Nineteen percent of patients with gene mutations showed hyperintensity along the corticospinal tract on T1 MR sequences. A global and statistically significative reduction in the whole white matter was found at TBSS analysis compared with healthy controls, in particular in the internal capsule, mean cerebellar peduncle, and pons. On FDG-PET scans, the familial ALS patients showed significant hypometabolism in the thalamus, anterior and posterior cingulate cortex, insula, caudate, left frontal and superior temporal cortex, and hypermetabolism in the pons, midbrain, and bilateral occipital cortex. The pons seems to be the structure where both metabolic alterations on PET scans and signal alterations on MR images can be found.

More recently (unpublished dates) our group studied 29 ALS patients carrying C9orf72 mutations by means 18F-FDG PET. The patients were divided in two subgroups with similar demographic profile but different in neuropsychological evaluation being the first group without cognitive deficits. The two groups were then crossmatched to 40 neurologically normal controls and 29 ALS without mutation. The C9orf72 ALS patients without cognitive deficits showed hypometabolism in the medial dorsal and anterior nuclei and pulvinar of thalamus with respect to the normal controls. C9orf72 ALS patients with cognitive deficits showed extensive hypometabolism in the bilateral frontal and temporal superior cortex, anterior cingulate cortex, bilateral thalamus, and caudate. The hypometabolism on the frontal cortex can be correlated with functional frontal deficits typically observed in FTD patients, but it is more widespread and severe than in ALS-FTD without gene mutation. Interestingly, neither ALS-FTD patients without mutation, as reported in previous study [67], nor the match between ALS without and ALS with C9orf72 mutations in this study showed hypometabolism in the thalamus (Fig. 14.3).

Bede and coworkers [70] confirmed thalamus implication in ALS C9orf72 hexanucleotide repeat expansion patients, together with other

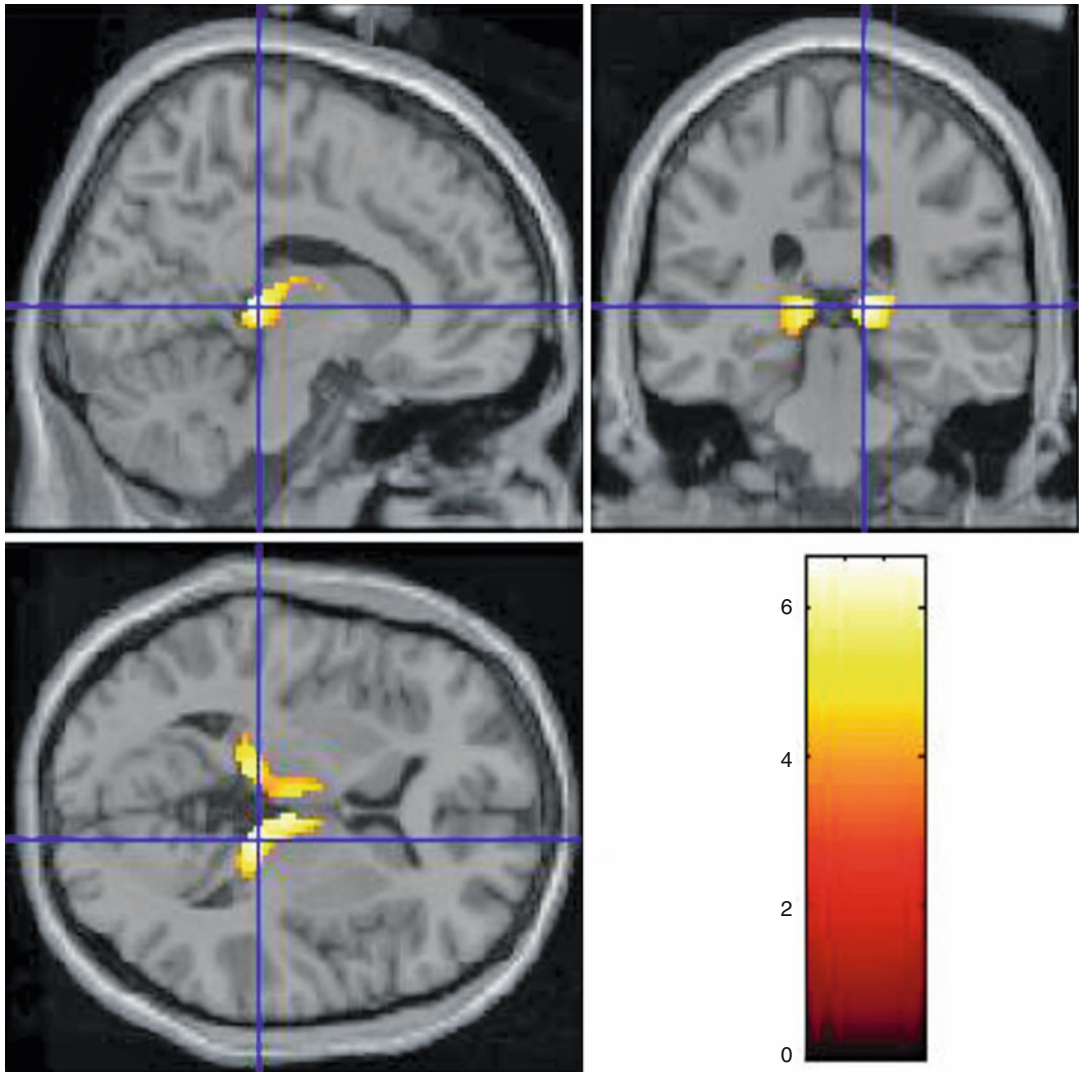

Fig. 14.3 Statistical parametric mapping (PET) findings in sporadic ALS patients compared with C9orf72 ALS patients. Statistically significant differences ($p<0.001$) are highlighted on a MRI T1 template. Hypometabolism: *top left sagittal view, top right coronal view, and bottom left transverse view*. Significant corrected clusters are seen in the bilateral thalamus: the medial dorsal nucleus, pulvinar, and left ventral anterior nucleus

structures, in a multiparametric MRI prospective study for cortical thickness analysis. Using voxel and surface-based morphometry, they described the patterns of cortical and subcortical changes in C9orf72 ALS patients with respect to ALS C9orf72-negative and healthy controls. A congruent pattern of cortical and subcortical involvement was identified in those with the C9orf72 genotype, affecting the thalamic, fusiform, supramarginal, and orbitofrontal regions and Broca's area. White matter abnormalities in the C9orf72-negative group were relatively confined to corticospinal and cerebellar pathways with limited extramotor expansion. The body of the corpus callosum and superior motor tracts were affected in both ALS genotypes.

Although previous reports have described thalamic changes in ALS [71], their significance has not been widely recognized, possibly due to the absence of convincing clinical and genetic

correlations. Our and Bede studies suggest that bilateral thalamus involvement is an important feature of C9orf72-positive ALS. Further classifier studies are warranted, as the thalamus could represent an important discriminating structure between C9pos and C9neg ALS.

14.4 Connectivity Analyses in Amyotrophic Lateral Sclerosis

A neural network can be defined as a population of interconnected nodes that perform a specific physiological function, just as the motor network controls muscle tone and movement. The properties and integrity of cortical neural networks can be explored using structural or functional measures [72].

Automated MRI structural connectivity analyses, which probe white matter (WM) connections linking various functionally cortical regions, have the potential to provide novel information about degenerative processes within multiple WM pathways. Whole brain probabilistic tractography can be applied to define specific WM pathways connecting discrete corticomotor targets generated from anatomical parcellation of structural MRI of the brain. The integrity of these connections can be interrogated by comparing the mean fractional anisotropy (FA) derived for each WM pathway. These structural measures can be combined with functional connectivity analysis of the motor network based on resting-state fMRI.

A study by Verstraete and coworkers [72], based on a network perspective, demonstrates a decline of structural integrity with preserved functional organization of the motor network in ALS. A reduced number of functional connections between the right and left motor cortex was found, but this reduction was not statistically significant, indicating relative sparing of functional connectivity. A significant reduction in microstructural organization was found in the corticospinal tracts, as the major efferent motor conduits to the spinal cord, mainly the rostral part. Furthermore, the corpus callosum, interconnecting the motor network, was found to be affected as a whole. Both the average cortical thickness of the precentral gyrus and the local connectedness were found to be related with disease progression. This suggests that strong functional connectivity allows for rapid spread of disease.

The functional correlates of the structural changes in ALS patients detected using advanced MRI techniques have been studied by Douaud and colleagues too [73]. Twenty-five patients with ALS were compared to healthy control subjects using MRI multimodal neuroimaging approach. A gray matter connection network was defined based upon the prominent corticospinal tract and corpus callosum involvement demonstrated by white matter tract-based spatial statistics. This "ALS-specific" network of decreased structural connectivity included motor, premotor, and supplementary motor cortices, pars opercularis, and motor-related thalamic nuclei. An analysis protocol was then used to assess changes in functional connectivity directly associated with this network. A spatial pattern of increased functional connectivity spanning sensorimotor, premotor, prefrontal, and thalamic regions was found. Therefore, this study identified apparently dichotomous processes characterizing the ALS cerebral network failure, in which there was increased functional connectivity within regions of decreased structural connectivity. Since patients with slower rates of disease progression showed connectivity measures with values closer to healthy controls, the authors suggest that functional connectivity increases might not simply represent a physiological compensation to reduced structural integrity. One alternative possibility is that increased functional connectivity reflects a progressive loss of inhibitory cortical influence as part of ALS pathogenesis.

More recently, higher functional connectivity correlating with greater structural damage to network-specific white matter tracts was described by Agosta and coworkers [74] in patients with primary lateral sclerosis compared with controls. Regions of increased functional connectivity were showed in the sensorimotor, frontal, and left frontoparietal and superior

temporal networks in patients with primary lateral sclerosis. Patients with more severe physical disability and a more rapid rate of disease progression had increased sensorimotor connectivity values. The increased functional connectivity within the frontal network was associated with executive dysfunction.

Until today, there are no studies examining the functional connectivity in ALS patients with PET [75]. Pagani and colleagues, providing a class III of evidence, confirmed in a greater sample the previous results of hypometabolism in the frontal, motor, and occipital cortices and hypermetabolism in the midbrain, temporal pole, and hippocampus in 195 patients with ALS compared to controls.

Thirty-four bulbar and 85 spinal onsets with confirmed diagnosis at 1-year follow-up were included in the study. Twenty-five bilateral cortical and subcortical volumes of interest plus cerebellum were taken into account for factorial and discriminant analyses. Discriminant analysis investigating sensitivity and specificity to discriminate patients from controls was performed using the 51 volumes of interest as well as age and sex. Metabolic connectivity was explored by voxel-wise interregional correlation analysis. The discriminant analysis showed a sensitivity of 95 % and a specificity of 83 % in separating patients from controls. Connectivity analysis found a highly significant positive correlation between the midbrain and white matter in corticospinal tracts in patients with ALS. The authors concluded that once validated by diseased-control studies, the present methodology might represent a potentially useful biomarker for ALS diagnosis.

The hypermetabolism in the midbrain might be interpreted as the neurobiological correlate of diffuse subcortical gliosis. The study supports a massive microglia activation and astrocytosis in regions of neurodegeneration [76]. The higher FDG accumulation in ALS can be related to the function of astrocytes as the preferential site of glucose metabolism along with their role in replacing the dead neurons. The strict correspondence between the motoneuron tracks and the hypermetabolic areas found in these ALS patients further supports this hypothesis.

14.5 Neuroinflammation in Amyotrophic Lateral Sclerosis

Evidence of microgliosis in ALS has mainly been obtained from postmortem studies and was focused on the final stages of the disease. Analysis of microglial activation at earlier stages and during the progression of the disease was technically limited until the development of neuroimaging ligands.

Neuroinflammation in ALS has been the focus of numerous studies using several approaches. These have mainly been based on the presence of the activated microglia, macrophages of the brain parenchyma, and infiltrates of lymphocytes in the areas of motor neuron loss in the motor cortex, brainstem, corticospinal tract, and anterior horn of the spinal cord [77–80].

Several explanations have been advanced to explain their role: decrease in the release of neurotrophic factors, excessive in the secretion of neurotoxic factors, and modulation of glutamatergic receptor expression [80].

Assessment of microglial activation and astrocytosis can be performed in vivo in ALS patients through neuroimaging of the peripheral benzodiazepine binding site or enzyme MAO-B, primarily located in astrocytes, and 18 kDa translocator protein (TSPO) overexpressed in activated microglia.

In the human brain, the enzyme MAO-B is primarily located in astrocytes. [11C](L)-deprenyl binds to MAO-B being useful for astrocytosis mapping. The first study of cerebral astrocytosis in vivo in ALS demonstrated an increased uptake rate of [11C](L)-deprenyl in pons and white matter [81]. Since the astrocytosis in ALS has also been demonstrated post-mortem in other parts of the corticospinal tract but pons has not been included [82, 83], the authors concluded that lacking neuropathological support in this region, the increased binding rate in pons must be interpreted cautiously. Nevertheless, the increased binding rate in pons, where the corticospinal tract fibers have converged, may reflect corticospinal tract astrocytosis.

Activated microglia is characterized by increased expression of the 18 kDa translocator protein (TSPO) in the brain and may be a useful biomarker of inflammation. TSPO, formerly named peripheral benzodiazepine receptor (PBR), is part of a multimeric "protein complex" associated with the outer mitochondrial membrane of many cells [84]. It is present in peripheral tissues and also in glia cells (astrocytes and microglia) when activated [85]. TSPO is involved in many processes such as apoptosis, regulation of cellular proliferation, immunomodulation, and steroidogenesis [86], and therefore it may be a useful biomarker of inflammation, since it is highly expressed in phagocytic inflammatory cells, such as activated microglia in the brain and macrophages in peripheral tissue.

A large number of positron emission tomography (PET) or single-photon emission computerized tomography (SPECT) radioligands selective for the TSPO have been developed, of which [11C]-PK11195 was the first TSPO radioligand to be evaluated [87, 88].

Using PK11195 [89] Turner and colleagues demonstrated in ten ALS patients a significantly increased binding in the motor cortex, pons, dorsolateral prefrontal cortex, and thalamus. There was a strong correlation between the individual binding potential values of the ALS patients and their clinical upper motor neuron (UMN) scores, both for the motor cortex and thalamus. No clear difference in the binding of [11C](R)-PK11195 between ALS patients with bulbar or limb onset and no significant correlation with either ALSFRS-R (revised ALS functional rating scale score) or disease duration for any region were seen.

Corcia P. and colleagues [90], comparing the 18F-DPA-714 binding, another radioligand of TSPO, in several cerebral regions between ten ALS patients, patients with probable or definite ALS, all right handed, without dementia, and untreated by riluzole or other medication, and a group of healthy controls, showed that the areas with the highest microglial activation in ALS patients were the in medial temporal cortex, motor cortex, and more specifically the supplementary motor area. In this study, the occipital and cerebellar regions were spared.

The involvement of the temporal lobe emphasized in this study might correspond to previous neuroimaging, neuropsychological, and neuropathology findings. Neuroimaging studies emphasized atrophy of the gray matter of the temporal lobe and of white matter adjacent to this area in voxel-based morphometric analysis [64, 91]. Neuropsychological assessment of verbal fluency also supported this assumption. Verbal fluency might be split into two components, i.e., phonemic fluency related to the frontal lobe and semantic fluency under the control of the temporal lobe. There is a significant decrease in semantic fluency in ALS compared to controls [92]. Finally, neuropathology studies have emphasized the presence of TDP-43 inclusions, the major disease protein in ALS, in around 40 % of the temporal lobe in ALS patients [93]. Finally, a postmortem study revealed the presence of neuronal loss and gliosis in 12.6 % of ALS patients without dementia [94].

The authors concluded that these results suggested an increased expression of TSPO on PET imaging using 18F-DPA-714 in untreated ALS patients. This increase is independent of the disease duration because it is present during the whole time of diagnosis phase, and this finding might be a surrogate marker of efficacy of treatment on microglial activation. Finally, the presence of extra motor microglial activation might corroborate theories suggesting that ALS is a prototypic motor neuron condition whose pathology is not limited to motor neurons.

More recently, the radioligand [11C]-PBR28 was shown to exhibit 80 times more specific binding compared to [11C]-(R)-PK11195 in rhesus macaques [95].

In a PET/MR study [96], voxel-wise analysis showed increased binding [11C]-PBR28 in the motor cortices and corticospinal tracts. Those values were positively correlated with UMN score and negatively correlated with ALSFRS. Further studies will determine the role of [11C]-PBR28 as a marker of treatments that target neuroinflammation.

14.6 Amyotrophic Lateral Sclerosis and Cognitive Deficits

Although the degeneration in ALS predominantly affects the motor system, cognitive and behavioral symptoms have been described for over a century. A subgroup of patients with ALS (5–15 %) meets the criteria for frontotemporal dementia (FTD), typically a frontal variant that predominantly causes executive dysfunction and behavioral changes. Many authors have suggested that ALS and FTD form a clinical and pathological spectrum [97]. There is no doubt that ALS and FTD have clinical, radiological, pathological, and genetic overlap. Cognitive decline in ALS is characterized by personality change, irritability, obsessions, poor insight, and pervasive deficits in frontal executive tests. The most consistently reported cognitive changes in ALS relate to dysfunction in components of the executive system, in particular in verbal fluency and attention, whereas abnormalities in memory and language are less well characterized. Understanding of cognitive impairment in ALS will improve care for patients and their families and provide valuable insights into the pathogenesis of neurodegeneration [98].

Ludolph and colleagues [99] studied the regional cerebral glucose utilization and the neuropsychological performance of 18 patients clinically displaying upper and lower motor neuron signs. In all ALS patients, significant changes were found in the entire and frontal cortex and also in subregions like the frontobasal and the superior parieto-occipital cortex. No changes were seen in the cerebellum. In fact glucose metabolism in the cerebellum was comparable in ALS and controls.

Comprehensive neuropsychological assessment of ALS patients compared to a pair-matched control group revealed mild frontal dysfunction which in part significantly correlated with reduced glucose metabolism in the cortex and subcortical structures. The authors concluded that in patients with ALS, glucose consumption is decreased in parts of the brain other than the motor cortex accompanied by mild neuropsychological deficits based on the tests employed in this study and that these findings support the hypothesis of mild cognitive deficits in early stages of ALS and may suggest the onset of a subcortical dementia.

Theory of mind (ToM) is defined by the ability to infer and understand the mental states of self and others. A distinction has been made between the so-called cognitive ToM (also known as mentalizing), which deals with the cognitive states, beliefs, thoughts, or intentions of other people [100], and affective ToM, which concerns their affective states, emotions, or feelings [101]. Carluer and colleagues designed a study to clarify the putative link between cognitive ToM deficits and executive dysfunction in 23 ALS using 18F-FDG PET and identify the dysfunctional brain regions responsible for any social cognition deficits. Using statistical parametric mapping, they showed that the cognitive ToM deficit correlated with the dorsomedial and dorsolateral prefrontal cortices, as well as the supplementary motor area [97].

Jeong et al. [102] investigated the FDG pattern of patients presenting both motor neuron disease (MND) and frontotemporal dementia (FTD). FTD/MND shows relatively symmetric hypometabolism in the frontal lobe, sparing the temporal lobe. In patients with FTD, the hypometabolism involves the frontal, anterior temporal, and parietal lobes and shows hemispheric asymmetry. The FTD group compared with patients with FTD/MND shows more hypometabolic in bilateral temporal regions. In a subsequent paper, of the same authors, hypometabolism was extensively documented in FTD patients in the prefrontal areas, anterior temporal regions, cingulate gyri, and left inferior parietal lobule and also, but less relevant, in the insula and uncus bilaterally, left putamen and globus pallidus, and medial thalamic structures [103]. In 2012, the group of Turku [104] investigated two siblings with clinical signs of ALS by means of PET imaging. In a patient clinical evaluation, MRI and FDG-PET failed to differentiate between FTD and Alzheimer's disease (AD), whereas 11C-Pittsburgh compound B (PiB) was negative for amyloid pathology. The patient later developed ALS symptoms, and postmortem

neuropathological examination was diagnostic of ALS-FTD, while no findings suggested AD. Of note, C9ORF72 expansion was detected in the patient and his sister. The authors suggest that 11C-PiB-PET may facilitate the early differential diagnosis between AD and FTD, including C9FTD/ALS.

Further confirmation regarding the utility 11C-PiB has been by Yamakawa et al. [105], in the cases of two patients with dementia associated with MND. One of the patients had FTD, whereas the other had AD. In the patient with FTD, the PIB-PET resulted to be negative, while in the AD patient PIB-PET documented the presence of amyloid accumulation in the frontoparietal cortex, lateral temporal lobes, posterior cingulate gyrus, and precuneus.

More recently, in a large survey on ALS including both neuropsychological assessment and 18F-FDG-PET, in order to identify the metabolic signature of the various levels of cognitive deficits in ALS using 18F-FDG-PET, Canosa and colleagues [106] investigated 170 patients with ALS. All patients were classified according to neuropsychological testing in 94 ALS normal cognition, 20 ALS full-blown FTD, 37 ALS executive or nonexecutive cognitive impairment not fulfilling FTD criteria (Ci), 9 ALS prevalent behavioral changes (Bi), and 10 ALS nonclassifiable impairment (Nc). We identified a decreasing gradient of frontal lobe metabolism going from ALS with normal cognition to ALS with FTD, through cases with intermediate cognitive deficits (ALS-Ci). According to these findings, ALS-Ci seems to represent a discrete category, showing less severe cognitive deficits and a distinct metabolic pattern as compared to ALS-FTD, being intermediate between pure ALS and ALS-FTD. The hypometabolic areas were included in the same left frontal regions found to be more severely hypometabolic in ALS-FTD as compared to ALS-Cn, suggesting a continuum between cognitive decline and metabolic activity in these areas.

Using statistical parametric mapping (SPM) analysis, the hypometabolism in frontal regions was associated in all comparisons to the hypermetabolism in the cerebellum, midbrain, and corticospinal tracts; the more severe the cognitive decline, the larger the size of the cluster and the statistical significance of 18F-FDG uptake differences. This finding supports the hypothesis that astrocytosis, mainly in white matter, is associated with ALS neurodegeneration and possibly anticipates cortical changes [62, 107–109].

This study has demonstrated in a large cohort of ALS patients a continuum of frontal lobe metabolic impairment reflecting the clinical and anatomic continuum ranging from pure ALS, through ALS with intermediate cognitive deficits, to ALS-FTD, and showing that patients with intermediate cognitive impairment display a characteristic metabolic pattern.

A neuropathological staging system of the spreading of brain pathology in ALS has been proposed, based on the propagation of phosphorylated TDP-43 (pTDP-43) proteinopathy, since pTDP-43 aggregates seem to be strictly linked to neuron degeneration. According to this model, pTDP-43 tends to spread with disease progression via axonal transport from the primary motor cortex to the prefrontal areas, suggesting that all ALS patients are susceptible to develop frontal cognitive impairment over time, according to disease duration and rate of progression [110].

Our findings are in keeping with MRI studies comparing ALS patients with different levels of cognitive impairment. A structural MRI study on 39 ALS cases reported that ALS-FTD patients display significantly more atrophy of prefrontal and anterior temporal cortex as compared to ALS with cognitive and behavioral symptoms not fulfilling FTD criteria (ALS plus) and that the ALS-plus group shows significantly more atrophy than the pure ALS group in various areas including the superior frontal gyrus and the left planum temporale, supporting the hypothesis of a gradient of atrophy across groups [111].

Another MRI study showed that both ALS-FTD and ALS patients with cognitive impairment display cortical thinning of the bilateral frontal and temporal cortex, with a more pronounced atrophy in the former group, suggesting the concept of a morphological continuum reflecting the clinical one [112].

Since ^{18}F-FDG-PEt allows to estimate the cerebral lesion load in vivo in neurodegenerative

diseases, it might be helpful to investigate in ALS its association with neuropsychological testing along the disease course to disclose the early metabolic signature of a possible cognitive impairment.

Acknowledgments We thank Mr. Piercarlo Fania and Dr. L. Cassalia for the supported artwork and for their useful discussions.

References

1. Cistaro A, Cuccurullo V, Quartuccio N, Pagani M, Valentini MC, Mansi L (2014) Role of PET and SPECT in the study of amyotrophic lateral sclerosis. Biomed Res Int 2014:237437
2. Kiernan M, Vucic S, Cheah B, Turner MR, Eisen A et al (2011) Amyotrophic lateral sclerosis. Lancet 377:942–955
3. Miller RG, Mitchell JD, Moore DH (2012) Riluzole for amyotrophic lateral sclerosis (ALS)/motor neuron disease (MND). Cochrane Database Syst Rev 3:CD001447
4. Mitchell JD, Borasio GD (2007) Amyotrophic lateral sclerosis. Lancet 369:2031–2041
5. Andersen PM, Al-Chalabi A (2011) Clinical genetics of amyotrophic lateral sclerosis: what do we really know? Nat Rev Neurol 7:603–615
6. Quartuccio N, Van Weehaeghe D, Cistaro A, Jonsson C, Van Leare K, Pagani M (2014) Positron emission tomography neuroimaging in amyotrophic lateral sclerosis: what is new? Q J Nucl Med Mol Imaging 58:344–354
7. Ravits JM, La Spada AR (2009) ALS motor phenotype heterogeneity, focality, and spread: deconstructing motor neuron degeneration. Neurology 73:805–811
8. Chio A, Calvo A, Moglia C, Mazzini L, Mora G (2011) Phenotypic heterogeneity of amyotrophic lateral sclerosis: a population based study. J Neurol Neurosurg Psychiatry 82:740–746
9. Al-Chalabi A, Hardiman O (2013) The epidemiology of ALS: a conspiracy of genes, environment and time. Nat Rev Neurol 9:617–628
10. Renton AE, Chio A, Traynor BJ (2014) State of play in amyotrophic lateral sclerosis genetics. Nat Neurosci 17:17–23
11. Rosen DR, Siddique T, Patterson D, Figlewicz DA, Sapp P et al (1993) Mutations in Cu/Zn superoxide dismutase gene are associated with familial amyotrophic lateral sclerosis. Nature 362:59–62, 5
12. Bruijn LJ, Miller TM, Cleveland DW (2004) Unravelling the mechanisms involved in motor neuron degeneration in ALS. Ann Rev Neurosci 27:723–749
13. Iwanaga K, Hayashi S, Oyake M et al (1997) Neuropathology of sporadic amyotrophic lateral sclerosis of long duration. J Neurol Sci 146(2):139–143
14. Castaigne P, Lhermitte F, Cambier J, Escourolle R, le Bigot P (1972) `Etude neuropathologique de 61 observations de sclerose laterale amyotrophique. Discussion nosologique. Rev Neurol 127(4):1–414
15. Sasaki S, Tsutsumi Y, Yamane K, Sakuma H, Maruyama S (1992) Sporadic amyotrophic lateral sclerosis with extensive neurological involvement. Acta Neuropathol 84(2):211–215
16. Kawamura Y, Dyck PJ, Shimono M (1981) Morphometric comparison of the vulnerability of peripheral motor and sensory neurons in amyotrophic lateral sclerosis. J Neuropathol Exp Neurol 40(6):667–675
17. Lomen-Hoerth C, Murphy J, Langmore S, Kramer JH, Olney RK, Miller B (2003) Are amyotrophic lateral sclerosis patients cognitively normal? Neurology 60(7):1094–1097
18. Gordon PH, Delgadillo D, Piquard A et al (2011) The range and clinical impact of cognitive impairment in French patients with ALS: a cross-sectional study of neuropsychological test performance. Amyotroph Lateral Scler 12(5):372–378
19. DeJesus-Hernandez M, Mackenzie IR, Boeve BF et al (2011) Expanded GGGGCC hexanucleotide repeat in noncoding region of C9ORF72 causes chromosome 9p-linked FTD and ALS. Neuron 72(2):245–256
20. Renton AE, Majounie E, Waite A et al (2011) A hexanucleotide repeat expansion in C9ORF72 is the cause of chromosome 9p21-linked ALS-FTD. Neuron 72(2):257–268
21. Pradat PF, Bruneteau G (2006) Differential diagnosis and atypical subsets of ALS. Rev Neurol 162(2):S81–S90
22. Gubbay SS, Kahana E, Zilber N, Cooper G, Pintov S, Leibowitz Y (1985) Amyotrophic lateral sclerosis. A study of its presentation and prognosis. J Neurol 232(5):295–300
23. Mitsumoto H, Chad DA, Pioro EP (1998) Clinical features: signs and symptoms. In: Amyotrophic lateral sclerosis. FA Davis Company, Philadelphie, pp 47–64
24. Li TM, Alberman E, Swash M (1988) Comparison of sporadic and familial disease amongst 580 cases of motor neuron disease. J Neurol Neurosurg Psychiatry 51(6):778–784
25. Moulard B, Camu W, Malafosse A, Billiard M, Baldy-Moulinier M (1997) Etude clinique des formes familiales de sclerose laterale amyotrophique: revue de la literature. Rev Neurol 153(5):314–324
26. Abe K, Aoki M, Ikeda M, Watanabe M, Hirai S, Itoyama Y (1996) Clinical characteristics of familial amyotrophic lateral sclerosis with Cu/Zn superoxide dismutase gene mutations. J Neurol Sci 136(1–2):108–116
27. Andersen PM, Forsgren L, Binzer M et al (1996) Autosomal recessive adult-onset amyotrophic lateral sclerosis associated with homozygosity for Asp90A1a CuZn-superoxide dismutase mutation A clinical and genealogical study of 36 patients. Brain 119(4):1153–1172

28. Camu W, Khoris J, Moulard B et al (1999) Genetics of familial ALS and consequences for diagnosis. J Neurol Sci 165(1):S21–S26
29. Jafari-Schluep HF, Khoris J, Mayeux-Portas V, Hand C, Rouleau R, Camu W (2004) Les anomalies du gene superoxide dismutase 1 dans la sclerose laterale amyotrophique familiale: correlations phenotype/genotype et implications pratiques. L'exp´erience franc¸aise et revue de la litt´erature. Rev Neurol 160(1):44–50
30. Kawata A, Kato S, Hayashi H, Hirai S (1997) Prominent sensory and autonomic disturbances in familial amyotrophic lateral sclerosis with a Gly93Ser mutation in the SOD1 gene. J Neurol Sci 153(1):82–85
31. Khoris J, Moulard B, Briolotti V et al (2000) Coexistence of dominant and recessive familial amyotrophic lateral sclerosis with the D90A Cu, Zn superoxide dismutase mutation within the same country. Eur J Neurol 7(2):207–211
32. Davenport RJ, Swingler RJ, Chancellor AM, Warlow CP (1996) Avoiding false positive diagnoses of motor neuron disease: lessons from the Scottish motor neuron disease register. J Neurol Neurosurg Psychiatry 60(2):147–151
33. Eisen A, Calne DB (1992) Amyotrophic lateral sclerosis, Parkinson's disease and Alzheimer's disease: phylogenetic disorders of the human neocortex sharing many characteristics. Can J Neurol Sci 19(1):117–120
34. Verma A, Bradley WG (2001) Atypical motor neuron disease and related motor syndromes. Semin Neurol 21(2):177–187
35. Zoccolella S, Palagano G, Fraddosio A et al (2002) ALS-plus: 5 cases of concomitant amyotrophic lateral sclerosis and parkinsonism. Neurol Sci 23(2):S123–S124
36. Desai J, Swash M (1999) Extrapyramidal involvement in amyotrophic lateral sclerosis: backward falls and retropulsion. J Neurol Neurosurg Psychiatry 67(2):214–216
37. Miwa H, Kajimoto M, Kondo T (2002) Chorea in motor neuron disease. Mov Disord 17(6):1397
38. Pradat PF, Salachas F, Lacomblez L et al (2002) Association of chorea and motor neuron disease. Mov Disord 17(2):419–420
39. Knirsch UI, Bachus R, Gosztonyi G, Zschenderlein R, Ludolph AC (2000) Clinicopathological study of atypical motor neuron disease with vertical gaze palsy and ballism. Acta Neuropathologica 100(3):342–346
40. Pradat PF, Bruneteau G, Munerati E et al (2009) Extrapyramidal stiffness in patients with amyotrophic lateral sclerosis. Mov Disord 24(14):2143–2148
41. Schimke N, Krampfl K, Petri S, Dengler R, Bufler J (2002) Cerebral symptoms with motor neuronal disorders: a special form of ALS-plus syndrome. Nervenarzt 73(8):751–753
42. Hayashi H, Kato S, Kawada T, Tsubaki T (1987) Amyotrophic lateral sclerosis: oculomotor function in patients in respirators. Neurology 37(8):1431–1432
43. Sharma R, Hicks S, Berna CM, Kennard C, Talbot K, Turner MR (2011) Oculomotor dysfunction in amyotrophic lateral sclerosis: a comprehensive review. Arch Neurol 68(7):857–861
44. Shimizu T, Kawata A, Kato S et al (2000) Autonomic failure in ALS with a novel SOD1 gene mutation. Neurology 54(7):1534–1537
45. Eisen A, Swash M (2001) Clinical neurophysiology of ALS. Clin Neurophysiol 112:2190–2201
46. Pradat PF, El Mendili MM (2014) Neuroimaging to investigate multisystem involvement and provide biomarkers in amyotrophic lateral sclerosis. Biomed Res Int 2014:467560. doi:10.1155/2014/467560, Epub 2014 Apr 17
47. Wijesekera LC, Leigh PN (2009) Amyotrophic lateral sclerosis. Orphanet J Rare Dis 34:3
48. Zoccolella S, Beghi E, Palagano G et al (2006) Predictors of delay in the diagnosis and clinical trial entry of amyotrophic lateral sclerosis patients: a population-based study. J Neurol Sci 250(1–2):45–49
49. Traynor BJ, Codd MB, Corr B, Forde C, Frost E, Hardiman OM (2000) Clinical features of amyotrophic lateral sclerosis according to the El Escorial and Airlie House diagnostic criteria: a population-based study. Arch Neurol 57(8):1171–1176
50. Riku Y, Atsuta N, Yoshida M et al (2014) Differential motor neuron involvement in progressive muscular atrophy: a comparative study with amyotrophic lateral sclerosis. BMJ Open 4:e005213
51. Rowland LP, Shneider NA (2001) Amyotrophic lateral sclerosis. N Emgl J Med 344:1688–1700
52. Patronas NJ, Di Chiro G, Smith BH, De La Paz R, Brooks RA, Milam HL, Kornblith PL, Bairamian D, Mansi L (1984) Depressed cerebellar glucose metabolism in supratentorial tumors. Brain Res 291:93–101
53. Hatazawa J, Brooks RA, Dalakas MC, Mansi L, Di Chiro G (1988) Cortical motor-sensory hypometabolism in amyotrophic lateral sclerosis: a PET study. J Comput Assist Tomogr 12:630–636
54. Sathasivam S (2010) Motor neurone disease: clinical features, diagnosis, diagnostic pitfalls and prognostic markers. Singapore Med J 51:367
55. Paganoni S, Macklin EA, Lee A et al (2014) Diagnostic timelines and delays in diagnosing amyotrophic lateral sclerosis (ALS). Amyotroph Lateral Scler Frontotemporal Degener 15:453–456
56. Verstraete E, Foerster BR (2015) Neuroimaging as a new diagnostic modality in amyotrophic lateral sclerosis. Neurotherapeutics 12(2):403–416
57. Turner MR, Kiernan MC, Leigh PN, Talbot K (2009) Biomarkers in amyotrophic lateral sclerosis. Lancet Neurol 8:94–109
58. Chiò A, Pagani M, Agosta F, Calvo A, Cistaro A, Filippi M (2014) Neuroimaging in amyotrophic lateral sclerosis: insight into structural and functional chances. Lancet Neurol 13:1228–1240
59. Dalakas MC, Hatazawa J, Brooks RA, Di Chiro G (1987) Lowered cerebral glucose utilization in amyotrophic lateral sclerosis. Ann Neurol 22:580–586.

Ludolph AC, Langen KJ, Regard M, Herzog H, Kemper B, Kuwert T et al (1992) Frontal lobe function in amyotrophic lateral sclerosis: a neuropsychologic and positron emission tomography study. Acta Neurol Scand 85:81–89
60. Lloyd CM, Richardson MP, Brooks DJ, Al-Chalabi A, Leigh PN (2000) Extramotor involvement in ALS: PET studies with the $GABA_A$ ligand [^{11}C]flumazenil. Brain 123:2289–2296
61. Abrahams S, Goldstein LH, Kew JJ, Brooks DJ, Lloyd CM, Frith CD, Leigh PN (1996) Frontal lobe dysfunction in amyotrophic lateral sclerosis: a PET study. Brain 119:2105–2120
62. Cistaro A, Valentini MC, Chiò A et al (2012) Brain hypermetabolism in amyotrophic lateral sclerosis: a FDG PET study in ALS of spinal and bulbar onset. Eur J Nucl Med Mol Imaging 39:251–259
63. Carrara G, Carapelli C, Venturi F, Ferraris MM et al (2012) A distinct MR imaging phenotype in amyotrophic lateral sclerosis: correlation between T1 magnetization transfer contrast hyperintensity along the corticospinal tract and diffusion tensor imaging analysis. AJNR Am J Neuroradiol 33:733–739
64. Filippini N, Douaud G, Mackay CE, Knight S et al (2010) Corpus callosum involvement is a consistent feature of amyotrophic lateral sclerosis. Neurology 75(18):1645–1652
65. Agosta F, Galantucci S, Riva N, Chiò A et al (2014) Intrahemispheric and interhemispheric structural network abnormalities in PLS and ALS. Hum Brain Mapp 35:1710–1722
66. Chiò A, Borghero G, Restagno G, Mora G, Drepper C, Traynor BJ et al (2012) Clinical characteristics of patients with familial amyotrophic lateral sclerosis carrying the pathogenic GGGGCC hexanucleotide repeat expansion of C9ORF72. Brain 135:784–793
67. Cistaro A, Pagani M, Montuschi A, Calvo A et al (2014) The metabolic signature of C9ORF72-related ALS: FDG PET comparison with nonmutated patients. EJNM Mol Imaging 41(5):844–852
68. Van Laere K, Vanhee A, Verschueren J, De Coster L, Driesen A, Dupont P, Robberecht W, Van Damme P (2014) Value of 18fluorodeoxyglucose-positron-emission tomography in amyotrophic lateral sclerosis: a prospective study. JAMA Neurol 71:553–561
69. Cistaro A, Fania P, Pagani M et al (2015) Integration between RMN and [18F]FDG PET brain imaging in familial amyotrophic lateral sclerosis patients. 2015 AIMN Annual Congress, Rimini, Italy
70. Bede P, Bokde ALW, Byrne S, Elamin M et al (2013) Multiparametric MRI study of ALS stratified for the C9ORF72 genotype. Neurology 81:361–369
71. Sharma KR, Saigal G, Maudsley AA, Govind V (2011) 1H MRS of basal ganglia and thalamus in amyotrophic lateral sclerosis. NMR Biomed 24:1270–1276
72. Verstraete E, van den Heuvel MP, Veldink JH, Blanken N, Mandl RC, Hulshoff Pol HE, van den Berg LH (2010) Motor network degeneration in amyotrophic lateral sclerosis: a structural and functional connectivity study. PLoS One 5(10):e13664
73. Douaud G, Filippini N, Knight S, Talbot K, Turner MR (2011) Integration of structural and functional magnetic resonance imaging in amyotrophic lateral sclerosis. Brain 134(Pt 12):3470–3479. doi:10.1093/brain/awr279, Epub 2011 Nov 10
74. Agosta F et al (2014) Resting state functional connectivity alterations in primary lateral sclerosis. Neurobiol Aging 35:916–925
75. Pagani M et al (2014) FDG-PET in amyotrophic lateral sclerosis – functional pattern and diagnostic accuracy. Neurology 83(12):1067–1074
76. Braak et al. 2013; Chio et al. 2014; Cistaro A, Valentini MC, Chiò A et al (2012) Brain hypermetabolism in amyotrophic lateral sclerosis: a FDG PET study in ALS of spinal and bulbar onset. Eur J Nucl Med Mol Imaging 39:251–259
77. Henkel J, Beers D, Zhao W, Appel SH (2009) Microglia in ALS: the good, the bad, and the resting. J NeuroimmunePharmacol 4:389–398
78. Philips T, Robberecht W (2011) Neuroinflammation in amyotrophic lateral sclerosis: role of glial activation in motor neuron disease. Lancet Neurol 10:253–263, 8
79. Appel SH, Zhao W, Beers DR, Henkel J (2011) The Microglial-Motoneuron dialogue in ALS. Acta Myologica 1:4–8
80. McGeer PL, McGeer EG (2002) Inflammatory process in amyotrophic lateral sclerosis. Muscle Nerve 26:459–470
81. Johanson A (2007) Evidence for astrocytosis in ALS demonstrated by (11C)(L)-deprenyl-D2 PET. J Neurol Sci 255:17–22
82. Schiffer D, Cordera S, Cavalla P, Migheli A (1996) Reactive astrogliosis of the spinal cord in amyotrophic lateral sclerosis. J Neurol Sci 139(Suppl):27–33
83. Aquilonius SM, Jossan SS, Ekblom JG, Askmark H, Gillberg PG (1992) Increased binding of 3H-L-deprenyl in spinal cords from patients with amyotrophic lateral sclerosis as demonstrated by autoradiography. J Neural Transm Gen Sect 89(1–2):111–122
84. Papadopoulos V, Baraldi M, Guilarte TR, Papadopoulos V, Baraldi M et al (2006) Translocator protein (18 kDa): new nomenclature for the peripheral-type benzodiazepine receptor based on its structure and molecular function. Trends Pharmacol Sci 27:402–409
85. Veenman L, Gavish M (2000) Peripheral-type benzodiazepine receptors: their implication in brain disease. Drug Dev Res 50:355–370
86. Veenman L, Gavish M (2012) The role of 18 kDa mitochondrial translocator protein (TSPO) in programmed cell death, and effects of steroids on TSPO expression. Curr Mol Med 12:398–412
87. Petit-Taboué MC, Baron JC, Barré L, Travère JM, Speckel D et al (1991) Brain kinetics and specific binding of [11C]PK 11195 to omega 3 sites in baboons: positron emission tomography study. Eur J Pharmacol 200:347–351

88. Hirvonen J, Roivainen A, Virta J, Helin S, Någren K et al (2010) Human biodistribution and radiation dosimetry of 11C-(R)-PK11195; the prototypic PET ligand to image inflammation. Eur J Nucl Med Mol Imaging 37:606–612
89. Turner MR (2004) Evidence of widespread cerebral microglial activation in amyotrophic lateral sclerosis: an (11C)(R)-PK11195 positron emission tomography study. Neurobiol Dis 15:601–609
90. Corcia P, Tauber C, Vercoullie J, Arlicot N et al (2012) Molecular imaging of microglial activation in amyotrophic lateral sclerosis. PLoS One 7:e52941
91. Agosta F, Pagani E, Rocca MA, Caputo D, Perini M et al (2007) Voxel-based morphometry study of brain volumetry and diffusivity in amyotrophic lateral sclerosis patients with mild disability. Hum Brain Mapp 28:1430–1438
92. Lepow L, Van Sweringen J, Strutt A, Jawaid A, MacAdam C et al (2010) Frontal and temporal lobe involvement on verbal fluency measures in amyotrophic lateral sclerosis. J Clin Exp Neuropsychol 32:913–922
93. Geser F, Brandmeir NJ, Kwong LK, Martinez-Lage M, Elman L et al (2008) Evidence of multisystem disorder in whole-brain map of pathological TDP-43 in amyotrophic lateral sclerosis. Arch Neurol 65:636–641
94. Piao YS, Wakabayashi K, Kakita A, Yamada M, Hayashi S et al (2003) Neuropathology with clinical correlations of sporadic amyotrophic lateral sclerosis 102 autopsy cases examined between 1962 and 2000. Brain Pathol 12:10–22
95. Kreisl WC, Fujita M, Fujimura Y, Kimura N, Jenko KJ, Kannan P et al (2010) Comparison of [(11) C]-(R)-PK 11195 and [(11)C]PBR28, two radioligands for translocator protein (18 kDa) in human and monkey: Implications for positron emission tomographic imaging of this inflammation biomarker. Neuroimage 49(4):2924–2932
96. Zucher NR, Loggia M, Lawson R, Chonde DB et al (2015) Increased in vivo glial activation in patients with amyotrophic lateral sclerosis: assessed with [11C]-PBR28. Neuroimage Clin 7:409–414
97. Carluer L, Mondou A, Buhour MS, Laisney M, Péelerin A, Eustache F, Viader F, Desgranges V (2015) Neural substrate of cognitive theory of mind impairment in amyotrophic lateral sclerosis. Cortex Cortex 65:19–30
98. Phukon J, Pender NP, Hardiman O (2007) Cognitive impairment in amyotrophic lateral sclerosis. Lancet Neurol 6:994–1003
99. Ludolph AC, Ludolph AC, Langen KJ, Regard M, Herzog H, Kemper B, Kuwert T, Böttger IG, Feinendegen L et al (1992) Frontal lobe function in amyotrophic lateral sclerosis: a neuropsychological and positron emission tomography. Acta Neurol Scand 85(2):81–89
100. Coricelli G (2005) Two-levels of mental states attribution: from automaticity to voluntariness. Neuropsychologia 43:294–300
101. Brothers L, Ring B (1992) A neuroethological framework for the representation of minds. J Cogn Neurosci 4(2):107–118
102. Jeong Y, Park KC, Cho SS, Kim EJ, Kang SJ, Kim SE, Kang E, Na DL (2005) Pattern of glucose hypometabolism in frontotemporal dementia with motor neuron disease. Neurology 64:734–736
103. Jeong Y, Cho SS, Park JM, Kang SJ, Lee JS, Kang E, Na DL, Kim SE (2005) 18F-FDG PET findings in frontotemporal dementia: an SPM analysis of 29 patients. J Nucl Med 46:233–239
104. Martikainen MH, Gardberg M, Jansson L, Röyttä M, Rinne JO, Kaasinen V (2014) Brain ^{18}F-FDG and ^{11}C-PiB PET findings in two siblings with FTD/ALS associated with the C9ORF72 repeat expansion. Neurocase 20:150–157
105. Yamakawa Y, Shimada H, Ataka S, Tamura A, Masaki H, Naka H, Tsutada T, Nakanishi A, Shiomi S, Watanabe Y, Miki T (2012) Two cases of dementias with motor neuron disease evaluated by Pittsburgh compound B-positron emission tomography. Neurol Sci 33:87–92
106. Canosa A, Pagani M, Cistaro A, Montuschi A, Iazzolino B, Fania P, Cammarosano S, Ilardi A, Moglia C, Calvo A, Chio A (2015) 18F-FDG-PET correlates of cognitive impairment in ALS. Neurology 86(1):44–49
107. Hall ED, Oostveen JA, Gurney ME (1998) Relationship of microglial and astrocytic activation to disease onset and progression in a transgenic model of familial ALS. Glia 23:249–256
108. Monk PN, Shaw PJ (2006) ALS: life and death in a bad neighborhood. Nat Med 12:885–887
109. Yamanaka K, Chun SJ, Boillee S, Fujimori-Tonou N et al (2008) Astrocytes as determinants of disease progression in inherited amyotrophic lateral sclerosis. Nat Neurosci 11:251–253
110. Brettschneider J, Del Tredici K, Toledo JB et al (2013) Stages of pTDP-43 pathology in amyotrophic lateral sclerosis. Ann Neurol 74:20–38
111. Mioshi E, Lillo P, Yew B et al (2013) Cortical atrophy in ALS is critically associated with neuropsychiatric and cognitive changes. Neurology 80:1117–1123
112. Schuster C, Kasper E, Dyrba M et al (2014) Cortical thinning and its relation to cognition in amyotrophic lateral sclerosis. Neurobiol Aging 35:240–246

Hybrid Imaging in Vegetative State

15

Carlo Cavaliere, Marco Aiello, and Andrea Soddu

Since the invention of the artificial respirator in the 1950s, the rate of patients that survive from traumatic accidents, prolonged cardiac arrest, and other brain-damaging conditions [1] has dramatically increased. This innovation has led to a wide and often undefined spectrum of clinical syndromes and disorders of consciousness (DOC) [2], including patients "awakening" from the acute phase of coma but without any sign of voluntary interaction with the environment.

Over time, different definitions have been coined for this condition, like apallic syndrome [3], coma vigil [4], or, in 1972, "persistent vegetative state (PVS)" [5]. Recently, the European Task Force on Disorders of Consciousness has coined a different more descriptive name for VS: "unresponsive wakefulness syndrome" (UWS) [2]. Two features are intrinsic in this definition: "unresponsive" to stress that VS patients are characterized by reflex movements without any sign of voluntary interaction and command following and "wakefulness" to illustrate the eye opening that can be spontaneous or induced by stimulation and differentiate this state by coma.

C. Cavaliere (✉) • M. Aiello
IRCCS SDN, Istituto Ricerca Diagnostica Nucleare, Via E. Gianturco 113, Naples, Italy
e-mail: ccavaliere@sdn-napoli.it

A. Soddu
Physics & Astronomy Department, Brain & Mind Institute, Western University, London, ON, Canada

Although by definition, the VS diagnosis is mainly clinical, and so possible to patient's bedside, the distinction among different DOC states (e.g., between VS and minimally conscious state (MCS)), is sometimes tricky, with high rates of diagnostic error to neurological assessment [6]. Nevertheless, accurate diagnosis in DOC remains critical for appropriate care and prognosis prediction of these chronic patients.

Despite the best clinical assessment [7], improved with the use of dedicated scales such as the Coma Recovery Scale – Revised (CRS-R) [8], some behaviorally unresponsive patients could be clinically underestimated in terms of assessment of residual consciousness and recovery prediction [9]. In this context, multimodal neuroimaging techniques can integrate bedside assessment, providing a valuable support for a correct workflow of VS patients [10]. In particular, morphological information about lesion site and extent (computed tomography, CT, and structural magnetic resonance, MR), structural connectivity and white matter integrity (diffusion tensor imaging, DTI), brain metabolism (magnetic resonance spectroscopy, MRS, and positron emission tomography with fluoro-18 fluorodeoxyglucose tracer, 18F-FDG PET), and hemodynamic response (functional magnetic resonance imaging, fMRI; arterial spin labeling, ASL; and positron emission tomography with oxygen-15 labelled water – 15O-H2O PET) can be achieved [11].

A. Ciarmiello, L. Mansi (eds.), *PET-CT and PET-MRI in Neurology*,
DOI 10.1007/978-3-319-31614-7_15

From a morphological point of view, MRI represents the gold standard to identify the site, characterize the typology, and evaluate the extent of brain lesions in DOC patients. Moreover, this tool is able to follow in a noninvasive manner cortical/subcortical atrophy [12], hydrocephalus, or lesion evolution that often characterize these kinds of patients and are predictive of unfavorable outcome [13, 14].

From a functional point of view, PET imaging has been the first neuroimaging technique to demonstrate massive decrease in brain metabolism in patients with DOC. Studies with 15H-H2O PET tracer [15, 16], confirmed by fMRI technique [17, 18], have demonstrated in VS patients a significant disconnection of several pathways following passive auditory or noxious stimulation. Moreover, studies with 18F-FDG PET during rest have demonstrated a cortical selective reduction of metabolic rate of glucose in VS patients, estimated in about 42 % of control values [19]. Also fMRI during resting state has introduced new evidences about VS differential diagnosis, identifying the so-called default mode network (DMN) as the brain network mainly correlated with the level of consciousness [20–22].

Other MRI sequences, like DTI or MRS, have been also applied to DOC patients [13, 23], reporting a significant reduction of fractional anisotropy values in predefined white matter regions (e.g., corpus callosum and thalamus) [24–26] or a reduction of both N-acetylaspartate to choline ratio (NAA/Cho) and N-acetylaspartate to creatine (NAA/Cr) ratio [13], respectively.

In this increasing amount of literature about neuroimaging role in DOC patients, only one study has recently compared MR and PET findings in the same population [27]. The authors examining 81 MCS and 41 VS patients by 18F-FDG PET and fMRI mental imagery task concluded that PET imaging is more accurate than fMRI for differential diagnosis and prediction outcome of DOC. Importantly, several considerations have been done according to the different paradigms and related informations used by these techniques. While 18F-FDG PET directly quantifies the brain metabolic activity during rest, fMRI task indirectly evaluates consciousness residuals through an intentional "command following" [28].

Although no evidences exist, the recent introduction of hybrid PET/MR imaging could overcome these issues, simultaneously acquiring both modalities. This neuroimaging tool could be used to assess the same phenomena, comparing PET and MR findings at the same time. For example, it could be interesting to compare 15H-H2O PET with ASL-MRI during rest to highlight perfusion discrepancies or 15H-H2O PET with fMRI during tasks to highlight network disconnections in DOC patients. The use of hybrid PET/MR for this aim results needed: considered the high temporal resolution of these phenomena, the sequential acquisition of both modalities is not a choice to really compare imaging findings.

A different more attractive possibility could be to compare different phenomena, employing the simultaneous acquisition of both imaging modalities. In this way it could be possible to characterize complementary features of patients with DOC, like metabolism by 18F-FDG PET and perfusion or cortical activation by ASL-MRI or fMRI, respectively.

References

1. Laureys S, Boly M (2008) The changing spectrum of coma. Nat Clin Pract Neurol 4(10):544–546
2. Laureys S, Celesia GG, Cohadon F, Lavrijsen J, León-Carrión J, Sannita WG, Sazbon L, Schmutzhard E, Von Wild KR, Zeman A, Dolce G (2010) Unresponsive wakefulness syndrome: a new name for the vegetative state or apallic syndrome. BMC Med 8:68
3. Kretschmer E (1940) Das apallische syndrom. Z Ges Neurol Psychiat 169:576–579
4. Calvet J, Coll J (1959) Meningitis of sinusoid origin with the form of coma vigil. Rev Otoneuroophtalmol 31:443–445
5. Jennett B, Plum F (1972) Persistent vegetative state after brain damage. A syndrome in search of a name. Lancet 1(7753):734–737
6. Schnakers C, Vanhaudenhuyse A, Giacino J, Ventura M, Boly M, Majerus S et al (2009) Diagnostic accuracy of the vegetative and minimally conscious state: clinical consensus versus standardized neurobehavioral assessment. BMC Neurol 9:35
7. American Congress of Rehabilitation Medicine, Brain Injury-Interdisciplinary Special Interest Group, Disorders of Consciousness Task Force, Seel R, Sherer M, Whyte J, Katz D, Giacino J, Rosenbaum A, Hammond F, Kalmar K, Pape T, Zafonte R, Biester R, Kaelin D, Kean J, Zasler N (2010) Assessment scales

for disorders of consciousness: evidence- based recommendations for clinical practice and research. Arch Phys Med Rehabil 91(12):795–813
8. Giacino JT, Kalmar K, Whyte J (2004) The JFK coma recovery scale-revised: measurement characteristics and diagnostic utility. Arch Phys Med Rehabil 85:2020–2029
9. Laureys S, Boly M (2007) What is it like to be vegetative or minimally conscious? Curr Opin Neurol 20(6):609–613
10. Giacino JT, Fins JJ, Laureys S, Schiff ND (2014) Disorders of consciousness after acquired brain injury: the state of the science. Nat Rev Neurol. Advance online publication 28 January 2014; doi:10.1038/nrneurol.2013.279
11. Di Perri C, Thibaut A, Heine L, Soddu A, Demertzi A, Laureys S (2014) Measuring consciousness in coma and related states. World J Radiol 6(8):589–597
12. Trivedi MA, Ward MA, Hess TM, Gale SD, Dempsey RJ, Rowley HA, Johnson SC (2007) Longitudinal changes in global brain volume between 79 and 409 days after traumatic brain injury: relationship with duration of coma. J Neurotrauma 24(5):766–771
13. Carpentier A, Galanaud D, Puybasset L, Muller JC, Lescot T, Boch AL et al (2006) Early morphologic and spectroscopic magnetic resonance in severe traumatic brain injuries can detect "invisible brain stem damage" and predict "vegetative states". J Neurotrauma 23:674–685
14. Choi SP, Park KN, Park HK, Kim JY, Youn CS, Ahn KJ, Yim HW (2010) Diffusion-weighted magnetic resonance imaging for predicting the clinical outcome of comatose survivors after cardiac arrest: a cohort study. Crit Care 14:R17
15. Laureys S, Faymonville ME, Peigneux P et al (2002) Cortical processing of noxious somatosensory stimuli in the persistent vegetative state. Neuroimage 17(2):732–741
16. Boly M, Faymonville ME, Schnakers C et al (2008) Perception of pain in the minimally conscious state with PET activation: an observation study. Lancet Neurol 7(11):1013–1020
17. Boly M, Faymonville ME, Peigneux P, Lambermont B, Damas F, Luxen A, Lamy M, Moonen G, Maquet P, Laureys S (2005) Cerebral processing of auditory and noxious stimuli in severely brain injured patients: differences between VS and MCS. Neuropsychol Rehabil 15(3–4):283–289
18. Fernandez-Espejo D, Junque C, Vendrell P, Bernabeu M, Roig T, Bargallo N, Mercader JM (2008) Cerebral response to speech in vegetative and minimally conscious states after traumatic brain injury. Brain Inj 22(11):882–890
19. Stender J, Kupers R, Rodell A et al (2015) Quantitative rates of brain glucose metabolism distinguish minimally conscious state from vegetative state patients. J Cereb Blood Flow Metab 35(1):58–65
20. Soddu A, Boly M, Nir Y, Noirhomme Q, Vanhaudenhuyse A, Demertzi A, Arzi A, Ovadia S, Stanziano M, Papa M, Laureys S, Malach R (2009) Reaching across the abyss: recent advances in functional magnetic resonance imaging and their potential relevance to disorders of consciousness. Prog Brain Res 177:261–274
21. Vanhaudenhuyse A, Noirhomme Q, Tshibanda L, Bruno M-A, Boveroux P, Schnakers C, Soddu A, Perlbarg V, Ledoux D, Brichant J-F, Moonen G, Maquet P, Greicius MD, Laureys S, Boly M (2010) Default network connectivity reflects the level of consciousness in non-communicative brain-damaged patients. Brain 133:161–171
22. Ovadia-Caro S et al (2012) Reduction in inter- hemispheric connectivity in disorders of consciousness. PLoS One 7:e37238
23. Cavaliere C, Aiello M, Di Perri C, Fernandez-Espejo D, Owen AM, Soddu A (2015) Diffusion tensor imaging and white matter abnormalities in patients with disorders of consciousness. Front Hum Neurosci 8:1028
24. Luyt CE, Galanaud D, Perlbarg V, Vanhaudenhuyse A, Stevens RD, Gupta R et al (2014) Diffusion tensor imaging to predict long-term outcome after cardiac arrest: a bicentric pilot study. Anesthesiology 117:1311–1321.doi:10.1097/ALN.0b013e318275148c
25. Edlow BL, Haynes RL, Takahashi E, Klein JP, Cummings P, Benner T et al (2013) Disconnection of the ascending arousal system in traumatic coma. J Neuropathol Exp Neurol 72:505–523
26. Fernández-Espejo D, Bekinschtein T, Monti MM, Pickard JD, Junque C, Coleman MR et al (2011) Diffusion weighted imaging distinguishes the vegetative state from the minimally conscious state. Neuroimage 54:103–112. doi:10.1016/j.neuroimage.2010.08.035
27. Stender J et al (2014) Diagnostic precision of PET imaging and functional MRI in disorders of consciousness: a clinical validation study. The Lancet 384(9942):514–522
28. Owen AM (2014) Diagnostic accuracy of brain imaging in the vegetative state. Nat Rev Neurol 10:370–371

Hybrid Imaging in Cerebrovascular Disease: Ischemic Stroke

16

Elisabetta Giovannini, Giampiero Giovacchini, and Andrea Ciarmiello

16.1 Background

Stroke represents a major health problem with a considerable human and economic burden [1].

Acute cerebral ischemia is one of the main causes of mortality and morbidity with incidence rate accounting for around 200 cases per 100,000 population/years [1]. Actually, stroke is positioned as the third cause of death in most Western countries. Furthermore, due to the aging of the population, the incidence and debilitating consequences of stroke are expected to increase dramatically [2, 3].

During the event of acute ischemia, cerebral blood flow (CBF) may drastically decrease. If hypoperfusion is prolonged in time, a cytotoxic cascade is activated producing focal or diffuse cerebral changes. The effects of ischemia depend on the duration of reduced cerebral blood flow. There are various possible outcomes, and tissue salvage may be achieved when reperfusion is established within a 6- to 8-h period [4]. When the CBF goes below 55 ml/100 g/min, protein synthesis begins to deteriorate, and when it drops below 35 ml/100 g/min, there is an increased glucose utilization and lactate accumulation. As CBF further declines below 26 ml/100 g/min, the resulting acidosis leads to the decline in phosphocreatine and adenosine triphosphate levels. As CBF reaches around 23 ml/100 g/min, neurological dysfunction and suppression of electrical activity in the brain appear. Further deterioration of CBF, to 5–18 ml/100 g/min, causes irreversible hemiparesis and infarction [4, 5].

Generally a central core of infarction with severely compromised CBF is surrounded by a rim of moderate ischemic tissue with impaired electrical activity but some preserved cellular metabolism and viability [6]. This area called "penumbra" commonly arises in the periphery of the brain when blood flow is significantly reduced causing hypoxia, but it is not severe enough to cause irreversible failure of energy metabolism and cellular necrosis (Fig. 16.1) [7, 8].

Tissue within the penumbra is functionally impaired and contributes to the clinical deficit, yet it is still viable and hence potentially salvageable by effective reperfusion. The extent of the penumbra, however, decreases over time by gradual recruitment into the core and as such represents a key target for therapeutic intervention, albeit with a progressively shrinking temporal window of opportunity [9]. The penumbra is functionally impaired, but potentially still viable brain tissue may survive if blood flow is restored.

E. Giovannini (✉) • A. Ciarmiello
Department of Nuclear Medicine, S. Andrea Hospital, La Spezia, Italy
e-mail: elisabetta.giovannini@asl5.liguria.it

G. Giovacchini
Institute of Radiology and Nuclear Medicine, Stadtspital Triemli, Zurich, Switzerland

A. Ciarmiello, L. Mansi (eds.), *PET-CT and PET-MRI in Neurology*,
DOI 10.1007/978-3-319-31614-7_16

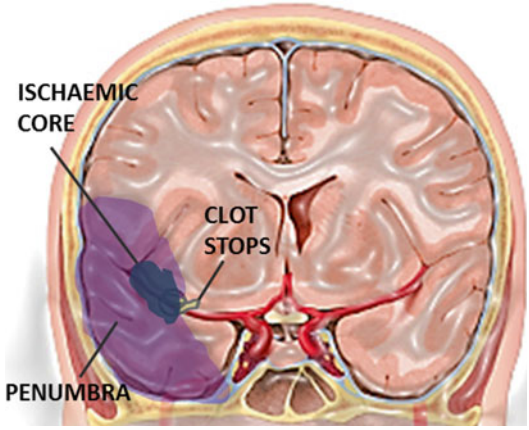

Fig. 16.1 Schematic representation of the (1) ischemic penumbra, the external area potential to reverse neurologic impairment with poststroke therapy, and (2) of the ischemic core, brain tissue deemed to evolve in infarction

The concept that a proportion of the brain subjected to ischemia is still viable and could recover marked a dramatic change in acute ischemic stroke management in the last decades [4].

There are two main types of stroke, that is, ischemic stroke and hemorrhagic stroke, which affect the brain in different ways and can have different causes. Ischemic strokes are the most common type of stroke and those where thrombolysis or thrombectomy is indicated [1, 2]. Ischemic clots occurs when a blood clot block the blood flow and oxygen diffusion to the brain. These blood clots typically form in areas where the arteries have been narrowed or blocked over time by fatty deposits known as plaques. Thrombolysis is nowadays performed. On the contrary, mechanical removal of the thrombus is indicated as thrombectomy. In the carotid artery, this procedure is called carotid endarterectomy; carotid angioplasty may also be performed alternatively [10]. The risk of stroke is correlated to the dimension of artery stenosis, as determined by the plaque. In symptomatic carotid artery disease, the grade of stenosis is a predictor for possible ischemic events, and it is the principal indication for intervention.

Histological studies have shown that plaque inflammation is a major prognosticator for ischemic stroke. Rupture of atherosclerotic plaques has been identified as the proximate event in the majority of cases of acute ischemic syndromes. Plaque rupture exposes thrombogenic components of the plaque activating the clotting cascade and promoting thrombus formation (Fig. 16.2) [11]. Although advanced atherosclerotic lesions are heterogeneous in nature, the majority is characterized by a large lipid core with a thin fibrous cap and increased numbers of inflammatory cells. There is a strong correlation between concentrations of macrophages localized in the site of plaque rupture and the occurrence of acute cardiovascular events [12, 13]. However, not every lesion progresses into a vulnerable or unstable plaque as there is a delicate equilibrium between degradation and the stabilization response of venous walls [14]. The understanding of plaque biology and the shortcoming of angiography in carotid stenosis imaging, as well as the concept of the penumbra during acute ischemic stroke have stimulated the development of novel imaging techniques. In the last decade several improvements have been made in neuroimaging technologies, which have made it possible to investigate the penumbra more accurately changing for the better acute ischemic stroke treatment.

Thrombolysis, such as with recombinant tissue plasminogen activator (rtPA), in acute ischemic stroke, when given within 3 h of symptom onset results in an overall benefit of 10 % with respect to living without disability [15, 16]. It does not, however, improve chances of survival [15]. Benefit is greater the earlier it is used. Between 3 and 4.5 h, the effects are less clear [10].

Imaging tools capable of providing insights into tissue viability continues to gain interest, which in turn may improve patient selection for reperfusion treatments [17]. The presence of neuroimaging-based evidence of salvageable brain tissue may help to identify the optimal time windows for which therapy of ischemic stroke is warranted [18].

16.2 PET/CT Imaging

PET, and subsequently PET/CT, has been employed as imaging tool to provide insights into brain tissue viability in vivo measuring the

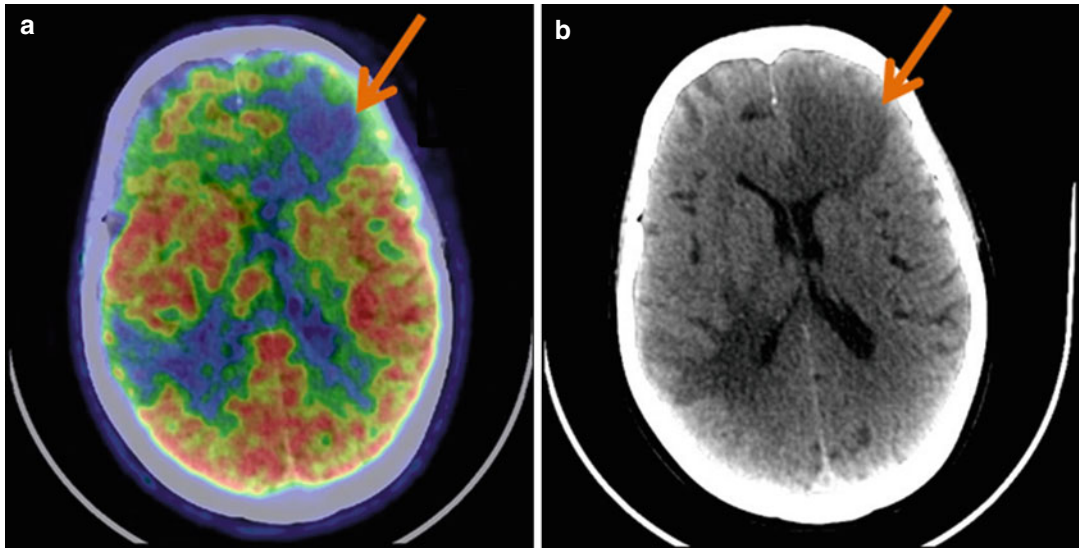

Fig. 16.2 Schematic representation of a stable plaque (*left*) and an unstable carotid plaque (*right*). The vulnerable carotid plaque is invaded by inflammatory cells that uptake [^{18}F]-FDG and allows its investigation by mean of PET

oxygen and glucose metabolism, the two main energy substrates of the brain. Quantitative measurements of cerebral hemodynamics CBF and oxygen metabolism (oxygen extraction fraction, OEF) and cerebral metabolic rate of oxygen utilization ($CMRO_2$) can be obtained using PET with the ^{15}O continuous inhalation method, which involved the sequential use of ^{15}O-labeled CO_2 and O_2 [19]. Experimental work on the ischemic flow thresholds of brain tissue demonstrated the existence of two critical levels of decreased perfusion: first, a level representing the flow threshold for reversible functional failure (functional threshold) and second, a lower threshold below which irreversible membrane failure and morphologic damage occur. The range of perfusion values between those limits was called the ischemic penumbra [8], which was characterized by the potential for functional recovery without morphologic damage, provided that sufficient local blood flow could be reestablished.

After an acute ischemic event, arterial vessels may be damaged and eventual reperfusion may then lead to postischemic hyperperfusion [20]. Such hyperperfusion may develop in viable tissue, where it is often mild and does not prevent a good outcome. However, it may also occur despite ischemic infarcts, known as "luxury perfusion." This phenomenon is a major reason for the inability of sole CBF measurements to predict tissue outcome reliably. Regarding OEF, clinical and preclinical studies have demonstrated that areas with compromised CBF but increased OEF may be indicative of ischemic penumbra, even though intersubject and inter-region values OEF may have substantial variability [21]. The $CMRO_2$ has been suggested as a highly promising parameter in predicting tissue fate in various stroke studies [22–26]. Specifically, it has been shown that brain regions with reduced CBF, but preserved $CMRO_2$, are associated with neuronal survival, whereas brain regions with reduced CBF and $CMRO_2$ reflect irreversible tissue damage. PET with ^{15}O-labeled tracers provides essential physiological information that could predict tissue final fate during acute cerebral ischemia. Unfortunately, the requirement of having a cyclotron to produce ultrashort half-life ^{15}O-labeled tracers (~2 min) significantly reduces its clinical utility [27].

Alternatively, fluorine-18 (or [^{18}F]) has a half-life of 110 min, and [^{18}F]-fluoro-2-deoxy-D-glucose ([^{18}F]-FDG) has been utilized extensively to reveal in vivo glucose utilization in different clinical settings. [^{18}F]-FDG is a glucose analogue

that is taken up by glucose-using cells and phosphorylated by hexokinase and intracellularly accumulated. In myocardial infarction patients, PET/CT with [^{18}F]-FDG has been routinely applied to discern viable myocardium before considering coronary artery bypass graft surgery [28, 29]. Likewise [^{18}F]-FDG-PET also offered valuable insights into cerebral glucose metabolism during cerebral ischemia discerning tissue viability. [^{18}F]-FDG has been employed in the study of cerebral ischemia, particularly in predicting tissue fate (Fig. 16.3) [30]. There are many other PET tracers used to analyze different parameters involved in cerebral ischemia. For example, markers of hypoxic tissue were also tested with respect to their capacity to identify penumbral tissue. [^{18}F]-fluoromisonidazole ([^{18}F]-FMISO) is a nitroimidazole compound that is selectively trapped within hypoxic but living cells [31–36]. The uptake of [^{18}F]-FMISO is detectable in the periphery and surrounding tissue of infarcts in 70 % of patients studied within 48 h of stroke, but it does not occur in patients studied at a later time point (between 6 and 11 days) after stroke, and where necrotic change had occurred [37]. Uptake of [^{18}F]-FMISO has been demonstrated to shift from the eventual infarct core (in patients studied in the first 6 h following the stroke) to the periphery and surrounding tissue (in patients studied from 6 to 48 h after stroke). Over time, the amount of hypoxic tissue declines. When imaged within 6 h of stroke onset, about 90 % of the region of [^{18}F]-FMISO is included in the eventual infarct, whereas this percentage falls to 50 % after 16 h [34, 38]. Clinical correlations exist between the volume of initially affected tissue and initial severity of the neurological deficit and between the proportion of initially affected tissue progressing to infarction and neurological deterioration during the first week following the stroke [38]. Since a variable portion of the tissue detected by [^{18}F]-FMISO does not develop into infarct if untreated, [^{18}F]-FMISO cannot accurately prevent infarction identification. So the interpretation of these data is that the level of hypoxia necessary for [^{18}F]-FMISO binding is less than that of the level which causes certain cell death [38].

Neuroimaging techniques can also be used to study cellular and functional mechanisms of

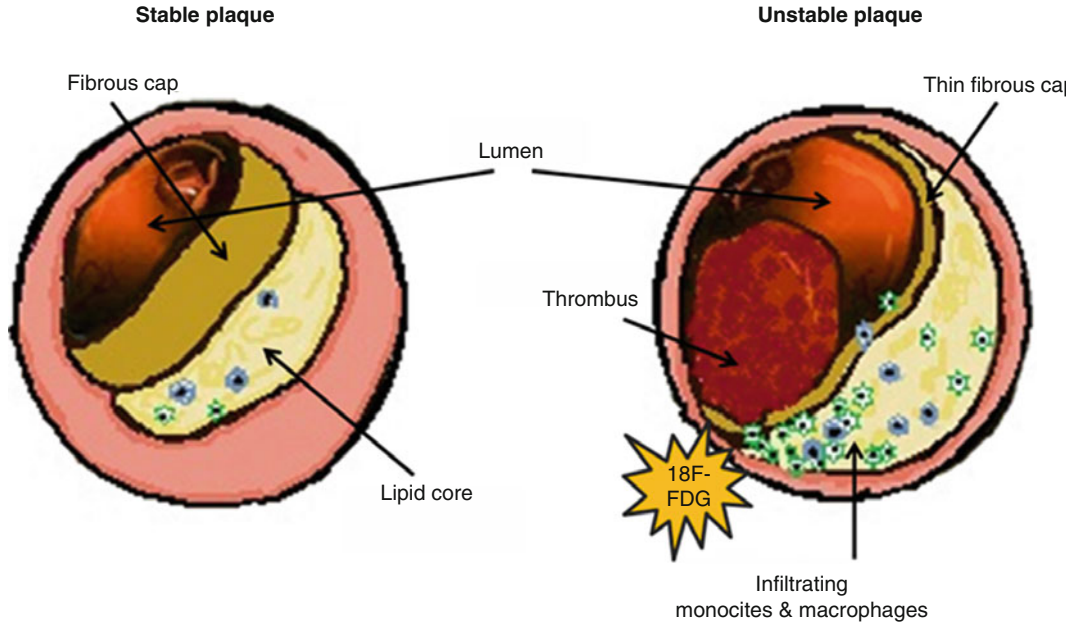

Fig. 16.3 [^{18}F]-FDG PET/CT scan of the brain showing a left frontal hypometabolism (*left image*), which is due to an acute ischemic stroke

poststroke recovery [18, 39]. Generally in a healthy brain, mechanisms that inhibit axonal sprouting are predominant in respect to stimulating factors. However, ischemic neuronal injury induces axonal sprouting. Bordering this glial scar is a larger "growth-permissive zone" of the peri-infarct cortex that expresses reduced levels of growth-inhibiting factors. In some human neuroimaging studies, increased signal in the peri-infarct zone correlates with good functional recovery [39, 40]. Most evidence indicates that functional recovery after stroke occurs primarily through reorganization of cortical activity in the vicinity of or connected to the infarct. Recent studies also suggest that recovery of motor function may involve alteration of intracortical wiring patterns. One potential role of these novel wiring patterns may be the recruitment of compensatory areas or areas of the brain that are not directly related to the damaged area [40]. The results of human neuroimaging studies suggest the formation of new connections between the peri-infarct cortex and the premotor, motor, and somatosensory cortical areas. This reorganization is accompanied by increased activity in the supplementary motor areas of the damaged side. Mechanisms of poststroke language recovery appear to be similar to the recovery after motor stroke; there is evidence of peri-infarct zone and contralateral homologue contributions to language recovery. Multiple mechanisms may exist for recovery of function after stroke. Evidence shows that recovery depends on the involvement of areas unaffected by stroke, either proximal to the damaged areas or in contralateral homologues. Many variables influence recovery, including age at the time of the stroke, the size of the stroke, and the poststroke training or therapy.

Brain-mapping techniques have dual roles in tracking recovery following a stroke. They provide information about the cellular and molecular processes arising naturally during stroke recovery and allow for the investigation of poststroke brain plasticity that may result from therapeutic interventions. In this scenario PET offers the unique opportunity to investigate the binding of specific neurotransmitter-like ligands to cell surface. Conducting PET imaging studies using radioactively labeled neurotransmitters or transporter ligands allows examination of the density and regional distribution of specific cell surface proteins in the brain. Information about receptor and transporter distribution or density can indicate the signaling viability of nerve cells in a given brain region. This can be quantified with different binding indices, namely, the distribution volume (V) and the binding potential (BP), either of which can be calculated using a multitude of methodological approaches [41–45].

Thus, ligand-based nuclear medicine techniques enable quantitative description of cellular neurotransmitter systems. Currently, ligand-based nuclear medicine techniques are not in widespread use in rehabilitation centers, but they appear to have a niche for examining acute stroke. A wide variety of PET ligands are available to the research community. All major neurotransmitter systems can be examined with one or more ligand. The gamma-aminobutyric acid (GABA) receptor, which has been extensively studied for epilepsy, has been evaluated also for stroke. [^{11}C]-flumazenil is a central benzodiazepine receptor radioligand that binds to GABA receptors on synapses of cortical neurons. Because GABA receptors are sensitive to ischemia, the reduction of [^{11}C]-flumazenil uptake has been used to provide an early indication of neuronal damage. However, the low density of central benzodiazepine receptors in subcortical gray and white matter restricts its ability to identify tissue damage in these regions [46–48]. In clinical studies evidence exists that the prognosis of aphasia recovery is related to the density of GABA receptor binding in language areas. GABA has been suggested as a marker of neuronal integrity [38, 49].

Both dopamine D_1 and D_2 receptors can also be visualized by PET. The D_2 form selectively binds [^{11}C]-raclopride and [^{18}F]-fallypride [49]. Dopamine function, being important to movement coordination in the striatum, could be affected by stroke, and dopamine imaging might provide a measure of improvement trough the rehabilitative therapy. For the dopamine transporter, for example, a PET tracer is represented by [^{18}F]-FPCIT, while [^{123}I]-FPCIT is available

for SPECT. [^{18}F]-altanserin or [^{18}F]-setoperone binds selectively to the serotonin receptor $5HT_{2A}$. Ligands also exist for a variety of other receptors, including nicotinic and muscarinic acetylcholine receptors, adenosine receptors, opioid receptors, and many others. Ligand-based imaging is likely to become more widespread in rehabilitation research, because it indicates the functionality of brain tissue with respect to specific neurotransmitter systems [49].

A main objective in cerebrovascular imaging is certainly the early assessment in patients with symptomatic carotid stenosis to decrease the risk of new or recurrent ischemic stroke. At present angiography is still the gold standard for the diagnosis of carotid stenosis providing high resolution definition of the anatomical affected site and severity of vessel luminal stenosis. However, this technique does not offer enough information about atherosclerotic plaques at risk of rupture. Some large randomized control trials have shown that the risk reduction for stroke by carotid endarterectomy is much lower for asymptomatic patients compared to symptomatic patients [50]. Carotid endarterectomy is a surgical procedure used to reduce the risk of stroke, by correcting stenosis in the common carotid artery or internal carotid artery. Endarterectomy is the removal of material on the inside of an artery. The absence of absolute risk reduction after carotid endarterectomy may accentuate the importance of other factors than plaque size and luminal obstruction. In fact atherosclerosis is a multifactorial disease combining metabolic alterations with inflammatory reactions such as activation of chemotactic proteins and monocytes recruitment [51, 52]. Pathology studies have shown that the immediate site of plaque rupture contains a high concentration of inflammatory cells. Inflammatory cells have high metabolic activity, especially when they are activated, which markedly enhances their glucose consumption. The imaging technique that enables quantification of vessel wall inflammation is PET with [^{18}F]-FDG [53]. [^{18}F]-FDG is known to accumulate in inflammatory lesions, a characteristic component of the atherosclerosis process (Fig. 16.4). So it was hypothesized that [^{18}F]-FDG-increased uptake in arteries was related to the severity of atherosclerosis. Detection of carotid plaque vulnerability by PET/CT may add important diagnostic information for both tailoring and monitoring treatment. In some studies it has been shown that carotid plaques can be imaged with [^{18}F]-FDG PET in patients with carotid stenosis [54]. The estimated [^{18}F]-FDG accumulation rate (plaque/integral plasma) in symptomatic lesions was higher than in contralateral asymptomatic lesions (around 25–30 %). There was no increased [^{18}F]-FDG uptake in normal carotid arteries. Other studies observed an actively vascular inflamed plaque, compatible with the clinical event, in approximatively 50 % of symptomatic patients [55]. Intensive [^{18}F]-FDG uptake was detected also in symptomatic patients previously submitted to surgical treatment, who suffered from an ischemic stroke, restenosis, or even death, during follow-up. Furthermore, it was observed that standardized uptake value (SUV) of [^{18}F]-FDG into the carotid artery was strongly related to the thickness of vessel circumference, high-density lipoprotein serum levels, and high-sensitivity C-reactive protein levels [56]. It was shown that simvastatin, and not the diet alone, attenuated carotid plaque [^{18}F]-FDG uptake [57].

16.3 Computed Tomography (CT)

In a clinical setting, the accurate determination of neurological examination and use of no contrast-enhanced CT scans are fundamental to rule out intracerebral hemorrhage and for selecting ischemic stroke patients who may benefit from reperfusion therapies [40]. Non-contrast CT was initially one of the only options in the acute setting of a radiology department to assess cerebral ischemia. However, in recent years, the development of multiple magnetic resonance imaging sequences (see below) provided insight into disease pathogenesis, mechanism, and evolution. Multimodal CT typically includes non-contrast CT, CT angiography of both the head and neck (CTA), as well as CT perfusion (CTP). Customization of imaging protocols in patients being evaluated for cerebral ischemia is typically

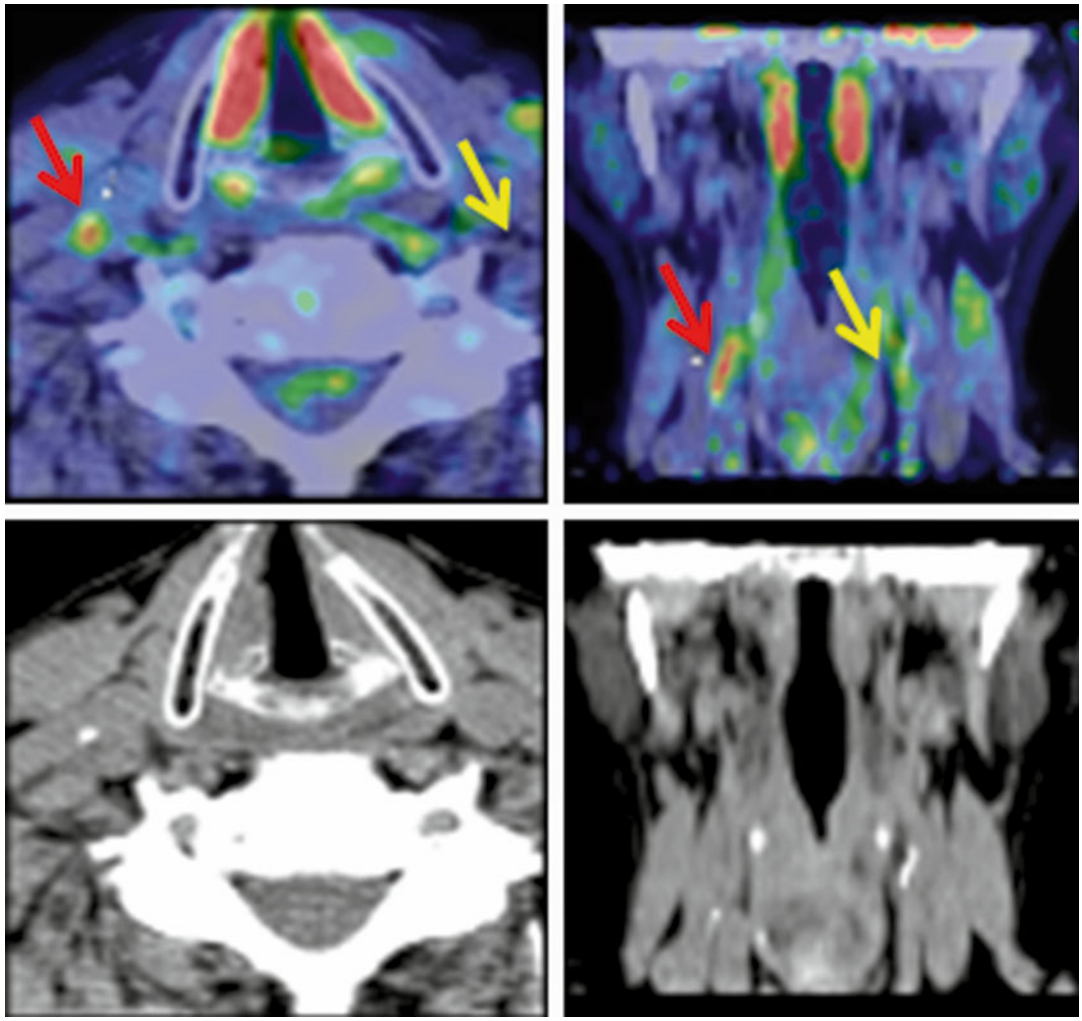

Fig. 16.4 [^{18}F]-FDG PET/CT carotid artery imaging. Transversal and coronal images display a vulnerable carotid plaque on the *right side* with intense tracer uptake. On the contrary, the uptake of [^{18}F]-FDG in the contralateral vessel is only negligible

tailored by institution. Multimodal imaging offers a comprehensive view of the patient's condition including integrity of brain parenchyma and extent of vascular involvement to a dynamic view of tissue viability based on the status of cerebral perfusion. The choice between CT versus magnetic resonance imaging can be tailored to the patient and to their symptoms at presentation. CT becomes the preferred imaging modality in patients who are unable to undergo MRI as in the case of those who have pacemaker devices or implanted metallic objects and for patients too unstable to sustain placement in a supine position for an extended period of time. CT has limited sensitivity in the detection of very early ischemic injury in the acute setting and is restricted in the ability to accurately visualize posterior fossa pathology [58]. However, due to the high specificity and to the wide availability of CT technology, in the community CT scanning continues to prevail as the first-line imaging modality. CTA and CTP, when combined with diagnostic CT, yield additional insight on early ischemia. In conjunction with a patient presentation and clinical exam, which is consistent with a vascular event, non-contrast CT may at least be helpful in ruling

out cerebral hemorrhage or an existing, nonvascular reason for presentation, such as mass-related to infection, malignancy, or other etiology. In the cases of suspected cerebral ischemia where non-contrast CT did not show abnormality, to repeat serial imaging with the evolution of the patient's symptoms is also critical [40].

CTP images are acquired in the cine mode after intravenous injection of an iodinated contrast agent, generating maps of cerebral blood flow (CBF), cerebral blood volume (CBV), as well as mean transit time (MTT) and time to peak (TTP) [59]. The maps are reproducible, especially when relative perfusion parameters are used, and reportedly have >90 % sensitivity and specificity for detecting large hemispheric stroke. Anatomical coverage, however, is typically restricted to 20 mm (two to four slices), reducing sensitivity to stroke not caused by proximal major artery occlusion [9]. Recent studies on CTP in acute stroke demonstrated that tissue with CBV <2 ml/100 g represents the core, while a relative MTT above 145 % of the normal hemisphere best outlines all at-risk tissue [60]. The penumbra can thus be estimated as the tissue existing between those two thresholds. Using this methodology, CTP parameters correlate very well with diffusion-weighted and perfusion-weighted MRI and are good predictors of the final infarct volume and clinical recovery [61]. In combination with CT angiography, CTP has comparable utility with that of MR in selecting patients for thrombolysis [9].

16.4 Magnetic Resonance Imaging (MRI)

Based on the complexity of distinguishing core and penumbra in the clinical setting, a multimodal approach to imaging that provides not only structural but also functional and hemodynamic information to aid the decision-making process is considered necessary also for MRI [62]. For MRI the approach includes a combination of conventional sequences (such as T1-weighted and T2-weighted sequences and fluid-attenuated inversion recovery) and T2-weighted, time-of-flight MR angiography, diffusion-weighted MRI (DWI), and perfusion-weighted MRI (PWI) [62].

Conventional (T1/T2) MRI sequences may not demonstrate an infarct for 6 h, and small infarcts may be difficult to appreciate on CT for days, especially without the benefit of prior imaging. Other MRI modalities, especially DWI and PWI, have been used with great success in many studies of cerebrovascular diseases and now are gradually entering in clinical use. DWI and PWI can detect brain ischemia within minutes from onset of stroke with high diagnostic accuracy, even for small areas of acute ischemia [63]. The DWI signal reflects restriction of the random motion of water in tissue and the decline of its apparent diffusion coefficient (ADC) – although the exact biological correlates are not completely understood, this probably involves energy failure and subsequent cytotoxic edema [9]. Increased DWI signal in ischemic brain tissue is observed within a few minutes after arterial occlusion and progresses through a stereotypic sequence of apparent diffusion coefficient reduction, followed by subsequent increase, pseudo-normalization, and, finally, permanent elevation. Parametric maps of TTP and MTT can be generated similarly to PCT. If comparison of the perfusion deficit depicted on these maps with the apparent diffusion coefficient on DWI (assumed to denote the core) yields a mismatch pattern (PWI >DWI), then the brain region is considered to indicate the existence of salvageable at-risk tissue and is found in about 70 % of all patients with anterior circulation stroke within 6 h of onset [9]. Reported sensitivity ranges from 88 to 100 % and specificity ranges from 86 to 100 %. Furthermore, these MRI modalities allow the follow-up of the ischemic lesion size over time with good spatial and temporal resolution, demonstrating perfusion deficit and reperfusion and the existence and the extent of penumbra. In contrast to the CT trials, MRI pilot studies demonstrate benefit of therapy up to 6 h after onset of symptoms [64]. DWI and PWI are not only of primary importance in the clinical setting for an early diagnosis of ischemic stroke, but they also can be used to define the therapeutic regimen and subsequently to monitor the therapeutic efficacy [65, 66].

16.5 Future Directions: PET/MRI

The development of magnetic field-insensitive PET detector technology paved the way from PET/CT to hybrid PET/MR systems, which have been commercially available since 2011. Due to the higher contrast between gray and white matter, MR provides a substantial advantage over CT for diagnosing CNS pathologies [40]. For scanning of neurological patients, the combination of both PET and MR has often proven to be superior to the single modality approach, improved workflow aspects and an increase in patient comfort, and regarding their research potential, the ability to characterize different pathophysiological aspects of diseases [67]. Acquisition of MR also allows correction for partial volume effect in PET studies. The first PET/MR studies with dedicated PET/MR scanners are now similarly providing evidence of the gained information and synergic effect of these two techniques. In particular hybrid [^{18}F]-FDG PET/MRI has proved to be a technology able to identify high-risk plaques and that may further improve vascular risk stratification in asymptomatic populations [68]. There are, however, clear advantages of using simultaneous PET/MRI scanners as compared to PET/CT and stand-alone MRI in this setting. The simultaneous acquisition diminishes the problem of the correct alignment between sequential examinations; this could be of particular importance in a follow-up trial where the expected plaque changes might be small. The information can be used not only for accurate diagnosis and determination of extent of disease but also for reasonable targeted therapy and monitoring treatment. Simultaneous PET/MRI may contribute in detecting the salvageable brain in patients with stroke, and it may facilitate the clinician in choosing the most appropriate short-term and long-term treatments [61].

Although PET is still considered a very accurate tool for noninvasively identifying the relevant regions of hemodynamic and metabolic compromise in ischemic stroke [69, 70], PET is not routinely integrated into the first-line diagnostic evaluation of patients with suspected cerebrovascular issues or stroke. Diagnosis is usually obtained by CT or increasingly also by MRI [67]. The MRI perfusion/diffusion-weighted mismatch is believed to reflect tissue that is potentially salvageable similar to the PET penumbra concept [39]. However, perfusion-weighted imaging does not correctly estimate the PET penumbra because it only assesses hypoperfusion in the vascular bed. A simultaneous determination of perfusion-weighted imaging hypoperfusion, a low flow preserved and oxygen extraction fraction by PET imaging, should be necessary to discriminate tissue that can benefit from therapies or to exclude patients who are not likely to benefit from thrombolytic therapy [67, 71]. Also in the follow-up of ischemic stroke, the simultaneous comparison between the progression of a lesion (the oxygen extraction or microglial activation using PET) and changes in brain perfusion (evaluating by perfusion- and diffusion-weighted images) is important. In fact these changes occur in small areas around the primary lesion and are transient so a simultaneous determination is necessary.

However, uncertainties about the meaning of DW image lesions have implications for the mismatch theory. Heiss compared [^{15}O]-water PET and [^{11}C]-flumazenil PET with MRI in patients with acute ischemic stroke [5]. They observed that DWI/PWI MRI mismatch overestimates the penumbra. Therefore, while MRI alone may not provide an accurate marker of the penumbra, combined PET and MRI provides complementary information about the penumbra that might enhance the accuracy of its measurement [46].

The use of [^{18}F]-FDG PET or MRI for imaging atherosclerosis has received much attention recently. [^{18}F]-FDG PET has been used as a molecular marker of inflammation, and thus perhaps vulnerability of plaques and MRI has been proven effective in differentiating plaque components based on signal intensities and morphological appearance of the plaque on different imaging sequences [72]. In the same study [^{18}F]-FDG PET fused with MRI identified additional highly inflamed lesions in the vascular territory of the remaining patients [72]. Recently,

the reproducibility results, using MRI for correction of partial volume error, are analyzed in patients with a recent transient ischemic attack [54, 73]. MRI-guided [^{18}F]-FDG PET resulted as a highly reproducible technique in the carotid artery providing excellent anatomical details. Using a combined PET/MRI system with [^{18}F]-FDG, it was recently shown that morphological and biological features of high-risk plaques can be detected with non-stenotic atherosclerotic plaques ipsilateral to the stroke, suggesting a causal role for these plaques in stroke. Combined [^{18}F]-FDG PET/MRI systems might help in the evaluation of patients with ischemic stroke classified as cryptogenic [74].

16.6 Final Remarks

PET [^{15}O] inhalation technique, which is hardly used nowadays also in research settings, has been fundamental since the early 1980s for first conceptualizing, imaging, and quantifying in vivo ischemic stroke and experimentally distinguishing the core from the penumbra. This distinction derived from clinical observations of reversible or partially reversible clinical deficits in some ischemic patients that received early revascularization. Owing to the limited availability, high costs, and extensive process of arterially input-derived parametric images, the development of multiparametric CT and MRI largely substituted this old but fascinating technique in the routine clinical settings and also in many clinical research applications. CT and MR are nowadays the standard for diagnosis, treatment, and follow-up of ischemia in many centers. Through the use of [^{18}F]-FDG or of different specific receptor tracers, such as [^{11}C]-flumazenil, [^{18}F]-fluoromisonidazole, [^{11}C]-raclopride, and [^{18}F]-fallypride, PET can nevertheless be used to quantify or predict the extent and severity of the ischemic neural damage; these studies do not require an input function, can be done outside the critical acute phase, and are logistically less complex. However, not providing a pure CBF information and for the inevitable logistic-limited availability, PET with either [^{18}F]-FDG or receptor ligand has still limited use for the differentiation between core and penumbra in the acute clinical setting. Dedicated centers with integrated PET/MRI scanners and ideally a cyclotron are equipped with a very potential tool that might combine information derived from the two modalities and might provide an increasing offer of diagnostic options for early therapy of cerebrovascular disorders of the brain. A realistic clinical application of these dedicated scanners is represented by the evaluation, using [^{18}F]-FDG, of the instability of the atherosclerotic plaque of carotid arteries. PET/MRI may also improve the physiological understanding of healthy and pathological brain functions, opening up new prospects for a more accurate assessment of brain disease in the acute phase and for monitoring the recovery of the brain functions. Therefore, a comeback of PET methodology in the management of acute cerebral vascular disease can be predicted.

References

1. Goldstein LB et al (2006) Primary prevention of ischemic stroke: a guideline from the American Heart Association/American Stroke Association Stroke Council: cosponsored by the Atherosclerotic Peripheral Vascular Disease Interdisciplinary Working Group; Cardiovascular Nursing Council; Clinical Cardiology Council; Nutrition, Physical Activity, and Metabolism Council; and the Quality of Care and Outcomes Research Interdisciplinary Working Group. Circulation 113(24):e873–e923
2. Soler EP, Ruiz VC (2010) Epidemiology and risk factors of cerebral ischemia and ischemic heart diseases: similarities and differences. Curr Cardiol Rev 6(3):138–149
3. Jauch EC et al (2013) Guidelines for the early management of patients with acute ischemic stroke: a guideline for healthcare professionals from the American Heart Association/American Stroke Association. Stroke 44(3):870–947
4. Hossmann KA (2008) Cerebral ischemia: models, methods and outcomes. Neuropharmacology 55(3): 257–270
5. Heiss WD (2014) Radionuclide imaging in ischemic stroke. J Nucl Med 55(11):1831–1841
6. Back T et al (2000) Penumbral tissue alkalosis in focal cerebral ischemia: relationship to energy metabolism, blood flow, and steady potential. Ann Neurol 47(4):485–492
7. Paciaroni M, Caso V, Agnelli G (2009) The concept of ischemic penumbra in acute stroke and therapeutic opportunities. Eur Neurol 61(6):321–330

8. Astrup J, Siesjo BK, Symon L (1981) Thresholds in cerebral ischemia – the ischemic penumbra. Stroke 12(6):723–725
9. Moustafa RR, Baron JC (2007) Clinical review: imaging in ischaemic stroke – implications for acute management. Crit Care 11(5):227
10. Alper BS et al (2015) Thrombolysis in acute ischaemic stroke: time for a rethink? BMJ 350:h1075
11. Shah PK (2003) Mechanisms of plaque vulnerability and rupture. J Am Coll Cardiol 41(4 Suppl S):15S–22S
12. Libby P et al (1997) Molecular determinants of atherosclerotic plaque vulnerability. Ann N Y Acad Sci 811:134–142; discussion 142–5
13. Libby P et al (1996) Macrophages and atherosclerotic plaque stability. Curr Opin Lipidol 7(5):330–335
14. Aikawa M, Libby P (2004) The vulnerable atherosclerotic plaque: pathogenesis and therapeutic approach. Cardiovasc Pathol 13(3):125–138
15. Wardlaw JM et al (2014) Thrombolysis for acute ischaemic stroke. Cochrane Database Syst Rev 7:CD000213
16. Emberson J et al (2014) Effect of treatment delay, age, and stroke severity on the effects of intravenous thrombolysis with alteplase for acute ischaemic stroke: a meta-analysis of individual patient data from randomised trials. Lancet 384(9958):1929–1935
17. Yamauchi H (2015) Evidence for cerebral hemodynamic measurement-based therapy in symptomatic major cerebral artery disease. Neurol Med Chir (Tokyo) 55(6):453–459
18. Guadagno JV, Calautti C, Baron JC (2003) Progress in imaging stroke: emerging clinical applications. Br Med Bull 65:145–157
19. Frackowiak RS et al (1980) Quantitative measurement of regional cerebral blood flow and oxygen metabolism in man using 15O and positron emission tomography: theory, procedure, and normal values. J Comput Assist Tomogr 4(6):727–736
20. Baron JC (1999) Mapping the ischaemic penumbra with PET: implications for acute stroke treatment. Cerebrovasc Dis 9(4):193–201
21. Baron JC et al (1981) Noninvasive tomographic study of cerebral blood flow and oxygen metabolism in vivo. Potentials, limitations, and clinical applications in cerebral ischemic disorders. Eur Neurol 20(3):273–284
22. Heiss WD et al (1994) Dynamic penumbra demonstrated by sequential multitracer PET after middle cerebral artery occlusion in cats. J Cereb Blood Flow Metab 14(6):892–902
23. Giffard C et al (2004) Outcome of acutely ischemic brain tissue in prolonged middle cerebral artery occlusion: a serial positron emission tomography investigation in the baboon. J Cereb Blood Flow Metab 24(5):495–508
24. Pappata S et al (1993) PET study of changes in local brain hemodynamics and oxygen metabolism after unilateral middle cerebral artery occlusion in baboons. J Cereb Blood Flow Metab 13(3):416–424
25. Touzani O et al (1995) Sequential studies of severely hypometabolic tissue volumes after permanent middle cerebral artery occlusion. A positron emission tomographic investigation in anesthetized baboons. Stroke 26(11):2112–2119
26. Shimosegawa E et al (2005) Metabolic penumbra of acute brain infarction: a correlation with infarct growth. Ann Neurol 57(4):495–504
27. Vespa P et al (2005) Metabolic crisis without brain ischemia is common after traumatic brain injury: a combined microdialysis and positron emission tomography study. J Cereb Blood Flow Metab 25(6):763–774
28. Baron JC (1985) Positron tomography in cerebral ischemia. A review. Neuroradiology 27(6):509–516
29. Heiss WD, Podreka I (1993) Role of PET and SPECT in the assessment of ischemic cerebrovascular disease. Cerebrovasc Brain Metab Rev 5(4):235–263
30. Bunevicius A, Yuan H, Lin W (2013) The potential roles of 18F-FDG-PET in management of acute stroke patients. Biomed Res Int 2013:634598
31. Riche F et al (2001) Nitroimidazoles and hypoxia imaging: synthesis of three technetium-99m complexes bearing a nitroimidazole group: biological results. Bioorg Med Chem Lett 11(1):71–74
32. Nunn A, Linder K, Strauss HW (1995) Nitroimidazoles and imaging hypoxia. Eur J Nucl Med 22(3):265–280
33. Markus R et al (2002) Statistical parametric mapping of hypoxic tissue identified by [(18)F]fluoromisonidazole and positron emission tomography following acute ischemic stroke. Neuroimage 16(2):425–433
34. Read SJ et al (2000) The fate of hypoxic tissue on 18F-fluoromisonidazole positron emission tomography after ischemic stroke. Ann Neurol 48(2):228–235
35. Sorger D et al (2003) [18F]Fluoroazomycinarabinofuranoside (18FAZA) and [18F]Fluoromisonidazole (18FMISO): a comparative study of their selective uptake in hypoxic cells and PET imaging in experimental rat tumors. Nucl Med Biol 30(3):317–326
36. Takasawa M et al (2007) Imaging of brain hypoxia in permanent and temporary middle cerebral artery occlusion in the rat using 18F-fluoromisonidazole and positron emission tomography: a pilot study. J Cereb Blood Flow Metab 27(4):679–689
37. Read SJ et al (1998) Identifying hypoxic tissue after acute ischemic stroke using PET and 18F-fluoromisonidazole. Neurology 51(6):1617–1621
38. Powers WJ, Zazulia AR (2010) PET in cerebrovascular disease. PET Clin 5(1):83106
39. Donnan GA, Davis SM (2002) Neuroimaging, the ischaemic penumbra, and selection of patients for acute stroke therapy. Lancet Neurol 1(7):417–425
40. Nour M, Liebeskind DS (2014) Imaging of cerebral ischemia: from acute stroke to chronic disorders. Neurol Clin 32(1):193–209
41. Mintun MA et al (1984) A quantitative model for the in vivo assessment of drug binding sites with positron emission tomography. Ann Neurol 15(3):217–227
42. Logan J et al (1996) Distribution volume ratios without blood sampling from graphical analysis of PET data. J Cereb Blood Flow Metab 16(5):834–840

43. Carson RE et al (1997) Quantification of amphetamine-induced changes in [11C]raclopride binding with continuous infusion. J Cereb Blood Flow Metab 17(4):437–447
44. Innis RB et al (2007) Consensus nomenclature for in vivo imaging of reversibly binding radioligands. J Cereb Blood Flow Metab 27(9):1533–1539
45. Koeppe RA et al (1991) Compartmental analysis of [11C]flumazenil kinetics for the estimation of ligand transport rate and receptor distribution using positron emission tomography. J Cereb Blood Flow Metab 11(5):735–744
46. Heiss WD, Sobesky J (2008) Comparison of PET and DW/PW-MRI in acute ischemic stroke. Keio J Med 57(3):125–131
47. Thiel A et al (2001) Estimation of regional cerebral blood flow levels in ischemia using [(15)O]water of [(11)C]flumazenil PET without arterial input function. J Comput Assist Tomogr 25(3):446–451
48. Yamauchi H et al (2005) Selective neuronal damage and borderzone infarction in carotid artery occlusive disease: a 11C-flumazenil PET study. J Nucl Med 46(12):1973–1979
49. Eliassen JC et al (2008) Brain-mapping techniques for evaluating poststroke recovery and rehabilitation: a review. Top Stroke Rehabil 15(5):427–450
50. Halliday A et al (2004) Prevention of disabling and fatal strokes by successful carotid endarterectomy in patients without recent neurological symptoms: randomised controlled trial. Lancet 363(9420):1491–1502
51. Bengel FM (2006) Atherosclerosis imaging on the molecular level. J Nucl Cardiol 13(1):111–118
52. Glass CK, Witztum JL (2001) Atherosclerosis: the road ahead. Cell 104(4):503–516
53. Yun M et al (2001) F-18 FDG uptake in the large arteries: a new observation. Clin Nucl Med 26(4):314–319
54. Rudd JH et al (2002) Imaging atherosclerotic plaque inflammation with [18F]-fluorodeoxyglucose positron emission tomography. Circulation 105(23):2708–2711
55. Davies JR et al (2005) Identification of culprit lesions after transient ischemic attack by combined 18F fluorodeoxyglucose positron-emission tomography and high-resolution magnetic resonance imaging. Stroke 36(12):2642–2647
56. Tahara N et al (2007) Vascular inflammation evaluated by [18F]-fluorodeoxyglucose positron emission tomography is associated with the metabolic syndrome. J Am Coll Cardiol 49(14):1533–1539
57. Tahara N et al (2006) Simvastatin attenuates plaque inflammation: evaluation by fluorodeoxyglucose positron emission tomography. J Am Coll Cardiol 48(9):1825–1831
58. Selco SL, Liebeskind DS (2005) Hyperacute imaging of ischemic stroke: role in therapeutic management. Curr Cardiol Rep 7(1):10–15
59. Wintermark M et al (2005) Comparative overview of brain perfusion imaging techniques. Stroke 36(9):e83–e99
60. Wintermark M et al (2006) Perfusion-CT assessment of infarct core and penumbra: receiver operating characteristic curve analysis in 130 patients suspected of acute hemispheric stroke. Stroke 37(4):979–985
61. Wintermark M et al (2007) Comparison of CT perfusion and angiography and MRI in selecting stroke patients for acute treatment. Neurology 68(9): 694–697
62. Muir KW et al (2006) Imaging of acute stroke. Lancet Neurol 5(9):755–768
63. Fiebach JB et al (2002) CT and diffusion-weighted MR imaging in randomized order: diffusion-weighted imaging results in higher accuracy and lower interrater variability in the diagnosis of hyperacute ischemic stroke. Stroke 33(9):2206–2210
64. Hjort N et al (2005) Magnetic resonance imaging criteria for thrombolysis in acute cerebral infarct. Stroke 36(2):388–397
65. Srinivasan A et al (2006) State-of-the-art imaging of acute stroke. Radiographics 26(Suppl 1):S75–S95
66. Allen LM et al (2012) Sequence-specific MR imaging findings that are useful in dating ischemic stroke. Radiographics 32(5):1285–1297; discussion 1297–9
67. Catana C et al (2012) PET/MRI for neurologic applications. J Nucl Med 53(12):1916–1925
68. Fernandez-Ortiz A et al (2013) The Progression and Early detection of Subclinical Atherosclerosis (PESA) study: rationale and design. Am Heart J 166(6):990–998
69. Heiss WD (2001) Imaging the ischemic penumbra and treatment effects by PET. Keio J Med 50(4):249–256
70. Heiss WD (2000) Ischemic penumbra: evidence from functional imaging in man. J Cereb Blood Flow Metab 20(9):1276–1293
71. Heiss WD (2003) Best measure of ischemic penumbra: positron emission tomography. Stroke 34(10):2534–2535
72. Arauz A et al (2007) Carotid plaque inflammation detected by 18F-fluorodeoxyglucose-positron emission tomography. Pilot study. Clin Neurol Neurosurg 109(5):409–412
73. Izquierdo-Garcia D et al (2009) Comparison of methods for magnetic resonance-guided [18-F]fluorodeoxyglucose positron emission tomography in human carotid arteries: reproducibility, partial volume correction, and correlation between methods. Stroke 40(1):86–93
74. Hyafil F et al (2016) High-risk plaque features can be detected in non-stenotic carotid plaques of patients with ischaemic stroke classified as cryptogenic using combined F-FDG PET/MR imaging. Eur J Nucl Med Mol Imaging 43(2):270–279

Hybrid Imaging in Emergency Room

17

Lorenzo Stefano Maffioli, Luca Dellavedova, and Luigia Florimonte

17.1 Introduction

The clinical role of nuclear medicine procedures in emergency department is largely limited by the frequent absence of gamma camera SPECT in this location and a lack of availability of a nuclear medicine physician 24 h per day.

All these practical problems and widespread availability of CT and MRI have eclipsed the utility of NM methods, even if specific acute indications of these methods remain.

The advent of hybrid modality (SPECT-CT) could open new perspectives and overcome these problems, especially for brain imaging in acute care: the goal is to obtain important coupled functional and anatomical information.

The added value of hybrid imaging is the possibility to accurately localize nuclear medicine findings in the corresponding anatomical structures and the correction of photon attenuation. In fact, the major limitation of brain SPECT study is the attenuation by the skull. The commonly used Chang method of attenuation correction is based on a simple mathematical algorithm, which is susceptible to technical variation. In diagnosis of dementia with SPECT, it can be difficult to separate the real defect from the attenuation artifact. Variation between images owing to the Chang attenuation correction may generate artifact when ictal-interictal subtraction SPECT scans are used for seizure localization: so SPECT-CT provides more accurate diagnostic results [1].

The possibility to perform both anatomical and functional images (high-quality CT scans simultaneously with brain SPECT) with one gantry in a single imaging session, without requiring additional space in an emergency room, may be of particular utility in detecting cerebral disorders.

In this way one can overcome a major disadvantage represented by the need to transport patient in unstable conditions from the intensive care unit to the imaging suite. In addition, the procedure can limit the time between diagnostic and therapeutic approach, thus shortening the hospital stays.

So, the presence of a SPECT-CT in an emergency department can result in a more rapid and accurate diagnosis.

Now we shortly review the main clinical indication in acute care setting (with particular attention to the evaluation of cerebral perfusion and cerebrospinal fluid flow).

L.S. Maffioli (✉) • L. Dellavedova
Nuclear Medicine Department,
ASST Ovest Milanese, Legnano, Milan, Italy
e-mail: lorenzo.maffioli@ao-legnano.it

L. Florimonte
Nuclear Medicine Department, Fondazione IRCCS
Ca' Granda Ospedale Maggiore Policlinico,
Milan, Italy

A. Ciarmiello, L. Mansi (eds.), *PET-CT and PET-MRI in Neurology*,
DOI 10.1007/978-3-319-31614-7_17

17.2 Perfusion Imaging

The first imaging procedure in the evaluation of brain perfusion in an emergency room is the SPECT-CT to early diagnose *brain death* [2, 3].

This ancillary examination serves after physical examination and apnea test to shorten the required interval to a second physical examination (or to avoid it). In other conditions SPECT-CT can be performed when physical examination and apnea test cannot be performed because of facial trauma, instability of vital signs, presence of drug intoxication (i.e., barbiturates), poisoning, neuromuscular blockade, hypothermia, and inadequate acoustic window through transcranial Doppler ultrasonography. Brain death scintigraphy may also be helpful in patients who are being considered as possible organ donors. In this case, the advantage is that donor organs are not exposed to the toxic effects of contrast media, thus preventing potential damage.

In addition, brain death could be investigated for forensic purposes in case of suspected criminal activities.

The delicate diagnosis has to be achieved by avoiding potential pitfalls that could generate misdiagnosis (e.g., lack of trapping because of radiopharmaceutical instability, extravasation during injection, or wrong injected radiopharmaceutical): the injected radioactive bolus must be clearly documented in the angioscintigraphic study as a transit throughout the common carotid arteries. This procedure, particularly important when lipophilic agents are used, allows for imaging with suboptimal patient positioning, which is often the case because of the presence of life support equipment.

When a non-lipophilic radiopharmaceutical (they do not pass the intact BBB, such as ^{99m}Tc-DTPA) is i.v. injected, normal finding results as a "trident appearance," due to the imaging of blood flow in the carotid and anterior and middle cerebral arteries. The blood pool demonstrates activity in dural venous sinuses. A lack of this sign reflects an absence of cerebral blood flow.

When a lipophilic radiopharmaceutical (they freely pass the BBB and accumulate and remain fixed in brain parenchyma with minimal redistribution) is injected, delayed imaging (parenchymal phase) provides information on cerebral perfusion. In case of brain death, the radiopharmaceutical (e.g., ^{99m}Tc bicisate [^{99m}Tc-ECD] or ^{99m}Tc-exametazime [^{99m}Tc-HMPAO]) is not trapped in cerebral tissue. The use of SPECT-CT, when feasible, makes image interpretation straightforward [4].

Thanks to an accurate co-registration of anatomical and functional images, the diagnostic value is increased by anatomical details.

So, SPECT-CT with ^{99m}Tc-HMPAO or ^{99m}Tc-ECD (two of which are the preferred imaging radiopharmaceuticals because they cross the BBB) can be used to confirm, but not diagnose, clinically suspected brain death [5].

Another important application of SPECT-CT in an emergency department is the study of *catastrophic or traumatic brain injury* (CBI or TBI).

Following CBI when some degree of residual brain stem function is demonstrated at physical examination, SPECT-CT brain perfusion can improve the assessment of the extent of injury with respect to the CT alone. In this, the neurologist/neurosurgeon can be helped in prognosing patient outcome prior to aggressive therapies [6].

TBI is characterized by various complex clinical phenomena with unclear definition (taxonomy, natural history, or pathology criteria). Usually it is divided in mild, moderate, or severe TBI on the basis of acute presentation that inconstantly predicts the long-term outcome. In this setting SPECT-CT can show focal hypoperfusion not matching with a normal CT or MRI [7]. This functional finding (not supported by anatomical changes) can early reveal post-injury neurocognitive or psychological deficits, possibly by revealing only mild changes in regional blood flow. So, SPECT was found to outperform both CT and MRI in both acute and chronic imaging of TBI, particularly mild TBI. It was also found to have a near 100 % negative predictive value [8]. SPECT-CT can be more accurate than CT or MRI alone in detecting lesion in TBI. Moreover SPECT-CT is related to neuropsychological and neurological outcomes and it can change treatment interventions. For these reasons Raji et al. conclude that SPECT should be mandatory in the diagnosis and management of TBI, according to the study by Chen et al. [9].

SPECT-CT can assist in the diagnosis, prognosis, and treatment of patients in the post-traumatic period. Moreover, SPECT-CT may also diagnose occult brain trauma in clinically confusing cases (symptoms can widely range in specificity and frequency) [10]. SPECT-CT in emergency room could help in revealing occult TBI in cases of treatment-resistant or treatment-unresponsive conditions (e.g., depression) [11, 12].

In *cerebrovascular acute diseases*, SPECT-CT plays an important potential role in acute setting, too. In fact, the gold standard in emergency room is the perfusion CT and/or MRI. However, these diagnostic tools allow to diagnose acute stroke only when the brain damage has yet occurred. At the contrary, perfusion SPECT-CT can give important early diagnostic and prognostic information, providing data on vasodilatory reserve, extension, and severity of the lesion. Moreover, it has an important added value in differentiating between nutritional reperfusion vs. luxury perfusion and allows to monitor the effects of surgical/interventional therapy [13].

Rescuing of viable tissue suffering ischemic penumbra is an important target of early therapeutic strategy.

The effects of drugs and interventions for ischemic stroke can be monitored by the imaging of the penumbra and cellular responses. This indicates that SPECT-CT could play a potential prognostic role as a marker of the efficacy of future therapies [14, 15].

Finally, since most of SPECT-CT tomographs are equipped with a multi-slice HR CT scanner, the new exciting frontier is the simultaneous acquisition of HR contrast-enhanced CT scan and perfusion SPECT, thus increasing the diagnostic performance of the study. In this context nuclear physician and radiologist can detect early vascular abnormalities (e.g., cerebral ischemia, stroke, or carotid stenosis), helping the clinician in rapid decision making.

However, it has to be remembered that the co-registration of functional and anatomical images increases radiation exposure to patients: the cost-effectiveness of the analysis must be kept in consideration. Anyway, the study has to be a priori justificated, and the CT ring should be optimized, e.g., by adapting dose reduction measures from SPECT-CT, and exposure levels should not exceed the national diagnostic reference levels for standard situations.

A further condition in which SPECT-CT has an incremental value in emergency room is in those cases in which a *poisoning from carbon monoxide* (CO) is suspected as a fatal event.

In fact, CO may damage multiple systems and, among these, especially those with high oxygen utilization (e.g., central nervous system – CNS). In general the clinical effects and prognosis of acute CO poisoning poorly correlate with blood carboxyhemoglobin (COHb) levels because of oxygen usually administered in ambulance (and in an emergency room before the blood withdrawal). In the early phase of CO intoxication, functional brain SPECT may be highly sensitive to brain injury due to CO poisoning. Its increasing role in evaluating the brain with acute CO intoxication is characterized by hypoperfusion in the basal ganglia **,** followed by the temporal, parietal, frontal, and occipital lobes and thalamus, but not in the cerebellum [16, 17].

Less common conditions in which SPECT-CT can be performed in acute setting are disorders that mimic stroke (toxic-metabolic pathologies, seizure disorders, multiple sclerosis, degenerative neurologic conditions, hemiplegic migraine, intracranial tumors, and peripheral neuropathies). Functional stroke mimics are an important subgroup admitted to acute stroke services and have a distinct demographic and clinical profile. Approximately one third of stroke mimics have been shown to be misdiagnosed (particularly in young people). The neurologist has to determine whether acute neurologic deficits represent a transient event or a stroke. Furthermore, their outcomes are poorly monitored, as demonstrated in a recent paper by Gargalas et al. [18], which concludes that "services should be developed to better diagnose and manage these patients."

Among the disorders that mimic stroke, SPECT-CT can play an important role in *hemiplegic migraine* (HM), an unusual type of migraine, with aura lasting less than 24 h. For this reason, the clinician does not check the variations of cerebral vascular flow. However, the regional cerebral blood flow in patient with migraine with aura is characterized by a hypoperfusion in the posterior

part of a hemisphere (according to symptoms). In migraine without aura, no blood flow changes occur.

So, SPECT-CT can help to make the differential diagnosis and to assess the cause of the neurological findings [19].

17.3 Cerebrospinal Fluid Flow

Another useful clinical indication of SPECT-CT in an emergency department is the evaluation of patients suspected of having *cerebrospinal fluid (CFS) leaks* that can occur after a trauma. Diagnosis and localization of CSF leak can be difficult. Planar images are affected by poor resolution and anatomic details. Co-registered SPECT-CT images allow accurate identification of the site of CFS leakage, thus avoiding the count of nasal pledget [1].

Integration of prolonged imaging protocols with co-registered anatomical/scintigraphic images seems to allow a precise and accurate diagnosis especially in slow or intermittent leaks. This is crucial for a prompt surgical or interventional closing of the dural defect, particularly if it is located at the base of the skull, because bacterial meningitis is the main cause of morbidity and mortality in these patients [20].

The *assessment of CSF shunt patency* is an important indication for a SPECT-CT in an emergency department, when a malfunction is suspected, because of nonspecific clinical symptoms and signs. The most common shunt systems are ventriculoperitoneal and ventriculoatrial shunts. Other systems are ventriculopleural and lumboperitoneal devices. After pertechnetate administration, shunt patency can be demonstrated by the flow activity to the distal end of the catheter. SPECT-CT can allow the precise localization of the stop and, possibly, its cause.

Conclusions

In conclusion, emergency room evaluation of patients presenting with brain disorders or injuries is common. The introduction of hybrid imaging modalities could probably increase the global accuracy of these evaluations, but its implementation is underdeveloped in most health systems, in spite of its clinical usefulness. The absence of specific HTA studies, and the consequent lack of clear evidence about the possible influence in the managing decision process, surely contributes to this delay.

Moreover, the rapid evaluation of patients in an emergency department requires a prompt availability of nuclear medicine staffing and radiopharmacy H24: this is still the most common and important limitation because they are considered not cost-effective and too slow in answering the clinical issue. However, the introduction of hybrid technology with SPECT coupled with multi (16–64)-slice CT (that could be used as a stand-alone device, too) could help the diffusion of nuclear medicine in emergency department: with recent advances in camera technology and changes in imaging protocols, in fact, nuclear medicine is becoming a more and more efficient way of providing functional diagnostic information.

Looking forward, we will probably have to evaluate if another recently developed hybrid imaging modality, as PET/MRI, could play a role in brain imaging also in an emergency department setting. MRI availability and utilization in emergency departments is increasing, mostly due to MRI and MR angiography examinations of the head (up to 70 % of the total number of scans). The limited soft-tissue specificity of CT, in fact, hinders its role in brain imaging in comparison to the greater anatomic detail of MRI that, in addition, does not implicate the use of ionizing radiation. Combining SPECT or PET and MRI holds great promise since the hybrid would be better than each stand-alone unit, allowing for simultaneous structural and functional data acquisition for diagnosis and treatment [21].

Anyway, no clear data have demonstrated whether the increase in MRI utilization in emergency departments results in better patient outcomes; moreover, many critics argue this is not a test needed on an emergency basis, supposing that it will only increase the risk of costly defensive medicine.

Thus, at the moment, the availability of PET/MRI or SPECT/MRI devices in an emergency setting seems to be an appealing but almost an infeasible option.

References

1. Bybel B, Brunken RC, DiFilippo FP, Neumann DR, Wu G, Cerqueira MD (2008) MDSPECT-CT imaging: clinical utility of an emerging technology. Radiographics 28:1097–1113
2. Donohoe KJ, Agrawal G, Frey KA, Gerbaudo VH, Mariani G, Nagel JS, Shulkin BL, Stabin MG, Stokes MK (2012) SNM practice guideline for brain death scintigraphy 2.0. J Nucl Med Technol 40(3):198–203
3. Sinha P, Conrad GR (2012) Scintigraphic confirmation of brain death. Semin Nucl Med 42:27–32
4. Zuckier LS, Sogbein OO (2013) Brain perfusion studies in the evaluation of acute neurologic abnormalities. Semin Nucl Med 43(2):129–138. doi:10.1053/j.semnuclmed.2012.12.003
5. Jolepalem P, Balon HR (2013) The role of scintigraphy in confirmation of suspected brain death. J Nucl Med Technol 41:306–307
6. Flowers WM, Patel BR (2000) Persistence of cerebral blood flow after brain death. South Med J 93(4):364–370
7. Kaloostian P, Robertson C, Gopinath SP, Stippler M, King CC et al (2012) Outcome prediction within twelve hours after severe traumatic brain injury by quantitative cerebral blood flow. J Neurotrauma 29:727–734
8. Raji CA, Tarzwell R, Pavel D, Schneider H, Uszler M, Thornton J, van Lierop M, Cohen P, Amen DG, Henderson T (2014) Clinical utility of SPECT neuroimaging in the diagnosis and treatment of traumatic brain injury: a systematic review. PLoS One 9(3):e91088
9. Chen Y, Huang W, Constantini S (2013) Concepts and strategies for clinical management of blast-induced traumatic brain injury and posttraumatic stress disorder. J Neuropsychiatry Clin Neurosci 25:103–110
10. Dikmen S, Machamer J, Fann JR, Temkin NR (2010) Rates of symptom reporting following traumatic brain injury. J Int Neuropsychol Soc 16:401–411
11. Fann JR, Hart T, Schomer KG (2009) Treatment for depression after traumatic brain injury: a systematic review. J Neurotrauma 26:2383–2402
12. Fann JR, Jones AL, Dikmen SS, Temkin NR, Esselman PC et al (2009) Depression treatment preferences after traumatic brain injury. J Head Trauma Rehabil 24:272–278
13. Imasaka K, Yasaka M, Tayama E, Tomita Y (2015) Obstructive carotid and/or intracranial artery disease rarely affects the incidence of haemodynamic ischaemic stroke during cardiac surgery: a study on brain perfusion single-photon emission computed tomography with acetazolamide. Eur J Cardiothorac Surg 48(5):739–746
14. Oku N, Kashiwagi T, Hatazawa J (2010) Nuclear neuroimaging in acute and subacute ischemic stroke. Ann Nucl Med 24(9):629–638. doi:10.1007/s12149-010-0421-7, Epub 2010 Oct 16
15. Brix G, Nekolla EA, Borowski M, Noßke D (2014) Radiation risk and protection of patients in clinical SPECT-CT. Eur J Nucl Med Mol Imaging 41(Suppl 1): S125–S136. doi:10.1007/s00259-013-2543-3, Epub 2013 Sep 20
16. Lu YY, Tsai SC, Kao CH, Lin WY (2012) Regional cerebral blood flow in patients with carbon monoxide intoxication. Ann Nucl Med 26(10):771–776
17. Mariani G, Bruselli L, Kuwert T, Kim EE, Flotats A, Israel O, Dondi M, Watanabe N (2010) A review on the clinical uses of SPECT-CT. Eur J Nucl Med Mol Imaging 37(10):1959–1985
18. Gargalas S, Weeks R, Khan-Bourne N, Shotbolt P, Simblett S, Ashraf L, Doyle C, Bancroft V, David AS (2015) Incidence and outcome of functional stroke mimics admitted to a hyperacute stroke unit. J Neurol Neurosurg Psychiatry. pii: jnnp-2015-311114. doi:10.1136/jnnp-2015-311114. [Epub ahead of print]
19. Jiménez-Hoyuela JM, Amrani-Raissouni T, Gallardo-Tur A, Moya-Espinosa F, Padilla-Parrado F (2013) Impact of 99mTc-HMPAO brain perfusion scan in the diagnosis of hemiplegic migraine. Clin Nucl Med 38(2):e103–e105
20. Slart RH, Koopmans KP, Gunneweg P, Luijckx GJ, de Jong BM (2006) Persistent aseptic meningitis due to post-surgical spinal CSF leakage: value of fused (111m) In-DTPA SPECT-CT cisternography. Eur J Nucl Med Mol Imaging 33(7):856
21. Abraham T, Feng J (2011) Evolution of brain imaging instrumentation. Semin Nucl Med 41:202–219

Part IV

SWOT Analysis

18 SWOT Analysis and Stakeholder Engagement for Comparative Evaluation of Hybrid Molecular Imaging Modalities

Andrea Ciarmiello and Luciano Hinna

18.1 Introduction

Strategic planning of technology development in healthcare is a complex process including the analysis of economic, medical, and social key elements. The main objective of the decision-making process in healthcare should be to promote effective and sustainable technological development, which effectively means a development able to produce a real improvement for research and patient's healthcare. It is conceivable that several key factors need to be identified to achieve this objective. Some of these are internal to the system (hospital, university, research clinic) where improvements should be realized, whereas others are external and depend on the economic environment, users (physicians, researchers), patients, manufacturers, and all other stakeholders that for various reasons are involved with these technologies. The involvement of different stakeholders is necessary in order to consider all possible relevant factors in a decision-making process and to legitimate the final decision [1–4]. Methods which include various stakeholders are based on public meetings, surveys, workshops, interviews, and e-participation through web platforms or other communication modalities. In this context, a factor can be considered a strength or a weakness, an opportunity or a threat, depending on the point of view or the expectations of each stakeholder. These differences describe more deeply the complex and dynamic scenario in which the evaluation must be carried out [5]. SWOT analysis is a decision supporting tool designed for incorporating internal (strengths and weaknesses) and external (opportunities and threats) factors into organizational or technological change planning. SWOT analysis is not only devoted to profit-seeking organizations but may also be used in any decision-making process where the proposed aim is clearly defined. SWOT analysis has been effectively used for strategy building and matching and converting purposes. The SWOT analysis has already been applied in some areas of medicine to address various organizational, technical, or scientific issues [6–10]. Only in a few cases was SWOT used for the strategic planning of technological development [11] or to promote the development and equal accessibility to technological resources potentially useful for population health [12]. Technological development has an important

A. Ciarmiello (✉)
Department of Nuclear Medicine, S. Andrea Hospital, La Spezia, Italy
e-mail: andrea.ciarmiello@asl5.liguria.it

L. Hinna
CSS – Consiglio Italiano per le Scienze Sociali, Rome, Italy

A. Ciarmiello, L. Mansi (eds.), *PET-CT and PET-MRI in Neurology*,
DOI 10.1007/978-3-319-31614-7_18

strategic role in terms of economic perspective as well as for the potential effect on population health and the availability of competitive tools for health research. Recent and latest generations of molecular hybrid modalities include high-cost technology and a potentially high impact on population health. Without considering the possible improvement of health research produced by cutting-edge technologies and the raising of competitiveness compared to other developed countries. We aimed to identify factors that could affect the success of a program of technological development and investigate the potential impact of technology development on quality improvement in healthcare. Therefore, we used the SWOT to compare internal (strengths and weaknesses) and external (opportunities or threats) main factors of the positron emission tomography (PET) associated with a CT scanner and a PET coupled to a magnetic resonance (MR) scanner. The analysis of the survey results has identified some internal and external factors useful to healthcare facilities for planning a strategic development plan and by manufacturers to improve scanner performance and market positioning.

18.2 SWOT Analysis Framework

18.2.1 Definition and Method

SWOT analysis is an analytical method which is used to identify and categorize significant internal (strengths and weaknesses) and external (opportunities and threats) factors involved in any kind of development project or planning activity. SWOT can be used by any public or private organization or firm with the aim of evaluating all pro and con factors of the project to be started. SWOT provides information helpful in matching the organizations' resources and capabilities to the competitive environment in which they operate thus providing an important contribution to the strategic planning process.

It should not be viewed as a static method with emphasis solely on its output, but should be used as a dynamic part of the management and business development process.

SWOT analysis involves the collection and portrayal of information about internal and external factors that have, or may have, an impact on the evolution of an organization or business. It generally provides a list of an organization's strengths and weaknesses as indicated by an analysis of its resources and capabilities, plus a list of the threats and opportunities identified by an analysis of its environment. Strategic logic requires that the future pattern of actions to be taken should match strengths with opportunities, ward off threats, and seek to overcome weaknesses.

SWOT analysis is not necessarily a foresight approach but can be a good starting point for the discussions of foresight. Another possibility is matching your own strengths and weaknesses against different foresight results. The different viewpoints can be a starting point for a discussion of the real threats and opportunities for those who want to improve the competitiveness of a company, region, or country.

This analytical approach was previously used mainly in policy research to systematically analyze organizations' environments and only recently has been introduced in healthcare systems [5, 11]. When properly used, SWOT analysis may provide decision-makers a strong and structured basis for strategy development.

Normally the people directly involved in various hierarchical levels of decision-making in an organization or business are part of the same organization or a wider sample of actors if the SWOT analysis concerns a whole region or nation. Representatives from a variety of internal stakeholder groups should be involved, as they would contribute to the analysis of their own particular perspectives. At least one expert in SWOT analysis should take part in or moderate the process.

Drawing up opportunity and threat matrices encourages an assessment of the likely probability and impact any factor may have on the organization. A scoring system can be used to assign importance to factors. A factor with a high score on both "probability of occurrence" and "likely impact on the organization or business" would

have to be one worthy of close attention and play a significant part in the development of a strategic plan. Similarly, strengths and weaknesses can be assessed against a scoring system that allows the factors to be identified according to their significance (i.e., major, minor, neutral) and level of importance (high, medium, low).

It is possible to represent this analysis in a performance-importance matrix that highlights those factors which are important and in which performance of the organization/business is low. It is toward these factors that strategy should be addressed.

To be more specific, the set of questions that need to be answered should be similar to the following:

- What are your advantages?
- What do you do well?
- What relevant resources do you have access to?
- What do other people see as your strengths?

Consider this from your own point of view and from the point of view of the people you deal with. Don't be modest. Be realistic. If you are having any difficulty with this, try writing down a list of your organization's characteristics. Some of these will hopefully be strengths!

In looking at your strengths, think about them in relation to your competitors, for example, if all your competitors provide high-quality products, then a high-quality production process is not a strength in the market, it is a necessity:

- What could you improve?
- What do you do badly?
- What should you avoid?

Again, consider this from an internal and external viewpoint: Do other people seem to perceive weaknesses that you do not see? Are your competitors doing any better than you? It is best to be realistic now and face any unpleasant truths as soon as possible:

- Where are the good opportunities in front of you?
- What are the interesting trends you are aware of?

Useful opportunities can come from such things as:

- Changes in technology and markets on both a broad and narrow scale
- Changes in government policy related to your field
- Changes in social patterns, population profiles, lifestyles, etc.
- Local events

A useful approach to looking at opportunities is to look at your strengths and ask yourself whether these open up any opportunities. Alternatively, look at your weaknesses and ask yourself whether you could open up opportunities by eliminating them:

- What obstacles do you face?
- What is your competition doing?
- Are the required specifications for your job, products, or services changing?
- Is changing technology threatening your position?
- Do you have bad debt or cash flow problems?

Could any of your weaknesses seriously threaten your business?

Carrying out this analysis will often be illuminating – both in terms of pointing out what needs to be done and in putting problems into perspective. A SWOT analysis is based on hard facts. These can be time consuming and costly to gather. People are needed who have a good knowledge of the sector, region, area, country, etc. under analysis in the specific exercise.

The main tangible output is a matrix presenting the most important strengths, weaknesses, opportunities, and threats for the area, sector, region, and country examined and aimed at giving a reasonable overview of major issues that can be taken into account when subsequently drawing up strategic plans for an organization.

A SWOT analysis could be performed in other contexts than those of an organization, for instance, in the case of an individual facing major decisions such as professional orientation.

The success of this method is mainly owed to its simplicity and its flexibility. Its implementation does not require technical knowledge and skills. SWOT analysis allows the synthesis and integration of various types of information which are generally known but still make it possible to organize and synthesize recent information as well.

It is worth pointing out that whereas SWOT analysis is often not seen strictly speaking as a foresight method, it is useful to consider it from this perspective. Indeed, foresight is particularly useful for addressing the opportunities and threats (OT) dimensions, whereas SWOT analyses Rhenman often fail because of poor OT examination.

A correlation is made between the internal factors, strengths and weaknesses (SW) of the organization, and the external factors, opportunities and threats. An effort can be made to exploit opportunities and overcome weaknesses and at the same time for the organization to protect itself from the threats of the external environment through the development of contingency plans.

The most common drawbacks of SWOT analysis are:

- The length of the lists of factors that have to be taken into account in the analysis
- Lack of prioritization of factors, there being no requirement for their classification and evaluation
- No suggestions for solving disagreements
- No obligation to verify statements or aspects based on the data or the analysis
- Analysis only at a single level (not multilevel analysis)
- No rational correlation with the implementation phases of the exercise

Moreover, there are risks of:

- Inadequate definition of factors
- Over-subjectivity in the generation of factors (compiler bias)
- The use of ambiguous and vague words and phrases

One has to be aware that this method is very commonly used by consulting firms and that for this reason some people in the public/quasi-public sector have an aversion to it.

In conclusion, the SWOT analysis is a management instrument used by the top management or consulting firm for the strategic positioning of a firm or product; in our context we intend to apply SWOT analysis to hybrid imaging. In addition, it is possible to use SWOT analysis in combination with other management instrument: stakeholder engagement.

18.2.2 The Stakeholder Engagement

Stakeholder engagement is the process by which an organization involves people who may be affected by the decisions it makes or can influence the implementation of its decisions. They may support or oppose the decisions, be influential in the organization or within the community in which it operates, hold relevant official positions, or be affected in the long term.

Normally stakeholder engagement is a part of corporate social responsibility (CSR) management. In fact, companies engage their stakeholders in the dialog to find out what social and environmental issues matter most to them about their performance in order to improve decision-making and accountability. The stakeholder engagement is also part of a quality process improvement, since the opinions of the stakeholders are useful to improve the quality of the product. The International Organization for Standardization (ISO) requires stakeholder engagement for all their new standards. The definition and the role of stakeholders within a company have changed in the last 30 years: if initially the stakeholder was conditioned by the company [13, 14], latterly they condition the company. The stakeholders, in fact, are now part of the process of creating the value of the company. The stakeholders contribute to the reputation of the company (an intangible asset), and their suggestions increase the quality of the product.

In general terms, the benefits of stakeholder engagement are:

Stakeholder engagement provides opportunities to further align organization practices with societal needs and expectations, helping to drive long-term sustainability and shareholder value. Stakeholder engagement is intended to help the practitioners fully realize the benefits of stakeholder engagement in their organization and to compete in an increasingly complex and ever-changing business environment while at the same time bringing about systemic change toward sustainable development.

Consequently, the behavior of stakeholders can be an opportunity or a threat for a company, for a product, including hybrid imaging, and the stakeholder engagement can be a technicality very useful for marketing reasons and for the strategic position of the product.

18.3 Research Steps and Statistical Sample

The survey included several stakeholders involved with hybrid technology at the meso-level on a worldwide basis. Meso- and micro-levels of involvement were defined according to WHO definition [15]. The meso-level included stakeholders involved in healthcare systems at organizational level in hospitals and academic institutions, physicians, researchers, and manufacturers of molecular imaging technology. This level also included international agencies aimed at promoting equal accessibility to these technologies in developing as well as developed countries. The micro-level such as citizens, patients, or local authorities was not included in this preliminary survey. Inclusion of different groups was deemed essential to obtain individual stakeholder perceptions and information on interactions between organizational levels, users, and manufacturers. Physicians and researchers were identified on the basis of a consolidated skill as evidenced by publication activity retrieved by scientific libraries (e.g. PubMed). Organizational stakeholders were identified through informal networking. We decided to conduct the survey on a sample of at least 50 experts distributed worldwide. To recruit 52 stakeholders, we have invited 200 experts. Manufacturers include three of the largest companies producing hybrid imaging technologies. The International Agency for Atomic Energy (IAEA) is an agency of the United Nations aimed at promoting the development of atomic energy-based technologies useful to people.

For the research we used the following framework:

- Phase 1: to identify stakeholder categories; in particular, we involved in the research manufacturing companies, decision-makers, researchers, clinical users, and promoter of healthcare technology [1]
- Phase 2: to identify the elements to take in(to) consideration for each category of stakeholder(s)
- Phase 3: to prepare a different questionnaire for each category of stakeholders using special matrix elements to take into consideration and position each element under the categories strengths, weaknesses, opportunities, and threats
- Phase 4: distribution of the questionnaire for a test
- Phase 5: modification of the questionnaire after the suggestions
- Phase 6: distribution of the questionnaire to all the identified stakeholder(s)
- Phase 7: collect the questionnaires
- Phase 8: analysis and comments of the results

The main drawback of this SWOT application is the limited statistical sample used in the survey which was composed by only 52 stakeholders. Instead, the greatest strength is given by the considerable experience gained in the field of hybrid imaging by the entire group of stakeholders.

18.4 Hybrid Modality Survey and Questionnaire

The survey data for SWOT analysis were collected by means of a specific stakeholder questionnaire. Questionnaire for each stakeholder category is showed in Tables 18.1, 18.2,

Table 18.1 Questionnaire used by the stakeholder group of users/IAEA in the survey on hybrid technologies

No.	Element	Strengths	Weaknesses	Opportunities	Threats
QU-01	Image evaluation and interpretation				
QU-02	Competition with established operating procedures				
QU-03	Competition with emerging imaging modalities				
QU-04	Competition with established imaging modalities				
QU-05	Imaging modality cost				
QU-06	Implementation cost of new hybrid modality				
QU-07	Simultaneous scanning of structural and functional images				
QU-08	Technical improvement for attenuation correction				
QU-09	Technical improvement for partial volume correction				
QU-10	Potential application or improvement of existing ones in radioguided surgery				
QU-11	Potential application or improvement of existing ones in emergency unit				
QU-12	Technical improvement for motion correction (PET-MR)				
QU-13	Image quality				
QU-14	Patients' compliance (one-stop shop, duration of the examination) (PET/CT)				
QU-15	Long work flow acquisition protocols (PET/MR)				
QU-16	Patient discomfort (PET/MR)				
QU-17	Patient radiation exposure (PET/CT)				
QU-18	Imaging in children and young adolescents (PET/MR)				
QU-19	Imaging in women of reproductive age (PET/MR)				
QU-20	Patients needing repeated scans				
QU-21	Radiotracers availability (other than 18F-FDG)				
QU-22	Research activities				
QU-23	Training for existing medical staff				
QU-24	Working in team with staff of different imaging units				
QU-25	Training existing for technical staff				
QU-26	Academic education needs				

Table 18.2 Questionnaire used by the stakeholder group of manufacturer in the survey on hybrid technologies

No.	Element	Strengths	Weaknesses	Opportunities	Threats
QC-01	Competition with established imaging modalities				
QC-02	Competition with emerging imaging modalities				
QC-03	Competition with established operating procedures				
QC-04	Need to promote the new technology				
QC-05	Selling modality				
QC-06	High development costs				
QC-07	High acquisition cost of hybrid as compared to standalone modality				
QC-08	High production costs				
QC-09	Cost of maintenance contracts				
QC-10	Installation costs				
QC-11	Potential cost reduction as a result of technology diffusion				
QC-12	Costs of new modality advertisement				
QC-13	Possible expansion of diagnostic field application				
QC-14	Potential application or improvement of existing ones in emergency unit				
QC-15	Improvement of image quality				
QC-16	Training for existing medical staff				
QC-17	Training existing for technical staff				
QC-18	Academic education needs				

and 18.3. The users/IAEA, manufacturers, and decision-maker questionnaire were composed of 26, 18, and 11 questions, respectively. In order to compare the points of view between the different groups of stakeholders, each element was allocated in 12 different categories (Table 18.4). The answers may vary from 1 to 3 indicating disagreement (1), neither (2), or agreement (3). In order to analyze the elements of interest within and between each stakeholder group, the results were grouped by stakeholder and category.

Table 18.3 Questionnaire used by the stakeholder group of decision-maker in the survey on hybrid technologies

No.	Element	Strengths	Weaknesses	Opportunities	Threats
QC-01	Payback time and number of scan to achieve the breakeven point				
QC-02	Cost of electric supply				
QC-03	Cost of maintenance contracts and service disruption				
QC-04	Installation costs				
QC-06	Impact on the time required to define the diagnosis				
QC-08	Impact on the diagnostic performance (accuracy)				
QC-09	Impact on the patient's waiting list				
QC-05	Hospital size and complexity of healthcare provided				
QC-07	Size of the spaces to install hybrid scanner				
QC-10	Training costs for technical staff				
QC-11	Training costs for medical staff				

Table 18.4 Categories covered by the survey on hybrid technologies explore the clinical, scientific, organizational, and economic impacts of hybrid modalities

No.	Category
1.	Clinical accuracy
2.	Comparison with existing modalities or clinical procedures
3.	Costs
4.	Future development
5.	Imaging quality
6.	Organization
7.	Patient's comfort
8.	Radiation exposure
9.	Radiotracer availability
10.	Research opportunities
11.	Staff training and education

18.5 Results

The survey to collect the information needed for the SWOT analysis on hybrid molecular imaging was conducted in the winter of 2015. The panel of stakeholders consisted of 22 clinical users, 16 researchers, 10 decision-makers, 1 promoter, and 3 manufacturers. The promoter included was the IAEA. The IAEA, a department of the United Nations (UN), aims at promoting equal accessibility to atomic energy for health in developed as well as in developing countries. Manufacturers included major companies producing diagnostic hybrid technologies (GE Healthcare Srl, Philips Spa, Siemens Healthcare Srl). The survey was based on a specific stakeholder questionnaire prepared to collect, analyze, and interpret the views of each target group. Each SWOT factor of every question was scored according to expert opinion. Users target group included 38 worldwide distributed physicians (Fig. 18.1). Fifty-eight percent of the physicians were involved in clinical and research activities, whereas 42 % of the sample was involved only in clinical activities. At the time of the survey, about two-thirds of the physicians were working in public hospitals while 11 % were working in research institutes and 24 % in universities. Figure 18.2 shows the radar plot of the scores assigned by the experts to each element of the SWOT analysis. Tables 18.5, 18.6, and 18.7 show the mean value of the scores obtained by each survey question in the group of users, manufacturers, and decision-makers, respectively. The higher value indicates the one

Fig. 18.1 Worldwide distribution of stakeholders involved in the survey on hybrid modalities

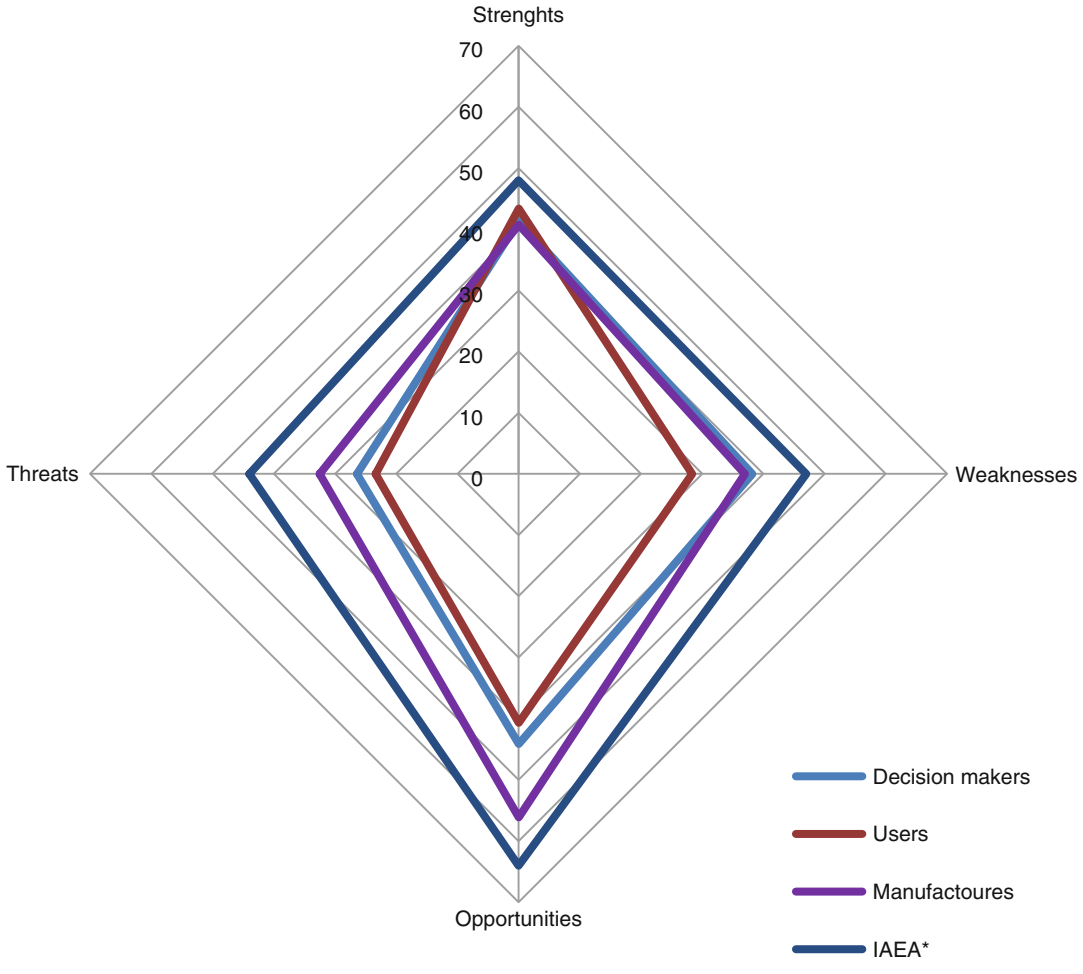

Fig.18.2 Plot of SWOT element as rated by stakeholders (* International Atomic Energy Agency)

Table 18.5 Results of the survey of hybrid technologies in the users group

Item	Questions	Strenghts	Weaknesses	Opportunities	Threats
QU-01	Simultaneous scanning of structural and functional images	2.8	0.5	1.7	0.8
QU-02	Patients' compliance (one-stop shop, duration of the examination) (PET/CT)	2.8	0.3	0.3	0.1
QU-03	Image evaluation & interpretation	2.7	0.6	2.1	0.7
QU-04	Image quality	2.6	0.7	2.2	0.6
QU-05	Technical improvement for attenuation correction	2.5	0.7	1.6	0.9
QU-06	Research activities	2.4	0.6	2.2	0.8
QU-07	Technical improvement for Partial volume correction	2.3	0.7	2.0	0.8
QU-08	Imaging in children and young adolescents (PET/MR)	2.0	1.1	1.8	1.0
QU-09	Long work flow acquisition protocols (PET/MR)	0.2	2.6	0.1	0.0
QU-10	Patient disconfort (PET/MR)	0.2	2.5	0.0	0.0
QU-11	Imaging modality cost	0.7	2.1	0.7	1.5
QU-12	Implementation cost of new hybrid modality	0.6	2.0	0.6	1.8
QU-13	Radiotracers availability (other than 18F-FDG)	1.0	1.5	1.4	0.8
QU-14	Potential application or improvement of existing ones in radioguided surgery	2.1	0.6	2.5	0.7
QU-15	Training for existing medical staff	2.0	0.7	2.3	0.7
QU-16	Working in team with staff of different imaging units	2.1	0.7	2.2	1.1
QU-17	Training existing for technical staff	2.0	0.8	2.2	0.6
QU-18	Potential application or improvement of existing ones in emergency unit	1.3	1.2	2.0	0.9
QU-19	Technical improvement for motion correction (PET-MR)	0.6	0.1	1.8	0.1
QU-20	Academic education needs	1.6	1.5	1.6	0.6
QU-21	Imaging in women of reproductive age (PET/MR)	1.5	1.2	1.6	1.2
QU-22	Patients needing repeated scans	1.3	1.2	1.5	1.2
QU-23	Competition with established operating procedures	1.2	1.1	1.4	1.1
QU-24	Patient radiation exposure (PET/CT)	1.0	1.5	0.7	1.8
QU-25	Competition with emerging imaging modalities	1.2	0.7	1.2	1.7
QU-26	Competition with established imaging modalities	1.3	0.9	1.4	1.5

Table shows the mean value based on the entire sample for each question and for each SWOT element. Higher score is showed in cyan. The possible answers ranged from 1 to 3 according to expert opinion (disagree = 1, neither = 2, agree = 3)

Table 18.6 Results of the survey of hybrid technologies in the manufacturers group

Item	Questions	Strenghts	Weaknesses	Opportunities	Threats
QC-01	Improvement of image quality	3.0	1.0	2.9	1.0
QC-02	Possible expansion of diagnostic field application	3.0	1.0	3.0	1.0
QC-03	Competition with established imaging modalities	3.0	1.3	2.8	1.3
QC-04	Selling modality	2.5	1.0	2.5	1.3
QC-05	Competition with emerging imaging modalities	2.5	1.3	2.3	1.8
QC-06	Competition with established operating procedures	1.8	1.0	1.7	1.0
QC-07	High development costs	1.0	3.0	1.5	2.0
QC-08	High acquisition cost of hybrid as compared to standalone modality	1.0	3.0	1.8	2.0
QC-09	High production costs	1.0	2.8	1.5	2.0
QC-10	Cost of maintenance contracts	1.0	2.8	1.3	2.0
QC-11	Installation costs	1.5	2.0	1.5	1.8
QC-12	Need to promote the new technology	2.3	1.0	3.0	1.3
QC-13	Potential cost reduction as result of technology diffusion	2.3	1.0	2.8	1.0
QC-14	Training for existing medical staff	1.0	1.5	2.8	1.8
QC-15	Training existing for technical staff	1.0	1.5	2.8	1.8
QC-16	Costs of new modality advertisement	1.3	1.8	2.5	1.3
QC-17	Academic education needs	1.5	1.3	2.5	1.0
QC-18	Potential application or improvement of existing ones in emergency unit	0.8	0.5	1.0	0.5

Table shows the mean value based on the entire sample for each question and for each SWOT element. Higher score is showed in cyan. The possible answers ranged from 1 to 3 according to expert opinion (disagree = 1, neither = 2, agree = 3)

Table 18.7 Results of the survey of hybrid technologies in the decision-makers group

Item	Questions	Strenghts	Weaknesses	Opportunities	Threats
QC-01	Impact on the diagnostic performance (accuracy)	3.0	0.3	2.3	0.3
QC-02	Impact on Impact on the time required to define the diagnosis	3.0	0.3	2.3	0.3
QC-03	Impact on the patients waiting list	2.3	0.3	1.5	0.3
QC-04	Hospital size and complexity of healthcare provided	2.0	1.0	1.8	1.0
QC-06	Payback time and number of scan to achieve the breakeven point	0.5	3.0	0.5	1.5
QC-08	Cost of electric supply	0.3	2.5	0.5	1.0
QC-09	Size of the spaces to install hybrid scanner	0.3	2.5	0.3	0.8
QC-05	Cost of maintenance contracts and service disruption	1.0	2.3	1.0	0.8
QC-07	Installation costs	0.8	1.8	0.3	1.5
QC-10	Training costs for technical staff	0.3	1.0	1.8	0.8
QC-11	Trainingcosts for medical staff	0.0	0.5	2.3	0.3

Table shows the mean value based on the entire sample for each question and for each SWOT element. Higher score is showed in cyan. The possible answers ranged from 1 to 3 according to expert opinion (disagree = 1, neither = 2, agree = 3)

Table 18.8 Results of the survey of hybrid technologies in all groups of stakeholders

Category	Users	Manufacturers	Decision Makers
Clinical and technological improvement[a]	2.6	3.0	3.0
Costs[a]	2.1	2.7	2.4
Future development[a]	2.3	2.0	3.0
Staff training & education[a]	2.1	2.6	2.0
Comparison with existing modalities or clinical procedures	1.5	2.6	–
Patient's comfort	2.6	–	–
Clinical accuracy	2.7	–	–
Research opportunities	2.4	–	–
Radiation exposure (PET/MR)	1.7	–	–
Radiation exposure (PET/CT)	1.8	–	–
Radiotracers availability	1.5	–	–
Organization	–	–	2.3

Legend
Strenghts
Weaknesses
Opportunities
Threats

Table shows the mean score of the questions included in each SWOT category. The colors indicate in which area of the SWOT lies each category according to the experts' assessment

[a]Questions common to all stakeholders

selected by the majority of experts as the most relevant between SWOT factors (Tables 18.4, 18.5, and 18.6). In order to compare the positions of different groups of stakeholders, mean score values were stratified by category and stakeholder groups. This assessment includes all the categories identified for the SWOT analysis and among them containing some questions common to all stakeholder groups. Table 18.8 shows the mean score of each category for each stakeholder group also using a color to indicate the SWOT class to which it has been allocated by the score reached. Interestingly, for all categories that include questions common to all groups of stakeholder, the results are the same for the SWOT factor positioning and slightly dissimilar for the score obtained. By contrast, the category "Comparison with existing modalities for clinical procedures" which includes questions common to users and manufacturers diverge for positioning and rating.

18.6 Conclusion and Future Directions

SWOT analysis and stakeholder engagement are management techniques normally used to assess firm strategic position and planning investments. This analytical approach could also be useful in areas other than those it has already been proved useful. Hybrid molecular imaging is a continuously evolving healthcare area with a high economic and social impact where SWOT analysis could provide a useful tool for planning development strategies. Preliminary obtained results

encourage to develop future research and application in healthcare especially in those marked by the most rapid changes and higher costs as that of hybrid imaging modalities in which we have experienced this first use of the SWOT analysis. In the future, this approach can also be combined with a more sophisticated systematic analytical model, such as value analysis [16–20], aimed to reduce time and costs of the hybrid molecular imaging application.

References

1. Reynolds CA, Wagner SL, Harder HG (2006) Physician-stakeholder collaboration in disability management: a Canadian perspective on guidelines and expectations. Disabil Rehabil 28(15):955–963
2. Nel AE et al (2013) A multi-stakeholder perspective on the use of alternative test strategies for nanomaterial safety assessment. ACS Nano 7(8):6422–6433
3. Droms CM, Ferguson M, Giuliano K (2014) The stakeholder approach: a new perspective on developing and marketing clinical trials. Health Mark Q 31(1):1–12
4. Stroetmann KA (2015) Patient-centric care and chronic disease management: a stakeholder perspective. Stud Health Technol Inform 208:324–330
5. van Wijngaarden JD, Scholten GR, van Wijk KP (2012) Strategic analysis for health care organizations: the suitability of the SWOT-analysis. Int J Health Plann Manage 27(1):34–49
6. Camden C et al (2009) SWOT analysis of a pediatric rehabilitation programme: a participatory evaluation fostering quality improvement. Disabil Rehabil 31(16):1373–1381
7. Terzic Z et al (2010) SWOT analysis: the analytical method in the process of planning and its application in the development of orthopaedic hospital department. Srp Arh Celok Lek 138(7–8):473–479
8. Dhawan BN (2011) Indian Pharmacological Society: a SWOT analysis. Indian J Pharmacol 43(6):621–623
9. Sharma R, Webster P, Bhattacharyya S (2014) Factors affecting the performance of community health workers in India: a multi-stakeholder perspective. Glob Health Action 7:25352
10. Ahmadi Q et al (2015) SWOT analysis of program design and implementation: a case study on the reduction of maternal mortality in Afghanistan. Int J Health Plann Manage. doi:10.1002/hpm.2288
11. Ciarmiello A et al (2014) Hybrid SPECT/CT imaging in neurology. Curr Radiopharm 7(1):5–11
12. Kashyap R et al (2013) Hybrid imaging worldwide-challenges and opportunities for the developing world: a report of a Technical Meeting organized by IAEA. Semin Nucl Med 43(3):208–223
13. Rhenman E (1964) Foeretagsdemokrati och foeretagsorganisation. Thule, Stockholm
14. Mitchell RK, Agle BR, Wood DJ (1997) Towards a theory of stakeholder identification and salience: defining the principle of who and what really counts. Acad Manage Rev 22(4):853–856
15. Gilson L (2013) Health policy and systems research: a methodology reader. Alliance for Health Policy and Systems Research/World Health Organization, Geneva. Accessed online 11 Jan 2013 via http://www.who.int/alliance-hpsr/alliancehpsr_reader.pdf
16. Cooper R, Slagmulder R, Barth C (1997) Target costing and value engineering, Strategies in confrontational cost management series. Productivity Press, Portland, Describes the combination of target costing process and value engineering in the new product development process (NPD). ISBN 1563271729
17. Gage WL (1967) Value analysis. McGraw Hill, London, * One of the first textbooks on VA. Easy to read, well structured and provides many examples
18. Shillito LM, Demarle DJ (1992) Value: its measurement, design and management. Wiley, New York, * Focuses on product development, and provides a structured approach to professionals. Contains four chapters: nature, measurement, design and management of value. ISBN 0471527386
19. Norton BR, McElligott WC (1995) Value management in construction: a practical guide. Macmillan, Basingstoke
20. Gibson JF (1968) Value analysis: the rewarding infection. Pergamon Press Limited, Oxford, * A 'quick-and-dirty' guide to VA

19 Worldwide Challenges and Opportunities of Hybrid Imaging: Perspective from the International Atomic Energy Agency (IAEA)

Diana Paez, Giuliano Mariani, T.N.B. Pascual, and R. Kashyap

19.1 Introduction

Imaging in general is currently playing a pivotal role in the clinical management of several serious diseases, either communicable or non-communicable, affecting the central nervous system (CNS). Regarding nuclear medicine imaging specifically, it must be emphasised that dating back as far as the mid-1970s, great advances in our understanding of the physiology of the brain, both in health and in disease, were achieved thanks to the unique capability of radionuclide methods to explore functional aspects.

The investigations mentioned above are typical of radionuclide imaging of brain physiology and/or of pathophysiologic changes based on properties that are intrinsic to functional imaging with nuclear medicine, which involves relatively non-specific bulk processes, such as diffusion, membrane permeability or electrostatic interactions. Functional imaging of the brain in the past was restricted to exploring diffusion, membrane permeability or electrostatic interactions using non-specific tracers, thus receiving insight into physiology and/or pathophysiology. The advancement in radiopharmaceuticals and instrumentation contributed to the enhanced understanding of the brain. The development of [^{18}F]FDG as an in vivo tracer of glucose metabolism marks the transition from classical functional radionuclide imaging to what is now called "molecular imaging" – a new scenario at the intersection of molecular biology and in vivo imaging, whereby radioactive tracers constitute new biomarkers of disease [1]. In the case of radionuclide imaging of the brain with single-photon emitters, the corresponding link is represented by the development of receptor-specific tracers for the dopaminergic system, to be utilised mainly for the characterisation of patients with movement disorders [2–4].

The area of molecular imaging has matured over the past decade and is still growing and evolving rapidly. Many concepts developed for molecular biology and cellular imaging have been successfully translated and applied to in vivo imaging of intact organisms. Molecular imaging enables the study of processes at a molecular level in their full biological context. Due to the high specificity of the molecular readouts, the approach bears a high potential in

D. Paez (✉) • T.N.B. Pascual • R. Kashyap
Nuclear Medicine and Diagnostic Imaging Section, Division of Human Health, International Atomic Energy Agency (IAEA), Wagramer Strasse 5, Vienna, Austria
e-mail: D.Paez@iaea.org

G. Mariani
Regional Center of Nuclear Medicine, University of Pisa Medical School, Via Roma 67, Pisa 56126, Italy

A. Ciarmiello, L. Mansi (eds.), *PET-CT and PET-MRI in Neurology*,
DOI 10.1007/978-3-319-31614-7_19

diagnostics. It is fair to say that molecular imaging has become an indispensable tool for biomedical research, drug discovery and development today.

Advances in the field have paved the way towards considering nuclear medicine as a prime actor in precision/personalised medicine, additionally because of the unique possibility of using radionuclide imaging with certain diagnostic tracers to predict with great accuracy the clinical outcome of treatment with the same biochemical agent labelled with an adequate particle-emitting radionuclide or simply with mass amounts of the cold, unlabelled drug (for instance, an antitumour chemotherapy agent or a drug utilised for treating patients with a certain degenerative CNS disease).

As a corollarium to the above considerations, most of the interest in these new avenues of technological development leading to better understanding and treatment of disease concerns oncological conditions. The underlying rationale is that the molecules of interest (either radiolabeled or nonradioactive) interact with molecular species that are distinctly present or absent in a disease state, such as a mutated locus of DNA or its protein or RNA product, a gene product that has normal sequence and structure but is aberrantly expressed in a given tissue or the product of a transcriptionally normal gene whose structure or function has been modified by abnormal RNA splicing or post-translational processing. Thus, as beautifully illustrated in an inspiring article by Britz-Cunningham and Adelstein [5], perhaps the definition "molecular targeting" is more suited than "molecular imaging" to identify the complex scenario in which nuclear medicine imaging takes on a primary role, in enabling the characterisation of disease states and the subsequent selection of the most adequate treatment according to the principles mentioned above. The use of genomic and proteomic methods is expected to accelerate the transition to this new scenario for more general use in clinical medicine.

The combined approach as alluded to above, which is especially but not exclusively suited for applications in oncology, is now termed "theranostics" and is providing important prognostic information not only on an individual patient by patient basis but also in the general process of developing new drugs for clinical use [6, 7].

Concerning nuclear medicine, recent advances in knowledge of molecular biology have contributed to important technological improvements in imaging, more specifically hybrid imaging. Hybrid imaging is a procedure, whereby the combined clinical outcome of two sets of co-registered images (typically emission images such as those obtained with PET or SPECT and transmission images obtained with CT – and more recently also with the non-transmission anatomic images provided by MRI) is far superior to the simple arithmetic sum of the two separate components (see Fig. 19.1). This process leads to improved characterisation – and hence better patient care – which is of paramount importance for brain tumours [8] as well as for degenerative CNS diseases such as dementias [9–11] and movement disorders among others [12–17].

Functional imaging has transformed considerably throughout the past decades, which is reflective of the shift in the causes of morbidity and mortality worldwide, mainly attributed to chronic

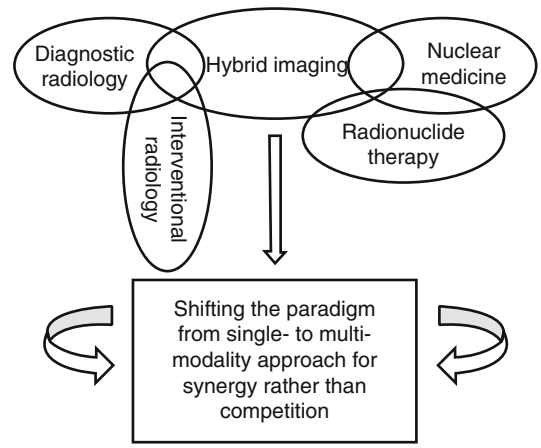

Fig. 19.1 Diagrammatic representation of the interaction and outcomes between radiologic imaging and nuclear medicine imaging as made possible by hybrid imaging that can be considered as the morpho-functional interface that not only leads to synergic diagnostic information but also has favourable consequences on planning and performing the therapy-related procedures traditionally included in the domains of radiology and nuclear medicine

and non-communicable diseases such as cardiovascular and neurological diseases and cancer. The vast and rapid research on the technology of hybrid imaging even increased the educational demands on the professionals involved [18]. Globalisation has brought forth increased efforts worldwide from experienced societies towards the harmonisation of procedures and the establishment of protocol guidelines and appropriate use of this modality, leading to increased sharing of information across all nations [19]. This indicates global cooperative efforts from practitioners and stakeholders in the field to strengthen the speciality through the sharing of new information, amidst the vast development. This dynamic medical speciality is highly technology dependent, and the appropriate practice of it greatly depends on a well-equipped facility with a highly skilled professional team of nuclear imaging professionals, technologists, radiochemists and medical physicists.

One major stakeholder committed to providing countries with opportunities for access to hybrid imaging technologies and its applications is the International Atomic Energy Agency (IAEA). The IAEA provides opportunities to member states (MSs) who need support in developing their hybrid imaging capacities, through equipment acquisition and human resources development among many other areas of support. Through a streamlined process, the synergy between the IAEA and MSs ensures that this emerging nuclear technology is delivered appropriately and serves its purpose.

This chapter provides a brief background on the epidemiologic considerations of neurological diseases and the role of hybrid imaging within this context. It then continues to describe the educational challenges encountered with the introduction of hybrid imaging within the standard nuclear medicine curriculum. It further explores the current state of implementing hybrid imaging technologies across major continents within the developing world and the associated challenges involved. Finally it provides an overview on how MSs can develop their hybrid imaging capacities from the perspective of the International Atomic Energy Agency (IAEA).

19.2 Epidemiologic Considerations of Neurological Diseases and the Role of Hybrid Imaging

Disease considerations in neurology from the imaging point of view are brain tumours, infections, degenerative diseases and movement disorders. The prevalence of most of these diseases is greater in countries with higher life expectancy at birth. Improvements in awareness and the ability to diagnose neurological conditions have reduced the underestimation of public health problems posed especially by degenerative CNS diseases, especially in low-income countries. Except for some brain tumours occurring in the paediatric age from 0 to 18 years of age, such as astrocytomas, medulloblastomas, ependymomas and some forms of gliomas, they tend to occur more frequently with increasing age. The pattern of increasing incidence in the ageing population is especially clear in the case of degenerative CNS diseases, typically dementias and movement disorders [20].

Nevertheless, as the low- and middle-income countries move towards higher levels on the ladder of socio-economic development, improvements both in life expectancy and in the capability of recognising and reporting certain diseases lead to an increasing incidence and/or prevalence of a variety of diseases previously thought to constitute public health problems only for high-income countries. Cardiovascular disease and degenerative CNS diseases are good paradigms for this changing pattern. Concerning in particular CNS diseases, many previously unrecognised neurological disorders, which cause significant disability but not mortality, are emerging as priority health problems also in low- and middle-income countries. Estimates by the World Health Organization (WHO, Geneva, Switzerland) in conjunction with the Harvard School of Public Health (Boston, Massachusetts, USA) indicate that the neurological disease burden will continue to increase, with a projected 12 % increase from 2005 to 2030 in disability adjusted life years [21]; this is the result of a 62 % increase in

dementias and movement disorders (chiefly Parkinson's disease) and 20 % increase in cerebrovascular diseases, despite a 57 % decrease in infectious diseases of the CNS. It is also estimated that, by the year 2040, 71 % of all dementia cases will be in the developing countries, with the highest growth projections for China and Southeast Asia (with a 300 % increase between 2001 and 2040) versus a 100 % increase in developed countries [22, 23].

19.3 Hybrid Imaging Modalities in Neurological Diseases

Leaving aside software-based co-registration of images obtained with different imaging equipments (typically one set of CT and one set of PET images acquired with two separate scanners and at different times), current terminology of hybrid imaging intrinsically implies the use of an integrated tomographic instrumentation that combines in a single gantry both a functional detection system and an anatomical imaging system, such as PET with CT (PET/CT), SPECT with CT (SPECT/CT) and more recently PET with MRI (PET/MR). The purpose of using these combined instrumentations is to correct the emission data (PET or SPECT) for attenuation correction as well as to provide anatomic correlates for the functional, molecular-based imaging data provided by PET or SPECT. The clinical impact derived from the combination of molecular imaging with anatomic imaging is clearly superior to the simple arithmetic sum of the two separate components, a feature that is especially important when investigating the CNS. The overall result translates into an added diagnostic value that has significant impact on clinical management of diseases.

Depending on the radioactive moiety of the tracer employed to map the different functions of the brain for molecular imaging, tomographic imaging is obtained either with SPECT (for single-photon emitters) or with PET (for positron emitters). The scanners currently available for hybrid imaging are SPECT/CT, PET/CT and PET/MR (although in principle a hybrid SPECT/MR scanner is technically feasible and putative imaging agents have been identified for such a combined imaging approach [24]; nevertheless, this option is not seriously pursued).

At variance with vast clinical evidence demonstrating the added value of SPECT/CT for whole-body examinations especially in the domains of oncology, cardiology and infectious diseases [25], there is little evidence that this hybrid imaging modality has a definite added value and a relevant clinical impact in patients with neurologic and psychiatric disorders [26]. Most of the experience with SPECT/CT applications for the CNS concerns the use of tracers of the dopaminergic system, typically ^{123}I-FP-CIT. In this case, it has been shown that CT-based attenuation correction yields a significantly greater signal recovery (up to 33 %) than the commonly applied phantom-based Chang attenuation correction [27]. This leads to improved semi-quantitative image analysis, therefore to greater accuracy in pathophysiologic measurements, to increased confidence in image interpretation and ultimately to more appropriate diagnosis [28, 29]. Better diagnostic performance of SPECT/CT compared to stand-alone SPECT has also been proven when imaging brain tumours with ^{99m}Tc-sestamibi [30].

By far more extensive than with SPECT/CT is the clinical experience with PET/CT in the investigation of the CNS, either for brain tumours, for dementias or for movement disorders [31–35]. Finally, even though the overall volume of examinations and of studies assessing clinical impact are currently still scarce because of the limited diffusion of such hybrid equipment worldwide, there is growing consensus that PET/MR imaging is the optimal combination to explore the multifaceted functions and morpho-functional correlates of CNS diseases [36–41]. In fact, in these scanners the high potential of molecular imaging for exploring the CNS with radioactive tracers using PET is combined with the high anatomic definition of MR imaging for the brain – coupled in turn with the possibility to explore some functional parameters linked to metabolic pathways within the CNS that are provided by both PET and functional MR.

As recently pointed out elsewhere [42, 43], distribution and operation of hybrid imaging equipments are very heterogeneous worldwide, mostly because of large discrepancies occurring in health resources available in countries with dramatically different incomes across the world. Direct cost of the equipment per se grows almost exponentially from SPECT/CT (in the range of USD 550,000–800,000), to PET/CT (in the range of USD 1,200,000–2,500,000) and finally to PET/MR (in the range of USD 5,000,000–6,500,000); for SPECT/CT and PET/CT, one of the main determinants of cost is the CT component. In addition of such direct cost of the equipment, there are other fundamental pillars on which to base the efficient and cost-effective operation of a clinical hybrid imaging diagnostic centre, i.e. a reliable technical maintenance service/assistance, a timely and reliable logistics of radiopharmaceuticals' supply and the availability of proper human resources (which includes physicians specialised in diagnostic imaging, technologists, radiochemists/radiopharmacists, health physicists and other ancillary personnel). Properly addressing these requirements is taken for granted in most countries where nuclear medicine is already deeply rooted in the medical community. However, such awareness is much lower in most of the developing/low-income countries, where health resources are in general poorer, and the predominant health priorities position nuclear medicine at a lower level in the range of the medical needs to be addressed; this makes it difficult in these countries to operate nuclear medicine, therefore also hybrid diagnostic imaging, in a timely accessible, cost-effective and sustainable manner.

19.4 Challenges in Education

Globalisation is a significant phenomenon and has produced an impact in a multitude of aspects, including science and technology, worldwide [44]. Within these realms, the rapid introduction of newer technologies such as hybrid imaging in the field of medical imaging has prompted a critical reflection on the current and future educational and social implications and its affect within the society.

Professional societies and certifying bodies (national and regional) involved in hybrid imaging (chiefly those devoted to nuclear medicine and diagnostic radiology) have explored potential issues regarding education and accreditation issues, with the declared purpose of optimising achievement of the full diagnostic information/potential offered by a hybrid imaging procedure (PET/CT, SPECT/CT, PET/MR) [42, 44].

Although the primary purpose of using SPECT/CT, PET/CT or PET/MR is to derive clinically useful information based on molecular imaging (i.e. the nuclear medicine component of the examination – SPECT or PET), nevertheless the hybrid scanners currently available are equipped with a fully state-of-the-art CT or MR component. Regarding in particular PET/CT and SPECT/CT (by far the hybrid scans most frequently and widely performed), even if the CT parameters employed for hybrid imaging are usually suboptimal in terms of kV and mA (and in general not using a radiologic contrast agent), the images obtained thereby can be considered of diagnostic quality. On one hand this feature makes it possible to detect previously unknown anatomic abnormalities that might have clinical relevance in addition to the purely metabolic/functional information provided by molecular imaging (PET or SPECT) [45–52]. On the other hand, abnormalities of some clinical relevance detectable in the CT component of the hybrid scan might be missed by specialists in molecular imaging who have not received adequate training in cross-sectional anatomic imaging – a possibility that can be important from both the clinical and legal points of view. In this regard, there are relevant differences across the world regarding the education and practice of nuclear medicine/hybrid imaging professionals [54].

The choice is therefore left to the individual countries regarding the specific model of education and training to be adopted, including comprehensive training in the two specialties (nuclear medicine and radiology), an adjusted period of training in the other specialty in addition to full training in the primary specialty (an option

whereby the two specialties would be obtained over a shorter period as opposed to the simple arithmetic sum of the two separate specialties) and finally the inclusion of training in the form of a cross-over or integrated training programme. Careful educational policy prescription should be tailored in order to maximise the competencies of professionals who will use the hybrid imaging technology within the context of the clinical practice.

19.5 Infrastructure of Hybrid Imaging in Different Regions of the World: Focus on Low- to Middle-Income Countries

19.5.1 Africa

This region of the world is characterised by a very high degree of heterogeneity among different countries concerning the healthcare infrastructure in general, with obvious consequences for imaging and in particular for hybrid imaging. In this specialty, adequate coordination/synergy among several different players (dependable power supply, instrumentation, technical servicing/maintenance, logistics of radiopharmaceuticals' supply, human resources, patients' referral, healthcare coverage) must perform at a sufficiently high level as to ensure regular and reliable operation of a centre delivering hybrid imaging services to patients and to the entire healthcare community at large. These requirements are met only in parts of Africa, in particular in those countries constituting the southern rim of the Mediterranean Sea (Egypt, Libya, Tunisia, Algeria, Morocco) and on the opposite side of the continent, South Africa. In terms of population, these countries altogether constitute only about 20 % of the entire population of the African region. Therefore, approximately 80 % of the estimated 1.153 billion people living in Africa do not have adequate access to general nuclear medicine and hybrid imaging procedures and sometimes not even to basic diagnostic imaging modalities such as plain X-ray. Concerning radionuclide imaging, 18 African countries have only one nuclear medicine centre per country, often non-functional.

According to the latest estimates collected by the IAEA through various national and international meetings, the overall nuclear medicine imaging equipment installed in Africa includes 267 scanners, 219 of which are stand-alone SPECT gamma cameras, 16 are hybrid SPECT/CT cameras and 32 are PET/CT installations. Concerning single-photon imaging, hybrid scanners therefore constitute less than 7 % of the overall gamma cameras installed, and it is estimated that they are mostly used for oncology, cardiology and infection localisation purposes outside the brain.

The vast majority of African countries do not have local/national training/residency programmes in nuclear medicine for physicians neither for technologists, nurses or medical physicists. Development of human resources is therefore based on training programmes of variable duration offered by more advanced countries within Africa (e.g. Algeria, Egypt, South Africa, Tunisia) or outside Africa (usually in Europe or in some Middle East countries).

19.5.2 Asia

The overall scenario of nuclear medicine imaging in Asia (excluding Australia and New Zealand) is on average more favourable than in Africa, although with a certain degree of heterogeneity among countries that have advanced levels of nuclear medicine operations (typically Japan, South Korea, Turkey), countries that have intermediate – but gradually improving – levels (typically, India, China, Thailand and Vietnam among others) and countries that have low levels of nuclear medicine. Altogether, in the Asian region (which also includes the Middle East countries), there are close to 1000 PET/CT installations. Geographic distribution of these installations is nevertheless quite variable population-wise, the highest absolute number being found in Japan, i.e. a total of 500 PET/CT scanners for a total population of over 126 million; this corresponds therefore to one PET/CT scanner every approximately

252,000 people. A similar scenario is seen in South Korea, with one PET/CT scanner every approximately 240,000 population. Intermediate scenarios are seen when the ratio of PET/CT installations to population remains within one scanner per million population, i.e. one every 502,000 population in Kuwait, one every 547,000 population in Singapore, one every 638,000 population in Lebanon, one every 932,000 population in Israel and one scanner every approximately one million population in Turkey. On the other hand, in the majority of the countries in the Asian region, the number of PET/CT scanners installed is far below the ideal proportion population-wise, with a wide range of distribution parameters that can be grouped in values anywhere between one scanner every approximately 1.37–8.52 million population (Jordan, Mongolia, Syria, Saudi Arabia, United Arab Emirates, Thailand, China, Kazakhstan), one scanner every approximately 11.55–26.69 million population (Vietnam, India, Philippines, Iran), one scanner every approximately 64.26–95 million population (Iran, Indonesia, Bangladesh, Pakistan) and finally no PET/CT scanner at all in the entire country (Nepal, Mongolia).

As far as SPECT/CT equipment is concerned, the recent trend to replace technically obsolete stand-alone SPECT gamma cameras with state-of-the art hybrid scanners is especially apparent in this region. In fact, SPECT/CT gamma cameras currently constitute approximately 60 % of all operating single-photon scanners installed in Asia, in strong contrast with, e.g. less than 7 % for Africa.

The overall number of nuclear medicine specialists reported in the Asian region is close to 7000, again with wide variations from country to country; in terms of absolute number, China comes first with approximately 2830 nuclear physicians, followed closely by Japan (approximately 2650 nuclear physicians – but covering an overall population which is over tenfold smaller than that of China). All other countries lag behind these numbers, from approximately 400 nuclear physicians in India (with a total population which is virtually equivalent to that of China), to a 100–300 range in South Korea, Pakistan, Taiwan, Philippines and Bangladesh, between 40 and 80 nuclear physicians per country (Thailand, Vietnam, Indonesia, Singapore), finally to single-digit numbers (Myanmar, Sri Lanka, Mongolia).

19.5.3 Europe

According to a survey conducted by the European Association of Nuclear Medicine (EANM) in 2012, the overall number of nuclear medicine centres/services in Europe is around 2000 – staffing approximately 6400 specialists. Of interest to hybrid imaging, some nuclear medicine departments include among their staff specialists in radiology – with a steadily growing number from approximately 550 in 2006 to about 750 in 2012. Other professionals forming the nuclear medicine staff include technologists (about 3400 in 2012), medical physicists (about 900), radiopharmacists (about 500) and nurses (about 1500) in addition to unspecified ancillary staff (about 1000 overall).

Of the 27 countries that provided this information, nuclear medicine is independent from radiology in 17 of them and belongs to radiology in 6, and in 4 countries nuclear medicine is in a department other than radiology. Regarding postgraduate education, in the majority of the European countries for which this information is available (19/27), nuclear medicine and radiology do not have a common educational core curriculum.

According to consolidated data available through the EANM, equipment for hybrid imaging installed up to 2012 included 684 SPECT/CT scanners, 551 PET/CT scanners and 19 PET/MR scanners; these numbers have clearly increased since the date of the 2012 survey. Although the EANM does not make available the country-by-country data, the general picture can perhaps be put into perspective considering an approximately even distribution of hybrid scanners throughout all nuclear medicine centres. In this regard, the average number of nuclear medicine centres in Europe on a population basis is about 4 per million population (with minor variations among high-income

countries); nevertheless, large discrepancies emerge among different countries with different income levels, from the lowest level of less than 1 centre per million population in some low-income countries to the peak value of 16 centres per million population (to be found in Greece, although this is probably linked to the large number of small nuclear medicine centres operated on a mere subsistence level). It is also to be noted that approximately 75 % of all gamma cameras installed between 2011 and 2013 are hybrid SPECT/CT (data supplied by the some manufacturers: GE Healthcare, Siemens, Philips).

19.5.4 Latin America and the Caribbean

Although the practice of nuclear medicine in the Latin American and the Caribbean region has grown considerably in the last decade, there exists a high degree of heterogeneity among different countries – and sometimes even within any given country. Detailed information on the overall status of hybrid imaging in this region has been published very recently [43] and data were extracted from that publication that are relevant to hybrid imaging, concerning both technology and human resources.

Official records show that in this region there are overall 1141 nuclear medicine centres, Brazil and Mexico (the two countries with the largest population size) accounting for more than half of the total number of nuclear medicine centres in Latin America and the Caribbean. On the other hand, Haiti has no nuclear medicine at all. The average number of nuclear medicine centres on a country-by-country basis is about 1.4 per million population across the entire region, therefore much lower than the corresponding figure in Europe (approximately 4 per million population); besides the case of Haiti, 9 out of the 21 countries in Latin America and the Caribbean region have less than 1 nuclear medicine centre per million population, while in 7 countries (Argentina, Brazil, Chile, Colombia, Mexico, Panama, Uruguay), this ratio approaches 2 nuclear medicine centres per million population (the highest value, 7.3, seen in Argentina). The SPECT/CT scanners constitute about 10 % of all the SPECT gamma cameras installed in this region; the highest absolute numbers are seen in Brazil (with 30 hybrid scanners) and Mexico ($n = 25$), followed by Argentina ($n = 8$) and Chile ($n = 6$); there is currently a high replacement rate in the region, with an increasing number of hybrid SPECT/CT scanners [42, 43]. Regarding PET/CT, the total number of installed scanners is 161, again the highest numbers seen in Brazil ($n = 68$) and Mexico ($n = 35$), followed by Argentina ($n = 23$), Chile ($n = 10$) and Colombia ($n = 9$). So far, there is no information on any PET/MR scanner already installed in this region, although some projects are under way.

As to the human resources, there are almost 1300 specialists in nuclear medicine in the Latina American and Caribbean region. Accredited training programmes for nuclear medicine conferring a nuclear medicine specialty are available in Argentina, Brazil, Chile, Colombia, Mexico, Peru, Uruguay and Venezuela. Nevertheless, there are wide variations among the different countries regarding duration of the programme (from 2 to 4 years) and total independence of the nuclear medicine specialty or affiliation as a subspecialty with either internal medicine or radiology (or part of a broader programme in radiation oncology, as it occurs in Venezuela).

19.6 Opportunities to Improve the Status of Hybrid Imaging in Developing Countries: IAEA Perspective

The IAEA is a specialised and independent organisation related to the United Nations family and is primarily concerned with the promotion of the peaceful use of atomic energy to peace. The IAEA reports its activities and governance to the UN General Assembly and Security Council [53]. As of February 2013, it has 164 member states. Its mandate lies in the Article II

of the Statute of the IAEA drafted in 1956 which states that:

> The Agency shall seek to accelerate and enlarge the contribution of atomic energy to peace, health and prosperity throughout the world. It shall ensure, so far as it is able, that assistance provided by it or at its request or under its supervision or control is not used in such a way as to further any military purpose. [53]

The objective of this mandate is to ensure that all agency activities supporting education and training are provided to member states (MSs) in a more integrated, consistent and optimised manner. This is achieved through improved coordination, cooperation, sharing of knowledge and experience and assisting concerned MSs in their efforts to build national capacity and to provide state-of-the-art education and training that meets their needs and priorities at national, regional or global levels.

Ever since its first inception, the IAEA has perceived the need to homogenise this diversity through inputs from professional organisations and international organisations [54, 55] and is carrying on initiatives specifically designed to fulfil this purpose [56–60]. Concerning in particular hybrid imaging, one should consider the requirements that must be met in order to ensure proper operation and self-sustaining management of such imaging procedures in such a manner that they would translate into clinical benefit to patients and into overall improvement in the healthcare system, thus providing the added value over single modality that the synergic effect of multimodality hybrid imaging is expected to induce. Besides obvious infrastructure factors that include both instrumentation-related parameters and logistic organisation, strong determinants in this process include the human resources (see Fig. 19.2), particularly the need to define new paradigms in education and training of medical and technical personnel, as well as the overall healthcare scenario that has to do with interaction between nuclear medicine staff (and also the diagnostic imaging staff at large) on one side and other specialties on the other side, such as neurology, cardiology, oncology, etc.

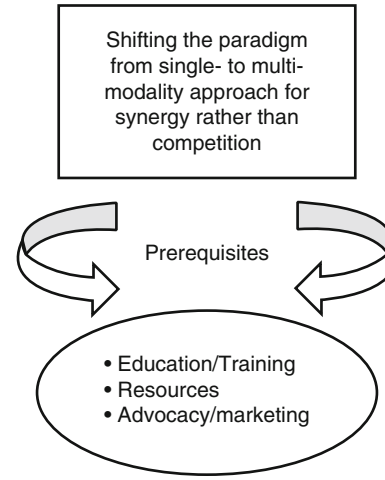

Fig. 19.2 Main determinants for the successful implementation of hybrid imaging programmes in the medical community and in the healthcare system at large (see text)

This undertaking is reflective of the current state of affairs or sociopolitical climate in the MSs, that is, there is acceptance of the country for the need to improve their nuclear technologies, existing or not, which is expressed in their respective country programme framework submitted to the IAEA. These technologies are therefore neither forced nor imposed upon any MS by the IAEA but are in fact a reflection of the need to build or improve the state of practice of these technologies, perhaps as a result of globalisation and the increasing necessity to address global health issues more effectively. The introduction of hybrid imaging technologies as a vital tool in the management of patients justifies inclusion of this technology within the countries' health frameworks wherein the IAEA can play a pivotal role in providing opportunities to MSs in realising their goals.

Activities are coordinated by the Nuclear Medicine and the Diagnostic Imaging Section at the Division of Human Health, which is part of the IAEA's Department of Nuclear Sciences and Applications, in collaboration with the IAEA's Department of Technical Cooperation. Through programmatic activities and national, regional or interregional technical cooperation projects, MSs engage in the development of hybrid imaging technologies in their countries. The ultimate goal

is to assist member states to build and maintain competent and sustainable human resources and institutional capacity matched to their current and future needs related to the peaceful use of atomic energy, in this case, the use of hybrid imaging modalities. The development of nuclear technologies as requested by developing MSs are carried out with the support of the IAEA, mainly as capacity building activities through the procurement of instrumentation and human resources development in the form of coordinated research projects, scientific visits, fellowships and further education mechanisms in the field of nuclear technology. With technical cooperation mechanisms alone, an approximate 54 million US dollars were allocated for capacity building in nuclear medicine (including hybrid imaging technologies) for over 180 projects in the past decade [57]. Projects are reflected within the country programme framework and are proposed, and these reflect mostly the effect of globalisation and its themes in the field of nuclear technology.

19.6.1 Equipment Procurement

The long-term objective of the IAEA projects in nuclear medicine (including hybrid imaging) is to provide human resource capacity building through education and training activities. In the case of some less-developed countries where nuclear medicine infrastructure is not well established, support through the procurement of appropriate equipment and its maintenance is also provided. This is reflected in the distribution of the budget wherein procurements account for nearly three-fifths of total disbursements, and human resource expenditures including fellowships, training courses, expert missions and scientific visits account for a little over two-fifths of the total [57]. Major equipment such as SPECT/CT, PET/CT and related devices are mainly procured through cost sharing basis between the IAEA and the recipient country, belonging to the low- and middle-income range.

19.6.2 Coordinated Research Projects

The IAEA is also committed to promote research using hybrid imaging technologies in neurodegenerative disorders or topics of recent relevance to MSs. Through a mechanism called coordinated research projects (CRPs), collaborative prospective researches between developed and low-middle-income countries are initiated in order to foster exchange of scientific data between MSs. This is articulated in the Article III of the IAEA's statute mandates that the IAEA should encourage and assist research on the development and practical application of atomic energy and its applications for peaceful purposes throughout the world and foster the exchange of scientific and technical information and exchange of scientists for peaceful uses of atomic energy [53].

19.6.3 Training Courses, Fellowships and Scientific Visits

The IAEA is also committed to provide learning opportunities to MSs through the mechanism of fellowships and scientific visits and training courses. Live educational events ranging from a minimum of 5 days are organised within the thematic programme of regional or interregional training courses or workshops. Within the scope of the role of hybrid imaging technologies in neurodegenerative disorders, these training courses provide a comprehensive live educational opportunity for participants, usually delivered via lectures and case discussions. Hands-on activities can be organised through fellowship and scientific programmes wherein individuals nominated by the eligible MS can gain from on-site visits to high-level institutions (university or hospital) and learn how the technology is utilised on-site. These visits or trainings can range from a minimum of 5 days to several months or years depending on the specific needs of the MS.

19.6.4 Advocacy and Outreach Publication/Guidelines

The IAEA promotes advocacy in the appropriate use of hybrid imaging technologies through several mechanisms. Through guidelines and technical documents published by the IAEA and experts in the field, MSs can remain updated on latest developments in the field of hybrid imaging and can use this information to implement the technology in their respective country, by translating these guidelines into policy prescriptions and eventually adopting the technology for their use. Similarly, expert missions (EM) can be organised by the IAEA to MSs, wherein experts and IAEA officers can offer direct advice on developing the technology to several MSs. The reports generated by these missions can then guide the stakeholders in the careful planning or interventions needed to introduce hybrid imaging modalities in their respective countries.

Conclusion

Hybrid imaging and its applications in neurodegenerative diseases have evolved rapidly throughout the last decade. Epidemiologic considerations of neurological diseases and the role of hybrid imaging should be understood in order to provide an in-depth perspective in applying these technologies to the current practice. With globalisation, educational challenges are being encountered with the introduction of hybrid imaging within the standard nuclear medicine curriculum. Aware of the crucial changes influencing the social and technological sphere on the use of hybrid imaging technologies, the IAEA provides support and opportunities through several mechanisms in order to promote capacity building in member states. Through appropriate guidance from the IAEA, MSs can take full advantage of implementing hybrid imaging technologies in their healthcare system.

References

1. James ML, Gambhir SS (2012) A molecular imaging primer: modalities, imaging agents, and applications. Physiol Rev 92:897–965
2. Costa DC, Verhoeff NP, Cullum ID et al (1990) In vivo characterisation of 3-iodo-6-methoxybenzamide ^{123}I in humans. Eur J Nucl Med 16:813–816
3. Abi-Dargham A, Gandelman MS, DeErausquin GA et al (1996) SPECT imaging of dopamine transporters in human brain with iodine-123-fluoroalkyl analogs of beta-CIT. J Nucl Med 37:1129–1133
4. Kung HF, Kim HJ, Kung MP, Meegalla SK, Plössl K, Lee HK (1996) Imaging of dopamine transporters in humans with technetium-99m TRODAT-1. Eur J Nucl Med 23:1527–1530
5. Britz-Cunningham SH, Adelstein SJ (2003) Molecular targeting with radionuclides: state of the science. J Nucl Med 44:1945–1961
6. Del Vecchio S, Zannetti A, Fonti R, Pace L, Salvatore M (2007) Nuclear imaging in cancer theranostics. Q J Nucl Med Mol Imaging 51:152–163
7. Srivastava SC (2012) Paving the way to personalized medicine: production of some promising theragnostic radionuclides at Brookhaven National Laboratory. Semin Nucl Med 42:151–163
8. Fink JR, Muzi M, Peck M, Krohn KA (2015) Multimodality brain tumor imaging: MR imaging, PET, and PET/MR imaging. J Nucl Med 56:1554–1561
9. Seibyl J, Zubal IG, Jennings D, Marek K, Doraiswamy PM (2011) Molecular PET imaging in multicenter Alzheimer's therapeutic trials: current trends and implementation strategies. Expert Rev Neurother 11:1783–1793
10. Jiménez Bonilla JF, Carril Carril JM (2013) Molecular neuroimaging in degenerative dementias. Rev Esp Med Nucl Imagen Mol 32:301–309
11. Heiss WD (2014) PET imaging in ischemic cerebrovascular disease: current status and future directions. Neurosci Bull 30:713–732
12. Peng S, Eidelberg D, Ma Y (2014) Brain network markers of abnormal cerebral glucose metabolism and blood flow in Parkinson's disease. Neurosci Bull 30:823–837
13. Politis M (2014) Neuroimaging in Parkinson disease: from research setting to clinical practice. Nat Rev Neurol 10:708–722
14. Ba F, Martin WR (2015) Dopamine transporter imaging as a diagnostic tool for parkinsonism and related disorders in clinical practice. Parkinsonism Relat Disord 21:87–94
15. Miller DB, O'Callaghan JP (2015) Biomarkers of Parkinson's disease: present and future. Metabolism 64(3 Suppl 1):S40–S46
16. Hirao K, Pontone GM, Smith GS (2015) Molecular imaging of neuropsychiatric symptoms in Alzheimer's

and Parkinson's disease. Neurosci Biobehav Rev 49:157–170
17. Weingarten CP, Sundman MH, Hickey P, Chen NK (2015) Neuroimaging of Parkinson's disease: expanding views. Neurosci Biobehav Rev 59:16–52
18. Hricak H, Choi BI, Scott AM, Sugimura K et al (2010) Global trends in hybrid imaging 1. Radiology 257:498–506
19. Segall G (2012) SNM and global cooperation. J Nucl Med 53:19N
20. Pringsheim T, Jette N, Frolkis A, Steeves TD (2014) The prevalence of Parkinson's disease: a systematic review and meta-analysis. Mov Disord 29:1583–1590
21. Disorders N (2006) Public health challenges. World Health Organization, Geneva
22. Kalaria RN, Maestre GE, Arizaga R et al (2008) Alzheimer's disease and vascular dementia in developing countries: prevalence, management, and risk factors. Lancet Neurol 7:812–826
23. World Health Organization. Dementia – A public health priority. Geneva: World Health Organization; 2012.
24. Park JA, Kim JY, Lee YJ et al (2012) Gadolinium complex of ^{125}I/^{127}I-RGD-DOTA conjugate as a tumor-targeting SPECT/MR bimodal imaging probe. ACS Med Chem Lett 4:216–219
25. Mariani G, Bruselli L, Kuwert T et al (2010) A review on the clinical uses of SPECT/CT. Eur J Nucl Med Mol Imaging 37:1959–1985
26. Buck AK, Nekolla S, Ziegler S et al (2008) SPECT/CT. J Nucl Med 49:1305–1319
27. Warwick JM, Rubow S, du Toit M, Beetge E, Carey P, Dupont P (2011) The role of CT-based attenuation correction and collimator blurring correction in striatal SPECT quantification. Int J Mol Imaging 2011:195037
28. Hayashi M, Deguchi J, Utsunomiya K et al (2005) Comparison of methods of attenuation and scatter correction in brain perfusion SPECT. J Nucl Med Technol 33:224–229
29. Ciarmiello A, Giovacchini G, Guidotti C et al (2013) Weighted registration of ^{123}I-FP-CIT SPECT images improves accuracy of binding potential estimates in pathologically low striatal uptake. J Cell Physiol 228:2086–2094
30. Schillaci O, Danieli R, Manni C, Simonetti G (2004) Is SPECT/CT with a hybrid camera useful to improve scintigraphic imaging interpretation? Nucl Med Commun 25:705–710
31. Berti V, Pupi A, Mosconi L (2011) PET/CT in diagnosis of movement disorders. Ann N Y Acad Sci 1228:93–108
32. Calabria F, Chiaravalloti A, Di Pietro B, Grasso C, Schillaci O (2012) Molecular imaging of brain tumors with ^{18}F-DOPA PET and PET/CT. Nucl Med Commun 33:563–570
33. Segtnan EA, Hess S, Grupe P, Høilund-Carlsen PF (2015) ^{18}F-fluorodeoxyglucose PET/computed tomography for primary brain tumors. PET Clin 10:59–73
34. Shivamurthy VK, Tahari AK, Marcus C, Subramaniam RM (2015) Brain FDG PET and the diagnosis of dementia. AJR Am J Roentgenol 204:W76–W85
35. Wray R, Solnes L, Mena E, Meoded A, Subramaniam RM (2015) ^{18}F-Flourodeoxy-glucose PET/computed tomography in brain tumors: value to patient management and survival outcomes. PET Clin 10:423–430
36. Heiss WD (2009) The potential of PET/MR for brain imaging. Eur J Nucl Med Mol Imaging 36(Suppl 1):S105–S112
37. Bisdas S, Nägele T, Schlemmer HP et al (2010) Switching on the lights for real-time multimodality tumor neuroimaging: the integrated positron-emission tomography/MR imaging system. AJNR Am J Neuroradiol 31:610–614
38. Garibotto V, Heinzer S, Vulliemoz S et al (2013) Clinical applications of hybrid PET/MRI in neuroimaging. Clin Nucl Med 38:e13–e18
39. Von Schulthess GK, Kuhn FP, Kaufmann P, Veit-Haibach P (2013) Clinical positron emission tomography/magnetic resonance imaging applications. Semin Nucl Med 43:3–10
40. Burgos N, Cardoso MJ, Thielemans K et al (2014) Attenuation correction synthesis for hybrid PET-MR scanners: application to brain studies. IEEE Trans Med Imaging 33:2332–2341
41. Barthel H, Schroeter ML, Hoffmann KT, Sabri O (2015) PET/MR in dementia and other neurodegenerative diseases. Semin Nucl Med 45:224–233
42. Kashyap R, Dondi M, Paez D, Mariani G (2013) Hybrid imaging worldwide – Challenges and opportunities for the developing world: a report of a technical meeting organized by the IAEA. Semin Nucl Med 43:208–223
43. Paez D, Orellana P, Gutierrez C, Ramirez R, Mut F, Torres L (2015) Current status of nuclear medicine practice in Latin America and the Caribbean. J Nucl Med 56:1629–1634
44. Olssen M, Codd JA, O'Neill A-M (2004) Education policy: globalization, citizenship and democracy. Sage Publications, London
45. Osman MM, Cohade C, Fishman EK et al (2005) Clinically significant incidental findings on the unenhanced CT portion of PET/CT studies: frequency in 250 patients. J Nucl Med 46:1352–1355
46. Bruzzi JF, Truong MT, Marom EM et al (2006) Incidental findings on integrated PET/CT that do not accumulate ^{18}F-FDG. AJR Am J Roentgenol 187:1116–1123
47. Goetze S, Pannu HK, Wahl RL (2006) Clinically significant abnormal findings on the "nondiagnostic" CT portion of low-amperage-CT attenuation-corrected myocardial perfusion SPECT/CT studies. J Nucl Med 47:1312–1318
48. Muzaffar R, Kudva G, Nguyen NC et al (2011) Incidental diagnosis of thrombus within an aneurysm on ^{18}F-FDG PET/CT: frequency in 926 patients. J Nucl Med 52:1408–1411
49. Fathala A, Aljefri A, Alsugair A et al (2011) Coronary artery calcification detected by PET/CT scan as a

marker of myocardial ischemia/coronary artery disease. Nucl Med Commun 32:273–278
50. Tootell A, Vinjamuri S, Elias M, Hogg P (2012) Clinical evaluation of the computed tomography attenuation correction map for myocardial perfusion imaging: the potential for incidental pathology detection. Nucl Med Commun 33:1122–1126
51. Zandieh S, Schütz M, Bernt R, Zwerina J, Haller J (2013) An incidentally found inflamed uterine myoma causing low abdominal pain, using Tc-99m-tektrotyd single photon emission computed tomography-CT hybrid imaging. Korean J Radiol 14: 841–844
52. Wuest W, Lell M, May MS, Saake M, Kuwert T, Uder M, Linke R (2015) Thoracic non-osseous lesions in cancer patients detected in low-dose CT images acquired as part of skeletal SPECT/CT examinations. Nuklearmedizin 54:173–177
53. International Atomic Energy Agency (IAEA) – Statute of the IAEA. Available online at http://www.iaea.org/About/about_statute.html. 1956. Last accessed online 10 May 2015.
54. Dondi M, Kashyap R, Paez D, Pascual T, Zaknun J, Mut Bastos F, Pynda Y (2011) Trends in nuclear medicine in developing countries. J Nucl Med 52(Suppl 2):16S–23S
55. Dondi M (2013) Guest editorial: IAEA approach to meet nuclear medicine needs of the emerging world. Semin Nucl Med 43:159–160
56. Pascual TN, Dondi M, Paez D, Kashyap R, Nunez-Miller R (2013) IAEA programs in empowering the nuclear medicine profession through online educational resources. Semin Nucl Med 43:161–166
57. Casas-Zamora JA, Kashyap R (2013) The IAEA technical cooperation programme and nuclear medicine in the developing world: objectives, trends, and contributions. Semin Nucl Med 43:172–180
58. Meghzifene A, Sgouros G (2013) IAEA support to medical physics in nuclear medicine. Semin Nucl Med 43:181–187
59. Duatti A, Bhonsle U (2013) Strengthening radiopharmacy practice in IAEA Member States. Semin Nucl Med 43:188–194
60. Patterson HE, Nunez M, Philotheou GM, Hutton BF (2013) Meeting the challenges of global nuclear medicine technologist training in the 21st century: the IAEA Distance Assisted Training (DAT) program. Semin Nucl Med 43:195–201

PET/CT Versus PET/MRI

20

Andrea Ciarmiello, Luigi Mansi, and Ignasi Carrio

20.1 Introduction

Molecular imaging (MI) is a diagnostic modality allowing the in vivo assessment of biological processes in normal and pathological conditions.

MI is based on the capability of a procedure to "follow" a molecular process using a labeled tracer detectable by an external probe. Theoretically, MI is feasible with computed tomography (CT) using iodinated tracers, magnetic resonance imaging (MRI) using paramagnetic labels, ultrasounds (US) with microbubbles, optical imaging (OI) using fluorescence, and nuclear medicine utilizing radiotracers. Being mandatory, to avoid an alteration on the system to be studied and/or toxicity, the administration of amounts of tracer in the order of pico/n moles, this possibility is only feasible at present with OI, NM, and, more rarely, MRI. Nevertheless, because fluorescent tracers cannot be imaged when they are deep, for the low/absent penetration of light photons through the matter, at the present MI in humans has to be intended prevalently as a prerogative of nuclear medicine, being rare the clinical diffusion of procedures based on OI and MRI.

MI is widely recognized as a tool which has an impact on the physician's intention to treat in oncology, neurology, and cardiology and in all the other fields of clinical interest. In the last decade, MI diagnostic potential was further strengthened by the availability of hybrid modalities able to couple functional (PET or PET) and structural (CT or MRI) modalities in the same scanner. Hybrid imaging offers several advantages for patients, health-care system, and caregivers. These include the availability of a single image containing structural and functional information and the opportunity to perform one-stop shop scan in full diagnostic modality. At the same time, the use of hybrid imaging (HI) is growing, driven by the scientific data that are accumulating on the potential clinical benefits and the progressive reduction of acquisition costs. Despite hybrid imaging has witnessed unprecedented change since the early 2000s, the risk deriving from extra patient's exposure to ionizing radiation and the overall acquisition and management costs are limiting the use of these modalities.

A. Ciarmiello (✉)
Department of Nuclear Medicine,
S. Andrea Hospital, La Spezia, Italy
e-mail: andrea.ciarmiello@asl5.liguria.it

L. Mansi
Nuclear Medicine, Second University of Naples,
Napoli, Italy

I. Carrio
Department of Nuclear Medicine, Autonomous
University of Barcelona, Hospital Sant Pau,
Sant Quintí 89, Barcelona 08025, Spain

A. Ciarmiello, L. Mansi (eds.), *PET-CT and PET-MRI in Neurology*,
DOI 10.1007/978-3-319-31614-7_20

This book is designed to provide base information on stand-alone and hybrid modalities to support strategic planning. Its content will also be of interest to government agencies aimed at promoting health care, patients, and industries. Several relevant issues are examined in the study including clinical need, impact on patient, educational need for medical staff and technicians, and hospital investment.

20.2 Clinical Context

A growing body of evidence and guidelines supports the use of PET imaging in the diagnosis of neurological diseases [1]. PET/CT combines functional and structural information into a single image which is reported to improve diagnostic accuracy and clinical outcome [2].

The added value of CT component of PET/CT in oncology has been extensively evaluated. PET/CT as compared with PET or CT alone is reported to improve diagnostic accuracy in lymphoma; in lung, colorectal, and head and neck cancers [3–5]; and in a variety of tumors such as melanoma; esophageal, thyroid, and gastrointestinal stroma tumors; and sarcoma [6, 7]. The significant increase of diagnostic accuracy of hybrid systems, as compared to stand-alone scanners, is estimated between 5 and 10 % on average over all cancers [1, 8].

Although the role of brain PET imaging in dementia disorders [9–11], neuro-oncology [12–14], epilepsy [15, 16], and movement disorders [17–20] has been established, data on the added value of combined PET/CT examinations is still under debate.

Due to the possibility of combining anatomical, functional, metabolic images and multiparametric images, PET/MRI scanner has the potential to become the latest frontier in multimodality imaging. At present there is not enough evidence to suggest clinical setting other than for the brain, but given the reduced exposure of the patients, it could be useful in younger adults, in nononcologic diseases, and for multiple repeated scans, having been already individuated a favorable field of utilization in regions as pelvis and head and neck, in which PET/MRI takes advantage of the superiority of MRI with respect to CT in evaluating lesions in these districts [21].

20.3 SWOT Analysis

20.3.1 Methods

SWOT analysis was used to identify strengths and weaknesses (SW) of hybrid imaging, as well as opportunities and threats (OT). To apply the SWOT a survey has been conducted with the aim of defining the most relevant factors influencing the use of hybrid modalities. The target group of this survey was composed of four group stakeholders involved at different levels with stand-alone and hybrid imaging. The panel of stakeholders consisted of users, decision-makers, promoters, and manufacturers. The survey was based on a specific stakeholder questionnaire prepared to collect, analyze, and interpret the views of each target group. Each SWOT factor of every question was scored according to expert opinion. Users included 38 worldwide distributed physicians (Fig. 20.1). In clinical and research activities, 93 % of the physicians were involved, whereas 5 % of the sample was involved only in research activities and 2 % in clinical work alone. At the time of the survey, about two-thirds of the physicians were working in public hospitals, while 11 % were working in research institutes and 24 % in universities. Decision-makers consisted of ten general managers of public institutions aimed at the production of health services for clinical and research purposes. Promoters included the International Agency of Atomic Energy (IAEA). The IAEA, a department of the United Nations (UN), aims at promoting equal accessibility to atomic energy for health in developed as well as in developing countries. Manufacturers included three of the major companies producing diagnostic hybrid technologies (GE, Philips, Siemens).

Fig. 20.1 Worldwide distribution of stakeholders involved in the survey on hybrid modalities

20.3.2 Results

The overall panel included 52 experts from different countries. Figure 20.2 shows the radar plot of the scores assigned by the experts to each element of the SWOT analysis. The survey highlighted some key elements across all the groups of stakeholders. Table 20.1 shows higher-scored factors of each SWOT class as rated by the experts. These elements were considered of particular interest by the experts and therefore represent in their opinion the main strengths and threats of multimodal imaging technologies. Because of this, the elements considered most important as a result of the total scores assigned by experts, they are individually discussed in the following paragraphs.

20.3.3 Major Strengths

20.3.3.1 Simultaneous Scanning of Structural and Functional Images

Hybrid systems provide functional and anatomical images in the same scanning session and patient position therefore limiting the drawbacks of software-based image registration [22]. Multimodality imaging allows the two images to be acquired with the same geometry and body position with minimal delay between the two studies and without the need for external reference markers. After acquisition, images are reconstructed with the same consistency, realigned and fused to generate a new image overlaying PET and CT data.

20.3.3.2 Improvement of Image Quality

Together with physiological, paraphysiological, and pathophysiological variations, physical factors as scattered photons [23], patient motion [24], attenuation of photons [25], and partial volume effect [26] may contribute to degrade image quality and reduce the accuracy of quantitative measures. Among them, tissue photon attenuation is one of the most important factors which contributes to depleting the image quality. The availability of CT images for attenuation correction (AC) of the PET images eliminates the need of an additional transmission scan [27, 28]. CT-based attenuation correction provides CT-measured attenuation correction factors which are noiseless compared

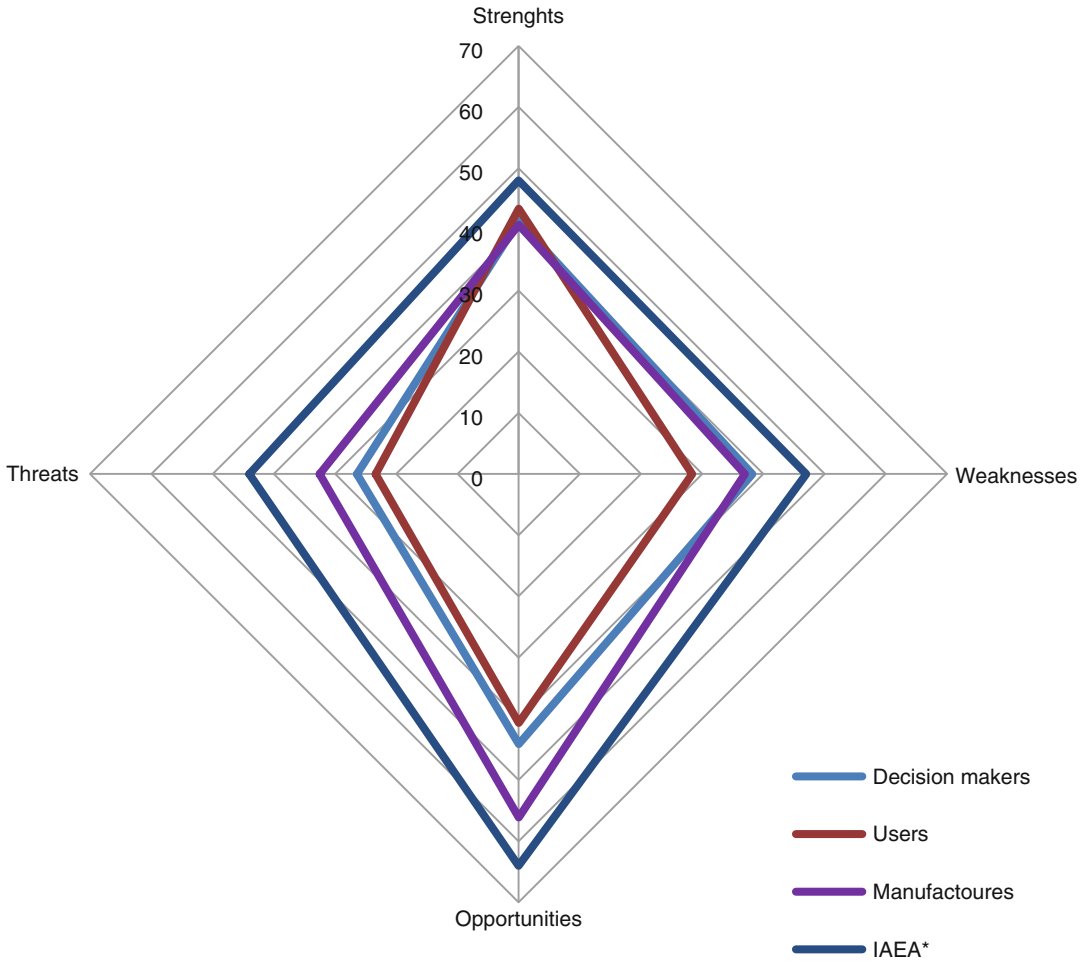

Fig. 20.2 Radar plot of SWOT element as rated by stakeholders (*International Atomic Energy Agency)

Table 20.1 Summary of higher-scored items of each SWOT factors according to experts' opinion

SWOT class	Users	Manufacturers	Decision-makers	IAEA[a]
Strengths	Simultaneous scanning of structural and functional image	Improvement of image quality	Impact on the diagnostic performance (accuracy)	Image quality
Weaknesses	Scan time (PET/MR) PET attenuation correction in PET/MR modality	High development costs	Payback time and number of scan to achieve the break-even point	Patient radiation exposure
Opportunities	Imaging in women in reproductive age, children, and young adolescent and serial scan (PET/MR)	Need to promote the new technology	Training of medical staff	Technical improvement for attenuation correction
Threats	Patient radiation exposure	Production costs	Installation costs	Imaging in women in reproductive age, children, and young adolescent and serial scan (PET/CT)

[a]International Atomic Energy Agency

to those measured with external radionuclide sources. Therefore CT-based AC influences image quality and both absolute and relative quantifications in cerebral PET [25, 29, 30]. Avoiding transmission scan, the overall scanning time and patient exposure significantly decrease. Different authors reported whole-body scanning times decrease by at least 40 % and patient radiation exposure reduction by about ~0.5–1.6 mrem [29].

20.3.3.3 Impact on Diagnostic Performance

Multimodality CT or MR-based imaging provides the anatomical template in which to localize the normal or pathological functional findings, thus allowing a more accurate image interpretation [2] and therefore offering to clinicians with a more accurate evaluation of disease which affects patient management [31]. In the diagnosis of head and neck cancer, as well as in many other fields, the evaluation of PET/CT as compared to PET and CT separately was reported to improve image interpretation and diagnostic accuracy [32].

20.3.4 Major Weaknesses

20.3.4.1 Scanning Times

Multimodality PET/MR research acquisition protocols may take as long as 60–90 mins. This makes the use of PET/MR in a clinical setting hardly imaginable. Unlike CT, the MR component of a multimodality scanner provides a higher number of pulse sequences than CT whose potential use may further increase acquisition time [33, 34]. Since a PET scan lasts 15 min, with a 60-min multimodality protocol, the PET would work only about 25 % compared to 75 % of the MR. This proportion tends to worsen with MR acquisition time increase. To be cost-effective in a clinical setting, the acquisition protocols should be completed within 1 h at the most [33]. Moreover the long acquisition time increases both the patient discomfort and probability of movement artifacts.

20.3.4.2 PET Attenuation Correction in PET/MR Modality

While added clinical added value of PET and MR simultaneous acquisition is still under evaluation, some relevant pitfalls in oncologic whole-body imaging are emerging. Many of them are dependent on an inaccurate MR-based attenuation correction [35]. The development of MR-based attenuation correction method is the real challenge of PET/MR imaging and is the main problem to address to obtain qualitatively and quantitatively accurate PET images [36]. Attenuation correction map in PET/CT hybrid modality is derived from CT scan by converting Hounsfield units to μ values for 511 keV photons using linear calibration curves [37, 38]. In PET/MR, attenuation maps cannot be calculated starting from MR signals because there is no linear correlation between proton density and magnetization relaxation properties and tissue attenuation. The majority of existing approaches consists in segmenting the tissues on the base of MR signal intensity and then assigning to each of them the corresponding tissue attenuation coefficient [39–41]. This approach was firstly proposed for brain studies and then modified for whole-body application [42]. Different segmentation approaches have been proposed so far to segment the MR images. Among them, the most used were atlas-based, template-based, direct segmentation approaches and sequence-based methods [42–46].

20.3.4.3 Patient Radiation Exposure

The growing spread of multimodality scanners using both X-rays and radiopharmaceuticals undoubtedly contributes toward clinical benefits and increased patient dose exposure. It is widely recognized that the CT portion of PET/CT results in additional radiation to the patient [47]. Based on phantom studies, the typical radiation dose from the CT with a hybrid PET/low-dose CT scan ranged from 1.3 mGy at the center of the phantom to 5 mGy at the surface compared to the 20 mGy for a typical diagnostic quality CT scan [48]. Effective dose for CT examinations is typically higher than the majority of other diagnostic imaging modalities [49–51].

However, the extra radiation exposure cannot cause deterministic effects, but in patients undergoing multiple studies, the stochastic effects could be significant [50].

It has to be pointed out that a dose reduction, determined through hardware, software, or modified procedures, represents one of the most relevant improvements achievable using the last commercial CT scanners.

Further studies are needed to clarify whether the high radiation exposure associated with the CT component of a hybrid scanner is acceptable given the potential benefits associated with multimodality approach.

20.3.5 Major Opportunities

20.3.5.1 PET/MR Imaging in Radiation-Sensitive Populations

Despite the clinical setting of multimodality, PET/MR imaging is not yet defined; the reduced patient dose exposure resulted from a non-x-ray-based multimodality scanner is one of the main recognized advantages. In some specific clinical settings, the availability of a multimodality scanner able to reduce the patient effective dose could be useful. These pathological conditions include children, young adults, and patients undergoing multiple imaging sessions. A possible cost-effectiveness could be reached also in women during pregnancy, in cases in which a clinical indication strongly supports the use of a PET study. Therefore, particularly in patients more sensitive to radiation, the overall radiation exposure dose could be kept as low as reasonably achievable [52].

Similarly a clinical justification, based on a more favorable cost-effectiveness, may be found in patients suspicious for a nononcologic disease. In particular PET/MR is preferred in patients with chronic inflammation, in which many follow-up studies may be requested to define extension, severity evolution, and activity of the disease.

In brain studies PET/MR was proposed for the high anatomical quality and metabolic assessment [53]. PET/MR provides a sophisticated multimodality scanner to trace molecular events with the best possible anatomical detail [54]. In neuro-oncology as well as in neurodegenerative diseases, PET/MR has been proposed as the latest frontier of neuroimaging for its ability to finely delineate structural details, thus facilitating the identification of PET activation sites [55].

In oncology settings, whole-body diffusion-weighted and metabolic images can be combined, thus avoiding radiation exposure from CT [56, 57]. Authors reported no significant differences between PET/CT and PET/MR for detection of malignant lesions. Moreover they found a strong correlation between the mean standardized uptake values measured by both imaging modalities [56].

PET/MR scanners deliver a lower dose than that released by PET/CT modality thus allowing to study patient populations at greater risk of dose exposure. These are the reasons why this key element of SWOT was chosen by almost all stakeholders as one of the major opportunities of this imaging technology.

20.3.5.2 Educational Needs

Multimodality imaging scanners require both physicians and technicians trained in both modalities. Unfortunately, there are neither common laws nor common guidelines in this regard. Therefore, to meet the need of training on multimodality scanner each country has adopted its own strategy. Although there are some differences between the training strategies, all are characterized by the need to provide nuclear medicine trainees some radiology skills and vice versa. As a result of the different training strategies adopted by various countries, the level of training is unbalanced across the states. In order to overcome these differences, the need for more consistent cross-training of hybrid-imaging physicians and technologists should be addressed by changes in government regulations and training curricula [58]. This element was considered an opportunity of continuous improvement for the staff working with hybrid technologies. It has to be noted that in most countries a different specialization is requested

to report nuclear medicine or CT studies, while a specific specialization is not needed for the evaluation of a MR scan. It means that a nuclear physician cannot report alone a PET/CT study, when CT is used as "full diagnostic procedure," as in the case of contrast-enhanced CT (CECT). Conversely a PET/MR may be analyzed "legally" only by a nuclear physician, although a professional expertise is mandatory either in nuclear medicine or in MR evaluation.

20.3.6 Major Threats

20.3.6.1 PET/CT Imaging in Radiation-Sensitive Populations

The association between increased exposure to radiation for diagnosis purposes and risk of solid cancer in specific target populations has been reported by several authors [59–61]. These populations include children, young adults, pregnant women, and patients undergoing multiple scans or suspicious for nononcologic diseases.

In children and young adults, the number of CT performed has increased rapidly between 1996 and 2005 and then slightly declined after 2007. In children under 5 years, the number of CT scans performed in the United States has doubled while for those between 5 and 14 years has tripled [59]. The risks of developing solid tumors linked to the radiation load increase were higher in younger patients and in girls than adults. Moreover, the risks of solid cancer were greater for patients who underwent abdomen and pelvis CT imaging than for those examined in other anatomical regions [59, 61].

In pregnant women the gestation period between the 8th and the 15th week is the most sensitive. Below the threshold of 100–200 mGy, deterministic effects such as abortion, abnormal growth, congenital malformations, and neurocognitive deficits are unlikely [62]. At the exposure dose of 50 mGy, the risk is reported to be negligible [63]. In women exposed to radiological examination at standard diagnostic dose, the risk of carcinogenesis is mildly higher than in the general population [64, 65]. Considering the possible effect of radiation on fetal development, X-ray-based imaging procedures should be avoided or limited to selected cases.

In patients candidate to multiple scans, the dose-exposure load increases significantly depending on the number of performed imaging procedures. In children with Hodgkin's disease (HD) and adults with non-Hodgkin's lymphoma (NHL), patients undergo several PET/CT imaging procedures. Due to multiple radiation exposure, the effective dose grows rapidly in malignant lymphoma patients [66]. As a result of effective dose increase, HD children and NHL adults showed only a mild increase of radiation-induced death that justifies the examination but suggests especially careful regard when treating children [66].

PET/CT scan delivers higher doses than that released by stand-alone PET and PET/MR modality. Considering the most recent published papers, it is easy to understand why this element has been reported by all stakeholders as a weakness or increased threat of CT-based multimodality. In these modalities it is possible to reduce the overall adsorbed dose paying attention to both CT imaging protocol and administered radiopharmaceutical activity without reducing image quality and the impact on patient care [67]. Therefore it is a priority to plan appropriate strategies to reduce the effective dose in order to reduce the number of radiation-induced tumors. This approach should be applied to all patients paying more attention to the most sensitive ones. A similar strategy has to be adopted also in patients in which a nononcologic disease is suspected, mainly when the analysis of pelvis and abdomen is included in the evaluation.

20.3.6.2 Acquisition Costs

Multimodality imaging scanners have a high structural and organizational impact. The structural impact is due to the resources for system acquisition and for structural changes needed to house the new technology. The organizational impact is due to the need to involve new highly qualified professionals as physics and engineers. The PET/MR overall costs are much

higher compared to PET/CT. Depending on manufacturers acquisition, costs of PET/MR scanners may vary between €3.800.000 and about €5.000.000. Maintenance costs per year are around 10 % of the system costs. Such a large investment needs a high productivity in terms of number of diagnostic procedures performed to reach the break-even point. While PET/CT is recommended by several clinical guidelines in the diagnosis of various oncology and neurology diseases, PET/MR has only a few possible clinical indications and at present has not yet entered into any clinical guideline. These are the main reasons that made these the major threats particularly for the decision-makers.

20.4 Clinical Impact

The clinical value of a diagnostic procedure depends more than on its capability alone, on the comparison with alternative techniques answering to the same question. Further indications may be achieved when it is possible to add complementary data to diagnosis, as in the case wherein an information better connectable with prognosis or with the therapeutic strategy may be acquired.

When many alternatives are available in defining the diagnostic course, being achievable a similar information through different techniques, the choice has to be done on the basis of the cost-effectiveness ratio that has to be calculated considering many issues involving either the diagnostic or the therapeutic strategy.

At first, it has to be remembered that *primum non nocere (first do no harm)*, i.e., that each diagnostic information has to be acquired in the presence of the minimum possible risk and never running an unjustified hazard. In this context, it has to be pointed out that, although techniques utilizing ionizing radiations, such as CT and nuclear medicine, are affected by the negative charge of the stochastic (low) probability to determine a cancer, many other even greater risks may be associated with diagnostic procedures outside of nuclear medicine. In particular, while there are no absolute contraindications against radionuclide examinations, which can be performed in all the subjects in the presence of a clinical justification, it is possible to die after the administration of contrast media and may be absolutely contraindicated to carry out an MR study in individuals with pacemakers and/or metallic components or a CECT in patients with a renal failure. Furthermore a greater risk may be determined by associated practices, as stress tests and narcosis, or by issues, particularly critical in emergency, as the duration of the examination or the incapability to immediately activate resuscitation maneuvers. Nevertheless the greatest risk in diagnosis is the mistake, dependent on an unsatisfactory sensitivity and/or specificity. In this sense techniques allowing an improvement in diagnostic accuracy may acquire a favorable cost-effectiveness ratio, mainly because of significant advantages which may be produced on patient's fate and in defining the best therapeutic strategy.

An improvement in diagnostic accuracy may also play an important role in reducing costs, which have to be calculated on the whole diagnostic and therapeutic course and not on the price of each procedure. For example, the adoption of PET/CT in staging of patients with lung cancer may increase the number of subjects correctly undergoing surgery with respect to stand-alone CT; at the same time, a staging procedure could be performed in a shorter period, also reducing hospitalization times.

In the definition of a cost-effectiveness, other relevant issues are connected with many other factors such as epidemiological conditions, favoring different choices in diverse contexts and local skills and supporting a preference for the procedure in which are locally involved more expert professionals, availability, age, and level of performance of equipments. Very important in clinical decisions is the accessibility to the examination, mainly dependent on waiting lists and therefore on the diffusion of the procedure.

For the reasons reported above, the choice of a diagnostic technique has to be done on the basis of many motivations that have to be calibrated either at general or local level. For example,

although MR, performed without ionizing radiations, shows a slightly better sensitivity in detecting breast lesions with respect to mammography (Mx), it cannot be used as first-line procedure in screening of breast cancer because it is scarcely diffuse, is operator dependent with a too low number of expert executors and evaluators in the local territory, and has a higher cost unjustified by the substantially overlapping diagnostic accuracy respect to Mx. Similarly, in the evaluation of cerebral diseases, although with the presence of ionizing radiations, CT has to be preferred in emergency with respect to MR, being faster, more easily performable, and at a lower cost, furthermore requiring less frequently narcosis. Moreover, a brain CT, being many of nervous cells perennials and therefore not subjected to mutations by rays, determines a lower rate of cancers associated with radiations with respect to a CT performed on pelvis.

Being this book dedicated to a SWOT analysis concerning hybrid imaging, at this point we focalize our attention in this field, starting with two statements already conclusive, i.e., which will be not be further discussed: (1) there is no doubt that PET/CT is preferable with respect to stand-alone PET, as it appears evident from the fact that in the commercial market hybrid machines are only available today; (2) SPET/CT is better than SPEt alone, but it didn't reach yet a value able to allow a complete replacement of SPET, also because gamma cameras continue to maintain a favorable cost-effectiveness in many cases, supporting their acquirement. As further demonstration, being cardiology still one of the major applications of traditional nuclear medicine, the industry has produced and continues to invest in dedicated cardiac SPET, not associated with CT. It means that, although the acquirement of a SPET/CT is strongly suggested, it may be not considered mandatory or always a priority in all the departments.

Conversely, the open question mark in the field of a SWOT analysis concerning hybrid machines is on the clinical impact of PET/MRI with respect to PET/CT to justify its acquisition: a contribution in answering to this question is one of the main aims of this book.

20.4.1 Which Institution Could Be Interested to Acquire a PET/MRI Scanner?

In this volume we focused our attention on a comparison at cerebral level, i.e., in the field in which PET/MR may more easily demonstrate a superiority with respect to PET/CT. Nevertheless, before comparing separately both hybrid systems in neurology and in whole-body applications, we want to try to answer to this relevant question: which institution could be today interested to acquire a PET/MRI scanner, considering its higher cost and the greater complexity with respect to PET/CT?

Our opinion is supported by data acquired in the SWOT analysis in which positive answers given by scientists/clinicians, with open minds to the future, are counterbalanced by the prevalence of weaknesses, mainly intended as acquisition and maintenance costs, and reported by decision-makers, answering on the basis of pragmatic opinions embedded in the present. Interestingly producing companies and promoting agency gave higher scores to related opportunity factors, demonstrating a "practical" interest in the diffusion of PET/MR, which justify a strong economical investment by industries.

20.4.2 PET/MRI and Research

What is already clear today is that PET/MR may be advantageous in research centers, in which it may optimize/complement the information achievable with PET/CT or open new fields of research, impossible or more difficult for its competitor. In this context, only at dawn in the present, the highest improvement with PET/MR could be achieved when the third eye will be "routinely" open [66], i.e., when PET/MR will be used acquiring simultaneously functional data obtained by PET together with morphostructural and functional information achievable with MRI. In fact, the golden added value of PET/MRI in the hybrid machine is the feasibility of fMRI, i.e., the possibility to create an interaction between metabolism/receptors/hypoxia, and so

on, which can be studied by PET and neo-angiogenesis/neural connections/biochemical issues, and so on, evaluable by MR.

In this way, new stimulating fields of research, with a hopefully fast application in the clinical practice, could be opened in oncology, in neuropsychiatry, and for many other applications. As an example in oncology, a better definition of the relationship between neo-angiogenesis and metabolism could allow the achievement of complementary data reliably defining tumor response to new therapeutic strategies. This indication could be immediately clinically relevant, because the RECIST, radiological method actually used in oncologic protocols, is unable to evaluate a tumor response to drugs not determining a reduction in tumor size. Similarly, in neuropsychiatry it is possible to individuate with PET/MR sub-centimetric alterations in structures neurologically connected with areas of dysmetabolism [68], evaluating through a tractography performed with diffusion tensor imaging (DTI) the connection with areas of altered metabolism, as seen by FDG, or of pathological deposits, using amyloid radiotracers.

Both the examples reported above are very effective in demonstrating that PET/MR could reach in the very near future a relevant impact in the health-care system. In fact, a reliable and early evaluation of tumor response may produce huge savings in spending for drugs; furthermore correctly individuating patients who may benefit from expensive medical treatments; at the same time the number of individuals subjected to unjustified toxicity, because they are nonresponders, may be significantly reduced. With respect to the neuropsychiatric example, PET/MR could earlier individuate and stratify patients with dementia, as those with Alzheimer's disease, diagnosed when affected with mild cognitive impairment (MCI): in this way, strategies allowing substantial savings for the health-care system could be adopted.

20.4.3 PET/MRI in the Clinical Arena

To determine a fast diffusion of PET/MR systems, it is important to justify their utilization more than in the research field, which offers the prospect of juicy fruits tomorrow, in the clinical arena today.

In this context, a major advantage, as clearly reported in previous chapters, is dependent on the lower dosimetry determined by the absence of ionizing radiations, over those issued by positron emitters, unlike what happens with CT. As it is well known, ionizing radiations may determine a risk of cancer which increases with the dose.

The benefit associated with PET/MR may play an important role in three different scenarios:

(1) Individuals with a higher risk of cancer because of the age, including pediatric patients and pregnant women. It is interesting to note that, in the presence of a strong clinical justification, contraindications actually proposed in infants and in pregnancy could be overcome in case an acceptable cost-effectiveness can be reached, also reducing radionuclide's dose.
(2) Populations with a benign pathological condition, including patients with inflammatory/infective diseases or with a low probability of cancer, as it happens in differential diagnosis of subjects with single pulmonary nodules.
(3) Patients undergoing serial scans. The preference for a procedure at a lower dosimetry, supporting the choice of PET/MR in the follow-up of oncologic patients in which the evaluation of a tumor response is requested, becomes almost "mandatory" in younger patients with chronic inflammation, as those with Crohn's disease, in which an FDG scan is requested to evaluate disease's activity during follow-up.

In the clinical arena, waiting for a wider and routinely reliable diffusion of PET/MR procedures utilizing also fMRI, most of the advantages of PET/MR with respect to PET/CT may be derived from the almost historic comparison between CT and MRI alone.

As it is well known, the most important field in which MR manifests a superiority with respect to CT is the brain and in previous chapters areas

in which PET/MR could consequently be preferred to PET/CT are individuated. In this context, major advantages seem identifiable in demyelinating diseases and in pathological conditions characterized by the presence of subcentimetric alterations or by pathological changes not determining significant variations in tissue density. In this sense, clinical applications for PET/MR could be mainly found in groups of patients as those affected with dementia, movement disorders, or pituitary microadenoma.

With respect to a whole-body evaluation, it has to be pointed out, as discussed in previous chapters, that PET/MR is negatively affected by technical problems, as those associated with a not yet standardized attenuation correction and with a greater duration of the examination, determining either a discomfort for the patient and artifacts, as those of movement. In this sense, although a whole-body PET/MR scan may be performed in an acceptable time [34], major advantages are achievable when the evaluation is requested at "regional level," being also achievable a multiparametric analysis. This evaluation may be particularly effective in districts with a complex anatomical organization, as head and neck, in which a pathological involvement of structures, as nerves and vessels, adjacent to a mass has to be very precisely individuated. Similarly a significant improvement may be obtained in pelvis, where pathological changes frequently do not result in structural variations of density, creating therefore problems at CT. At the present useful clinical indications may be already achievable mainly in this group of patients as those with prostate cancer or pelvic tumors and in head and neck region [69]. Not yet defined at the moment is the role in breast cancer, being PET/MR a promising tool for an earlier diagnosis of local relapse.

Other fields of application of PET/MR could be stimulated by a wider diffusion of PET radiotracers beyond FDG, but it is too early to evaluate their clinical application, but in prostate cancer where the most diffuse radiotracer is already radio-choline.

Only by way of example of possible perspectives associated with easily available radiotracers will it be interesting to refer to PET/MRI with ^{18}F-fluoride (NaF). Its applications could define new indications in oncology, as in patients with lung cancer in which bone metastases could be found either by NaF, when osteoblastic, or by MRI, when exclusively intramedullary. A further exciting field of application, which has to be verified on the basis of a wide clinical experience, could be found in the evaluation of active atherosclerotic plaques, in which the NaF's uptake has been demonstrated [70]. It has to be reported that for this indication interesting perspectives are also connected with PET/MR with FDG [71].

20.5 Final Comment

The future of PET/MR could be extremely bright in a health-care system without economical problems, being already now identifiable many motivations justifying its diffusion either in research or in the clinical practice. Unfortunately, being in the present, an age in which there are limited economical resources, the acquirement of a PET/MR system has to compete with many alternatives, first of all the consolidated favorable experience with PET/CT which present major advantages such as (1) lower cost, (2) easier management, (3) higher number of expert readers, and (4) radiological culture, mainly based on a morphostructural evaluation.

In our opinion there are already fields in which PET/MR may reach a cost-effectiveness justifying its acquirement in a limited number of specialized institutions.

At first, PET/MR is certainly a very effective tool in evaluating cerebral diseases, with a major improvement achievable when fMRI will be more frequently applied in the clinical practice. Interestingly the "cerebral field" is advantaged by the shorter time of evaluation with respect to a whole-body scan, determining feasibility for a multiparametric analysis, being also practically absent two major problems associated with PET/MR: attenuation correction and movement artifacts. Conversely, when a whole-body study is requested, the longer time of acquisition acts against the possibility

of acquiring a comprehensive study, being also present technical problems, which have not yet been solved in the routine practice. A major improvement could be obtained either increasing the speed of the whole-body scan, working either on hardware or software, or defining "segmental procedures," in which it is possible to dedicate more time to the region really important for the clinical question, renouncing to an optimal whole-body information, if not requested. It is interesting to note that the technological evolution requested by hybrid MR is having a relevant impact also on PET technology. At the present are already available detectors with higher sensitivity with respect to the traditional ones, allowing a higher sensitivity and previously unreachable performances, mainly when a TOF acquisition using a fully digital system is available.

It has also to be pointed that at the present PET/CT maintains a superiority with respect to PET/MR in oncology in detecting pulmonary metastases. A technical or procedural improvement in MR, also associated with the adoption of functional techniques or of contrast media, could give a further support to the definition of a more favorable cost-effective ratio with respect to PET/CT also in this particular aspect.

Finally, it is clear that the major determinant against a wide diffusion of PET/MR equipments is the unsatisfactory economical condition of the health-care system that acts against investments in high-cost technologies. The road to change this opinion is very long and has to be based on a cultural revolution; the best way to optimize the health-care balance is in targeted cuts, which may produce funds for new investments.

Hybrid machines, and between them PET/MR, may increase diagnostic accuracy. Therefore they can optimize the choice of therapeutic strategies, reducing unjustified surgery or useless toxic and expensive therapies. They may earlier diagnose diseases, as dementia, creating conditions favorable to a significant reduction of costs associated with millions of patients affected with these pathologies. They may better define activity in patients with chronic diseases, in which a therapy can be activated only in cases when it is really useful. Briefly, hybrid machines and in particular PET/MR may act in the direction of tailored medicine, a context where each patient could be treated with the best therapy, individually defined.

In this new scenario, a health-care system could improve remaining sustainable through investments in new technologies, if a cultural revolution having at the center of the new universe no longer structural data but functional/molecular information will be applied.

References

1. http://www.ncbi.nlm.nih.gov/books/n/cadthrdcollect/. 2014
2. Even-Sapir E, Keidar Z, Bar-Shalom R (2009) Hybrid imaging (SPECT/CT and PET/CT)–improving the diagnostic accuracy of functional/metabolic and anatomic imaging. Semin Nucl Med 39(4):264–275
3. Facey K et al (2007) Overview of the clinical effectiveness of positron emission tomography imaging in selected cancers. Health Technol Assess 11(44):iii–iv, xi-267
4. Brush J et al (2011) The value of FDG positron emission tomography/computerised tomography (PET/CT) in pre-operative staging of colorectal cancer: a systematic review and economic evaluation. Health Technol Assess 15(35):1–192, iii–iv
5. Poeppel TD et al (2013) Differential uptake of (68)Ga-DOTATOC and (68)Ga-DOTATATE in PET/CT of gastroenteropancreatic neuroendocrine tumors. Recent Results Cancer Res 194:353–371
6. Poeppel TD et al (2009) PET/CT for the staging and follow-up of patients with malignancies. Eur J Radiol 70(3):382–392
7. Poeppel TD et al (2011) 68Ga-DOTATOC versus 68Ga-DOTATATE PET/CT in functional imaging of neuroendocrine tumors. J Nucl Med 52(12):1864–1870
8. Czernin J, Allen-Auerbach M, Schelbert HR (2007) Improvements in cancer staging with PET/CT: literature-based evidence as of September 2006. J Nucl Med 48(Suppl 1):78S–88S
9. Herholz K, Carter SF, Jones M (2007) Positron emission tomography imaging in dementia. Br J Radiol 80 Spec No 2:S160–S167
10. Herholz K et al (2002) Discrimination between Alzheimer dementia and controls by automated analysis of multicenter FDG PET. Neuroimage 17(1):302–316
11. Mosconi L et al (2008) Multicenter standardized 18F-FDG PET diagnosis of mild cognitive impairment, Alzheimer's disease, and other dementias. J Nucl Med 49(3):390–398

12. Kaschten B et al (1998) Preoperative evaluation of 54 gliomas by PET with fluorine-18-fluorodeoxyglucose and/or carbon-11-methionine. J Nucl Med 39(5):778–785
13. Alkonyi B et al (2012) Accurate differentiation of recurrent gliomas from radiation injury by kinetic analysis of alpha-11C-methyl-L-tryptophan PET. J Nucl Med 53(7):1058–1064
14. Aki T et al (2012) Evaluation of brain tumors using dynamic (11)C-methionine-PET. J Neurooncol 109(1):115–122
15. Henry TR, Votaw JR (2004) The role of positron emission tomography with [18F]fluorodeoxyglucose in the evaluation of the epilepsies. Neuroimaging Clin N Am 14(3):517–535, ix
16. Van Paesschen W et al (2007) The use of SPECT and PET in routine clinical practice in epilepsy. Curr Opin Neurol 20(2):194–202
17. Eckert T et al (2005) FDG PET in the differential diagnosis of parkinsonian disorders. Neuroimage 26(3):912–921
18. Eckert T et al (2008) Abnormal metabolic networks in atypical parkinsonism. Mov Disord 23(5):727–733
19. Ciarmiello A et al (2006) Brain white-matter volume loss and glucose hypometabolism precede the clinical symptoms of Huntington's disease. J Nucl Med 47(2):215–222
20. Ciarmiello A et al (2012) 18F-FDG PET uptake in the pre-Huntington disease caudate affects the time-to-onset independently of CAG expansion size. Eur J Nucl Med Mol Imaging 39(6):1030–1036
21. Beyer T et al (2011) The future of hybrid imaging-part 3: PET/MR, small-animal imaging and beyond. Insights Imag 2(3):235–246
22. von Schulthess GK, Pelc NJ (2002) Integrated-modality imaging: the best of both worlds. Acad Radiol 9(11):1241–1244
23. Zaidi H (2001) Scatter modelling and correction strategies in fully 3-D PET. Nucl Med Commun 22(11):1181–1184
24. Osman MM et al (2003) Respiratory motion artifacts on PET emission images obtained using CT attenuation correction on PET-CT. Eur J Nucl Med Mol Imaging 30(4):603–606
25. Zaidi H, Hasegawa B (2003) Determination of the attenuation map in emission tomography. J Nucl Med 44(2):291–315
26. Rousset OG, Ma Y, Evans AC (1998) Correction for partial volume effects in PET: principle and validation. J Nucl Med 39(5):904–911
27. Kinahan PE, Hasegawa BH, Beyer T (2003) X-ray-based attenuation correction for positron emission tomography/computed tomography scanners. Semin Nucl Med 33(3):166–179
28. Kluetz PG et al (2000) Combined PET/CT imaging in oncology. Impact on patient management. Clin Positron Imag 3(6):223–230
29. Weinzapfel BT, Hutchins GD (2001) Automated PET attenuation correction model for functional brain imaging. J Nucl Med 42(3):483–491
30. Reza Ay M, Zaidi H (2006) Computed tomography-based attenuation correction in neurological positron emission tomography: evaluation of the effect of the X-ray tube voltage on quantitative analysis. Nucl Med Commun 27(4):339–346
31. Delbeke D et al (2009) Hybrid imaging (SPECT/CT and PET/CT): improving therapeutic decisions. Semin Nucl Med 39(5):308–340
32. Branstetter BF et al (2005) Head and neck malignancy: is PET/CT more accurate than PET or CT alone? Radiology 235(2):580–586
33. von Schulthess GK, Veit-Haibach P (2014) Workflow considerations in PET/MR imaging. J Nucl Med 55(Suppl 2):19S–24S
34. Barbosa Fde G, von Schulthess G, Veit-Haibach P (2015) Workflow in simultaneous PET/MRI. Semin Nucl Med 45(4):332–344
35. Attenberger U et al (2015) Whole-body FDG PET-MR oncologic imaging: pitfalls in clinical interpretation related to inaccurate MR-based attenuation correction. Abdom Imaging 40(6):1374–1386
36. Wagenknecht G et al (2013) MRI for attenuation correction in PET: methods and challenges. MAGMA 26(1):99–113
37. Burger C et al (2002) PET attenuation coefficients from CT images: experimental evaluation of the transformation of CT into PET 511-keV attenuation coefficients. Eur J Nucl Med Mol Imaging 29(7):922–927
38. Carney JP et al (2006) Method for transforming CT images for attenuation correction in PET/CT imaging. Med Phys 33(4):976–983
39. Vontobel J et al (2015) MR-based attenuation correction for cardiac FDG PET on a hybrid PET/MRI scanner: comparison with standard CT attenuation correction. Eur J Nucl Med Mol Imaging 42(10):1574–1580
40. Juttukonda MR et al (2015) MR-based attenuation correction for PET/MRI neurological studies with continuous-valued attenuation coefficients for bone through a conversion from R2* to CT-Hounsfield units. Neuroimage 112:160–168
41. Shandiz MS et al (2014) A hybrid method for generation of attenuation map for MR-based attenuation correction of PET data in prostate PET/MR imaging. EJNMMI Phys 1(Suppl 1):A77
42. Montandon ML, Zaidi H (2005) Atlas-guided non-uniform attenuation correction in cerebral 3D PET imaging. Neuroimage 25(1):278–286
43. Schreibmann E et al (2010) MR-based attenuation correction for hybrid PET-MR brain imaging systems using deformable image registration. Med Phys 37(5):2101–2109
44. Catana C et al (2010) Toward implementing an MRI-based PET attenuation-correction method for neurologic studies on the MR-PET brain prototype. J Nucl Med 51(9):1431–1438
45. Keereman V et al (2010) MRI-based attenuation correction for PET/MRI using ultrashort echo time sequences. J Nucl Med 51(5):812–818

46. Aitken AP et al (2014) Improved UTE-based attenuation correction for cranial PET-MR using dynamic magnetic field monitoring. Med Phys 41(1):012302
47. Mattsson S, Andersson M, Soderberg M (2015) Technological advances in hybrid imaging and impact on dose. Radiat Prot Dosimetry 165(1–4):410–415
48. Bocher M et al (2000) Gamma camera-mounted anatomical X-ray tomography: technology, system characteristics and first images. Eur J Nucl Med 27(6):619–627
49. Wall BF, Hart D (1997) Revised radiation doses for typical X-ray examinations. Report on a recent review of doses to patients from medical X-ray examinations in the UK by NRPB. National Radiological Protection Board. Br J Radiol 70(833):437–439
50. Larkin AM et al (2011) Quantifying the increase in radiation exposure associated with SPECT/CT compared to SPECT alone for routine nuclear medicine examinations. Int J Mol Imag 2011:897202
51. Sharma P et al (2012) SPECT-CT in routine clinical practice: increase in patient radiation dose compared with SPECT alone. Nucl Med Commun 33(9):926–932
52. Jadvar H, Colletti PM (2014) Competitive advantage of PET/MRI. Eur J Radiol 83(1):84–94
53. Schlemmer HP et al (2008) Simultaneous MR/PET imaging of the human brain: feasibility study. Radiology 248(3):1028–1035
54. Schwenzer NF et al (2012) Simultaneous PET/MR imaging in a human brain PET/MR system in 50 patients–current state of image quality. Eur J Radiol 81(11):3472–3478
55. Cho ZH et al (2013) In-vivo human brain molecular imaging with a brain-dedicated PET/MRI system. MAGMA 26(1):71–79
56. Drzezga A et al (2012) First clinical experience with integrated whole-body PET/MR: comparison to PET/CT in patients with oncologic diagnoses. J Nucl Med 53(6):845–855
57. Catalano OA et al (2013) Clinical impact of PET/MR imaging in patients with cancer undergoing same-day PET/CT: initial experience in 134 patients–a hypothesis-generating exploratory study. Radiology 269(3):857–869
58. Hricak H et al (2010) Global trends in hybrid imaging. Radiology 257(2):498–506
59. Miglioretti DL et al (2013) The use of computed tomography in pediatrics and the associated radiation exposure and estimated cancer risk. JAMA Pediatr 167(8):700–707
60. Bahadori A et al (2015) Calculation of organ doses for a large number of patients undergoing CT examinations. AJR Am J Roentgenol 205(4):827–833
61. Smith-Bindman R et al (2015) Radiation doses in consecutive CT examinations from five University of California Medical Centers. Radiology 277(1):134–141
62. McCollough CH et al (2007) Radiation exposure and pregnancy: when should we be concerned? Radiographics 27(4):909–917; discussion 917–8
63. Lin EC (2010) Radiation risk from medical imaging. Mayo Clin Proc 85(12):1142–1146; quiz 1146
64. De Santis M et al (2005) Ionizing radiations in pregnancy and teratogenesis: a review of literature. Reprod Toxicol 20(3):323–329
65. Gomes M, Matias A, Macedo F (2015) Risks to the fetus from diagnostic imaging during pregnancy: review and proposal of a clinical protocol. Pediatr Radiol 45(13):1916–1929
66. Nievelstein RA et al (2012) Radiation exposure and mortality risk from CT and PET imaging of patients with malignant lymphoma. Eur Radiol 22(9):1946–1954
67. Gelfand MJ (2009) Dosimetry of FDG PET/CT and other molecular imaging applications in pediatric patients. Pediatr Radiol 39(Suppl 1):S46–S56
68. Cho ZH et al (2010) Substructural hippocampal glucose metabolism observed on PET/MRI. J Nucl Med 51(10):1545–1548
69. Kuwert T, Ritt P (2016) PET/MRI and PET/CT: is there room for both at the top of the food chain? Eur J Nucl Med Mol Imaging 43(2):209–211
70. Kang WJ (2015) F-18 fluoride positron emission tomography-computed tomography for detecting atherosclerotic plaques. Korean J Radiol 16(6):1257–1261
71. Hyafil F et al (2016) High-risk plaque features can be detected in non-stenotic carotid plaques of patients with ischaemic stroke classified as cryptogenic using combined (18)F-FDG PET/MR imaging. Eur J Nucl Med Mol Imaging 43(2):270–279

Index

A. Ciarmiello, L. Mansi (eds.), *PET-CT and PET-MRI in Neurology*,
DOI 10.1007/978-3-319-31614-7